REFINING THE INTERPRETATION OF NITROGEN ISOTOPES IN DEEP TIME SYSTEMS

EDITED BY: Magali Ader, Thomas Algeo, Pierre Sansjofre, Eva Stüeken and Shucheng Xie

PUBLISHED IN: Frontiers in Earth Science

frontiers Research Topics

ISSN 1664-8714
ISBN 978-2-88976-671-0
DOI 10.3389/978-2-88976-671-0

About Frontiers

Frontiers is more than just an open-access publisher of scholarly articles: it is a pioneering approach to the world of academia, radically improving the way scholarly research is managed. The grand vision of Frontiers is a world where all people have an equal opportunity to seek, share and generate knowledge. Frontiers provides immediate and permanent online open access to all its publications, but this alone is not enough to realize our grand goals.

Frontiers Journal Series

The Frontiers Journal Series is a multi-tier and interdisciplinary set of open-access, online journals, promising a paradigm shift from the current review, selection and dissemination processes in academic publishing. All Frontiers journals are driven by researchers for researchers; therefore, they constitute a service to the scholarly community. At the same time, the Frontiers Journal Series operates on a revolutionary invention, the tiered publishing system, initially addressing specific communities of scholars, and gradually climbing up to broader public understanding, thus serving the interests of the lay society, too.

Dedication to Quality

Each Frontiers article is a landmark of the highest quality, thanks to genuinely collaborative interactions between authors and review editors, who include some of the world's best academicians. Research must be certified by peers before entering a stream of knowledge that may eventually reach the public - and shape society; therefore, Frontiers only applies the most rigorous and unbiased reviews.
Frontiers revolutionizes research publishing by freely delivering the most outstanding research, evaluated with no bias from both the academic and social point of view. By applying the most advanced information technologies, Frontiers is catapulting scholarly publishing into a new generation.

What are Frontiers Research Topics?

Frontiers Research Topics are very popular trademarks of the Frontiers Journals Series: they are collections of at least ten articles, all centered on a particular subject. With their unique mix of varied contributions from Original Research to Review Articles, Frontiers Research Topics unify the most influential researchers, the latest key findings and historical advances in a hot research area! Find out more on how to host your own Frontiers Research Topic or contribute to one as an author by contacting the Frontiers Editorial Office: frontiersin.org/about/contact

REFINING THE INTERPRETATION OF NITROGEN ISOTOPES IN DEEP TIME SYSTEMS

Topic Editors:
Magali Ader, UMR7154 Institut de Physique du Globe de Paris (IPGP), France
Thomas Algeo, University of Cincinnati, United States
Pierre Sansjofre, Muséum National d'Histoire Naturelle, France
Eva Stüeken, University of St Andrews, United Kingdom
Shucheng Xie, China University of Geosciences Wuhan, China

Citation: Ader, M., Algeo, T., Sansjofre, P., Stüeken, E., Xie, S., eds. (2022). Refining the Interpretation of Nitrogen Isotopes in Deep Time Systems. Lausanne: Frontiers Media SA. doi: 10.3389/978-2-88976-671-0

Table of Contents

frontiers | Frontiers in Earth Science

EDITORIAL
published: 05 July 2022
doi: 10.3389/feart.2022.966090

Editorial: Refining the Interpretation of Nitrogen Isotopes in Deep Time Systems

Magali Ader[1], Eva Stüeken[2], Pierre Sansjofre[3], Thomas J. Algeo[4,5,6] and Shucheng Xie[4]*

[1]Institut de Physique Du Globe de Paris, Université Paris Cité, CNRS, Paris, France, [2]School of Earth and Environmental Sciences, University of St Andrews, St Andrews, United Kingdom, [3]Muséum National D'Histoire Naturelle, Institut de Physique des Matériaux et de Cosmochimie, Sorbonne Université, Paris, France, [4]State Key Laboratory of Biogeology and Environmental Geology and School of Earth Sciences, China University of Geosciences, Wuhan, China, [5]State Key Laboratory of Geological Processes and Mineral Resources, China University of Geosciences, Wuhan, China, [6]Department of Geology, University of Cincinnati, Cincinnati, OH, United States

Keywords: nitrogen biogeochemical cycle, modern analog studies, paleoenvironments reconstructions, post depositional alteration, nitrogen isotopes ($d^{15}N$)

Editorial on the Research Topic

Refining the Interpretation of Nitrogen Isotopes in Deep-Time Systems

The nitrogen stable isotope composition in sedimentary rocks ($\delta^{15}N$) is increasingly used in deep-time studies for reconstructing changes in the N-biogeochemical cycle (*e.g.,* reviews in Algeo et al., 2014; Ader et al., 2016; Stüeken et al., 2016). Analytical advances in EA-IRMS systems have greatly decreased the $\delta^{15}N$ measurement time, complexity, and detection limit, while allowing simultaneous $\delta^{13}C$ measurements, making the $\delta^{15}N$ proxy a standard procedure in paleo-environmental studies (Mulvaney, 2012). Hence, it has already provided some insight into the Precambrian evolution of the marine nitrogen cycle (*e.g.,* Thomazo et al., 2011; Ader et al., 2014; Stüeken et al., 2015, 2016, 2021a, Stüeken et al.; Michiels et al., 2017; Zerkle et al., 2017; Kipp et al., 2018; Luo et al., 2018) and its linkage to the history of Earth-surface oxygenation (Lyons et al., 2014) and biotic evolution (Stüeken, 2013). For the more recent Phanerozoic times, it has yielded detailed reconstructions of nitrogen cycling at the regional scale (*e.g.,* Sachs and Repeta, 1999; Fulton et al., 2012), and documented wholesale reorganization of the marine nitrogen cycle in conjunction with major Phanerozoic biocrises (*e.g.,* Xie et al., 2010, 2017; Luo et al., 2011; Schoepfer et al., 2016) as well as systematic changes related to major climate events (*e.g.,* Algeo et al., 2008, 2014; Yao et al., 2015; Luo et al., 2016).

However, many uncertainties remain in the application of this proxy. The goals of the contributions to this Research Topic are thus to further refine the applicability of the $\delta^{15}N$ proxy in sedimentary rocks and develop more nuanced interpretations and research questions for paleo-environmental reconstructions.

As reviewed in several studies (Ader et al., 2006; Robinson et al., 2012; Thomazo and Papineau, 2013; Ader et al., 2016; Stüeken et al.), including two of the present Research Topic (Stüeken et al.; Quan and Adeboye), one of the key uncertainties is the poor knowledge of the impact of diagenesis, catagenesis, metamorphism and fluid migration on primary $\delta^{15}N$ signatures. Yet, it is of utmost importance to be able to precisely reconstruct primary $\delta^{15}N$ values in order to make reliable paleo-environmental reconstructions, these aspects will therefore need to be better charaterized.

Another important uncertainty is the fact that, although the nitrogen fluxes operating at any given time in an ecosystem depend on the presence, absence or abundance of oxygen, several isotopic fractionations associated with N-cycling are not diagnostic of a particular redox state and hence of nitrogen speciation as nitrate or ammonium (Brandes et al., 2007; Thamdrup, 2012; Quan and Adeboye).

OPEN ACCESS

Edited and reviewed by:
Martyn Tranter,
Aarhus University, Denmark

****Correspondence:***
Magali Ader
ader@ipgp.fr

Specialty section:
This article was submitted to Geochemistry, a section of the journal Frontiers in Earth Science

Received: *10 June 2022*
Accepted: *15 June 2022*
Published: *05 July 2022*

Citation:
Ader M, Stüeken E, Sansjofre P, Algeo TJ and Xie S (2022) Editorial: Refining the Interpretation of Nitrogen Isotopes in Deep Time Systems. Front. Earth Sci. 10:966090. doi: 10.3389/feart.2022.966090

In addition, most of the current underlying assumptions supporting $\delta^{15}N$ interpretation in the sedimentary rock record rely heavily on analogies with the present-day marine nitrogen cycle (*e.g.,* Galbraith et al., 2008; Sigman et al., 2009; Robinson et al., 2012; Tesdal et al., 2013), which may not be the best analogue for deep-time lakes, restricted basins and oceans.

Two papers address the goal of refining the applicability of the $\delta^{15}N$ proxy via the study of modern systems: the Dziani Dzaha, a saline and alkaline lake (Cadeau et al.), and the Coorong lagoon showing a strong salinity gradient (Priestley et al.). The results show that, while in the Coorong lagoon sediment $\delta^{15}N$ records as expected the $\delta^{15}N$ of primary producers (Priestley et al.), in the Dziani Dzaha lake the sediment $\delta^{15}N$ values are more positive by three‰ compared to primary producers, possibly as a result of ^{15}N-enriched ammonium assimilation in alkaline bottom waters (Cadeau et al.). Taken together, these two studies highlight that not only redox conditions but also salinity and pH may influence the nitrogen cycle. These aspects will need to be better integrated into future studies of deep-time nitrogen cycling.

The remaining papers address the goal of developing more nuanced interpretation of the $\delta^{15}N$ proxy in deep-time by coupling it to other proxies, such as redox indicators, C/N ratio, $\delta^{13}C_{org}$ and $\delta^{13}C_{carb}$ and biomarker $\delta^{15}N$. Two papers characterize nitrogen speciation (ammonium or nitrate) in the water column by coupling $\delta^{15}N$ to other aqueous redox proxies. Johnson et al. use concentrations of U, V and Mo, along with Fe-speciation, in sedimentary successions of the Yangtze Platform during the Neoproterozoic Cryogenian Period, allowing them to show that nitrate was stable in the water column and to identify temporal variations in denitrification rates. Riquier et al. in a detailed multi-proxy study ($\delta^{13}C_{org}$, $\delta^{15}N_{bulk}$, Rock-Eval and trace metals) of the oceanic anoxic event (OAE-2) of the DSDP 367 succession from Cape Verde, show that $\delta^{15}N$ values can be interpreted as evidence of ammonium assimilation. This implies that ammonium (and hence anoxia) reached the photic zone, corroborating molecular studies indicating photic zone anoxia at that time (Higgins et al., 2012).

Three studies identify feedbacks between the C- and N-cycles by coupling $\delta^{15}N$ to $\delta^{13}C_{carb}$ and/or $\delta^{13}C_{org}$ at high stratigraphic resolution. Xu et al. identify subtle changes in $\delta^{15}N$ in the Yangtze platform that coincided with the Shuram Excursion, *i.e.*, the largest negative $\delta^{13}C_{carb}$ excursion in Earth history (Grotzinger et al., 2011; Cao et al., 2020). This work is novel in that it highlights the variability in fractionation factors as a possible driver of subtle $\delta^{15}N$ shifts in the paleoenvironment. Fraga-Ferreira et al. this volume also identify subtle changes in the $\delta^{15}N$ values that coincided with the onset of an extreme $\delta^{13}C_{carb}$ positive isotope excursion and with variations in Sr isotope ratios and redox tracers in several sections of the Ediacarian/Cambrian Bambui Group (Brazil) (Caetano-Filho et al., 2021), further highlighting the close linkage between nitrogen and carbon cycling. In the same vein, Mercuzot et al. explore a combination of several proxies ($\delta^{15}N_{bulk}$ to C/N, $\delta^{13}C_{org}$, Rock-Eval and palynofacies analyses) to deconvolute terrestrial from autochthonous organic matter in several sections of Late Carboniferous to Early Permian continental basins, providing insights into nitrogen cycling during times of enhanced autochthonous organic matter accumulation.

Finally, Hallmann et al., following the lead of a handful of previous studies (e.g., Sachs and Repeta, 1999; Higgins et al., 2012) reaffirmed the power of coupling of $\delta^{15}N$ in bulk rocks and kerogens to that of N-containing biomarkers. In the case of Ediacaran sedimentary successions from Oman, the authors were also able to show that primary producers assimilated ammonium at a shallow redoxcline during times of enhanced water-column stratification. Furthermore, they identify and tentatively quantify the biomass produced by eukaryotic and cyanobacterial oxygenic primary producers, as well as anoxygenic primary producers.

The findings reported in these contributions show that providing context using other proxies allows the interpretation of even subtle changes in $\delta^{15}N$. Collectively, the studies in this Research Topic serve to further our understanding of the deep-time marine nitrogen cycle, providing a baseline for evaluating present-day anthropogenic changes in nitrogen cycling and their impacts on the environment and biosphere (Fowler et al., 2013).

AUTHOR CONTRIBUTIONS

MA drafted a first version of this editorial. All authors contributed to and approved the final version.

ACKNOWLEDGMENTS

We deeply thank all the authors, reviewers and Editors of Frontiers in Earth Sciences, who have participated in this Research Topic.

REFERENCES

Ader, M., Cartigny, P., Boudou, J. P., Oh, J. H., Petit, E., and Javoy, M. (2006). Nitrogen Isotopic Evolution of Carbonaceous Matter during Metamorphism: Methodology and Preliminary Results. *Chem. Geol.* 232 (3-4), 152–169. doi:10.1016/j.chemgeo.2006.02.019

Ader, M., Sansjofre, P., Halverson, G. P., Busigny, V., Trindade, R. I. F., Kunzmann, M., et al. (2014). Ocean Redox Structure across the Late Neoproterozoic Oxygenation Event: A Nitrogen Isotope Perspective. *Earth Planet. Sci. Lett.* 396, 1–13. doi:10.1016/j.epsl.2014.03.042

Ader, M., Thomazo, C., Sansjofre, P., Busigny, V., Papineau, D., Laffont, R., et al. (2016). Interpretation of the Nitrogen Isotopic Composition of Precambrian Sedimentary Rocks: Assumptions and Perspectives. *Chem. Geol.* 429, 93–110. doi:10.1016/j.chemgeo.2016.02.010

Algeo, T. J., Meyers, P. A., Robinson, R. S., Rowe, H., and Jiang, G. Q. (2014). Icehouse-greenhouse Variations in Marine Denitrification. *Biogeosciences* 11 (4), 1273–1295. doi:10.5194/bg-11-1273-2014

Algeo, T., Rowe, H., Hower, J. C., Schwark, L., Herrmann, A., and Heckel, P. (2008). Changes in Ocean Denitrification during Late Carboniferous Glacial-Interglacial Cycles. *Nat. Geosci.* 1 (10), 709–714. doi:10.1038/ngeo307

Brandes, J. A., Devol, A. H., and Deutsch, C. (2007). New Developments in the Marine Nitrogen Cycle. *Chem. Rev.* 107 (2), 577–589. doi:10.1021/cr050377t

Caetano-Filho, S., Sansjofre, P., Ader, M., Paula-Santos, G. M., Guacaneme, C., Babinski, M., et al. (2021). A Large Epeiric Methanogenic Bambuí Sea in the Core of Gondwana Supercontinent? *Geosci. Front.* 12 (1), 203–218. doi:10.1016/j.gsf.2020.04.005

Cao, M., Daines, S. J., Lenton, T. M., Cui, H., Algeo, T. J., Dahl, T. W., et al. (2020). Comparison of Ediacaran Platform and Slope δ238U Records in South China: Implications for Global-Ocean Oxygenation and the Origin of the Shuram Excursion. *Geochimica Cosmochimica Acta* 287, 111–124. doi:10.1016/j.gca.2020.04.035

Fowler, D., Coyle, M., Skiba, U., Sutton, M. A., Cape, J. N., Reis, S., et al. (2013). The Global Nitrogen Cycle in the Twenty-First Century. *Phil. Trans. R. Soc. B* 368 (1621), 20130164. doi:10.1098/rstb.2013.0164

Fulton, J. M., Arthur, M. A., and Freeman, K. H. (2012). Black Sea Nitrogen Cycling and the Preservation of Phytoplankton δ^{15}N Signals during the Holocene. *Glob. Biogeochem. Cycles* 26 (2), GB2030. doi:10.1029/2011gb004196

Galbraith, E. D., Sigman, D. M., Robinson, R. S., and Pedersen, T. F. (2008). Nitrogen in Past Marine Environments. *Nitrogen Mar. Environ.* 2, 1497–1535. doi:10.1016/b978-0-12-372522-6.00034-7

Grotzinger, J. P., Fike, D. A., and Fischer, W. W. (2011). Enigmatic Origin of the Largest-Known Carbon Isotope Excursion in Earth's History. *Nat. Geosci.* 4 (5), 285–292. doi:10.1038/ngeo1138

Higgins, M. B., Robinson, R. S., Husson, J. M., Carter, S. J., and Pearson, A. (2012). Dominant Eukaryotic Export Production during Ocean Anoxic Events Reflects the Importance of Recycled NH 4 +. *Proc. Natl. Acad. Sci. U.S.A.* 109 (7), 2269–2274. doi:10.1073/pnas.1104313109

Kipp, M. A., Stüeken, E. E., Yun, M., Bekker, A., and Buick, R. (2018). Pervasive Aerobic Nitrogen Cycling in the Surface Ocean across the Paleoproterozoic Era. *Earth Planet. Sci. Lett.* 500, 117–126. doi:10.1016/j.epsl.2018.08.007

Luo, G., Junium, C. K., Izon, G., Ono, S., Beukes, N. J., Algeo, T. J., et al. (2018). Nitrogen Fixation Sustained Productivity in the Wake of the Palaeoproterozoic Great Oxygenation Event. *Nat. Commun.* 9 (1), 978–979. doi:10.1038/s41467-018-03361-2

Luo, G., Algeo, T. J., Zhan, R., Yan, D., Huang, J., Liu, J., et al. (2016). Perturbation of the Marine Nitrogen Cycle during the Late Ordovician Glaciation and Mass Extinction. *Palaeogeogr. Palaeoclimatol. Palaeoecol.* 448, 339–348. doi:10.1016/j.palaeo.2015.07.018

Luo, G., Wang, Y., Algeo, T. J., Kump, L. R., Bai, X., Yang, H., et al. (2011). Enhanced Nitrogen Fixation in the Immediate Aftermath of the Latest Permian Marine Mass Extinction. *Geology* 39 (7), 647–650. doi:10.1130/g32024.1

Lyons, T. W., Reinhard, C. T., and Planavsky, N. J. (2014). The Rise of Oxygen in Earth's Early Ocean and Atmosphere. *Nature* 506 (7488), 307–315. doi:10.1038/nature13068

Michiels, C. C., Darchambeau, F., Roland, F. A. E., Morana, C., Llirós, M., García-Armisen, T., et al. (2017). Iron-dependent Nitrogen Cycling in a Ferruginous Lake and the Nutrient Status of Proterozoic Oceans. *Nat. Geosci.* 10 (3), 217–221. doi:10.1038/ngeo2886

Mulvaney, R. L. (2012). "Mass Spectrometry," in *Nitrogen Isotope Techniques*. Editors E. Paul, J. Melillo, R. Knowles, and H. Blackburn (Amsterdam: Elsevier), 11–58.

Robinson, R. S., Kienast, M., Luiza Albuquerque, A., Altabet, M., Contreras, S., De Pol Holz, R., et al. (2012). A Review of Nitrogen Isotopic Alteration in Marine Sediments. *Paleoceanography* 27 (4), 002321. doi:10.1029/2012pa002321

Sachs, J. P., and Repeta, D. J. (1999). Oligotrophy and Nitrogen Fixation during Eastern Mediterranean Sapropel Events. *Science* 286 (5449), 2485–2488. doi:10.1126/science.286.5449.2485

Schoepfer, S. D., Algeo, T. J., Ward, P. D., Williford, K. H., and Haggart, J. W. (2016). Testing the Limits in a Greenhouse Ocean: Did Low Nitrogen Availability Limit Marine Productivity during the End-Triassic Mass Extinction? *Earth Planet. Sci. Lett.* 451, 138–148. doi:10.1016/j.epsl.2016.06.050

Sigman, D. M., Karsh, K. L., and Casciotti, K. L. (2009). *Ocean Process Tracers: Nitrogen Isotopes in the Ocean*. San Francisco: Academia.

Stüeken, E. E., Buick, R., Guy, B. M., and Koehler, M. C. (2015). Isotopic Evidence for Biological Nitrogen Fixation by Molybdenum-Nitrogenase from 3.2 Gyr. *Nature* 520 (7549), 666–669. doi:10.1038/nature14180

Stüeken, E. E. (2013). A Test of the Nitrogen-Limitation Hypothesis for Retarded Eukaryote Radiation: Nitrogen Isotopes across a Mesoproterozoic Basinal Profile. *Geochimica Cosmochimica Acta* 120, 121–139. doi:10.1016/j.gca.2013.06.002

Stüeken, E. E., Gregory, D. D., Mukherjee, I., and McGoldrick, P. (2021). Sedimentary Exhalative Venting of Bioavailable Nitrogen into the Early Ocean. *Earth Planet. Sci. Lett.* 565, 116963. doi:10.1016/j.epsl.2021.116963

Stüeken, E. E., Kipp, M. A., Koehler, M. C., and Buick, R. (2016). The Evolution of Earth's Biogeochemical Nitrogen Cycle. *Earth-Science Rev.* 160, 220–239. doi:10.1016/j.earscirev.2016.07.007

Stüeken, E. E., Zaloumis, J., Meixnerová, J., and Buick, R. (2017). Differential Metamorphic Effects on Nitrogen Isotopes in Kerogen Extracts and Bulk Rocks. *Geochimica Cosmochimica Acta* 217, 80–94. doi:10.1016/j.gca.2017.08.019

Tesdal, J.-E., Galbraith, E. D., and Kienast, M. (2013). Nitrogen Isotopes in Bulk Marine Sediment: Linking Seafloor Observations with Subseafloor Records. *Biogeosciences* 10 (1), 101–118. doi:10.5194/bg-10-101-2013

Thamdrup, B. (2012). New Pathways and Processes in the Global Nitrogen Cycle. *Annu. Rev. Ecol. Evol. Syst.* 43, 407–428. doi:10.1146/annurev-ecolsys-102710-145048

Thomazo, C., Ader, M., and Philippot, P. (2011). Extreme 15N-Enrichments in 2.72-Gyr-Old Sediments: Evidence for a Turning Point in the Nitrogen Cycle. *Geobiology* 9, 107–120. doi:10.1111/j.1472-4669.2011.00271.x

Thomazo, C., and Papineau, D. (2013). Biogeochemical Cycling of Nitrogen on the Early Earth. *Elements* 9 (5), 345–351. doi:10.2113/gselements.9.5.345

Xie, S., Algeo, T. J., Zhou, W., Ruan, X., Luo, G., Huang, J., et al. (2017). Contrasting Microbial Community Changes during Mass Extinctions at the Middle/Late Permian and Permian/Triassic Boundaries. *Earth Planet. Sci. Lett.* 460, 180–191. doi:10.1016/j.epsl.2016.12.015

Xie, S., Pancost, R. D., Wang, Y., Yang, H., Wignall, P. B., Luo, G., et al. (2010). Cyanobacterial Blooms Tied to Volcanism during the 5 m.Y. Permo-Triassic Biotic Crisis. *Geology* 38 (5), 447–450. doi:10.1130/g30769.1

Yao, L., Qie, W., Luo, G., Liu, J., Algeo, T. J., Bai, X., et al. (2015). The TICE Event: Perturbation of Carbon-Nitrogen Cycles during the Mid-Tournaisian (Early Carboniferous) Greenhouse-Icehouse Transition. *Chem. Geol.* 401, 1–14. doi:10.1016/j.chemgeo.2015.02.021

Zerkle, A. L., Poulton, S. W., Newton, R. J., Mettam, C., Claire, M. W., Bekker, A., et al. (2017). Onset of the Aerobic Nitrogen Cycle during the Great Oxidation Event. *Nature* 542, 465–467. doi:10.1038/nature20826

Conflict of Interest: The authors declare that the research was conducted in the absence of any commercial or financial relationships that could be construed as a potential conflict of interest.

Publisher's Note: All claims expressed in this article are solely those of the authors and do not necessarily represent those of their affiliated organizations, or those of the publisher, the editors and the reviewers. Any product that may be evaluated in this article, or claim that may be made by its manufacturer, is not guaranteed or endorsed by the publisher.

frontiers in Earth Science

ORIGINAL RESEARCH
published: 30 April 2021
doi: 10.3389/feart.2021.675726

Reconstructing Nitrogen Sources to Earth's Earliest Biosphere at 3.7 Ga

Eva E. Stüeken[1], Toby Boocock[1], Kristoffer Szilas[2], Sami Mikhail[1] and Nicholas J. Gardiner[1,3]*

[1] School of Earth and Environmental Sciences, University of St Andrews, St Andrews, United Kingdom, [2] Department of Geosciences and Natural Resource Management, University of Copenhagen, Copenhagen K, Denmark, [3] School of Earth, Atmosphere and Environment, Monash University, Melbourne, VIC, Australia

Earth's sedimentary record has preserved evidence of life in rocks of low metamorphic grade back to about 3.2–3.5 billion years ago (Ga). These lines of evidence include information about specific biological metabolisms, permitting the reconstruction of global biogeochemical cycles in the early Archean. Prior to 3.5 Ga, the geological record is severely compromised by pervasive physical and chemical alteration, such as amphibolite-granulite facies metamorphic overprinting. Despite this alteration, evidence of biogenic organic matter is preserved in rare localities, including meta-turbidites from the 3.8 to 3.7 Ga Isua Supracrustal Belt, Western Greenland. But detailed insights into metabolic strategies and nutrient sources during the time of deposition of these Eoarchean meta-sedimentary rocks are lacking. Here we revisit the Isua meta-turbidites and provide new data for metal abundances as well as organic carbon and nitrogen isotope values. Our results reveal mixing between authigenic and detrital nitrogen phases with the authigenic phase likely fractionated by metamorphic degassing. Rayleigh fractionation models of these 3.7 Ga samples indicate pre-metamorphic $\delta^{15}N$ values of between −1 and −10‰. The most plausible initial values are below −5‰, in agreement with a prior study. While the upper endmember of −1‰ could indicate biological N_2 fixation at 3.7 Ga, the more plausible lighter values may point toward a distinct biogeochemical nitrogen cycle at that time, relative to the rest of Earth's history. In light of recent experimental and phylogenetic data aligned with observations from the modern atmosphere, we tentatively conclude that lightning and/or high-energy photochemical reactions in the early atmosphere may have contributed isotopically light nitrogen to surface environment(s) preserved in the Isua turbidites. In this case, recycling of Eoarchean sediments may have led to the isotopically light composition of the Earth's upper mantle dating back to at least 3.2 Ga.

Keywords: Eoarchean, Isua, metamorphism, lightning, nitrogen isotopes

OPEN ACCESS

Edited by:
Naohiko Ohkouchi, Japan Agency for Marine-Earth Science and Technology (JAMSTEC), Japan

Reviewed by:
Tsuyoshi Komiya, The University of Tokyo, Japan
Huan Cui, Université de Paris, France

****Correspondence:***
Eva E. Stüeken
ees4@st-andrews.ac.uk

Specialty section:
This article was submitted to Biogeoscience, a section of the journal Frontiers in Earth Science

Received: *03 March 2021*
Accepted: *06 April 2021*
Published: *30 April 2021*

Citation:
Stüeken EE, Boocock T, Szilas K, Mikhail S and Gardiner NJ (2021) Reconstructing Nitrogen Sources to Earth's Earliest Biosphere at 3.7 Ga. Front. Earth Sci. 9:675726. doi: 10.3389/feart.2021.675726

INTRODUCTION

Signatures of life on Earth have previously been identified in some of the oldest rocks on Earth, dating back to almost 4 billion years ago (reviewed by Lepot, 2020). These signatures include carbon isotope values indicative of biological CO_2 fixation (Rosing, 1999), which today plays a major role in the global carbon cycle and may have done so for most of Earth's history (Schidlowski, 2001). In

contrast, the antiquity of other metabolic pathways (e.g., nitrogen, phosphorus, or sulfur uptake) is more elusive, because metamorphic alteration severely impacts our ability to extract primary information from the oldest paleobiological records. For example, in the case of nitrogen, evidence of biological N_2 fixation has so far been taken back to ca. 3.2 Ga (Beaumont and Robert, 1999; Stüeken et al., 2015; Homann et al., 2018; Koehler et al., 2019a), though phylogenetic data suggest that this metabolism already existed in the last universal common ancestor, possibly as early as 3.8 Ga (Weiss et al., 2016).

A widely used geochemical tool to reconstruct nitrogen cycling in deep time are nitrogen isotopes (Ader et al., 2016; Stüeken et al., 2016); however, primary isotopic values are easily perturbed during metamorphism at greenschist facies grades and above (reviewed by Thomazo and Papineau, 2013), which prohibits detecting specific nitrogen metabolisms in Eoarchean rocks. A lack of knowledge about the primary $\delta^{15}N$ composition of the sedimentary cover in the earliest intervals of Earth's history also has important implications for our understanding of the geological nitrogen cycle through time. In the modern Earth system, biogenic nitrogen buried in sediments can be subducted into Earth's mantle in significant quantities, which, if true in the past, may have had important implications on the evolution of atmospheric N_2 pressure, and therefore planetary habitability, over billion-year timescales (e.g., Mikhail and Sverjensky, 2014; Barry and Hilton, 2016; Busigny et al., 2019). However, constraining the onset of biogenic nitrogen burial requires better constraints on the biogenic $\delta^{15}N$ endmember in the past, because this endmember is required to distinguish sedimentary from mantle-derived nitrogen sources. In short, there is a significant need to determine the primary $\delta^{15}N$ composition of Eoarchean sediments.

To address this knowledge gap, we revisited some of the world's oldest metasedimentary rocks located in the Eoarchean Isua Supracrustal Belt, West Greenland, where previous studies documented graphitic schists with $\delta^{13}C$ values and elemental compositions diagnostic of a biogenic origin (Rosing, 1999; Hassenkam et al., 2017). We analyzed these rocks for nitrogen isotopes and abundances and determined a best-estimate initial composition via a Rayleigh fractionation model. Albeit indirect, our approach allows us to place new constraints on plausible nitrogen sources to Earth's earliest biosphere.

GEOLOGICAL SETTING

The Eoarchean Isua Supracrustal Belt (ISB) of South Western Greenland (**Figure 1**) represents the oldest meta-sedimentary and meta-volcanic sequence on Earth and has therefore been intensively studied since the 1970s (e.g., Moorbath et al., 1973; Moorbath et al., 1975; Baadsgaard et al., 1984; Nutman and Friend, 2009; Nutman et al., 2019). The ISB is hosted by the >3.6 Ga Itsaq Gneiss Complex, which is the world's most extensive domain of Early Archean crustal rocks, and forms part of the North Atlantic Craton (Nutman et al., 1996). This craton represents the amalgamation of several distinct tectonomagmatic crustal blocks, and therefore experienced a long and complex deformation and thermal history (Friend and Nutman, 2019). The complex nature of the Itsaq Gneiss Complex and the ISB in particular, complicates the interpretation of the protoliths and the degree to which these rocks preserves primary features (Myers, 2001; Whitehouse et al., 2009).

The metamorphic mineral assemblages recorded by the ISB documents a polymetamorphic history with thermal events in both the early and late Archean (Boak and Dymek, 1982; Rollinson, 2002; Rollinson, 2003). Rocks with garnet-hornblende-plagioclase-quartz and garnet–epidote–biotite–muscovite–quartz–graphite assemblages (Boak and Dymek, 1982; Rosing, 1999) support a prograde peak metamorphic temperature of ∼550°C and pressure of ∼5 to 7 kbar (∼15 km burial depth) before 3.6 Ga (Boak and Dymek, 1982). Recently it has been proposed that contrasting metamorphic T/P regimes are recorded in the ISB, resembling modern paired metamorphic belts, which support the hypothesis that the ISB formed at a convergent margin with peak pressure above 1 GPa (Nutman et al., 2020; Guotana, submitted). Thus, overwhelmingly, the ISB has been interpreted in the context of having formed by subduction zone processes (Hanmer and Greene, 2002; Polat et al., 2002; Jenner et al., 2009; Hoffmann et al., 2010). However, recent studies questioned this long-held model based on a new structural analysis of the ISB (Webb et al., 2020), and due to a detailed investigation of the metamorphic regimes that ISB experienced (Ramírez-Salazar et al., 2021). The latter authors found evidence for three distinct metamorphic events (M_i) with peak conditions of 550–600°C and 0.5–0.7 GPa at M_1, <540°C and <0.5 GPa at M_2, and finally low temperature retrogression of <500°C at M_3. M_1 and M_2 likely occurred at >3.5 and >2.9 Ga, whereas M_3 is currently not well-constrained.

For this study, we focused on a succession of metamorphosed siliciclastic sedimentary rocks (**Figure 2**) that have previously been interpreted as a meta-turbidite and yielded organic carbon isotope values indicative of biogenic organic matter (Nutman et al., 1984; Rosing et al., 1996; Rosing, 1999). The succession is approximately 50 m thick; individual beds are 10–70 cm in thickness and defined by sharp bases and normal grading. The meta-turbidite rests on top of meta-basalts with pillow structures. Prior work on U abundances was interpreted as evidence of oxic conditions conducive of U mobilization in the depositional basin (Rosing and Frei, 2004). The U would then have been trapped in locally anoxic sediments represented by roughly 10 cm-thick organic-rich slates of the turbidite succession (**Figure 2**). The U abundance data were thus used to infer the presence of oxygenic photosynthetic bacteria at 3.7 Ga. In this study, we sampled the same slate horizons for analyses of organic carbon and nitrogen isotopes as well as major and minor element abundances.

METHODS

The rock samples were cut with a water-cooled diamond saw to remove any weathered surfaces. The interiors were then hammered into sub-cm sized chips with a steel pestle on a steel plate, and the chips were subsequently washed with methanol

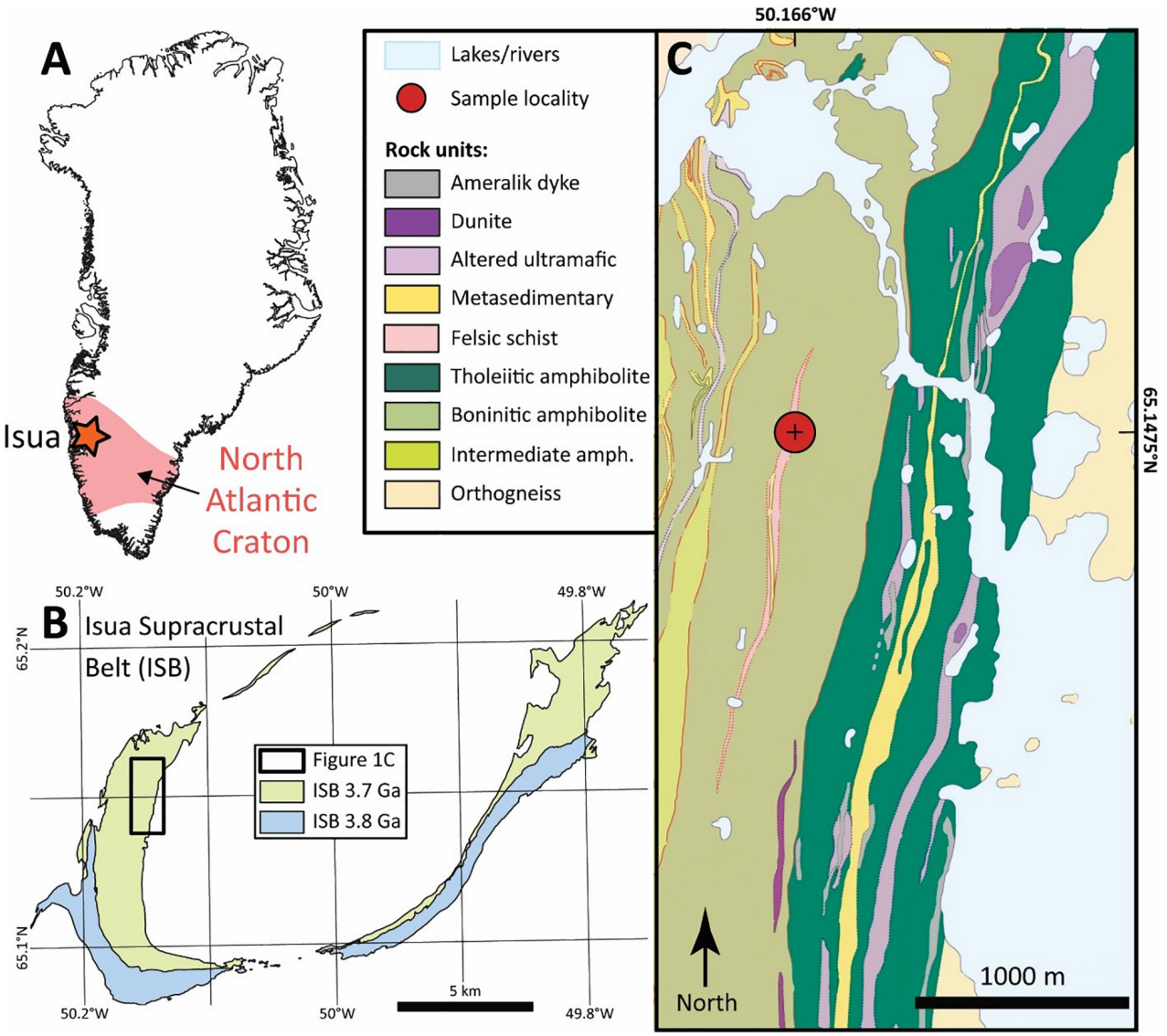

FIGURE 1 | Geological map of the Isua Supracrustal Belt. **(A)** Shows the extent of the Archean North Atlantic Craton in Greenland, with the position of Isua marked by the star. **(B)** Overview map of the Isua Supracrustal Belt, with the two distinct sequences shown in blue and green colors. The study area is outlined by the box. **(C)** Detailed geological map of the locality from which the samples of the present study were collected. Modified after and Nutman and Friend (2009) and Waterton (submitted).

(reagent grade), 1M HCl (reagent grade) and 18 MΩ/cm^{-1} DI-water. The clean chips were dried overnight in an oven at 70°C and then pulverized in an agate ball mill. The milling vessels were cleaned with pre-combusted silica sand (500°C overnight) in between samples, wiped with DI-water and methanol, and blow-dried with compressed air. The rock powders were stored in pre-combusted scintillation vials. Prior to isotopic analyses, an aliquot of ∼0.5 g of each sample was decarbonated with 2M HCl in pre-combusted Pyrex centrifuge tubes and then washed three times with DI-water. The decarbonated residue was dried in a closed oven at 70°C. For organic carbon and total sulfur analyses, around 50 mg of each decarbonated powder were weighed into tin capsules (8 × 5 mm^2 in cross section, Thermo Fisher), mixed with ∼5 mg of V_2O_5 (Elemental Microanalysis), and analyzed by flash-combustion with an elemental analyzer (EA IsoLink, Thermo Fisher) coupled to a gas source mass spectrometer (MAT253, Thermo Fisher) via a ConFlo IV (Thermo Fisher). The data were calibrated with the international reference materials USGS-40 and USGS-41 for carbon and IAEA-S2 and IAEA-S3 for sulfur. Results are expressed in standard delta notation (δ [‰] = [($R_{sample}/R_{standard}$) − 1] × 1000), where R = $^{13}C/^{12}C$ for $\delta^{13}C$ and R = $^{34}S/^{32}S$ for $\delta^{34}S$. Reference standards are VPDB for carbon and VCDT for sulfur. The average reproducibility of replicate analyses of the same sample was ±0.4‰ for $\delta^{13}C$ and ±0.6‰ for $\delta^{34}S$. Peak areas were calibrated for total organic carbon (TOC) and total sulfur (TS) abundances.

FIGURE 2 | Photo of the main outcrop of the turbidite locality from which the studied samples were taken, which is the same locality that was documented by Rosing (1999). The graphitic slate is the obvious dark layer in the middle, with the proposed meta-turbidites on either side of it displaying gradational lamination. This outcrop is a protected site, and hence the samples for this study are from the continuation of the strata a couple of meters above and behind this rock face. Backpack for scale.

For nitrogen abundance and isotopes, analyses were done by offline combustion, which allows accurate isotopic analyses down to low nitrogen abundances (<10 ppm) in hard-to-combust silicate phases (Boocock et al., 2020). Quartz glass tubes were cleaned by combustion at 1,000°C for >6 h before use. Similarly, CuO wire was prepared by pre-combustion at 800°C for >6 h to ensure that any adsorbed N_2 impurities were volatilized before introducing samples, hence minimizing the reagent nitrogen blank. Approximately 300 mg of sample powder were then weighed into the quartz tubes and mixed with 0.5 g of CuO wire. Sample tubes were attached to a custom-built vacuum line and evacuated overnight to $<10^{-5}$ mbar. During the evacuation, the samples and quartz tubes were heated to 120°C to remove adsorbed moisture and volatile contaminants. The next day, the quartz tubes were sealed with an oxy-acetylene blow torch. Sealed evacuated tubes containing sample powders were then placed into a muffle furnace at 950°C for 4 h, followed by 2 h at 600°C and slow cooling to room temperature. This procedure converts all rock-bound nitrogen into N_2 gas. The gas samples were analyzed with a tube cracker attached to the same ConFlo and mass spectrometer as the elemental analyzer used for carbon and sulfur analyses. Analyses were calibrated with USGS-61 and USGS-62 and are reported as $\delta^{15}N = [(^{15}N/^{14}N)_{sample}/(^{15}N/^{14}N)_{air}) - 1] \times 1000$. Procedural blanks were measured throughout the analytical campaign and had an average composition of 20.1 nmol total N at with a $\delta^{15}N$ value of $-2.1 \pm 0.9‰$. This average value was subtracted from all standard and sample data. To assess analytical accuracy, we analyzed three aliquots of BHVO-2 and obtained an isotopic value of $+2.3 \pm 0.3‰$ and a total nitrogen abundance of 20.8 ± 0.9 ppm, which agrees well with previous studies (Feng et al., 2018; Boocock et al., 2020).

For major and minor elemental abundance analyses, untreated rock powders were sent to Australian Laboratory Services in Dublin. Here, samples were dissolved in HF, $HClO_4$, HNO_3 and HCl and analyzed by ICP-MS and ICP-OES. The reproducibility (1SD) of major elements was generally better than 4% (relative error) and better than 11% for minor elements.

RESULTS

The results are summarized in **Tables 1**, **2**. Eight of the nine samples contain moderate amounts of organic carbon (TOC = 0.05 – 0.80 wt.%, **Figure 3B**) and show a tight distribution of carbon isotope values around a mean of $-18.1 \pm 0.5‰$ (1SD), which is in good agreement with previous measurements on the same stratigraphic unit (-14 to $-20‰$, Rosing, 1999). The remaining sample had too little TOC (0.003 wt.%) for reliable carbon isotope determinations. Total nitrogen abundances (TN) and $\delta^{15}N$ values show two populations, one with low abundances (4.8 ± 1.3 ppm) and $\delta^{15}N$ around $+2.3 \pm 0.7‰$ and a second with slightly higher abundances (26.2 ± 6.4 ppm) and an average $\delta^{15}N$ of $+6.1 \pm 0.7‰$ (**Figure 3A**). TN and $\delta^{15}N$ thus positively correlate with each other, which is opposite to the negative correlation that would be expected from metamorphic devolatilization of a homogeneous starting composition (Haendel et al., 1986). To assess the degree of lab-derived contamination, pure minerals (quartz, plagioclase, orthoclase, biotite, muscovite, kaolinite) and baked silica sand were processed through the same rock crushing and

TABLE 1 | Major and minor element abundances.

	Al	Ca	Ce	Co	Cr	Cu	Fe	K	La	Mg	Mn	Mo	Na	Ni	P	Pb	Sc	Th	Ti	U	V	Y	Zn	Zr
	%	%	ppm	ppm	ppm	ppm	%	%	ppm	%	ppm	ppm	%	ppm	ppm	ppm	ppm	ppm	%	ppm	ppm	ppm	ppm	ppm
208288	6.9	0.82	4.18	14.3	51	59.6	4.68	0.85	1.7	1.07	565	0.36	2.58	88.5	310	1.7	6.5	2.52	0.221	0.6	35	7.3	36	87
208289	8.22	1.1	30.9	16.9	19	0.2	4.92	0.62	13	1.7	777	0.02*	4.29	24.7	440	2.1	9.7	3.2	0.365	0.7	70	10.5	95	119
208290	6.33	2.37	7.95	3.5	45	4.1	2.03	3.21	3.8	0.52	1,290	0.07	0.12	16.4	330	1.4	8.1	2.02	0.234	0.6	47	7.7	18	76
208291	8.86	2.93	20.4	9.4	89	0.1*	4.75	3.58	9.1	1.42	1,290	0.02*	0.46	66.9	470	2.4	11.9	3.08	0.36	0.7	72	9.8	46	94
208292	9.23	1.47	29	9.3	97	0.1*	5.49	3.83	12.1	1.69	1,400	0.02*	0.35	71.5	490	1.7	12.3	3.44	0.387	0.7	78	9.8	54	119
208293	7.83	2.78	22.7	12.6	123	0.1*	4.51	2.34	9.1	1.86	1,720	0.07	1.44	101	440	2.7	12	2.52	0.349	0.7	75	9.5	54	115
208294	5.92	0.83	4.34	21.7	41	80.9	3.83	0.59	1.7	0.76	428	0.46	2.76	101.5	350	1.6	5	2.66	0.196	0.9	22	5.7	28	110
208295	9.04	2.85	24.9	11.3	84	0.1*	7.45	4	10.1	1.04	929	0.09	0.39	66	400	3.3	9.4	2.47	0.319	0.7	65	10	66	32
208296	9.19	0.4	6.07	15.6	97	8.5	8.37	2.31	2.2	1.68	2,510	0.14	1.2	116	440	1.1	10.8	3.29	0.338	0.7	66	20.6	59	115

** = measurements were below detection limit and are reported as 0.5 × the limit of detection.*

TABLE 2 | Organic carbon, total nitrogen and total sulfur data.

	TOC	$\delta^{13}C$	TN	$\delta^{15}N$	TS	$\delta^{34}S$	C/N
	(wt.%)	(‰)	(ppm)	(‰)	(wt.%)	(‰)	(mol/mol)
208288	0.323	−18.83	6.1	3.02	0.23	1.81	620
208289	0.003		3.4	1.75	0.00		10
208290	0.395	−17.54	25.1	5.89	0.01	−0.29	183
208291	0.117	−18.34	30.9	5.96	0.00		44
208292	0.119	−17.95	36.6	6.93	0.00		38
208293	0.045	−18.42	19.7	6.10	0.00		27
208294	0.622	−18.25	4.8	2.05	0.23	1.90	1509
208295	0.797	−17.41	23.4	6.75	0.00		397
208296	0.427	−18.05	21.6	5.06	0.00		230

decarbonation protocol and found to accumulate a maximum of 1 ppm N; some specimens lost N compared to a hand-crushed aliquot due to the washing step and acid-treatment of the rock powder (Stüeken et al., 2021). Hence contamination in the laboratory is not a major contributor of N to the samples. The covariance between TN and $\delta^{15}N$ is therefore indigenous to the rocks.

Molar ratios of organic carbon to total nitrogen (hereafter C/N) vary widely with C/N ratios from 10 to 1,509. TN is not correlated with TOC (r^2 = 0.01) but strongly correlated with potassium abundances (r^2 = 0.89) (**Figures 3C,D**), indicating that the nitrogen contained in these rocks is now mostly silicate-bound as opposed to organic-bound. Total sulfur concentrations range from 0.001 to 0.230 wt.%. Only three samples yielded enough sulfur for isotopic analyses and showed $\delta^{34}S$ values around a mean of +1.1 ± 1.2‰. Total sulfur is not correlated with TOC (**Figure 4A**) but covaries with Cu and Mo (**Figures 4B,D**), indicating that these metals are dominantly sulfide-bound. Molybdenum shows no correlation with TOC (**Figure 4C**), counter to what is observed in modern marine sediments (Wilde et al., 2004). Ratios of Ni/Co (mean 5.9 ± 2.1), Th/Sc (0.3 ± 0.1), Fe/Al (0.6 ± 0.2) and U/Th (0.3 ± 0.0) fall in between those of average upper continental crust (Rudnick and Gao, 2014), average oceanic crust (White and Klein, 2014), and average komatiite (Ptáček et al., 2020; **Figure 5**).

DISCUSSION

Sedimentary Provenance and Redox Conditions

Sedimentary provenance, mild hydrothermal alteration and metasomatism have affected the major and minor element distribution in these rocks, and therefore need to be addressed. Regarding sedimentary provenance, mapping has shown that the turbidites analyzed in this study sit on top of mafic volcanic rocks (Rosing et al., 1996), and our Th/Sc, U/Th and Fe/Al ratios are indeed consistent with a strong contribution of mafic detritus. These element ratios were selected because they have previously been shown to be good discriminators for distinguishing between mafic, ultramafic and felsic provenance (Ptáček et al., 2020). All three ratios fall in between those of average upper continental crust and average oceanic crust (Rudnick and Gao, 2014; White and Klein, 2014), which suggest mixing of material from sources of similar compositions. The relatively high Ni/Co ratios may further indicate contributions of ultramafic material, such as komatiite (**Figure 5A**), consistent with previous studies of other Archean siliciclastic rocks (Ptáček et al., 2020). This interpretation is overall in line with previous trace element work on metasedimentary rocks from the Isua Supracrustal Belt (Kamber et al., 2005).

In the case of U/Th and Fe/Al, input of mafic or ultramafic detritus has important implications for the utility of these elements as redox proxies. We briefly address this topic here, because previous work found geochemical evidence of biological oxygen production in rocks from this same geological unit (Rosing and Frei, 2004). A high Fe/Al ratio above ∼0.5 in sedimentary rocks, i.e., elevated relative to upper continental crust, is typically interpreted as evidence of anoxic conditions during the time of deposition that favored the accumulation of authigenic iron minerals, including sulfides, carbonates or oxides (Lyons and Severmann, 2006; Raiswell et al., 2019). However, in settings with significant contributions of iron-rich siliciclastic material or detrital iron sulfides or iron oxides, such as mafic rock-forming minerals and their weathering products, this empirically defined threshold is no longer applicable (Stüeken et al., 2017; Stüeken et al., 2020). It is therefore not possible to

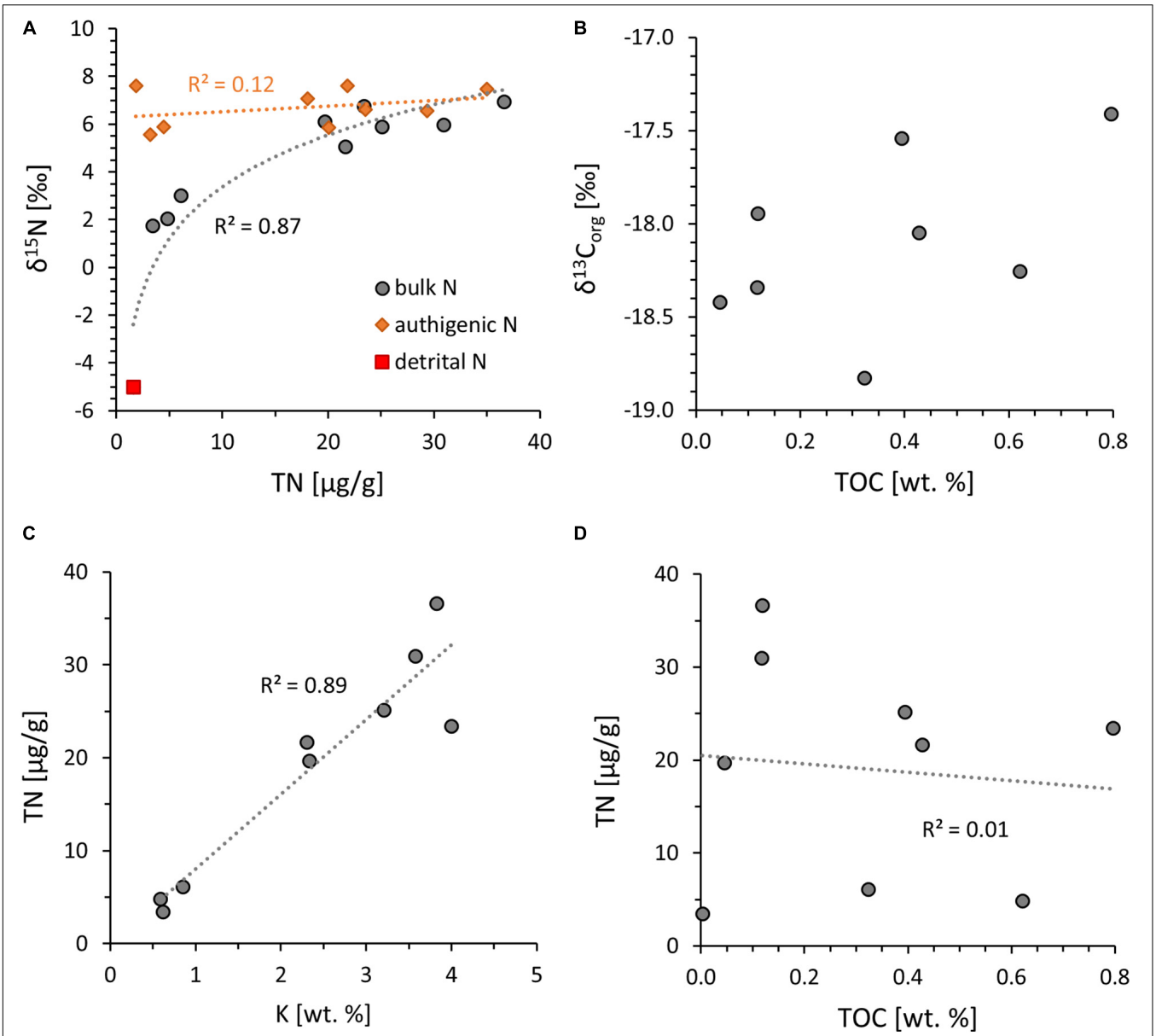

FIGURE 3 | Organic carbon and nitrogen data. **(A)** $\delta^{15}N$ vs. total nitrogen (TN). Gray circles = measured data; red square = assumed detrital endmember; orange diamonds = calculated authigenic nitrogen component (see text for details). **(B)** $\delta^{13}C_{org}$ vs. total organic carbon (TOC). **(C)** Measured TN vs. K with strong covariance, indicating that most N is now bound to potassic minerals. **(D)** TN vs. TOC, showing no correlation, suggesting that only minor amounts of nitrogen are bound to organic matter.

infer redox conditions during the time of deposition on the basis on Fe/Al ratios. Other commonly used redox proxies include Mo abundances and U/Th ratios (Tribovillard et al., 2006). Both Mo(VI) and U(VI) are soluble under oxic conditions and can thus become enriched in anoxic sediments as Mo(IV) and U(IV), respectively. However, we find no evidence for enrichments in either of these proxies above the level of detrital background. Molybdenum would be expected to correlate with TOC, because adsorption of thiolated Mo to organic matter is the major pathway for Mo burial in sediments (Wilde et al., 2004; Helz et al., 2011). The absence of such a correlation in our data (**Figure 4C**) prohibits any inferences about Mo levels in the water column during the time of organic matter deposition. We can therefore not confirm previous suggestions for the presence of biogenic O_2 production during the time of deposition of these meta-sedimentary rocks (cf. Rosing and Frei, 2004).

It is, however, likely that these rocks have undergone some degree of hydrothermal alteration. Previous workers documented chalcopyrite in this geological unit (Rosing, 1999), and our good correlation between Cu and S (**Figure 4B**) is likely evidence for the presence of chalcopyrite. Copper [both Cu(I) and Cu(II)] is most soluble in saline and/or hot fluids, such as hydrothermal

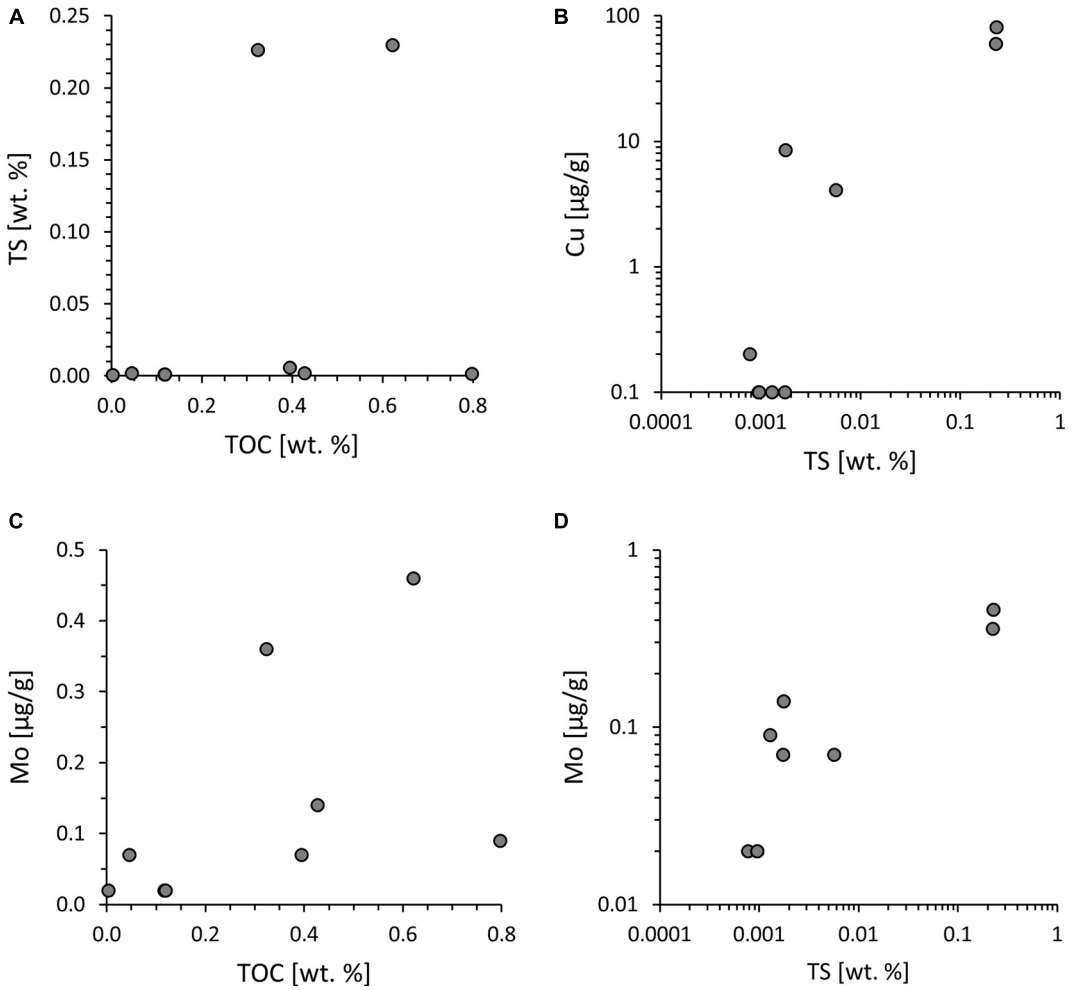

FIGURE 4 | Redox and hydrothermal alteration indicators. **(A)** Total sulfur (TS) vs. total organic carbon (TOC), showing no correlation. **(B)** Cu vs. TS. Given previous observations of chalcopyrite in these rocks (Rosing, 1999), the covariance between Cu and TS suggests a hydrothermal source of sulfur. **(C)** Mo vs. TOC, showing no correlation, counter to what is commonly observed in unaltered sedimentary rocks (Wilde et al., 2004). **(D)** Mo vs. TS, indicating that Mo may have been introduced by hydrothermal fluids along with Cu and sulfur.

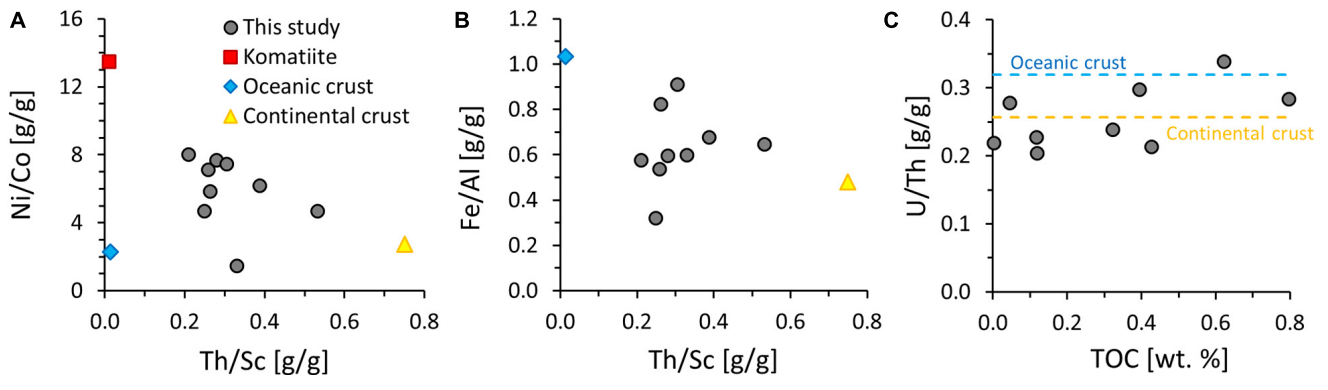

FIGURE 5 | Geochemical provenance and redox indicators. **(A)** Ni/Co vs. Th/Sc. **(B)** Fe/Al vs. Th/Sc. **(C)** U/Th vs. total organic carbon (TOC). Reference values for average crust and komatiite are taken from the literature (Rudnick and Gao, 2014; White and Klein, 2014; Ptáček et al., 2020).

effluents and relatively insoluble in cold seawater (Zhong et al., 2015). The Cu and S abundances in our samples are overall relatively low, and it is conceivable that Cu sulfides are detrital in origin. However, given the association of Cu with S, we cannot rule out minor hydrothermal overprinting. This conclusion is also consistent with our sulfur isotope data which plot close to the average upper mantle value of -1 ± 0.5 ‰ (Labidi et al., 2012) and may thus reflect contributions of hydrothermal H_2S derived from magmatic processes (Seal, 2006). Such hydrothermal fluids may have also introduced slightly elevated amounts of Mo into some of the samples, which also covaries with S (**Figure 4D**). Whether this hydrothermal activity was syn- or post-depositional cannot be resolved from our data, but its implications require consideration in the interpretation of the nitrogen isotope data.

Nitrogen Sources

In the form of ammonium (NH_4^+), nitrogen has the same charge and size as K^+ and Rb^+ and therefore partitions into similar mineral phases (Busigny and Bebout, 2013). This notion explains our dataset where the abundances for TN and K show a strong correlation ($R^2 = 0.89$; **Figure 3C**). It is thus conceivable that one major source of N are detrital mineral grains that were eroded from K-bearing igneous rocks (e.g., Hall, 1999). However, organic $\delta^{13}C$ values as well as previous hydrogen and nitrogen detections in the graphite in these rocks point toward the presence of biomass during the deposition of the turbidites (Rosing, 1999; Hassenkam et al., 2017). This graphitized biomass is thought to be derived from living organisms that were thriving on the seafloor or within the water column. When biomass gets buried in sediments and undergoes diagenesis, ammonium is released into porewaters, where it may accumulate to high concentrations in the mM range (e.g., Rosenfeld, 1979; Boudreau and Canfield, 1988). At such high concentrations, significant amounts of ammonium can substitute into K-bearing minerals, such as illite (Müller, 1977; Schroeder and McLain, 1998). This mechanism thus effectively transfers N from organic matter into silicate minerals and has even been invoked to explain elevated N abundances in granitoids (Hall, 1999). Hence if the graphite in our samples does indeed represent ancient biomass, then it is very likely that N was initially introduced in the form of organic molecules and later transferred to potassic minerals during diagenesis and/or metamorphism. The correlation between TN and K could therefore represent a diagenetic artifact rather than provenance.

However, we cannot rule out that the N-poor samples in our set contain significant contributions of detrital nitrogen. In fact, mixing between a detrital and authigenic component could well explain the correlation between TN and $\delta^{15}N$ that is difficult to explain by metamorphic effects alone. We can calculate this detrital endmember, if we make an assumption for its isotopic composition. As a first plausible guess, we assume that it has a composition of -5‰, i.e., similar to Earth's upper mantle and mafic crust (Cartigny and Marty, 2013). Two-endmember mixing of (i) detrital nitrogen with a composition of -5‰ and (ii) authigenic nitrogen with a composition of $+6.1$‰ (i.e., the mean value of the N-rich samples) would thus imply that the authigenic component of the three N-poor samples makes up between 61 and 72% while the rest is detrital; the detrital fraction would make up 1.6 ppm on average (range 1.4–1.7 ppm). It is likely that also the N-rich samples contain a similar detrital component, but if we correct the measured data under the assumption that 1.6 ppm of the total nitrogen is detrital in origin, the resulting $\delta^{15}N$ values increase only slightly from a mean of $+6.1$ to $+6.9$‰. Across all samples, the authigenic component would thus have a composition of $+6.7 \pm 0.8$‰ (**Figure 3A**). Hence detrital contributions are probably negligible for these relatively N-rich samples in our sample set (4–8% of total N).

Importantly, using a value of -5‰ for the detrital contribution, based on the composition of mantle-derived magmatic rocks (Cartigny and Marty, 2013), requires that this detrital component has not been affected by metamorphism in the same manner as the authigenic nitrogen in the same samples (see section "Metamorphic Effects on Nitrogen Geochemistry"). This assumption is plausible, because detrital minerals eroded from magmatic rocks have already been exposed to high temperatures and pressures and may therefore be resistant to metamorphism. Of course, magmatic rocks do undergo metamorphism as well, but magmatic N is likely fully lattice bound as the high temperatures under which the minerals formed would volatilize loosely bound material. Therefore, metamorphism of magmatic materials likely results in a smaller loss of N compared to materials in which N is predominantly organic-bound. Hence detrital magmatic minerals are expected to lose relatively less N during thermal metamorphism. However, if we take the more radical view that all three of the N-poor samples are 100% composed of detrital N with an average of 4.8 ppm and an isotopic value of $+2.3$‰ (i.e., allowing for metamorphic alteration and isotopic enrichment of detrital minerals), it would mean that the N-rich population contains between 76 and 87% authigenic N, and this authigenic N would have an isotopic value of $+7.0 \pm 0.8$‰. This result is very similar to the value of $+6.7 \pm 0.8$‰ calculated above, meaning that the uncertainty about the size and isotopic composition of the detrital component does not impact our overall conclusions. We will therefore proceed with the assumption that the authigenic N component in these samples falls around a mean $\delta^{15}N$ value of 6–7‰.

Metamorphic Effects on Nitrogen Geochemistry

The rocks investigated in this study have undergone metamorphic alteration up to mid-amphibolite facies (Rosing, 1999; Ramírez-Salazar et al., 2021), and it is well known that metamorphism strongly impacts N abundances and isotopic ratios in sedimentary rocks (Haendel et al., 1986; Bebout and Fogel, 1992; Boyd and Phillippot, 1998; Jia, 2006; Palya et al., 2011). The measured data do therefore not represent primary values. However, it is possible to quantify the degree of metamorphic alteration and to estimate the pre-metamorphic starting value, because the isotopic fractionation factors associated with partial N volatilization during metamorphism have been constrained in previous studies. For a temperature around 527°C, Hanschmann (1981) estimated $\alpha = 1.0073$ for N-loss as NH_3 (i.e., for the reaction NH_3–NH_4^+) and

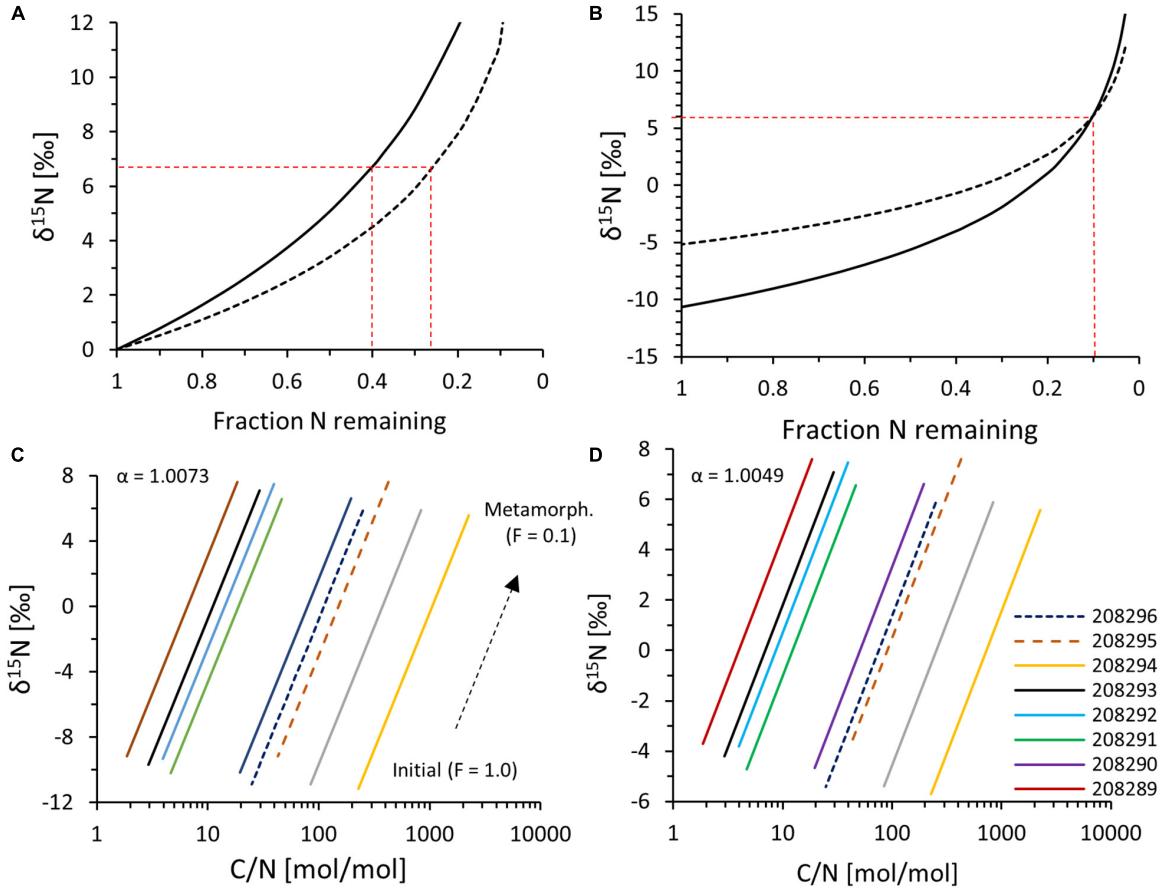

FIGURE 6 | (A) Rayleigh fractionation model with fixed $\delta^{15}N_{initial}$ = 0‰ and fractionation factors (α) of either 1.0049 (dashed line) or 1.0073 (solid line). Red dashed lines = F values corresponding to $\delta^{15}N$ = +6.7‰, which is the average authigenic N component. **(B)** Rayleigh fractionation model, adjusting $\delta^{15}N_{initial}$ such that $\delta^{15}N_{metamorphic}$ = +6.7‰ at F = 0.1. **(C)** Evolution of authigenic $\delta^{15}N$ and C/N ratios at α = 1.0073. **(D)** Evolution of authigenic $\delta^{15}N$ and C/N ratios at α = 1.0049.

α = 1.0049 for N-loss as N_2 (for the reaction N_2–NH_3), where $\alpha = (^{15}N/^{14}N)_{residue}/(^{15}N/^{14}N)_{volatile}$ (summarized by Haendel et al., 1986). These fractionation factors were found to be applicable to Archean rocks by Pinti et al. (2001). As the nitrogen speciation in our scenario is not known, we plot the maximum and minimum fractionation factors (**Figure 6**). We used a standard Rayleigh distillation equation $(\delta^{15}N_{metamorphic}/1000 + 1)/(\delta^{15}N_{initial}/1000 + 1) = F^{(1-\alpha)}$ where F = fraction nitrogen remaining, $\delta^{15}N_{initial}$ = initial $\delta^{15}N$ value, and $\delta^{15}N_{metamorphic}$ = metamorphic $\delta^{15}N$ value. Either F or $\delta^{15}N_{initial}$ can be calculated by assuming reasonable bounds for the respective other parameter.

At first, we fixed $\delta^{15}N_{initial}$ and calculated F. A plausible assumption for $\delta^{15}N_{initial}$ may be the composition of biological N_2-fixing organisms, which dominate $\delta^{15}N$ signals of younger Archean sedimentary rocks (Stüeken et al., 2016). We therefore set $\delta^{15}N_{initial}$ to 0‰ and calculated how much nitrogen would need to remain in the system (F) such that the calculated metamorphosed values ($\delta^{15}N_{metamorphic}$) match our observation (+6.7‰ for average authigenic N). The results suggest that about 24–40% (average 33%) of TN would have needed to be retained to shift authigenic $\delta^{15}N$ from 0 to +6.7‰ with a fractionation factor (α) of 1.0049–1.0073 (**Figure 6A**). However, such a high retention is inconsistent with previous studies that documented down to only 10% nitrogen retention at amphibolite facies (Haendel et al., 1986). The average TN retention found by Haendel et al. (1986) was 20%, while the maximum was around 10%. In a second calculation we therefore assumed that only 10% of TN has remained in the sample (i.e., F = 0.1) and varied $\delta^{15}N_{initial}$ until the isotopic composition of the residual measured nitrogen ($\delta^{15}N_{metamorphic}$) was equal to the calculated authigenic $\delta^{15}N$ value for each sample. The results point toward a starting composition of −4.6 ± 0.8‰ for α = 1.0049 and −10.1 ± 0.8‰ for α = 1.0073 with a mean of −7.3 ± 1.1‰ (**Figure 6B**). This value is close to the value of −7.1‰ that Pinti et al. (2001) reconstructed from a single sample of the same geological unit, using a stepwise combustion technique paired with argon isotope measurements. If we assume 20% N retention, our initial $\delta^{15}N$ values would fall between −1.2 and −5.2‰, which does not overlap with the value derived by Pinti et al. (2001). To further constrain TN retention, we looked at the reconstructed C/N ratios, which were calculated by changing

TN while holding TOC constant. In reality, some TOC is likely to have been lost as well during metamorphism, and so the reconstructed values represent an upper limit of the true initial C/N Redfield ratio. In the case of 10% retention, reconstructed C/N ratios fall around an average of 15 for the N-rich sample population, which is close to the Redfield ratio (C/N = 7–10) of microbial biomass (Godfrey and Glass, 2011; Algeo et al., 2014). For the case of 20% retention, the C/N ratios would be 30 on average and therefore further removed from the expected value of microbial biomass. This offset would be even larger if we account for loss of some TOC during metamorphism. A scenario with only 10% nitrogen retention, i.e., 90% TN loss during metamorphism, therefore appears more likely. In any case, the reconstructed C/N ratios vary widely between samples (range 2–226 for the 10% retention scenario, median 20, **Figures 6C,D**), but this variability may simply reflect diagenetic ammonium migration from organic-rich to organic-lean laminae, which is commonly observed in younger sedimentary successions (e.g., Koehler et al., 2019b). Overall, paired with the one data point collected by Pinti et al. (2001), our data suggest a starting $\delta^{15}N$ value that was significantly less ^{15}N-enriched than in younger Archean sedimentary rocks.

Pre-metamorphic Alteration

A pre-metamorphic $\delta^{15}N$ value around −1 to −10 ‰ in these Isua turbidites (Pinti et al., 2001, this study) may not necessarily represent the composition of biomass during the time of deposition. As noted above, we cannot rule out that these rocks have been exposed to at least mild hydrothermal alteration over their complex metamorphic history, as suggested by the presence of possibly hydrothermally-derived chalcopyrite. However, it is unlikely that post-depositional fluid circulation led to these light isotopic values by either subtraction or addition of nitrogen. First, experimental work has shown that the interaction between hot fluids and organic-bound N imparts minimal isotopic fractionation (<1‰) (Boudou et al., 2008). Hydrothermal leaching of N from these rocks is therefore unlikely to have induced such a large isotopic perturbation. Second, hydrothermal fluids are N-poor unless they circulate through sedimentary packages and mobilized ammonium from older organic matter (Lilley et al., 1993), for which there is no evidence in this field area. And even if older sedimentary rocks existed and provided a source of nitrogen to hydrothermal fluids, which was then added to our sample set, those older rocks would themselves have needed to contain isotopically light nitrogen. Hence there is no obvious mechanism by which hydrothermal fluids could have shifted initial $\delta^{15}N$ values downward by several permil.

Other studies of hydrothermally altered Precambrian rocks show strong isotopic perturbations, where organic-bound nitrogen has become isotopically depleted by up to 15‰ (Godfrey et al., 2013); however, in that case, the silicate-bound nitrogen fraction incorporated the complementary heavy nitrogen pool, such that the bulk rock value was within 2–3‰ of contemporaneous unaltered strata from the same basin. As we measured bulk rock values rather than kerogen isolates, this mechanism can therefore not explain our data. Therefore, we find no evidence for significant hydrothermal alteration of the ammonium contained in these samples, suggesting that the pre-metamorphic $\delta^{15}N$ value was between −1 and −10‰.

Eoarchean Biogeochemical Nitrogen Cycling

If primary $\delta^{15}N$ values were as high as −1‰, as inferred for 20% TN retention and a relatively small isotopic fractionation factor (section "Metamorphic Effects on Nitrogen Geochemistry"), this may be evidence for the presence of biological N_2 fixation as far back as 3.7 Ga. This interpretation would be consistent with phylogenetic data indicating an early evolution and ecological radiation of this metabolism, possibly dating back to the last universal common ancestor of life on Earth (Weiss et al., 2016; Parsons et al., 2020). However, if the lighter values are correct, which agree better with the previous estimate by Pinti et al. (2001) and are consistent with reconstructed C/N ratios, this may point toward a distinct geobiological N cycle at the time. First, such a low $\delta^{15}N$ value could reflect a different source of N to biological communities compared to later periods in Earth's history where $\delta^{15}N$ rarely drops below −2‰ (Stüeken et al., 2016). One possible explanation may be biological N_2 fixation with a so-called alternative nitrogenase. These enzymes contain either V or Fe instead of Mo in their catalytic center and impart isotopic fractionation down to −8 ‰ during the conversion of N_2 to NH_4^+ (Zhang et al., 2014). They are rarely expressed in natural environments today, but Mo scarcity in the early Archean ocean may potentially have favored V- or Fe-based nitrogenase (Raymond et al., 2004; Scott et al., 2008). However, the scarcity of similarly light $\delta^{15}N$ values throughout the rest of the Archean then becomes puzzling. Furthermore, phylogenetic data suggest that V- and Fe-based nitrogenases may not have radiated until the late Proterozoic (Parsons et al., 2020), making it unlikely that they were important players in the Eoarchean N cycle. Alternatively, isotopically light N may have been derived from atmospheric rainout of lightning products or HCN. HCN can form during photolysis in the upper atmosphere (Tian et al., 2011), and experimental data revealed an isotopic composition of −15 to −25‰ (Kuga et al., 2014). The composition of lightning products such as NOx is so far poorly constrained, but some existing measurements from the modern atmosphere show light values around −5 to −15‰ (Moore, 1977). Atmospheric N-bearing molecules could thus be a plausible explanation for our results. Phylogenetic data are consistent with early utilization of NOx species, possibly derived from lightning (Parsons et al., 2020). If so, it would imply that the atmospheric nitrogen source declined in relative importance between the Eoarchean and younger Archean (3.2 Ga onward) where such light values are no longer observed and N metabolisms are dominated by anaerobic pathways (Parsons et al., 2020). A third possible explanation for light $\delta^{15}N$ in biomass is partial assimilation of ammonium from a large, dissolved ammonium pool in seawater. Culturing experiments with modern microorganisms show fractionation factors of

−4 to −27‰ if ammonium concentrations exceed ca. 10–20 μM (Hoch et al., 1992). However, given the high metabolic costs of converting N_2 into ammonium and the inefficiency of abiotic ammonium accumulation in seawater (Stüeken, 2016), it is unlikely that such a large ammonium pool existed. In summary, the meaning of these light values in Eoarchean rocks, if correct, remains elusive, but atmospheric rainout of isotopically light bioavailable N species is at present perhaps the most plausible explanation.

Nitrogen Recycling Into Earth's Mantle?

If our reconstruction is correct, and if these values are representative of the Eoarchean (which we cannot confirm from a single outcrop), then this may have implications for the secular evolution of key geological N reservoirs over Earth's history. Today Earth's lower mantle, upper mantle and surface reservoirs show striking and intriguing isotopic imbalances. The upper mantle shows an average $\delta^{15}N$ value of ca. -5 ± 3‰, as determined by measurements of diamonds, kimberlite xenoliths and mid-ocean ridge basalt (Cartigny and Marty, 2013). This negative upper mantle value is thought to date back to the Archean as indicated by diamonds from 3.3 to 2.9 Ga which display a mode around -5 ± 3‰ (Richardson et al., 2001; Cartigny, 2005). In contrast, plume sources for ocean island basalts—assumed to originate from lower mantle domains below the upper mantle—are weakly positive in $\delta^{15}N$, similar to post-Archean crustal reservoirs (Marty and Dauphas, 2003). Since the Great Oxidation Event in the Paleoproterozoic (∼2.5 Ga), crustal materials are dominantly enriched in ^{15}N (>+2‰) (Zerkle et al., 2017; Kipp et al., 2018), and most of the Archean sedimentary record between 3.2 and 2.5 Ga falls around values of 0‰ (Stüeken et al., 2015; Homann et al., 2018; Koehler et al., 2019a; Ossa Ossa et al., 2019). Isotopically lighter values are rare in open marine settings and mostly restricted to organic extracts, which are distinct from bulk rock values (Beaumont and Robert, 1999; Yang et al., 2019). Hence Earth's upper mantle and exterior (crust + atmosphere) appear to have displayed an isotopic imbalance for the last 3.2 billion years (Boyd and Pillinger, 1994). This is intriguing, because degassing of the upper mantle and/or the subduction of sedimentary nitrogen should generate a more ^{15}N-enritched upper mantle (Boyd and Pillinger, 1994).

However, if the positive $\delta^{15}N$ values in plumes from the lower mantle are primary and reflect the initial mantle $\delta^{15}N$ value, then one possible explanation for the isotopic imbalance of the upper mantle is the subduction of isotopically light sedimentary rocks in the Eoarchean This hypothesis is not new (Marty and Dauphas, 2003; Cartigny, 2005; Cartigny and Marty, 2013), but has perhaps lost momentum because several recent studies of Mesoarchean rocks revealed sedimentary $\delta^{15}N$ values 0‰ (Stüeken et al., 2015; Homann et al., 2018; Koehler et al., 2019a; Ossa Ossa et al., 2019). However, our new findings open up the possibility that the Eoarchean N cycle may have been distinct, in particular if it involved a stronger involvement of atmospheric products that were incorporated into ancient biomass. It is therefore conceivable that during the first one billion years of Earth's history nitrogen in sediments was more akin to the modern upper mantle $\delta^{15}N$ value. If correct, this may fuel the idea that the mantle inherited its light value from Eoarchean sediment recycling. We stress that a geodynamic mechanism for such a model is so far ambiguous, and it remains to be determined if the total volume of isotopically light sedimentary rocks would have been large enough to change the isotopic value of the mantle. For example, the subduction of sedimentary N with negative $\delta^{15}N$ values would only control the upper mantle $\delta^{15}N$ value if the mass of subducted sedimentary N is far greater than the N abundance of the upper mantle to account for loss by degassing. The abundance and distribution of nitrogen throughout the deep silicate Earth is a topic of much debate (Zerkle and Mikhail, 2017), but our results suggest that this may be a worthwhile avenue to pursue in future studies.

CONCLUSION

Reconstructing the conditions under which life emerged and thrived on the early Earth is pivotal for delineating constraints on the habitability of other worlds. The poor preservation of the oldest sedimentary rock record presents a clear impediment to this line of research; however, our results add to a growing body of literature showing that some information can be extracted if metamorphic effects are appropriately accounted for. In this case, we find that amphibolite-grade meta-sedimentary rocks from the Isua Supracrustal Belt contain several μg N per g of bulk rock with an average $\delta^{15}N$ value of +6.1‰, and most of this nitrogen appears to be bound in potassic phases. However, knowledge of the diagenetic and metamorphic behavior of nitrogen allows us to reconstruct that the initial nitrogen endowment of these rocks was likely derived from buried biomass, and this biogenic nitrogen appears to have been isotopically depleted with $\delta^{15}N$ values down to −1 to −10‰ and most likely below −5‰. This result is consistent with previous work that estimated a value of −7‰ (Pinti et al., 2001). Hydrothermal alteration cannot easily be evoked to explain such a light initial value. Instead, we speculate that the Eoarchean nitrogen cycle was strongly influenced by atmospheric rainout of NOx species and/or HCN, which could explain these light $\delta^{15}N$ values (Moore, 1977; Kuga et al., 2014). This conclusion supports the idea that recycling of Eoarchean sedimentary rocks may have created the isotopic dichotomy between Earth's exterior and interior that appears to have existed since at least 3.2 Ga (Richardson et al., 2001; Cartigny, 2005; Cartigny and Marty, 2013), although we stress that a geodynamic model in support of this view requires significant developmental work (beyond the scope of this study).

Importantly, the imprint of isotopically light atmospheric products is absent from the younger Archean record (Ader et al., 2016; Stüeken et al., 2016). From the Mesoarchean onward Earth's biosphere appears to have been fueled by biological Mo-based nitrogenase-driven N_2 fixation (Parsons et al., 2020). We speculate that the transition from mostly abiotic N sources to biological N_2 fixation reflects an increase in biological productivity, which "encouraged" the invention and expansion of N_2-fixing enzymes. If so, then atmospheric processes may have been important for origin of life, but they were perhaps not sufficient for sustaining a large biosphere over geologic timescales.

DATA AVAILABILITY STATEMENT

The original contributions presented in the study are included in the article/supplementary material, further inquiries can be directed to the corresponding author/s.

AUTHOR CONTRIBUTIONS

KS collected the samples. NG established the connections between researchers. ES and TB analyzed the samples. SM contributed to the interpretation of the data. ES wrote the manuscript with inputs from all authors. All authors contributed to the article and approved the submitted version.

FUNDING

ES acknowledges support from the School of Earth and Environmental Sciences at St Andrews. TB was funded by a NERC IAPETUS Doctoral Training Program (NE/R012253/1) studentship. Fieldwork at Isua was supported by the Carlsberg Foundation through grant CF18-0090 to KS.

REFERENCES

Ader, M., Thomazo, C., Sansjofre, P., Busigny, V., Papineau, D., Laffont, R., et al. (2016). Interpretation of the nitrogen isotopic composition of precambrian sedimentary rocks: assumptions and perspectives. *Chem. Geol.* 429, 93–110. doi: 10.1016/j.chemgeo.2016.02.010

Algeo, T. J., Meyers, P. A., Robinson, R. S., Rowe, H., and Jiang, G. Q. (2014). Icehouse-greenhouse variations in marine denitrification. *Biogeosciences* 11, 1273–1295. doi: 10.5194/bg-11-1273-2014

Baadsgaard, H., Nutman, A. P., Bridgwater, D., Rosing, M., McGregor, V. R., and Allaart, J. H. (1984). The zircon geochronology of the akilia association and Isua supracrustal belt, West Greenland. *Earth Planetary Sci. Lett.* 68, 221–228. doi: 10.1016/0012-821x(84)90154-7

Barry, P. H., and Hilton, D. R. (2016). Release of subducted sedimentary nitrogen throughout Earth's mantle. *Geochem. Perspect. Lett.* 2, 148–159. doi: 10.7185/geochemlet.1615

Beaumont, V., and Robert, F. (1999). Nitrogen isotope ratios of kerogens in Precambrian cherts: a record of the evolution of atmosphere chemistry? *Precambrian Res.* 96, 63–82. doi: 10.1016/s0301-9268(99)00005-4

Bebout, G. E., and Fogel, M. L. (1992). Nitrogen-isotopic composition of metasedimentary rocks in the Catalina Schist, California: implications for metamorphic devolatilization history. *Geochimica et Cosmochimica Acta* 56, 2839–2849. doi: 10.1016/0016-7037(92)90363-n

Boak, J. L., and Dymek, R. F. (1982). Metamorphism of the ca. 3800 Ma supracrustal rocks at Isua, West Greenland: implications for early Archaean crustal evolution. *Earth Planetary Sci. Lett.* 59, 155–176. doi: 10.1016/0012-821x(82)90123-6

Boocock, T. J., Mikhail, S., Prytulak, J., Di Rocco, T., and Stüeken, E. E. (2020). Nitrogen mass fraction and stable isotope ratios for fourteen geological reference materials: evaluating the applicability of elemental analyser versus sealed tube combustion methods. *Geostand. Geoanal. Res.* 44, 537–551. doi: 10.1111/ggr.12345

Boudou, J. P., Schimmelmann, A., Ader, M., Mastalerz, M., Sebilo, M., and Gengembre, L. (2008). Organic nitrogen chemistry during low-grade metamorphism. *Geochimica et Cosmochimica Acta* 72, 1199–1221. doi: 10.1016/j.gca.2007.12.004

Boudreau, B. P., and Canfield, D. E. (1988). A provisional diagenetic model for pH in anoxic porewaters: application to the FOAM site. *J. Mar. Res.* 46, 429–455. doi: 10.1357/002224088785113603

Boyd, S. R., and Phillippot, P. (1998). Precambrian ammonium biogeochemistry: a study of the moine metasediments, Scotland. *Chem. Geol.* 144, 257–268. doi: 10.1016/s0009-2541(97)00135-6

Boyd, S. R., and Pillinger, C. T. (1994). A preliminary study of 15N/14N in octahedral growth form diamonds. *Chem. Geol.* 116, 43–59. doi: 10.1016/0009-2541(94)90157-0

Busigny, V., and Bebout, G. E. (2013). Nitrogen in the silicate earth: speciation and isotopic behavior during mineral–fluid interactions. *Elements* 9, 353–358. doi: 10.2113/gselements.9.5.353

Busigny, V., Cartigny, P., Laverne, C., Teagle, D., Bonifacie, M., and Agrinier, P. (2019). A re-assessment of the nitrogen geochemical behavior in upper oceanic crust from Hole 504B: implications for subduction budget in Central America. *Earth Planetary Sci. Lett.* 525:115735. doi: 10.1016/j.epsl.2019.115735

Cartigny, P. (2005). Stable isotopes and the origin of diamond. *Elements* 1, 79–84. doi: 10.2113/gselements.1.2.79

Cartigny, P., and Marty, B. (2013). Nitrogen isotopes and mantle geodynamics: the emergence of life and the atmosphere–crust–mantle connection. *Elements* 9, 359–366. doi: 10.2113/gselements.9.5.359

Feng, L., Li, H., and Liu, W. (2018). Nitrogen Mass fraction and isotope determinations in geological reference materials using sealed-tube combustion coupled with continuous-flow isotope-ratio mass spectrometry. *Geostand. Geoanal. Res.* 42, 539–548. doi: 10.1111/ggr.12234

Friend, C. R., and Nutman, A. P. (2019). Tectono-stratigraphic terranes in Archaean gneiss complexes as evidence for plate tectonics: the Nuuk region, southern West Greenland. *Gondwana Res.* 72, 213–237. doi: 10.1016/j.gr.2019.03.004

Godfrey, L. V., and Glass, J. B. (2011). The geochemical record of the ancient nitrogen cycle, nitrogen isotopes, and metal cofactors. *Methods Enzymol.* 486, 483–506. doi: 10.1016/b978-0-12-381294-0.00022-5

Godfrey, L. V., Poulton, S. W., Bebout, G. E., and Fralick, P. W. (2013). Stability of the nitrogen cycle during development of sulfidic water in the redox-stratified late Paleoproterozoic ocean. *Geology* 41, 655–658.

Guotana. (submitted). Deserpentinization and high pressure (eclogite-facies) metamorphic features in the Eoarchean ultramafic body from Isua, Greenland. *Geosci. Front.*

Haendel, D., Muehle, K., Nitzsche, H.-M., Stiehl, G., and Wand, U. (1986). Isotopic variations of the fixed nitrogen in metamorphic rocks. *Geochimica et Cosmochimica Acta* 50, 749–758.

Hall, A. (1999). Ammonium in granites and its petrogenetic significance. *Earth Sci. Rev.* 45, 145–165.

Hanmer, S., and Greene, D. C. (2002). A modern structural regime in the Paleoarchean (3.64 Ga); Isua greenstone belt, southern West Greenland. *Tectonophysics* 346, 201–222. doi: 10.1016/s0040-1951(02)00029-x

Hanschmann, G. (1981). Berechnung von Isotopieeffekten auf quantenchemischer Grundlage am beispiel stickstoffhaltiger molecule. *Zfl-Mitteilungen* 41, 19–39.

Hassenkam, T., Andersson, M. P., Dalby, K. N., Mackenzie, D. M. A., and Rosing, M. T. (2017). Elements of eoarchean life trapped in mineral inclusions. *Nature* 548, 78–81. doi: 10.1038/nature23261

Helz, G. R., Bura-Nakic, E., Mikac, N., and Ciglenecki, I. (2011). New model for molybdenum behavior in euxinic waters. *Chem. Geol.* 284, 323–332. doi: 10.1016/j.chemgeo.2011.03.012

Hoch, M. P., Fogel, M. L., and Kirchman, D. L. (1992). Isotope fractionation associated with ammonium uptake by a marine bacterium. *Limnol. Oceanogr.* 37, 1447–1459. doi: 10.4319/lo.1992.37.7.1447

Hoffmann, J. E., Münker, C., Polat, A., König, S., Mezger, K., and Rosing, M. T. (2010). Highly depleted Hadean mantle reservoirs in the sources of early Archean arc-like rocks, Isua supracrustal belt, southern West Greenland. *Geochimica et Cosmochimica Acta* 74, 7236–7260. doi: 10.1016/j.gca.2010.09.027

Homann, M., Sansjofre, P., Van Zuilen, M., Heubeck, C., Gong, J., Killingsworth, B., et al. (2018). Microbial life and biogeochemical cycling on land 3,220 million years ago. *Nat. Geosci.* 11, 665–671. doi: 10.1038/s41561-018-0190-9

Jenner, F. E., Bennett, V. C., Nutman, A. P., Friend, C. R. L., Norman, M. D., and Yaxley, G. (2009). Evidence for subduction at 3.8 Ga: geochemistry of arc-like

metabasalts from the southern edge of the Isua Supracrustal Belt. *Chem. Geol.* 261, 83–98. doi: 10.1016/j.chemgeo.2008.09.016

Jia, Y. (2006). Nitrogen isotope fractionations during progressive metamorphism: a case study from the Paleozoic Cooma metasedimentary complex, southeastern Australia. *Geochimica et Cosmochimica Acta* 70, 5201–5214. doi: 10.1016/j.gca.2006.08.004

Kamber, B. S., Whitehouse, M. J., Bolhar, R., and Moorbath, S. (2005). Volcanic resurfacing and the early terrestrial crust: zircon U–Pb and REE constraints from the Isua Greenstone Belt, southern West Greenland. *Earth Planetary Sci. Lett.* 240, 275–290.

Kipp, M. A., Stüeken, E. E., Yun, M., Bekker, A., and Buick, R. (2018). Pervasive aerobic nitrogen cycling in the surface ocean across the Paleoproterozoic Era. *Earth Planetary Sci. Lett.* 500, 117–126. doi: 10.1016/j.epsl.2018.08.007

Koehler, M. C., Buick, R., and Barley, M. E. (2019a). Nitrogen isotope evidence for anoxic deep marine environments from the mesoarchean mosquito creek formation, Australia. *Precambrian Res.* 320, 281–290. doi: 10.1016/j.precamres.2018.11.008

Koehler, M. C., Stüeken, E. E., Hillier, S., and Prave, A. R. (2019b). Limitation of fixed nitrogen and deepening of the carbonate-compensation depth through the Hirnantian at Dob's Linn, Scotland. *Palaeogeogr. Palaeoclimatol. Palaeoecol.* 534:109321. doi: 10.1016/j.palaeo.2019.109321

Kuga, M., Carrasco, N., Marty, B., Marrocchi, Y., Bernard, S., Rigaudier, T., et al. (2014). Nitrogen isotopic fractionation during abiotic synthesis of organic solid particles. *Earth Planetary Sci. Lett.* 393, 2–13. doi: 10.1016/j.epsl.2014.02.037

Labidi, J., Cartigny, P., Birck, J. L., Assayag, N., and Bourrand, J. J. (2012). Determination of multiple sulfur isotopes in glasses: a reappraisal of the MORB δ34S. *Chem. Geol.* 334, 189–198. doi: 10.1016/j.chemgeo.2012.10.028

Lepot, K. (2020). Signatures of early microbial life from the Archean (4 to 2.5 Ga) eon. *Earth Sci. Rev.* 209:103296. doi: 10.1016/j.earscirev.2020.103296

Lilley, M. D., Butterfield, D. A., Olson, E. J., Lupton, J. E., Macko, S. A., and McDuff, R. E. (1993). Anomalous CH4 and NH4+ concentrations at an unsedimented mid-ocean-ridge hydrothermal system. *Nature* 364, 45–47. doi: 10.1038/364045a0

Lyons, T. W., and Severmann, S. (2006). A critical look at iron paleoredox proxies: new insights from modern euxinic marine basins. *Geochimica et Cosmochimica Acta* 70, 5698–5722. doi: 10.1016/j.gca.2006.08.021

Marty, B., and Dauphas, N. (2003). The nitrogen record of crust-mantle interaction and mantle convection from Archean to present. *Earth Planetary Sci. Lett.* 206, 397–410. doi: 10.1016/s0012-821x(02)01108-1

Mikhail, S., and Sverjensky, D. A. (2014). Nitrogen speciation in upper mantle fluids and the origin of Earth's nitrogen-rich atmosphere. *Nat. Geosci.* 7, 816–819. doi: 10.1038/ngeo2271

Moorbath, S., O'nions, R. K., and Pankhurst, R. J. (1973). Early archaean age for the isua iron formation, west greenland. *Nature* 245, 138–139. doi: 10.1038/245138a0

Moorbath, S., O'nions, R. K., and Pankhurst, R. J. (1975). The evolution of early Precambrian crustal rocks at Isua, West Greenland—geochemical and isotopic evidence. *Earth Planetary Sci. Lett.* 27, 229–239. doi: 10.1016/0012-821x(75)90034-5

Moore, H. (1977). The isotopic composition of ammonia, nitrogen dioxide and nitrate in the atmosphere. *Atmos. Environ.* 11, 1239–1243. doi: 10.1016/0004-6981(77)90102-0

Müller, P. J. (1977). CN ratios in Pacific deep-sea sediments: effect of inorganic ammonium and organic nitrogen compounds sorbed by clays. *Geochimica et Cosmochimica Acta* 41, 765–776. doi: 10.1016/0016-7037(77)90047-3

Myers, J. S. (2001). Protoliths of the 3.8–3.7 Ga Isua greenstone belt, west Greenland. *Precambrian Res.* 105, 129–141. doi: 10.1016/s0301-9268(00)00108-x

Nutman, A. P., Allaart, J. H., Bridgwater, D., Dimroth, E., and Rosing, M. (1984). Stratigraphic and geochemical evidence for the depositional environment of the early Archaean Isua supracrustal belt, southern West Greenland. *Precambrian Res.* 25, 365–396. doi: 10.1016/0301-9268(84)90010-x

Nutman, A. P., and Friend, C. R. (2009). New 1: 20,000 scale geological maps, synthesis and history of investigation of the Isua supracrustal belt and adjacent orthogneisses, southern West Greenland: a glimpse of Eoarchaean crust formation and orogeny. *Precambrian Res.* 172, 189–211. doi: 10.1016/j.precamres.2009.03.017

Nutman, A. P., Bennett, V. C., Friend, C. R., and Van Kranendonk, M. (2019). The Eoarchean legacy of Isua (Greenland) worth preserving for future generations. *Earth Sci. Rev.* 198:102923. doi: 10.1016/j.earscirev.2019.102923

Nutman, A. P., Bennett, V. C., Friend, C. R., and Yi, K. (2020). Eoarchean contrasting ultra-high-pressure to low-pressure metamorphisms (<250 to >1000°C/GPa) explained by tectonic plate convergence in deep time. *Precambrian Res.* 344:105770. doi: 10.1016/j.precamres.2020.105770

Nutman, A. P., McGregor, V. R., Friend, C. R., Bennett, V. C., and Kinny, P. D. (1996). The Itsaq gneiss complex of southern West Greenland; the world's most extensive record of early crustal evolution (3900-3600 Ma). *Precambrian Res.* 78, 1–39. doi: 10.1016/j.gca.2020.03.043

Ossa Ossa, F., Hofmann, A., Spangenberg, J. E., Poulton, S. W., Stüeken, E. E., Schoenberg, R., et al. (2019). Limited oxygen production in the Mesoarchean ocean. *Proc. Natl. Acad. Sci. U.S.A.* 116, 6647–6652. doi: 10.1073/pnas.1818762116

Palya, A. P., Buick, I. S., and Bebout, G. E. (2011). Storage and mobility of nitrogen in the continental crust: evidence from partially melted metasedimentary rocks, Mt. Stafford, Australia. *Chem. Geol.* 281, 211–226. doi: 10.1016/j.chemgeo.2010.12.009

Parsons, C., Stüeken, E. E., Rosen, C., Mateos, K., and Anderson, R. (2020). Radiation of nitrogen-metabolizing enzymes across the tree of life tracks environmental transitions in Earth history. *Geobiology* 19, 18–34. doi: 10.1111/gbi.12419

Pinti, D. L., Hashizume, K., and Matsuda, J. I. (2001). Nitrogen and argon signatures in 3.8 to 2.8 Ga metasediments: clues on the chemical state of the Archean ocean and the deep biosphere. *Geochimica et Cosmochimica Acta* 65, 2301–2315. doi: 10.1016/s0016-7037(01)00590-7

Polat, A., Hofmann, A. W., and Rosing, M. T. (2002). Boninite-like volcanic rocks in the 3.7–3.8 Ga Isua greenstone belt, West Greenland: geochemical evidence for intra-oceanic subduction zone processes in the early Earth. *Chem. Geol.* 184, 231–254. doi: 10.1016/s0009-2541(01)00363-1

Ptáček, M. P., Dauphas, N., and Greber, N. D. (2020). Chemical evolution of the continental crust from a data-driven inversion of terrigenous sediment compositions. *Earth Planetary Sci. Lett.* 539:116090. doi: 10.1016/j.epsl.2020.116090

Raiswell, R., Hardisty, D. S., Lyons, T. W., Canfield, D. E., Owens, J., Planavsky, N., et al. (2019). The iron paleoredox proxies: a guide to the pitfalls, problems and proper practice. *Am. J. Sci.* 318, 491–526. doi: 10.2475/05.2018.03

Ramírez-Salazar, A., Müller, T., Piazolo, S., Webb, A. A. G., Hauzenberger, C., Zuo, J., et al. (2021). Tectonics of the Isua supracrustal belt 1: P-T-X-d constraints of a poly-metamorphic terrane. *Tectonics* 40:e2020TC006516.

Raymond, J., Siefert, J. L., Staples, C. R., and Blankenship, R. E. (2004). The natural history of nitrogen fixation. *Mol. Biol. Evol.* 21, 541–554.

Richardson, S. H., Shirey, S. B., Harris, J. W., and Carlson, R. W. (2001). Archean subduction recorded by Re–Os isotopes in eclogitic sulfide inclusions in kimberley diamonds. *Earth Planetary Sci. Lett.* 191, 257–266. doi: 10.1016/s0012-821x(01)00419-8

Rollinson, H. (2002). The metamorphic history of the Isua greenstone belt, West Greenland. *Geol. Soc. Lond. Special Publications* 199, 329–350. doi: 10.1144/gsl.sp.2002.199.01.16

Rollinson, H. (2003). Metamorphic history suggested by garnet-growth chronologies in the Isua Greenstone Belt, West Greenland. *Precambrian Res.* 126, 181–196. doi: 10.1016/s0301-9268(03)00094-9

Rosenfeld, J. K. (1979). Ammonium adsorption in nearshore anoxic sediments. *Limnol. Oceanogr.* 24, 356–364. doi: 10.4319/lo.1979.24.2.0356

Rosing, M. T. (1999). 13C-depleted carbon microparticles in > 3700-Ma sea-floor sedimentary rocks from West Greenland. *Science* 283, 674–676. doi: 10.1126/science.283.5402.674

Rosing, M. T., and Frei, R. (2004). U-rich Archaean sea-floor sediments from Greenland–indications of >3700 Ma oxygenic photosynthesis. *Earth Planetary Sci. Lett.* 217, 237–244. doi: 10.1016/s0012-821x(03)00609-5

Rosing, M. T., Rose, N. M., Bridgwater, D., and Thomsen, H. S. (1996). Earliest part of Earth's stratigraphic record: a reappraisal of the> 3.7 Ga Isua (Greenland) supracrustal sequence. *Geology* 24, 43–46. doi: 10.1130/0091-7613(1996)024<0043:epoess>2.3.co;2

Rudnick, R. L., and Gao, S. (2014). Composition of the continental crust. *Treatise Geochem.* 4, 1–51. doi: 10.1016/b0-08-043751-6/03016-4

Schidlowski, M. (2001). Carbon isotopes as biogeochemical recorders of life over 3.8 Ga of earth history: evolution of a concept. *Precambrian Res.* 106, 117–134. doi: 10.1016/s0301-9268(00)00128-5

Schroeder, P. A., and McLain, A. A. (1998). Illite-smectites and the influence of burial diagenesis on the geochemical cycling of nitrogen. *Clay Miner.* 33, 539–546. doi: 10.1180/000985598545877

Scott, C., Lyons, T. W., Bekker, A., Shen, Y., Poulton, S. W., Chu, X., et al. (2008). Tracing the stepwise oxygenation of the Proterozoic ocean. *Nature* 452, 456–459. doi: 10.1038/nature06811

Seal, R. R. (2006). Sulfur isotope geochemistry of sulfide minerals. *Rev. Mineral. Geochem.* 61, 633–677. doi: 10.1515/9781501509490-013

Stüeken, E. E. (2016). Nitrogen in ancient mud: a biosignature? *Astrobiology* 16, 730–735. doi: 10.1089/ast.2016.1478

Stüeken, E. E., Boocock, T. J., Robinson, A., Mikhail, S., and Johnson, B. W. (2021). Hydrothermal recycling of sedimentary ammonium into oceanic crust and the Archean ocean at 3.24 Ga. *Geoloy* 49. doi: 10.1130/G48844.1

Stüeken, E. E., Buick, R., Anderson, R. E., Baross, J. A., Planavsky, N., and Lyons, T. W. (2017). Environmental niches and biodiversity in Neoarchean lakes. *Geobiology* 15, 767–783. doi: 10.1111/gbi.12251

Stüeken, E. E., Buick, R., Guy, B. M., and Koehler, M. C. (2015). Isotopic evidence for biological nitrogen fixation by Mo-nitrogenase at 3.2 Gyr. *Nature* 520, 666–669. doi: 10.1038/nature14180

Stüeken, E. E., Jones, S., Raub, T. D., Prave, A. R., Rose, C. V., Linnekogel, S., et al. (2020). Geochemical fingerprints of seawater in the Late Mesoproterozoic Midcontinent Rift, North America: life at the marine-land divide. *Chem. Geol.* 553:119812. doi: 10.1016/j.chemgeo.2020.119812

Stüeken, E. E., Kipp, M. A., Koehler, M. C., and Buick, R. (2016). The evolution of earth's biogeochemical nitrogen cycle. *Earth Sci. Rev.* 160, 220–239. doi: 10.1016/j.earscirev.2016.07.007

Thomazo, C., and Papineau, D. (2013). Biogeochemical cycling of nitrogen on the early earth. *Elements* 9, 345–351. doi: 10.2113/gselements.9.5.345

Tian, F., Kasting, J. F., and Zahnle, K. (2011). Revisiting HCN formation in Earth's early atmosphere. *Earth Planetary Sci. Lett.* 308, 417–423. doi: 10.1016/j.epsl.2011.06.011

Tribovillard, N., Algeo, T. J., Lyons, J., and Riboulleau, A. (2006). Trace metals as paleoredox and paleoproductivity proxies: an update. *Chem. Geol.* 232, 12–32.

Waterton, (submitted). A cumulate origin for Isua dunites rules out formation as an Eoarchaean ophiolite. *Geology*.

Webb, A. A. G., Müller, T., Zuo, J., Haproff, P. J., and Ramírez-Salazar, A. (2020). A non–plate tectonic model for the Eoarchean Isua supracrustal belt. *Lithosphere* 12, 166–179.

Weiss, M. C., Sousa, F. L., Mrnjavac, N., Neukirchen, S., Roettger, M., Nelson-Sathi, S., et al. (2016). The physiology and habitat of the last universal common ancestor. *Nat. Microbiol.* 1:16116.

White, W. M., and Klein, E. M. (2014). Composition of the oceanic crust. *Treatise Geochem.* 4, 457–496. doi: 10.1016/b978-0-08-095975-7.00315-6

Whitehouse, M. J., Myers, J. S., and Fedo, C. M. (2009). The akilia controversy: field, structural and geochronological evidence questions interpretations of> 3.8 Ga life in SW Greenland. *J. Geol. Soc.* 166, 335–348. doi: 10.1144/0016-76492008-070

Wilde, P., Lyons, T. W., and Quinby-Hunt, M. S. (2004). Organic carbon proxies in black shales: molybdenum. *Chem. Geol.* 206, 167–176. doi: 10.1016/j.chemgeo.2003.12.005

Yang, J., Junium, C. K., Grassineau, N. V., Nisbet, E. G., Izon, G., Mettam, C., et al. (2019). Ammonium availability in the Late Archaean nitrogen cycle. *Nat. Geosci.* 12, 553–557. doi: 10.1038/s41561-019-0371-1

Zerkle, A. L., and Mikhail, S. (2017). The geobiological nitrogen cycle: from microbes to the mantle. *Geobiology* 15, 343–352. doi: 10.1111/gbi.12228

Zerkle, A. L., Poulton, S. W., Newton, R. J., Mettam, C., Claire, M. W., Bekker, A., et al. (2017). Onset of the aerobic nitrogen cycle during the great oxidation event. *Nature* 542, 465–467. doi: 10.1038/nature20826

Zhang, X., Sigman, D. M., Morel, F. M., and Kraepiel, A. M. (2014). Nitrogen isotope fractionation by alternative nitrogenases and past ocean anoxia. *Proc. Natl. Acad. Sci. U.S.A.* 111, 4782–4787. doi: 10.1073/pnas.1402976111

Zhong, R., Brugger, J., Chen, Y., and Li, W. (2015). Contrasting regimes of Cu, Zn and Pb transport in ore-forming hydrothermal fluids. *Chem. Geol.* 395, 154–164. doi: 10.1016/j.chemgeo.2014.12.008

Conflict of Interest: The authors declare that the research was conducted in the absence of any commercial or financial relationships that could be construed as a potential conflict of interest.

frontiers in Earth Science

ORIGINAL RESEARCH
published: 25 May 2021
doi: 10.3389/feart.2021.678149

Feedback Between Carbon and Nitrogen Cycles During the Ediacaran Shuram Excursion

Dongtao Xu[1], Xinqiang Wang[1,2], Xiaoying Shi[1,2], Yongbo Peng[3,4] and Eva E. Stüeken[5]*

[1]School of Earth Science and Resources, China University of Geosciences (Beijing), Beijing, China, [2]State Key Laboratory of Biogeology and Environmental Geology, China University of Geosciences (Beijing), Beijing, China, [3]International Center for Isotope Effect Research, Nanjing University, Nanjing, China, [4]School of Earth Sciences and Engineering, Nanjing University, Nanjing, China, [5]School of Earth and Environmental Sciences, University of St Andrews, St Andrews, United Kingdom

The middle Ediacaran Period records one of the deepest negative carbonate carbon isotope ($\delta^{13}C_{carb}$) excursions in Earth history (termed the Shuram excursion). This excursion is argued by many to represent a large perturbation of the global carbon cycle. If true, this event may also have induced significant changes in the nitrogen cycle, because carbon and nitrogen are intimately coupled in the global ocean. However, the response of the nitrogen cycle to the Shuram excursion remains ambiguous. Here, we reported high resolution bulk nitrogen isotope ($\delta^{15}N$) and organic carbon isotope ($\delta^{13}C_{org}$) data from the upper Doushantuo Formation in two well-preserved sections (Jiulongwan and Xiangerwan) in South China. The Shuram-equivalent excursion is well developed in both localities, and our results show a synchronous decrease in $\delta^{15}N$ across the event. This observation is further supported by bootstrapping simulations taking into account all published $\delta^{15}N$ data from the Doushantuo Formation. Isotopic mass balance calculations suggest that the decrease in $\delta^{15}N$ during the Shuram excursion is best explained by the reduction of isotopic fractionation associated with water column denitrification (ε_{wd}) in response to feedbacks between carbon and nitrogen cycling, which were modulated by changes in primary productivity and recycled nutrient elements through remineralization of organic matter. The study presented here thus offers a new perspective for coupled variations in carbon and nitrogen cycles and sheds new light on this critical time in Earth history.

Keywords: Ediacaran, South China, Doushantuo Formation, Shuram excursion, nitrogen isotopes

OPEN ACCESS

Edited by:
Jon Telling,
Newcastle University, United Kingdom

Reviewed by:
Qing Li,
Qingdao Institute of Marine Geology (QIMG), China
Christophe Thomazo,
Université de Bourgogne, France

****Correspondence:***
Xinqiang Wang
wxqiang307@126.com

Specialty section:
This article was submitted to Geochemistry, a section of the journal Frontiers in Earth Science

Received: *09 March 2021*
Accepted: *11 May 2021*
Published: *25 May 2021*

Citation:
Xu D, Wang X, Shi X, Peng Y and Stüeken EE (2021) Feedback Between Carbon and Nitrogen Cycles During the Ediacaran Shuram Excursion. Front. Earth Sci. 9:678149. doi: 10.3389/feart.2021.678149

INTRODUCTION

Unraveling the global carbon cycle in deep time of Earth history mostly relies on the analyses of carbon isotope compositions in carbonate rocks ($\delta^{13}C_{carb}$) and organic matter ($\delta^{13}C_{org}$) (Kump and Arthur, 1999). With the expansion of $\delta^{13}C_{carb}$ datasets over the past 2 decades (cf. Lyons et al., 2014), a general $\delta^{13}C_{carb}$ picture from the Archean to present has become evident. A major feature of this curve is that the magnitude of isotopic variation in the Precambrian is much larger than that of the Phanerozoic, as exemplified by the notable Shuram negative $\delta^{13}C_{carb}$ excursion documented in the middle Ediacaran (Burns and Matter, 1993; Fike et al., 2006; Le Guerroué et al., 2006a, 2006b). This excursion and its possible equivalents are widely distributed in Ediacaran successions all over the world and have been generally used as a tie-point for the stratigraphic correlations across different

continents (Jiang et al., 2007; Zhu et al., 2007; Halverson et al., 2010; Grotzinger et al., 2011; Wang et al., 2012; Lu et al., 2013; Husson et al., 2015; Wang et al., 2016; Zhou et al., 2017), although whether they are truly synchronous remains to be tested independently by precise radiometric ages (Grotzinger et al., 2011; Zhou et al., 2017).

Among all negative $\delta^{13}C_{carb}$ excursions from the Archean to Phanerozoic, the Shuram excursion is remarkable for two reasons: first, it is one of the largest negative excursions in Earth history, with $\delta^{13}C_{carb}$ decreasing from +5‰ to as low as −12‰ (Grotzinger et al., 2011); second, it may have lasted for millions of years (~5–50 Myr) before returning to positive values (Le Guerroué et al., 2006a, 2006b; Bowring et al., 2007; Jiang et al., 2007; Cui et al., 2015; Sui et al., 2019; Canfield et al., 2020; Gong and Li, 2020; Rooney et al., 2020). The anomalously low $\delta^{13}C_{carb}$ values (down to −12‰) during the Shuram excursion are below the mantle-derived carbon isotope value of −6‰ (Melezhik et al., 2005) and can therefore not be readily explained by the conventional steady-state mass balance model of carbon isotopes (Kump and Arthur, 1999). Several non-steady-state models link the Shuram excursion to the rise of oxygen in the atmosphere-ocean system, which may have resulted in the oxidation of an inferred large dissolved organic carbon (DOC) reservoir in deep ocean (Rothman et al., 2003; Fike et al., 2006; Jiang et al., 2007; McFadden et al., 2008) and/or other reduced carbon sources, including terrestrial organic matter (Kaufman et al., 2007; Shi et al., 2018), methane hydrates (Bjerrum and Canfield, 2011) and expelled hydrocarbons (Lee et al., 2015). These models imply that the Shuram excursion recorded the primary isotopic composition of seawater, which is further supported by a recent *in situ* carbon isotope study from the Wonoka Formation in Australia (Husson et al., 2020). These hypotheses have been challenged on the basis that the oxidant budget may have been insufficient if the Shuram excursion lasted for more than 5 Myr (Bristow and Kennedy, 2008); however, recent biogeochemical modeling results suggest that the oxidants required for the oxidiation of DOC could have derived from the weathering of sulfate evaporites (Shields et al., 2019). Alternatively, the Shuram excursion has been interpreted as reflecting secondary processes such as meteoric alteration (Knauth and Kennedy, 2009; Swart and Kennedy, 2012), burial diagenesis (Derry, 2010), or the contribution from authigenic carbonates (Schrag et al., 2013; Cui et al., 2017; Jiang et al., 2019). However, these diagenetic processes, which are essentially local phenomena, are difficult to reconcile with the global distribution of the Shuram excursion and its unique occurrence in the Ediacaran (Grotzinger et al., 2011). Additionally, Paulsen et al. (2017) argued that the Shuram excursion may be partially attributed to extensive release of mantle ^{12}C-enriched carbon associated with carbonatite and alkaline magmatism during the Ediacaran period, but the extremely low $\delta^{13}C_{carb}$ values of the Shuram excursion still require additional input from surface processes.

The carbon cycle has intimate relationships with the nitrogen and oxygen cycles in the global ocean (Fennel et al., 2005). Nitrogen is one of the major nutrient elements required for all life. In the excess of bioavailable P, fixed N may become an important limiting nutrient in the ocean and thereby control the amount of carbon sequestered into sediments and the rate of oxygen production through photosynthesis (Falkowski, 1997; Tyrrell, 1999). Conversely, the concentration of fixed N is mainly determined by the balance between N_2 fixation, the major pathway of N into aquatic ecosystems, and the reconversion of fixed nitrogen to N_2 gas mainly via denitrification (stepwise reduction of nitrate to N_2) and anammox (coupled oxidation of ammonium with reduction of nitrite) (Sigman et al., 2009; Devol, 2015), which in turn is largely dependent on the ocean redox structure (Quan et al., 2013; Ader et al., 2016; Stüeken et al., 2016). During denitrification, organic matter is an important electron donor (Sigman et al., 2009), although it can be replaced by ferrous Fe(II) or hydrogen sulfide (H_2S) (Lam and Kuypers, 2011; Michiels et al., 2017). Coupled nitrate (NO_3^-) reduction and the oxidation of organic matter through denitrification would result in the transformation of ^{12}C-enriched organic carbon to inorganic carbon, and the preferential release of light ^{14}N to the atmosphere, thereby elevating the $\delta^{15}N$ in the fixed N pool and lowering the $\delta^{13}C$ of the dissolved inorganic carbon pool (Sigman et al., 2009; Kump et al., 2011). Further, the remineralization of organic matter in the oceans would release the organic-bound N into seawater with limited nitrogen isotopic fractionation (−1 to +2‰, Ader et al., 2016; Stüeken et al., 2016), which could serve as new nutrient N source to fuel productivity (Higgins et al., 2012; Xu et al., 2020).

The Shuram excursion, if recording a large perturbation in the carbon cycle, provides an excellent window into the feedback between carbon, oxygen and nitrogen cycles in deep time. However, the role of the nitrogen cycle in the Shuram excursion has not been systematically investigated. Kikumoto et al. (2014) reported nitrogen isotope data from the Ediacaran to early Cambrian in a drill core in the Yangtze Gorges area, South China, and found a coherent decrease in $\delta^{15}N$ along with the Shuram excursion in the upper Doushantuo Formation (Locally named as N3, EN3 or DOUNCE, Jiang et al., 2007; Zhou and Xiao, 2007; Zhu et al., 2013). This negative $\delta^{15}N$ excursion was interpreted as evidence for an increased nitrate pool which may have resulted in the partial assimilation of NO_3^- (Kikumoto et al., 2014; Nishizawa et al., 2019). Nitrogen isotope data have also been reported from the other Ediacaran sections in South China and other continents (e.g., Ader et al., 2014; Spangenberg et al., 2014; Wang et al., 2017; Chen et al., 2019; Lan et al., 2019; Nishizawa et al., 2019), but the Shuram excursion is poorly developed or missing in these sections. In this contribution, we report high resolution $\delta^{15}N$ and $\delta^{13}C_{org}$ data from the upper Doushantuo Formation in two sections (Jiulongwan and Xiangerwan) in the Yangtze Gorges area, South China, where the Shuram-EN3 excursion is well recorded (Jiang et al., 2007; An et al., 2015; Zhou et al., 2017). The new data presented here, along with previous ones, will shed new light on the origin of the Shuram excursion and the coevolution of carbon and nitrogen cycles during this critical interval.

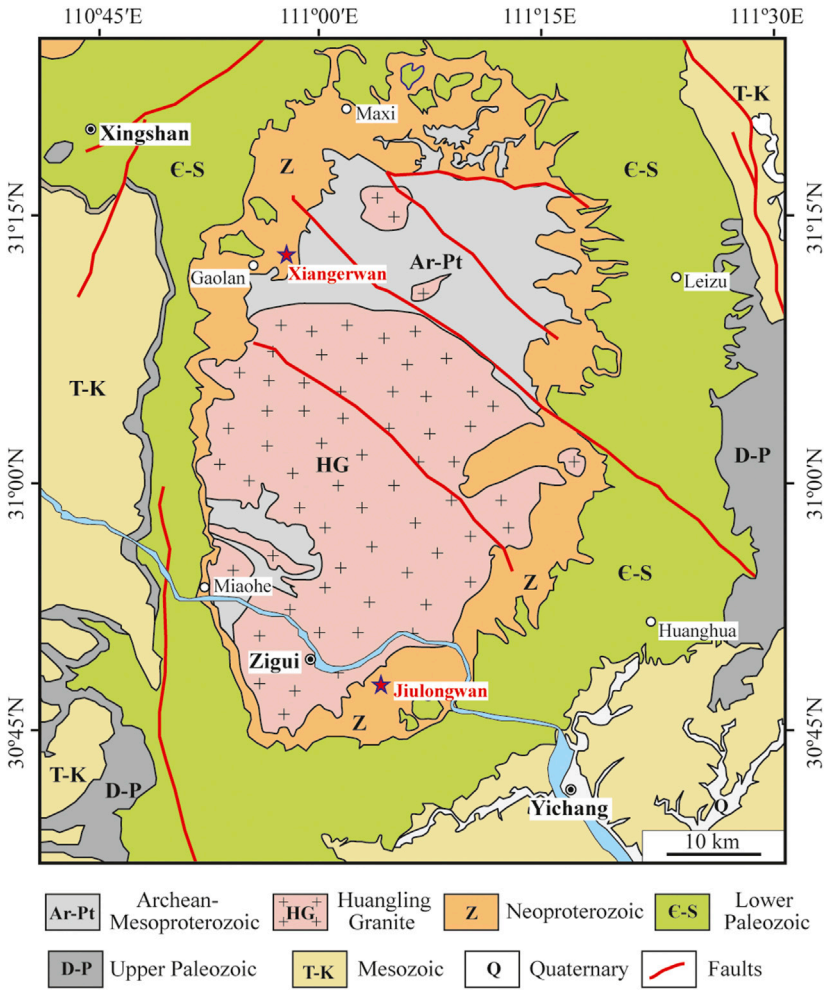

FIGURE 1 | Simplified geological map in the Yangtze Gorges area (modified from An et al., 2015). Red stars show the locations of two study sections.

GEOLOGICAL SETTING AND STUDY SECTIONS

The Ediacaran Doushantuo Formation was deposited in an inferred passive continental margin setting along the southeast part of the South China Block, following the termination of the Marinoan glaciation (Wang and Li, 2003; Jiang et al., 2011). In the Yangtze Gorges area, western Hubei Province, the Doushantuo Formation in the stratotype (Jiulongwan) section can be divided into four lithological members: Member I is a 3–5 m thick cap carbonate, Member II is characterized by interlayered black shale and muddy limestone with abundant centimeter-scaled chert nodules, Member III is dominated by carbonate deposits, and Member IV consists mainly of black shales with meter-scale carbonate concretions (e.g., Jiang et al., 2011). Abundant microfossils and macrofossils have been reported from the Doushantuo Formation, providing a unique window into eukaryotic evolution leading up to the Cambrian Explosion, as well as a valuable tool for biostratigraphic subdivision (Liu et al., 2014; Xiao et al., 2016; Zhou et al., 2019 and references therein). Geochronologically, the depositional age of the Doushantuo Formation has previously been constrained to ca. 635–551 Ma based on U-Pb zircon dating (Condon et al., 2005; Zhang et al., 2005). Regional stratigraphic correlation suggest that the ca. 551 Ma tuffaceous layer within the Miaohe Member, which was traditionally correlated with Member IV, is likely located in the overlying Dengying Formation (An et al., 2015), implying that the upper boundary of the Doushantuo Formation is older than 551 Ma. However, a more detailed investigation of $\delta^{13}C_{carb}$ of multiple sections around the Huangling Anticline (Zhou et al., 2017) and the $\delta^{13}C_{org}$ study from the Miaohe member (Xiao et al., 2017) argue against the correlation scheme proposed by An et al. (2015).

Our samples were collected from the upper part of the Doushantuo Formation in the Jiulongwan and Xiangerwan sections in the Yangtze Gorges area (**Figure 1**). These two sections were chosen for nitrogen isotope analyses due to the excellent preservation of the Shuram-EN3 carbon isotope excursion (Jiang et al., 2007; An et al., 2015; Zhou et al., 2017). Paleogeographically, the two sections were both

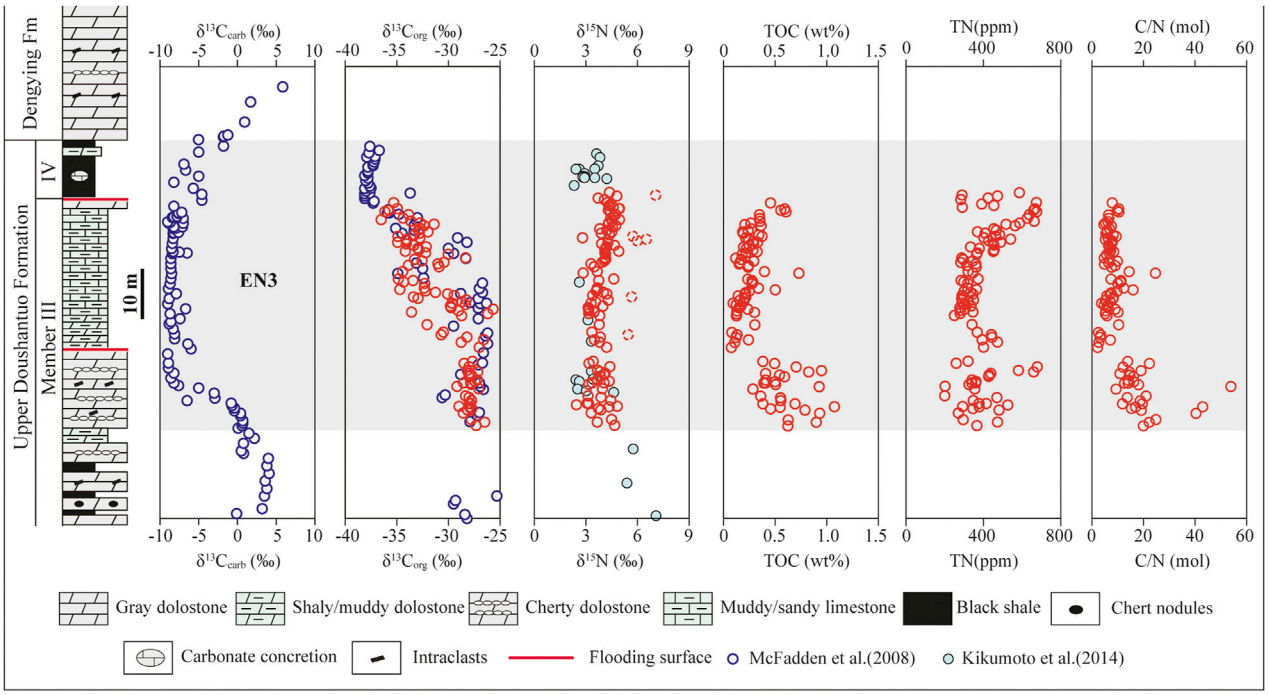

FIGURE 2 | The geochemical profiles of $\delta^{13}C_{carb}$, $\delta^{13}C_{org}$, $\delta^{15}N$, TOC, TN and MC/N spanning the Shuram-EN3 excursion in the Jiulongwan section. The data points with dashed outline fall away from the general trend.

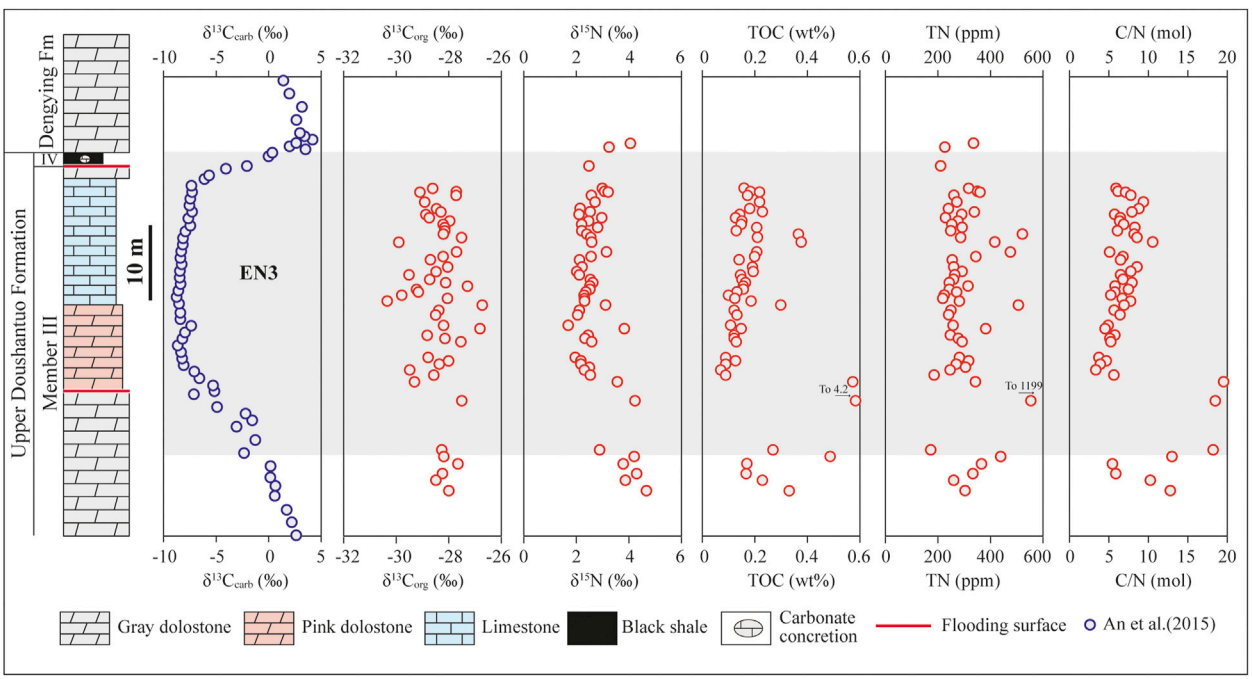

FIGURE 3 | The geochemical profiles of $\delta^{13}C_{carb}$, $\delta^{13}C_{org}$, $\delta^{15}N$, TOC, TN and MC/N spanning the Shuram-EN3 excursion in the Xiangerwan section.

deposited in proximal settings of an intrashelf basin (Jiang et al., 2011; An et al., 2015). The Jiulongwan section, located in the southern part of the Huangling Anticline (**Figure 1**), has been extensively studied to characterize the ocean redox structure (e.g., Jiang et al., 2007; McFadden et al., 2008; Li et al., 2010; Zhou et al., 2012; Ling et al., 2013; Wei et al., 2018; Fan et al., 2020, 2021). The upper Doushantuo Formation in the Jiulongwan section is dominated by cherty dolostone, muddy limestone/dolostone and black shales (**Figure 2**). The Shuram-EN3 excursion begins in the middle part of Member III, continued upwards through the rest of the Doushantuo Formation until return to positive $\delta^{13}C_{carb}$ values at the Doushantuo/Dengying boundary (**Figure 2**). The Xiangerwan section is located in the northwestern part of the Huangling Anticline (**Figure 1**), about 60 km away from the Jiulongwan section. The upper Doushantuo Formation in this section is mainly composed of medium-thick bedded dolostone, pink dolostone and thinly bedded limestone with subordinate black shales (**Figure 3**). The pink dolostone was interpreted as the precipitate of a primary marine red bed enabled by ocean oxygenation (Song et al., 2017). The pattern of the Shuram-EN3 excursion in the Xiangerwan section is similar to that of the Jiulongwan section (**Figure 3**).

ANALYTICAL METHOD

We performed measurements of $\delta^{15}N$ and $\delta^{13}C_{org}$, total nitrogen (TN) contents, and total organic carbon (TOC) contents for 162 samples. Fresh sample chips without any weathering surfaces or visible veins were ground into powders below 200 mesh in an agate mortar. About 10 g of powders from each sample were treated with 2 M excess HCl to ensure the complete removal of carbonate. The carbonate-free samples were then rinsed with deionized water multiple times until a near-neutral pH value was reached. After centrifuging, the decarbonated sample residue was dried at 70°C in an oven before analysis. The isotopic and elemental compositions were measured in the Oxy-Anion Stable Isotope Consortium (OASIC) at Louisiana State University (LSU), using a Vario Microcube Elemental Analyzer (EA) connected to an Isoprime 100 isotope ratio mass spectrometer (IRMS). Because most of our samples are TOC-lean carbonate rocks, approximately 50–100 mg sample powders (based on TOC estimation) were wrapped in tin capsules and combusted in the EA to enhance the N signal. The organic carbon isotope compositions are reported as δ values with reference to the Vienna Pee Dee Belemnite standard (VPDB). The nitrogen isotope compositions are reported in standard δ notation in per mil (‰) deviations from atmospheric N_2 (0‰, Air). Reference standard acetanilide-OASIC ($\delta^{13}C$ = −27.62‰, $\delta^{15}N$ = +1.61‰) was used to calibrate the analytical results. Measurements of C and N concentrations of blanks were below detection limits, suggesting that contamination from capsules did not contribute much to our results. A few samples (n = 10) with N peaks much lower than that of the reference standard were excluded from the dataset and from the discussion. The reproducibility monitored by the reference material was better than 0.1‰ for $\delta^{13}C_{org}$ and 0.3‰ for $\delta^{15}N$.

RESULTS

The analytical results of $\delta^{15}N$, $\delta^{13}C_{org}$, TN, TOC and C/N are shown in **Figures 2**, **3** and **Supplementary Tables S1, S2**. The $\delta^{13}C_{org}$ variations in the Jiulongwan section are well matched with previously published data by McFadden et al. (2008) (**Figure 2**). In the prelude and lower part of the Shuram-EN3 excursion, $\delta^{13}C_{org}$ is relatively high and centers around −28‰. It becomes more variable but shows an overall decreasing trend in the rest of Member III. Low and stable $\delta^{13}C_{org}$ values cluster around -38‰ in the Member IV black shale. The $\delta^{15}N$ data of our samples in the Jiulongwan section largely overlap with those reported from the equivalent interval in the nearby (within 3 km) Wuhe drillcore (**Figure 2**; Kikumoto et al., 2014). Before the Shuram-EN3 excursion, a few data points show relatively high $\delta^{15}N$ values from +5.4‰ to +6.7‰. During the main phase of the Shuram-EN3 excursion, most of $\delta^{15}N$ values fall in the range of +3‰ to +5.5‰, except for a few outliers, with an average of +3.8 ± 0.8‰ (n = 123) (**Figure 2**; this study; Kikumoto et al., 2014). The variability in $\delta^{15}N$ is independent of lithological changes.

In the Xiangerwan section, $\delta^{13}C_{org}$ does not show any clear stratigraphic trend across the Shuram-EN3 excursion. It varies between −30.3‰ and −26.7‰, with an average of −28.4 ± 0.7‰ (n = 49) (**Figure 3**). Variations in $\delta^{15}N$ from this section generally mirror the trend of $\delta^{13}C_{carb}$ reported by An et al. (2015), although the magnitude of change is small (**Figure 3**). Prior to the Shuram-EN3 excursion, $\delta^{15}N$ varies from +3.0‰ to +4.7‰ and the mean value is +4.0 ± 0.6‰ (n = 6). During the main stage of excursion, most samples have $\delta^{15}N$ values between +2.0‰ and +3.8‰. The average value (+2.5 ± 0.4‰, n = 43) is about 1.5‰ lower than that of the pre-excursion interval. An increase of $\delta^{15}N$ relative to pre-excursion values is observed in the upper Doushantuo Formation, coincident with the rising branch of the Shuram-EN3 excursion. Overall, the $\delta^{15}N$ values from the Xiangerwan section are 1–2‰ lower than those from the Jiulongwan section.

DISCUSSION

Evaluation of the Preservation of Primary Isotopic Signals

Whether $\delta^{15}N$ and $\delta^{13}C_{org}$ in sedimentary rocks record primary autochthonous signatures is dependent on several factors, including paleogeographic setting, diagenesis, metamorphism, and potential contributions of allochthonous materials (Ader et al., 2009; Ader et al., 2016; Robinson et al., 2012; Stüeken et al., 2016). In modern oceans, sedimentary $\delta^{15}N$ of organic matter may show large offsets compared to sinking organic particles at sites located off continental margins due to extended remineralization of organic matter in the water column and upper sediment. In contrast, on continental shelves with high sediment accumulation rates and/or organic matter content, sedimentary organic matter generally displays $\delta^{15}N$ values similar to that of sinking particles (Robinson et al., 2012). The two study sections were deposited in shallow shelf environments (Jiang et al., 2011; An et al., 2015), minimizing this

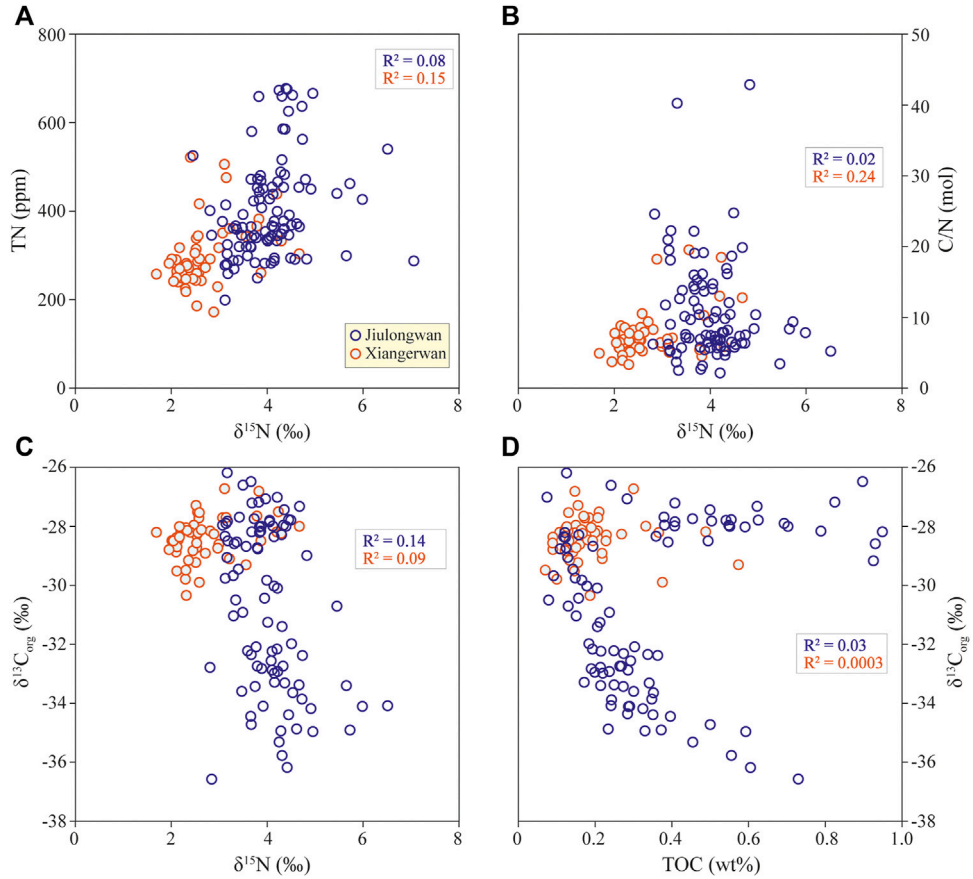

FIGURE 4 | Cross plots of TN vs. $\delta^{15}N$ **(A)**, C/N vs. $\delta^{15}N$ **(B)**, $\delta^{13}C_{org}$ vs. $\delta^{15}N$ **(C)**, and $\delta^{13}C_{org}$ vs. TOC **(D)** in study sections.

effect on sedimentary $\delta^{15}N$ as well as $\delta^{13}C_{org}$. However subsequent biological decomposition and thermal maturation of sedimentary organic matter during early and burial diagenesis can still perturb the original $\delta^{15}N$ and $\delta^{13}C_{org}$ values (Ader et al., 2009; Ader et al., 2016; Stüeken et al., 2016). Several lines of evidence, however, argue against these processes as major controls on our data. First, the isotopic alteration by biological decomposition during early diagenesis is generally small for $\delta^{13}C_{org}$ (Ader et al., 2009 and references therein). Although this effect could be large for $\delta^{15}N$ (up to 4‰) when bottom water was oxic (Altabet et al., 1999; Freudenthal et al., 2001; Lehmann et al., 2002; Prokopenko et al., 2006), Fe speciation data, I/(Ca + Mg) ratios and Ce anomales (Ce/Ce*) from the Jiulongwan and Xiangerwan sections indicate oxygen-depleted bottom water conditions (Li et al., 2010; Zhou et al., 2012; Ling et al., 2013; Wei et al., 2019). Second, Raman spectra and equivalent vitrinite reflectance data suggested that the peak heating temperature of the Doushantuo Formation was <300°C (Chang et al., 2020), and at such low metamorphic grade thermal alterations of isotopic composition would be limited for both $\delta^{15}N$ and $\delta^{13}C_{org}$ (Ader et al., 2009; Ader et al., 2016; Stüeken et al., 2016; Stüeken et al., 2017). Lastly, if the original $\delta^{13}C_{org}$ and $\delta^{15}N$ were largely modified by the preferential loss of light ^{12}C and/or ^{14}N during early and burial diagenesis, one would expect correlation between $\delta^{15}N$, TN, C/N, and $\delta^{13}C_{org}$ as well as $\delta^{13}C_{org}$ and TOC. No significant correlations, however, are observed between these parameters (**Figure 4**). A subset of samples show a negative correlation between $\delta^{13}C_{org}$ and TOC commonly seen in Precambrian rocks, but the reason of this is unknown based on current research and warrants further investigation.

The addition of material from allochthonous sources is another factor that can affect sedimentary $\delta^{13}C_{org}$ and $\delta^{15}N$. These allochthonous sources include hydrothermal fluids and detrital input. Hydrothermal fluids are unlikely to increase the organic carbon to sedimentary rocks, but they could contain some inorganic N that can be trapped by sedimentary clay when moving along the fractures, thereby affecting the bulk $\delta^{15}N$ (e.g., Zerkle et al., 2017; Luo et al., 2018). However, no clear correlation is observed between potassium abundance (Wang, 2019) and $\delta^{15}N$ and in the Xiangerwan section (**Figure 5A**), suggesting that exchange with hydrothermal fluids was limited and did not severely bias our $\delta^{15}N$ values. For sedimentary rocks with low authigenic TOC contents, detrital organic matter could be a major component and overprint the primary $\delta^{13}C_{org}$ (Jiang et al., 2010). It is difficult to quantify the contribution of detrital organic matter and detrital clay-bound N to our samples; however, $\delta^{15}N$, $\delta^{13}C_{org}$ and TOC do not show

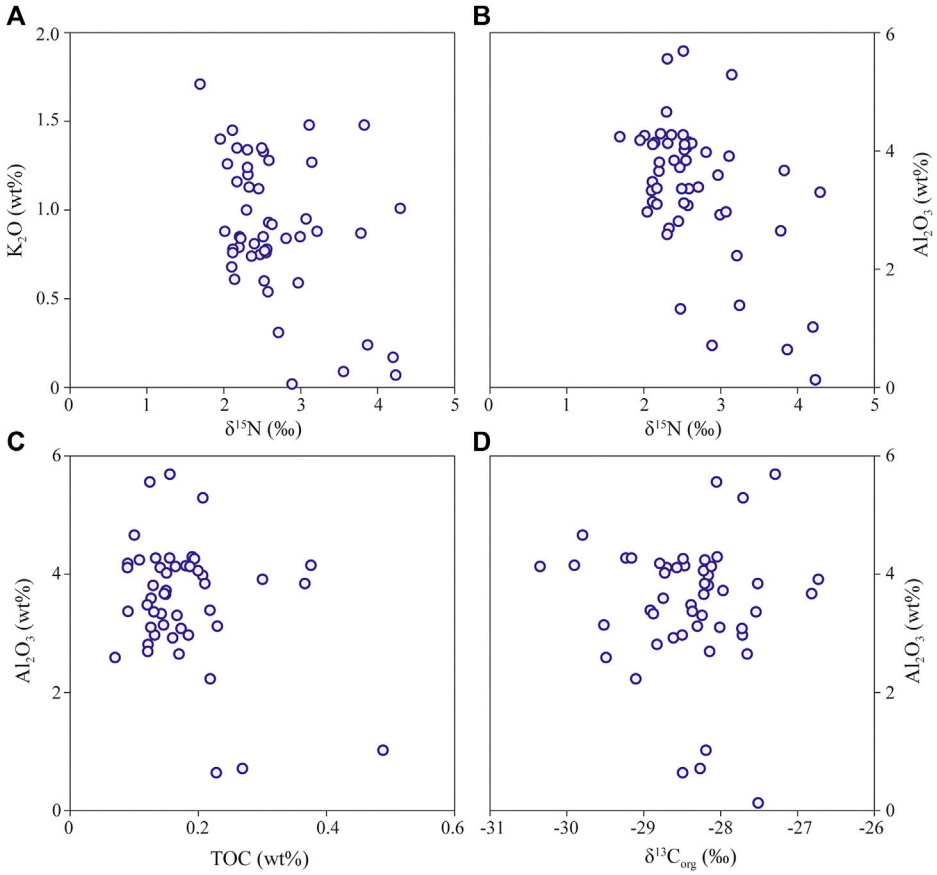

FIGURE 5 | Cross plots of K_2O vs. $\delta^{15}N$ **(A)**, Al_2O_3 vs. $\delta^{15}N$ **(B)**, Al_2O_3 vs. TOC **(C)**, and Al_2O_3 vs. $\delta^{13}C_{org}$ **(D)** in the Xiangerwan section. The Al_2O_3 and K_2O data are from Wang (2019).

correlations with Al content in the Xiangerwan section (Wang, 2019)—an indicator of detrital input (**Figures 5B–D–D**). Therefore, we suggest that detrital input did not significantly affect our data. Nevertheless, this question can be further clarified in a future dedicated study.

Variations of $\delta^{15}N$-$\delta^{13}C_{carb}$ Pattern in the Upper Doushantuo Formation

The upper Doushantuo Formation in South China is characterized by a prominent negative $\delta^{13}C_{carb}$ excursion (N3, EN3 or DOUNCE) that is widely accepted to be equivalent to the Shuram excursion (Jiang et al., 2007; Zhou and Xiao, 2007; Zhu et al., 2007; Zhu et al., 2013; McFadden et al., 2008; Wang et al., 2012; Lu et al., 2013; An et al., 2015; Wang et al., 2016; Li et al., 2017; Zhou et al., 2017; Wei et al., 2019). Although the Shuram-EN3 excursion has a wide paleogeographic distribution from the inner shelf to upper slope setting, it shows large spatial variations in its pattern, magnitude and stratigraphic coverage (Wang et al., 2016; Zhou et al., 2017). In some sections, this excursion is completely absent (Zhou et al., 2017). The discrepancy of the Shuram-EN3 excursion between different sections has been attributed to facies change, stratigraphic truncation, the diachronous nature of the Doushantuo/Dengying boundary and/or diagenetic overprinting of primary isotope signatures (Cui et al., 2015; Wang et al., 2016; Zhou et al., 2017).

$\delta^{15}N$ data for the Ediacaran Doushantuo Formation were first reported from the Wuhe drillcore in Yangtze Gorges area by Kikumoto et al. (2014). They found a synchronous decrease in $\delta^{15}N$ from ca. +6‰ to ca. +3.2‰ along with the Shuram-EN3 excursion (**Figure 6B**; Kikumoto et al., 2014). Our new $\delta^{15}N$ data from the upper Doushantuo Formation in the Jiulongwan section, which is <3 km away from the Wuhe drillcore, are well consistent with the trend reported by Kikumoto et al. (2014) when excluding a few outliers (**Figure 6B**). In the inner shelf Xiangerwan section about 60 km north of the Jiulongwan section, the Shuram-EN3 excursion is well developed and shows striking similarity with that in the Jiulongwan section (**Figure 6A**; An et al., 2015). The $\delta^{15}N$ data also mirror the trend observed in the Wuhe drillcore, although the absolute values are overall 1–2‰ lower than those of the Wuhe drillcore both before and during the Shuram-EN3 excursion. The $\delta^{15}N$-$\delta^{13}C_{carb}$ pattern from the upper Doushantuo Formation in the outer shelf Wangjiapeng drillcore section shows some differences compared to the Wuhe (Jiulongwan) and Xiangerwan sections (**Figure 6C**; Lan et al., 2019). The Shuram-EN3 excursion in this

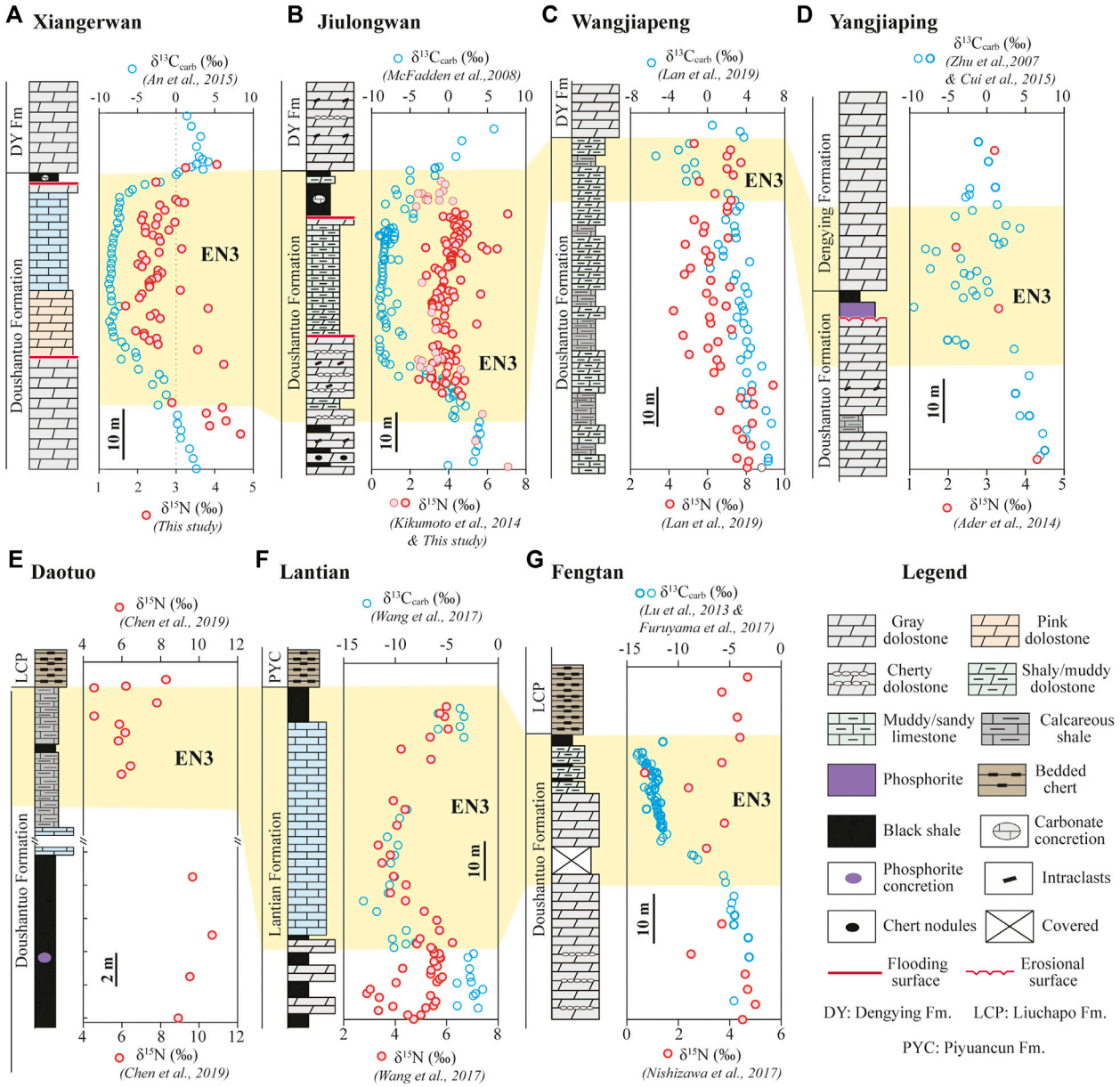

FIGURE 6 | Correlation of $\delta^{15}N$ variations across the Shuram-EN3 excursion in different sections.

section is marked by a sharp decrease of $\delta^{13}C_{carb}$ to a minimum value of −5.4‰, followed by a quick return to positive values, while the associated $\delta^{15}N$ in this interval shows an opposite (increasing) trend. It should be noted that $\delta^{15}N$ in the Wangjiapeng section shows a small negative excursion in the 'uppermost' Doushantuo Formation, clearly postdating the Shuram-EN3 excursion (Lan et al., 2019). Whether this negative $\delta^{15}N$ excursion can be correlated with that in the Wuhe and Xiangerwan sections is questionable and requires further investigation.

In the Yangjiaping section on the shelf margin, Ediacaran $\delta^{13}C_{carb}$ data were reported by several research groups (Zhu et al., 2007; Ader et al., 2009; Kunimitsu et al., 2011; Cui et al., 2015). Here the Shuram-EN3 excursion spans the upper Doushantuo Formation and the lower part of the overlying Dengying Formation, but the data show large sample-to-sample variations (Wang et al., 2016). A few $\delta^{15}N$ data points from this interval show a decreasing trend from ~ +4.3‰ to ~ +3.0‰ (**Figure 6D**; Ader et al., 2014). More data are needed to confirm this variation. Chen et al. (2019) reported $\delta^{15}N$ data from the Doushantuo Formation in an upper slope drill core section (zk 2012) in the Daotuo area, northeastern Guizhou Province. A conspicuous decline in $\delta^{15}N$ was observed in the upper Doushantuo Formation (**Figure 6E**; Chen et al., 2019). Although no $\delta^{13}C_{carb}$ data were reported in zk 2012, the $\delta^{13}C_{carb}$ profile from an adjacent drill core verifies the

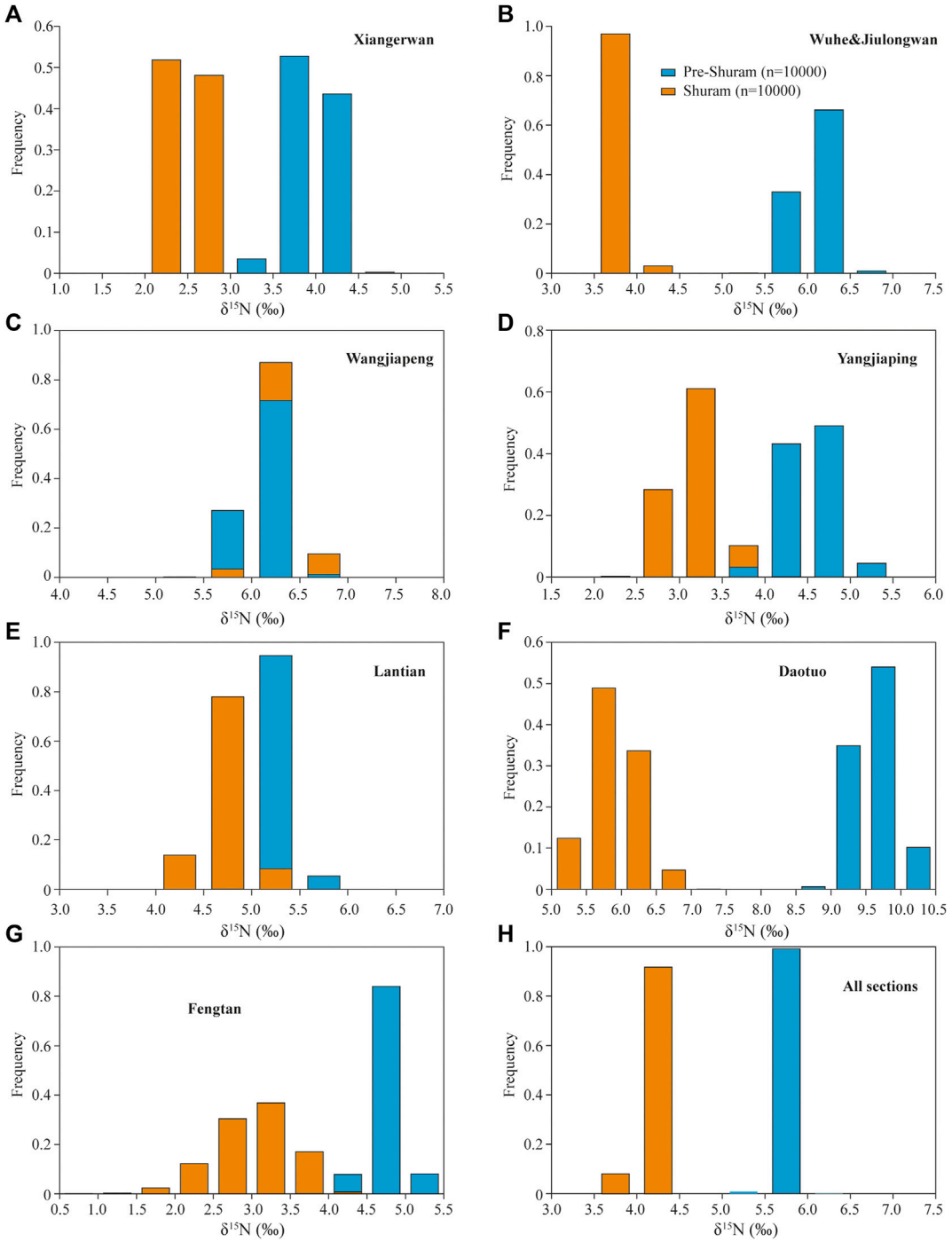

FIGURE 7 | Bootstrap distribution of $\delta^{15}N$ before and during the Shuram-EN3 excursion in the Xiangerean section **(A)**, Jiulongwan section **(B)**, Wangjiapeng drill core **(C)**, Yangjiaping section **(D)**, Lantian drill core **(E)**, Daotuo drill core **(F)**, Fengtan section **(G)**, and all sections **(H)**.

presence of the Shuram-EN3 excursion in the upper Doushantuo Formation (Wei et al., 2019). Coupled $\delta^{15}N$-$\delta^{13}C_{carb}$ data have also been reported from the Lantian Formation in southern Anhui, which is equivalent to the Doushantuo Formation (Wang et al., 2017). The $\delta^{13}C_{carb}$ from this unit is dominated by negative values and show a negative excursion in the upper Lantian Formation that is considered to be correlative to the Shuram excursion. However, the $\delta^{15}N$ data from this interval do not show a clear stratigraphic trend (**Figure 6F**; Wang et al., 2017). In the basinal Fentan section, the Shuram-EN3 excursion is documented in the upper Doushantuo Formation (**Figure 6G**; Lu et al., 2013; Furuyama et al., 2017). In the same interval, the

$\delta^{15}N$ also show a clear decreasing trend from ~ +4.5‰ to nadir +0.7‰ (**Figure 6G**; Nishizawa et al., 2019). Recently, a $\delta^{15}N$ study was performed for the Doushantuo Formation in the proximal E-Shan section (Peng et al., 2020), However, this section is not included in our correlation (**Figure 6**) because the Dousantuo Formation is dominated by siliciclastic rocks and do not contain the Shuram excursion.

To better characterize the overall $\delta^{15}N$ trend during this critical time interval, we simulate the $\delta^{15}N$ variations before and during the Shuram excursion for each section using a bootstrap resampling method. Out of seven sections, six sections are characterized by a bimodal $\delta^{15}N$ distribution (**Figure 7**). Notably, although the $\delta^{15}N$ data from the Lantian section do not show a clear stratigraphic trend (Wang et al., 2017), the model result indicates that $\delta^{15}N$ during the Shuram excursion are statistically 0.6‰ lower than prior to the excursion (**Figure 7E**). In the Wangjiapeng section, the mean $\delta^{15}N$ distributions obtained from bootstrap resampling largely overlap for pre- and syn-excursion strata (**Figure 7C**). This is likely due to a prominent negative $\delta^{15}N$ excursion in the lower part of the Doushantuo Formation (Lan et al., 2019). The bimodal $\delta^{15}N$ distribution becomes even more evident when the bootstrap method is applied to all data from the seven sections (**Figure 7H**), providing evidence for a synchronous decrease of $\delta^{15}N$ associated with the Shuram excursion. This covariation pattern could be attributed to a feedback between nitrogen and carbon cycles that will be discussed in the following section.

Feedback Between Nitrogen and Carbon Cycles

Modeled results indicate that $\delta^{15}N$ data from the Ediacaran Doushantuo Formation show contrasting distributions before and during the Shuram excursion (**Figure 7**). High $\delta^{15}N$ values from the lower-middle Doushantuo Formation prior to the Shuram excursion have been attributed to incomplete denitrification that preferentially removed light ^{14}N from the ocean (Kikumoto et al., 2014; Ader et al., 2014; Wang et al., 2017, 2018; Chen et al., 2019; Lan et al., 2019; Xu et al., 2020). The decrease of $\delta^{15}N$ associated with the Shuram excursion was previously interpreted as partial assimilation of NO_3^- from an expanding nitrate pool in response to a rise of oxygen levels in the ocean-atmosphere system, implying that dissolved P rather than N was the limiting nutrient during the excursion interval (Kikumoto et al., 2014; Nishizawa et al., 2019). We challenge this explanation for the following reasons. First, if the decrease in $\delta^{15}N$ was caused by partial assimilation of NO_3^-, the ^{15}N-enriched residual NO_3^- would be quantitatively utilized in other parts of the basin. One should expect a positive $\delta^{15}N$ excursion in the upper Doushantuo Formation in some sections, which, however, has not been observed in sections studied to date (**Figure 7**); Second, the upper Doushantuo Formation contains abundant phosphatized fossils and phosphorite deposits (Xiao et al., 1998; Xiao et al., 2014; Liu et al., 2014; She et al., 2014; Yin et al., 2015; Zhang Y. et al., 2019), possibly indicating high dissolved P level in coeval seawater (e.g., Laakso et al., 2020). Thus, it is unlikely that P was severely limited during the Shuram excursion.

Alternatively, the isotopic shift could have been caused by a shift in the location of denitrification changes in the relative proportions of water column denitrification vs. sedimentary denitrification can affect the seawater $\delta^{15}N$ and accordingly sedimentary $\delta^{15}N$ (Sigman et al., 2009; Algeo et al., 2014; Stüeken et al., 2016). In the modern oceans, water column denitrification accounts for 25–32% of total denitrification and is generally accompanied by large isotope fractionation ($\varepsilon \approx \delta^{15}N_{reactant} - \delta^{15}N_{product}$). The remaining 68–75% of denitrification occurs within sedimentary porewaters with small or negligible isotope fractionation. The balance between these two processes and N_2 fixation determines the isotope composition of modern seawater (average ca. +5‰) (Sigman et al., 2009; Algeo et al., 2014; Stüeken et al., 2016). Assuming a steady isotope scenario, a high fraction of water column denitrification would thus increase the $\delta^{15}N$ of seawater nitrate, and vice versa (Sigman et al., 2009; Algeo et al., 2014; Stüeken et al., 2016). Hence, the decrease of $\delta^{15}N$ coupled with the Shuram excursion on the Yangtze Platform could have resulted from the decrease of the fraction of water column denitrification. This requires a more widely oxygenated ocean than today, i.e. a complete absence of oxygen minimum zones, which is not supported by any current geochemical and geological evidence. However, the nitrogen isotope mass balance can potentially also be affected by sea level. Algeo et al. (2014) compiled $\delta^{15}N$ data from the Cryogenian to present and found a long-term decrease in $\delta^{15}N$ from the Cryogenian to the Cambrian, which they attributed to a first-order climate-driven sea level change. According to this model, high eustatic sea level could have resulted in relatively low $\delta^{15}N$ if the dominant locus of denitrification shifted to sediments (Algeo et al., 2014). However, this model is difficult to reconcile with the relatively stable positive $\delta^{15}N$ values from ca. 750 Ma to 570 Ma, spanning from the Tonian through the Cryogenian to the middle Ediacaran (Ader et al., 2014). Particularly, after the deglaciation of the Marinoan Snowball Earth, which represented a global sea level rise, $\delta^{15}N$ remains high for at least 60 Myr or even longer until the onset of the Shuram excursion (Xiang et al., 2018; Chen et al., 2019; Xu et al., 2020). Further, from the Ediacaran to early Cambrian the ocean was characterized by predominately anoxic environments with multiple short-term oxygenation events (Sahoo et al., 2016; Li et al., 2018). Under such conditions, the fraction of water column denitrification should always have been much higher than it is in more oxygenated oceans like today, even during intervals of high eustatic sea level. Therefore, changes in proportion of water column denitrification alone cannot readily explain the decrease in $\delta^{15}N$ during the Shuram excursion.

Variation in the isotope fractionation associated with water column denitrification is another factor that can modulate seawater $\delta^{15}N$. According to the mass balance model for the nitrogen cycle (Sigman et al., 2009; Algeo et al., 2014; Stüeken et al., 2016), the seawater nitrate $\delta^{15}N$ is determined by the isotopic balance between input and output processes, which can be described in the following formulation:

$$\delta^{15}N_{atmosphere} - \varepsilon_{fix} = \delta^{15}N_{nitrate} - \varepsilon_{den} \quad (1)$$

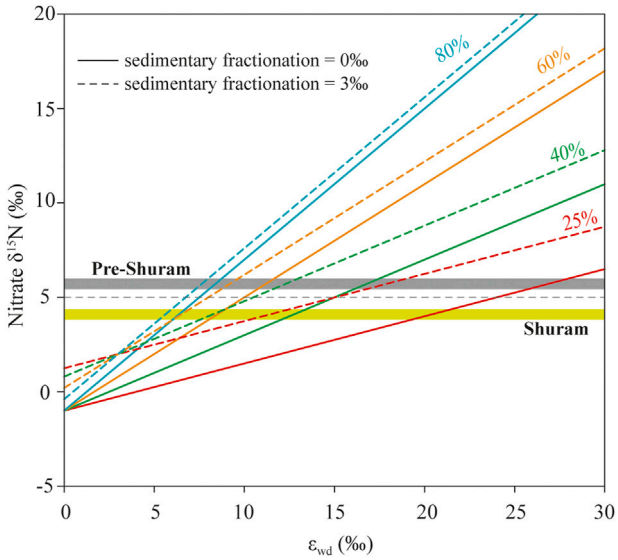

FIGURE 8 | Mass balance model showing seawater nitrate $\delta^{15}N$ as function of ε_{wd}. Colored oblique lines represent the fraction of water column denitrification (f_{wd}) from 25% (red line) to 80% (blue line). Horizontal dash line indicates the average $\delta^{15}N$ and modern seawater. Shaded zones show the bootstrap $\delta^{15}N$ range (same as in **Figure 7H**) before and during the Shuram excursion.

where ε_{fix} refers to isotopic fractionation of N_2 fixation, and ε_{den} represents net isotope fractionation of total denitrification which can be expressed as:

$$\varepsilon_{den} = f_{wd} \cdot \varepsilon_{wd} + (1 - f_{wd}) \cdot \varepsilon_{sd} \quad (2)$$

where the subscripts *wd* and *sd* refer to water column denitrification and sedimentary denitrification, respectively, and f_{wd} represents the fraction of water column denitrification. In modern oceans, the ε_{wd} can vary from 0‰ for quantitative denitrification to 30‰ (Sigman et al., 2009 and references therein). To model seawater nitrate $\delta^{15}N$ as a function of ε_{wd}, we set ε_{fix} to be +1‰ and ε_{sd} to be 0‰ (Sigman et al., 2009 and references therein). If the fraction of water column denitrification was 25% during the Ediacaran as generally suggested for today (Sigman et al., 2009), the mean $\delta^{15}N$ of pre-Shuram samples corresponds to ε_{wd} of 26–28%, and the decrease of $\delta^{15}N$ during the Shuram excursion would require a decrease of ε_{wd} to 19–21% (**Figure 8**). The ε_{wd} could have been smaller if f_{wd} increased (**Figure 8**). For example, ε_{wd} for the mean $\delta^{15}N$ of the Shuram interval would be 12–13‰, if f_{wd} increased to 40%, and it would decrease to ca. 6‰ when increasing f_{wd} to 80%. A high fraction of f_{wd} was possible for the Ediacaran when anoxic marine environments were more extensive than today. Modifying ε_{sd} to 3‰ as observed in some modern sediment (Kessler et al., 2014) would require a lower ε_{wd} to produce the same $\delta^{15}N$. This difference would be large when f_{wd} was low but small as f_{wd} increased (**Figure 8**).

As discussed above, the decrease of $\delta^{15}N$ associated with the Shuram excursion can be well explained by the decrease of ε_{wd}. We argue that this change may have been caused by a feedback between the nitrogen and carbon cycles at that time. Enhanced continental weathering before the Shuram excursion, as evidenced by the increase of $^{87}Sr/^{86}Sr$ (Sawaki et al., 2010; Wang et al., 2014; Cui et al., 2015; Xiao et al., 2016; Lan et al., 2019), would have delivered substantial amounts of nutrients to the ocean, promoting primary productivity (Williams et al., 2019). High primary productivity would have resulted in an expansion of anoxic bottom waters on productive continental shelves. These anoxic waters would have been capped by oxic surface waters, leading to extensive aerobic respiration or organic matter along the redox interface. An ensuing consequence of this combined effect would have been the significant consumption of nitrate through enhanced denitrification. Stoichiometric relationships indicate that remineralization of 1 mol of organic carbon through denitrification would consume 85 mol or even more nitrate (Altabet, 2006). The shrinkage of the nitrate pool may have reduced ε_{wd} due to reservoir effects, as has been documented from modern microbial cultures, where ε_{wd} decreased when nitrate levels dropped to a few μM (compared to ~30 μM in the modern open ocean) (Kritee et al., 2012). Additionally, the decrease of nitrate levels would inevitably shift the nitrogen cycle towards N_2 fixation and ammonium assimilation, which may also partially contribute to the lower $\delta^{15}N$ during the Shuram excursion, as evidenced by a near zero value observed in the Fengtan section (Nishizawa et al., 2019). In the long time scale, an increase in organic burial in the context of high primary productivity would have led to rising O_2 levels (e.g., Alcott et al., 2019). This inference is consistent with the increase of I/(Ca + Mg) ratios (Hardisty et al., 2017; Wei et al., 2019), a large positive $\delta^{238}U$ excursion (Zhang F. et al., 2019; Cao et al., 2020), and a negative excursion of thallium isotope composition ($\varepsilon^{205}Tl$) (Fan et al., 2020) during the Shuram interval. The rise of oxygen would have resulted in partial oxidation of dissolved organic carbon stored in the anoxic deep ocean (Rothman et al., 2003) or of other forms of reduced carbon (e.g., Bjerrum and Canfield, 2011), lowering the $\delta^{13}C$ of inorganic carbon in seawater, as documented in the Shuram excursion. Further, the recycled N and P from the oxidation of organic matter could have been upwelled to the photic zone, providing new nutrient input for organisms and further stimulating primary productivity. Although we cannot completely rule out the possibility of diagenetic overprint over the Shuram signal in individual cases, the coupled variations of $\delta^{13}C_{carb}$ and $\delta^{15}N$ in multiple sections across the Yangtze Platform suggest that they may partially record changes in primary seawater signals in response to the complex feedback between carbon and nitrogen cyclings during this critical period.

CONCLUSION

High resolution $\delta^{15}N$ and $\delta^{13}C_{org}$ data are reported from the upper part of the Ediacaran Doushantuo Formation in two well-preserved sections in the Yangtze Gorges area, South China. These data, coupled with previously published $\delta^{13}C_{carb}$ in the same sections, are used to elucidate the inherent relationship between carbon and nitrogen cycling during the Shuram-EN3 excursion—the deepest negative $\delta^{13}C_{carb}$ excursion in Earth history. The $\delta^{15}N$ data in the studied sections show concurrent variations with $\delta^{13}C_{carb}$, although the magnitude of change is much smaller. Bootstrapping simulations

further demonstrate a clear decrease of $\delta^{15}N$ associated with the Shuram-EN3 excursion. We argue that the decrease in $\delta^{15}N$ during the Shuram-EN3 excursion can be reasonably explained by the reduction of isotopic fractionation associated with water column denitrification rather than the partial assimilation of nitrate. The parallel changes in $\delta^{13}C_{carb}$ and $\delta^{15}N$ may have resulted from feedbacks between carbon and nitrogen cycles.

DATA AVAILABILITY STATEMENT

The original contributions presented in the study are included in the article/**Supplementary Material**, further inquiries can be directed to the corresponding author.

AUTHOR CONTRIBUTIONS

XW and XS designed research. DX and XW collected samples. DX, XW, and YP performed lab analyses. XW, DX, XS, YP, and ES wrote the paper.

FUNDING

This research is supported by the National Natural Science Foundation of China (41872032, 41830215, 41930320) and the Chinese '111' project (B20011).

ACKNOWLEDGMENTS

Haoming Wei and Lijing Wang participated part of field trip and sample collection. We are indebted to Hao Yan for the kind help with the carbon and nitrogen isotope analyses. Thanks are given to two reviewers for valuable comments that improve the quality of this paper.

SUPPLEMENTARY MATERIAL

The Supplementary Material for this article can be found online at: https://www.frontiersin.org/articles/10.3389/feart.2021.678149/full#supplementary-material

REFERENCES

Ader, M., Macouin, M., Trindade, R. I. F., Hadrien, M.-H., Yang, Z., Sun, Z., et al. (2009). A Multilayered Water Column in the Ediacaran Yangtze Platform? Insights from Carbonate and Organic Matter Paired $\delta^{13}C$. *Earth Planet. Sci. Lett.* 288, 213–227. doi:10.1016/j.epsl.2009.09.024

Ader, M., Sansjofre, P., Halverson, G. P., Busigny, V., Trindade, R. I. F., Kunzmann, M., et al. (2014). Ocean Redox Structure across the Late Neoproterozoic Oxygenation Event: A Nitrogen Isotope Perspective. *Earth Planet. Sci. Lett.* 396, 1–13. doi:10.1016/j.epsl.2014.03.042

Ader, M., Thomazo, C., Sansjofre, P., Busigny, V., Papineau, D., Laffont, R., et al. (2016). Interpretation of the Nitrogen Isotopic Composition of Precambrian Sedimentary Rocks: Assumptions and Perspectives. *Chem. Geol.* 429, 93–110. doi:10.1016/j.chemgeo.2016.02.010

Alcott, L. J., Mills, B. J. W., and Poulton, S. W. (2019). Stepwise Earth Oxygenation Is an Inherent Property of Global Biogeochemical Cycling. *Science* 366, 1333–1337. doi:10.1126/science.aax6459

Algeo, T. J., Meyers, P. A., Robinson, R. S., Rowe, H., and Jiang, G. Q. (2014). Icehouse-greenhouse Variations in marine Denitrification. *Biogeosciences* 11, 1273–1295. doi:10.5194/bg-11-1273-2014

Altabet, M. A. (2006). "Isotopic Tracers of the Marine Nitrogen Cycle: Present and Past," in *Marine Organic Matter: Biomarkers, Isotopes and DNA. The Handbook of Environmental Chemistry, Vol 2N*. Editor J.K. Volkman (Berlin, Heidelberg: Springer), 251–293. doi:10.1007/698_2_008

Altabet, M. A., Pilskaln, C., Thunell, R., Pride, C., Sigman, D., Chavez, F., et al. (1999). The Nitrogen Isotope Biogeochemistry of Sinking Particles from the Margin of the Eastern North Pacific. *Deep Sea Res. Oceanographic Res. Pap.* 46, 655–679. doi:10.1016/S0967-0637(98)00084-3

An, Z., Jiang, G., Tong, J., Tian, L., Ye, Q., Song, H., et al. (2015). Stratigraphic Position of the Ediacaran Miaohe Biota and its Constrains on the Age of the Upper Doushantuo $\delta^{13}C$ Anomaly in the Yangtze Gorges Area, South China. *Precambrian Res.* 271, 243–253. doi:10.1016/j.precamres.2015.10.007

Bjerrum, C. J., and Canfield, D. E. (2011). Towards a Quantitative Understanding of the Late Neoproterozoic Carbon Cycle. *Proc. Natl. Acad. Sci.* 108, 5542–5547. doi:10.1073/pnas.1101755108

Bowring, S. A., Grotzinger, J. P., Condon, D. J., Ramezani, J., Newall, M. J., and Allen, P. A. (2007). Geochronologic Constraints on the Chronostratigraphic Framework of the Neoproterozoic Huqf Supergroup, Sultanate of Oman. *Am. J. Sci.* 307, 1097–1145. doi:10.2475/10.2007.01

Bristow, T. F., and Kennedy, M. J. (2008). Carbon Isotope Excursions and the Oxidant Budget of the Ediacaran Atmosphere and Ocean. *Geol* 36, 863–866. doi:10.1130/g24968a.1

Burns, S. J., and Matter, A. (1993). Carbon Isotopic Record of the Latest Proterozoic from Oman. *Eclogae Geologicae Helv.* 86, 595–607.

Canfield, D. E., Knoll, A. H., Poulton, S. W., Narbonne, G. M., and Dunning, G. R. (2020). Carbon Isotopes in Clastic Rocks and the Neoproterozoic Carbon Cycle. *Am. J. Sci.* 320, 97–124. doi:10.2475/02.2020.01

Cao, M., Daines, S. J., Lenton, T. M., Cui, H., Algeo, T. J., Dahl, T. W., et al. (2020). Comparison of Ediacaran platform and slope δ238U records in South China: Implications for global-ocean oxygenation and the origin of the Shuram Excursion. *Geochimica et Cosmochimica Acta* 287, 111–124. doi:10.1016/j.gca.2020.04.035

Chang, B., Li, C., Liu, D., Foster, I., Tripati, A., Lloyd, M. K., et al. (2020). Massive Formation of Early Diagenetic Dolomite in the Ediacaran Ocean: Constraints on the "Dolomite Problem". *Proc. Natl. Acad. Sci. USA* 117, 14005–14014. doi:10.1073/pnas.1916673117

Chen, Y., Diamond, C. W., Stüeken, E. E., Cai, C., Gill, B. C., Zhang, F., et al. (2019). Coupled Evolution of Nitrogen Cycling and Redoxcline Dynamics on the Yangtze Block across the Ediacaran-Cambrian Transition. *Geochimica et Cosmochimica Acta* 257, 243–265. doi:10.1016/j.gca.2019.05.017

Condon, D., Zhu, M. Y., Bowring, S., Wang, W., Yang, A. H., and Jin, Y. G. (2005). U-pb Ages from the Neoproterozoic Doushantuo Formation, China. *Science* 308, 95–98. doi:10.1126/science.1107765

Cui, H., Kaufman, A. J., Xiao, S., Zhou, C., and Liu, X.-M. (2017). Was the Ediacaran Shuram Excursion a Globally Synchronized Early Diagenetic Event? Insights from Methane-Derived Authigenic Carbonates in the Uppermost Doushantuo Formation, South China. *Chem. Geol.* 450, 59–80. doi:10.1016/j.chemgeo.2016.12.010

Cui, H., Kaufman, A. J., Xiao, S., Zhu, M., Zhou, C., and Liu, X.-M. (2015). Redox Architecture of an Ediacaran Ocean Margin: Integrated Chemostratigraphic ($\delta^{13}C$-$\Delta^{34}S$-$^{87}Sr/^{86}Sr$-Ce/Ce*) Correlation of the Doushantuo Formation, South China. *Chem. Geol.* 405, 48–62. doi:10.1016/j.chemgeo.2015.04.009

Derry, L. A. (2010). A Burial Diagenesis Origin for the Ediacaran Shuram-Wonoka Carbon Isotope Anomaly. *Earth Planet. Sci. Lett.* 294, 152–162. doi:10.1016/j.epsl.2010.03.022

Devol, A. H. (2015). Denitrification, Anammox, and N2Production in Marine Sediments. *Annu. Rev. Mar. Sci.* 7, 403–423. doi:10.1146/annurev-marine-010213-135040

Falkowski, P. G. (1997). Evolution of the Nitrogen Cycle and its Influence on the Biological Sequestration of CO_2 in the Ocean. *Nature* 387, 272–275. doi:10.1038/387272a0

Fan, H., Fu, X., Ward, J. F., Yin, R., Wen, H., and Feng, X. (2021). Mercury Isotopes Track the Cause of Carbon Perturbations in the Ediacaran Ocean. *Geol.* 49, 248–252. doi:10.1130/g48266.1

Fan, H., Nielsen, S. G., Owens, J. D., Auro, M., Shu, Y., Hardisty, D. S., et al. (2020). Constraining Oceanic Oxygenation during the Shuram Excursion in South China Using Thallium Isotopes. *Geobiol.* 18, 348–365. doi:10.1111/gbi.12379

Fennel, K., Follows, M., and Falkowski, P. G. (2005). The Co-evolution of the Nitrogen, Carbon and Oxygen Cycles in the Proterozoic Ocean. *Am. J. Sci.* 305, 526–545. doi:10.2475/ajs.305.6-8.526

Fike, D. A., Grotzinger, J. P., Pratt, L. M., and Summons, R. E. (2006). Oxidation of the Ediacaran Ocean. *Nature* 444, 744–747. doi:10.1038/nature05345

Freudenthal, T., Wagner, T., Wenzhöfer, F., Zabel, M., and Wefer, G. (2001). Early Diagenesis of Organic Matter from Sediments of the Eastern Subtropical Atlantic: Evidence from Stable Nitrogen and Carbon Isotopes. *Geochimica et Cosmochimica Acta* 65, 1795–1808. doi:10.1016/S0016-7037(01)00554-3

Furuyama, S., Kano, A., Kunimitsu, Y., Ishikawa, T., Wang, W., and Liu, X. (2017). Chemostratigraphy of the Ediacaran Basinal Setting on the Yangtze Platform, South China: Oceanographic and Diagenetic Aspects of the Carbon Isotopic Depth Gradient. *Isl. Arc* 26, e12196. doi:10.1111/iar.12196

Gong, Z., and Li, M. (2020). Astrochronology of the Ediacaran Shuram Carbon Isotope Excursion, Oman. *Earth Planet. Sci. Lett.* 547, 116462. doi:10.1016/j.epsl.2020.116462

Grotzinger, J. P., Fike, D. A., and Fischer, W. W. (2011). Enigmatic Origin of the Largest-Known Carbon Isotope Excursion in Earth's History. *Nat. Geosci* 4, 285–292. doi:10.1038/ngeo1138

Halverson, G. P., Wade, B. P., Hurtgen, M. T., and Barovich, K. M. (2010). Neoproterozoic Chemostratigraphy. *Precambrian Res.* 182, 337–350. doi:10.1016/j.precamres.2010.04.007

Hardisty, D. S., Lu, Z., Bekker, A., Diamond, C. W., Gill, B. C., Jiang, G., et al. (2017). Perspectives on Proterozoic Surface Ocean Redox from Iodine Contents in Ancient and Recent Carbonate. *Earth Planet. Sci. Lett.* 463, 159–170. doi:10.1016/j.epsl.2017.01.032

Higgins, M. B., Robinson, R. S., Husson, J. M., Carter, S. J., and Pearson, A. (2012). Dominant Eukaryotic export Production during Ocean Anoxic Events Reflects the Importance of Recycled NH4+. *Proc. Natl. Acad. Sci.* 109, 2269–2274. doi:10.1073/pnas.1104313109

Husson, J. M., Linzmeier, B. J., Kitajima, K., Ishida, A., Maloof, A. C., Schoene, B., et al. (2020). Large Isotopic Variability at the Micron-Scale in 'Shuram' Excursion Carbonates from South Australia. *Earth Planet. Sci. Lett.* 538, 116211. doi:10.1016/j.epsl.2020.116211

Husson, J. M., Maloof, A. C., Schoene, B., Chen, C. Y., and Higgins, J. A. (2015). Stratigraphic Expression of Earth's Deepest $\delta^{13}C$ Excursion in the Wonoka Formation of South Australia. *Am. J. Sci.* 315, 1–45. doi:10.2475/01.2015.01

Jiang, G., Kaufman, A. J., Christie-Blick, N., Zhang, S., and Wu, H. (2007). Carbon Isotope Variability across the Ediacaran Yangtze Platform in South China: Implications for a Large Surface-To-Deep Ocean δ13C Gradient. *Earth Planet. Sci. Lett.* 261, 303–320. doi:10.1016/j.epsl.2007.07.009

Jiang, G., Shi, X., Zhang, S., Wang, Y., and Xiao, S. (2011). Stratigraphy and Paleogeography of the Ediacaran Doushantuo Formation (Ca. 635-551Ma) in South China. *Gondwana Res.* 19, 831–849. doi:10.1016/j.gr.2011.01.006

Jiang, G., Wang, X., Shi, X., Zhang, S., Xiao, S., and Dong, J. (2010). Organic Carbon Isotope Constraints on the Dissolved Organic Carbon (DOC) Reservoir at the Cryogenian-Ediacaran Transition. *Earth Planet. Sci. Lett.* 299, 159–168. doi:10.1016/j.epsl.2010.08.031

Jiang, L., Planavsky, N., Zhao, M., Liu, W., and Wang, X. (2019). Authigenic Origin for a Massive Negative Carbon Isotope Excursion. *Geol.* 47, 115–118. doi:10.1130/g45709.1

Kaufman, A. J., Corsetti, F. A., and Varni, M. A. (2007). The Effect of Rising Atmospheric Oxygen on Carbon and Sulfur Isotope Anomalies in the Neoproterozoic Johnnie Formation, Death Valley, USA. *Chem. Geol.* 237, 47–63. doi:10.1016/j.chemgeo.2006.06.023

Kessler, A. J., Bristow, L. A., Cardenas, M. B., Glud, R. N., Thamdrup, B., and Cook, P. L. M. (2014). The Isotope Effect of Denitrification in Permeable Sediments. *Geochimica et Cosmochimica Acta* 133, 156–167. doi:10.1016/j.gca.2014.02.029

Kikumoto, R., Tahata, M., Nishizawa, M., Sawaki, Y., Maruyama, S., Shu, D., et al. (2014). Nitrogen Isotope Chemostratigraphy of the Ediacaran and Early Cambrian Platform Sequence at Three Gorges, South China. *Gondwana Res.* 25, 1057–1069. doi:10.1016/j.gr.2013.06.002

Knauth, L. P., and Kennedy, M. J. (2009). The Late Precambrian Greening of the Earth. *Nature* 460, 728–732. doi:10.1038/nature08213

Kritee, K., Sigman, D. M., Granger, J., Ward, B. B., Jayakumar, A., and Deutsch, C. (2012). Reduced Isotope Fractionation by Denitrification under Conditions Relevant to the Ocean. *Geochimica et Cosmochimica Acta* 92, 243–259. doi:10.1016/j.gca.2012.05.020

Kump, L. R., and Arthur, M. A. (1999). Interpreting Carbon-Isotope Excursions: Carbonates and Organic Matter. *Chem. Geol.* 161, 181–198. doi:10.1016/S0009-2541(99)00086-8

Kump, L. R., Junium, C., Arthur, M. A., Brasier, A., Fallick, A., Melezhik, V., et al. (2011). Isotopic Evidence for Massive Oxidation of Organic Matter Following the Great Oxidation Event. *Science* 334, 1694–1696. doi:10.1126/science.1213999

Kunimitsu, Y., Setsuda, Y., Furuyama, S., Wang, W., Kano, A., et al. (2011). Ediacaran chemostratigraphy and paleoceanography at a shallow marine setting in northwestern Hunan Province, South China. *Precambrian Res.* 191, 194–208. doi:10.1016/j.precamres.2011.09.006

Laakso, T. A., Sperling, E. A., Johnston, D. T., and Knoll, A. H. (2020). Ediacaran Reorganization of the marine Phosphorus Cycle. *Proc. Natl. Acad. Sci. USA* 117, 11961–11967. doi:10.1073/pnas.1916738117

Lam, P., and Kuypers, M. M. M. (2011). Microbial Nitrogen Cycling Processes in Oxygen Minimum Zones. *Annu. Rev. Mar. Sci.* 3, 317–345. doi:10.1146/annurev-marine-120709-142814

Lan, Z., Sano, Y., Yahagi, T., Tanaka, K., Shirai, K., Papineau, D., et al. (2019). An Integrated Chemostratigraphic (δ13C-Δ18o-87Sr/86Sr-Δ15n) Study of the Doushantuo Formation in Western Hubei Province, South China. *Precambrian Res.* 320, 232–252. doi:10.1016/j.precamres.2018.10.018

Le Guerroué, E., Allen, P. A., and Cozzi, A. (2006a). Chemostratigraphic and Sedimentological Framework of the Largest Negative Carbon Isotopic Excursion in Earth History: The Neoproterozoic Shuram Formation (Nafun Group, Oman). *Precambrian Res.* 146, 68–92. doi:10.1016/j.precamres.2006.01.007

Le Guerroué, E., Allen, P. A., Cozzi, A., Etienne, J. L., and Fanning, M. (2006b). 50 Myr Recovery from the Largest negativeδ13C Excursion in the Ediacaran Ocean. *Terra Nova* 18, 147–153. doi:10.1111/j.1365-3121.2006.00674.x

Lee, C., Love, G. D., Fischer, W. W., Grotzinger, J. P., and Halverson, G. P. (2015). Marine Organic Matter Cycling during the Ediacaran Shuram Excursion. *Geol.* 43, 1106. doi:10.1130/g37236.1

Lehmann, M. F., Bernasconi, S. M., Barbieri, A., and McKenzie, J. A. (2002). Preservation of Organic Matter and Alteration of its Carbon and Nitrogen Isotope Composition during Simulated and *In Situ* Early Sedimentary Diagenesis. *Geochimica et Cosmochimica Acta* 66, 3573–3584. doi:10.1016/S0016-7037(02)00968-7

Li, C., Cheng, M., Zhu, M., and Lyons, T. W. (2018). Heterogeneous and Dynamic marine Shelf Oxygenation and Coupled Early Animal Evolution. *Emerging Top. Life Sci.* 2, 279–288. doi:10.1042/etls20170157

Li, C., Hardisty, D. S., Luo, G., Huang, J., Algeo, T. J., Cheng, M., et al. (2017). Uncovering the Spatial Heterogeneity of Ediacaran Carbon Cycling. *Geobiol.* 15, 211–224. doi:10.1111/gbi.12222

Li, C., Love, G. D., Lyons, T. W., Fike, D. A., Sessions, A. L., and Chu, X. (2010). A Stratified Redox Model for the Ediacaran Ocean. *Science* 328, 80–83. doi:10.1126/science.1182369

Ling, H.-F., Chen, X., Li, D., Wang, D., Shields-Zhou, G. A., and Zhu, M. (2013). Cerium Anomaly Variations in Ediacaran-Earliest Cambrian Carbonates from the Yangtze Gorges Area, South China: Implications for Oxygenation of Coeval Shallow Seawater. *Precambrian Res.* 225, 110–127. doi:10.1016/j.precamres.2011.10.011

Liu, P., Xiao, S., Yin, C., Chen, S., Zhou, C., and Li, M. (2014). Ediacaran Acanthomorphic Acritarchs and Other Microfossils from Chert Nodules of the Upper Doushantuo Formation in the Yangtze Gorges Area, South China. *J. Paleontol.* 88, 1–139. doi:10.1666/13-009

Lu, M., Zhu, M., Zhang, J., Shields-Zhou, G., Li, G., Zhao, F., et al. (2013). The DOUNCE Event at the Top of the Ediacaran Doushantuo Formation, South China: Broad Stratigraphic Occurrence and Non-diagenetic Origin. *Precambrian Res.* 225, 86–109. doi:10.1016/j.precamres.2011.10.018

Luo, G., Junium, C. K., Izon, G., Ono, S., Beukes, N. J., Algeo, T. J., et al. (2018). Nitrogen Fixation Sustained Productivity in the Wake of the Palaeoproterozoic Great Oxygenation Event. *Nat. Commun.* 9, 978. doi:10.1038/s41467-018-03361-2

Lyons, T. W., Reinhard, C. T., and Planavsky, N. J. (2014). The Rise of Oxygen in Earth's Early Ocean and Atmosphere. *Nature* 506, 307–315. doi:10.1038/nature13068

McFadden, K. A., Huang, J., Chu, X., Jiang, G., Kaufman, A. J., Zhou, C., et al. (2008). Pulsed Oxidation and Biological Evolution in the Ediacaran Doushantuo Formation. *Proc. Natl. Acad. Sci.* 105, 3197–3202. doi:10.1073/pnas.0708336105

Melezhik, V., Fallick, A., Pokrovsky, B. G., and Pokrovsky, B. (2005). Enigmatic Nature of Thick Sedimentary Carbonates Depleted in C beyond the Canonical Mantle Value: The Challenges to Our Understanding of the Terrestrial Carbon Cycle. *Precambrian Res.* 137, 131–165. doi:10.1016/j.precamres.2005.03.010

Michiels, C. C., Darchambeau, F., Roland, F. A. E., Morana, C., Llirós, M., García-Armisen, T., et al. (2017). Iron-dependent Nitrogen Cycling in a Ferruginous lake and the Nutrient Status of Proterozoic Oceans. *Nat. Geosci* 10, 217–221. doi:10.1038/ngeo2886

Nishizawa, M., Tsuchiya, Y., Du, W., Sawaki, Y., Matsui, Y., Wang, Y., et al. (2019). Shift in Limiting Nutrients in the Late Ediacaran-Early Cambrian marine Systems of South China. *Palaeogeogr. Palaeoclimatol. Palaeoecol.* 530, 281–299. doi:10.1016/j.palaeo.2019.05.036

Paulsen, T., Deering, C., Sliwinski, J., Bachmann, O., and Guillong, M. (2017). Evidence for a Spike in Mantle Carbon Outgassing during the Ediacaran Period. *Nat. Geosci* 10, 930–934. doi:10.1038/s41561-017-0011-6

Peng, Y., Dong, L., Ma, H., Wang, R., Lang, X., Peng, Y., et al. (2020). Surface Ocean Nitrate-Limitation in the Aftermath of Marinoan Snowball Earth: Evidence from the Ediacaran Doushantuo Formation in the Western Margin of the Yangtze Block, South China. *Precambrian Res.* 347, 105846. doi:10.1016/j.precamres.2020.105846

Prokopenko, M., Hammond, D., Berelson, W., Bernhard, J., Stott, L., and Douglas, R. (2006). Nitrogen Cycling in the Sediments of Santa Barbara basin and Eastern Subtropical North Pacific: Nitrogen Isotopes, Diagenesis and Possible Chemosymbiosis between Two Lithotrophs (Thioploca and Anammox)-"riding on a Glider". *Earth Planet. Sci. Lett.* 242, 186–204. doi:10.1016/j.epsl.2005.11.044

Quan, T. M., Wright, J. D., and Falkowski, P. G. (2013). Co-variation of Nitrogen Isotopes and Redox States through Glacial-Interglacial Cycles in the Black Sea. *Geochimica Et Cosmochimica Acta* 112, 305–320. doi:10.1016/j.gca.2013.02.029

Robinson, R. S., Kienast, M., Luiza Albuquerque, A., Altabet, M., Contreras, S., De Pol Holz, R., et al. (2012). A Review of Nitrogen Isotopic Alteration in marine Sediments. *Paleoceanography* 27, PA4203. doi:10.1029/2012pa002321

Rooney, A. D., Cantine, M. D., Bergmann, K. D., Gómez-Pérez, I., Al Baloushi, B., Boag, T. H., et al. (2020). Calibrating the Coevolution of Ediacaran Life and Environment. *Proc. Natl. Acad. Sci. USA* 117, 16824–16830. doi:10.1073/pnas.2002918117

Rothman, D. H., Hayes, J. M., and Summons, R. E. (2003). Dynamics of the Neoproterozoic Carbon Cycle. *Pnas* 100, 8124–8129. doi:10.1073/pnas.0832439100

Sahoo, S. K., Planavsky, N. J., Jiang, G., Kendall, B., Owens, J. D., Wang, X., et al. (2016). Oceanic Oxygenation Events in the Anoxic Ediacaran Ocean. *Geobiol.* 14, 457–468. doi:10.1111/gbi.12182

Sawaki, Y., Ohno, T., Tahata, M., Komiya, T., Hirata, T., Maruyama, S., et al. (2010). The Ediacaran Radiogenic Sr Isotope Excursion in the Doushantuo Formation in the Three Gorges Area, South China. *Precambrian Res.* 176, 46–64. doi:10.1016/j.precamres.2009.10.006

Schrag, D. P., Higgins, J. A., Macdonald, F. A., and Johnston, D. T. (2013). Authigenic Carbonate and the History of the Global Carbon Cycle. *Science* 339, 540–543. doi:10.1126/science.1229578

She, Z.-B., Strother, P., and Papineau, D. (2014). Terminal Proterozoic Cyanobacterial Blooms and Phosphogenesis Documented by the Doushantuo Granular Phosphorites II: Microbial Diversity and C Isotopes. *Precambrian Res.* 251, 62–79. doi:10.1016/j.precamres.2014.06.004

Shi, W., Li, C., Luo, G., Huang, J., Algeo, T. J., Jin, C., et al. (2018). Sulfur Isotope Evidence for Transient marine-shelf Oxidation during the Ediacaran Shuram Excursion. *Geol.* 46, 267–270. doi:10.1130/G39663.1

Shields, G. A., Mills, B. J. W., Zhu, M., Raub, T. D., Daines, S. J., and Lenton, T. M. (2019). Unique Neoproterozoic Carbon Isotope Excursions Sustained by Coupled Evaporite Dissolution and Pyrite Burial. *Nat. Geosci.* 12, 823–827. doi:10.1038/s41561-019-0434-3

Sigman, D. M., Casciotti, K. L., and Casciotti, K. L. (2001). "Nitrogen Isotopes in the Ocean," in *Encyclopedia of Ocean Science* (Amsterdam: Elsevier), 1884–1894. doi:10.1006/rwos.2001.0172

Song, H., Jiang, G., Poulton, S. W., Wignall, P. B., Tong, J., Song, H., et al. (2017). The Onset of Widespread marine Red Beds and the Evolution of Ferruginous Oceans. *Nat. Commun.* 8, 399. doi:10.1038/s41467-017-00502-x

Spangenberg, J. E., Bagnoud-Velásquez, M., Boggiani, P. C., and Gaucher, C. (2014). Redox Variations and Bioproductivity in the Ediacaran: Evidence from Inorganic and Organic Geochemistry of the Corumbá Group, Brazil. *Gondwana Res.* 26, 1186–1207. doi:10.1016/j.gr.2013.08.014

Stüeken, E. E., Kipp, M. A., Koehler, M. C., and Buick, R. (2016). The Evolution of Earth's Biogeochemical Nitrogen Cycle. *Earth-Science Rev.* 160, 220–239. doi:10.1016/j.earscirev.2016.07.007

Stüeken, E. E., Zaloumis, J., Meixnerová, J., and Buick, R. (2017). Differential Metamorphic Effects on Nitrogen Isotopes in Kerogen Extracts and Bulk Rocks. *Geochimica et Cosmochimica Acta* 217, 80–94. doi:10.1016/j.gca.2017.08.019

Sui, Y., Huang, C., Zhang, R., Wang, Z., and Ogg, J. (2019). Astronomical Time Scale for the Middle-Upper Doushantuo Formation of Ediacaran in South China: Implications for the Duration of the Shuram/Wonoka Negative δ13C Excursion. *Palaeogeogr. Palaeoclimatol. Palaeoecol.* 532, 109273. doi:10.1016/j.palaeo.2019.109273

Swart, P. K., and Kennedy, M. J. (2012). Does the Global Stratigraphic Reproducibility of δ13C in Neoproterozoic Carbonates Require a marine Origin? A Pliocene-Pleistocene Comparison. *Geol.* 40, 87–90. doi:10.1130/g32538.1

Tyrrell, T. (1999). The Relative Influences of Nitrogen and Phosphorus on Oceanic Primary Production. *Nature* 400, 525–531. doi:10.1038/22941

Wang, J., and Li, Z.-X. (2003). History of Neoproterozoic Rift Basins in South China: Implications for Rodinia Break-Up. *Precambrian Res.* 122, 141–158. doi:10.1016/S0301-9268(02)00209-7

Wang, L. (2019). *Variations of Trace Elements in the Upper Part of the Ediacaran Doushantuo Formation and Environmental Implication*. Beijing: China University of Geosciences. Master Thesis (in Chinese with English abstract). doi:10.1130/abs/2019am-336558

Wang, W., Guan, C., Zhou, C., Peng, Y., Pratt, L. M., Chen, X., et al. (2017). Integrated Carbon, Sulfur, and Nitrogen Isotope Chemostratigraphy of the Ediacaran Lantian Formation in South China: Spatial Gradient, Ocean Redox Oscillation, and Fossil Distribution. *Geobiol.* 15, 552–571. doi:10.1111/gbi.12226

Wang, W., Zhou, C., Guan, C., Yuan, X., Chen, Z., and Wan, B. (2014). An Integrated Carbon, Oxygen, and Strontium Isotopic Studies of the Lantian Formation in South China with Implications for the Shuram Anomaly. *Chem. Geol.* 373, 10–26. doi:10.1016/j.chemgeo.2014.02.023

Wang, W., Zhou, C., Yuan, X., Chen, Z., and Xiao, S. (2012). A Pronounced Negative δ13C Excursion in an Ediacaran Succession of Western Yangtze Platform: A Possible Equivalent to the Shuram Event and its Implication for Chemostratigraphic Correlation in South China. *Gondwana Res.* 22, 1091–1101. doi:10.1016/j.gr.2012.02.017

Wang, X., Jiang, G., Shi, X., Peng, Y., and Morales, D. C. (2018). Nitrogen Isotope Constraints on the Early Ediacaran Ocean Redox Structure. *Geochimica et Cosmochimica Acta* 240, 220–235. doi:10.1016/j.gca.2018.08.034

Wang, X., Jiang, G., Shi, X., and Xiao, S. (2016). Paired Carbonate and Organic Carbon Isotope Variations of the Ediacaran Doushantuo Formation from an Upper Slope Section at Siduping, South China. *Precambrian Res.* 273, 53–66. doi:10.1016/j.precamres.2015.12.010

Wei, H., Wang, X., Shi, X., Jiang, G., Tang, D., Wang, L., et al. (2019). Iodine Content of the Carbonates from the Doushantuo Formation and Shallow Ocean Redox Change on the Ediacaran Yangtze Platform, South China. *Precambrian Res.* 322, 160–169. doi:10.1016/j.precamres.2019.01.007

Wei, W., Frei, R., Gilleaudeau, G. J., Li, D., Wei, G.-Y., Chen, X., et al. (2018). Oxygenation Variations in the Atmosphere and Shallow Seawaters of the Yangtze Platform during the Ediacaran Period: Clues from Cr-Isotope and Ce-Anomaly in Carbonates. *Precambrian Res.* 313, 78–90. doi:10.1016/j.precamres.2018.05.009

Williams, J. J., Mills, B. J. W., and Lenton, T. M. (2019). A Tectonically Driven Ediacaran Oxygenation Event. *Nat. Commun.* 10, 2690. doi:10.1038/s41467-019-10286-x

Xiang, L., Schoepfer, S. D., Zhang, H., Cao, C.-q., and Shen, S.-z. (2018). Evolution of Primary Producers and Productivity across the Ediacaran-Cambrian Transition. *Precambrian Res.* 313, 68–77. doi:10.1016/j.precamres.2018.05.023

Xiao, S., Bykova, N., Kovalick, A., and Gill, B. C. (2017). Stable Carbon Isotopes of Sedimentary Kerogens and Carbonaceous Macrofossils from the Ediacaran Miaohe Member in South China: Implications for Stratigraphic Correlation and Sources of Sedimentary Organic Carbon. *Precambrian Res.* 302, 171–179. doi:10.1016/j.precamres.2017.10.006

Xiao, S., Narbonne, G. M., Zhou, C., Laflamme, M., Grazhdankin, D. V., Moczydlowska-Vidal, M., et al. (2016). Towards an Ediacaran Time Scale: Problems, Protocols, and Prospects. *Episodes* 39, 540–555. doi:10.18814/epiiugs/2016/v39i4/103886

Xiao, S., Zhang, Y., and Knoll, A. H. (1998). Three-dimensional Preservation of Algae and Animal Embryos in a Neoproterozoic Phosphorite. *Nature* 391, 553–558. doi:10.1038/35318

Xiao, S., Zhou, C., Liu, P., Wang, D., and Yuan, X. (2014). Phosphatized Acanthomorphic Acritarchs and Related Microfossils from the Ediacaran Doushantuo Formation at Weng'an (South China) and Their Implications for Biostratigraphic Correlation. *J. Paleontol.* 88, 1–67. doi:10.1666/12-157r

Xu, D., Wang, X., Shi, X., Tang, D., Zhao, X., Feng, L., et al. (2020). Nitrogen Cycle Perturbations Linked to Metazoan Diversification during the Early Cambrian. *Palaeogeogr. Palaeoclimatol. Palaeoecol.* 538, 109392. doi:10.1016/j.palaeo.2019.109392

Yin, Z., Zhu, M., Davidson, E. H., Bottjer, D. J., Zhao, F., and Tafforeau, P. (2015). Sponge Grade Body Fossil with Cellular Resolution Dating 60 Myr before the Cambrian. *Proc. Natl. Acad. Sci. USA* 112, E1453–E1460. doi:10.1073/pnas.1414577112

Zerkle, A. L., Poulton, S. W., Newton, R. J., Mettam, C., Claire, M. W., Bekker, A., et al. (2017). Onset of the Aerobic Nitrogen Cycle during the Great Oxidation Event. *Nature* 542, 465–467. doi:10.1038/nature20826

Zhang, F., Xiao, S., Romaniello, S. J., Hardisty, D., Li, C., Melezhik, V., et al. (2019a). Global marine Redox Changes Drove the Rise and Fall of the Ediacara Biota. *Geobiol.* 17, 594–610. doi:10.1111/gbi.12359

Zhang, S., Jiang, G., Zhang, J., Song, B., Kennedy, M. J., and Christie-Blick, N. (2005). U-pb Sensitive High-Resolution Ion Microprobe Ages from the Doushantuo Formation in south China: Constraints on Late Neoproterozoic Glaciations. *Geol* 33, 473–476. doi:10.1130/g21418.1

Zhang, Y., Pufahl, P. K., Du, Y., Chen, G., Liu, J., Chen, Q., et al. (2019b). Economic Phosphorite from the Ediacaran Doushantuo Formation, South China, and the Neoproterozoic-Cambrian Phosphogenic Event. *Sediment. Geol.* 388, 1–19. doi:10.1016/j.sedgeo.2019.05.004

Zhou, C., Jiang, S., Xiao, S., Chen, Z., and Yuan, X. (2012). Rare Earth Elements and Carbon Isotope Geochemistry of the Doushantuo Formation in South China: Implication for Middle Ediacaran Shallow marine Redox Conditions. *Chin. Sci. Bull.* 57, 1998–2006. doi:10.1007/s11434-012-5082-6

Zhou, C., and Xiao, S. (2007). Ediacaran δ13C Chemostratigraphy of South China. *Chem. Geol.* 237, 89–108. doi:10.1016/j.chemgeo.2006.06.021

Zhou, C., Xiao, S., Wang, W., Guan, C., Ouyang, Q., and Chen, Z. (2017). The Stratigraphic Complexity of the Middle Ediacaran Carbon Isotopic Record in the Yangtze Gorges Area, South China, and its Implications for the Age and Chemostratigraphic Significance of the Shuram Excursion. *Precambrian Res.* 288, 23–38. doi:10.1016/j.precamres.2016.11.007

Zhou, C., Yuan, X., Xiao, S., Chen, Z., and Hua, H. (2019). Ediacaran Integrative Stratigraphy and Timescale of China. *Sci. China Earth Sci.* 62, 7–24. doi:10.1007/s11430-017-9216-2

Zhu, M., Lu, M., Zhang, J., Zhao, F., Li, G., Aihua, Y., et al. (2013). Carbon Isotope Chemostratigraphy and Sedimentary Facies Evolution of the Ediacaran Doushantuo Formation in Western Hubei, South China. *Precambrian Res.* 225, 7–28. doi:10.1016/j.precamres.2011.07.019

Zhu, M., Zhang, J., and Yang, A. (2007). Integrated Ediacaran (Sinian) Chronostratigraphy of South China. *Palaeogeogr. Palaeoclimatol. Palaeoecol.* 254, 7–61. doi:10.1016/j.palaeo.2007.03.025

Conflict of Interest: The authors declare that the research was conducted in the absence of any commercial or financial relationships that could be construed as a potential conflict of interest.

frontiers in Earth Science

ORIGINAL RESEARCH
published: 19 July 2021
doi: 10.3389/feart.2021.705351

Carbon and Nitrogen Cycle Dynamic in Continental Late-Carboniferous to Early Permian Basins of Eastern Pangea (Northeastern Massif Central, France)

Mathilde Mercuzot[1], Christophe Thomazo[2,3], Johann Schnyder[4], Pierre Pellenard[2], François Baudin[4], Anne-Catherine Pierson-Wickmann[1], Pierre Sans-Jofre[5], Sylvie Bourquin[1], Laurent Beccaletto[6], Anne-Lise Santoni[2], Georges Gand[2], Matthieu Buisson[4,7], Laure Glé[2], Thomas Munier[2], Antonios Saloume[4], Mohamed Boussaid[4] and Tracy Boucher[4]*

[1]Univ Rennes, CNRS, Géosciences Rennes - UMR 6118, Rennes, France, [2]Biogéosciences UMR uB/CNRS 6282, Université Bourgogne Franche-Comté, Dijon, France, [3]Institut Universitaire de France, Paris, France, [4]Institut des Sciences de la Terre de Paris (ISTeP), UMR 7193 CNRS, Sorbonne Université, Paris, France, [5]MNHN, CNRS UMR 7590, IRD, Institut de minéralogie, Physique des Matériaux et de Cosmochimie, Sorbonne Université, Paris, France, [6]BRGM, Orléans, France, [7]Université de Paris - Institut de physique du globe de Paris - CNRS, UMR 7154, Paris, France

OPEN ACCESS

Edited by:
Jean-louis Vigneresse, Université de Lorraine, France

Reviewed by:
Jean-Marc Lardeaux, Université Côte d'Azur, France
Alain Izart, UMR7359 GéoRessources (GEORESSOURCES), France

***Correspondence:**
Mathilde Mercuzot
mathilde.mercuzot@outlook.com

Specialty section:
This article was submitted to Geochemistry, a section of the journal Frontiers in Earth Science

Received: *05 May 2021*
Accepted: *07 July 2021*
Published: *19 July 2021*

Citation:
Mercuzot M, Thomazo C, Schnyder J, Pellenard P, Baudin F, Pierson-Wickmann A-C, Sans-Jofre P, Bourquin S, Beccaletto L, Santoni A-L, Gand G, Buisson M, Glé L, Munier T, Saloume A, Boussaid M and Boucher T (2021) Carbon and Nitrogen Cycle Dynamic in Continental Late-Carboniferous to Early Permian Basins of Eastern Pangea (Northeastern Massif Central, France). Front. Earth Sci. 9:705351. doi: 10.3389/feart.2021.705351

Late Carboniferous to early Permian organic-rich sedimentary successions of late-orogenic continental basins from the northeastern Massif Central (France) coincide with both the Variscan mountain dismantling and the acme of the long-lasting Late Paleozoic Ice Age. Here, we investigate the carbon and nitrogen cycles in the newly dated sedimentary successions of the Decize–La Machine and Autun basins during these geodynamic and climate upheavals. The sedimentary organic matter has been analyzed through Rock-Eval pyrolysis, palynofacies and elemental and isotope geochemistry along cored-wells and outcropping sections, previously accurately defined in terms of paleo-depositional environments. Rock-Eval and palynofacies data have evidenced two origins of organic matter: a phytoplanktonic/bacterial lacustrine origin (Type I organic matter, organic $\delta^{13}C$ values around −23.5‰), and a terrestrial origin (vascular land plants, Type III organic matter, organic $\delta^{13}C$ values around −20‰), mixed in the deltaic-lacustrine sediments during background sedimentation (mean organic $\delta^{13}C$ values around −22‰). Episodes of high organic matter storage, reflected by black shales and coal-bearing deposits (total organic carbon up to 20 and 70%, respectively) are also recognized in the successions, and are characterized by large negative organic carbon isotope excursions down to −29‰. We suggest that these negative isotope excursions reflect secondary processes, such as organic matter remineralization and/or secondary productivity varying under strict local controls, or possibly larger scale climate controls. At times, these negative $\delta^{13}C$ excursions are paired with positive $\delta^{15}N$ excursions up to +10‰, reflecting water column denitrification and anammox during lake-water stratification episodes. Together, these isotopic signals (i.e., low sedimentary organic $\delta^{13}C$ associated with high bulk $\delta^{15}N$ values) indicate periods of high primary productivity of

surface waters, where nitrogen and carbon cycles are spatially decoupled. These local processes on the sedimentary isotope archives may partially blur our ability to directly reconstruct paleoclimate variations in such continental settings using only C and N isotopes. At last, we explore an organic $\delta^{13}C$-based mixing model to propose ways to disentangle autochthonous versus allochthonous origin of organic matter in lacustrine continental settings.

Keywords: late Paleozoic, continental basin, carbon, nitrogen, isotope geochemistry, organic matter, paleoclimate, paleoenvironment

INTRODUCTION

The late Carboniferous to early Permian period (~300 Ma) is largely recognized for its high primary productivity on lands, and witnesses the highest rates of global organic carbon burial of the Phanerozoic Eon preserved in the sedimentary rocks (e.g., Klemme and Ulmishek, 1991; Maynard et al., 1997; Berner, 2003; Schwarzbauer and Jovančićević, 2015; Montañez, 2016). Indeed, coal forests (wetland biome) occupied large areas within the intertropical zone during this time interval (Cleal and Thomas, 2005).

The continental sediments archived during this time window reflect different parameters including first-order tectonics, controlling the structure and subsidence history of sedimentary basins of the late Variscan orogenic setting, and paleoclimate. During the Carboniferous–Permian transition (CPT), the latter is characterized by the acme of the Late Paleozoic Ice Age (LPIA, late Devonian to late Permian, Isbell et al., 2003; Fielding et al., 2008; Isbell et al., 2012; Montañez and Poulsen, 2013; Soreghan et al., 2019), associated with humid belts promoting organic-matter (OM) production in the intertropical zone (e.g., Scotese, 2016) and followed by global warming and aridification until the early Triassic. The onset and duration of the LPIA resulted from several parameters such as paleogeographic and geodynamic changes (landmass merging towards southern high latitudes, erection of reliefs at the equator, Powell and Veevers 1987; Veevers, 1994; Opdyke et al., 2001; Frank et al., 2008; Isbell et al., 2012; Domeier and Torsvik, 2014), an increase in chemical weathering of Variscan reliefs (Goddéris et al., 2017), astronomical forcing (e.g., low incident solar luminosity, albedo feedbacks, Crowley and Baum, 1992; Hyde et al., 1999), and an enhanced volcanic activity (sulfate aerosols, Soreghan et al., 2019). Thus, relief erosion and alteration products triggered high sedimentary fluxes, which are recorded in the CPT basins.

The late Carboniferous to early Permian period exhibits substantial variations in the global carbon cycle, with the highest ^{13}C enrichment in carbonates of the Phanerozoic, with carbonate $\delta^{13}C$ values as high as 5‰ (Strauss and Peters-Kottig, 2003). This isotope excursion is usually interpreted as reflecting a carbon cycle dominated by a very high burial rate of OM in the sediments, in agreement with OM-rich deposit evidences (Berner and Raiswell, 1983; Beauchamp et al., 1987; Berner, 1989; Bruckschen et al., 1999; Hayes et al., 1999; Mii et al., 1999; Mii et al., 2001; Saltzman et al., 2004; Saltzman, 2005; Peters-Kottig et al., 2006; Frank et al., 2008, Grossman et al., 2008; Liu et al., 2017; Liu et al., 2018).

While sedimentological context of northeastern Massif Central CPT basins (France) has been recently updated (Ducassou et al., 2019; Mercuzot et al., 2021; Mercuzot et al., submitted), both the dynamics of OM production and preservation are poorly documented in these areas, except for a few studies (Elsass-Damon 1977; Garel et al., 2017). Moreover, the OM isotopic characterization is still lacking in most studies on continental series from this period, although many studies have successfully demonstrated that carbon and nitrogen isotope signals of OM help to decipher its production (primary productivity), preservation (remineralization), and paleoclimate dynamics (e.g., Hollander and McKenzie, 1991; Hollander et al., 1993; Altabet and Francois, 1994; Schubert and Calvert, 2001; Sephton et al., 2002; Deutsch et al., 2004; Algeo et al., 2008; Kashiyama et al., 2008; Ramaswamy et al., 2008; Schnyder et al., 2009; Thomazo et al., 2009; Jenkyns, 2010; Ader et al., 2014; Ader et al., 2016; Wang et al., 2017).

In this study, we aim to describe the sedimentary dynamics of OM and associated geochemical signatures from recently radio-isotopically-dated continental series of the northeastern Massif Central (Pellenard et al., 2017; Ducassou et al., 2019).

Using elemental and isotope ($\delta^{13}C$ and $\delta^{15}N$) geochemistry through Rock Eval pyrolysis and Isotope Ratio Mass Spectrometry (IRMS), paired with OM characterization through palynofacies analyses, we discuss the origin and preservation of archived OM in the CPT northeastern Massif Central basins, and describe the processes associated with the biogeochemical cycling of carbon and nitrogen through time and space in deep-time lacustrine-dominated environments. Local, facies-related controls on the OM sedimentation relative to global signals are also considered in the light of known trends in the carbon and nitrogen global cycle across the LPIA period.

GENERAL GEOLOGICAL SETTING

The late Variscan orogenic evolution of Western Europe is characterized by two syn-to late- extensional tectonic events (i.e. D4 and D5 events from Faure et al., 2009): 1) a mid-Carboniferous syn-orogenic ductile extensional event, synchronous with pluton emplacement, widespread crustal-derived plutonism and volcanism, and local development of volcano-sedimentary basins, and 2) a late Carboniferous-early

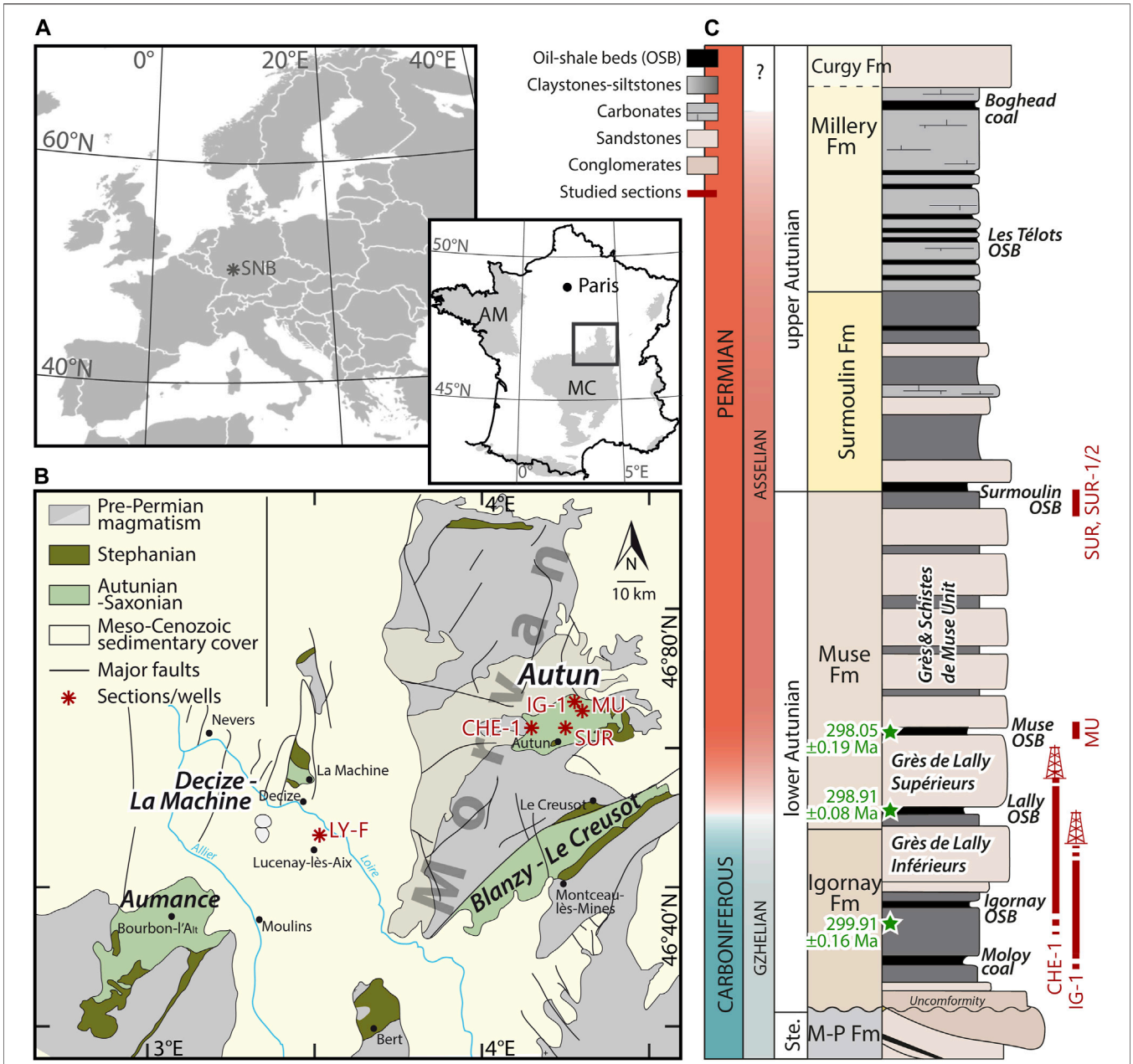

FIGURE 1 | (A) Map of Europe, with a zoom on France where the Variscan remains are displayed in grey. AM, Armorican Massif; MC, Massif Central; SNB, Saar-Nahe Basin. **(B)** Simplified map of the north-eastern Massif Central, showing four late Carboniferous to Permian basins, including the Autun and the Decize-La Machine basins described in this study (modified from Elsass-Damon, 1977). **(C)** Lithostratigraphic column of the Autun Basin showing the location of the studied wells and sections in the stratigraphy. Fm, Formation; Ste., Stephanian; M-P Fm, Mont-Pelé Fm (modified from Pellenard et al., 2017).

Permian late-orogenic extension, characterized by the uplift of high-grade metamorphic domes and related faults and detachments, and the development of mainly half-graben basins, like the Autun Basin. These two events were triggered by the collapse of the Variscan mountain belt (Ménard and Molnar, 1988; Valle et al., 1988; Van Den Driessche and Brun, 1989; Burg et al., 1990; Malavieille et al., 1990; Van Den Driessche and Brun, 1992; Faure and Becq-Giraudon 1993; Burg et al., 1994; Faure 1995; Becq-Giraudon et al., 1996; Choulet et al., 2012). This WE-oriented mountain belt was located in equatorial position and has influenced the late Paleozoic global climate dynamics (e.g., Goddéris et al., 2017) reflected by the LPIA, constituting a major glaciation on a vegetated Earth (Gastaldo et al., 1996; Montañez et al., 2007). The paroxysmal phase of the LPIA occurred at the end of the Carboniferous and during the earliest Permian (ca. 305–290 Ma, Isbell et al., 2003; Fielding et al., 2008; Isbell et al., 2012; Montañez and Poulsen, 2013; Soreghan et al., 2019), a period that records both extremely low CO_2 levels (roughly equivalent to

present-day levels, between 100 and 1,000 ppm, Berner, 2001; Montañez et al., 2007; Foster et al., 2017) and the highest O_2 levels (nearly twice the present-day atmospheric level) in probably the entire Earth history (Berner and Canfield, 1989).

The Decize–La Machine and Autun basins, located in the northeastern French Massif Central (**Figures 1A,B**) record the collapse of the Variscan mountain through their late CPT sedimentary successions (Pellenard et al., 2017; Ducassou et al., 2019). These basins have recently been re-investigated to improve their sedimentological and chronological settings (Garel et al., 2017; Pellenard et al., 2017; Ducassou et al., 2019; Mercuzot et al., 2021; Mercuzot et al., submitted), but their biogeochemical characteristics remain poorly documented to date.

Recently, Mercuzot et al. (2021) have proposed that the Decize–La Machine and Autun basins may have been connected at the time of their filling, and that they probably reflect paleo-depocenters of a larger sedimentary basin, encompassing other nearby basins, notably the southward Blanzy–Le Creusot Basin and the eastward Aumance Basin (**Figure 1B**), and possibly the Carboniferous–Permian series beneath the Meso-Cenozoic sedimentary cover of the Paris Basin (Contres, Brécy and Arpheuilles basins, Beccaletto et al., 2015; Mercuzot et al., 2021; Mercuzot et al., submitted). Consequently, the sedimentary successions of the Decize–La Machine and Autun basins could be part of a much larger sedimentary area than previously considered and could have archived and participated in the secular evolution of the global carbon cycle at that time. It is therefore interesting to investigate the organic geochemical signals recorded in these areas.

The Decize–La Machine Basin is partly outcropping (La Machine area), and partly located beneath the Meso-Cenozoic sedimentary cover of the Paris Basin (Lucenay-lès-Aix area, **Figure 1B**). Our work is based on the study of the reference LY-F cored-well (**Figure 1B**), whose sediments were deposited between 299 ± 2 and 294 ± 2/−7 Ma—ages obtained by LA-ICP-MS dating (Laser Ablation–Induced Coupled Plasma–Mass Spectrometry) on zircon and apatite by Ducassou et al. (2019).

In the Autun Basin, five sections are investigated, respectively the IG-1, CHE-1, MU, SUR-1, SUR-2 cored-wells and the SUR outcrop (**Figure 1C**). The base of the IG-1 core has been dated at 299.91 ± 0.16 Ma and the top of the Muse outcrop (approximatively corresponding to the top of the MU core) at 298.05 ± 0.19 Ma, using the U-Pb CA-ID-TIMS method (Chemical Abrasion–Isotopic Dilution–Thermal Ionization Mass Spectrometry, Pellenard et al., 2017).

DEPOSITIONAL ENVIRONMENTS IN THE NORTHEASTERN MASSIF CENTRAL BASINS

The Lucenay-lès-Aix area presents a variety of continental depositional environments, ranging from coastal plain, with coal-bearing levels formed in swamps, to lake, with occurrences of deltaic systems that evolve to deep lake deposits toward the east, according to the observations of sedimentological facies and seismic profiles in this part of the basin (Ducassou et al., 2019; Mercuzot et al., 2021). The general depositional context is typical of differentiated Gilbert-type deltas, with inclined foreset and bottomset features (mostly coarse-grained), sinking into a lake environment characterized by fine-grained deposits (**Figure 2**). This lacustrine environment is located either at the end of the deltaic complexes or laterally to the sediment input. In the second case, microbial deposits may be found, indicating a water depth within the photic zone.

The sedimentological setting of the Autun Basin was firstly investigated by Marteau (1983), and recently by Mercuzot et al. (submitted). The sedimentary succession shows mainly lacustrine facies with occurrences of deltaic facies and OM-rich levels corresponding to black shales, namely oil-shale beds, OSBs (**Figure 2**). The base of the Autun Basin sedimentary succession is characterized by deep lacustrine deposits, showing well-developed OSBs alternating with episodic distal turbidites, and the sediment supply is provided to the basin by deltaic distributaries (Mercuzot et al., submitted). Three main depositional environments have been defined, based on the classification of Bohacs et al. (2000) (**Figure 2**): the profundal, the sublittoral and the littoral lake environments, from the more distal to the more proximal, the two latter encompassing deltaic deposits. Due to the dominance of sublittoral to profundal lacustrine facies in this area (Mercuzot et al., submitted), and the consistence with the chronostratigraphic framework, it has been suggested that the Autun Basin could be the distal equivalent of the Lucenay-lès-Aix area proximal series, with major sedimentary supplies coming from the west (Mercuzot et al., 2021).

In both areas, where sediment supply is minimal, OM-rich deposits are observed as coal accumulations in the Lucenay-lès-Aix area and OSBs in the Autun Basin (**Figure 2**). The coal levels were formed in a supralittoral environment (floodplain), mainly by accumulation of vascular land plant remains, whereas OSBs were deposited in a profundal lake environment, mainly fed by primary productivity in the water column (phytoplankton) with additional terrestrial OM (Garel et al., 2017).

MATERIAL AND METHODS

Geochemical analyses were carried out on samples collected in both areas, from cored-well and outcrop sections. The sections are from the Lucenay-lès-Aix area (LY-F well, 329 m) and from the Autun Basin (IG-1 well, 200 m; CHE-1 well, 365 m; MU well, 7.5 m; SUR 1 and 2 wells, 14 m in total; SUR outcrop, 17 m). The SUR-1 and SUR-2 cores were acquired for this study at the base of the SUR outcrop. The cores were drilled vertically, using a modified portable Shawtool Drill machine (diamond bit, 41 mm diameter) lubricated by fresh water from an adjacent river. It is important to note that the MU and SUR sections represent sedimentary intervals of very short duration compared to the 3 other wells. Each section was sampled every 1–2 m in fine-grained lithologies (sometimes with significantly higher resolution such as for the MU core and the Igornay OSBs of the IG-1 core, i.e., each 10 cm). The samples were then ground with a ring and puck mill at the Biogéosciences

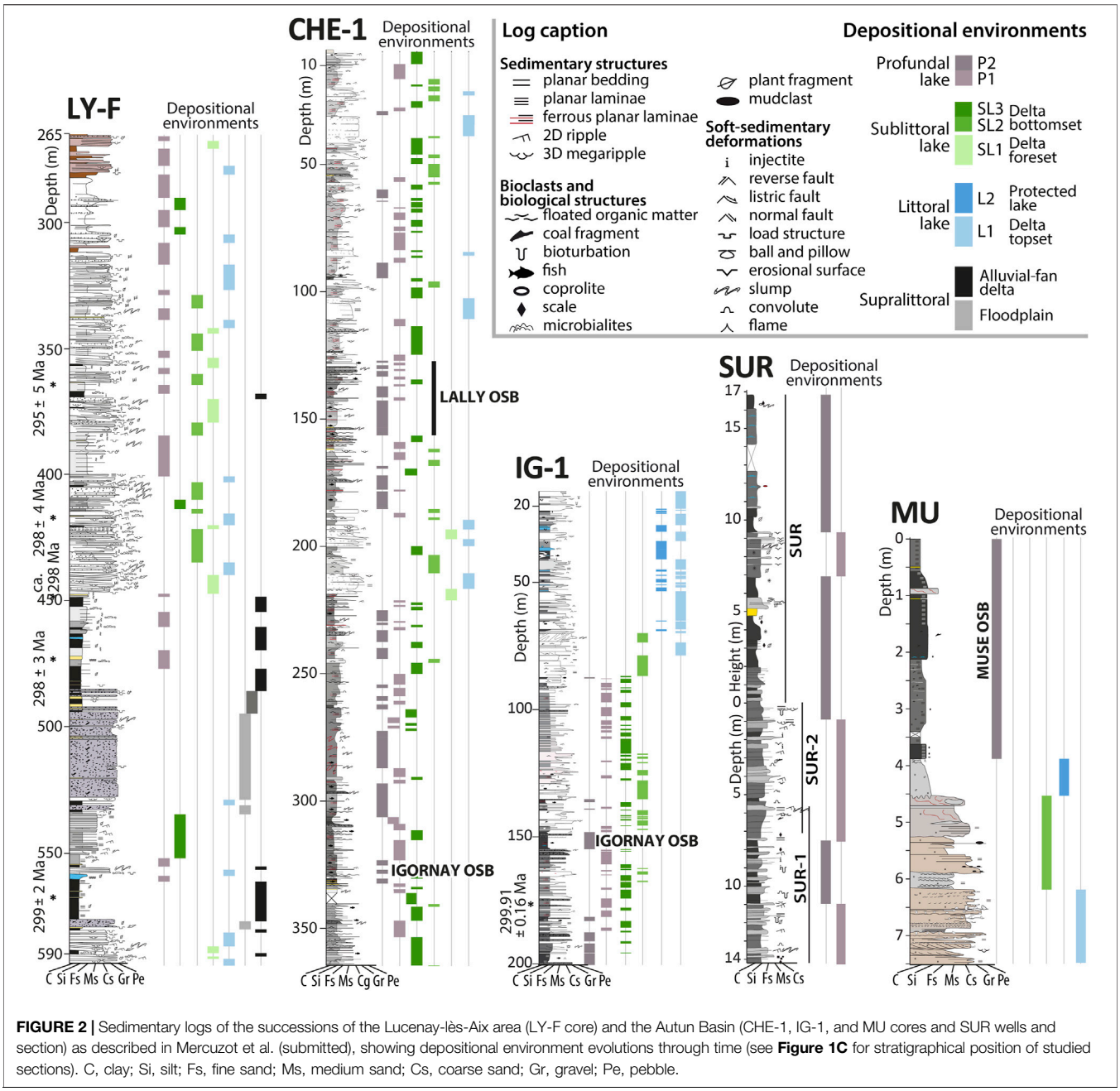

FIGURE 2 | Sedimentary logs of the successions of the Lucenay-lès-Aix area (LY-F core) and the Autun Basin (CHE-1, IG-1, and MU cores and SUR wells and section) as described in Mercuzot et al. (submitted), showing depositional environment evolutions through time (see **Figure 1C** for stratigraphical position of studied sections). C, clay; Si, silt; Fs, fine sand; Ms, medium sand; Cs, coarse sand; Gr, gravel; Pe, pebble.

laboratory (Université Bourgogne–Franche-Comté, France) in order to obtain a 60-µm sample powder.

Rock-Eval Pyrolysis

Samples from IG-1 (215 samples), CHE-1 (329 samples), MU (34 samples), SUR (42 samples) and SUR 1 and 2 (8 samples) sections were analyzed using a Rock-Eval 6 Turbo apparatus (Vinci Technologies) at the ISTeP laboratory (Sorbonne Université) following the method described by Behar et al. (2001). These measurements were obtained from the successive pyrolysis and oxidation of ~60 µg of powder. The amount of free hydrocarbons is given by the S1 signal, while the S2 signal corresponds to the hydrocarbons generated from the cracking of the kerogen between 300 and 650°C. The temperature at which the maximum hydrocarbon yield occurs (Tmax) is used to monitor the OM thermal maturation. The quantity of CO_2 and CO generated during pyrolysis and oxidation is continuously detected and related to organic and inorganic carbon contents, depending on decomposition temperature. The total organic carbon (TOC, wt.%) is calculated as the sum of pyrolzsed and oxidized organic carbon. Hydrogen (HI) and oxygen (OI) indexes are expressed in mgHC/gTOC (HC: hydrocarbon) and mgCO_2/gTOC, respectively, and result from the S2/TOC × 100 and from the S3/TOC × 100 calculations.

Palynofacies Characterization

Palynofacies aim to study the organic constituents of a sediment under optical microscope (Combaz, 1964; Tyson, 1995), in order to assess their origin(s) and preservation state (Batten, 1982; McArthur et al., 2016; Schnyder et al., 2017). In order to remove carbonates and silicates, bulk-rock samples were treated by HCl-HF using standard method developed by Steffen and Gorin (1993). The organic residues were then used to make total, non-filtered and filtered slides (the latter using a 10-µm sieve mesh). Palynofacies observations were performed using an Axioplan2 Imaging Zeiss microscope in transmitted light at the ISTeP laboratory. Five samples were selected from the IG-1 core, six samples from the MU core and ten samples from the CHE-1 core, in order to obtain a general and qualitative assessment of the particulate OM. The samples were selected to document the range of varying TOC and HI values obtained through Rock-Eval pyrolysis.

Elemental and Isotope Analyses

Organic carbon and bulk nitrogen isotopic compositions were analyzed on the LY-F (98 samples), IG-1 (222 samples), CHE-1 (98 samples), MU (32 samples) and SUR, SUR-1 and SUR-2 (21 samples) sections. For IG-1, CHE-1, MU, and SUR samples, containing some carbonates such as calcite, dolomite and siderite, carbonate-free residues were produced by mixing sample powders with 6N HCl during 24 h. The powder was then rinsed with deionized distilled water to a neutral pH and oven-dried at 50°C for 12 h. The total carbonate content, expressed in weight percent (wt.%), was evaluated by gravimetric quantification. The residues were then poured into tin capsules (2–200 mg) using a Sartorius M2P ultra-balance before isotope measurements were performed using a Vario MICRO cube (Elementar GmbH, Hanau, Germany) elemental analyser, coupled to an Isoprime (Elementar, Manchester, United Kingdom) isotope ratio mass spectrometer (EA-IRMS) at the Biogéosciences laboratory. Certified USGS40 ($\delta^{13}C_{org}$ = −26.2‰, C_{org} = 40.82 wt.% and $\delta^{15}N$ = −4.5‰, N = 9.52 wt.%) and caffeine IAEA-600 ($\delta^{13}C_{org}$ = −27.77‰, and $\delta^{15}N$ = 1‰) reference materials were used for the calibration. Isotope results are reported in delta-notation relative to V-PDB and to AIR for carbon and nitrogen isotopes, respectively. Replicates were made for each sample except for the LY-F sample set. The external reproducibility (1σ), based on sample replicate analyses, is better than ±0.06‰ for the $\delta^{13}C_{org}$ and ±0.17‰ for the $\delta^{15}N_{bulk}$. Total organic carbon (TOC) and total nitrogen (organic and mineral nitrogen, TN) contents are expressed in dry weight percentage (wt.%) of the bulk powder, and have a mean 1 σ reproducibility of ±0.11 wt.% and ±0.18 wt.%, respectively.

For LY-F samples, carbonate-free residues were produced by mixing sample powder with 2N HCl in an ultrasonic bath before rinsing and drying at 60°C. The $\delta^{13}C_{org}$ values were determined using an elemental analyser (VarioCube) interfaced with an isotope ratio mass spectrometer (VG Isoprime), at the Stable Isotope Laboratory of the PEGASE Joint Research Unit (INRAE, Saint-Gilles, France). International standards USGS 24 (with $\delta^{13}C$ = −16.5 ± 0.1‰, n = 36) and ANU sucrose (with $\delta^{13}C$ = −10.5 ± 0.1‰, n = 35) were used as reference materials. The reproducibility of $\delta^{13}C$ values is better than ±0.2‰, based on repeated measurements of samples and standards.

RESULTS

Rock-Eval Pyrolysis

All the following mean values for the analysis panel are given associated with their standard deviation (±1σ).

In the IG-1 core, Tmax values range from 369 to 520°C with a mean value of 437 ± 12°C, TOC values range from 0.12 to 20.36 wt.% with a mean value of 4.76 ± 4.58 wt.% (**Figure 3**), HI values range from 28 to 587 mgHC/gTOC with a mean value of 231 ± 151 mgHC/gTOC and OI values range between 0 and 131 $mgCO_2$/gTOC with a mean value of 14 ± 18 $mgCO_2$/gTOC (**Supplementary Table 1**). The TOC curve displays five intervals of very high values (>5 wt.%, **Figure 3**), between ~200 and 180 m, ~160 and 130 m, ~90 and 70 m–35 and 45 m, and at ~22 m.

In the CHE-1 core, Tmax values range from 413 to 460°C with a mean value of 443 ± 9°C, TOC values range from 0.47 to 12.43 wt.% with a mean value of 2.59 ± 2.40 wt.% (**Figure 4**), HI values range from 22 to 382 mgHC/gTOC with a mean value of 104 ± 88 mgHC/gTOC and OI values range between 4 and 673 $mgCO_2$/gTOC with a mean value of 99 ± 133 $mgCO_2$/gTOC (**Supplementary Table 1**). TOC variations (**Figure 4**) fluctuate more than in the IG-1 core record (**Figure 3**). Nonetheless, a first interval of high values (up to 10 wt.%) can be recognized from the base to ~320 m and a second interval from ~240 to 120 m, in which TOC values fluctuate significantly and reach values up to 21 wt.% at 139 m (**Figure 4**).

In the MU core, Tmax values range from 345 to 440°C with a mean value of 418 ± 30°C, TOC values range from 0.18 to 28.03 wt.% with a mean value of 14.01 ± 8.30 wt.% (**Figure 5**), HI values range from 22 to 715 mgHC/gTOC with a mean value of 424 ± 206 mgHC/gTOC and OI values range between 2 and 154 $mgCO_2$/gTOC with a mean value of 30 ± 47 $mgCO_2$/gTOC (**Supplementary Table 1**). TOC values are stable around a few percent from the base of the core up to 4 m (**Figure 5**), before progressively increasing up to 30 wt.% at ~2 m. The TOC decreases towards the top of the core with values down to 5 wt.%.

In the SUR section, Tmax values range from 384 to 438°C with a mean value of 423 ± 11°C, TOC values range from 0.06 to 15.82 wt.% with a mean value of 4.55 ± 4.35 wt.% (**Figure 6**), HI values range from 38 to 568 mgHC/gTOC with a mean value of 304 ± 179 mgHC/gTOC and OI values between 3 and 332 $mgCO_2$/gTOC with a mean value of 33 ± 65 $mgCO_2$/gTOC (**Supplementary Table 1**). TOC chemostratigraphic variations (**Figure 6**) display 3 peaks of ~10 wt.% at −8 m, ~25 wt.% at 0 m and ~20 wt.% at 7 m.

Palynofacies Analyses

The palynofacies slides selected from the IG-1 core (IG-5, 11, 12, 48, and 54) and from the MU core (MU-3, 5, 13, 14, 15, 24) represent HI values ranging from 100 to up to 700 mgHC/gTOC. In all slides, terrestrial-derived organic particles (phytoclasts, coming from wood tissues), and palynomorphs (spores and pollens, comprising *Botryococcus* algae, as already reported by

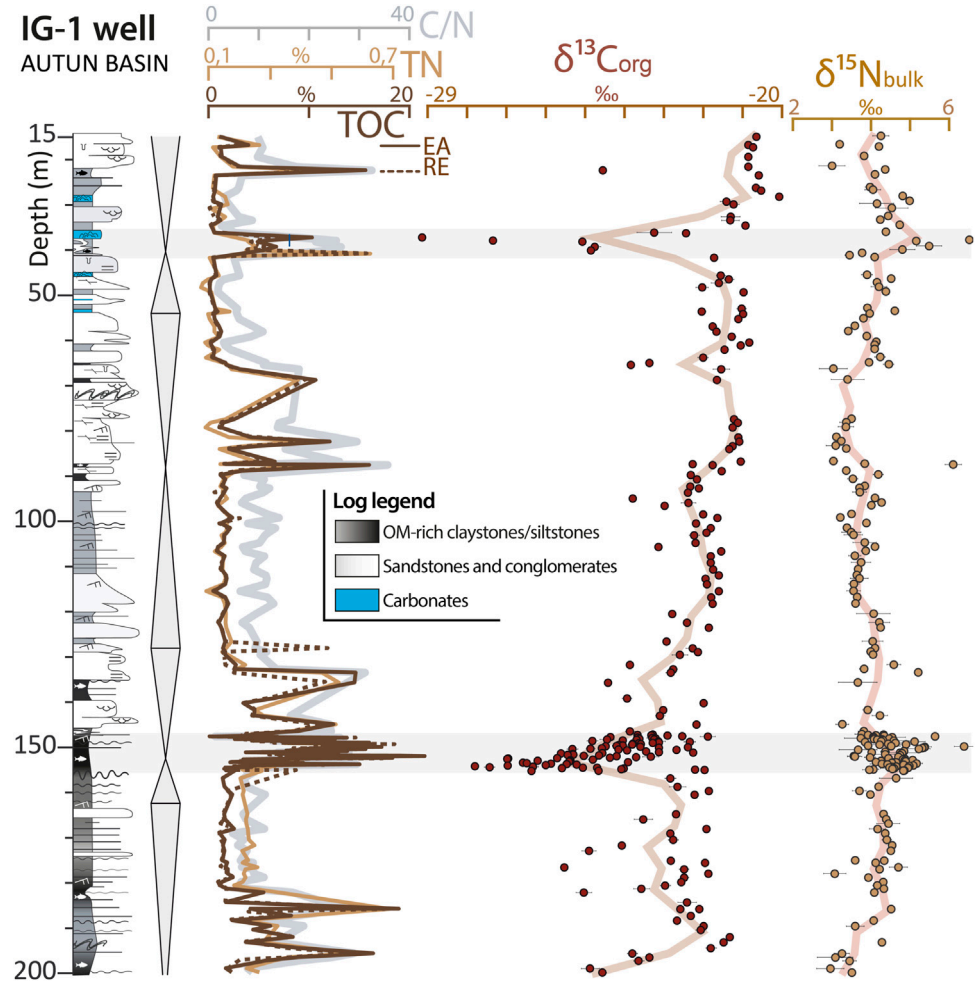

FIGURE 3 | Sedimentary section, sequence stratigraphy of the IG-1 core (Autun Basin) and organic signal evolution (total organic carbon TOC, total nitrogen TN, C/N atomic ratio, $\delta^{13}C_{org}$ and $\delta^{15}N_{bulk}$ variations). The log caption is displayed on **Figure 2**. RE, Rock-Eval pyrolysis.

Izart et al., 2012; Garel et al., 2017) are present in varying proportions, but remain quite minor. Amorphous organic matter (AOM) particles, probably algal/bacterial-derived, are the dominant component.

The 10 palynofacies slides selected from CHE-1 core correspond to HI values ranging from 73 to 326 mgHC/gTOC. As in IG-1 and MU cores, a mixture of OM of terrestrial (phytoclasts, palynomorphs) and probably algal-bacterial (AOM) origin is observed (**Figure 7**). Half of the sample set shows AOM particles dominating the terrestrial components (**Figures 7A,B**). The remaining slides show an enhanced composition of organic particles of terrestrial origin (**Figures 7C,D**), suggesting a more contrasted OM source when compared to IG-1 and MU cores.

Elemental and Isotope Geochemical Signals

The TOC content measured with EA-IRMS is consistent with those found by Rock-Eval analyses (**Figure 8**); the R^2 coefficient between TOC values obtained by Rock-Eval pyrolysis and those obtained by elemental analyser is greater than 0.92 for most of sections, except for the SUR section where an outlier pulls the R^2 coefficient towards lower value (R^2 = 0.53, **Figure 8D**).

Total nitrogen (TN) and total organic carbon (TOC) contents are presented in **Figures 3–6**, **9** for the different sections (detailed dataset is available on **Supplementary Table 1**). The TN content ranges from 0.07 to 0.76 wt.% in the IG-1 core with a mean value of 0.26 ± 0.14 wt.% (**Figure 3**), from 0.16 to 0.55 wt.% in the CHE-1 core, with a mean value of 0.29 ± 0.08 wt.% (**Figure 4**), from 0.07 to 0.79 wt.% for the MU core, with a mean value of 0.42 ± 0.19 wt.% (**Figure 5**), from 0.15 to 0.68 wt.% for the SUR section, with a mean value of 0.34 ± 0.12 wt.% (**Figure 6**) and from 0.02 to 1.64 wt.% in the LY-F core, with a mean value of 0.47 ± 0.53 wt.% (**Figure 9**). The C/N atomic ratio, calculated from the elemental composition of the organic carbon and total nitrogen, is also shown in **Figures 3–6**, **9**. It ranges between 1 and 36 for the IG-1 core, with a mean value of 14 ± 8, between 2 and 26 for the CHE-1 core, with a mean value of 9 ± 6, between 1 and 47 for the MU core, with a mean value of 31 ± 12, between 2 and 42 for the SUR section, with a mean value of 18 ± 14, and between 0 and 86 for the LY-F core, with a mean value of 27 ±

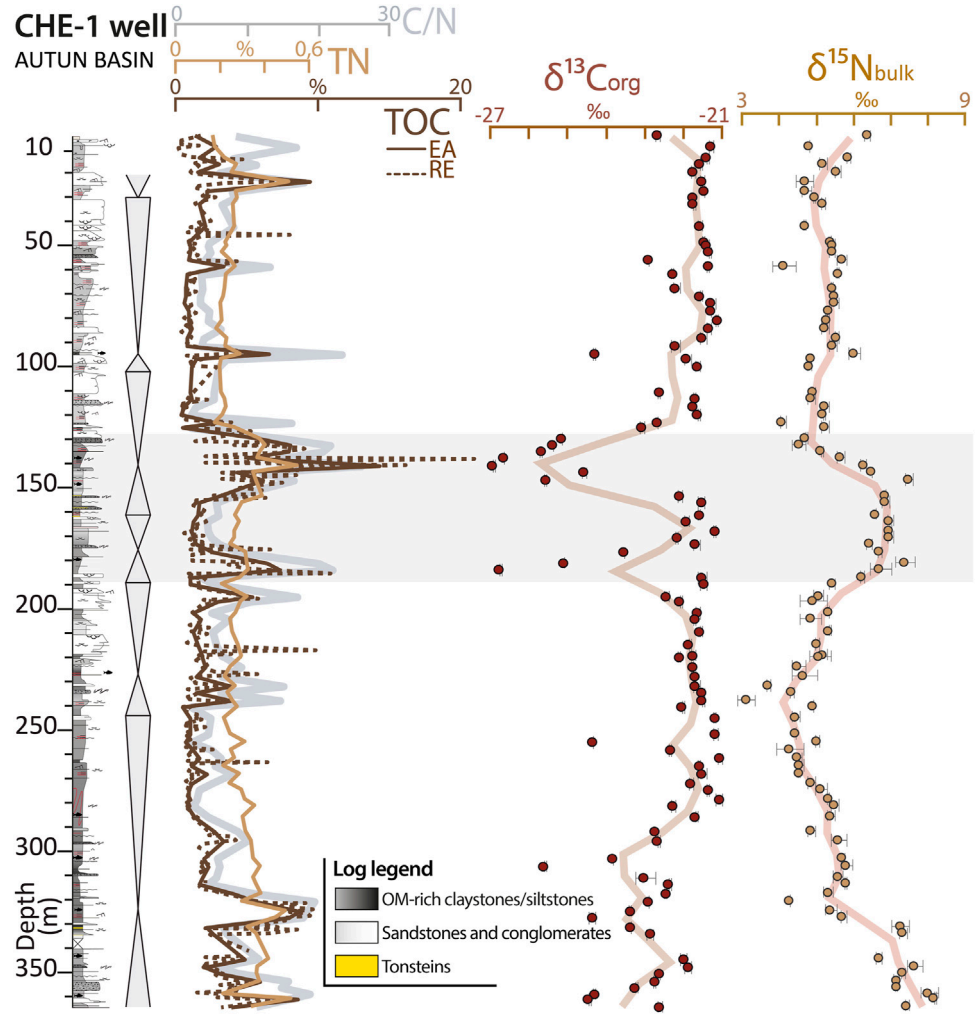

FIGURE 4 | Sedimentary section, sequence stratigraphy of the CHE-1 core (Autun Basin) and organic signal evolution (total organic carbon TOC, total nitrogen TN, C/N atomic ratio, $\delta^{13}C_{org}$ and $\delta^{15}N_{bulk}$ variations). The log caption is displayed on **Figure 2**. RE, Rock-Eval pyrolysis.

18. For each section, C/N variations primarily reflect the TOC evolution.

In the IG-1 core (**Figure 3**), the $\delta^{13}C_{org}$ values gradually increase from −24 to −20‰, with a mean value of −23.1 ± 1.7‰, with large-amplitude negative shifts down to −29.4‰ and −27.3‰ near 150 m (Igornay OSB, clayey facies) and 40 m, respectively. The $\delta^{15}N$ values show less variation, with values ranging from 2.7 to 6.5‰, with a mean value of 4.1 ± 0.62‰. The highest $\delta^{15}N_{bulk}$ values are encountered with the lowest $\delta^{13}C_{org}$, i.e., 6.4‰ close to 150 m and 6.5‰ close to 40 m.

In the CHE-1 core (**Figure 4**), values progressively increase from −24.0 to −21.0‰, with a mean value of −22.5 ± 1.4‰, with negative shifts down to −25.5‰ at ~300 m and −26.8‰ at ~180 m and −27.0‰ at 140 m. These values remain in the same range as those of the IG-1 core. The $\delta^{15}N_{bulk}$ values range from 2.9 to 8.2‰, with a mean value of 5.6 ± 1.1‰, with positive shifts up to 8.3‰ at ~330 m, 7.6‰ at ~190 m and 7.1‰ at ~150 m.

In the MU core, the base is characterized by ^{13}C-enriched OM, with $\delta^{13}C_{org}$ values averaging −20‰, and then sharply dropped by 8‰, down to ~−28‰ all along the core. The $\delta^{15}N_{bulk}$ values present a relatively narrow range from 3.5 to 6.7‰, with a mean value of 4.7 ± 0.7‰ all along the core, with a slight decrease (from 5 to 4‰) towards the top (**Figure 5**).

In the SUR section (**Figure 6**), the $\delta^{13}C_{org}$ curve presents a wavy evolution from −27.5 to −20.6‰, with a mean value of −24.3 ± 2.7‰, and shows a sharp decrease between the cores and the following outcrop at ~−1 m from −20.8 to −26‰. $\delta^{15}N_{bulk}$ values range between 5.3 and 10.1‰, with a mean value of 7.2 ± 1.3‰. The values remain relatively constant (~6‰) up to ~−1 m, with a shift to ~+10‰ at 7 m, followed by a slight decrease towards the top down to ~6‰.

Finally, in the LY-F core (**Figure 9**), $\delta^{13}C_{org}$ values slowly increase from −26.4 to −20‰, with a mean value of −22.2 ± 1.8‰, with two outliers reaching values up to −15.5‰. $\delta^{15}N_{bulk}$ values range from 1 to 4.4‰, with a mean value of

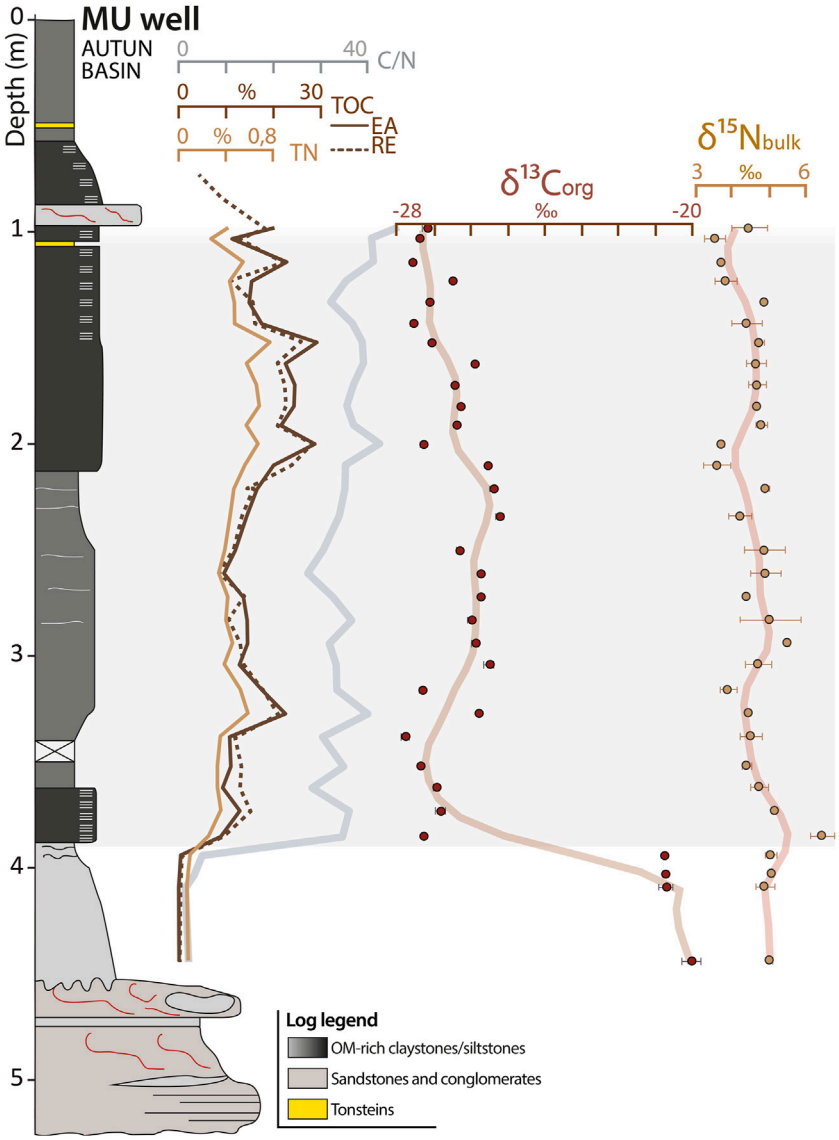

FIGURE 5 | Sedimentary section of the MU core (Autun Basin) and organic signal evolution (total organic carbon TOC, total nitrogen TN, C/N atomic ratio, $\delta^{13}C_{org}$ and $\delta^{15}N_{bulk}$ variations). The log caption is displayed on **Figure 2**. RE, Rock-Eval pyrolysis.

2.8 ± 0.7‰. $\delta^{15}N_{bulk}$ values are stable around 3‰ from the base of the core up to ~400 m, and then show a continuous increase up to ~4.5‰ towards the top of the core.

The dispersion of the elemental results obtained through EA-IRMS are synthesized on **Figure 10** for each section.

DISCUSSION

Organic-Matter Characterization

Lacustrine sedimentary OM generally consists of a mixture of remains of aquatic primary producers, vascular land plants, palynomorphs and of heterotrophic bacterial biomass thriving in the water column and sediments (Meyers and Ishiwatari, 1995). The OM origin, separated here in autochthonous (i.e., lacustrine algal/bacterial-derived OM) and allochthonous (i.e., terrestrial-derived OM), is appreciated through Rock-Eval pyrolysis results and palynofacies observations. In a lacustrine system such as Autun, AOM is generally considered to originate from primary algal and/or bacterial bio-production in surface waters (Tyson, 1995), whereas in some rarer cases it could have been derived from fixed or floating vegetation installed at the edges of shallow lakes or marshes (Schnyder et al., 2009).

In a pseudo van Krevelen diagram grouping all the sections (**Figure 11**), the HI vs. OI values obtained by Rock-Eval pyrolysis also indicate two types of OM: 1) a Type I OM (autochthonous OM) characterized by high HI and low OI values, and 2) a Type III OM (allochthonous OM) when HI values are low and OI

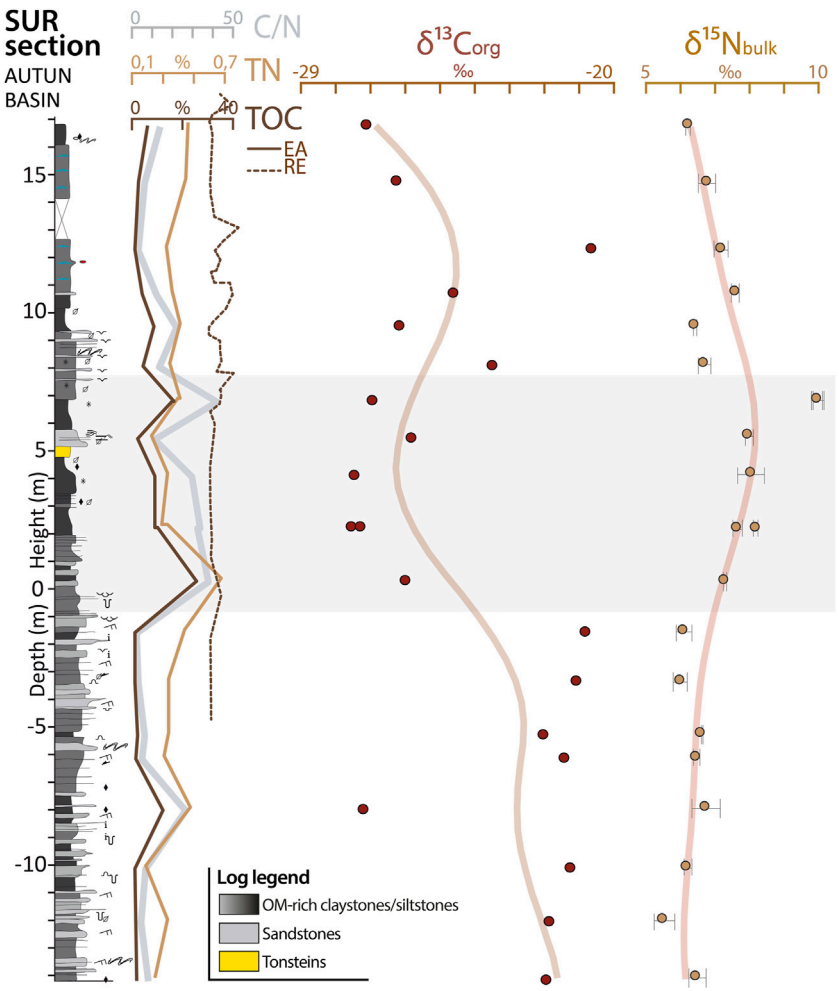

FIGURE 6 | Sedimentary section of the SUR, SUR-1 and SUR-2 cores and outcrop (Autun Basin) and organic signal evolution (total organic carbon TOC, total nitrogen TN, C/N atomic ratio, $\delta^{13}C_{org}$ and $\delta^{15}N_{bulk}$ variations). The log caption is displayed on **Figure 2**. RE, Rock-Eval pyrolysis.

values are high. At the end of the Paleozoic, the Type III OM consists exclusively of vascular land plants with a Calvin-Benson C3 metabolism, the C4 and CAM metabolisms evolving between the Cretaceous and the Tertiary (Thomasson et al., 1986; Bocherens et al., 1993; Cerling, 1999; Kuypers et al., 1999; Sage, 2004). The occurrence of altered Type I OM produced during degradation or oxidation, e.g., under aerobic conditions in the water column, may also explain some of the low HI-high OI endmembers (e.g., Type III, **Figure 11**).

The palynofacies observations confirm the occurrence of mixed sources of OM in the Autun Basin. In most cases, autochthonous AOM seems to predominate over allochthonous terrestrial components in samples with high HI values, notably in IG-1 and MU cores. Intermediate HI and OI values obtained from Rock-Eval mimic a Type II OM (marine OM), but palynofacies observations rather indicate mixture between Type I and Type III. These results are consistent with previous biomarker analyses by gas chromatography mass spectrometry (GC-MS) realized in the Autun Basin, as well as in the Aumance, Lodève (France) and Saar (Germany) basins by Izart et al. (2012), that reveal a bimodal OM origin (algal and bacterial vs vascular land plants). Moreover, the studies of Doubinger and Elsass (1975), Broutin et al. (1986), Broutin et al. (1990), Becq-Giraudon (1993), conducted in the Autunian facies of the Autun Basin and some other French Massif Central basins, also point out two OM-source endmembers, with fluctuations through time of the vascular land-plant species endmember, depending on their ecology in terms of water needs (i.e. hygrophile vs xerophile plants, well-adapted for wetness and dryness, respectively).

The C/N atomic ratio is usually a good proxy to approximate the OM sources and their relative contribution in lacustrine sediments (Meyers and Ishiwatari, 1993; Meyers, 1994; Meyers and Ishiwatari, 1995; Meyers and Teranes, 2001; Meyers, 2003; Lamb et al., 2006; Birgenheier et al., 2010; Baudin et al., 2017). Indeed, C/N ratios between 4 and 10 characterize autochthonous OM (algae and cyanobacteria, Type I and Type II OM, **Figure 12A**), and values higher than 20 indicate an

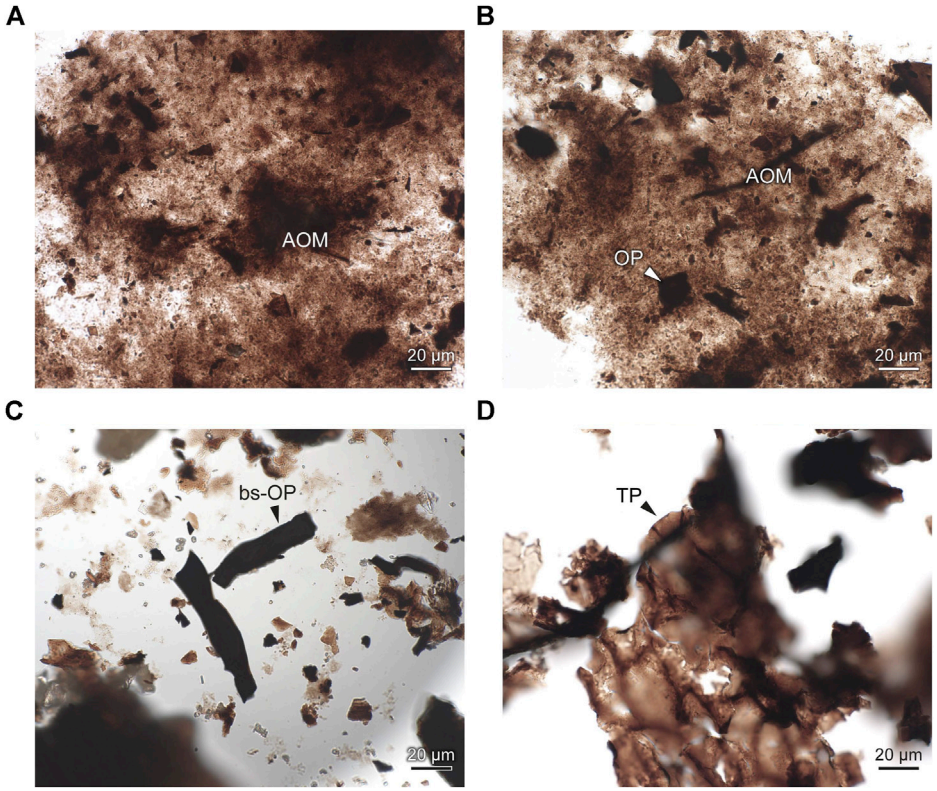

FIGURE 7 | Palynofacies microphotographs from the CHE-1 core. **(A)** amorphous organic matter (AOM – probably algal-bacterial-derived), 245.6 m; **(B)** AOM and opaque phytoclasts (OP), 245.6 m; **(C)** details of blade-shaped opaque phytoclasts (bs-OP), 219.45 m; **(D)** details of translucent phytoclast (TP), 210.6 m.

allochthonous source (Type III OM). However, the C/N ratio can be altered over time due to degradation of unstable nitrogen compounds in aquatic OM and the loss of carbon-rich sugars and lipids in terrestrial OM (Lamb et al., 2004). This ratio can be also modified during the earliest diagenesis which tends to decrease the nitrogen content (highly reactive and volatile) and hence increase the C/N ratio (Thomazo et al., 2009). Moreover, this ratio is directly impacted by the presence of mineral nitrogen when nitrogen is measured in bulk material, particularly for samples with a low OM content, where mineral lattice-bound nitrogen (i.e., primarily K-bearing phyllosilicates) can represent a significant fraction of the bulk nitrogen (e.g., Capone et al., 2006). In this study, a fraction of nitrogen (<0.1%) is indeed under fixed form, probably in illite and illite-smectite mixed-layers interlayers as shown by a TN vs. TOC diagram (**Figure 12A**), where the linear regression lines do not intercept the origin of the graph (nitrogen in excess relatively to organic carbon), especially for the MU, LY-F and IG-1 cores. In the case of the MU core, which shows a well-defined regression line (**Figure 12A**), almost 0.1 wt.% of nitrogen is likely fixed in K-bearing minerals, which represents a significant amount (~12%) when compared to the highest value of bulk nitrogen content of ~0.8 wt.%. The nitrogen retention efficiency in K-bearing minerals appears to be even higher in the CHE and SUR sections with 0.2–0.3% of mineral nitrogen (**Figure 12A**), but these values may be biased by poorly-defined regression slopes when compared to other sections. Moreover, the **Figure 12B** shows an exponential pattern of C/N ratio vs. TOC curves that would not be expected in the absence of mineral nitrogen. Thus, the presence of mineral nitrogen implies that the C/N ratio cannot simply be interpreted in terms of OM sources. In our study, it rather indicates an efficient mechanism of retention of ammonium in K-bearing minerals after the processes of diagenesis and denitrification (i.e., nitrogen loss). Another way to assess the presence of mineral nitrogen in the TN fraction is the C/N values below 1 displayed in the LY-F core, indicating that more nitrogen than carbon is preserved (**Figures 9**, **10**).

For some cores, TN and TOC contents are significantly correlated, such as for the LY-F and MU cores. Such a correlation may suggest an increased input of Type III OM to the aquatic system due to enhanced soil erosion from the lake catchment, associated with a significant clastic input to the lake. However, early diagenetic processes may also be involved in the modification of the sedimentary C/N ratio due to the escape of N_2 during denitrification, leading to a higher C/N ratio (exceeding 10). This remineralization of nitrogen also depends on the type of OM, being highly proteinic and thus N-rich for Type I, while more recalcitrant in case of Type III (highly cellulosic, e.g., Ertel and Hedges, 1985; Meyers, 1994). These two possible interpretations of a sedimentary C/N increase (i.e., variation in nitrogen cycling in the water column or sediments or mixed origin of OM) make a direct

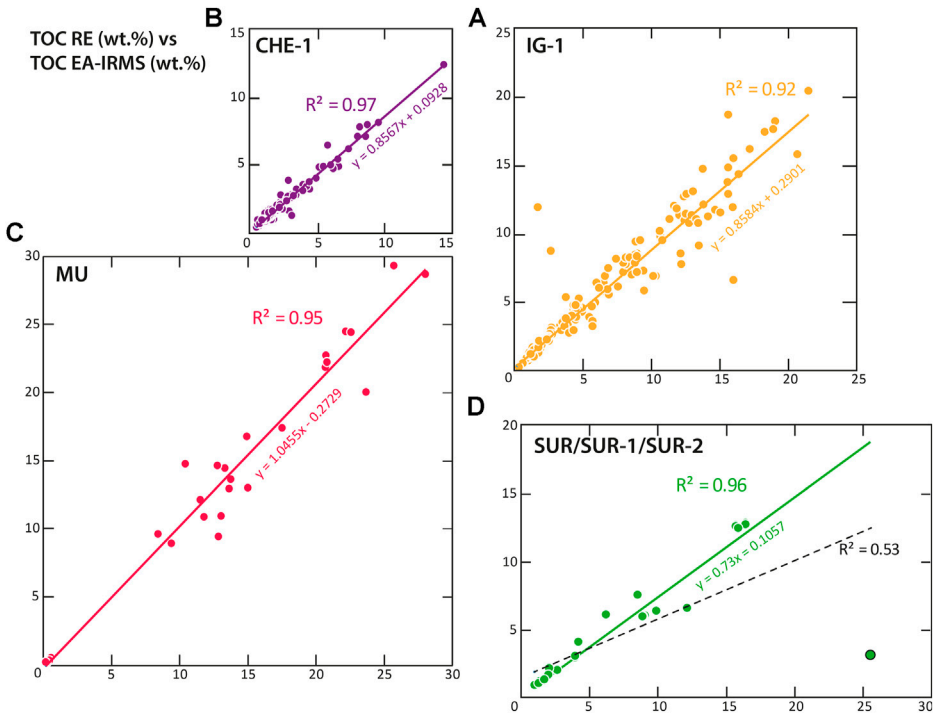

FIGURE 8 | Total Organic Carbon (TOC) values obtained by Rock-Eval pyrolysis (RE, ordinate) vs TOC values obtained by elemental analyzer (EA-IRMS, abscissa) showing a proportionality between the two measurements. **(A)** IG-1 well, $R^2 = 0.92$. **(B)** CHE-1 well, $R^2 = 0.97$. **(C)** MU well, $R^2 = 0.95$. **(D)** SUR section and SUR-1 and SUR-2 well for which two regression lines are calculated: one comprising all the points ($R^2 = 0.53$) and a second without the outlier (point with black circle, $R^2 = 0.96$), showing that there is probably a measurement error with this point given the difference higher than 20% between the two methods.

interpretation of the C/N signal even more confusing (e.g., Van Mooy et al., 2002).

The IG-1 Well (Autun Basin)

Previous Rock-Eval and palynofacies analyses (Elsass-Damon, 1977; Marteau, 1983; Garel et al., 2017) have shown that the OM of Igornay OSB (P2 environment on **Figure 11A**) is mostly composed of a Type I OM. Palynofacies tend to confirm these results, as AOM dominates over phytoclasts and palynomorphs. Very low HI values, such as observed in the delta topset environment (littoral lake L1 environment, **Figure 11A**) could be interpreted as Type III OM input, but palynofacies analyses show generally minor but constant plant-derived components in palynofacies. Thus, low HI values represent more altered Type I OM in proximal environment where the water column is thin, allowing OM degradation by aerobic heterotrophic micro-organisms and the reworking of sediments (which increases sedimentary oxygen depth penetration). Inversely, in the distal environments, OM anaerobic remineralization (including bacterial sulphate reduction and denitrification) is less effective and results in higher TOC contents and higher HI values.

The CHE-1 Well (Autun Basin)

Rock-Eval data show two endmembers, the first one with high HI and low OI values, and conversely a second with low HI and high OI values (**Figure 11B**). This dichotomy may arise from a variable mixture of Type I and a Type III OM or a strongly altered trend in Type I OM after oxidative processes.

The distal-proximal alteration gradient found in the IG-1 core is less distinguishable in the CHE-1 core (**Figure 11B**), as distal lacustrine facies are this time associated with either high or low HI values. The presence of both Type I and Type III OM in distal lacustrine sediments is marked by very variable OI and HI. The palynofacies data indicate that the OM of the CHE-1 core is composed of a mixture of terrestrial-derived and algal/bacterial OM. Judging from our limited palynofacies dataset, the terrestrial component seems higher in CHE-1 when compared to IG-1 and MU cores, which may correspond to lower average HI values, suggesting a higher allochthonous contribution and/or a higher average oxygen level in the water column.

The MU Well (Autun Basin)

As shown by Garel et al. (2017) and this work, Muse OSB (MU well, **Figures 2**, **5**) is composed by a Type I OM with some samples showing a mixture with Type III OM, characterized by gelified OM corresponding to cuticles of land plants. This is confirmed by macroscopic observations showing land plant fragments in the blackest levels. This cuticle-Type III OM has the particularity to present high HI which can reach more than 500 mgHC/gTOC (e.g., Garel et al., 2017), induced by the presence of cuticular wax.

The MU core is composed at its base by proximal environments (from the base to ~4 m, coarse-grained

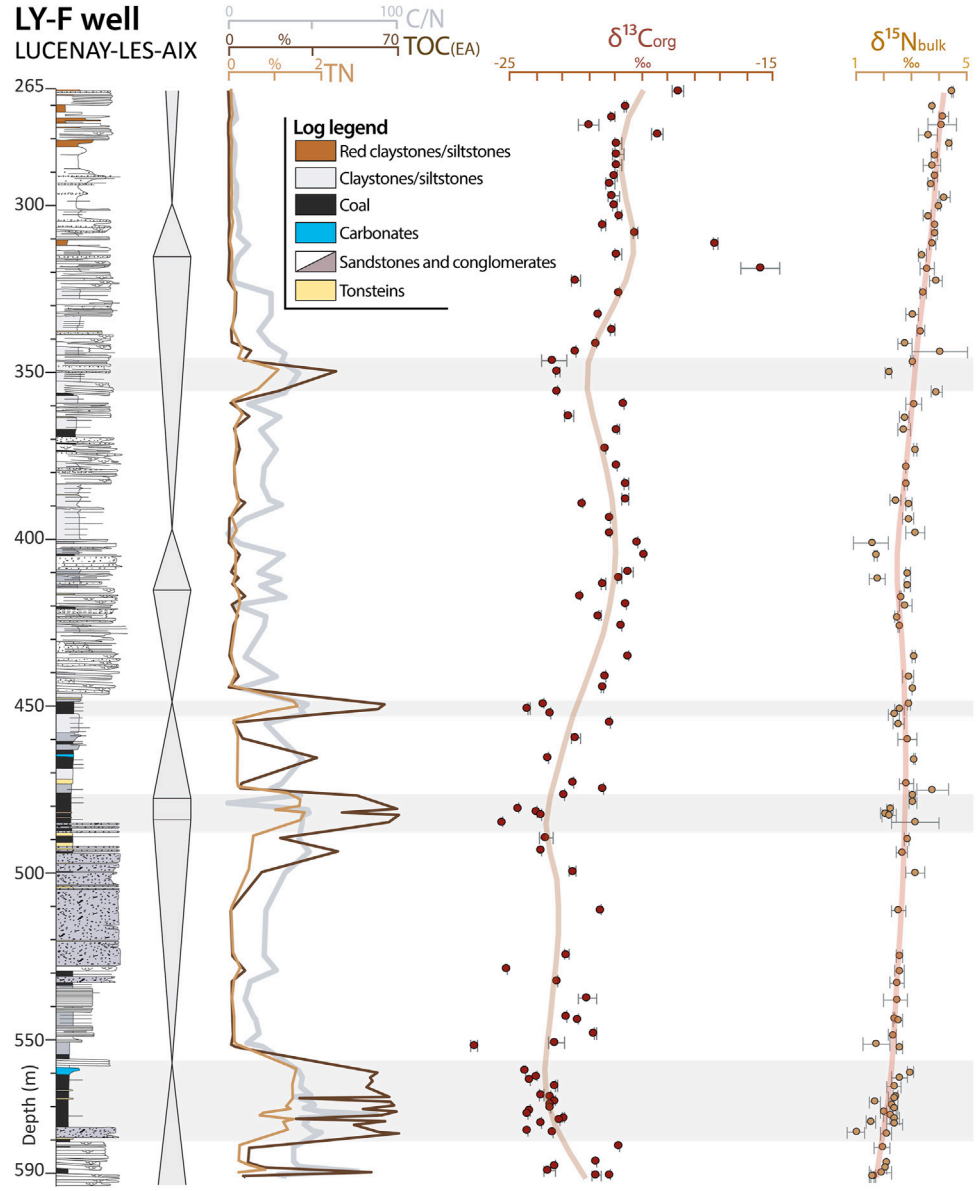

FIGURE 9 | Sedimentary section, sequence stratigraphy of the LY-F core (Lucenay-lès-Aix area, Decize–La Machine Basin) and organic signal evolution (TOC, TN, C/N atomic ratio, $\delta^{13}C_{org}$ and $\delta^{15}N_{bulk}$ variations). The log caption is displayed on **Figure 2**.

lithologies corresponding to a deltaic topset environment L1 and fine-grained grey lithologies characterising a protected littoral lake environment L2, **Figure 2**), followed by a probable profundal lacustrine P2 environment corresponding to the Muse OSB (from ~4 to 0 m, fine-grained dark lithologies, **Figure 2**). On a pseudo van Krevelen diagram (**Figure 11C**), the distinction between the protected littoral lake and the profundal lake P2 depositional environments is very clear. The OM of the protected littoral lake environment is oxidized compared to those of the profundal lake environment. HI values are not relevant for two of these points because of very low TOC values (<0.25%, **Figure 11C**). However, the macroscopic features of the protected littoral lake environment level display large land plant fragments, confirming an allochthonous Type III OM, compared to the profundal lake characterized by a dominant autochthonous Type I OM.

The SUR Section (Autun Basin)

Although very few palynofacies data are available for the SUR section excepted the two samples characterized by Garel et al. (2017), showing that bacterial-derived OM (Type I) is largely dominant, the HI values measured in our study mostly sign a Type I OM (**Figure 11D**). The observed low HI-high OI values could be tentatively assigned to Type III OM, but could also reflect a degraded Type I OM.

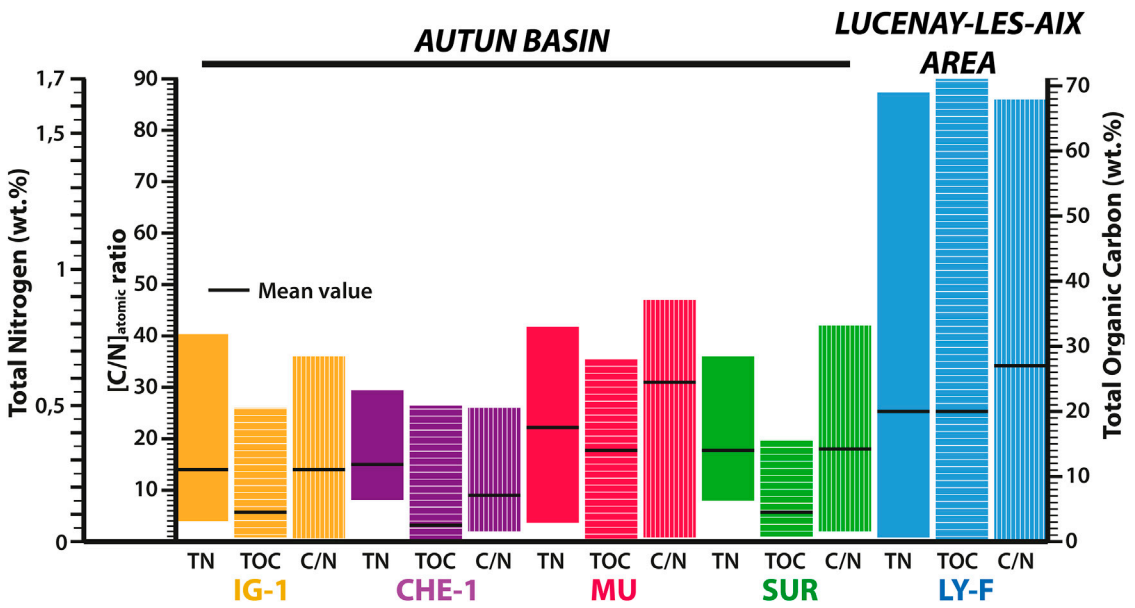

FIGURE 10 | Histograms of the dispersion of total nitrogen (TN), total organic carbon (TOC) and C/N atomic ratio values for all the sections studied; mean values are represented by black horizontal lines; the C and N content is obtained by EA-IRMS. The values display approximatively the same ranges in the Autun Basin, whereas ranges for those of the Lucenay-lès-Aix area are wider.

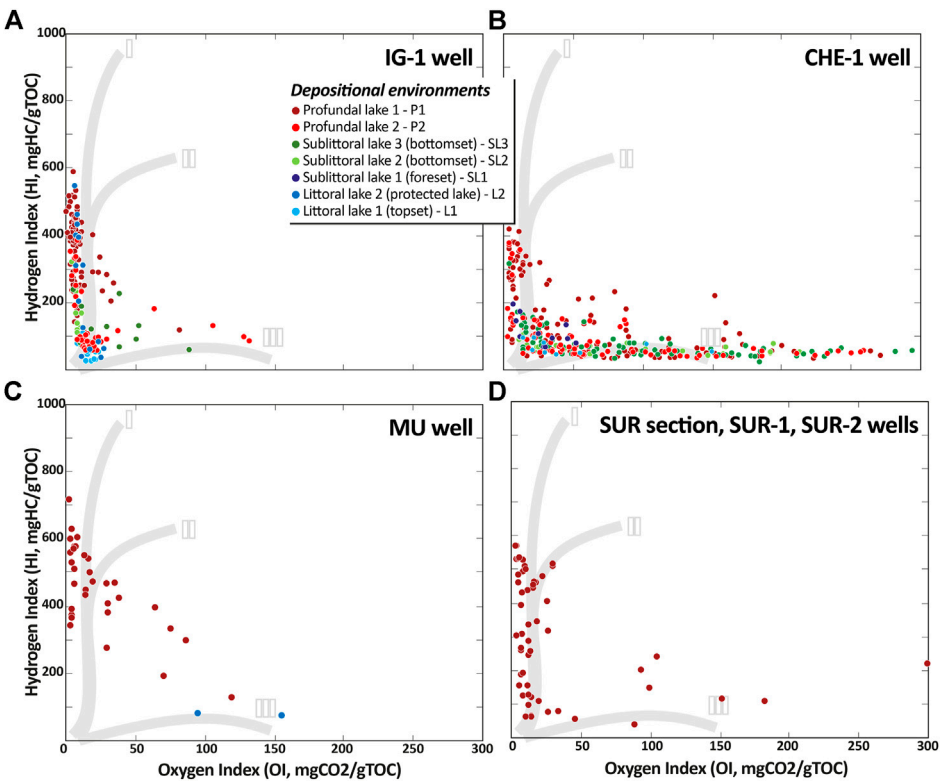

FIGURE 11 | Pseudo-van Krevelen diagrams displaying HI and OI values for the studied section samples depending on the depositional environments. **(A)** In the IG-1 well samples, the more distal facies display the highest HI values, whereas environments submitted to high sediment supply and oxidation processes show lower values. **(B)** In the CHE-1 core samples, the facies distribution is not as marked as for the IG-1 well, with more oxidized samples. **(C,D)** In the MU and SUR cores and section, the environment is only lacustrine (either littoral or profundal) with minimal sediment supply and samples mostly display high HI-low OI values.

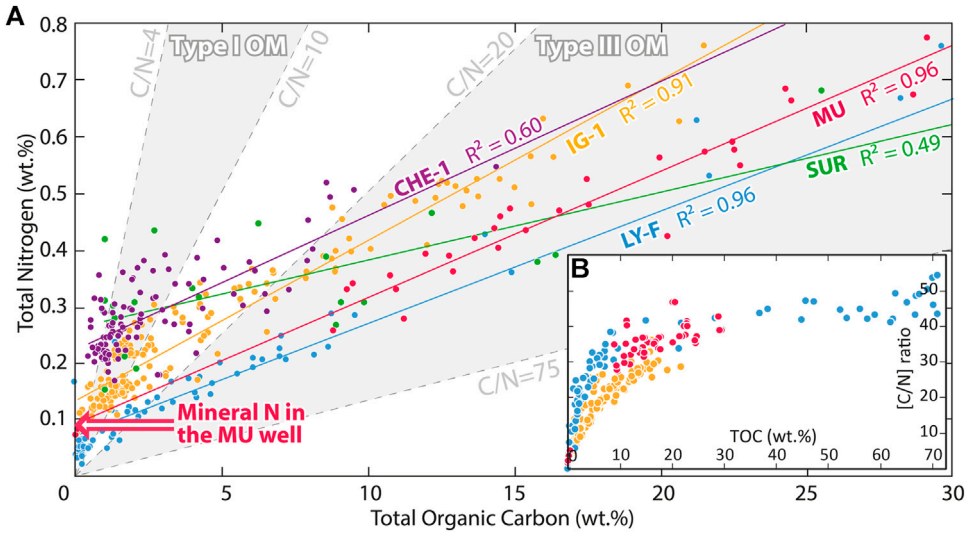

FIGURE 12 | (A) TN vs TOC for the IG-1, CHE-1, MU, SUR, SUR-1, SUR-2, and LY-F sections. Grey areas display the intervals where points for Type I and Type III OM should be found if this signal is not altered by the presence of mineral nitrogen or denitrification processes. The regression lines for the SUR, SUR-1, SUR-2, and CHE-1 sections cannot be extrapolated at the origin to calculate the mineral nitrogen, because of a too low R^2. **(B)** C/N atomic ratio vs Total Organic Carbon (TOC) for the LY-F, IG-1, and MU wells showing an exponential pattern induced by the presence of mineral nitrogen.

The LY-F Well (Lucenay-lès-Aix Area)

Despite the absence of Rock-Eval pyrolysis and palynofacies data for the LY-F well, the core presents a different geochemical pattern from sections of the Autun Basin. Indeed, this core is composed by an autochthonous lacustrine and allochthonous terrestrial OM mixing, but also by floodplain OM (coal-bearing levels), contrary to the other sections composed dominantly by the mixture of lacustrine and terrestrial OM (**Figures 2**, **9**). **Figure 12A** also indicates that mineral nitrogen is present in the samples, but in lower amounts than in the Autun Basin. According to the high $\delta^{13}C_{org}$ values (**Figure 9**), it is likely that allochthonous OM dominates the bulk OM (i.e., the Type I and Type III OM mixing) signal; this core, unlike the sections in the Autun Basin, is dominated by coarse-grained clastic inputs that may indeed contribute a large amount of allochthonous Type III OM to the basin. By comparison, a study in the Western-European Carboniferous to Permian continental Saar-Nahe Basin (Germany, **Figure 1A**) evidenced that such high $\delta^{13}C_{org}$ values (~−21‰) are associated with a dominant Type III OM, based on Rock-Eval and palynofacies analyses, contrary to the Type I OM which is associated to $\delta^{13}C_{org}$ values close to −27‰ (Müller et al., 2006). A similar amplitude between $\delta^{13}C_{org}$ values of autochthonous and allochthonous OM has been observed in an early Cretaceous lacustrine system at Bernissart (Mons Basin, Belgium), were the Type III, allochthonous OM, corresponds to $\delta^{13}C_{org}$ values around −24.5‰, whereas autochthonous primary productivity-derived OM is associated with more negative $\delta^{13}C_{org}$ values, close to −28‰ (Schnyder et al., 2009). The $\delta^{13}C_{org}$ values close to −24‰ for the three coal intervals (i.e. located at ~575, 490, and 450 m in the LY-F well, **Figure 9**) are consistent with $\delta^{13}C_{org}$ values of humic Permian coal from the Australian Sydney Basin (Grice et al., 2007; Ahmed et al., 2009; Retallack et al., 2011).

Preservation of Isotope Organic Signals

Early diagenesis at the sediment-water interface having a low impact on the OM isotope signal preservation (Lehmann et al., 2002), the preservation of OM isotope signal can also be assessed by several parameters: 1) $\delta^{13}C_{org}$ values are consistent with those expected for primary productivity OM (~−25 to −30‰, Schidlowski et al., 1983; Kump and Arthur, 1999), and particularly those expected during this time-window (between −20 and −27‰, Strauss and Peters-Kottig, 2003; Müller et al., 2006; Peters-Kottig et al., 2006; Nordt et al., 2016; Cui et al., 2017) and 2) the Tmax parameter, showing values ranging from 423 to 443°C in the studied sections, indicates moderate burial diagenesis. With respect to the petroleum generation, this reflects a relatively immature OM, or at the beginning of the oil window for the highest Tmax values. Moreover, the absence of correlation between the $\delta^{15}N_{bulk}$ and the TN content in all sections shows that the OM isotope signals are probably not pervasively altered by late secondary processes (the nitrogen content being more prone than the carbon to vary during OM alteration, Meyers and Ishiwatari, 1993; Meyers, 2014). Similarly, the $\delta^{15}N_{bulk}$ values obtained are those expected for non-marine sediments, usually between −3 and +7‰ (Peters et al., 1978) and are also within the range of biological signals measured in ancient and modern environments (e.g., Tramoy et al., 2016a; Bouton et al., 2020). $\delta^{13}C_{org}$ negative excursions (**Figures 3–6**) also appear to be of primary origin because diagenesis is expected to induce positive values (Hoefs and Frey, 1976; Monin et al., 1981; Hayes et al., 1983), yet lower than +2‰ (Busigny et al., 2013), and without altering the initial trends (des Marais et al., 1992).

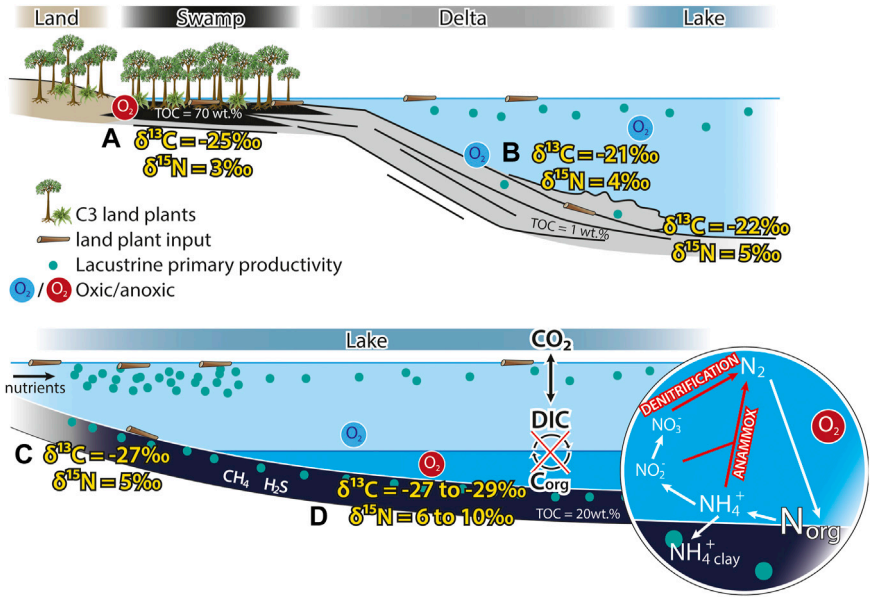

FIGURE 13 | Synthetic sketch showing the different ways to obtain TOC, $\delta^{13}C_{org}$ and $\delta^{15}N_{bulk}$ values depending on depositional environments and lake water physic and chemical parameters. **(A)** Swamp environment materialized by a dominant Type III OM constituting the coal deposits, with moderate $\delta^{13}C_{org}$ and $\delta^{15}N_{bulk}$. **(B)** Deltaic to lacustrine environment dominated by terrigenous land plants inputs, displaying high $\delta^{13}C_{org}$ (depending on the mixing of the two OM) and low $\delta^{15}N_{bulk}$ values. **(C)** Shallow lake environment (littoral lake) dominated by lacustrine OM with some terrigenous land plant inputs, marked by very low $\delta^{13}C_{org}$ and $\delta^{15}N_{bulk}$ values, indicating anoxic sediments but the absence of a developed chemocline. The low water column prevents the oxidation of OM during sinking. **(D)** Deep lacustrine environment with a well-developed chemocline, leading to anoxia in bottom waters and sediments, favouring the lacustrine OM preservation, and the denitrification and anammox processes.

$\delta^{15}N_{bulk}$ Variations

In the modern nitrogen cycle, di-nitrogen (N_2) is withdrawn from the atmosphere during biological fixation by autotrophs as ammonia (NH_3) by the nitrogenase enzyme. Subsequently, the OM sedimentation is followed its mineralization under aerobic or anaerobic conditions with a first step, namely ammonification, consisting in the reduction of organic nitrogen into ammonium (NH_4^+). Then, in aerobic context, NH_4^+ is oxidized to nitrite (NO_2^-) and nitrate (NO_3^-) during nitrification. The produced nitrates can also be biologically assimilated. In anaerobic context (low O_2 in the water column or in sediments, or high sedimentation rates), two processes can occur: anaerobic oxidation of NH_4^+ by an anammox reaction that converts NH_4^+ and NO_2^- to N_2 (**Figure 13**), and denitrification, i.e., a respiratory process that converts NO_3^- to N_2 (Van Mooy et al., 2002; Ader et al., 2016). While nitrification is a moderately fractionating process in modern environments when NH_4^+ oxidation is quantitative, the denitrification pathway is associated with a strong ^{15}N-enrichment of the residual NO_3^-, leading to an increase of $\delta^{15}N_{bulk}$ values owning to the balance between NO_3^- assimilation and N_2 fixation (Peters et al., 1978; Sigman et al., 2009; Ader et al., 2016). Indeed, denitrification induces a fractionation between the residual NO_3^- and released gaseous N_2 and N_2O of about −3‰ in the sediment and up to −25 to −30‰ in the water column (Ader et al., 2016). This process is therefore associated with a ^{15}N-enrichment of the $\delta^{15}N_{bulk}$ values archived in sediments (i.e., positive $\delta^{15}N_{bulk}$ excursions). Similarly, the anammox reaction leads to a ^{15}N-enriched residual NH_4^+ and so higher $\delta^{15}N_{bulk}$ signal if a sufficient amount of this NH_4^+ is fixed by biological activity or in K-bearing minerals (Prokopenko et al., 2006).

Therefore, positive $\delta^{15}N_{bulk}$ excursions usually indicate an increase in denitrification and/or anammox processes and are associated with the establishment or expansion of strong redox gradient in the water column. Indeed, both processes require chemical stratification of the water column and are often associated with the development of anoxia, at least in the lower part of the water column or in a zone of oxygen minimum in the water column.

In the sedimentary successions studied, positive nitrogen excursions are sometimes associated with increases in TOC and decreases in $\delta^{13}C_{org}$ values, while generally $\delta^{15}N_{bulk}$ and $\delta^{13}C_{org}$ values are not related. Yet, this relation can be explained by several mechanisms under anoxic conditions, including 1) an increase in Type I OM associated with anoxic OM remineralization processes shifting the isotope signal mass balance towards ^{12}C-enriched isotope signal, and/or 2) the build-up of a large dissolved organic carbon reservoir subsequently used by secondary productivity (e.g., Hayes, 1983; Kah et al., 1999; Hayes, 2001; Guo et al., 2013). This coevolution is observed in the IG-1 core in the Igornay OSB at ~155 m and at ~40 m, and also in the CHE-1 core, between ~190 and 130 m. However, periods of high TOC and low $\delta^{13}C_{org}$ values without positive $\delta^{15}N_{bulk}$ excursions (e.g., IG-1 core, ~70 m and MU core, from 4 to 1 m) represent periods when denitrification or anammox processes are absent or less efficient

(i.e., limited to the sediment), indicating that the chemocline is not sustained. This likely indicates a thin water column, promoting the water homogenization, but paired with a substantial primary productivity in surface water, compensating OM degradation during its sinking and before reaching the anoxic sediments, and thus favouring OM-rich deposits. This interpretation is consistent with the protected littoral lake environment (i.e., thin water column) inferred from several sedimentological features for the OM-rich deposits located at ~70 m in the IG-1 core, such as their association with microbial deposits formed in the photic zone (Mercuzot et al., submitted), but differs from the depositional environment inferred for the Muse OSB, firstly considered as deposited in a profundal lake (Mercuzot et al., submitted, based on the classification of Bohacs et al., 2000). These results and interpretations highlight that paired carbon and nitrogen isotope geochemistry can be an additional helpful tool to depositional paleoenvironment determinations, often solely based on sedimentological facies interpretations.

$\delta^{13}C_{org}$ Variations

Whereas the $\delta^{13}C$ of carbonates ($\delta^{13}C_{carb}$) is thought to reflect the $\delta^{13}C$ of the dissolved inorganic carbon (DIC) reservoir, the OM carbon isotope signal ($\delta^{13}C_{org}$) in a lake can be affected by a large combination of factors such as: 1) the isotope composition of the DIC (depending on the isotope composition of the dissolved CO_2 contained in the water compared to atmospheric CO_2), 2) metabolisms of primary producers, their species and growth rates (Mayer and Schwark, 1999), 3) OM sources (allochthonous vs autochthonous, Schnyder et al., 2009; Yans et al., 2010), 4) the water pCO_2 (Herczeg and Fairbanks, 1987), 5) the degradation of particulate organic carbon below the sediment-water interface, 6) the remineralization of dissolved organic carbon in the water column and sediments (e.g., Hayes, 1983; Kah et al., 1999; Hayes, 2001; Guo et al., 2013), and 7) the post-depositional OM thermal decomposition (Strauss et al., 1992; Tocqué et al., 2005; Derry, 2010). Moreover, $\delta^{13}C_{org}$ values in OM-rich environments can be influenced by secondary productivity developing in anoxic bottom waters or within the sediments (e.g., Hayes et al., 1999). In the present study, because of the low burial and the resulting moderate thermal diagenesis state, it is unlikely that $\delta^{13}C_{org}$ variations result from thermal decomposition of OM.

According to the U–Pb dating of the Autun Basin by Pellenard et al. (2017), the sediments from IG-1 and CHE-1 cores are susceptible to have been deposited in less than a million year, revealing high sedimentation rates and thus very short-term $\delta^{13}C_{org}$ variations. The origin of these isotope events is not constrained, but could be related to short-term climate variations, through a direct impact on the lake level and chemistry, or a more indirect impact on sedimentary fluxes, controlling the origin of OM (e.g., terrestrial vs. lacustrine bioproduction, Schnyder et al., 2009; Yans et al., 2010) supplied to the basin.

We considered here that at first order, the $\delta^{13}C_{org}$ variations observed in this study are due to three main parameters: 1) variations of OM sources through time (autochthonous vs. allochthonous), 2) variations in primary productivity and storage efficiency of OM under a thin water column, or 3) variations in OM remineralization in the water column under a developed chemocline and at the water–sediment interface, associated with fluctuating contribution of secondary heterotrophic biomass to the sedimentary OM. Those parameters may either vary under autocyclic conditions, or be indirectly controlled by climate changes, through fluctuations of the lake level or of the erosion intensity in the catchment area. Furthermore, at second order, these perturbations could also reflect direct climate variations recorded in the basins: in Australian Permian basin, Retallack et al. (2011) have shown that short-term negative carbon excursions in terrestrial OM are synchronous with warmer and wetter "greenhouse crises." This pattern is also observed in United States and South African basins (Retallack, 2013). At a longer time-scale (i.e. 5–7 Myr), $\delta^{13}C_{org}$ variations in bulk OM marine sediments seem to indicate pCO_2 fluctuations, with increases at the beginning of icehouse intervals (ice-caps waxing) and decreases in the second part of the icehouse intervals up to the interglacial (ice-caps waning, Birgenheier et al., 2010). Unfortunately, the pCO_2 evolution is not available through the $\Delta^{13}C$ proxy (i.e., the difference between $\delta^{13}C$ of carbonates and $\delta^{13}C$ of OM), because of the mixing of the OM sources, and the substantial diagenetic overprint on the scarce carbonates preserved in the basins.

Accumulation of OM can be derived from both lacustrine productivity and terrestrial inputs with varying degrees of mixing. In this study, terrigenous OM can even be subdivided into two different origins: one representing the exported terrestrial (allochthonous) OM, the second being direct accumulation of vascular land plants in swamp (i.e., coal). The $\delta^{13}C_{org}$ signature of vascular land plants is evidenced in the coal levels of the Lucenay-lès-Aix area with values around −24‰ (**Figures 9**, **13A**). The remaining $\delta^{13}C_{org}$ variations observed in this study may therefore reflect the interaction of varying degree of mixing between autochthonous productivity and allochthonous OM delivery and secondary processes (e.g., remineralization and secondary productivity). Mixing between OM types with different $\delta^{13}C_{org}$ can be independently inferred based on Rock Eval and palynofacies data, while secondary processes can be evidenced when rapid variations of the $\delta^{13}C_{org}$ are deciphered and cannot be linked to changes in OM types. Within this framework of interpretations, and as supported by the palynofacies data, we observe that periods of low OM accumulation are associated with $\delta^{13}C_{org}$ mean values close to −22‰ (**Figures 3–6**, **9**) and are dominated by Type III OM, and that periods of increasing TOC show ^{12}C-enriched $\delta^{13}C_{org}$ values (down to −29‰) reflecting lake OM production and processing. In addition, OM anaerobic remineralization by bacterial acetotrophic methanogenesis, and to a lesser extent by sulfate reduction, could still lead to lower sedimentary $\delta^{13}C_{org}$ values (Meyers and Ishiwatari, 1995; Müller et al., 2006). However, it can be challenging to distinguish the respective impact of these two secondary processes in the fossil record.

In order to disentangle the various contributions of different sources of OM and the internal lacustrine OM cycling, we explore the relationship between OM-type concentrations and their

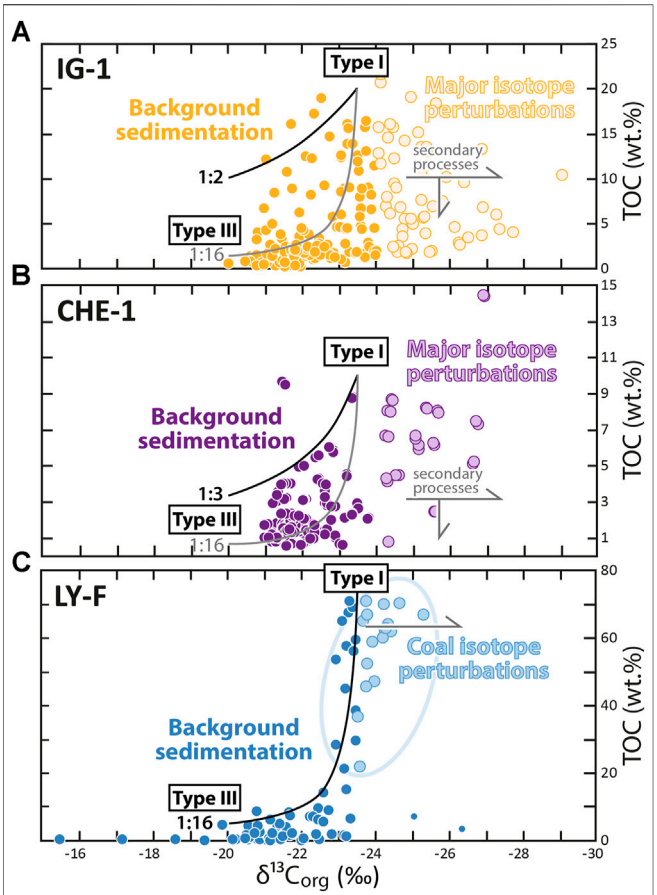

FIGURE 14 | Mixing model of Johnston et al. (2012) applied to the three major studied sections: Total organic carbon (TOC) depending on the $\delta^{13}C_{org}$; only background sedimentation values are taken into account. In each case, the mean value for the Type III OM pole is −20‰, and for the Type I OM pole, −23.5‰. **(A)** The IG-1 data present a mixing Type III: Type I ratio of ~1:2, **(B)** the CHE-1 data a ratio of ~1:3 (high mixing), whereas **(C)** the LY-F data fit with a ~1:16 ratio (low mixing). On Figure **(A,B)**, this 1:16 ratio has been determined for the IG-1 core and CHE-1 core data in order to highlight the difference in the modelled curves which would occur in case of a lower mixing.

isotope signals using the concept developed by Johnston et al. (2012) in the following section.

Another Method to Sort $\delta^{13}C_{org}$ Variation Origins?

Common methods have been previously used to constrain the OM types preserved in the sediments of the studied sections, through Rock-Eval pyrolysis interpretations and palynofacies characterization. However, it is difficult to identify secondary cycling OM with this combined method. Johnston et al. (2012) have elaborated a new methodology based on patterns of TOC and ε_{TOC} values, the latter approximated here using the $\delta^{13}C_{org}$ signal, to quantitatively infer the respective proportions in a mixture of two OM types (type a and type b). For instance, when a sample consists of a-type and b-type OM in roughly same proportions (i.e., characterized by a a:b ratio close to 1:1), the TOC vs ε_{TOC} (or $\delta^{13}C_{org}$) pattern shows a horizontal straight line. In contrast, when the sample is dominated by one OM type (e.g., 1:100 ratio), the pattern shows an exponential curve. This methodology was applied to our OM data from the longest cores (IG-1, CHE-1, and LY-F wells). The model described the isotopic mass balance of the mixing of two OM sources, based on their respective $\delta^{13}C_{org}$ values (fixed at −20‰ for the Type III OM and at −23.5‰ for the Type I OM), their organic contents (i.e., TOC) and their relative fractions (evolving from 0 to 1, see Johnston et al., 2012 **Supplementary Material** for the detailed equation). The modelled mixing lines are then plotted in the same diagrams than the $\delta^{13}C_{org}$ and TOC measured values, for each well (**Figures 14A–C**). For the IG-1 samples, the best fit corresponds to a Type I: Type III OM ratio close to 1:2 (**Figure 14A**); for the CHE-1 samples, this ratio is close to 1:3 (**Figure 14B**), and for the LY-F, the samples is close to 1:16 (**Figure 14C**). This clearly indicates that in the Autun Basin, during background sedimentation, the OM mixing is composed in nearly equal proportions of Type I and Type III OM, contrary to the Lucenay-lès-Aix Area, where the Type III OM largely dominates the sedimentary OM. Moreover, values departing from the modelled line correspond to the major isotope excursions (i.e., $\delta^{13}C_{org}$ values lower than −23.5‰) recognized in chemostratigraphic profiles. These $\delta^{13}C_{org}$ values are most likely impacted by secondary processes in the case of the IG-1 and CHE-1 samples, that could result from secondary productivity and/or remineralization in anoxic setting.

Therefore, this model seems accurate in identifying and quantify 1) a two-component OM mixing during background sedimentation in the Autun Basin and in the Lucenay-lès-Aix area and 2) punctual isotope excursions reflecting changes in the lake water column functioning, hence expanding the domain of application of this isotope mass balance methodology from Neoproterozoic marine series to Phanerozoic deltaic-lacustrine deposits.

Nitrogen and Carbon Cycling and Depositional Environment Refinement

Considering the exploitable dataset, several cases can be individualized in the two basins studied: 1) periods with $\delta^{13}C_{org}$ values between ~−20 and −22‰, representing the background sedimentation, with a mixture of Type I and Type III OM, sometimes largely dominated by Type III OM as in the Lucenay-lès-Aix area (**Figure 13B**); 2) periods of negative carbon-isotope excursions but not linked with positive nitrogen-isotope excursions, as observed at 70 m in the IG-1 core or in the Muse OSB of the MU core in the Autun Basin (**Figures 3**, **5**, **13C**); 3) periods where $\delta^{13}C_{org}$ values show sharp negative isotope excursions down to ~−29‰, related to high TOC content and during which positive $\delta^{15}N_{bulk}$ excursions are recorded (Autun Basin).

In the second case (negative $\delta^{13}C_{org}$ excursions only), these periods are attributed to high lacustrine primary productivity in surface waters (represented by high HI values) with a reduced chemocline, in a relatively low water column preventing OM

oxidation during sinking. The bottom waters are not anoxic, within the photic zone, possibly due to the thinness of the water column or the seasonal vertical diffusion of waters observed in some meromictic to polymictic lakes.

In the third case ($\delta^{13}C_{org}$ negative excursions associated with $\delta^{15}N_{bulk}$ positive excursions), these periods are associated with maximum flooding surfaces (MFSs, **Figures 3**, **4**, **9**) and are attributed to reduced OM remineralization under anoxic conditions (minimal sedimentary input and developed chemocline close to the euphotic zone), preventing the equilibrium of the carbon and nitrogen cycles with the atmosphere. Denitrification and/or anammox processes can occur (high $\delta^{15}N_{bulk}$ values), as same as possible sulfate-reduction or methanogenesis (low $\delta^{13}C_{org}$ values, **Figure 13D**). Sometimes, the negative carbon-isotope excursions display a relatively higher duration than their associated positive nitrogen-isotope excursions, at it is the case for the event at ~150 m in the CHE-1 core (**Figure 4**). This pattern was already observed by Algeo et al. (2008), who assume that the recovery of the negative carbon-isotope excursion demands more time than that of the nitrogen positive excursion. In this study, positive nitrogen-isotope excursions are restrained to retrogradational cycles (i.e., periods preceding the MFS) and to MFSs (periods of lowest sediment supply favouring dysoxic/anoxic conditions), and disappear during progradational cycles (i.e., periods following the MFS). By contrast, negative carbon-isotope excursions persist during a part of the progradational cycle, which is also observed in the CHE-1 core between ~150 and 130 m. This can be due to an increasing reoxygenation of the bottom waters when the lake level begins to fall (chemocline demise, high clastic inputs), minimizing denitrification and anammox processes.

The Lucenay-lès-Aix area represents the proximal pole on a depositional environment profile compared to the sections of the Autun Basin, with the presence of supralittoral deposits (coal-bearing sequences deposited in floodplain environments) indicating periods close to the emersion. High $\delta^{13}C_{org}$ values of the enclosing background sedimentation (~−20 to −22‰) indicate the mixture between a lacustrine OM and material derived from terrestrial OM, as observed at a macroscopic scale. However, the Johnston et al. (2012) model previously discussed highlights a higher proportion of Type III OM compare to Type I OM. This feature is consistent with the more proximal depositional environment (i.e., increased terrigenous fluxes) of the Lucenay-lès-Aix area compare to those of the Autun Basin. The coal levels of the Lucenay-lès-Aix area are represented by slight negative carbon-isotope excursions (**Figure 9**) indicating strong OM accumulation and storage of lighter carbon. The $\delta^{15}N_{bulk}$ values do not show significant fluctuations, indicating that the nitrogen cycle is not perturbed, unlike in the Autun OSBs formed in the distal part of the depositional environment profile. Such a geochemical feature is consistent with the absence of a developed chemocline in the environments characterized by very thin water column required for peat accumulation.

Paleoclimate Control

This work shows that it is not simple to assess direct paleoclimate variations from continental late Paleozoic sedimentary successions based solely on OM geochemistry, including carbon and nitrogen isotopes, Rock-Eval and palynofacies analyses, as these signals are highly affected by OM-sources and autocyclic and secondary processes (e.g., variations in intensity of the primary productivity, secondary productivity overprint, OM remineralization). Moreover, in the context of the European Permian basins, the high sedimentation rates (e.g., 300 m/Ma in the Saar-Nahe Basin, Stollhofen et al., 1999), probably linked to the dismantling of the Variscan belt, induce fast-changing depositional environments along the sedimentary sections, thus adding complexity to record and decipher long-term paleoclimate modifications.

Although the infilling of European Carboniferous to Permian basins is synchronous of the peak icehouse period of the LPIA (Crowley and Baum, 1992; Isbell et al., 2003; Montañez et al., 2007; Fielding et al., 2008; Isbell et al., 2012; Montañez and Poulsen, 2013; Soreghan et al., 2019), some of them record relatively short-term climate variations. Retallack (2013) evidenced two "greenhouse crises" during the Asselian, associated with increasing global temperatures and precipitations. Roscher and Schneider (2006) suggest wet phases during late Carboniferous and Permian in Europe, including one at the base of the Asselian, also recognized by Trümper et al. (2020) in Germany. Retallack et al. (2011) also indicate that negative $\delta^{13}C_{org}$ excursions in Australian Permian sediments are synchronous with warmer and wetter periods. In the Autun Basin, palynology analyses of Doubinger and Elsass (1975) indicate alternating wet and dry periods during the whole filling of the basin. However, these climate variations are likely occurring at longer time scale than the carbon and nitrogen isotope trends presented in our study, but it seems that some shorter-term climate modifications can also be inferred from our sedimentary successions, when 1) taking into account sequence stratigraphy features, and 2) comparing our dataset to previous studies and discussions.

In the Autun Basin, OSBs correspond to maximum flooding intervals, underpinning an increase in the relative lake level, either due to 1) a subsidence increase (i.e., tectonic-control hypothesis), or 2) wetter periods (i.e. climate-control hypothesis). Given the radiometric ages obtained for the lower Autunian in the Autun Basin by Pellenard et al. (2017), the whole studied sedimentary successions of IG-1 and CHE-1 wells necessarily correspond to a time-interval shorter than 10^6 yr, thus reflecting geochemical perturbations within a range of ~10^5 yr. As tectonic processes occur on a longer time scale (10^6–10^8 yr), the subsidence hypothesis appears unlikely, and climate forcing may thus explain part of the lake-level variations and OM-rich level deposits. Moreover, the results of cyclostratigraphy tests, notably performed on the TOC values of the CHE-1 core, show a cyclic pattern (Schnyder et al., 2020), that would suggest that the OM accumulation and the local and secondary processes may have been indirectly controlled by climate variations. Such an hypothesis is consistent with the work of Izart et al. (2012), who analyzed biomarkers in several

Carboniferous to Permian European basins, and shown that in the Autun and Saar-Nahe basins, δD values of mid- and long-chain n-alkanes coming from vascular land plants are higher than δD values of short-chain n-alkanes coming from algal OM. This pattern, also discussed in modern and recent sediments, in the Jurassic and in the late Paleozoic (Dawson et al., 2004; Sachse et al., 2004; Tramoy et al., 2016b), seems to indicate that black shales deposits would form during wetter periods occurring in an overall dry tropical, i.e., during more sustained monsoonal episodes, thus linking OM-rich deposits with wet climate episodes. A high-resolution dedicated study on deuterium isotope of biomarkers in the Autun and Decize–La Machine basins may therefore represent an interesting perspective.

CONCLUSION

This study evidences perturbations in the carbon and nitrogen cycles in the late Carboniferous to early Permian Autun and Decize–La Machine continental basins located in the eastern Pangea. These biogeochemical variations have been attributed to diverse physical and chemical lacustrine conditions in relation with depositional environments. At first order, increases in TOC and TN contents are associated with periods of enhanced OM storage in sediments during high lake level events. These events are accompanied by negative carbon-isotope excursions, and sometime positive nitrogen-isotope excursions. Long-term variations in $\delta^{13}C_{org}$ values indicate changes in OM sources to the basin through time, with very low values (~−29 to −23.5‰) associated with *in-situ* lacustrine production (autochthonous Type I OM) and higher values (~−22 to −20‰) with terrestrial input (allochthonous Type III OM). This interpretation is consistent on a regional scale (i.e., when comparing with the contemporaneous German Saar-Nahe Basin). Variations of the $\delta^{15}N_{bulk}$ signal inform on the chemical stratification of the water column, with high values reflecting denitrification or anammox processes occurring in anoxic water bodies, below a well-developed chemocline. Associated with black shale deposits, this water stratification prevents the equilibrium between the $\delta^{13}C$ of the dissolved carbon in bottom waters and the $\delta^{13}C$ of the atmospheric CO_2. This feature is due to the secondary productivity metabolisms driving the low $\delta^{13}C_{org}$ signal of anoxic sediments (probable bacterial methanogenesis and/or sulfate reduction).

Low sedimentary $\delta^{13}C_{org}$ values associated with constant $\delta^{15}N_{bulk}$ values indicate periods of high primary productivity of surface waters and spatially-decoupled nitrogen and carbon cycles (i.e., the nitrogen cycle recording the water column processes while the carbon cycle records sedimentary processes and diagenesis imprints). For more proximal environments (i.e., swamps in floodplain environments), negative $\delta^{13}C_{org}$ excursions are explained by Type III OM accumulation as coal deposits.

Finally, this work demonstrates that in lake-dominated paleoenvironments, global paleoclimate reconstructions based on organic carbon and nitrogen biogeochemical cycles can only be attempted when the OM source mixing and the secondary processes (i.e., occurring in the water column and the sediments and linked to various internal factors) are precisely determined, and that geochemically-based interpretations can help to detail or refine previous sedimentologically-based paleoenvironment reconstructions. Even if some studies indicate that negative carbon-isotope excursions can be accounted during wetter climate intervals, and therefore that the imprint of climate was probable on OM sedimentation in the Autun and Decize-La Machin basins, complementary methods should be used to deconvolute in detail the influence of OM origins and water-column reprocessing on the C and N sedimentary isotope signals, linked to local controls, from climate variations.

DATA AVAILABILITY STATEMENT

The original contributions presented in the study are included in the article/**Supplementary Material**, further inquiries can be directed to the corresponding author.

AUTHOR CONTRIBUTIONS

MM, PP, JS, FB, A-CP-W, MBu, and LG collected the samples and realized geochemical analyses with TM, AS, MBo, and TB. A-LS managed the analytical process. PS-J helped with core-drilling process. MM, CT, JS, PP, SB, LB, GG, MBu, and LG contributed to sedimentological and stratigraphical descriptions of the sections. MM and CT wrote the manuscript with inputs from all authors. All authors contributed to the interpretation of the data and approved the submitted version.

FUNDING

The sources of funding for this research are the TelluS-Syster program of the Institut National des Sciences de l'Univers (INSU-CNRS, GEOPERM project), and the French geological survey (BRGM) and the Région Bretagne (support for MM's PhD).

ACKNOWLEDGMENTS

We are grateful to the TelluS-Syster program of the Institut National des Sciences de l'Univers (INSU-CNRS, GEOPERM project), and the French geological survey (BRGM) and the Région Bretagne for financial support (MM's PhD). The authors also thank Dominique Chabard (MNHA) for the accesses to the CHE-1 core, Florence Savignac (ISTeP) for her help during the Rock-Eval analyses, Guy Barnay (SHNA), Frédéric Fluteau (IPGP, Paris, France) for assistance in the field (authorizations and drilling), and Søren Basbøll for English proofreading. The authors acknowledge J-ML and AI for their constructive reviews which have greatly improved the manuscript.

SUPPLEMENTARY MATERIAL

The Supplementary Material for this article can be found online at: https://www.frontiersin.org/articles/10.3389/feart.2021.705351/full#supplementary-material

REFERENCES

Ader, M., Sansjofre, P., Halverson, G. P., Busigny, V., Trindade, R. I. F., Kunzmann, M., et al. (2014). Ocean Redox Structure Across the Late Neoproterozoic Oxygenation Event: A Nitrogen Isotope Perspective. *Earth Planet. Sci. Lett.* 396, 1–13. doi:10.1016/j.epsl.2014.03.042

Ader, M., Thomazo, C., Sansjofre, P., Busigny, V., Papineau, D., Laffont, R., et al. (2016). Interpretation of the Nitrogen Isotopic Composition of Precambrian Sedimentary Rocks: Assumptions and Perspectives. *Chem. Geol.* 429, 93–110. doi:10.1016/j.chemgeo.2016.02.010

Ahmed, M., Volk, H., George, S. C., Faiz, M., and Stalker, L. (2009). Generation and Expulsion of Oils from Permian Coals of the Sydney Basin, Australia. *Org. Geochem.* 40, 810–831. doi:10.1016/j.orggeochem.2009.04.003

Algeo, T., Rowe, H., Hower, J. C., Schwark, L., Herrmann, A., and Heckel, P. (2008). Changes in Ocean Denitrification During Late Carboniferous Glacial-Interglacial Cycles. *Nat. Geosci.* 1, 709–714. doi:10.1038/ngeo307

Altabet, M. A., and Francois, R. (1994). Sedimentary Nitrogen Isotopic Ratio as a Recorder for Surface Ocean Nitrate Utilization. *Glob. Biogeochem. Cycles* 8, 103–116. doi:10.1029/93GB03396

Batten, D. J. (1982). Palynofacies, Palaeoenvironments and Petroleum. *J. Micropalaeontol.* 1, 107–114. doi:10.1144/jm.1.1.107

Baudin, F., Tribovillard, N., and Trichet, J. (2017). *Géologie de la matière organique*. Les Ulis: EDP Sciences.

Beauchamp, B., Oldershaw, A. E., and Krouse, H. R. (1987). Upper Carboniferous to Upper Permian 13C-Enriched Primary Carbonates in the Sverdrup basin, Canadian Arctic: Comparisons to Coeval Western North American Ocean Margins. *Chem. Geology. Isotope Geosci. section* 65, 391–413. doi:10.1016/0168-9622(87)90016-9

Beccaletto, L., Capar, L., Serrano, O., and Marc, S. (2015). Structural Evolution and Sedimentary Record of the Stephano-Permian Basins Occurring beneath the Mesozoic Sedimentary Cover in the Southwestern Paris Basin (France). *Bull. Soc. Géol. Fr.* 186, 429–450. doi:10.2113/gssgfbull.186.6.429

Becq-Giraudon, J.-F., Montenat, C., and Van Den Driessche, J. (1996). Hercynian High-Altitude Phenomena in the French Massif Central: Tectonic Implications. *Palaeogeogr. Palaeoclimatol. Palaeoecol.* 122, 227–241. doi:10.1016/0031-0182(95)00081-X

Becq-Giraudon, J.-F. (1993). Problèmes de la biostratigraphie dans le Paléozoïque supérieur continental (Stéphanien - Autunien) du Massif Central. *Geodinamica Acta* 6, 219–224. doi:10.1080/09853111.1993.11105249

Behar, F., Beaumont, V., and De B. Penteado, H. L. (2001). Rock-Eval 6 Technology: Performances and Developments. *Oil Gas Sci. Technol.* 56, 111–134. doi:10.2516/ogst:2001013

Berner, R. A. (2001). "The Effect of the Rise of Land Plants on Atmospheric CO2 During the Paleozoic," in *Plants Invade the Land: Evolutionary and Environmental Perspectives*. Editors P. G. Gensel and D. Edwards (New York, NY: Columbia University Press), 173–178.

Berner, R. A. (1989). Biogeochemical Cycles of Carbon and Sulfur and Their Effect on Atmospheric Oxygen Over Phanerozoic Time. *Glob. Planet. Change* 1, 97–122. doi:10.1016/0921-8181(89)90018-0

Berner, R. A., and Canfield, D. E. (1989). A New Model for Atmospheric Oxygen over Phanerozoic Time. *Am. J. Sci.* 289, 333–361. doi:10.2475/ajs.289.4.333

Berner, R. A., and Raiswell, R. (1983). Burial of Organic Carbon and Pyrite Sulfur in Sediments over Phanerozoic Time: a New Theory. *Geochim. Cosmochim. Acta* 47, 855–862. doi:10.1016/0016-7037(83)90151-5

Berner, R. A. (2003). The Long-Term Carbon Cycle, Fossil Fuels and Atmospheric Composition. *Nature* 426, 323–326. doi:10.1038/nature02131

Birgenheier, L. P., Frank, T. D., Fielding, C. R., and Rygel, M. C. (2010). Coupled Carbon Isotopic and Sedimentological Records from the Permian System of Eastern Australia Reveal the Response of Atmospheric Carbon Dioxide to Glacial Growth and Decay during the Late Palaeozoic Ice Age. *Palaeogeogr. Palaeoclimatol. Palaeoecol.* 286, 178–193. doi:10.1016/j.palaeo.2010.01.008

Bocherens, H., Friis, E. M., Mariotti, A., and Pedersen, K. R. (1993). Carbon Isotopic Abundances in Mesozoic and Cenozoic Fossil Plants: Palaeoecological Implications. *Lethaia* 26, 347–358. doi:10.1111/j.1502-3931.1993.tb01541.x

Bohacs, K. M., Carroll, A. R., Neal, J. E., and Mankiewicz, P. J. (2000). Lake-Basin Type, Source Potential, and Hydrocarbon Character: An Integrated Sequence-Stratigraphic-Geochemical Framework," in *Lake Basins Through Space and Time*. Editors Gierlowski-Kordesch, E. H., and Kelts, K. (American Association of Petroleum Geologists), 3–34.

Bouton, A., Vennin, E., Thomazo, C., Mathieu, O., Garcia, F., Jaubert, M., et al. (2020). Microbial Origin of the Organic Matter Preserved in the Cayo Coco Lagoonal Network, Cuba. *Minerals* 10, 143. doi:10.3390/min10020143

Broutin, J., Doubinger, J., Farjanel, G., Freytet, P., Kerp, H., Langiaux, J., et al. (1990). Le renouvellement des flores au passage Carbonifère Permien: approches stratigraphique, biologique, sédimentologique. *Comptes Rendus de l'Académie des Sci. Paris* 311, 1563–1569.

Broutin, J., Doubinger, J., Langiaux, J., and Primey, D. (1986). Conséquences de la coexistence de flores à caractères stéphaniens et autuniens dans les bassins limniques d'Europe occidentale. *Mémoires de la Société Géologique de France Nouvelle Série* 149, 15–25.

Bruckschen, P., Oesmann, S., and Veizer, J. (1999). Isotope Stratigraphy of the European Carboniferous: Proxy Signals for Ocean Chemistry, Climate and Tectonics. *Chem. Geology.* 161, 127–163. doi:10.1016/S0009-2541(99)00084-4

Burg, J. P., Brun, J. P., and Van Den Driessche, J. (1990). "Le sillon houiller du Massif Central français: faille de transfert pendant l'amincissement crustal de la chaîne," in *Comptes rendus de l'Académie des sciences. Série 2, Mécanique, Physique, Chimie, Sciences de l'univers, Sciences de la Terre*, 147–152.

Burg, J. P., van den Driessche, J., and Brun, J. P. (1994). Syn-to post-thickening Extension in the Variscan Belt of Western Europe: Modes and Structural Consequences. *Géologie de la France* 3, 33–51.

Busigny, V., Lebeau, O., Ader, M., Krapež, B., and Bekker, A. (2013). Nitrogen Cycle in the Late Archean Ferruginous Ocean. *Chem. Geol.* 362, 115–130. doi:10.1016/j.chemgeo.2013.06.023

Capone, D. G., Popa, R., Flood, B., and Nealson, K. H. (2006). GEOCHEMISTRY: Follow the Nitrogen. *Science* 312, 708–709. doi:10.1126/science.1111863

Cerling, T. E. (1999). "Paleorecords of C4 Plants and Ecosystems," in *Paleorecords of C4 Plants and Ecosystems*. Editors R. F. Sage and R. K. Monson (San Diego, CA: Academic Press), 445–469.

Choulet, F., Faure, M., Fabbri, O., and Monié, P. (2012). Relationships between Magmatism and Extension along the Autun-La Serre Fault System in the Variscan Belt of the Eastern French Massif Central. *Int. J. Earth Sci.* 101, 393–413. doi:10.1007/s00531-011-0673-z

Cleal, C. J., and Thomas, B. A. (2005). Palaeozoic Tropical Rainforests and Their Effect on Global Climates: Is the Past the Key to the Present?. *Geobiology* 3, 13–31. doi:10.1111/j.1472-4669.2005.00043.x

Combaz, A. (1964). Les Palynofaciès. *Revue de Micropaléontologie* 7, 205–218.

Crowley, T. J., and Baum, S. K. (1992). Modeling Late Paleozoic Glaciation. *Geology* 20, 507–510. doi:10.1130/0091-7613(1992)020<0507:MLPG>2.3.CO;2

Cui, Y., Bercovici, A., Yu, J., Kump, L. R., Freeman, K. H., Su, S., et al. (2017). Carbon Cycle Perturbation Expressed in Terrestrial Permian-Triassic Boundary Sections in South China. *Glob. Planet. Change* 148, 272–285. doi:10.1016/j.gloplacha.2015.10.018

Dawson, D., Grice, K., Wang, S. X., Alexander, R., and Radke, J. (2004). Stable Hydrogen Isotopic Composition of Hydrocarbons in Torbanites (Late Carboniferous to Late Permian) Deposited under Various Climatic Conditions. *Org. Geochem.* 35, 189–197. doi:10.1016/j.orggeochem.2003.09.004

Derry, L. A. (2010). On the Significance of δ13C Correlations in Ancient Sediments. *Earth Planet. Sci. Lett.* 296, 497–501. doi:10.1016/j.epsl.2010.05.035

des Marais, D. J., Strauss, H., Summons, R., and Hayes, J. M. (1992). The Proterozoic Carbon Isotopic Record of Organic Burial Rates, Changing Redox Conditions and Atmospheric CO2 Levels. Cincinnati: Geological Society of America.

Deutsch, C., Sigman, D. M., Thunell, R. C., Meckler, A. N., and Haug, G. H. (2004). Isotopic Constraints on Glacial/Interglacial Changes in the Oceanic Nitrogen Budget. *Glob. Biogeochem. Cycles* 18. doi:10.1029/2003GB002189

Domeier, M., and Torsvik, T. H. (2014). Plate Tectonics in the Late Paleozoic. *Geosci. Front.* 5, 303–350. doi:10.1016/j.gsf.2014.01.002

Doubinger, J., and Elsass, F. (1975). Nouvelles données minéralogiques et palynologiques sur les sédiments permiens du bassin d'Autun. *Bull. de la Société d'Histoire naturelle des amis du musée d'Autun* 76, 13–28.

Ducassou, C., Mercuzot, M., Bourquin, S., Rossignol, C., Pellenard, P., Beccaletto, L., et al. (2019). Sedimentology and U-Pb Dating of Carboniferous to Permian continental Series of the Northern Massif Central (France): Local Palaeogeographic Evolution and Larger Scale Correlations. *Palaeogeogr. Palaeoclimatol. Palaeoecol.* 533, 109228. doi:10.1016/j.palaeo.2019.06.001

Elsass-Damon, F. (1977). Les «schistes bitumineux» du bassin d'Autun: Pétrographie, Minéralogie, Cristallochimie, Pyrolise. Dissertation thesis. Paris (France): Université Pierre et Marie Curie.

Ertel, J. R., and Hedges, J. I. (1985). Sources of Sedimentary Humic Substances: Vascular Plant Debris. *Geochim. Cosmochim. Acta* 49, 2097–2107. doi:10.1016/0016-7037(85)90067-5

Faure, M., and Becq-Giraudon, J. F. (1993). "Sur la succession des épisodes extensifs au cours du désépaississement carbonifère du Massif central français," in *Comptes rendus de l'Académie des sciences. Série 2, Mécanique, Physique, Chimie, Sciences de l'univers, Sciences de la Terre* (Paris: Gauthier-Villars), 967–973.

Faure, M., Lardeaux, J.-M., and Ledru, P. (2009). A Review of the Pre-permian Geology of the Variscan French Massif Central. *Comptes rendus Geosci.* 341, 202–213. doi:10.1016/j.crte.2008.12.001

Faure, M. (1995). Late Orogenic Carboniferous Extensions in the Variscan French Massif Central. *Tectonics* 14, 132–153. doi:10.1029/94TC02021

Fielding, C. R., Frank, T. D., Birgenheier, L. P., Rygel, M. C., Jones, A. T., and Roberts, J. (2008). Stratigraphic Imprint of the Late Palaeozoic Ice Age in Eastern Australia: a Record of Alternating Glacial and Nonglacial Climate Regime. *J. Geol. Soc.* 165, 129–140. doi:10.1144/0016-76492007-036

Foster, G. L., Royer, D. L., and Lunt, D. J. (2017). Future Climate Forcing Potentially without Precedent in the Last 420 Million Years. *Nat. Commun.* 8, 1–8. doi:10.1038/ncomms14845

Frank, T. D., Thomas, S. G., and Fielding, C. R. (2008). On Using Carbon and Oxygen Isotope Data from Glendonites as Paleoenvironmental Proxies: a Case Study from the Permian System of Eastern Australia. *J. Sediment. Res.* 78, 713–723. doi:10.2110/jsr.2008.081

Garel, S., Behar, F., Schnyder, J., and Baudin, F. (2017). Palaeoenvironmental Control on Primary Fluids Characteristics of Lacustrine Source Rocks in the Autun Permian Basin (France). *Bull. Soc. Géol. Fr.* 188, 29. doi:10.1051/bsgf/2017187

Gastaldo, R. A., DiMichele, W. A., and Pfefferkorn, H. W. (1996). Out of the Icehouse into the Greenhouse: A Late Paleozoic Analogue for Modern Global Vegetational Change. *Gsa today* 6, 1–7.

Goddéris, Y., Donnadieu, Y., Carretier, S., Aretz, M., Dera, G., Macouin, M., et al. (2017). Onset and Ending of the Late Palaeozoic Ice Age Triggered by Tectonically Paced Rock Weathering. *Nat. Geosci.* 10, 382–386. doi:10.1038/ngeo2931

Grice, K., Nabbefeld, B., and Maslen, E. (2007). Source and Significance of Selected Polycyclic Aromatic Hydrocarbons in Sediments (Hovea-3 Well, Perth Basin, Western Australia) Spanning the Permian-Triassic Boundary. *Org. Geochem.* 38, 1795–1803. doi:10.1016/j.orggeochem.2007.07.001

Grossman, E. L., Yancey, T. E., Jones, T. E., Bruckschen, P., Chuvashov, B., Mazzullo, S. J., et al. (2008). Glaciation, Aridification, and Carbon Sequestration in the Permo-Carboniferous: The Isotopic Record from Low Latitudes. *Palaeogeogr. Palaeoclimatol. Palaeoecol.* 268, 222–233. doi:10.1016/j.palaeo.2008.03.053

Guo, H., Du, Y., Kah, L. C., Huang, J., Hu, C., Huang, H., et al. (2013). Isotopic Composition of Organic and Inorganic Carbon from the Mesoproterozoic Jixian Group, North China: Implications for Biological and Oceanic Evolution. *Precambrian Res.* 224, 169–183. doi:10.1016/j.precamres.2012.09.023

Hayes, J. M. (2001). Fractionation of Carbon and Hydrogen Isotopes in Biosynthetic Processes. *Rev. Mineral. Geochem.* 43, 225–277. doi:10.2138/gsrmg.43.1.225

Hayes, J. M. (1983). "Geochemical Evidence Bearing on the Origin of Aerobiosis, a Speculative Hypothesis," in *Earth's Earliest Biosphere: Its Origin and Evolution*. Editor J. W. Schopf (Princeton, NJ: Princeton University Press), 291–301.

Hayes, J. M., Strauss, H., and Kaufman, A. J. (1999). The Abundance of 13C in marine Organic Matter and Isotopic Fractionation in the Global Biogeochemical Cycle of Carbon during the Past 800 Ma. *Chem. Geol.* 161, 103–125. doi:10.1016/S0009-2541(99)00083-2

Hayes, J. M., Wedeking, K. W., and Kaplan, I. R. (1983). "Precambrian Organic Geochemistry-Preservation of the Record," in *Organic Geochemistry, Principles and Applications*. Editors M. H. Engel and S. A. Macko (Boston, MA: Springer), 657–684.

Herczeg, A. L., and Fairbanks, R. G. (1987). Anomalous Carbon Isotope Fractionation between Atmospheric CO2 and Dissolved Inorganic Carbon Induced by Intense Photosynthesis. *Geochim. Cosmochim. Acta* 51, 895–899. doi:10.1016/0016-7037(87)90102-5

Hoefs, J., and Frey, M. (1976). The Isotopic Composition of Carbonaceous Matter in a Metamorphic Profile from the Swiss Alps. *Geochim. Cosmochim. Acta* 40, 945–951. doi:10.1016/0016-7037(76)90143-5

Hollander, D. J., and McKenzie, J. A. (1991). CO_2 Control on Carbon-Isotope Fractionation During Aqueous Photosynthesis: A Paleo-pCO_2 Barometer. *Geology* 19, 929–932. doi:10.1130/0091-7613(1991)019%3C0929:CCOCIF%3E2.3.CO;2)

Hollander, D. J., McKenzie, J. A., Hsu, K. J., and Huc, A. Y. (1993). Application of an Eutrophic Lake Model to the Origin of Ancient Organic-Carbon-Rich Sediments. *Glob. Biogeochem. Cycles* 7, 157–179. doi:10.1029/92GB02831

Hyde, W. T., Crowley, T. J., Tarasov, L., and Peltier, W. R. (1999). The Pangean Ice Age: Studies with a Coupled Climate-Ice Sheet Model. *Clim. Dyn.* 15, 619–629. doi:10.1007/s003820050305

Isbell, J. L., Henry, L. C., Gulbranson, E. L., Limarino, C. O., Fraiser, M. L., Koch, Z. J., et al. (2012). Glacial Paradoxes During the Late Paleozoic Ice Age: Evaluating the Equilibrium Line Altitude as a Control on Glaciation. *Gondwana Res.* 22, 1–19. doi:10.1016/j.gr.2011.11.005

Isbell, J. L., Lenaker, P. A., Askin, R. A., Miller, M. F., and Babcock, L. E. (2003). Reevaluation of the Timing and Extent of Late Paleozoic Glaciation in Gondwana: Role of the Transantarctic Mountains. *Geol* 31, 977–980. doi:10.1130/G19810.1

Izart, A., Palhol, F., Gleixner, G., Elie, M., Blaise, T., Suarez-Ruiz, I., et al. (2012). Palaeoclimate Reconstruction from Biomarker Geochemistry and Stable Isotopes of n-Alkanes from Carboniferous and Early Permian Humic Coals and Limnic Sediments in Western and Eastern Europe. *Org. Geochem.* 43, 125–149. doi:10.1016/j.orggeochem.2011.10.004

Jenkyns, H. C. (2010). Geochemistry of Oceanic Anoxic Events. *Geochem. Geophys. Geosyst.* 11. doi:10.1029/2009GC002788

Johnston, D. T., Macdonald, F. A., Gill, B. C., Hoffman, P. F., and Schrag, D. P. (2012). Uncovering the Neoproterozoic Carbon Cycle. *Nature* 483, 320–323. doi:10.1038/nature10854

Kah, L. C., Sherman, A. G., Narbonne, G. M., Knoll, A. H., and Kaufman, A. J. (1999). δ13C Stratigraphy of the Proterozoic Bylot Supergroup, Baffin Island, Canada: Implications for Regional Lithostratigraphic Correlations. *Can. J. Earth Sci.* 36, 313–332. doi:10.1139/e98-100

Kashiyama, Y., Ogawa, N. O., Kuroda, J., Shiro, M., Nomoto, S., Tada, R., et al. (2008). Diazotrophic Cyanobacteria as the Major Photoautotrophs during Mid-cretaceous Oceanic Anoxic Events: Nitrogen and Carbon Isotopic Evidence from Sedimentary Porphyrin. *Org. Geochem.* 39, 532–549. doi:10.1016/j.orggeochem.2007.11.010

Klemme, H. D., and Ulmishek, G. F. (1991). Effective Petroleum Source Rocks of the World: Stratigraphic Distribution and Controlling Depositional Factors. *AAPG Bull.* 75, 1809–1851. doi:10.1306/0C9B2A47-1710-11D7-8645000102C1865D

Kump, L. R., and Arthur, M. A. (1999). Interpreting Carbon-Isotope Excursions: Carbonates and Organic Matter. *Chem. Geol.* 161, 181–198. doi:10.1016/S0009-2541(99)00086-8

Kuypers, M. M. M., Pancost, R. D., and Damsté, J. S. S. (1999). A Large and Abrupt Fall in Atmospheric CO2 Concentration during Cretaceous Times. *Nature* 399, 342–345. doi:10.1038/20659

Lamb, A. L., Leng, M. J., Umer Mohammed, M., and Lamb, H. F. (2004). Holocene Climate and Vegetation Change in the Main Ethiopian Rift Valley, Inferred from the Composition (C/N and δ13C) of Lacustrine Organic Matter. *Quat. Sci. Rev.* 23, 881–891. doi:10.1016/j.quascirev.2003.06.010

Lamb, A. L., Wilson, G. P., and Leng, M. J. (2006). A Review of Coastal Palaeoclimate and Relative Sea-Level Reconstructions Using δ13C and C/N Ratios in Organic Material. *Earth Sci. Rev.* 75, 29–57. doi:10.1016/j.earscirev.2005.10.003

Lehmann, M. F., Bernasconi, S. M., Barbieri, A., and McKenzie, J. A. (2002). Preservation of Organic Matter and Alteration of its Carbon and Nitrogen Isotope Composition during Simulated and *In Situ* Early Sedimentary Diagenesis. *Geochim. Cosmochim. Acta* 66, 3573–3584. doi:10.1016/S0016-7037(02)00968-7

Liu, C., Du, Y., Jarochowska, E., Yan, J., Munnecke, A., and Lu, G. (2018). A Major Anomaly in the Carbon Cycle during the Late Cisuralian (Permian): Timing, Underlying Triggers and Implications. *Palaeogeogr. Palaeoclimatol. Palaeoecol.* 491, 112–122. doi:10.1016/j.palaeo.2017.11.061

Liu, C., Jarochowska, E., Du, Y., Vachard, D., and Munnecke, A. (2017). Stratigraphical and δ13C Records of Permo-Carboniferous Platform Carbonates, South China: Responses to Late Paleozoic Icehouse Climate and Icehouse-Greenhouse Transition. *Palaeogeogr. Palaeoclimatol. Palaeoecol.* 474, 113–129. doi:10.1016/j.palaeo.2016.07.038

Malavieille, J., Guihot, P., Costa, S., Lardeaux, J. M., and Gardien, V. (1990). Collapse of the Thickened Variscan Crust in the French Massif Central: Mont Pilat Extensional Shear Zone and St. Etienne Late Carboniferous basin. *Tectonophysics* 177, 139–149. doi:10.1016/0040-1951(90)90278-G

Marteau, P. (1983). Le bassin permo-carbonifère d'Autun: stratigraphie, sédimentologie et aspects structuraux. Dissertation thesis. Dijon (France): Université de Bourgogne.

Mayer, B., and Schwark, L. (1999). A 15,000-Year Stable Isotope Record from Sediments of Lake Steisslingen, Southwest Germany. *Chem. Geol.* 161, 315–337. doi:10.1016/S0009-2541(99)00093-5

Maynard, J. R., Hofmann, W., Dunay, R. E., Benthan, P. N., Dean, K. P., and Watson, I. (1997). The Carboniferous of Western Europe; the Development of a Petroleum System. *Pet. Geosci.* 3, 97–115. doi:10.1144/petgeo.3.2.97

McArthur, A. D., Kneller, B. C., Wakefield, M. I., Souza, P. A., and Kuchle, J. (2016). Palynofacies Classification of the Depositional Elements of Confined Turbidite Systems: Examples from the Gres d'Annot, SE France. *Mar. Pet. Geol.* 77, 1254–1273. doi:10.1016/j.marpetgeo.2016.08.020

Ménard, G., and Molnar, P. (1988). Collapse of a Hercynian Tibetan Plateau into a Late Palaeozoic European Basin and Range Province. *Nature* 334, 235–237. doi:10.1038/334235a0

Mercuzot, M., Bourquin, S., Beccaletto, L., Ducassou, C., Rubi, R., and Pellenard, P. (2021). Palaeoenvironmental Reconstitutions at the Carboniferous-Permian Transition South of the Paris Basin, France: Implications on the Stratigraphic Evolution and basin Geometry. *Int. J. Earth Sci.* 110, 9–33. doi:10.1007/s00531-020-01940-7

Meyers, P. A. (2003). Applications of Organic Geochemistry to Paleolimnological Reconstructions: A Summary of Examples from the Laurentian Great Lakes. *Org. Geochem.* 34, 261–289. doi:10.1016/S0146-6380(02)00168-7

Meyers, P. A., and Ishiwatari, R. (1993). Lacustrine Organic Geochemistry-An Overview of Indicators of Organic Matter Sources and Diagenesis in lake Sediments. *Org. Geochem.* 20, 867–900. doi:10.1016/0146-6380(93)90100-P

Meyers, P. A., and Ishiwatari, R. (1995). "Organic Matter Accumulation Records in Lake Sediments," in *Physics and Chemistry of Lakes*. Editors A. Lerman, D. Imboden, and J. Gat (Berlin, Germany: Springer), 279–328.

Meyers, P. A. (1994). Preservation of Elemental and Isotopic Source Identification of Sedimentary Organic Matter. *Chem. Geol.* 114, 289–302. doi:10.1016/0009-2541(94)90059-0

Meyers, P. A., and Teranes, J. L. (2001). "Sediment Organic Matter," in *Tracking Environmental Change Using Lake Sediments 2: Physical and Geochemical Methods*. Editors W. M. Last and J. P. Smol (Dordrecht, Netherlands: Kluwer Academic Publishers), 239–269.

Meyers, P. A. (2014). Why are the δ13Corgvalues in Phanerozoic Black Shales More Negative Than in Modern marine Organic Matter?. *Geochem. Geophys. Geosyst.* 15, 3085–3106. doi:10.1002/2014GC005305

Mii, H.-S., Grossman, E. L., Yancey, T. E., Chuvashov, B., and Egorov, A. (2001). Isotopic Records of Brachiopod Shells from the Russian Platform - Evidence for the Onset of Mid-carboniferous Glaciation. *Chem. Geol.* 175, 133–147. doi:10.1016/S0009-2541(00)00366-1

Mii, H. S., Grossman, E. L., and Yancey, T. E. (1999). Carboniferous Isotope Stratigraphies of North America: Implications for Carboniferous Paleoceanography and Mississippian Glaciation. *Geol. Soc. Am. Bull.* 111, 960–973. doi:10.1130/0016-7606(1999)111<0960:CISONA>2.3.CO;2

Monin, J. C., Boudou, J. P., Durand, B., and Oudin, J. L. (1981). Example of the Enrichment of Carbon-13 in Coals in the Process of Coalification. *Fuel* 60, 957–960. doi:10.1016/0016-2361(81)90091-0

Montañez, I. P. (2016). A Late Paleozoic Climate Window of Opportunity. *Proc. Natl. Acad. Sci. USA* 113, 2334–2336. doi:10.1073/pnas.1600236113

Montañez, I. P., and Poulsen, C. J. (2013). The Late Paleozoic Ice Age: an Evolving Paradigm. *Annu. Rev. Earth Planet. Sci.* 41, 629–656. doi:10.1146/annurev.earth.031208.100118

Montañez, I. P., Tabor, N. J., Niemeier, D., DiMichele, W. A., Frank, T. D., Fielding, C. R., et al. (2007). CO2-forced Climate and Vegetation Instability during Late Paleozoic Deglaciation. *Science* 315, 87–91. doi:10.1126/science.1134207

Müller, A. B., Strauss, H., Hartkopf-Fröder, C., and Littke, R. (2006). Reconstructing the Evolution of the Latest Pennsylvanian-Earliest Permian Lake Odernheim Based on Stable Isotope Geochemistry and Palynofacies: A Case Study from the Saar-Nahe Basin, Germany. *Palaeogeogr. Palaeoclimatol. Palaeoecol.* 240, 204–224. doi:10.1016/j.palaeo.2006.03.049

Nordt, L., Tubbs, J., and Dworkin, S. (2016). Stable Carbon Isotope Record of Terrestrial Organic Materials for the Last 450 Ma yr. *Earth Sci. Rev.* 159, 103–117. doi:10.1016/j.earscirev.2016.05.007

Opdyke, N. D., Mushayandebvu, M., and De Wit, M. J. (2001). A New Palæomagnetic Pole for the Dwyka System and Correlative Sediments in Sub-saharan Africa. *J. Afr. Earth Sci.* 33, 143–153. doi:10.1016/S0899-5362(01)90095-8

Pellenard, P., Gand, G., Schmitz, M., Galtier, J., Broutin, J., and Stéyer, J.-S. (2017). High-precision U-Pb Zircon Ages for Explosive Volcanism Calibrating the NW European Continental Autunian Stratotype. *Gondwana Res.* 51, 118–136. doi:10.1016/j.gr.2017.07.014

Peters, K. E., Sweeney, R. E., and Kaplan, I. R. (1978). Correlation of Carbon and Nitrogen Stable Isotope Ratios in Sedimentary Organic Matter 1. *Limnol. Oceanogr.* 23, 598–604. doi:10.4319/lo.1978.23.4.0598

Peters-Kottig, W., Strauss, H., and Kerp, H. (2006). The Land Plant δ13C Record and Plant Evolution in the Late Palaeozoic. *Palaeogeogr. Palaeoclimatol. Palaeoecol.* 240, 237–252. doi:10.1016/j.palaeo.2006.03.051

Powell, C. M., and Veevers, J. J. (1987). Namurian Uplift in Australia and South America Triggered the Main Gondwanan Glaciation. *Nature* 326, 177–179. doi:10.1038/326177a0

Prokopenko, M. G., Hammond, D. E., and Stott, L. (2006). Lack of Isotopic Fractionation of $\delta^{15}N$ of Organic Matter During Long-Term Diagenesis in marine Sediments, ODP Leg 202, Sites 1234 and 1235. *Proc. Ocean Drill. Program Sci. Results* 202..

Ramaswamy, V., Gaye, B., Shirodkar, P. V., Rao, P. S., Chivas, A. R., Wheeler, D., et al. (2008). Distribution and Sources of Organic Carbon, Nitrogen and Their Isotopic Signatures in Sediments from the Ayeyarwady (Irrawaddy) continental Shelf, Northern Andaman Sea. *Mar. Chem.* 111, 137–150. doi:10.1016/j.marchem.2008.04.006

Retallack, G. J. (2013). Permian and Triassic Greenhouse Crises. *Gondwana Res.* 24, 90–103. doi:10.1016/j.gr.2012.03.003

Retallack, G. J., Sheldon, N. D., Carr, P. F., Fanning, M., Thompson, C. A., Williams, M. L., et al. (2011). Multiple Early Triassic Greenhouse Crises Impeded Recovery from Late Permian Mass extinctionHydrogen Isotope Ratios of Recent Lacustrine Sedimentary n-Alkanes Record Modern Climate Variability. *Palaeogeogr. Palaeoclimatol. Palaeoecol.* 308, 233–251. doi:10.1016/j.palaeo.2010.09.022

Roscher, M., and Schneider, J. W. (2006). Permo-Carboniferous Climate: Early Pennsylvanian to Late Permian Climate Development of Central Europe in a Regional and Global Context. *Geol. Soc. Spec. Publ.* 265, 95–136. doi:10.1144/GSL.SP.2006.265.01.05

Sachse, D., Radke, J., and Gleixner, G. (2004). Hydrogen Isotope Ratios of Recent Lacustrine Sedimentary n-1137 Alkanes Record Modern Climate Variability. *Geochim. Cosmochim. Acta* 68, 4877–4889. doi:10.1016/j.gca.2004.06.004

Sage, R. F. (2004). The Evolution of C4photosynthesis. *New Phytol.* 161, 341–370. doi:10.1111/j.1469-8137.2004.00974.x

Saltzman, M., Groessens, E., and Zhuravlev, A. (2004). Carbon Cycle Models Based on Extreme Changes in δ13C: An Example from the Lower Mississippian. *Palaeogeogr. Palaeoclimatol. Palaeoecol.* 213, 359–377. doi:10.1016/j.palaeo.2004.07.01910.1016/s0031-0182(04)00389-x

Saltzman, M. R. (2005). Phosphorus, Nitrogen, and the Redox Evolution of the Paleozoic Oceans. *Geology* 33, 573–576. doi:10.1130/G21535.1

Schidlowski, M., Hayes, J. M., and Kaplan, I. R. (1983). "Isotopic Inferences of Ancient Biochemistries-Carbon, Sulfur, Hydrogen, and Nitrogen," in *Earth's Earliest Biosphere: Its Origin and Evolution*. Editors J. W. Schopf (Princeton, NJ: Princeton University Press), 149–186.

Schnyder, J., Dejax, J., Keppens, E., Nguyen Tu, T. T., Spagna, P., Boulila, S., et al. (2009). An Early Cretaceous Lacustrine Record: Organic Matter and Organic Carbon Isotopes at Bernissart (Mons Basin, Belgium). *Palaeogeogr. Palaeoclimatol. Palaeoecol.* 281, 79–91. doi:10.1016/j.palaeo.2009.07.014

Schnyder, J., Martinez, M., Baudin, F., Mercuzot, M., Pellenard, P., Thomazo, C., et al. (2020). *Long-Term Lacustrine Paleo-Productivity And/or Paleo-Anoxia Trends Controlled by Eccentricity Cycles in the continental Autun Basin (France) at the Carboniferous/Permian Boundary*, Vienna.

Schnyder, J., Stetten, E., Baudin, F., Pruski, A. M., and Martinez, P. (2017). Palynofacies Reveal Fresh Terrestrial Organic Matter Inputs in the Terminal Lobes of the Congo Deep-Sea Fan. *Deep Sea Res. Part Top. Stud. Oceanogr.* 142, 91–108. doi:10.1016/j.dsr2.2017.05.008

Schubert, C. J., and Calvert, S. E. (2001). Nitrogen and Carbon Isotopic Composition of marine and Terrestrial Organic Matter in Arctic Ocean Sediments:. *Deep Sea Res. Oceanographic Res. Pap.* 48, 789–810. doi:10.1016/S0967-0637(00)00069-8

Schwarzbauer, J., and Jovančićević, B. (2015). *Fundamentals in Organic Geochemistry – Fossil Matter in the Geosphere*. Cham, CH: Springer.

Scotese, C. R. (2016). PALEOMAP PaleoAtlas for GPlates and the PaleoData Plotter Program, PALEOMAP Project. Available at: http://www.earthbyte.org/paleomap-paleoatlas-for-gplates (Accessed June 17, 2021).

Sephton, M. A., Amor, K., Franchi, I. A., Wignall, P. B., Newton, R., and Zonneveld, J. P. (2002). Carbon and Nitrogen Isotope Disturbances and an End-Norian (Late Triassic) Extinction Event. *Geology* 30, 1119–1122. doi:10.1130/0091-7613(2002)030%3C1119:CANIDA%3E2.0.CO;2

Sigman, D. M., Karsh, K. L., and Casciotti, K. L. (2009). "Ocean Process Tracers: Nitrogen Isotopes in the Ocean," in *Encyclopedia of Ocean Sciences*. Editor J. H. Steele (London, Elsevier Ltd), 40–54.

Soreghan, G. S., Soreghan, M. J., and Heavens, N. G. (2019). Explosive Volcanism as a Key Driver of the Late Paleozoic Ice Age. *Geology* 47, 600–604. doi:10.1130/G46349.1

Steffen, D., and Gorin, G. E. (1993). "Sedimentology of Organic Matter in Upper Tithonian-Berriasian Deep-Sea Carbonates of Southeast France: Evidence of Eustatic Control," in *Source Rocks in a Sequence Stratigraphic Framework*. Editors B. J. Katz and L. M. Pratt (Tulsa, OK: AAPG Studies on Geology), 49–65.

Stollhofen, H., Frommherz, B., and Stanistreet, I. G. (1999). Volcanic Rocks as Discriminants in Evaluating Tectonic versus Climatic Control on Depositional Sequences, Permo-Carboniferous continental Saar-Nahe Basin. *J. Geol. Soc.* 156, 801–808. doi:10.1144/gsjgs.156.4.0801

Strauss, H., Des Marais, D. J., Hayes, J. M., and Summons, R. E. (1992). "Proterozoic Organic Carbon—Its Preservation and Isotopic Record," in *Early Organic Evolution*. Editor M. Schidlowski, S. Golubic, M. M. Kimberley, D. M. McKirdy, and P. A. Trudinger (Berlin: Springer), 203–211. doi:10.1007/978-3-642-76884-2_14

Strauss, H., and Peters-Kottig, W. (2003). The Paleozoic to Mesozoic Carbon Cycle Revisited: The Carbon Isotopic Composition of Terrestrial Organic Matter. *Geochem. Geophys. Geosyst.* 4, 1083. doi:10.1029/2003GC000555

Thomasson, J. R., Nelson, M. E., and Zakrzewski, R. J. (1986). A Fossil Grass (Gramineae: Chloridoideae) from the Miocene with Kranz Anatomy. *Science* 233, 876–878. doi:10.1126/science.233.4766.876

Thomazo, C., Pinti, D. L., Busigny, V., Ader, M., Hashizume, K., and Philippot, P. (2009). Biological Activity and the Earth's Surface Evolution: Insights from Carbon, Sulfur, Nitrogen and Iron Stable Isotopes in the Rock Record. *Comptes Rendus Palevol* 8, 665–678. doi:10.1016/j.crpv.2009.02.003

Tocqué, E., Behar, F., Budzinski, H., and Lorant, F. (2005). Carbon Isotopic Balance of Kerogen Pyrolysis Effluents in a Closed System. *Org. Geochem.* 36, 893–905. doi:10.1016/j.orggeochem.2005.01.007

Tramoy, R., Salpin, M., Schnyder, J., Person, A., Sebilo, M., Yans, J., et al. (2016b). Stepwise Palaeoclimate Change across the Eocene–Oligocene Transition Recorded in continental NW Europe by Mineralogical Assemblages and $\delta^{15}N_{org}$ (Rennes Basin, France). *Terra Nova* 28, 212–220. doi:10.1111/ter.12212

Tramoy, R., Schnyder, J., Nguyen Tu, T. T., Yans, J., Jacob, J., Sebilo, M., et al. (2016a). The Pliensbachian-Toarcian Paleoclimate Transition: New Insights from Organic Geochemistry and C, H, N Isotopes in a continental Section from Central Asia. *Palaeogeogr. Palaeoclimatol. Palaeoecol.* 461, 310–327. doi:10.1016/j.palaeo.2016.08.020

Trümper, S., Germann, S., Schneider, J. W., Mertmann, D., Götze, J., and Rößler, R. (2020). Petrified Trees of the Kyffhäuser (Pennsylvanian, Thuringia): Growth Habitat, Fossilisation and Palaeoclimatic-Palaeoecological Implications. *Zeitschrift der Dtsch. Gesellschaft fur Geowissenschaften.* 171, 277–321. doi:10.1127/zdgg/2020/0238

Tyson, R. V. (1995). Palynological Kerogen Classification. *Sediment. Org. Matter* 341–365. doi:10.1007/978-94-011-0739-6_20

Valle, B., Courel, L., and Gelard, J. P. (1988). Les Marqueurs de la tectonique synsedimentaire et syndiagenetique dans le bassin stephanien a regime cisaillant de Blanzy-Montceau (Massif Central, France). *Bull. Soc. Géol. Fr.* 4, 529–540. doi:10.2113/gssgfbull.iv.4.529

Van Den Driessche, J., and Brun, J.-P. (1992). Tectonic Evolution of the Montagne Noire (French Massif Central): A Model of Extensional Gneiss Dome. *Geodinamica Acta* 5, 85–97. doi:10.1080/09853111.1992.11105221

Van Den Driessche, J., and Brun, J. P. (1989). "Un modèle cinématique de l'extension paléozoïque supérieur dans le Sud du Massif Central," in *Comptes rendus de l'Académie des sciences. Série 2, Mécanique, Physique, Chimie, Sciences de l'univers, Sciences de la Terre*. 1607–1613.

Van Mooy, B. A. S., Keil, R. G., and Devol, A. H. (2002). Impact of Suboxia on Sinking Particulate Organic Carbon: Enhanced Carbon Flux and Preferential Degradation of Amino Acids via Denitrification. *Geochim. Cosmochim. Acta* 66, 457–465. doi:10.1016/S0016-7037(01)00787-6

Veevers, J. J. (1994). "Pangea: Evolution of a Supercontinent and its Consequences for Earth's Paleoclimate and Sedimentary Environments," in *Pangea: Paleoclimate, Tectonics, and Sedimentation during Accretion, Zenith, and Breakup of a Supercontinent*. Editor G. O. Klein (Boulder, CO: Geological Society of America Special Paper 288), 13–24.

Wang, W., Guan, C., Zhou, C., Peng, Y., Pratt, L. M., Chen, X., et al. (2017). Integrated Carbon, Sulfur, and Nitrogen Isotope Chemostratigraphy of the Ediacaran Lantian Formation in South China: Spatial Gradient, Ocean Redox Oscillation, and Fossil Distribution. *Geobiology* 15, 552–571. doi:10.1111/gbi.12226

Yans, J., Gerards, T., Gerrienne, P., Spagna, P., Dejax, J., Schnyder, J., et al. (2010). Carbon-Isotope Analysis of Fossil wood and Dispersed Organic Matter from the Terrestrial Wealden Facies of Hautrage (Mons Basin, Belgium). *Palaeogeogr. Palaeoclimatol. Palaeoecol.* 291, 85–105. doi:10.1016/j.palaeo.2010.01.014

Conflict of Interest: The authors declare that the research was conducted in the absence of any commercial or financial relationships that could be construed as a potential conflict of interest.

frontiers in Earth Science

ORIGINAL RESEARCH
published: 03 August 2021
doi: 10.3389/feart.2021.692895

The Nitrogen Cycle in an Epeiric Sea in the Core of Gondwana Supercontinent: A Study on the Ediacaran-Cambrian Bambuí Group, East-central Brazil

Paula Luiza Fraga-Ferreira[1], Magali Ader[2], Sérgio Caetano-Filho[1], Pierre Sansjofre[3], Gustavo Macedo Paula-Santos[4], Marly Babinski[1], Cristian Guacaneme[1], Carolina Bedoya-Rueda[1], Virginia Rojas[2], Humberto L. S. Reis[5], Matheus Kuchenbecker[6] and Ricardo I. F. Trindade[7]*

[1]Instituto de Geociências, Universidade de São Paulo, São Paulo, Brazil, [2]Université de Paris, Institut de Physique du Globe de Paris, CNRS, Paris, France, [3]Institut de Minéralogie, de Physique des Matériaux et de Cosmochimie, MNHN, Sorbonne Université, Paris, France, [4]MARUM – Center for Marine Environmental Sciences, University of Bremen, Bremen, Germany, [5]Laboratório de Modelagem Tectônica, Departamento de Geologia, Universidade Federal de Ouro Preto, Ouro Preto, Brazil, [6]Laboratório de Estudos Tectônicos, Centro de Estudos em Geociências, Instituto de Ciência e Tecnologia, Universidade Federal do Vale do Jequitinhonha e Mucuri, Diamantina, Brazil, [7]Instituto de Astronomia, Geofísica e Ciências Atmosféricas, Universidade de São Paulo, São Paulo, Brazil

OPEN ACCESS

Edited by:
Graham Shields,
University College London,
United Kingdom

Reviewed by:
Xinqiang Wang,
China University of Geosciences,
China
Fabricio Caxito,
Federal University of Minas Gerais,
Brazil

***Correspondence:**
Paula Luiza Fraga-Ferreira
paulafraga@usp.br

Specialty section:
This article was submitted to Geochemistry, a section of the journal Frontiers in Earth Science

Received: 09 April 2021
Accepted: 26 July 2021
Published: 03 August 2021

Citation:
Fraga-Ferreira PL, Ader M, Caetano-Filho S, Sansjofre P, Paula-Santos GM, Babinski M, Guacaneme C, Bedoya-Rueda C, Rojas V, Reis HLS, Kuchenbecker M and Trindade RIF (2021) The Nitrogen Cycle in an Epeiric Sea in the Core of Gondwana Supercontinent: A Study on the Ediacaran-Cambrian Bambuí Group, East-central Brazil. Front. Earth Sci. 9:692895. doi: 10.3389/feart.2021.692895

The Ediacaran-Cambrian transition is marked by the diversification of metazoans in the marine realm. However, this is not recorded by the Ediacaran-Cambrian Bambuí Group of the São Francisco basin, Brazil. Containing the sedimentary record of a partially confined foreland basin system, the Bambuí strata bear rare metazoan remnants and a major carbon isotope positive excursion decoupled from the global record. This has been explained by changes in the paleogeography of the basin, which became a restricted epicontinental sea in the core of the Gondwana supercontinent, promoting episodes of shallow water anoxia. Here, we report new $\delta^{15}N_{bulk}$ data from the two lowermost second-order transgressive-regressive sequences of the Bambuí Group. The results show a rise of $\delta^{15}N$ values from +2 to +5‰ in the transgressive system tract of the basal sequence, which was deposited when the basin was connected to other marginal seas. Such excursion is interpreted as an oxygenation event in the Bambuí sea. Above, in the regressive systems tract, $\delta^{15}N$ values vary from +2 to +5‰, pointing to instabilities in the N-cyle that are concomitant with the onset of basin restrictions, higher sedimentary supply/accommodation ratios, and the episodic anoxia. In the transgressive systems tract, the $\delta^{15}N$ values stabilise at ~+3.5‰, pointing to the establishment of an appreciable nitrate pool in shallow waters in spite of the basin full restriction as marked by the onset of a positive carbon isotope excursion. In sum, our data show that the N-cycle and its fluctuations were associated with variations in sedimentary supply/accommodation ratios induced by tectonically-related paleogeographic changes. The instability of the N-cycle and redox conditions plus the scarcity of nitrate along regression episodes might have hindered the development of early benthic metazoans within the Bambuí seawater

and probably within other epicontinental seas during the late Ediacaran-Cambrian transition.

Keywords: nitrogen isotopes, paleoenviroments, Bambuí Group, Ediacaran-Cambrian, epeiric sea, chemostratigraphy

INTRODUCTION

Nitrogen (N) has two stable isotopes, ^{14}N and ^{15}N, and they occur in a proportion of 99.633 and 0.337%, respectively (Meija et al., 2016). Due to its abundance, ability to build chemical bonds with carbon, and to join redox reactions when it is dissolved in liquid water, nitrogen is an important component in Earth's life system (Stüeken et al., 2016). In seawater, N is found mostly as N_2 (di-nitrogen), NO_2^- (nitrite), NO_3^- (nitrate), NH_4^+ (ammonium) and N_{org} (dissolved or particulate organic nitrogen) (Thomazo et al., 2011) depending on the redox structure of the water column, which controls most of the reactions operating the N-biogeochemical cycle. These reactions impart nitrogen isotope fractionation, hence, they also control the nitrogen isotope composition of these nitrogen species. Based on the study of modern systems, it is commonly assumed that the measured $\delta^{15}N$ of a rock/sediment reflects the isotopic signature of primary producers (i.e. superficial waters) which itself reflects the $\delta^{15}N$ of the N species they have assimilated (*see* review in Ader et al., 2016). Hence, $\delta^{15}N$ in past sedimentary rocks enables to obtain valuable information about changes in both redox structure of ancient water bodies (e.g., Godfrey and Falkowski, 2009; Quan et al., 2013; Ader et al., 2014; Wang et al., 2015; Chen et al., 2019) and past N-biogeochemical cycle paths (e.g., Cremonese et al., 2013; Stüeken et al., 2015; Cox et al., 2019; Sun et al., 2019; Xu et al., 2020).

To understand the biogeochemical cycle of nitrogen in the past, it is important to understand how it operates now, since, even if not accurate, our knowledge of the modern N cycle is used as the basis of comparison to understand ancient systems. When they are not completed, the reactions of this cycle produce isotopic fractionation ($\varepsilon = \delta^{15}N_{product} - \delta^{15}N_{reactant}$) and the modern biogeochemical cycle of N in the oceans operates as follows (**Figure 1**):

i) Nitrogen enters the ocean when N_2 is fixed by bacteria and archaea, the diazotrophs (ε = −7 to +1‰, Zhang et al., 2014; Sigman and Fripiat, 2019). Subsequently, N_2 is converted to a biologically available form of N, the NH_3 gas, which is quickly converted to the soluble NH_4^+ (Glass et al., 2009). The fractionation on this step depends strongly on which cofactor is used by the nitrogenase enzyme. Mo-based nitrogenase imparts a small fractionation (−2 to +1‰), while Fe or V-based ones lead to a much larger isotopic differentiation, reaching values as low as −7‰ (Zhang et al., 2014).

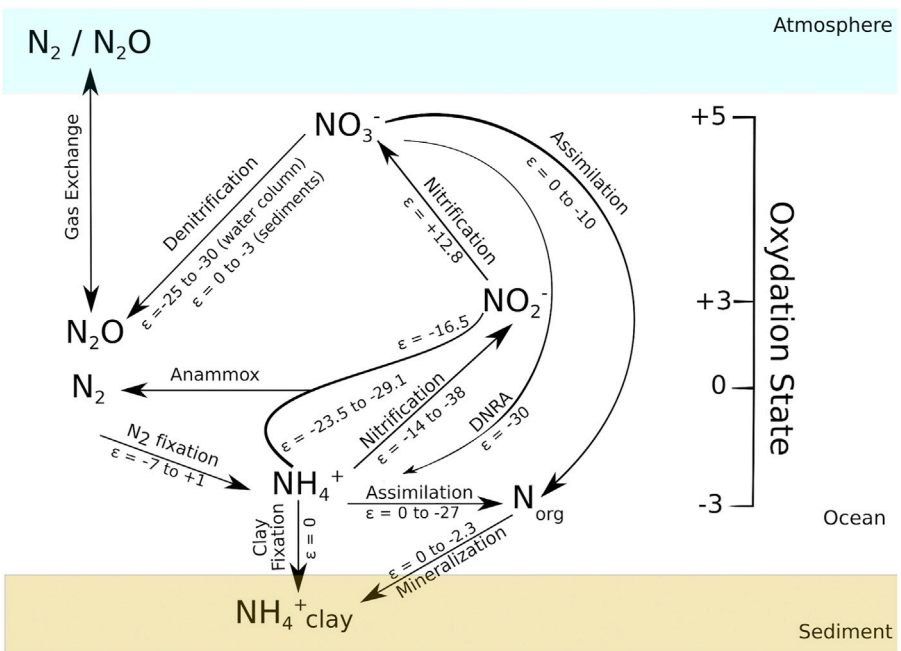

FIGURE 1 | Schematic diagram of the modern marine nitrogen cycle. Oxidation state of nitrogen species is shown on the vertical axis going from −3 (NH_4^+) to +5 (NO_3^-). Nitrogen isotopic fractionation of the pathways of the N-cycle are detailed in the text and are expressed in ‰. Modified after Ader et al. (2016).

ii) During organic matter mineralization, N_{org} is converted into NH_4^+ (ε = 0 to −2.3‰, Möbius, 2013). This NH_4^+ can be fixed into clays (ε = 0, Ader et al., 2016), since its ionic radius is similar to the potassium one (Müller, 1977; Greenfield, 1992) or it can be assimilated by organisms (ε = 0 to −27‰, Hoch et al., 1992; Pennock et al., 1996; Liu et al., 2013). NH_4^+ can also be nitrified, i.e. NH_4^+ is oxidized to NO_2^- (ε = −14 to −38‰, Casciotti, 2009) and NO_2^- is rapidly oxidized to NO_3^- (ε = +12.8‰, Casciotti, 2009). Finally, NH_4^+ can contribute to the loss of fixed N in the ocean in a process called anammox, in which NO_2^- is used to oxidize NH_4^+, generating N_2 (ε = −23.5 to −29.1‰ for $\varepsilon_{NH_4^+ - N_2}$ and ε = −16.5‰ for $\varepsilon_{NO_2^- - N_2}$, Brunner et al., 2013).

iii) Denitrification (ε = −25 to −30‰ in the water column and 0 to −3‰ in sediments, Granger et al., 2008; Casciotti, 2009; Kessler et al., 2014), the conversion of NO_3^- to N_2/N_2O, is the major sink of fixed N in modern oceans. It occurs in the sediments and in the water column where oxygen levels are low. The remarkable difference in the fractionation of N in the two environments where the process happens is explained by the fact that in sediment pore waters nitrate is almost fully consumed, leading to a small fractionation (Sigman and Fripiat, 2019). NO_3^- is an important nutrient, accounting for most of the fixed N in marine ecosystems. When it is assimilated by microorganisms (ε = 0 to −10‰, Casciotti, 2009; Granger et al., 2010) its fractionation depends on the abundance of the species, the scarcer is the nutrient, the closer to 0‰ the kinetic isotopic effect is (Fogel and Cifuentes, 1993).

iv) The direct conversion of NO_3^- to NH_4^+, known as dissimilatory nitrate reduction to ammonium (DNRA). Although the isotopic effect of this process is not very well known, it can account for fractionations larger than −30‰ (McCready et al., 1983).

Many sedimentary basins worldwide record the transition from the Ediacaran to Cambrian with a rich fossil assemblage, however this does not happen in the Bambuí Group, east-central Brazil, which is almost fossil-barren. This Neoproterozoic unit is situated in the São Francisco Craton and was deposited in a foreland basin, which was generated in response to the uplift of the Brasília and Aracuaí belts (Reis et al., 2017). The Bambuí Group encompasses carbonates and siliciclastic rocks that were deposited above glaciogenic units (Alkmim and Martins-Neto, 2001, 2012; Martins-Neto and Hercos, 2002; Martins-Neto, 2009; Reis and Alkmim, 2015) and lately, it has been a matter of intense research regarding the conditions that could have prevented the Ediacaran fauna to thrive at the core of West Gondwana (e.g., Paula-Santos et al., 2017, 2020; Uhlein et al., 2017, 2019; Okubo et al., 2018, 2020; Paula-Santos and Babinski, 2018; Caetano-Filho et al., 2019, 2021; Crockford et al., 2019). Geochronological and chemostratigraphic data suggest that the Bambuí evolved from a sea connected to the global ocean to a fully restricted environment (Paula-Santos et al., 2015, 2017), which might have influenced its paleoenvironmental conditions, leading to very high $\delta^{13}C_{carb}$ values (Iyer et al., 1995; Martins and Lemos, 2007; Kuchenbecker et al., 2016b; Guacaneme et al., 2017; Caetano-Filho et al., 2019; Uhlein et al., 2019) and anoxia (Paula-Santos et al., 2017; Hippertt et al., 2019; Uhlein et al., 2019). These in turn may have prevented complex life forms to thrive (Hippertt et al., 2019). Further knowledge on the interplay between the redox state of Bambuí seawater and the biological metabolic paths could help understanding the limiting conditions for life during the Ediacaran-Cambrian boundary, and thus on the comprehension of how life may have progressed to more complex forms at that period. Aiming to contribute to this debate, we present a new redox proxy on the Bambuí Group sediments: nitrogen isotopic composition ($\delta^{15}N$). The nature of $\delta^{15}N$ data have the potential to provide important information on the Bambuí seawater chemistry, its redox state and prevailing metabolisms.

GEOLOGICAL SETTING

The São Francisco Basin and the Bambuí Group

The São Francisco Basin (SFB) is a long-lasting sedimentary locus in east-central Brazil, whose records cover a large area (~350.000 km^2) of the São Francisco craton (**Figure 2**). This intracratonic basin encompasses many first order sedimentary cycles younger than 1.8 Ga, which record important tectonic and climate events (Reis et al., 2017). The basement of SFB present three main structural domains: two structural highs, named Januária (north) and Sete Lagoas (south) highs, separated by a deep NW-trending aulacogen, called Pirapora aulacogen. During the Neoproterozoic-Phanerozoic transition, the SFB hosted a complex foreland system, which evolved in response to the growth of the Brasília and Araçuaí orogens around the São Francisco craton in the context of the Gondwana supercontinent assembly (e.g. Alkmim and Martins Neto, 2001; Martins-Neto, 2009; Reis and Suss, 2016; Reis et al., 2017; Uhlein et al., 2017; Kuchenbecker et al., 2020). The records of such important foreland system are encompassed in the Bambuí Group, which cover a large area of the São Francisco basin, presenting mostly carbonates, pelites, sandstones and conglomerates. Regarding the lithostratigraphy of the Bambuí Group, Dardenne (1978), after Costa and Branco (1961), divided the unit into six units: A diamictite at its base and the Sete Lagoas, Serra de Santa Helena, Lagoa do Jacaré, Serra da Saudade and Três Marias formations. Other units of the Bambuí Group are the Samburá (Barbosa et al., 1970), Lagoa Formosa (Seer et al., 1989) and Gorutuba formations (Kuchenbecker et al., 2016a). The Bambuí has been interpreted as a first-order sequence subdivided into four second-order progradational-retrogradational sequences (**Figure 3**) (Martins and Lemos 2007; Martins-Neto, 2009; Reis and Alkmim, 2015; Caetano-Filho et al., 2019). The basal second-order sequence comprises the Carrancas Formation and the base of the Sete Lagoas Formation. The Carrancas Formation is composed of conglomerates with a sandy-calcareous matrix, whose glacial origin has been discussed (e.g. Martins-Neto et al., 2001; Uhlein et al., 2016; Delpomdor et al., 2020) and the overlying Sete Lagoas Formation consists mainly of marine dolostones, limestones and organic-rich shales (e.g. Iglesias and Uhlein, 2009; Reis and Suss, 2016). The basal limestones of the Sete Lagoas Formation have been interpreted as

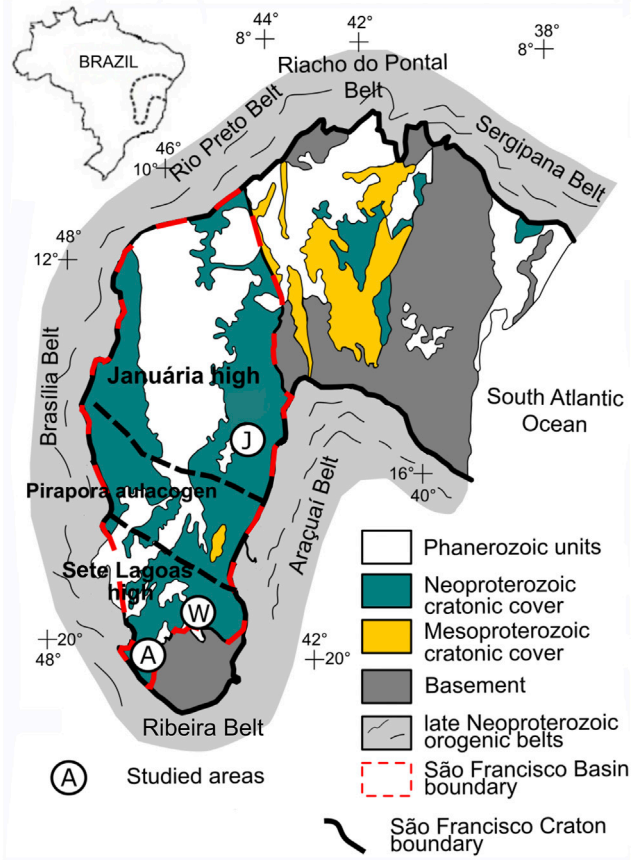

FIGURE 2 | The São Francisco Craton geological map and the São Francisco Basin. Studied sections: A, Arcos; W, Well 1; J, Januária. Modified after Caetano-Filho et al. (2019).

a cap carbonate related to a Neoproterozoic glaciation (e.g. Babinski et al., 2007; Vieira et al., 2007b; Caxito et al., 2012; Kuchebecker et al., 2016a). The two-following second-order sequences are the upper part of the Sete Lagoas, Serra de Santa Helena, Lagoa do Jacaré, and the lower Serra da Saudade formations, which also record marine environments. The Serra de Santa Helena Formation is composed of siltites, pelites, shales and minor limestones, whereas the Lagoa do Jacaré Formation is characterized by pisolitic and oolitic limestones, marbles, intraclastic breccias, shales and siltites and the Serra da Saudade Formation is a succession of siltites and greenish shales, with minor limestones and dolostones (Dardenne, 1978). The uppermost second-order sequence encompasses the upper Serra da Saudade and the shallow marine/continental deposits of the Três Marias and Gorotuba formations (Kuchenbecker et al., 2016a; Reis and Suss, 2016). At the western portion of the basin, the Samburá and Lagoa Formosa formations are interpreted as the deposits of fan-deltas and submarine-fans, representing the gravitational flows associated to the intermediate second-order sequences (Uhlein et al., 2011; Reis et al., 2017).

Chemo and Sequence Stratigraphy of the Bambuí Group

Many chemostratigraphic studies were done on the Bambuí Group applying ^{13}C isotopes on carbonate rocks ($\delta^{13}C_{carb}$) (Iyer et al., 1995; Santos et al., 2004; Martins and Lemos, 2007; Vieira et al., 2007a; Caxito et al., 2012; Kuchenbecker et al., 2016b; Guacaneme et al., 2017; Paula-Santos et al., 2017; Caetano-Filho et al., 2019; Uhlein et al., 2019). Considering $\delta^{13}C_{carb}$ and also $^{87}Sr/^{86}Sr$ ratios, Paula-Santos et al. (2017) divided the basal Bambuí into three chemostratigraphic intervals (CIs) and interpreted the shifts in the measurements in terms of oceanic connection and restriction of the basin (**Figure 3**). The first interval (CI-1) comprises the Sete Lagoas cap carbonates, in which $\delta^{13}C_{carb}$ values records a negative excursion (−3 to −5‰) followed by a positive excursion (−5 to 0‰). Also, at CI-1, the $^{87}Sr/^{86}Sr$ ratio increases from 0.7074 to 0.7082. At CI-2, which corresponds to the middle of the Sete Lagoas Formation, both $\delta^{13}C_{carb}$ and $^{87}Sr/^{86}Sr$ are stable, around 0‰ and 0.7082, respectively. At the CI-2 the marine late Ediacaran index fossil *Cloudina sp*. (Grotzinger et al., 1995) was reported by Warren et al. (2014), suggesting that the São Francisco basin was connected to other Gondwana marine basins through a sea pathway, allowing the migration of metazoans and C-isotope homogenization with global seawater. Finally, the third interval (CI-3), encompasses the upper Sete Lagoas, Serra de Santa Helena, and Lagoa do Jacaré formations. At CI-3, $\delta^{13}C_{carb}$ reaches very high values (up to +16‰) and $^{87}Sr/^{86}Sr$ ratios decrease when compared to CI-2, being close to 0.7075. The reported $^{87}Sr/^{86}Sr$ ratios are low for the late Ediacaran/early Cambrian, suggesting restriction and lack of homogenization with external seawaters, hence, its Sr signature was mostly controlled by weathering of ancient carbonate platforms (Paula-Santos et al., 2015, 2017). Such restriction was probably caused by the progressive uplift of the marginal orogens of the São Francisco Craton (Paula-Santos et al., 2017), which isolated the basin. Uhlein et al. (2019) named these very high $\delta^{13}C_{carb}$ values reported in CI-3 interval as MIBE (Middle Bambuí Excursion). They were mostly interpreted as the result of enhanced burial of organic matter and active methanogenesis coupled to methane emissions to the atmosphere (Iyer et al., 1995; Paula-Santos et al., 2017; Caetano-Filho et al., 2021) or the consequence of a change in carbon input due to weathering of ancient sedimentary carbonates and higher burial rates of authigenic carbonates due to organic matter oxidation (Uhlein et al., 2019; Cui et al., 2020). The chemostratigraphic division made by Paula-Santos et al. (2017) was later corroborated by Paula-Santos et al. (2018) since the Rare Earth Elements + Yttrium (REY) patterns that were reported by the authors present secular trends that matches the intervals CI-1, CI,-2 and CI-3. Using geochemical data and two major stratigraphic surfaces, the maximum flooding surface (MFS) and the first sequence boundary (SB1), which are recognizable throughout the basin, Caetano-Filho et al. (2019) established correlations between the sections used in this work, classifying its basal units in terms of systems tracts identified both at the Sete Lagoas and at the Januária highs. The authors defined a transgressive system tract (TST), an early highstand system tract

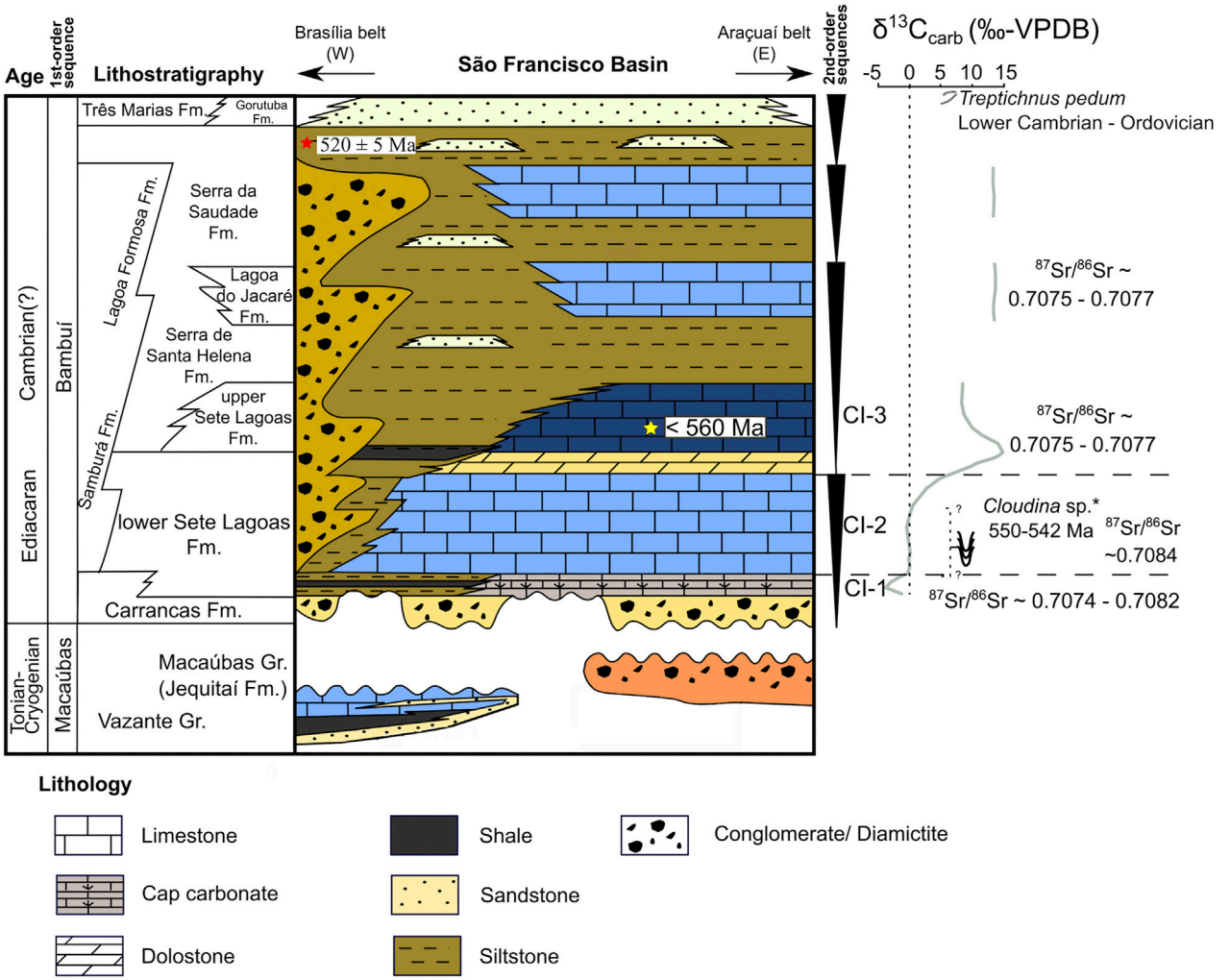

FIGURE 3 | Litho-sequence and chemostratigraphy of the São Francisco Basin. Yellow Star represents maximum depositional age obtained in detrital zircons in the upper Sete Lagoas Formation (Paula-Santos et al., 2015); The red star represents a Serra da Saudade Concordia Age obtained by Moreira et al. (2020). Chemostratigraphic intervals (CIs) were defined by Paula-Santos et al. (2017). Cloudina occurrences are reported in Warren et al. (2014) and Perrella Júnior et al. (2017) and *Treptichnus pedum* occurrences are reported in Sanchez et al. (2020). Modified after Caetano-Filho et al. (2019).

(EHST) and a late highstand system tract (LHST) and also a second transgression at the base of the upper second-order sequence. The TST corresponds to a retrogradational pattern that marks a transgression over the forebulge of the Bambuí domain and its connection to the global ocean, and it comprises deposits of diamictites from Carrancas and carbonates from the basal Sete Lagoas Formation. This sequence ends at MFS, which in the Sete Lagoas High is marked by a succession of shale and mudstones, whilst in Januária bindstones lacking structures related to flows were chosen as the limiting surface, this interval is associated to the CI-1 of Paula-Santos et al. (2017). Above it, a progradational pattern shows that a regression occurred, marking the EHST. At this stage, the Bambuí was still connected to the global ocean. Carbonates are the main lithology of this stage and represent a stable marine ramp. The boundary between EHST and LHST was defined by a sharp increase in the Sr/Ca ratio since the latter present an average value of 0.004, while the former the value of 0.001 and this increment was interpreted as the beginning of the restriction of the Bambuí seaway. LHST comprises very pure carbonates that become coarser towards the top of the sequence. Despite the rise in Sr/Ca ratios, Paula-Santos et al. (2017) defined that the CI-2 covers both EHST and LHST, which places the beginning of the restriction later than it was suggested by Caetano-Filho et al. (2019). The LHST ends with the surface identified as SB1 marking the beginning of the second second-order sequence, which corresponds to the CI-3 of Paula-Santos et al. (2017). The SB1 is defined by subaerial features in shallow environments, whereas in deeper it is defined by an erosional surface at the base of peritidal channels limestones.

Age of the Bambuí Group

A large set of data show that the deposition of the Bambuí Group largely took place between the late Ediacaran and Cambrian. Paula-Santos et al. (2015) determined U-Pb ages in detrital zircons from pelites intercalated with carbonates from the upper part of the Sete Lagoas Formation and obtained a maximum depositional age around 560 Ma. The discovery of fossils of *Cloudina sp*. and *Corumbella Werneri* (550–542 Ma) (Grotzinger et al., 1995) in the middle Sete Lagoas Formation (Warren et al., 2014; Perrella Júnior et al., 2017) corroborate Paula-Santos et al. (2015) ages. Recently, Moreira et al. (2020) reported that ten prismatic zircon grains extracted from a K-bentonite volcanoclastic bed in the upper Serra da Saudade Formation defined a U-Pb Concordia age of 520 Ma ± 5 Ma. Finally, the fossil *Treptichnus pedum* was reported in the upper Três Marias formation, which places the deposition age of this unit in the early Paleozoic (Sanchez et al., 2020).

MATERIALS AND METHODS

Studied Sections

Three stratigraphic sections from the Bambuí Group were studied in this work: Januária (~130 m-thick), an assemblage of three minor sections in the central-east portion of the São Francisco Basin in Januária High domain, Arcos (180 m-thick) and Well 1 (430 m-thick), the latter two sections corresponding to drill cores, at the South of the Basin, in the Sete Lagoas High domain (**Figure 2**). Januária and Arcos represent shelf environments of the Bambuí, while Well 1 represents a forebulge graben setting. For detailed lithostratigraphy and sedimentological features of Januária, Arcos and Well 1, *see* Caetano-Filho et al. (2019), Kuchenbecker et al. (2011, 2013) and Reis and Suss (2016), respectively. The samples analyzed here correspond to the two lowermost second-order sequences of the Bambuí Group.

Januária Section

The Januária composite section (**Figure 4**) is composed of three minor sections, Cônego Marinho (CM), Barreiro (BAR) and Januária-Lontra (JL), all located at the North of Minas Gerais State, Brazil. Above the unconformity that separates the Bambuí Group from the basement, grey calcilutites (0–4 m) presenting aragonite pseudomorphs (cap carbonates) are overlapped by pink carbonates (4–19 m) that transition to light grey fine-grained carbonates (19–25 m) interleaved with pelitic siliciclastic layers. The presence of such layers was interpreted as evidence for a deep environment, therefore, at this interval, Caetano-Filho et al. (2019) set the maximum flood surface for the section. Overlying the light grey limestones, there are dark grey calcisiltites (25–58 m) intercalated with thin beds of clay. From 58 to 98 m, carbonates become gradually coarser and flat pebble breccias. At the top of the Sete Lagoas Formation, there are dolostones (98–100 m) with intraclasts and vugular porosity, which are interpreted as the result of a shallow to subaerial conditions (Caetano-Filho et al., 2019). Above them, an unconformity marks the end of the first second-order sequence. Following a gap of unknown thickness, the Serra de Santa Helena Fm. outcrops in a 20 m-thick succession of laminated to massive siltstones and mudstones and it is overlapped by the 20 m-thick package of limestones of the Lagoa do Jacaré Formation, which shows features such as oolites, intraclastic breccias and planar-parallel lamination. This section is detailed described in Caetano-Filho et al. (2019).

Arcos Section

The Arcos section (**Figure 5**) consists of two drillcores of about 200 m that were obtained by mining companies within the area of the city of Arcos, Minas Gerais, Brazil. Its detailed description can be found in Kuchenbecker et al. (2011, 2013) and will be summarized here. The basement comprises slightly deformed dark-green to grey granodiorites, above it, in an irregular contact, a 0.5 m-thick layer of the Carrancas diamictite occurs, containing clasts from the basement, besides clasts of limestones, siltite and quartz. The next 9 m of the section encompasses light-grey impure limestone intercalated with calcilutites. Microbial lamination is present so as fenestral porosity, commonly filled with sparry calcite and more rarely with crysptocrystalline silica. From 600 to 608 m, the terrigenous content diminishes and calcilutites are the dominant lithology and, occasionally, there is the occurrence of impure calcarenite. Stylolites and other dissolution structures are present, and at the top of this segment, there are aragonite pseudomorphs. Pyrite crystals, euhedric or framboidal, are also a common feature. Between 608 and 627 m the detrital content increases remarkably and the interval is marked by mudstones and siltstones, and, more rarely, by calcilutites. Such enhance in the detrital content was used as a guide to determine the maximum flood surface of the Arcos section (Caetano-Filho et al., 2019). Again, from 627 to 668 m, the terrigenous content is very low and limestones featuring microbial laminations predominate. However, from time to time, intraclastic calcarenites are also found. At the segment that goes from 668 to 705 m, calcilutite exhibiting microbial structures intercalates with black shaly rocks presenting a crinkled lamination. Then, until 718 m, calcilutites are the major lithology. From 718 to 738 m there are oolitic and intraclastic calcarenites. The interval between 738 and 761 m is heavily dolomitized, featuring oolitic and intraclastic doloarenites, sometimes laminated. The dolomitization is evidence of regression; therefore, at this interval, there is an unconformity that marks the end of the first second-order sequence and the beginning of the second second-order sequence. Following the dolomitic rocks, the Arcos section comprises, again, calcilutites with microbial structures, until the end of the section.

Well 1 Section

The Well 1 section (**Figure 6**) is a continuous drill core that was drilled in the southern São Francisco basin during hydrocarbon exploration campaigns. The detailed stratigraphy and depositional environment of Well 1 is present by Reis and Suss (2016). Its base, which will be investigated in this work, is approximately 430 m-thick, consisting of the thickest studied section presented here. An erosional unconformity marks the appearance of the Carrancas diamictite (muddy matrix sustaining

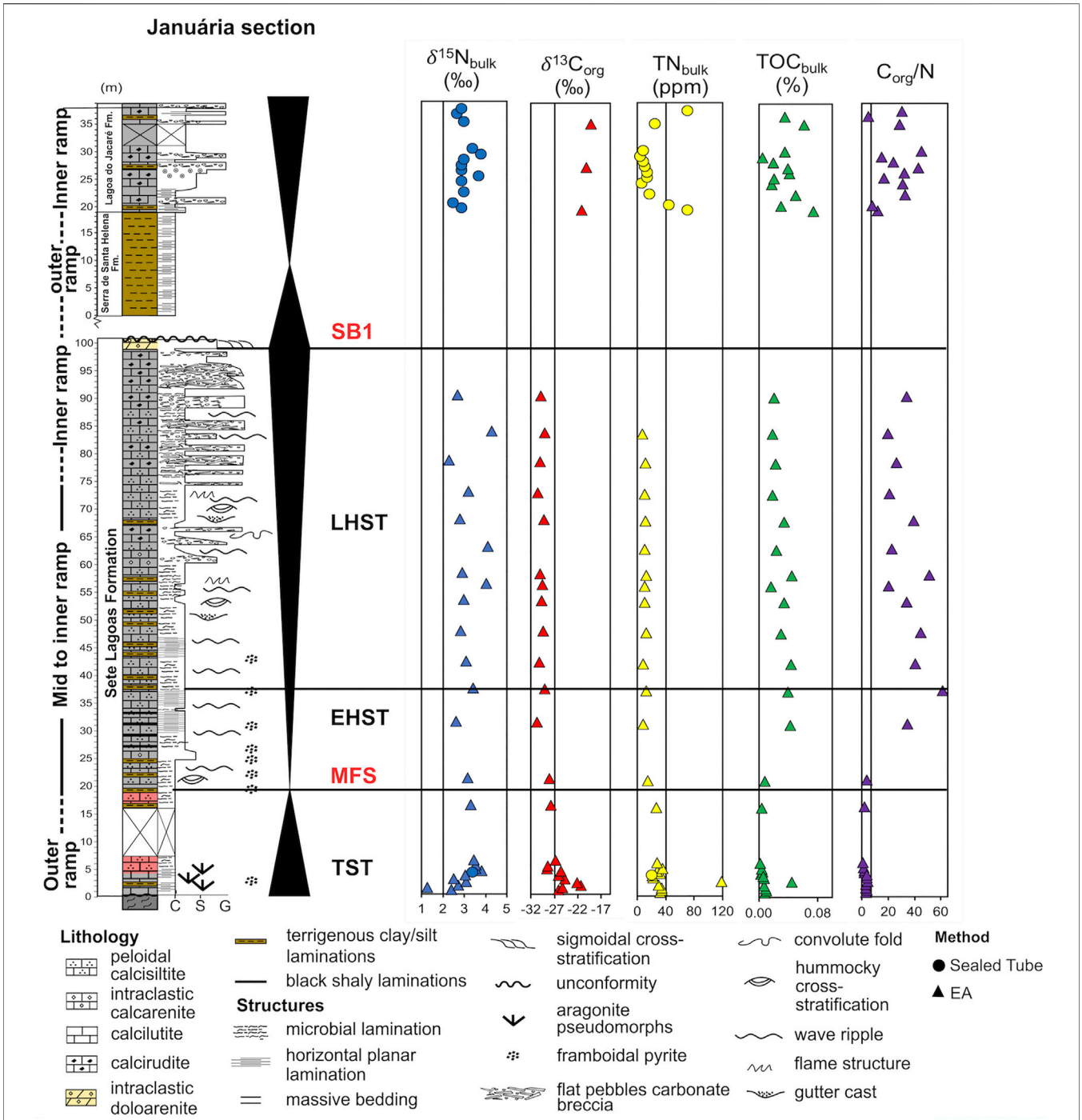

FIGURE 4 | Januária section: Depositional environments, lithologies, structures and sequence stratigraphy framework. $\delta^{15}N$ data was obtained in this study and $\delta^{13}C_{org}$ was published by Caetano-Filho et al. (2021). The axis on the C_{org}/N column is fixed on the Redfield ratio (6.6). System tracts: TST, Transgressive System Tract; MFS, Maximum Flooding Surface; EHST, Early Highstand System Tract; LHST, Late Highstand System Tract; SB1, Sequence Boundary. Granulometry scale: C, clay; S, sand; G, gravel. Adapted after Caetano-Filho et al. (2019).

clasts of metasedimentary rocks, granitoids and quartz veins) above the basement. The conglomerate grades upward to recrystallized dolomites ~80 m-thick) cemented by sparry dolomite and chert; wave ripples and hummocky stratification are present as well. From 1100 to 1075 m-depth dark shales intercalate with limestones, and from 1075 to 1045 m-depth a thick layer of shale containing pyrite closes this portion of the drill core. In the middle of this interval, the maximum flood surface was set (Caetano-Filho et al., 2019), as it represents deeper facies. Above the shaly interval, until approximately 880 m-depth,

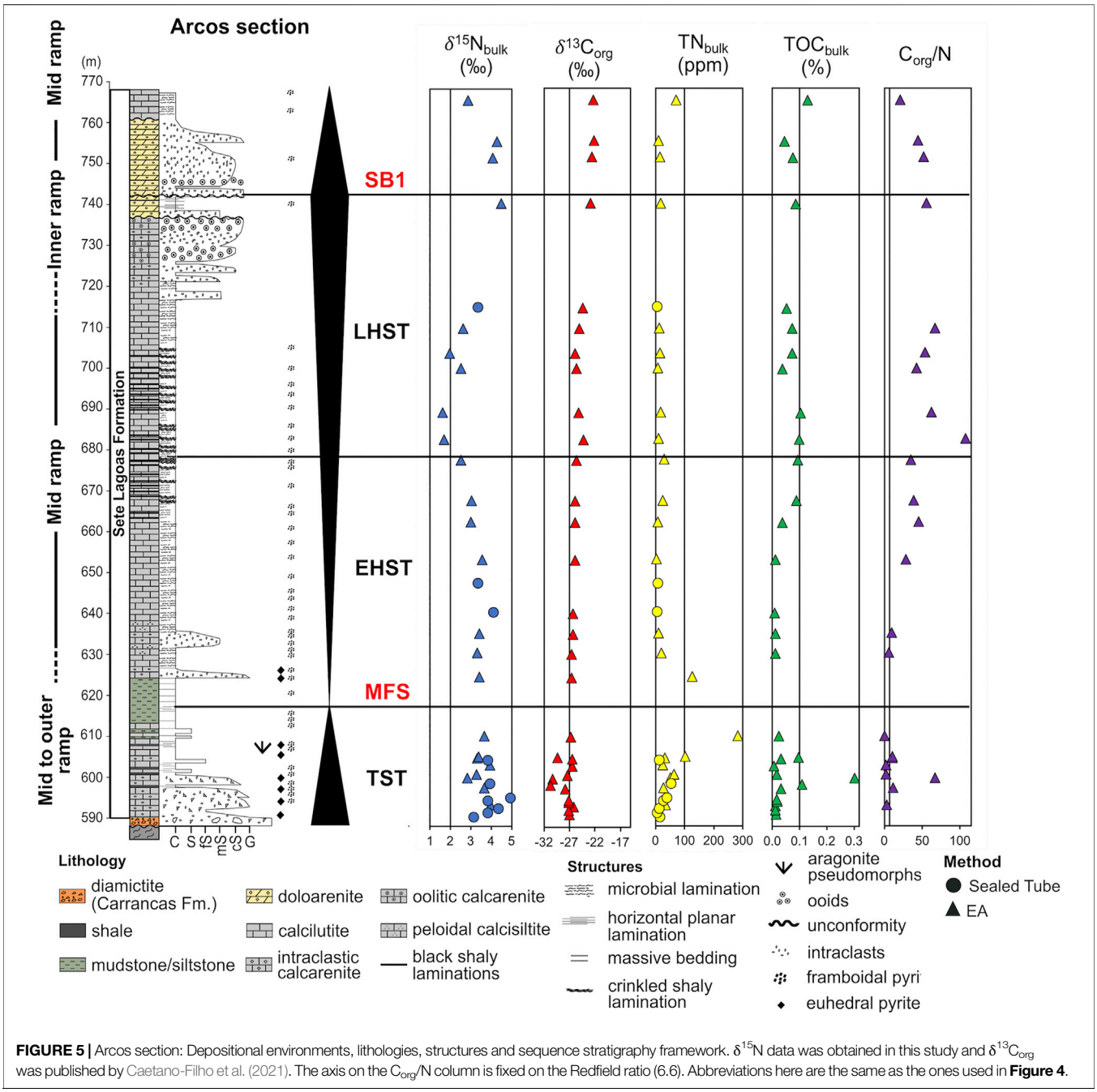

FIGURE 5 | Arcos section: Depositional environments, lithologies, structures and sequence stratigraphy framework. $\delta^{15}N$ data was obtained in this study and $\delta^{13}C_{org}$ was published by Caetano-Filho et al. (2021). The axis on the C_{org}/N column is fixed on the Redfield ratio (6.6). Abbreviations here are the same as the ones used in **Figure 4**.

greenish siltstones intercalate with calcilutites, calcarenites and calcirudites. Structures such as wavy, lisen and flaser beddings, wave ripples and hummocky stratification are reported. From 880 to 720 m-depth the section comprises dark-limestones of varied granulometry, in which wavy ripples, gutter casts, hummocky and horizontal planar lamination are described at the base of this segment and ooids, trough cross-bedding, planar cross-stratification and microbial lamination at the top. Also, associated with these microbial laminations, there is the limit of the first second-order sequence, an erosional surface at the base of peritidal channels limestones (Caetano-Filho et al., 2019).This is the only studied section in which there are no dolostones associated with the end of the first second-order sequence. The uppermost 30 m of Well 1 comprises shales with minor intercalations of calcirudites and calcarenites, pyrite is a common feature.

Preparation of the Samples for Analysis

In total, 177 samples were analysed, from these, 86 were from Well 1, 46 from Januária and 45 from Arcos. A stratigraphic resolution of 1 m was deployed for the cap carbonate interval, except Well 1, in which the resolution was 3 m. Also, for the

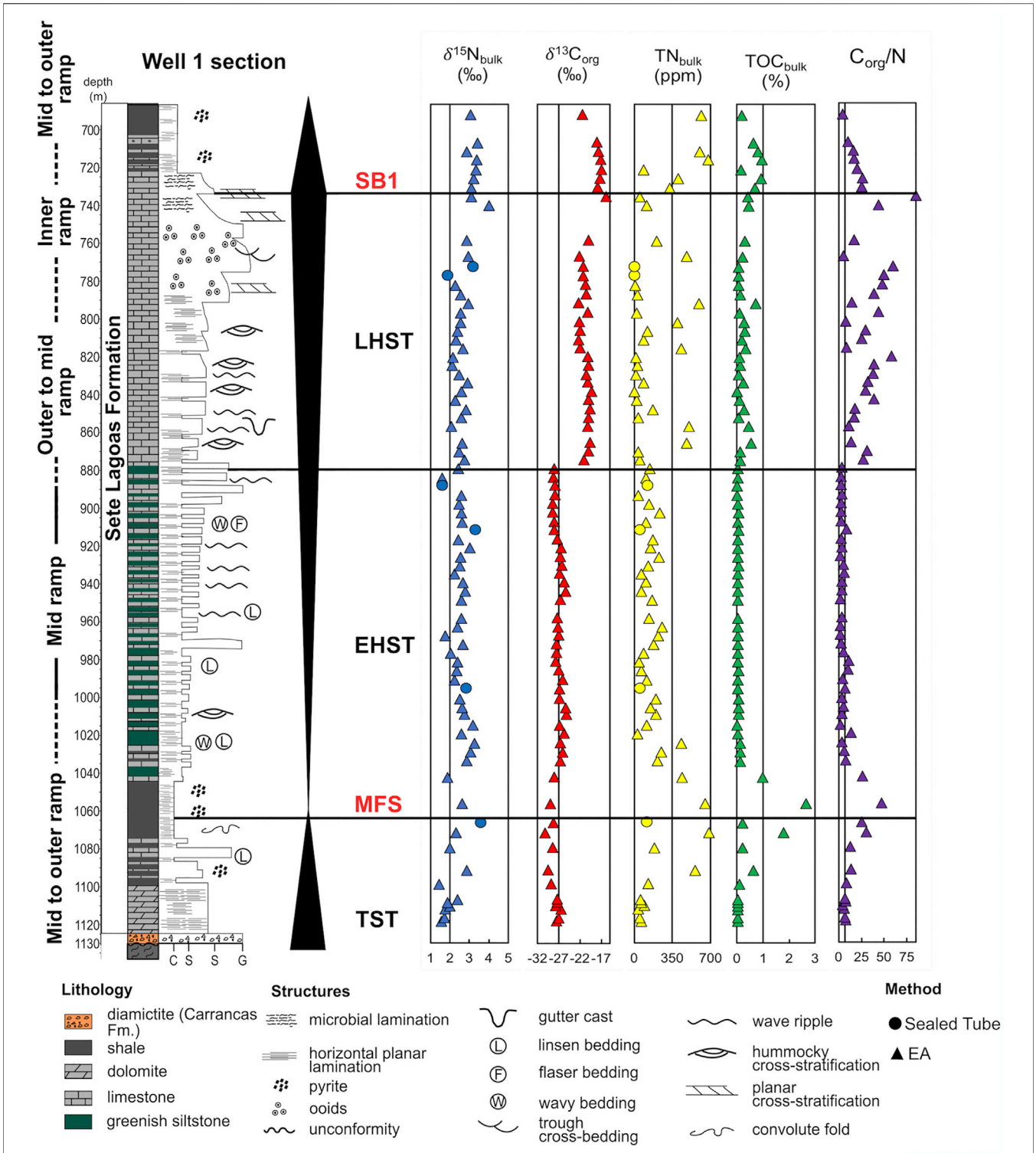

FIGURE 6 | Well 1 section: Depositional environments, lithologies, structures and sequence stratigraphy framework. $\delta^{15}N$ data was obtained in this study and $\delta^{13}C_{org}$ was published by Caetano-Filho et al. (2021). The axis on the C_{org}/N column is fixed on the Redfield ratio (6.6). Abbreviations here are the same as the ones used in **Figure 4**.

second sequence of the Januária section, the resolution of sampling was 1 m. For the rest of the sections, the interval was of 5 m, encompassing all the systems tract intervals defined by Caetano-Filho et al. (2019). To acquire $\delta^{15}N_{bulk}$ (N bounded to clays + N bounded to kerogen) data, the rocks were crushed into smaller pieces using mortar and pestle and were

subsequently pulverized using a tungsten carbide mill. The carbonate fraction was removed by adding 25 ml of 5 N HCl to 3–15 g of sample for 12 h at 25°C. The reaction proceeded after that at 80°C for 2 h. Leachate was centrifuged and discarded and the residue of this procedure was rinsed with distilled water until its pH was neutral and was then dried in an oven at 50°C. This allowed to concentrate N in the residue, a necessary step given the high carbonate content and very low TOC of most samples.

$\delta^{15}N$, Total N and Total Carbon – Elemental Analyzer

To obtain the $\delta^{15}N_{bulk}$ data, samples were analyzed on an elemental analyser Thermo Scientific EA Flash 2000 coupled to a Thermo Scientific Delta V+, at Pôle de Spectométrie Océan, University of Western Brittany, France. For this, 5–10 mg of the insoluble residue of each sample was weighted in tin capsules and dropped by an autosampler into an oxidation furnace at 1020°C. An 8 s injection time of dioxygen at a flux of 240 ml/min was used to accomplish the flash combustion. To avoid incomplete oxidation of the flash combustion products, chromium(III) oxide and silver-plated cobalt oxide were added to the oxidation reactor. The produced gas was transported by continuous helium flow (100 ml/min) to a reducing column containing activated copper (heated at 650°C), which enabled the removal of oxygen in excess and the conversion of NO_x to N_2. Water vapor was removed from the gas using anhydrous magnesium perchlorate. The rest of the gases were separated using gas chromatography and were introduced into the mass spectrometer *via* a Thermo Scientific ConFlo IV universal interface. Total nitrogen (TN) was measured by the Thermal Conductivity Detector of the Flash EA 2000 and in this work, we report TN_{decarb} as the measured N concentration in the insoluble residue obtained after HCl leaching. $\delta^{15}N_{bulk}$ data is reported in per mil (‰) deviation from the atmospheric N isotopic composition ($\delta^{15}N_{air}$ = 0‰). The average uncertainty was calculated based on repeated measurements of the reference standard SED-IVA (sediment; + 4.42‰) and the in-house standard LIPG (yeast; −0.16‰) and it was better than 0.15‰ (2σ) for $\delta^{15}N_{bulk}$ and better than 0.03% (2σ) for N total concentration. This work also reports total nitrogen in samples (TN_{bulk}), which was calculated gravimetrically based on the amount of mass of sample remaining after the HCl leaching. Most of the total carbon data used here was published by Caetano-Filho et al. (2021), except for 11 samples from the second second-order sequence of Januária and one sample from Arcos that were measured at the Institut de Physique du Globe de Paris using a Flash EA 1112 coupled to a Thermo-Fisher Delta + XP isotope ratio mass spectrometer. The analytical procedure is similar to the one already described in Caetano-Filho et al. (2021) and the reproducibility of duplicate samples was better than 0.02% (2σ).

$\delta^{15}N_{bulk}$ and Total N – Sealed Tube Combustion + Dual Inlet Mass Spectrometer

For some of the samples from Arcos, Well 1 and Januária the nitrogen content was too low to obtain accurate results using the EA method. In these cases, when there was still enough material, samples were measured using what is known as the classical sealed tube method (Ader et al., 1998, 2016) at the Institut de Physique du Globe de Paris. In this method, the N_2 is extracted and purified using a vacuum line (Ader et al., 1998, 2016). For this purpose, quartz tubes were filled with previously purified CuO, Cu wires and sample. Then, the tubes were attached to the vacuum line and were degassed under 150°C until high vacuum conditions were obtained. Subsequently, the tubes were flame-sealed and proceeded to the combustion step, in which the tubes were heated in a furnace at 950°C for 6 h to allow the CuO to decompose into Cu and O, as the liberated O causes the combustion of the sample, which generates water, dinitrogen, carbon dioxide and nitrogen oxides as products. Then, the tubes are cooled down until 600°C for 2 h, to allow for the NO_x to react with Cu to generate N_2 and CuO. After the combustion, the generated gas was extracted and purified using the vacuum line. CO_2 and H_2O were separated from N_2 using a liquid nitrogen trap. After the purification step, the gas was concentrated and pushed into a sample vessel using a Toepler pump, which also allows the quantification of the extracted N_2. To assess possible contaminations coming from the vacuum line, blanks were commonly done, yielding less than 0.02 μmol of gas within the vacuum line system, which is negligible considering the amount of N_2 in Bambuí samples. The extracted gas was analyzed using a Thermo-Fisher Delta + XP mass spectrometer with a dual inlet introduction system to determine the nitrogen isotope composition. Nitrogen isotopes are measured in masses 28, 29 and 30 and masses 12 (C), 32 (O_2), 40 (Ar) and 44 (CO_2) are tracked to check for possible contaminations. The precision of $\delta^{15}N_{bulk}$ values was better than 0.5‰ (2σ), estimated from multiple measurements of a batch of samples. Accuracy was monitored by measuring certified materials IAEA-N1(+0.4 ± 0.2‰) and IAEA-N2 (+20.3 ± 0.2‰) and IPGP internal standard MS#5 (+14.9 ± 0.5‰).

K and Al Contents

K and Al contents were measured using a portable XRF device Thermo Scientific Niton XL3t provided by the Geological Survey of Brazil (CPRM). Sample slabs were polished and veins or terrigenous laminations were avoided during measurements. A blank (SiO_2) and a certified reference material (QC 180-673; Thermo) were run after every batch of 30 samples. The blanks present K content that was less than 0.01 ppm and the reproducibility of the standard was better than 0.2% (1σ). The Al blanks were lower than the detection limits and the reproducibility of standards was better than 0.5% (1σ). K and Al content are reported in percentage (%).

RESULTS

$\delta^{15}N$ and Total N

From the initial batch of 177 samples, we obtained 152 results. 39 from Januária section, 34 from Arcos section and 79 from Well 1 section (**Figures 4–6**). The results of the isotopic compositions of bulk nitrogen ($\delta^{15}N_{bulk}$), total nitrogen samples in residues (TN_{decarb}) and total nitrogen in bulk rock (TN_{bulk}) are shown

in **Supplementary Table S1**. The results were paired with total organic carbon in the insoluble residue (TOC_{decarb}), total carbon in bulk rock (TOC_{bulk}) and $\delta^{13}C_{org}$ data published by Caetano-Filho et al. (2021) except for 11 samples from the second sequence of Januária and one from Arcos, whose TOC_{decarb} and TOC_{bulk} were obtained in this work. C_{org}/N ratios were calculated from measured TOC_{decarb} and TN_{decarb} on an atomic basis and are also reported in **Supplementary Table S1**; **Figures 4–6**. $\delta^{15}N_{bulk}$ values are fairly constant on the three sections ranging from a minimum of +1.3‰ in Januária to a maximum of +5.0‰ in Arcos, with an average value of +2.9‰ (n = 152). TN_{bulk} (ppm) values are low in all sections, with an average value of 119.3 ppm (n = 152). In respect of C_{org}/N ratios, they range from 0.63, in Januária, to a maximum of 107.4, in Arcos, while the average value for the three sections is 20.3 (n = 152), which is above the Redfield Ratio (6.6) for C_{org}/N. Even if our average C_{org}/N value is low for Precambrian rocks, similar C_{org}/N ratios have been reported on the Ediacaran/Cambrian transition in China (Kikumoto et al., 2014). In all sections, the lowermost samples display a remarkable enrichment in N compared to the Redfield value and this enrichment ends near the transition to the LHST, except in Well 1, in which occasionally samples with low C_{org}/N are reported in the upper segments of the section (**Figures 4–6**; **Supplementary Table S1**).

Januária Section

Januária section samples average $\delta^{15}N_{bulk}$ is +3.1‰ (n = 39), ranging from +1.3 to +4.3‰ (**Figure 4**). In its TST interval, a pronounced positive $\delta^{15}N_{bulk}$ excursion from +1.2 to +3.8‰ occurs on the post-glacial carbonates of this section. In the EHST interval, Januária values form a plateau around +3.0‰, however, in the LHST interval, the $\delta^{15}N_{bulk}$ data of Januária oscillate between ~+2 and ~+4‰. Meanwhile, during the second second-order sequence, the average $\delta^{15}N_{bulk}$ of Januária is +3.0‰ (n = 13). Januária average TN_{bulk} and C_{org}/N is 29 ppm and 20 (n = 39), respectively. In Januária, the low C_{org}/N interval is present in its 13 lowermost samples, with an average C_{org}/N of 2.7, which corresponds to the cap carbonates and the upper limit of the EHST interval.

Arcos Section

Considering the three studied sections, Arcos has the heaviest N mean isotopic composition, +3.4‰ (n = 34) with $\delta^{15}N_{bulk}$ going from +1.6 to +5.0‰ (**Figure 5**). Some excursions are present along Arcos profile. The TST interval of this section presents a shift in which $\delta^{15}N_{bulk}$ values go from +3.2 to 5.0‰. In the EHST interval, $\delta^{15}N_{bulk}$ values are stable (~+3.0‰), but in the LHST interval they fall to a minimum of +1.6‰ near EHST/LHST boundary and then they return to +3.4‰. During the second second-order sequence, the $\delta^{15}N_{bulk}$ values of Arcos section rise and its mean value during this interval is +3.8‰ (n = 3). Arcos section average TN_{bulk} and C_{org}/N is 37 ppm and 31 (n = 34), respectively. Here, the low C_{org}/N interval ends earlier than in the other sections, in the middle of the EHST interval. One sample is an exception in this segment, with a C_{org}/N ratio of 67, which drives the mean value of this interval to 12. Without this sample, the average value for Arcos low C_{org}/N interval would be 8.

Well 1 Section

Well 1 section has the lowest $\delta^{15}N_{bulk}$ mean, +2.5‰ (n = 79), with N signatures going from +1.4 to +4.0‰ (**Figure 6**). In the TST interval, the cap carbonates from Well 1 present a little positive $\delta^{15}N_{bulk}$ shift going from +1.5 to +2.8‰ and during the EHST and LHST intervals, the $\delta^{15}N_{bulk}$ values of the Well 1 section are around a plateau of +2.5‰. In the second second-order sequence, $\delta^{15}N_{bulk}$ values rise and the average N isotopic composition is +3.2‰ (n = 6). Well 1 section is enriched in N when compared to the other two sections, with a TN_{bulk} of 198 ppm (n = 79). Also, TN_{bulk} concentrations increase as the amount of carbonate minerals diminish (**Supplementary Table S1**). This feature generated a remarkable zigzag pattern on the EHST interval of Well 1 section, in which limestones more or less rich in insoluble residue intercalates (**Figure 6**). In Well 1 the low C_{org}/N interval extends from the bottom of the section until the EHST/LHST boundary, except for values >6.6 that occurs near to the Maximum Flood surface (**Figure 5**) and rise the mean value of this interval to 7.

K and Al Contents

The average K content of samples is 0.4, 0.6 and 2.9%, whilst the average Al content is 1.0, 1.3 and 2.1% in Januária, Arcos and Well 1, respectively. Higher K and Al contents are reported during transgressive tracts, while the regressions show lower values (**Table 1**).

DISCUSSION

Preservation of $\delta^{15}N$ Primary Signals

We must evaluate the effects of diagenesis and metamorphism on the rock samples to check if the measured $\delta^{15}N_{bulk}$ values represent primary signals. In sedimentary rocks, N occurs mainly in two phases: within the organic fraction or present as clay-bound NH_4^+ substituting K^+ in crystal lattices (Müller, 1977; Greenfield, 1992), together, they compose the N_{bulk} reservoir. The clay-bound NH_4^+ comes mainly from the *in-situ* degradation of organic matter, although it can come from external fluid circulations (e.g. Schimmelmann et al., 2009). During the early diagenesis, as organic matter is degraded and N_{org} is liberated as NH_4^+ with minimum isotopic fractionation (Möbius, 2013), a pool of ammonium within the pore waters is generated. This NH_4^+, depending on the mineralogy, permeability and porosity of sediments (Stüeken et al., 2017), can either be fixed into clay minerals substituting K (Müller, 1977; Greenfield, 1992) without fractionation (Ader et al., 2016) or/and it can be oxidized into NO_2^-, NO_3^- and N_2, which depends on the O_2 concentrations of the environment. Since partial oxidation of NH_4^+ leads to isotopic fractionation, diagenetic effects on $\delta^{15}N_{bulk}$ are enhanced under oxic conditions, as it favors the instability of ammonium. Under anoxic environments, studies have shown that diagenetic effects increase primary $\delta^{15}N$ signal of bulk sediments by less than +1‰, while in oxic environments the increment can reach +4‰ (Altabet et al., 1999; Lehmann et al., 2002). Studies using Rare Earth Elements and iron speciation indicate that the bottom

TABLE 1 | Al and K content average values during the transgressions and regressions.

Section	Average K content – TST and 2nd-sequence (%)	Average K content - HST (%)	Average Al content – TST and 2nd-sequence (%)	Average Al content - HST (%)
Januária	0.4	0.3	1.1	0.6
Arcos	0.7	0.4	1.7	0.6
Well 1	4.6	0.7	2.9	1.9

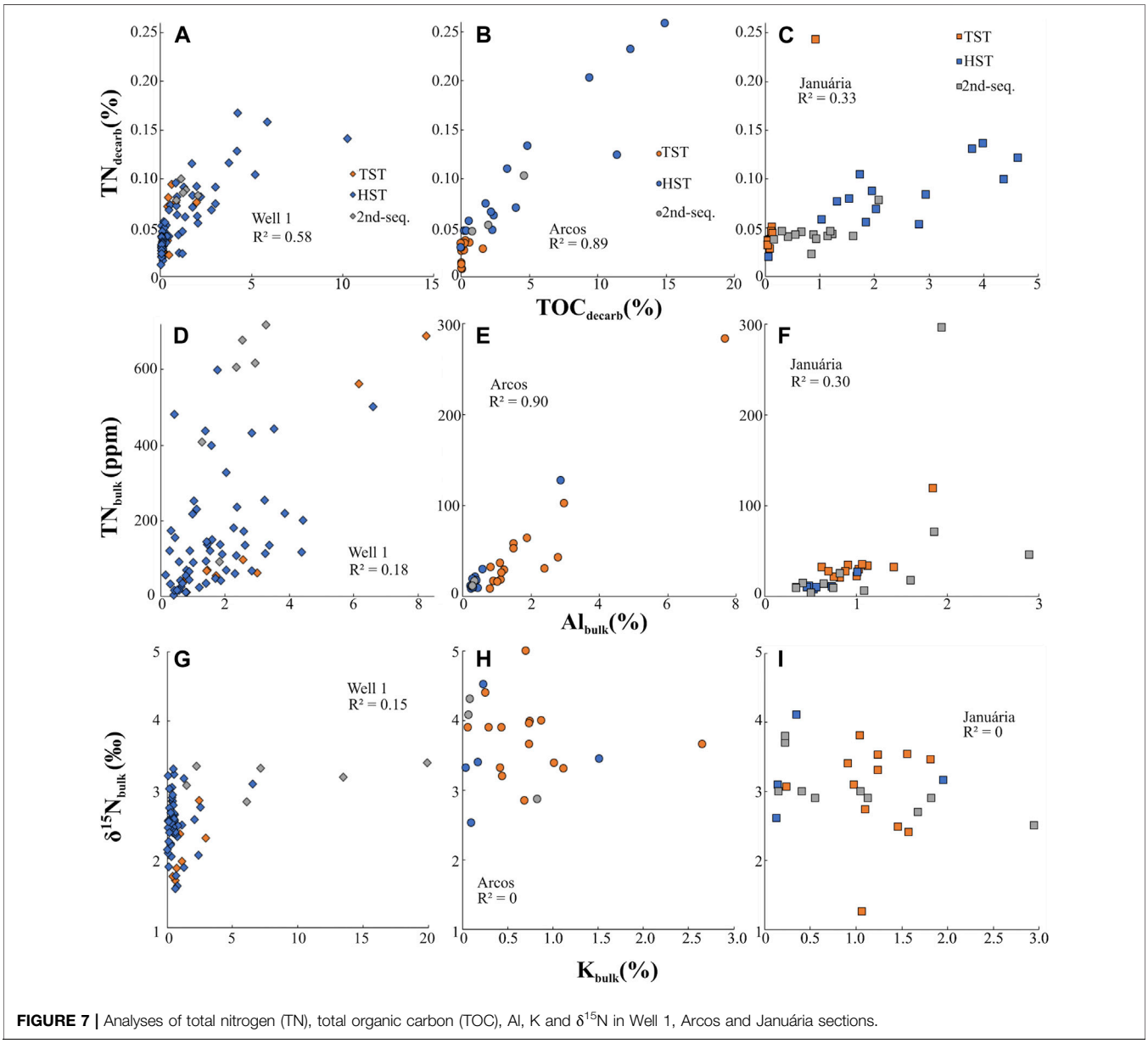

FIGURE 7 | Analyses of total nitrogen (TN), total organic carbon (TOC), Al, K and $\delta^{15}N$ in Well 1, Arcos and Januária sections.

waters of the Bambuí sea were anoxic in the intervals reported on this paper (Paula-Santos et al., 2018; Hippertt et al., 2019), which likely diminished the effects of diagenesis on the N isotopic signatures of the samples. Well 1 and Arcos section samples show a moderate and strong correlation (R^2 = 0.57 and 0.89, respectively) between TN_{decarb} and TOC_{decarb} (**Figures 7A,B**), indicating that N came mainly from the primary organic matter (Calvert, 2004). In Januária, the correlation is weaker, R^2 = 0.33 (**Figure 7C**), however, its coefficient of determination is influenced by an outlier heavily enriched in N. When the outlier

is removed, R^2 rises to 0.75. None of the trendlines of TN_{decarb} and TOC_{decarb} plots pass through the origin, which shows that a fraction of N in the samples is clay-bound. The presence of NH_4^+ linked to clay minerals is also notable when Al_{bulk} values are plotted against N_{bulk} concentrations. In Well 1 (**Figure 7D**) a correlation between these proxies is not seen during the HST interval, which drives its R^2 to 0.18, however, the correlation is clear during the TST and second-sequence interval of this section. In Arcos (**Figure 7E**) and Januária (**Figure 7F**), the correlation is also clear, with an R^2 of 0.90 and 0.30, respectively. The apparently low R^2 of Januária is caused by one N_{bulk}-rich sample present in its second second-order sequence. One remarkable feature in all sections is the C_{org}/N ratio at their base. The ratios are low when compared to the modern redfield ratio (6.6), which might indicate that the samples are enriched in N compared to the organic matter from which they were generated. This enrichment of N, when coupled to the fact that some N may be linked to clays and not to organic matter, must be investigated since the excess in N can be non-primary. Alternatively, excess of N can be a result of N preservation at the expense of C. If the first alternative is true, the samples cannot be used for paleoenvironmental reconstruction.

Metasomatic alteration can add non-primary NH_4^+ to the rocks and this could have happened in the sections, especially along intervals in which lithological heterogeneities facilitate fluid percolation, such as in the EHST interval of the Well 1 section. However, such external ammonium would have been preserved in clay minerals substituting K, and the lack of correlation between K_{bulk} and $\delta^{15}N$ in all three sections (**Figures 7G–I**) argues against such external N contamination. Therefore, the low C_{org}/N observed in the base of the sections was likely caused by exceptional preservation of N, which occurred due to the *in-situ* degradation of organic matter and releasement of NH_4^+ that was later trapped by clay-rich sediments while C was lost. Another evidence for this is that the Al_{bulk}/TOC_{bulk} ratios are higher in the low C_{org}/N intervals (**Table 2**). This ratio shows that clays are abundant when compared to organic matter, which creates favourable condition for the preservation of N in the form of NH_4^+. The conversion of N_{org} to mineralized NH_4^+ that is subsequently trapped into clays does not imply significant changes on the original primary $\delta^{15}N_{bulk}$ signal, especially under anoxic conditions. This hypothesis also is corroborated by the strong correlation observed between TOC_{decarb} and C_{org}/N ratios of the sections (**Figures 8A–C**) (Calvert, 2004), pointing that carbon loss is the major responsible for C_{org}/N variations. Such scenario requires a process that oxidizes C and preserves N, which can be achieved *via* microbial sulfate reduction, a plausible process considering the visual abundance of pyrite in the base of all sections decreasing towards the top of the basal sequence (Caetano-Filho et al., 2019). As sulfate cannot oxidize NH_4^+ under most conditions, NH_4^+ tends to accumulate in anoxic pore waters (Stüeken et al., 2016) and then it is trapped in clay minerals. Metamorphism effects on $\delta^{15}N$ signatures increase with metamorphic grade, as ^{14}N is preferentially volatilized (reviewed by Thomazo and Papineau, 2013; Ader et al., 2016). Fortunately, samples from the Bambuí Group are metamorphosed under greenschist facies and their signature was unlikely altered by more than 1‰ (Ader et al., 2016). A negative correlation between $\delta^{15}N$ and TN_{decarb} is also an indicator of metamorphic effects on $\delta^{15}N$ due to metamorphism, as during thermal alteration mainly ^{14}N is lost from the system, lowering N content and enhancing $\delta^{15}N$ primary signatures. Except for Arcos, which presents a moderate negative $\delta^{15}N$ and TN_{decarb} correlation (R^2 = 0.48; **Figure 8E**), the other sections do not present such a negative trend (**Figures 8D,F**). However, Arcos average $\delta^{15}N_{bulk}$ values (+3.4‰, n = 34) are similar to ones of Well 1 (+2.5‰, n = 79) and Januária (+3.1‰, n = 39), which discredits the hypothesis of heavy alteration of primary $\delta^{15}N$. Furthermore, the sections do not show relevant $\delta^{15}N$ and C_{org}/N correlations (**Figures 8G–I**), which would be expected if metamorphic alteration of N signals was relevant. Arcos shows a weak negative trend (R^2 = 0.34), the opposite expected for a metamorphism influence, as N is preferentially lost in higher temperatures when compared to C (Ader et al., 2006). Lastly, C_{org}/N ratios are mainly under 100, which is consistent with Proterozoic data with little $\delta^{15}N_{bulk}$ alteration (e.g, Beaumont and Robert, 1999; Chen et al., 2019). Hence, it is reasonable to consider that $\delta^{15}N_{bulk}$ of the Bambuí Group reflects mainly the primary signals of the organic matter and the data can be used for paleoenvironmental reconstructions.

TABLE 2 | Al_{bulk}/TOC ratios in low and high C_{org}/N ratios interval.

Section	Al_{bulk}/TOC_{bulk} in low C_{org}/N segments	Al_{bulk}/TOC_{bulk} in high C_{org}/N segments
Januária	~112	~17
Arcos	~46	~4
Well 1	~112	~17

The Nitrogen Biogeochemical Cycle in the Bambuí Sea

Increasing Oxygenation During the Deposition of the TST Interval

All the studied sections present a positive $\delta^{15}N_{bulk}$ excursion, from a minimum of +1‰ to a maximum +5‰, depending on the section, during the first transgression registered in the Bambuí Group (**Figure 9**). Two scenarios can generate $\delta^{15}N_{bulk}$ values comprehended between ~−2 and ~+1‰ (e.g., Casciotti, 2009; Quan et al., 2013; Sigman and Fripiat, 2019).

(i) assimilation of NO_3^- from an ocean where denitrification occurs only in the sediments. This would require a fully oxygenated water column to prevent the conversion of NO_3^- to N_2 while the former is transported/sunk.
(ii) biological N_2 fixation using Mo-based nitrogenase as a dominant path of the N cycle;

In the Bambuí Group, the reported low values on the TST interval (~+1‰) cannot be explained by a fully oxygenated ocean without denitrification on the water column. This scenario is not only unrealistic for the Precambrian (Canfield et al., 2010; Ader et al., 2016; Stüeken et al., 2016), it does not fit the published

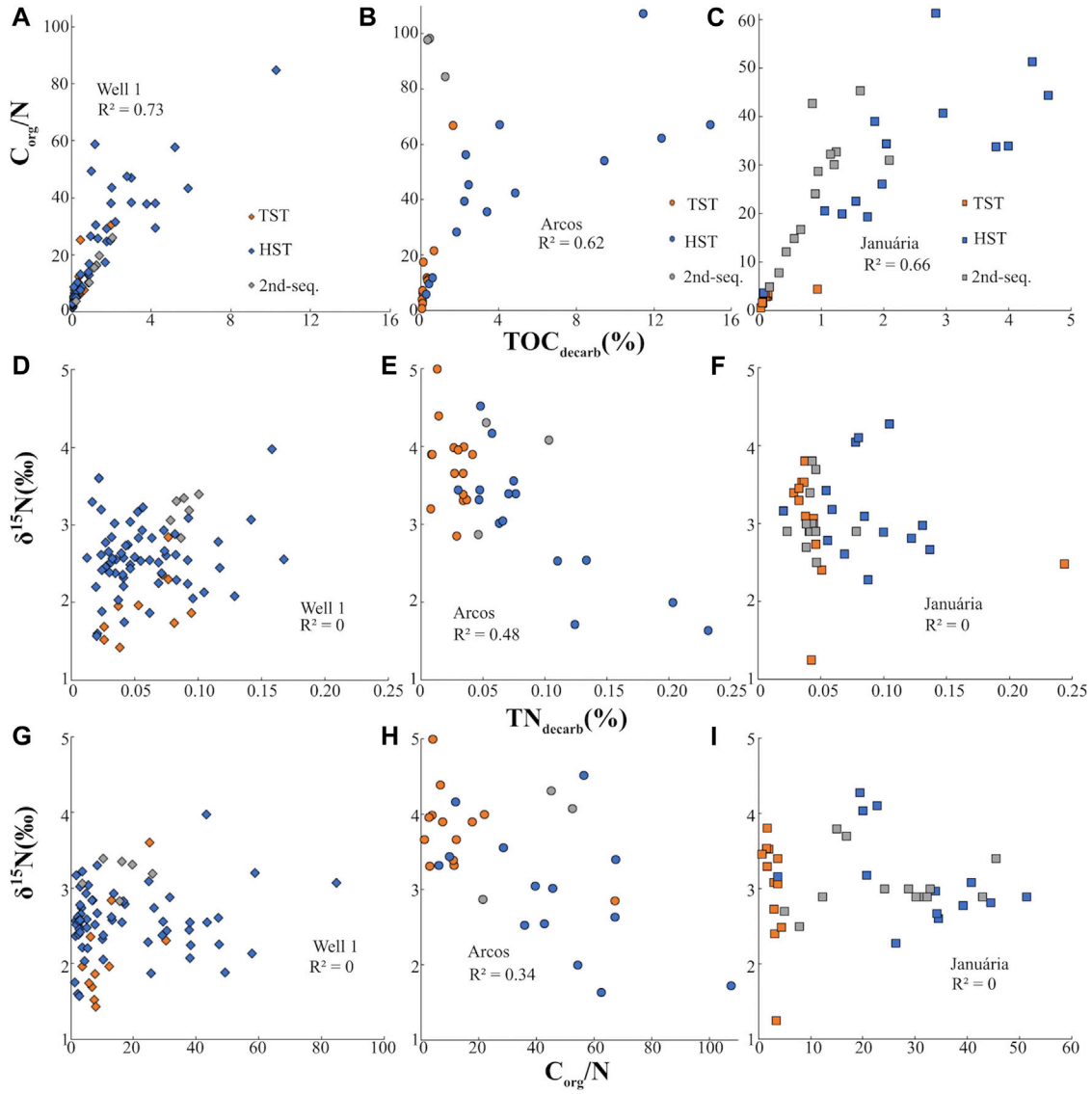

FIGURE 8 | Analyses of total nitrogen (TN), total organic carbon (TOC), C_{org}/N and $\delta^{15}N_{bulk}$ in Well 1, Arcos and Januária sections.

geochemical data available for the Bambuí which indicate bottom water anoxia (e.g. Caxito et al., 2018; Paula-Santos et al., 2018; Hippertt et al., 2019). Hence, the reported low $\delta^{15}N_{bulk}$ signature of Well 1 and Januária sections was likely caused by N_2 fixation using Mo-based nitrogenase in a redox stratified water body. The covalent bonds present in the N_2 molecule makes the conversion of N_2 to NH_3 energetically costly. Consequently, N_2 fixation requires more energy than NO_3^-/NH_4^+ direct assimilation to be processed (Alexander, 1984) and can only happen when no other form of N nutrient (NH_4^+ or NO_3^-) is available. As N_2 fixers are sensitive to O_2 (Gallon, 1981) anoxic conditions favours diazotroph and the presence of nutrient phosphorous (Tyrrell, 1999) and Mo (Seefeldt et al., 2009) are also important for the success of Mo-based N_2 fixation. Hence, $\delta^{15}N_{bulk}$ data points that at the beginning of the deposition of the cap carbonates from Well 1 and Januária sections (both presenting $\delta^{15}N_{bulk}$ values near +1‰ at their base) the water column was mainly anoxic which made N_2 fixation a main path of N-assimilation. NH_4^+ and NO_3^- would be near quantitatively consumed at the redoxcline by anammox and denitrification respectively. Phosphorus would also be in abundant supply as melting glaciers would deliver it to the Bambuí sea, however this hypothesis must be tested using other proxies. Besides that, as anoxic conditions enhance P residence time in the water column, environmental conditions prevented it from binding with Fe oxyhydroxides and being sequestered into sediments (Van Cappellen and Ingall, 1994). Finally, previous studies on the Bambuí Group show that Mo availability was high enough to support N_2 fixation (Hippertt et al., 2019). In fact, despite microbiological culture studies showing that low Mo-conditions might harm nitrogenase

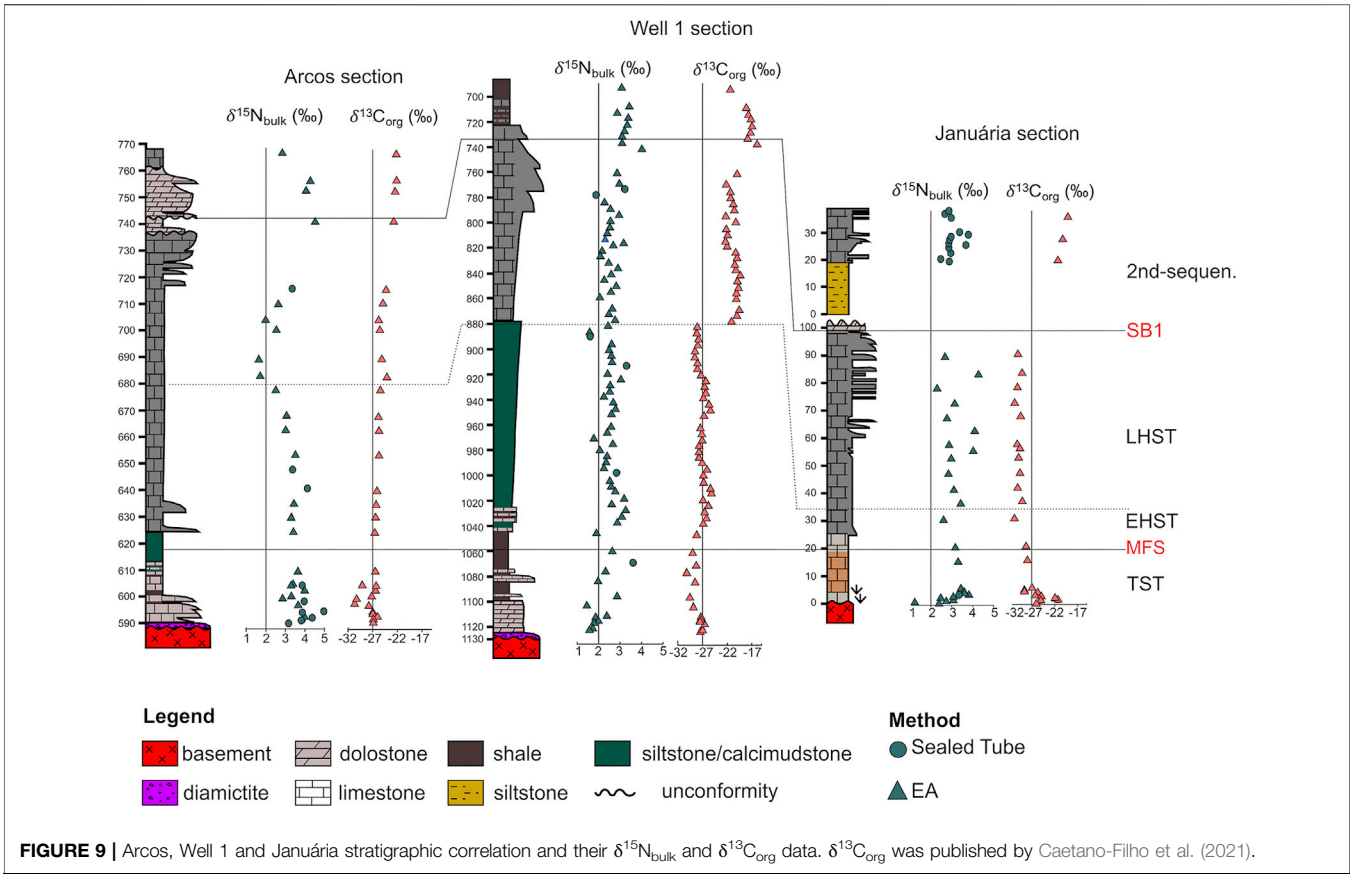

FIGURE 9 | Arcos, Well 1 and Januária stratigraphic correlation and their $\delta^{15}N_{bulk}$ and $\delta^{13}C_{org}$ data. $\delta^{13}C_{org}$ was published by Caetano-Filho et al. (2021).

enzyme operation (Zerkle, 2005), there is no evidence that Mo-scarcity played a role in diazotrophy activity in geological time (Stüeken et al., 2016).

As along the TST interval $\delta^{15}N_{bulk}$ values increase, another N-assimilation pathway must have competed with N_2 direct fixation. Two possibilities can be envisaged depending on redox state of the euphotic zone. In an anoxic photic zone (i.e. NH_4^+ is the main dissolved N species) $\delta^{15}N_{bulk}$ >+2‰ can be interpreted as:

(i) assimilation of NH_4^+ from a reservoir in which NH_3 dissociated from NH_4^+ and was volatilized (e.g. Stüeken et al., 2015);
(ii) non-quantitative assimilation of upwelled NH_4^+;
(iii) assimilation from an NH_4^+ pool that faced non-quantitative nitrification while the resultant nitrite and nitrate were completely reduced (e.g. Thomazo et al., 2011).

NH_4^+ can be dissociated to H^+ and volatile NH_3 and, as this reaction proceeds, ^{14}N-rich NH_3 is lost to the atmosphere and the remaining ammonium pool becomes strongly enriched in ^{15}N (Li et al., 2012). Thus, when this enriched NH_4^+ is assimilated, the sediments will yield very high $\delta^{15}N$ values. However, this process is observed only in highly alkaline lakes (pH > 9.25), which is not the case of Bambuí Group rocks (Li et al., 2012; Stüeken et al., 2015). The second alternative, non-quantitative assimilation of upwelled NH_4^+ is also unlikely. Microorganisms prefer to assimilate ^{14}N, which would generate more negative $\delta^{15}N$ values while enriching the residual NH_4^+ pool in ^{15}N. The absence of negative $\delta^{15}N$ values reported in any section is not in favour of this hypothesis. Finally, partial ammonium oxidation happens even when oxygen concentrations are in nanomolar levels (Füssel et al., 2012) and it is usually a quantitative reaction. Very few records of incomplete nitrification are reported on the geological history (Thomazo et al., 2011; Morales et al., 2014) and none of them for the Ediacaran/Cambrian, which discredit the third alternative. Moreover, all these paths involving NH_4^+ as the main nutrient are associated with big fractionation factors and should intuitively lead to significant stratigraphic $\delta^{15}N$ variability, which does not match the mild and consistent fractionation data reported on the Bambuí rocks. Hence, we assume in the following that samples from the TST interval which $\delta^{15}N_{bulk}$ values are higher than +2‰ do not reflect ammonium as a main nutrient.

In an oxidized photic zone (i.e. nitrate is stable), values of $\delta^{15}N_{bulk}$ >+2‰ is usually interpreted as:

(i) non-quantitative assimilation of NO_3^- (e.g. Sigman et al., 1999).
(ii) assimilation from a nitrate reservoir that experienced some degree of denitrification (e.g. Godfrey and Falkowski, 2009; Tesdal et al., 2013);
(iii) assimilation from a nitrate reservoir that experienced dissimilatory nitrate reduction (DNRA) (e.g. An and Gardner, 2002; Dong et al., 2011; Jensen et al., 2011);

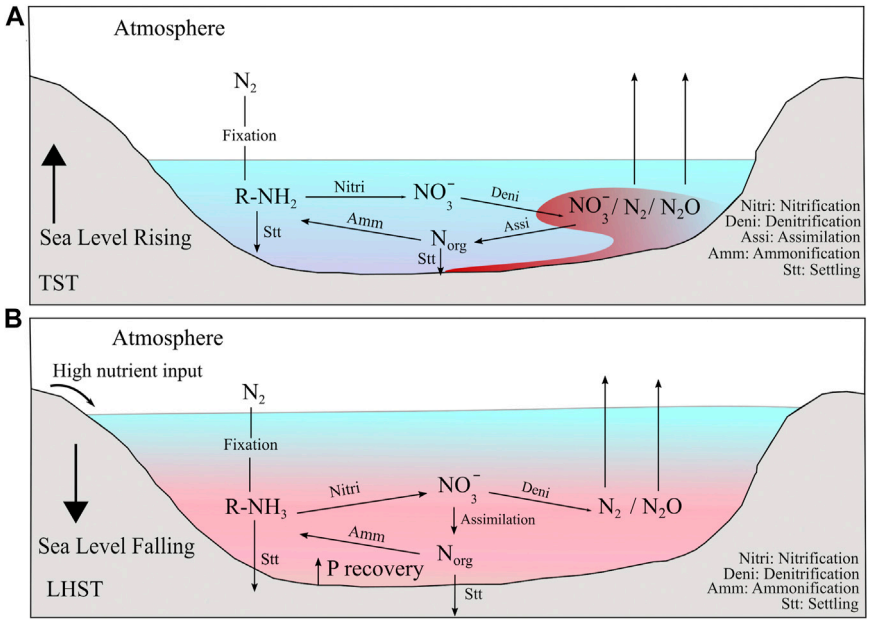

FIGURE 10 | Possible scenario of the N-cycle on the Bambuí Basin during the deposition of its basal sequences. **(A)** During the TST, a stable nitrate pool was established and the most dominant form of N available was nitrate that went through partial denitrification on zones of low oxygenation. **(B)** During the LHST, the high input of nutrients coming from the continent and P recovery under anoxic bottom water conditions, caused the limitation of NO_3^- in superficial waters, making N_2 fixation the main form of N acquisition by phytoplankton.

In the Bambuí, non-quantitative assimilation of upwelled NO_3^- is improbable. This alternative would require a large reservoir of nitrate to have built on deep oxygenated waters, which is not the case. Therefore, it is likely that $\delta^{15}N_{bulk}$ >+2‰ reported on TST interval is linked to the assimilation of a NO_3^- reservoir that faced dissimilatory nitrate reduction and/or denitrification. However, in DNRA, differently from denitrification, N does not escape from the water column, but it is converted to light bioavailable NH_4^+. Hence, if DNRA was a main path, one would expect to find in other samples a complementary light reservoir opposing the enriched $\delta^{15}N_{bulk}$ reported here. As the light reservoir was not found in any section, the importance of DNRA was likely minimal. Hence, discarded all others possibilities, the positive $\delta^{15}N_{bulk}$ excursion reported at the basal Januária and Well 1 section represents a shallow sea that was initially dominated by Mo-based N_2 fixation and later was enough oxygenated to support nitrate accumulation and assimilation from a pool that faced denitrification (Sigman and Fripiat, 2019) (**Figure 10A**). The built-up of a nitrate reservoir in the oxygenated surface waters during the transgressive tract on the euphotic zone matches geochemical data that suggests progressive oxygenation of the Bambuí seawater associated with the input of oxygenated freshwater. For instance, positively fractionated $\delta^{53}Cr$ (Caxito et al., 2018), punctual negative Ce anomalies (Caxito et al., 2018; Hippertt et al., 2019; Paula-Santos et al., 2020) and iron speciation/redox-sensitive elements data indicating locally oxygenated conditions (Hippertt et al., 2019) are reported in this interval. Importantly, in Januária and Well 1, $\delta^{15}N_{bulk}$ values associated with nitrate assimilation are low (maximum value of +3.8‰ in Januária) when compared to the mean value of modern nitrate (~+5‰, Tesdal et al., 2013). This implies that N_2 fixation was still playing an important role in bioproduction and also that the nitrate reservoir was small and denitrification occurred nearly quantitatively, i.e., with a reduced isotope fractionation at a shallow redoxcline. The lowermost sample from the Arcos section presents a $\delta^{15}N_{bulk}$ value of +3.2‰, which means that at the beginning of the transgression there was already a nitrate reservoir in this part of the basin. Moreover, Arcos' values rise to 5‰, implying reduced N_2 fixation and a large nitrate reservoir compared to the other sites. This points to more oxygenated surface waters in the South of the São Francisco basin paleohighs (Arcos section), compared to the forebulge grabens area (Well 1 section). Oxygenation in Arcos TST interval was also observed by Paula-Santos et al. (2020) using Ce anomalies.

Increasing Anoxia During the Highstand System Tract Interval

In the EHST interval, the $\delta^{15}N_{bulk}$ data point to a stable N-cycle, as no significant shift is N isotopic signature is observed in any of the sections (**Figure 9**). The $\delta^{15}N_{bulk}$ average values for the EHST are +2.9, +3.3 and +2.5‰ in Januária, Arcos and Well 1, respectively, suggesting the maintenance of the nitrate reservoir established in surface waters during the TST interval. Also, REY data shows that freshwater input was still happening during the EHST (Paula-Santos et al., 2020) deposition, which might have contributed to the maintenance of nitrate on surface waters. However, oxygenation was not pervasive, as $\delta^{15}N_{bulk}$ values are still low when compared to the modern nitrate reservoir, pointing to a shallow redoxcline and nitrate loss

compensated by N_2 Mo-based fixation. The $\delta^{15}N_{bulk}$ values from Arcos and Januária sections are slightly higher than in Well 1, indicating that surface waters were more oxygenated in shallow domains than in forebulge grabens.

In the LHST interval, the sections present different trends. Many geochemical proxies mark significant paleoenvironmental changes in this interval that are linked to the progressive restriction of this unit (e.g. Paula-Santos and Babinski, 2018; Paula-Santos et al., 2020). The LHST may also record a period of higher bioproductivity, a hypothesis that is further corroborated by its slightly higher TOC when compared to the other system tracts (**Figures 4–6**; Caetano-Filho et al., 2021). This could have been induced by a change to more congruent weathering regimes at the surrounding orogenic fronts that led to higher total alkalinity of seawater during the LHST (Paula-Santos et al., 2020), although proxies to quantify weathering fluxes are still required. These environmental changes are also tracked by N data. A negative excursion is present at the lower Arcos LHST and sometimes its $\delta^{15}N_{bulk}$ values are within the N_2 fixation range (<+2‰). As in the TST interval, there is no evidence that ammonium incomplete assimilation was a main path during the LHST, as the reported fractionation values are mild and constant, differently from large fractionations usually associated with NH_4^+ assimilation (e.g. Thomazo et al., 2011; Stüeken et al., 2015). Therefore the negative shift at the transition from the EHST to the LHST in Arcos section could be caused either by *1*) excess of nitrate and its incomplete assimilation or *2*) exhaustion of the nitrate reservoir forcing microorganisms to fix N. The first alternative is unlikely. In modern oceans, excess of nitrate is only achieved in zones named high-nutrient, low chlorophyll (HNLC) zones, where despite the abundance of macronutrients, the phytoplankton biomass is low, due to a shortage of iron, which seems not to occur in the Bambuí (Hippertt et al., 2019). Also, HNLC conditions are usually met in open oceans, a different scenario from the restricted Bambuí sea during the LHST (Edwards et al., 2004). Then, the drop in the $\delta^{15}N_{bulk}$ values during Arcos EHST/LHST transition is probably an effect of enhanced bioproductivity, as the nitrate reservoir that was built during the EHST was not able to support the high productivity related to high input of nutrients. In this scenario, the input of P due to the enhanced weathering disturbed the normal 16:1 ratio of $[NO_3^-]$:$[PO_4^{3-}]$ on seawater. Consequently, diazotrophic activity rose to restore this ratio (Tyrrell, 1999), which is reflected by low $\delta^{15}N_{bulk}$ values (**Figure 10B**). Also, at this stage, not only the input of phosphorus *via* weathering was high, but progressively anoxic conditions also favored the recycling of this nutrient (Van Cappellen and Ingall, 1994; Ingall and Jahnke, 1997), making it abundant when compared to nitrate. In addition to that, the restriction likely disturbed the circulation patterns of the basin, diminishing the amount of NH_4^+ that is upwelled and nitrified, making the supply of NO_3^- even shorter. As the availability of NO_3^- diminished, the energetic costly N_2 fixation became the main path to acquire N. High productivity associated to high N_2 fixation rates was also observed in modern environments, such as the Black Sea (Quan et al., 2013) and the Cariaco Basin (Haug et al., 1998). Importantly, as the Bambuí, these two settings are also restricted. Up section, in the LHST, the $\delta^{15}N_{bulk}$ values from Arcos rises from +1.6 to +3.4‰, implying that the nitrate reservoir was re-established, but it does not reach the +5.0‰ values reported in the TST interval. In Januária, there is not an abrupt shift in $\delta^{15}N_{bulk}$ during the transition from the EHST to the LHST interval as in Arcos. However, when one observes the $\delta^{15}N_{bulk}$ profile of the LHST interval in the Januária section, the most striking feature are the rapid changes of $\delta^{15}N_{bulk}$, as sometimes they interchange between values around +2.5 and +4.0‰, which creates a zigzag pattern (**Figure 4**). These increased variability indicate that in the central part of the São Francisco Basin shallow domains also faced instability of a limited superficial nitrate pool during regression, which was compensated by N_2 fixation. Also, the average $\delta^{15}N_{bulk}$ of the LHST from Januária (+3.2‰, $n = 12$) and Arcos (+3.3‰, $n = 9$) is low, which means that even when redox conditions permitted the stability of NO_3^-, the pool was not large and $\delta^{15}N_{bulk}$ still reflects a mix between N_2 fixation and NO_3^- assimilation. It is important to access that the fossil *Cloudina* sp. was reported (Warren et al., 2014) in this section and it is associated to the LHST interval (Caetano-Filho et al., 2019). The $\delta^{15}N_{bulk}$ values show that even if deep waters were anoxic (Hippertt et al., 2019), superficial waters could intermittently sustain a small nitrate reservoir, which is important given the fact that major *Cloudina* sp. reports are found in oxic contexts (Bowyer et al., 2017). The record of the LHST from Well 1 section differs from the other two, as no shift in the $\delta^{15}N_{bulk}$ values is observed in comparison to the EHST interval. The values reported for Well 1 section in the entire HST are low, nearly at the boundary of N_2 fixation and NO_3^- assimilation. The stability of $\delta^{15}N_{bulk}$ during the regression stages points that progressive restriction and relative changes in accommodation and sediment supply did not influence the N cycle in the forebulge graben setting compared with shallower domains. It also implies that during the regression stage, local controls affected the nitrogen cycle in the forebulge grabens, despite changes in sea level. One of those controls may have been poor wind mixing effects inside the extensional depocenters, which would have prevented the vertical mixing of superficial waters and enhance stratification in deep environments (Yang et al., 2018). Also, if the rates of sinking organic matter are low, this can move the redoxcline to shallower depths (Meyer et al., 2016). The TOC_{bulk} content of Well 1 during the HST is three times higher than the ones from Januária and Arcos section for the same interval, which suggests that bioproduction could be one of the local factors that caused consistent low values of $\delta^{15}N_{bulk}$. Finally, if we consider that the chemocline was at the same level in all the Bambuí sea, Well 1 would have a larger anoxic water column than the other two sections (**Figure 11**), which might have contributed to its consistent low values. In the LHST interval, the Bambuí was physically restricted and circulation was very inefficient. Therefore, the bioavailable NO_3^- recharge of surface waters was limited to diffusion from deeper waters or by induced water column mixing caused by storms (Ader et al., 2016). There are evidences of storms in Arcos and Well 1 LHST interval (Hummocky Cross-stratification, **Figures 5**, **6**), which explains why the $\delta^{15}N_{bulk}$ values are not entirely within the N_2-fixation range. However, such storms are occasional events and the NO_3^- reservoir was small. The scarcity of NO_3^- during the LHST is also corroborated by episodes of euxinia observed during this interval (Hippertt et al., 2019). Nitrate and sustained euxinia can never coexist because

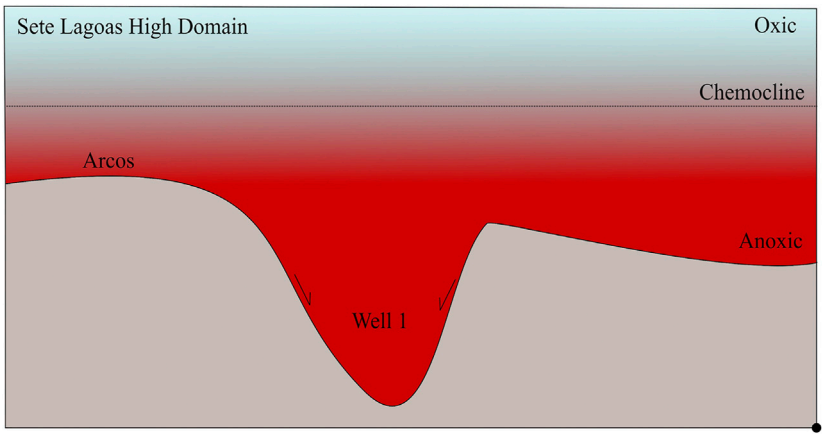

FIGURE 11 | Schematic representation of the Sete Lagoas High Domain. Well 1 is located inside a forebulge graben and Arcos in a shallower part of the Sete Lagoas Domain. Hence, if we consider that the chemocline was at the same level, Well 1 had a deeper anoxic water column than Arcos.

denitrification produce more free energy per mole of carbon than microbial sulfate reduction (MSR), being therefore a preferred respiratory pathway when SO_4^{2-} and NO_3^- coexist. For that reason, nitrate concentrations exert a primary role in the rates of MSR and this mechanism is prohibited when NO_3^- is available (Canfield, 2006). However, a form of N acquisition is essential to fuel the production of the organic matter that will be respired by MSR and consequently generate an H_2S pool. As this species cannot be NO_3^-, Boyle et al. (2013) argued that intermediate euxinic waters must be coupled to superficial waters in which the main path of the N-cycle is direct N_2 fixation, which is a plausible scenario in the Bambuí Group geological context.

Oxygenated Euphotic Zone During the Second second-Order Sequence

The sedimentary rocks from the second second-order sequence of the Bambuí Group are considered to be deposited under a fully restricted sea and this interval is marked by very high $\delta^{13}C_{org}$ values interpreted to be caused by high methanogenic activity under anoxic conditions (Caetano-Filho et al., 2021) and/or recycling of ancient carbonate platforms, higher burial rate of authigenic carbonate, and low-sulfate conditions (Uhlein et al., 2019; Cui et al., 2020). When one compares the $\delta^{15}N_{bulk}$ and the $\delta^{13}C_{org}$ data of the Bambuí during the second second-order sequence it is clear that they are decoupled, which shows that despite big changes in the carbon cycle, the nitrogen cycle was not much affected (**Figure 9**). Still, minor changes occurred. The $\delta^{15}N_{bulk}$ data from this sequence suggests that a nitrate pool was buildup, although smaller and not stable as the one from the basal TST interval, which implies that at least superficial waters were oxygenated. Furthermore, samples from this interval do not present a consistent REY pattern, which shows that freshwater input might have happened during its deposition (Paula-Santos et al., 2020), influencing superficial oxygenation. In all sections, in the second second-order sequence $\delta^{15}N_{bulk}$ values are around ~+3‰. Even in Well 1 section, whose $\delta^{15}N_{bulk}$ data were stable during the EHST/LHST, $\delta^{15}N_{bulk}$ values rise during the second transgression. Since values of $\delta^{15}N_{bulk}$ higher than +2.0‰ can be interpreted as assimilation from a nitrate pool that went through partial denitrification, $\delta^{15}N_{bulk}$ values suggest that during the second second-order sequence transgression there was more oxygen dissolved in superficial waters of forebulge grabens than during the EHST/LHST. As both transgressions recorded in the Bambuí basal second-order sequences present a rise in $\delta^{15}N_{bulk}$ values, which contrast with the regressive tract data, one must think if there is a relationship between transgression and oxygenation. In fact, it was suggested that in the Ediacaran Nama Group persistent oxygenation in mid-ramp settings was controlled by basin hydrodynamics, as data from this unit implies that ventilation was favored by highly energetical flooding events (Wood et al., 2015). Although the tectonic setting of the Bambuí (restricted epicontinental sea) and Nama groups (open sea connected to global ocean) are different, the data presented here show that sea-level changes affected oxygenation and the N-cycle of the former. However, the nitrate pool of the second transgression was not as stable or large as the one from the first TST, which can be inferred by their lower values and also $\delta^{15}N_{bulk}$ oscillation, especially in Arcos section. This is probably a response to a heavily stratified water column, as proposed by other studies (Hippertt et al., 2019; Caetano-Filho et al., 2021).

The Nitrogen Cycle and its Implications for Life Systems

The metazoan fossil record of the Bambuí Group is scarce when compared to other geological Ediacaran/Cambrian units (e.g. Nama Group, Doushantuo Formation). It was hypothesized that such scarcity could be related to anoxia, euxinia, hypersaline and methane-rich conditions of the Bambuí seawater (Hippertt et al., 2019; Caetano-Filho et al., 2021). In addition to this, $\delta^{15}N_{bulk}$ points out that as expected in such a situation, the N-cycle (and hence redox conditions) functioned with a reduced nitrate pool, which could have contributed to hinder the sustainability of complex forms of life. The link between

oxygenation and the Cambrian explosion has been discussed for more than 60 yr (e.g., Nursall, 1959; Wood et al., 2020). Metazoans can indeed habit environments with low oxygen concentrations and some studies even suggest that the amount of O_2 necessary for their metabolism was achieved much earlier than the first appearance of animals on the fossil record (e.g., Mills et al., 2014). However, poorly oxygenated environments cannot support complex life systems or large organisms (Sperling et al., 2013), and concordantly, most of the Ediacaran/Cambrian Fauna is recorded at oxygenated habitats, even if oxygenation was transient (Bowyer et al., 2017; Wood et al., 2019). Therefore, the fluctuations of the generally shallow chemocline's depth in the Bambuí basin may have been one of the drivers of its low macrofauna diversity. In fact, the metazoans reported at the Bambuí Group were found on the Januária's LHST interval, which is, if $\delta^{15}N_{bulk}$ values are considered, the most nitrate rich and oxygenated site during this stage, although with a strong variability, indicating that conditions were unstable (*see* **section 5.2.2**). Redox conditions control the availability of nitrate, which is the form of nitrogen preferred by eukaryotes, as they cannot process direct N_2 fixation and other forms of fixed-N, such as NH_4^+, are mainly consumed by prokaryotes (Fawcett et al., 2011). Complex and large-celled phytoplankton communities generate food webs that are more effective to transfer nutrients and energy to higher trophic levels (Irwin et al., 2006) and the rise of eukaryotes is linked to the development of metazoans as they have higher energetic demands (Brocks et al., 2017). As the $\delta^{15}N_{bulk}$ values from Bambuí Group suggest that nitrate pools were not large or stable, especially during regressions, this could have affected the large-celled plankton and consequently metazoans. In addition, if a large eukaryote community do not develop and the phytoplankton is dominated by prokaryotes, due to their low mass, the sinking rate of the organic matter particulates is low and remineralization of this organic matter is faster and occurs within the water column, enhancing anoxia (Lenton et al., 2014). The relation between nitrate and complex life forms during the Ediacaran/Cambrian transition has been studied mainly in South China (e.g., Wang et al., 2018; Xiang et al., 2018; Liu et al., 2020; Xu et al., 2020) and although it is not possible to link the Bambuí Group to global trends, due to its marine isolation, this study brings more data to clarify how the N-cycle operated at that time. These episodes of nitrate limitation reported here are probably one of the many factors that might have driven the inhospitality of the Bambuí sea, associated with phases of methane or free H_2S in the water column (Caetano-Filho et al., 2021).

CONCLUSION

Relative sea-level variations seem to exert control in the Bambuí N-Cycle. During the first transgression interval (TST), in all the studied sections $\delta^{15}N_{bulk}$ values rise from a minimum of ~+1.0‰ to a maximum of ~+5.0‰, which is parsimoniously explained as a rise of the nitrate reservoir and hence oxygen levels in surface waters. As the restriction of the Bambuí increases (LHST) the NO_3^- stability is disturbed, which is shown by a negative excursion observed in the transition of Arcos EHST to LHST and by increased variability in the $\delta^{15}N_{bulk}$ values of Januária. The low $\delta^{15}N_{bulk}$ observed in the LHST interval of both sections is interpreted as the result of N_2 fixation using Mo as cofactor, indicating a small NO_3^- reservoir. Finally, the slightly higher $\delta^{15}N_{bulk}$ values of the second second-order transgressions show that the nitrate pool increased again, but not to the level that prevailed during the first transgression. In this latter interval, N_2 fixation still played a significant role, maybe due to the restriction of the Bambuí seawater at this stage. Hence, the $\delta^{15}N_{bulk}$ data shows that the basin operated in periods in which N_2 fixation and NO_3^- assimilation intercalated as the dominant path of nitrogen assimilation by primary producers, which can be interpreted in terms of more or less oxygen within superficial waters. Nitrate is a very important nutrient for eukaryotes primary producers and eukaryotes are necessary to fuel higher trophic levels, its depletion in some intervals might be one of the factors that drove the hostile conditions for metazoans in the Bambuí seawater.

DATA AVAILABILITY STATEMENT

The raw data supporting the conclusions of this article will be made available by the authors, without undue reservation.

AUTHOR CONTRIBUTIONS

PF-F analyzed the nitrogen isotopic composition of the samples, interpreted the data and wrote the manuscript. SC-F, MA, PS, and VR acquired N data. SC-F, GP-S, CG, and CB-R obtained K and Al data and also did fieldwork. MB, MK, HR, and RT assisted with tectonic, stratigraphic, petrographic, geochemical information regarding the Bambuí Group and also with the conceptualization of this project. MK and HR provided samples from the sections of Arcos and Well 1 respectively. All the authors collaborated on the final version of the manuscript and assisted with geological interpretations.

FUNDING

This study was funded by the São Paulo Research Foundation (FAPESP) thematic project The Neoproterozoic Earth System and the rise of biological complexity grant 2016/06114-6. PF-F holds a FAPESP scholarship grant #2019/13228-6.

ACKNOWLEDGMENTS

We acknowledge to Lhoist and Petra Energia S.A. for providing drill core samples, Brazilian Geological Service (CPRM) for providing the XRF device, CAPES for institutional support and Pôle de Spectométrie Océan and Institut de Physique du Globe de Paris staff for the technical support in data acquisition. PF-F holds a FAPESP scholarship grant #2019/13228-6. MB, RT, and MK are

fellows of the Brazilian Research Council (#307563/2013-8, #206997/2014-0 and #309106/2017-6, respectively). We are also thankful to the reviewers Dr. Xinqiang Wang and Dr. Fabricio Caxito for constructive suggestions, and to Dr. Graham Shields for the editorial handling of the manuscript.

SUPPLEMENTARY MATERIAL

The Supplementary Material for this article can be found online at: https://www.frontiersin.org/articles/10.3389/feart.2021.692895/full#supplementary-material

REFERENCES

Ader, M., Boudou, J.-P., Javoy, M., Goffe, B., and Daniels, E. (1998). Isotope Study on Organic Nitrogen of Westphalian Anthracites from the Western Middle Field of Pennsylvania (U.S.A.) and from the Bramsche Massif (Germany). *Org. Geochem.* 29, 315–323. doi:10.1016/S0146-6380(98)00072-2

Ader, M., Cartigny, P., Boudou, J.-P., Oh, J.-H., Petit, E., and Javoy, M. (2006). Nitrogen Isotopic Evolution of Carbonaceous Matter During Metamorphism: Methodology and Preliminary Results. *Chem. Geology.* 232, 152–169. doi:10.1016/j.chemgeo.2006.02.019

Ader, M., Sansjofre, P., Halverson, G. P., Busigny, V., Trindade, R. I. F., Kunzmann, M., et al. (2014). Ocean Redox Structure Across the Late Neoproterozoic Oxygenation Event: A Nitrogen Isotope Perspective. *Earth Planet. Sci. Lett.* 396, 1–13. doi:10.1016/j.epsl.2014.03.042

Ader, M., Thomazo, C., Sansjofre, P., Busigny, V., Papineau, D., Laffont, R., et al. (2016). Interpretation of the Nitrogen Isotopic Composition of Precambrian Sedimentary Rocks: Assumptions and Perspectives. *Chem. Geology.* 429, 93–110. doi:10.1016/j.chemgeo.2016.02.010

Alexander, M. (1984). *Biological Nitrogen Fixation: Ecology, Technology and Physiology*. Boston, MA: Springer, 1–258. Available at: https://doi.org/10.1007/978-1-4613-2747-9 (Accessed May 22, 2020).

Alkmim, F. F., and Martins-Neto, M. (2001). "Bacia Intracratônica Do São Francisco: Arcabouço Estrutural e Cenários Evolutivos," in *Bacia do São Francisco: Geologia e Recursos Naturais*. Editors C. P. Pinto and M. Martins-Neto (Belo Horizonte: SBG/MG).

Alkmim, F. F., and Martins-Neto, M. A. (2012). Proterozoic First-Order Sedimentary Sequences of the São Francisco Craton, Eastern Brazil. *Mar. Pet. Geology.* 33, 127–139. doi:10.1016/j.marpetgeo.2011.08.011

Altabet, M. A., Pilskaln, C., Thunell, R., Pride, C., Sigman, D., Chavez, F., et al. (1999). The Nitrogen Isotope Biogeochemistry of Sinking Particles from the Margin of the Eastern North Pacific. *Deep Sea Res. Oceanographic Res. Pap.* 46, 655–679. doi:10.1016/S0967-0637(98)00084-3

An, S., and Gardner, W. (2002). Dissimilatory Nitrate Reduction to Ammonium (DNRA) as a Nitrogen Link, Versus Denitrification as a Sink in a Shallow Estuary (Laguna Madre/Baffin Bay, Texas). *Mar. Ecol. Prog. Ser.* 237, 41–50. doi:10.3354/meps237041

Babinski, M., Vieira, L. C., and Trindade, R. I. F. (2007). Direct Dating of the Sete Lagoas Cap Carbonate (Bambuí Group, Brazil) and Implications for the Neoproterozoic Glacial Events. *Terra Nova* 19, 401–406. doi:10.1111/j.1365-3121.2007.00764.x

Barbosa, O., Braun, O. P. G., Dyer, R. C., and Cunha, C. A. B. M. (1970). *Geologia da região do Triângulo Mineiro*. Rio de Janeiro: DNPM/CPRM.

Beaumont, V., and Robert, F. (1999). Nitrogen Isotope Ratios of Kerogens in Precambrian Cherts: A Record of the Evolution of Atmosphere Chemistry? *Precambrian Res.* 96, 63–82. doi:10.1016/S0301-9268(99)00005-4

Bowyer, F., Wood, R. A., and Poulton, S. W. (2017). Controls on the Evolution of Ediacaran Metazoan Ecosystems: A Redox Perspective. *Geobiology* 15, 516–551. doi:10.1111/gbi.12232

Boyle, R. A., Clark, J. R., Poulton, S. W., Shields-Zhou, G., Canfield, D. E., and Lenton, T. M. (2013). Nitrogen Cycle Feedbacks as a Control on Euxinia in the Mid-proterozoic Ocean. *Nat. Commun.* 4, 1533. doi:10.1038/ncomms2511

Brocks, J. J., Jarrett, A. J. M., Sirantoine, E., Hallmann, C., Hoshino, Y., and Liyanage, T. (2017). The Rise of Algae in Cryogenian Oceans and the Emergence of Animals. *Nature* 548, 578–581. doi:10.1038/nature23457

Brunner, B., Contreras, S., Lehmann, M. F., Matantseva, O., Rollog, M., Kalvelage, T., et al. (2013). Nitrogen Isotope Effects Induced by Anammox Bacteria. *Proc. Natl. Acad. Sci.* 110, 18994–18999. doi:10.1073/pnas.1310488110

Caetano-Filho, S., Paula-Santos, G. M., Guacaneme, C., Babinski, M., Bedoya-Rueda, C., Peloso, M., et al. (2019). Sequence Stratigraphy and Chemostratigraphy of an Ediacaran-Cambrian Foreland-Related Carbonate Ramp (Bambuí Group, Brazil). *Precambrian Res.* 331, 105365. doi:10.1016/j.precamres.2019.105365

Caetano-Filho, S., Sansjofre, P., Ader, M., Paula-Santos, G. M., Guacaneme, C., Babinski, M., et al. (2021). A Large Epeiric Methanogenic Bambuí Sea in the Core of Gondwana Supercontinent? *Geosci. Front.* 12, 203–218. doi:10.1016/j.gsf.2020.04.005

Calvert, S. E. (2004). Beware Intercepts: Interpreting Compositional Ratios in Multi-Component Sediments and Sedimentary Rocks. *Org. Geochem.* 35, 981–987. doi:10.1016/j.orggeochem.2004.03.001

Canfield, D. E., Glazer, A. N., and Falkowski, P. G. (2010). The Evolution and Future of Earth's Nitrogen Cycle. *Science* 330, 192–196. doi:10.1126/science.1186120

Canfield, D. E. (2006). Models of Oxic Respiration, Denitrification and Sulfate Reduction in Zones of Coastal Upwelling. *Geochimica et Cosmochimica Acta* 70, 5753–5765. doi:10.1016/j.gca.2006.07.023

Casciotti, K. L. (2009). Inverse Kinetic Isotope Fractionation During Bacterial Nitrite Oxidation. *Geochimica et Cosmochimica Acta* 73, 2061–2076. doi:10.1016/j.gca.2008.12.022

Caxito, F. A., Frei, R., Uhlein, G. J., Gonçalves Dias, T., Árting, T. B., and Uhlein, A. (2018). Multiproxy Geochemical and Isotope Stratigraphy Records of a Neoproterozoic Oxygenation Event in the Ediacaran Sete Lagoas Cap Carbonate, Bambuí Group, Brazil. *Chem. Geology.* 481, 119–132. doi:10.1016/j.chemgeo.2018.02.007

Caxito, F. d. A., Halverson, G. P., Uhlein, A., Stevenson, R., Gonçalves Dias, T., Uhlein, G. J., et al. (2012). Marinoan Glaciation in East Central Brazil. *Precambrian Res.* 200-203, 38–58. doi:10.1016/j.precamres.2012.01.005

Chen, Y., Diamond, C. W., Stüeken, E. E., Cai, C., Gill, B. C., Zhang, F., et al. (2019). Coupled Evolution of Nitrogen Cycling and Redoxcline Dynamics on the Yangtze Block Across the Ediacaran-Cambrian Transition. *Geochimica et Cosmochimica Acta* 257, 243–265. doi:10.1016/j.gca.2019.05.017

Costa, M. T., and Branco, J. J. R. (1961). "Roteiro para a excursão Belo Horizonte - Brasília," in *Anais do Congresso Brasileiro de Geologia*. Editor J. J. R. Branco (Belo Horizonte: SBG), 1–119.

Cox, G. M., Sansjofre, P., Blades, M. L., Farkas, J., and Collins, A. S. (2019). Dynamic Interaction Between Basin Redox and the Biogeochemical Nitrogen Cycle in an Unconventional Proterozoic Petroleum System. *Sci. Rep.* 9, 5200. doi:10.1038/s41598-019-40783-4

Cremonese, L., Shields-Zhou, G., Struck, U., Ling, H.-F., Och, L., Chen, X., et al. (2013). Marine Biogeochemical Cycling During the Early Cambrian Constrained by a Nitrogen and Organic Carbon Isotope Study of the Xiaotan Section, South China. *Precambrian Res.* 225, 148–165. doi:10.1016/j.precamres.2011.12.004

Crockford, P. W., Wing, B. A., Paytan, A., Hodgskiss, M. S. W., Mayfield, K. K., Hayles, J. A., et al. (2019). Barium-isotopic Constraints on the Origin of Post-Marinoan Barites. *Earth Planet. Sci. Lett.* 519, 234–244. doi:10.1016/j.epsl.2019.05.018

Cui, H., Warren, L. V., Uhlein, G. J., Okubo, J., Liu, X.-M., Plummer, R. E., et al. (2020). Global or Regional? Constraining the Origins of the Middle Bambuí Carbon Cycle Anomaly in Brazil. *Precambrian Res.* 348, 105861. doi:10.1016/j.precamres.2020.105861

Dardenne, M. A. (1978). "Síntese sobre a estratigrafia Do Grupo Bambuí no Brasil Central," in Proceedings of the 30th Congresso Brasileiro de Geologia, November, 1978 (Recife: SBG), 507–610.

Delpomdor, F. R. A., Ilambwetsi, A. M., Caxito, F. A., and Pedrosa-Soares, A. C. (2020). New Interpretation of the Basal Bambuí Group, Sete Lagoas High (Minas Gerais, E Brazil) by Sedimentological Studies and Regional Implications for the Aftermath of the Marinoan Glaciation: Correlations Across Brazil and Central Africa. *Geol. Belg.* 23, 1–17. doi:10.20341/gb.2019.010

Dong, L. F., Sobey, M. N., Smith, C. J., Rusmana, I., Phillips, W., Stott, A., et al. (2011). Dissimilatory Reduction of Nitrate to Ammonium, Not Denitrification

or Anammox, Dominates Benthic Nitrate Reduction in Tropical Estuaries. *Limnol. Oceanogr.* 56, 279–291. doi:10.4319/lo.2011.56.1.0279

Edwards, A. M., Platt, T., and Sathyendranath, S. (2004). The High-Nutrient, Low-Chlorophyll Regime of the Ocean: Limits on Biomass and Nitrate Before and After Iron Enrichment. *Ecol. Model.* 171, 103–125. doi:10.1016/j.ecolmodel.2003.06.001

Fawcett, S. E., Lomas, M. W., Casey, J. R., Ward, B. B., and Sigman, D. M. (2011). Assimilation of Upwelled Nitrate by Small Eukaryotes in the Sargasso Sea. *Nat. Geosci* 4, 717–722. doi:10.1038/ngeo1265

Fogel, M. L., and Cifuentes, L. A. (1993). "Isotope Fractionation During Primary Production," in *Organic Geochemistry*. Editors M. H. Engel and S. A. Macko (Boston, MA: Springer), 73–98. doi:10.1007/978-1-4615-2890-6_3

Füssel, J., Lam, P., Lavik, G., Jensen, M. M., Holtappels, M., Günter, M., et al. (2012). Nitrite Oxidation in the Namibian Oxygen Minimum Zone. *ISME J.* 6, 1200–1209. doi:10.1038/ismej.2011.178

Gallon, J. R. (1981). The Oxygen Sensitivity of Nitrogenase: A Problem for Biochemists and Micro-organisms. *Trends Biochem. Sci.* 6, 19–23. doi:10.1016/0968-0004(81)90008-6

Glass, J. B., Wolfe-Simon, F., and Anbar, A. D. (2009). Coevolution of Metal Availability and Nitrogen Assimilation in Cyanobacteria and Algae. *Geobiology* 7, 100–123. doi:10.1111/j.1472-4669.2009.00190.x

Godfrey, L. V., and Falkowski, P. G. (2009). The Cycling and Redox State of Nitrogen in the Archaean Ocean. *Nat. Geosci* 2, 725–729. doi:10.1038/ngeo633

Granger, J., Sigman, D. M., Lehmann, M. F., and Tortell, P. D. (2008). Nitrogen and Oxygen Isotope Fractionation During Dissimilatory Nitrate Reduction by Denitrifying Bacteria. *Limnol. Oceanogr.* 53, 2533–2545. doi:10.4319/lo.2008.53.6.2533

Granger, J., Sigman, D. M., Rohde, M. M., Maldonado, M. T., and Tortell, P. D. (2010). N and O Isotope Effects During Nitrate Assimilation by Unicellular Prokaryotic and Eukaryotic Plankton Cultures. *Geochimica et Cosmochimica Acta* 74, 1030–1040. doi:10.1016/j.gca.2009.10.044

Greenfield, L. G. (1992). Acid Hydrolysis and the Release of Fixed Ammonium From Soils. *Soil Biol. Biochem.* 24, 271–273. doi:10.1016/0038-0717(92)90229-Q

Grotzinger, J. P., Bowring, S. A., Saylor, B. Z., and Kaufman, A. J. (1995). Biostratigraphic and Geochronologic Constraints on Early Animal Evolution. *Science* 270, 598–604. doi:10.1126/science.270.5236.598

Guacaneme, C., Babinski, M., Paula-Santos, G. M. d., and Pedrosa-Soares, A. C. (2017). C, O, and Sr Isotopic Variations in Neoproterozoic-Cambrian Carbonate Rocks from Sete Lagoas Formation (Bambuí Group), in the Southern São Francisco Basin, Brazil. *Braz. J. Geol.* 47, 521–543. doi:10.1590/2317-4889201720160126

Haug, G. H., Pedersen, T. F., Sigman, D. M., Calvert, S. E., Nielsen, B., and Peterson, L. C. (1998). Glacial/interglacial Variations in Production and Nitrogen Fixation in the Cariaco Basin During the Last 580 Kyr. *Paleoceanography* 13, 427–432. doi:10.1029/98PA01976

Hippertt, J. P., Caxito, F. A., Uhlein, G. J., Nalini, H. A., Sial, A. N., Abreu, A. T., et al. (2019). The Fate of a Neoproterozoic Intracratonic Marine Basin: Trace Elements, TOC and IRON Speciation Geochemistry of the Bambuí Basin, Brazil. *Precambrian Res.* 330, 101–120. doi:10.1016/j.precamres.2019.05.001

Hoch, M. P., Fogel, M. L., and Kirchman, D. L. (1992). Isotope Fractionation Associated with Ammonium Uptake by a Marine Bacterium. *Limnol. Oceanogr.* 37, 1447–1459. doi:10.4319/lo.1992.37.7.1447

Iglesias, M., and Uhlein, A. (2009). Estratigrafia Do Grupo Bambuí e coberturas fanerozóicas no vale Do rio São Francisco, norte de Minas Gerais. *RBG* 39, 256–266. doi:10.25249/0375-7536.2009392256266

Ingall, E., and Jahnke, R. (1997). Influence of Water-Column Anoxia on the Elemental Fractionation of Carbon and Phosphorus During Sediment Diagenesis. *Mar. Geology.* 139, 219–229. doi:10.1016/S0025-3227(96)00112-0

Irwin, A. J., Finkel, Z. V., Schofield, O. M. E., and Falkowski, P. G. (2006). Scaling-up from Nutrient Physiology to the Size-Structure of Phytoplankton Communities. *J. Plankton Res.* 28, 459–471. doi:10.1093/plankt/fbi148

Iyer, S., Babinski, M., Krouse, H., and Chemalejr, F., Jr (1995). Highly 13C-Enriched Carbonate and Organic Matter in the Neoproterozoic Sediments of the BambuíGroup, Brazil. *Precambrian Res.* 73, 271–282. doi:10.1016/0301-9268(94)00082-3

Jensen, M. M., Lam, P., Revsbech, N. P., Nagel, B., Gaye, B., Jetten, M. S., et al. (2011). Intensive Nitrogen Loss over the Omani Shelf Due to Anammox Coupled with Dissimilatory Nitrite Reduction to Ammonium. *ISME J.* 5, 1660–1670. doi:10.1038/ismej.2011.44

Kessler, A. J., Bristow, L. A., Cardenas, M. B., Glud, R. N., Thamdrup, B., and Cook, P. L. M. (2014). The Isotope Effect of Denitrification in Permeable Sediments. *Geochimica et Cosmochimica Acta* 133, 156–167. doi:10.1016/j.gca.2014.02.029

Kikumoto, R., Tahata, M., Nishizawa, M., Sawaki, Y., Maruyama, S., Shu, D., et al. (2014). Nitrogen Isotope Chemostratigraphy of the Ediacaran and Early Cambrian Platform Sequence at Three Gorges, South China. *Gondwana Res.* 25, 1057–1069. doi:10.1016/j.gr.2013.06.002

Kuchenbecker, M., Atman, D., Costa, R. D. d., Pedrosa-Soares, A., and Babinski, M. (2016a). A Formação Gorutuba: sedimentação litorânea a continental na margem leste da Bacia Bambuí (MG). *Geol. USP. Sér. Cient.* 16, 67. doi:10.11606//issn.2316-9095.v16i2p67-81

Kuchenbecker, M., Babinski, M., Pedrosa-Soares, A. C., Lopes-Silva, L., and Pimenta, F. (2016b). Chemostratigraphy of the Lower Bambuí Group, Southwestern São Francisco Craton, Brazil: Insights on Gondwana Paleoenvironments. *Braz. J. Geol.* 46, 145–162. doi:10.1590/2317-488920160030285

Kuchenbecker, M., Costa, R. D. d., Babinski, M., Pedrosa-Soares, A. C., Lopes-Silva, L., and Pimenta, F. (2013). Proveniência e análise sedimentar da porção basal Do Grupo Bambuí em Arcos (MG). *Geol. Usp, Sér. Cient.* 13, 49–61. doi:10.5327/Z1519-874X201300040003

Kuchenbecker, M., Lopes-Silva, L., Pimenta, F., Pedrosa-Soares, A. C., and Babinski, M. (2011). Estratigrafia da porção basal Do grupo Bambuí na região de Arcos (MG): uma contribuição a partir de testemunhos de sondagem. *Geol. Usp, Sér. Cient.* 11, 45–54. doi:10.5327/Z1519-874X2011000200003

Kuchenbecker, M., Pedrosa-Soares, A. C., Babinski, M., Reis, H. L. S., Atman, D., and Costa, R. D. d. (2020). Towards an Integrated Tectonic Model for the Interaction Between the Bambuí basin and the Adjoining Orogenic Belts: Evidences from the Detrital Zircon Record of Syn-Orogenic Units. *J. South Am. Earth Sci.* 104, 102831. doi:10.1016/j.jsames.2020.102831

Lehmann, M. F., Bernasconi, S. M., Barbieri, A., and McKenzie, J. A. (2002). Preservation of Organic Matter and Alteration of its Carbon and Nitrogen Isotope Composition during Simulated and In Situ Early Sedimentary Diagenesis. *Geochimica et Cosmochimica Acta* 66, 3573–3584. doi:10.1016/S0016-7037(02)00968-7

Lenton, T. M., Boyle, R. A., Poulton, S. W., Shields-Zhou, G. A., and Butterfield, N. J. (2014). Co-evolution of Eukaryotes and Ocean Oxygenation in the Neoproterozoic Era. *Nat. Geosci* 7, 257–265. doi:10.1038/ngeo2108

Li, L., Lollar, B. S., Li, H., Wortmann, U. G., and Lacrampe-Couloume, G. (2012). Ammonium Stability and Nitrogen Isotope Fractionations for -NH3(aq)-NH3(gas) Systems at 20-70°C and pH of 2-13: Applications to Habitability and Nitrogen Cycling in Low-Temperature Hydrothermal Systems. *Geochimica et Cosmochimica Acta* 84, 280–296. doi:10.1016/j.gca.2012.01.040

Liu, K.-K., Kao, S.-J., Chiang, K.-P., Gong, G.-C., Chang, J., Cheng, J.-S., et al. (2013). Concentration Dependent Nitrogen Isotope Fractionation during Ammonium Uptake by Phytoplankton under an Algal Bloom Condition in the Danshuei Estuary, Northern Taiwan. *Mar. Chem.* 157, 242–252. doi:10.1016/j.marchem.2013.10.005

Liu, Y., Magnall, J. M., Gleeson, S. A., Bowyer, F., Poulton, S. W., and Zhang, J. (2020). Spatio-temporal Evolution of Ocean Redox and Nitrogen Cycling in the Early Cambrian Yangtze Ocean. *Chem. Geology.* 554, 119803. doi:10.1016/j.chemgeo.2020.119803

Martins, M., and Lemos, V. B. (2007). Análise estratigráfica das seqüências neoproterozóicas da Bacia Do São Francisco. *RBG* 37, 156–167. doi:10.25249/0375-7536.200737S4156167

Martins-Neto, M. A., and Hercos, C. M. (2002). "Sedimentation and Tectonic Setting of Early Neoproterozoic Glacial Deposits in South-Eastern Brazil," in *Precambrian Sedimentary Environments*. Editors W. Altermann and P. L. Corcoran (Oxford, UK: Blackwell Publishing Ltd.), 383–403. doi:10.1002/9781444304312.ch18

Martins-Neto, M. A., Pedrosa-Soares, A. C., and Lima, S. A. A. (2001). Tectono-sedimentary Evolution of Sedimentary Basins from Late Paleoproterozoic to Late Neoproterozoic in the São Francisco Craton and Araçuaí Fold belt, Eastern Brazil. *Sediment. Geology.* 141-142, 343–370. doi:10.1016/S0037-0738(01)00082-3

Martins-Neto, M. A. (2009). Sequence Stratigraphic Framework of Proterozoic Successions in Eastern Brazil. *Mar. Pet. Geology.* 26, 163–176. doi:10.1016/j.marpetgeo.2007.10.001

McCready, R. G. L., Gould, W. D., and Barendregt, R. W. (1983). Nitrogen Isotope Fractionation During the Reduction of NO3− to NH4+ by Desulfovibrio Sp. *Can. J. Microbiol.* 29, 231–234. doi:10.1139/m83-038

Meija, J., Coplen, T. B., Berglund, M., Brand, W. A., De Bièvre, P., Gröning, M., et al. (2016). Isotopic Compositions of the Elements 2013 (IUPAC Technical Report). *Pure Appl. Chem.* 88, 293–306. doi:10.1515/pac-2015-0503

Meyer, K. M., Ridgwell, A., and Payne, J. L. (2016). The Influence of the Biological Pump on Ocean Chemistry: Implications for Long-term Trends in Marine Redox Chemistry, the Global Carbon Cycle, and Marine Animal Ecosystems. *Geobiology* 14, 207–219. doi:10.1111/gbi.12176

Mills, D. B., Ward, L. M., Jones, C., Sweeten, B., Forth, M., Treusch, A. H., et al. (2014). Oxygen Requirements of the Earliest Animals. *Proc. Natl. Acad. Sci.* 111, 4168–4172. doi:10.1073/pnas.1400547111

Möbius, J. (2013). Isotope Fractionation During Nitrogen Remineralization (Ammonification): Implications for Nitrogen Isotope Biogeochemistry. *Geochimica et Cosmochimica Acta* 105, 422–432. doi:10.1016/j.gca.2012.11.048

Morales, L. V., Granger, J., Chang, B. X., Prokopenko, M. G., Plessen, B., Gradinger, R., et al. (2014). Elevated 15N/14N in Particulate Organic Matter, Zooplankton, and Diatom Frustule-Bound Nitrogen in the Ice-Covered Water Column of the Bering Sea Eastern Shelf. *Deep Sea Res. Part Topical Stud. Oceanography* 109, 100–111. doi:10.1016/j.dsr2.2014.05.008

Moreira, D. S., Uhlein, A., Dussin, I. A., Uhlein, G. J., and Pimentel Misuzaki, A. M. (2020). A Cambrian Age for the Upper Bambuí Group, Brazil, Supported by the First U-Pb Dating of Volcaniclastic Bed. *J. South Am. Earth Sci.* 99, 102503. doi:10.1016/j.jsames.2020.102503

Müller, P. J. (1977). Ratios in Pacific Deep-Sea Sediments: Effect of Inorganic Ammonium and Organic Nitrogen Compounds Sorbed by Clays. *Geochimica et Cosmochimica Acta* 41, 765–776. doi:10.1016/0016-7037(77)90047-3

Nursall, J. R. (1959). Oxygen as a Prerequisite to the Origin of the Metazoa. *Nature* 183, 1170–1172. doi:10.1038/1831170b0

Okubo, J., Muscente, A. D., Luvizotto, G. L., Uhlein, G. J., and Warren, L. V. (2018). Phosphogenesis, Aragonite Fan Formation and Seafloor Environments Following the Marinoan Glaciation. *Precambrian Res.* 311, 24–36. doi:10.1016/j.precamres.2018.04.002

Okubo, J., Warren, L. V., Luvizotto, G. L., Varejão, F. G., Quaglio, F., Uhlein, G. J., et al. (2020). Evidences of Seismic Events During the Sedimentation of Sete Lagoas Formation (Bambuí Group - Ediacaran, Brazil). *J. South Am. Earth Sci.* 98, 102461. doi:10.1016/j.jsames.2019.102461

Paula-Santos, G. M., Babinski, M., Kuchenbecker, M., Caetano-Filho, S., Trindade, R. I., and Pedrosa-Soares, A. C. (2015). New Evidence of an Ediacaran Age for the Bambuí Group in Southern São Francisco Craton (Eastern Brazil) from Zircon U-Pb Data and Isotope Chemostratigraphy. *Gondwana Res.* 28, 702–720. doi:10.1016/j.gr.2014.07.012

Paula-Santos, G. M., Caetano-Filho, S., Babinski, M., and Enzweiler, J. (2018). Rare Earth Elements of Carbonate Rocks from the Bambuí Group, Southern São Francisco Basin, Brazil, and Their Significance as Paleoenvironmental Proxies. *Precambrian Res.* 305, 327–340. doi:10.1016/j.precamres.2017.12.023

Paula-Santos, G. M., Caetano-Filho, S., Babinski, M., Trindade, R. I. F., and Guacaneme, C. (2017). Tracking Connection and Restriction of West Gondwana São Francisco Basin Through Isotope Chemostratigraphy. *Gondwana Res.* 42, 280–305. doi:10.1016/j.gr.2016.10.012

Paula-Santos, G. M., Caetano-Filho, S., Enzweiler, J., Navarro, M. S., Babinski, M., Guacaneme, C., et al. (2020). Rare Earth Elements in the Terminal Ediacaran Bambuí Group Carbonate Rocks (Brazil): Evidence for High Seawater Alkalinity during Rise of Early Animals. *Precambrian Res.* 336, 105506. doi:10.1016/j.precamres.2019.105506

Paula-Santos, G. M. d., and Babinski, M. (2018). Sedimentary Provenance in the Southern Sector of the São Francisco Basin, SE Brazil. *Braz. J. Geol.* 48, 51–74. doi:10.1590/2317-4889201820170061

Pennock, J. R., Velinsky, D. J., Ludlam, J. M., Sharp, J. H., and Fogel, M. L. (1996). Isotopic Fractionation of Ammonium and Nitrate during Uptake by Skeletonema Costatum : Implications for δ15N Dynamics Under Bloom Conditions. *Limnol. Oceanogr.* 41, 451–459. doi:10.4319/lo.1996.41.3.0451

Perrella Júnior, P., Uhlein, A., Uhlein, G. J., Sial, A. N., Pedrosa-Soares, A. C., and Lima, O. N. B. d. (2017). Facies Analysis, Sequence Stratigraphy and Chemostratigraphy of the Sete Lagoas Formation (Bambui Group), Northern Minas Gerais State, Brazil: Evidence of a Cap Carbonate Deposited on the Januária Basement High. *Braz. J. Geol.* 47, 59–77. doi:10.1590/2317-4889201720160112

Quan, T. M., Wright, J. D., and Falkowski, P. G. (2013). Co-variation of Nitrogen Isotopes and Redox States Through Glacial-Interglacial Cycles in the Black Sea. *Geochimica et Cosmochimica Acta* 112, 305–320. doi:10.1016/j.gca.2013.02.029

Reis, H. L. S., and Alkmim, F. F. (2015). Anatomy of a Basin-controlled Foreland Fold-Thrust Belt Curve: The Três Marias Salient, São Francisco Basin, Brazil. *Mar. Pet. Geology.* 66, 711–731. doi:10.1016/j.marpetgeo.2015.07.013

Reis, H. L. S., Suss, J. F., Fonseca, R. C. S., and Alkmim, F. F. (2017). Ediacaran Forebulge Grabens of the Southern São Francisco Basin, SE Brazil: Craton Interior Dynamics During West Gondwana Assembly. *Precambrian Res.* 302, 150–170. doi:10.1016/j.precamres.2017.09.023

Reis, H. L. S., and Suss, J. F. (2016). Mixed Carbonate-Siliciclastic Sedimentation in Forebulge Grabens: An Example from the Ediacaran Bambuí Group, São Francisco Basin, Brazil. *Sediment. Geology.* 339, 83–103. doi:10.1016/j.sedgeo.2016.04.004

Sanchez, E. A. M., Uhlein, A., and Fairchild, T. R. (2021). Treptichnus Pedum in the Três Marias Formation, South-central Brazil, and its Implications for the Ediacaran-Cambrian Transition in South America. *J. South Am. Earth Sci.* 105, 102983. doi:10.1016/j.jsames.2020.102983

Santos, R. V., Souza de Alvarenga, C. J., Babinski, M., Ramos, M. L. S., Cukrov, N., Fonseca, M. A., et al. (2004). Carbon Isotopes of Mesoproterozoic-Neoproterozoic Sequences from Southern São Francisco Craton and Araçuaí Belt, Brazil: Paleographic Implications. *J. South Am. Earth Sci.* 18, 27–39. doi:10.1016/j.jsames.2004.08.009

Schimmelmann, A., Mastalerz, M., Gao, L., Sauer, P. E., and Topalov, K. (2009). Dike Intrusions into Bituminous Coal, Illinois Basin: H, C, N, O Isotopic Responses to Rapid and Brief Heating. *Geochimica et Cosmochimica Acta* 73, 6264–6281. doi:10.1016/j.gca.2009.07.027

Seefeldt, L. C., Hoffman, B. M., and Dean, D. R. (2009). Mechanism of Mo-dependent Nitrogenase. *Annu. Rev. Biochem.* 78, 701–722. doi:10.1146/annurev.biochem.78.070907.103812

Seer, H. J., Moraes, L. C., and Fogaça, A. C. C. (1989). *Roteiro Geológico para a região de Lagoa Formosa-Chumbo-Carmo do Paranaíba, MG*. Belo Horizonte: SBG/MG.

Sigman, D. M., Altabet, M. A., McCorkle, D. C., Francois, R., and Fischer, G. (1999). The δ15N of Nitrate in the Southern Ocean: Consumption of Nitrate in Surface Waters. *Glob. Biogeochem. Cycles* 13, 1149–1166. doi:10.1029/1999GB900038

Sigman, D. M., and Fripiat, F.. (2019). Nitrogen Isotopes in the Ocean. *Encyclopedia of Ocean Sciences* 1, 263–278. doi:10.1016/B978-0-12-409548-9.11605-7

Sperling, E. A., Frieder, C. A., Raman, A. V., Girguis, P. R., Levin, L. A., and Knoll, A. H. (2013). Oxygen, Ecology, and the Cambrian Radiation of Animals. *Proc. Natl. Acad. Sci. U S A.* 110, 13446–13451. doi:10.1073/pnas.1312778110

Stüeken, E. E., Buick, R., and Schauer, A. J. (2015). Nitrogen Isotope Evidence for Alkaline Lakes on Late Archean Continents. *Earth Planet. Sci. Lett.* 411, 1–10. doi:10.1016/j.epsl.2014.11.037

Stüeken, E. E., Kipp, M. A., Koehler, M. C., and Buick, R. (2016). The Evolution of Earth's Biogeochemical Nitrogen Cycle. *Earth-Science Rev.* 160, 220–239. doi:10.1016/j.earscirev.2016.07.007

Stüeken, E. E., Zaloumis, J., Meixnerová, J., and Buick, R. (2017). Differential Metamorphic Effects on Nitrogen Isotopes in Kerogen Extracts and Bulk Rocks. *Geochimica et Cosmochimica Acta* 217, 80–94. doi:10.1016/j.gca.2017.08.019

Sun, Y. D., Zulla, M. J., Joachimski, M. M., Bond, D. P. G., Wignall, P. B., Zhang, Z. T., et al. (2019). Ammonium Ocean Following the End-Permian Mass Extinction. *Earth Planet. Sci. Lett.* 518, 211–222. doi:10.1016/j.epsl.2019.04.036

Tesdal, J.-E., Galbraith, E. D., and Kienast, M. (2013). Nitrogen Isotopes in Bulk Marine Sediment: Linking Seafloor Observations with Subseafloor Records. *Biogeosciences* 10, 101–118. doi:10.5194/bg-10-101-2013

Thomazo, C., Ader, M., and Philippot, P. (2011). Extreme 15N-Enrichments in 2.72-Gyr-Old Sediments: Evidence for a Turning Point in the Nitrogen Cycle. *Geobiology* 9, 107–120. doi:10.1111/j.1472-4669.2011.00271.x

Thomazo, C., and Papineau, D. (2013). Biogeochemical Cycling of Nitrogen on the Early Earth. *Elements* 9, 345–351. doi:10.2113/gselements.9.5.345

Tyrrell, T. (1999). The Relative Influences of Nitrogen and Phosphorus on Oceanic Primary Production. *Nature* 400, 525–531. doi:10.1038/22941

Uhlein, A., Baptista, M. C., Seer, H. J., Caxito, F. de. A., Uhlein, G. J., and Dardenne, M. A. (2011). A Formação Lagoa Formosa, Grupo Bambuí (MG): Sistema Deposicional De Leque Submarino Em Bacia De Ante-país. *Geonomos* 19 (2), 163–172. doi:10.18285/geonomos.v19i2.51

Uhlein, G. J., Uhlein, A., Halverson, G. P., Stevenson, R., Caxito, F. A., Cox, G. M., et al. (2016). The Carrancas Formation, Bambuí Group: A Record of Pre-marinoan Sedimentation on the Southern São Francisco Craton, Brazil. *J. South Am. Earth Sci.* 71, 1–16. doi:10.1016/j.jsames.2016.06.009

Uhlein, G. J., Uhlein, A., Pereira, E., Caxito, F. A., Okubo, J., Warren, L. V., et al. (2019). Ediacaran Paleoenvironmental Changes Recorded in the Mixed Carbonate-Siliciclastic Bambuí Basin, Brazil. *Palaeogeogr. Palaeoclimatol. Palaeoecol.* 517, 39–51. doi:10.1016/j.palaeo.2018.12.022

Uhlein, G. J., Uhlein, A., Stevenson, R., Halverson, G. P., Caxito, F. A., and Cox, G. M. (2017). Early to Late Ediacaran Conglomeratic Wedges from a Complete Foreland Basin Cycle in the Southwest São Francisco Craton, Bambuí Group, Brazil. *Precambrian Res.* 299, 101–116. doi:10.1016/j.precamres.2017.07.020

Van Cappellen, P., and Ingall, E. D. (1994). Benthic Phosphorus Regeneration, Net Primary Production, and Ocean Anoxia: A Model of the Coupled Marine Biogeochemical Cycles of Carbon and Phosphorus. *Paleoceanography* 9, 677–692. doi:10.1029/94PA01455

Vieira, L. C., Almeida, R. P., Trindade, R. I. F., Nogueira, A. C. R., and Janikian, L. (2007a). A Formação Sete Lagoas em sua área-tipo: fácies, estratigrafia e sistemas deposicionais. *RBG* 37, 1–14. doi:10.25249/0375-7536.200737S4114

Vieira, L. C., Trindade, R. I. F., Nogueira, A. C. R., and Ader, M. (2007b). Identification of a Sturtian Cap Carbonate in the Neoproterozoic Sete Lagoas Carbonate Platform, Bambuí Group, Brazil. *Comptes Rendus Geosci.* 339, 240–258. doi:10.1016/j.crte.2007.02.003

Wang, D., Struck, U., Ling, H.-F., Guo, Q.-J., Shields-Zhou, G. A., Zhu, M.-Y., et al. (2015). Marine Redox Variations and Nitrogen Cycle of the Early Cambrian Southern Margin of the Yangtze Platform, South China: Evidence from Nitrogen and Organic Carbon Isotopes. *Precambrian Res.* 267, 209–226. doi:10.1016/j.precamres.2015.06.009

Wang, X., Jiang, G., Shi, X., Peng, Y., and Morales, D. C. (2018). Nitrogen Isotope Constraints on the Early Ediacaran Ocean Redox Structure. *Geochimica et Cosmochimica Acta* 240, 220–235. doi:10.1016/j.gca.2018.08.034

Warren, L. V., Quaglio, F., Riccomini, C., Simões, M. G., Poiré, D. G., Strikis, N. M., et al. (2014). The Puzzle Assembled: Ediacaran Guide Fossil Cloudina Reveals an Old Proto-Gondwana Seaway. *Geology* 42, 391–394. doi:10.1130/G35304.1

Wood, R. A., Poulton, S. W., Prave, A. R., Hoffmann, K.-H., Clarkson, M. O., Guilbaud, R., et al. (2015). Dynamic Redox Conditions Control Late Ediacaran Metazoan Ecosystems in the Nama Group, Namibia. *Precambrian Res.* 261, 252–271. doi:10.1016/j.precamres.2015.02.004

Wood, R., Donoghue, P. C. J., Lenton, T. M., Liu, A. G., and Poulton, S. W. (2020). The Origin and Rise of Complex Life: Progress Requires Interdisciplinary Integration and Hypothesis Testing. *Interf. Focus.* 10, 20200024. doi:10.1098/rsfs.2020.0024

Wood, R., Liu, A. G., Bowyer, F., Wilby, P. R., Dunn, F. S., Kenchington, C. G., et al. (2019). Integrated Records of Environmental Change and Evolution Challenge the Cambrian Explosion. *Nat. Ecol. Evol.* 3, 528–538. doi:10.1038/s41559-019-0821-6

Xiang, L., Schoepfer, S. D., Zhang, H., Cao, C.-q., and Shen, S.-z. (2018). Evolution of Primary Producers and Productivity Across the Ediacaran-Cambrian Transition. *Precambrian Res.* 313, 68–77. doi:10.1016/j.precamres.2018.05.023

Xu, D., Wang, X., Shi, X., Tang, D., Zhao, X., Feng, L., et al. (2020). Nitrogen Cycle Perturbations Linked to Metazoan Diversification During the Early Cambrian. *Palaeogeogr. Palaeoclimatol. Palaeoecol.* 538, 109392. doi:10.1016/j.palaeo.2019.109392

Yang, Y., Wang, Y., Zhang, Z., Wang, W., Ren, X., Gao, Y., et al. (2018). Diurnal and Seasonal Variations of Thermal Stratification and Vertical Mixing in a Shallow Fresh Water Lake. *J. Meteorol. Res.* 32, 219–232. doi:10.1007/s13351-018-7099-5

Zerkle, A. L. (2005). Biogeochemical Signatures through Time as Inferred from Whole Microbial Genomes. *Am. J. Sci.* 305, 467–502. doi:10.2475/ajs.305.6-8.467

Zhang, X., Sigman, D. M., Morel, F. M. M., and Kraepiel, A. M. L. (2014). Nitrogen Isotope Fractionation by Alternative Nitrogenases and Past Ocean Anoxia. *Proc. Natl. Acad. Sci. USA* 111, 4782–4787. doi:10.1073/pnas.1402976111

Conflict of Interest: The authors declare that the research was conducted in the absence of any commercial or financial relationships that could be construed as a potential conflict of interest.

Publisher's Note: All claims expressed in this article are solely those of the authors and do not necessarily represent those of their affiliated organizations, or those of the publisher, the editors and the reviewers. Any product that may be evaluated in this article, or claim that may be made by its manufacturer, is not guaranteed or endorsed by the publisher.

frontiers in Earth Science

REVIEW
published: 12 August 2021
doi: 10.3389/feart.2021.705691

Interpretation of Nitrogen Isotope Profiles in Petroleum Systems: A Review

Tracy M. Quan and Oyeleye O. Adeboye*

Boone Pickens School of Geology, Oklahoma State University, Stillwater, OK, United States

Bulk sedimentary nitrogen isotope profiles are often used as proxies for depositional redox conditions, nitrogen cycling, and nutrient uptake in modern and ancient marine systems. The general preference in terms of analysis is that the sediments measured have undergone minimal thermal alteration, as post-depositional processes might have altered the initial $\delta^{15}N$ signal, thus complicating the interpretation of these records. Although not a traditional proxy for petroleum evaluation purposes, recently the use of nitrogen isotopes in petroleum systems has been investigated as potential proxies to reconstruct paleoenvironmental conditions such as redox, and for organic matter evaluation. In this paper we review the use of nitrogen isotope data in petroleum systems, their interpretations, and factors that may complicate their use as proxies. We review the evidence for nitrogen isotopic fractionation during diagenesis, catagenesis, and fluid migration as determined by lab experiments, and how these might impact interpretation of $\delta^{15}N$ data in petroleum systems. We also analyze the use and interpretation of $\delta^{15}N$ data from petroleum-producing reservoir units, including unconventional reservoirs and lacustrine basins. Lastly, we discuss potential applications for nitrogen isotopes in petroleum systems with regards to their use as both geochemical proxies and as tools to evaluate petroleum reservoirs.

Keywords: nitrogen isotopes, petroleum systems, diagenesis, redox, catagenesis, organic matter transformation

OPEN ACCESS

Edited by:
Thomas Algeo,
University of Cincinnati, United States

Reviewed by:
Michael Tuite,
NASA Jet Propulsion Laboratory (JPL), United States
Aiguo Dong,
China University of Geosciences, China

****Correspondence:***
Tracy M. Quan
tracy.quan@okstate.edu

Specialty section:
This article was submitted to Geochemistry, a section of the journal Frontiers in Earth Science

Received: *06 May 2021*
Accepted: *02 August 2021*
Published: *12 August 2021*

Citation:
Quan TM and Adeboye OO (2021) Interpretation of Nitrogen Isotope Profiles in Petroleum Systems: A Review. Front. Earth Sci. 9:705691. doi: 10.3389/feart.2021.705691

INTRODUCTION

Nitrogen isotopes are being used in an increasing number of recent sedimentary system studies as paleoenvironmental proxies. Nitrogen isotope ($\delta^{15}N$) measurements of sediments have been shown to record processes occurring in the water column, allowing them to serve as proxies for paleoredox conditions and nitrogen cycling (Altabet and Francois, 1994). As a result, sedimentary $\delta^{15}N$ data have been used to investigate the causes of mass extinctions, the extent of ocean anoxic events, and changes in oxygen minimum zones on glacial-interglacial time scales (e.g., Ganeshram et al., 1995; Calvert et al., 2001; Jenkyns et al., 2001; Quan et al., 2008; Ryabenko et al., 2012). Sedimentary $\delta^{15}N$ profiles have also been used to identify intervals and locations where the nitrogen cycle and nutrient regimes appear to have been significantly altered from that for the modern-day, including Precambrian conditions and Mediterranean sapropel deposits (e.g., Godfrey and Falkowski, 2009; Higgins et al., 2010; Ader et al., 2016). These evaluations of paleoredox conditions and changes in the nitrogen cycle can provide critical evidence for the occurrence of larger biogeochemical cycle changes or geological events,

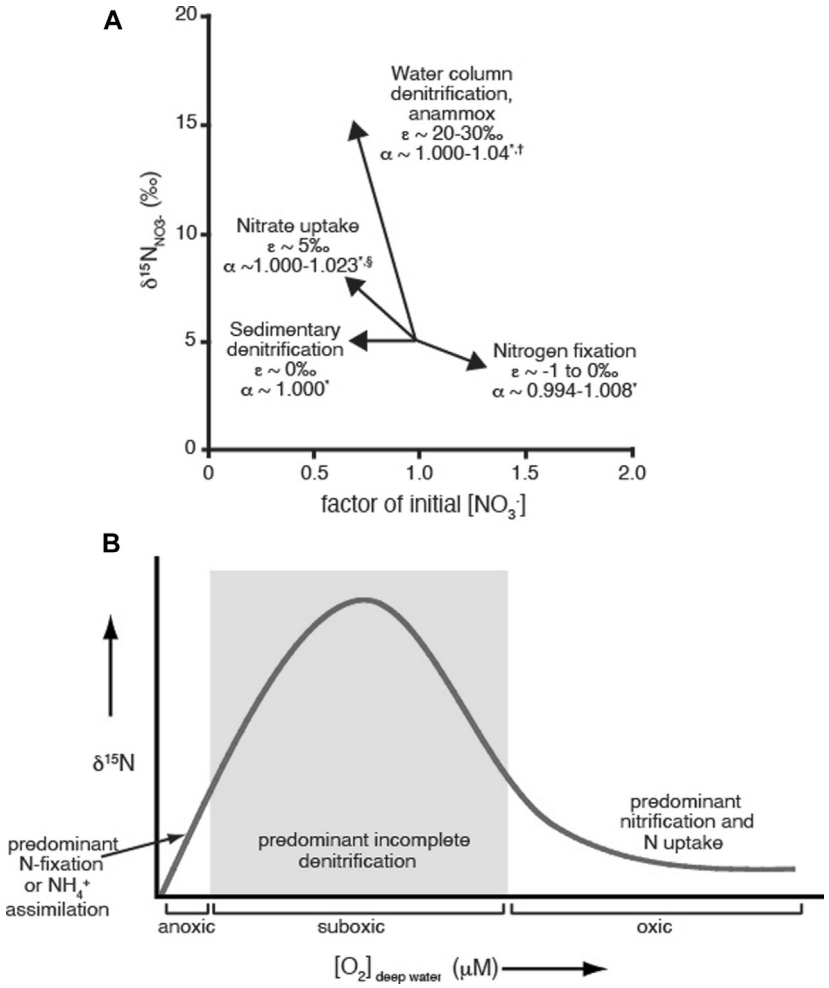

FIGURE 1 | (A): Illustration of selected nitrogen reactions that occur in marine systems showing their instantaneous impact on nitrate $\delta^{15}N$ value and concentration (assuming initial $\delta^{15}N_{NO3-}$ = 5‰). Isotope effect (ε) values are from Sigman and Casciotti (2001); fractionation factor (α) ranges are taken from *Wada et al. 1980 and references therein, †Brunner et al. 2013 and §Talbot 2001 and references therein. Reprinted (modified) from the Encyclopedia of Ocean Sciences, Sigman DM, and Casciotti KL, Nitrogen Isotopes in the Ocean, *p*. 1884–1894, Copyright 2001, with author permission. **(B)**: Conceptual model illustrating how $\delta^{15}N$ values can be used as a paleoredox proxy. As the predominant water column nitrogen reactions change in response to oxygen concentrations, the $\delta^{15}N$ values for organic matter deposited in the sediment is altered due to the characteristic isotopic fractionation factors for each reaction. Reprinted (modified) from *Chemical Geology* **360**, Quan TM, Adigwe EN, Riedinger N, and Puckette J, Evaluating nitrogen isotopes as proxies for depositional environmental conditions in shales: Comparing Caney and Woodford Shales in the Arkoma Basin, Oklahoma, p. 231–240 Copyright 2013, with permission from Elsevier.

such as emplacement of large igneous provinces, climate change, changes in export production, or the timing of the Great Oxygenation Event (e.g., Holloway and Dahlgren, 2002; Meyers et al., 2009; Algeo et al., 2014; Ader et al., 2016; Danzelle et al., 2020).

Nitrogen is an essential bionutrient for all living creatures, and is a critical component of many biological compounds, including proteins, enzymes, and nucleic acids. Nitrogen can also be found in a range of oxidation states ranging from -III in NH_3 and organic N compounds to + V in NO_3^-. Nitrogen has two isotopes: ^{14}N (99.63% abundance) and ^{15}N (0.37% abundance); due to the much higher abundance of ^{14}N, measured isotopic values are reported as $\delta^{15}N$ in parts per thousand (per mil; ‰):

$$\delta^{15}N = \left[\frac{(^{15}N/^{14}N)_{sample}}{(^{15}N/^{14}N)_{standard}} - 1 \right] \times 1000 \quad (1)$$

The reference standard is atmospheric nitrogen gas, set by definition to $\delta^{15}N$ = 0‰. Measured samples that are depleted in ^{15}N relative to the standard have negative $\delta^{15}N$ values, while samples that are relatively enriched in ^{15}N have positive $\delta^{15}N$ values. Transformation of nitrogen between oxidation states and between organic and inorganic forms is predominantly mediated by organisms. Due to differences in bond strengths between ^{14}N and ^{15}N, isotopic fractionation occurs during these reactions, and therefore nitrogen isotopes can be used to provide information about the reactions involved and the larger nitrogen cycle. The

fractionation factor (α) for any reaction can be calculated as the difference in $^{15}N/^{14}N$ ratios between reactants (R) and products (P):

$$\alpha_{N_R \rightarrow N_P} = \frac{(^{15}N/^{14}N)_R}{(^{15}N/^{14}N)_P} \quad (2)$$

If no fractionation takes place, $\alpha = 1$; reactions that favor the light isotope have $\alpha > 1$, and reactions that favor the heavier isotope have $\alpha < 1$. Similarly, kinetic fractionation can be assessed using the kinetic isotope effect (ε), which is the difference in rates of reaction for each isotope. For reactions taking place in natural systems, ε is essentially the difference between the $\delta^{15}N$ value of the reactant and that of the instantaneous product formed. **Figure 1A** shows a schematic of isotope effects for nitrogen reactions that are important to the geologic aquatic nitrogen cycle, along with their associated fractionation factors (α) and isotope effects (ε) (Delwiche and Steyn, 1970; Wada et al., 1980; Sigman and Casciotti, 2001; Talbot, 2001; Brunner et al., 2013). Measured fractionation factors for nitrogen processes may vary depending on the reaction pathway, culture or field measurement, and the specific species measured (Delwiche and Steyn, 1970; Wada et al., 1980 and references therein; Talbot, 2001 and references therein). If a reaction proceeds to completion, no fractionation is observed.

The interpretations of $\delta^{15}N$ data with regards to paleoredox conditions and nitrogen cycling rely on the fractionation factors for different nitrogen reactions (**Figure 1A**), which are in turn set by environmental conditions, particularly oxygen concentrations. The details have been discussed in several papers (e.g., Delwiche and Steyn, 1970; Wada et al., 1980; Altabet and Francois, 1994; Talbot, 2001; Robinson et al., 2012), but in brief, the sedimentary $\delta^{15}N$ values reflect the $\delta^{15}N$ of sinking organic matter, which is in turn influenced by the nitrogen reactions and environmental conditions occurring in the water column. In general, higher sedimentary $\delta^{15}N$ values are representative of low oxygen/suboxic water column conditions, because these conditions favor strongly fractionating denitrification and anammox reactions that result in organic matter enriched in ^{15}N, which is recorded in the sediments as higher $\delta^{15}N$ values (Altabet and Francois, 1994; Robinson et al., 2012 and references within). Lower $\delta^{15}N$ values can represent either anoxic systems dominated by nitrogen fixation or ammonium assimilation, or oxic systems utilizing nitrate as the main source of nitrogen; the nitrogen reactions for both of these conditions have smaller fractionation factors, and therefore generate organic matter depleted in ^{15}N. The conceptual model of how sedimentary $\delta^{15}N$ values vary with oxygen levels is shown in **Figure 1B**. Since sedimentary $\delta^{15}N$ values represent the average of all nitrogen processes occurring in the water column at a particular location, nitrogen isotopes are a local proxy. Nitrogen isotope values in sedimentary systems also reflect the $\delta^{15}N$ values of the initial nitrate or ammonium used to produce the organic matter, so variations in the $\delta^{15}N$ record may reflect the input of different sources of nitrogen into the system (Altabet and Francois, 1994; Robinson et al., 2012 and references within). Therefore, correlating specific $\delta^{15}N$ values to exact O_2 concentrations can be difficult, particularly for historical records.

One of the main concerns in the interpretation of sedimentary $\delta^{15}N$ records is whether the sedimentary $\delta^{15}N$ values measured accurately reflect the water column processes, or whether there is alteration of the record either during the initial organic matter sedimentation or through post-depositional processes. In brief, loss of nitrogen compounds could result in altering the original $\delta^{15}N$ signal through removal of compounds that are either enriched or depleted in ^{15}N (Robinson et al., 2012 and references within). This could result in measured $\delta^{15}N$ values that do not correspond to the original environmental conditions and nitrogen reactions. Remineralization of nitrogen compounds is most likely to occur at locations at which the water column and sediments are predominantly oxic, sedimentation rates are particularly slow, or productivity is low, so use of nitrogen isotopes as proxies in these environments may not be straightforward. Isotopic alteration may also occur at the sediment-water interface, with some evidence for preferential loss of nitrogen compounds with lower $\delta^{15}N$ values, resulting in a shift to higher $\delta^{15}N$ values measured in the sediment (Freudenthal et al., 2001; Robinson et al., 2012 and references within). Other processes that may alter the initial $\delta^{15}N$ signal include input of NH_4^+ or terrestrial nitrogen from outside sources into the sediments. These alterations to the bulk sedimentary $\delta^{15}N$ signal may be identified by isolating and measuring specific fractions that are more resistant to alteration such as compounds derived from chlorophyll, or that have been physically protected, such as microfossil bound compounds. Bulk sedimentary $\delta^{15}N$ measurements from areas where the organic matter is well-preserved are generally considered to be accurate proxies of water-column processes, so measurements from suboxic to anoxic environments or high sedimentation rate locations can be used for reconstruction of paleoenvironmental conditions with a high degree of confidence. In order to conform to the tenets of Fretwell's Law (as cited by Kendall and Caldwell, 1998), which cautions against using stable isotope data as the sole source of information, other redox and environmental proxies, such as biomarkers, paleontological evidence, and element enrichment, should be used to provide additional support and context for interpretation of $\delta^{15}N$ data (e.g., Lee et al., 2019; Adeboye et al., 2020).

Given the caveats associated with interpretation of $\delta^{15}N$ profiles for modern and ancient sedimentary systems that have not undergone significant post-depositional alteration, the potential use of nitrogen isotopes as paleoenvironmental and nitrogen cycle proxies in petroleum systems deserves additional analysis. In this paper, we review the recent research on nitrogen isotopes in petroleum systems, including fractionation due to diagenesis and catagensis, and the influence of kerogen type, and highlight applications of $\delta^{15}N$ data as paleoenvironmental proxies in petroleum systems.

POST-DEPOSITIONAL NITROGEN FRACTIONATION

The reliability of proxies to be used to decipher paleoenvironmental conditions relies on the ability to identify

TABLE 1 | List of previously published $\delta^{15}N$ values for a representative range of petroleum systems and petroleum-related samples.

OM type	Geographic location	Formation	Range of $\delta^{15}N$ values	Reporting reference(s)
Bituminous sediment	Various	Various	+4.2 to +10.7‰	Stiehl and Lehmann (1980)
Coal	Antarctica	Beaver Lake	+3.0‰	Rigby and Batts (1986)
Coal	Australia	Various	+0.3 to +3.7‰	Rigby and Batts (1986)
Coal	Canada	Various	−3.2 to 1.4‰	Whiticar (1996)
Coal	China	Various	−2.9 to +3.6‰	Ding et al. (2018)
Coal	China	Huainan	+3.7 to +7.7‰	Xie et al. (2021) and references therein
Coal	Various	Various	+3.5 to +6.3‰	Stiehl and Lehmann (1980)
Coal	Netherlands	State Mine Maurits	+2‰	Bokhoven and Theeuwen (1966)
Coal	New Zealand	Stockton	+1.3‰	Rigby and Batts (1986)
Coal after pyrolysis	Zwickau		+3.9 to 5.1‰	Stiehl and Lehmann (1980)
Crude oil	China	Various	−5.79 to +18.11‰	Chen et al. (2005)
Crude oil	Japan	Various	+2.3 to +5.1‰	Wada et al. (1975)
Crude oil	United States	Various	+1 to +6.7‰	Hoering and Moore (1958)
Neutral, low polarity oil fraction	China	Liaohe Basin	+10.6 to +12.2‰	Oldenburg et al. (2007)
Neutral, high polarity oil fraction	China	Liaohe Basin	+9.0 to +11.3‰	Oldenburg et al. (2007)
Basic oil fraction	China	Liaohe Basin	+4.1 to +5.8‰	Oldenburg et al. (2007)
Kerogen (undifferentiated)	Australia	Various	−2.25 to +5.34‰	Stüeken et al. (2017) and references therein
Kerogen (undifferentiated)	Canada	Sulphur Mountain Formation	+2.92 to +7.42‰	Stüeken et al. (2017) and references therein
Kerogen (undifferentiated)	China	Various	−0.48 to +7.50‰	Chen et al. (2005)
Kerogen (undifferentiated)	Mexico	Bandaras Bay	+2.4 to +4.2‰	Peters et al. (1978)
Kerogen (undifferentiated)	South Africa	Witwatersrand Supergroup	−4.44 to −0.48‰	Stüeken et al. (2017) and references therein
Kerogen (undifferentiated)	Switzerland	Serpiano Oil Shale	−0.9‰	Chicarelli et al. (1993)
Kerogen (undifferentiated)	Unite States	Various	−1.67 to +9.9‰	Peters et al. (1978) and Stüeken et al. (2017) and references therein; Williams et al. (1995)
Type I Kerogen	Russia	Shungite	+3.4‰	Boudou et al. (2008) and references therein
Type I Kerogen	United States	Mahogany Shale, Green River Formation	+16.8‰	Schimmelmann and Lis (2010) and references therein
Type II Kerogen	United States	New Albany Shale	−1.3 to +1.2‰	Boudou et al. (2008) and references therein; Schimmelmann and Lis (2010) and references therein
Type II-S Kerogen	Jordan	Sononian Ghareb limestone	+9.0‰	Schimmelmann and Lis (2010) and references therein
Type III Kerogen	Various	Various	+2.2 to +6.0‰	Boudou et al. (2008) and references therein; Schimmelmann and Lis (2010) and references therein
Sapropelic kerogen	Mexico	Laguna Mormona Algal mats	+1.87 to +6.18‰	Peters et al. (1981)
Humic kerogen	United States	Staten Island Peaty Soil Kerogen	+1.15 to +5.31‰	Peters et al. (1981)
Mudstone	United States	Fordoche Field	+0.7 to +4.5‰	Williams et al. (1995)
Natural gas	China	Yinggehai Basin	−9.0‰ to −1.8‰	Zhu et al. (2000)
Natural gas	Germany	Mid-European Basin	+6.5 to +18.0‰	Zhu et al. (2000) and references therein
Natural gas	Netherlands	Slochteren	+12 to +18‰	Bokhoven and Theeuwen (1966)
Natural gas	Poland	Zechstein Main Dolomite	+9.2 to +15.9‰	Kotarba et al. (2020) and references therein
Natural gas	Russia	West Siberian Basin	−19.0 to −10.7‰	Zhu et al. (2000) and references therein
Natural gas	United States	Various	−10.5 to +14.4‰	Hoering and Moore (1958) and Zhu et al. (2000) and references therein
Oil shale	Australia	Various	−2.5 to +12.7‰	Rigby and Batts (1986)
Organic extract	Poland	Various	−1.7 to +1.8‰	Bauersachs et al. (2009)
Organic extract	Switzerland	Serpiano oil Shale	−3.97‰	Chicarelli et al. (1993)
Organic matter	Germany	Wealden shale	+10.11 to +15.03‰	Froidl et al. (2021)
Porphyrins	Switzerland	Serpiano oil Shale	−3.04 to −3.38‰	Chicarelli et al. (1993)
Shale	Oklahoma	Caney	+8.2 to +11.2‰	Quan et al. (2013)
Shale	Oklahoma	Woodford	+1.5 to +9.5‰	Quan et al. (2013) and Rivera et al. (2015)
Shale	Virginia	Chattanooga	−0.7 to 3.0‰	Tuite et al. (2019)

For analytical and sample details, please refer to the original articles. Please note that this is not an exhaustive list of all published $\delta^{15}N$ values from petroleum-focused nitrogen isotope studies.

and constrain the relationship between the measured proxy and the parameter it represents. In the case of bulk sedimentary $\delta^{15}N$ profiles in petroleum systems, this means trying to characterize any deviations from the initial $\delta^{15}N$ value set by nitrogen reactions in response to paleoenvironmental conditions during deposition to those measured in the bulk sediment from core samples and outcrops. Since the organic matter has undergone significant transformation from fresh organic matter to

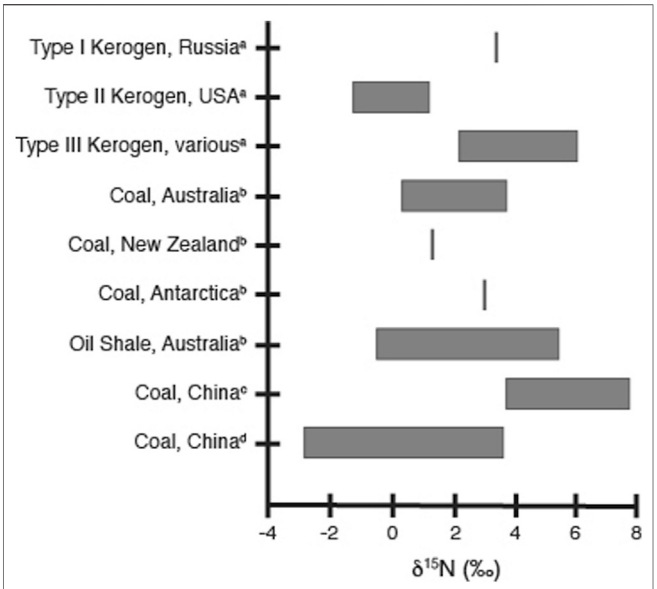

FIGURE 2 | Ranges of measured $\delta^{15}N$ values for selected kerogen and coal samples, as referred to in the text. Values shown are from [a]Boudou et al. 2008 and references therein, [b]Rigby and Batts 1986, [c]Xie et al. 2021 and references therein, and [d]Ding et al. 2018; for analytical and sample details, please refer to the original articles.

petroleum, it is likely that the nitrogen isotope values have also been altered by these same processes. Unfortunately, identification and quantification of these transformation processes and the nitrogen isotope fractionation factors associated with them are not easy to determine or constrain. The heterogeneity of organic matter, the difficulty in characterizing elemental and compositional changes during diagenesis and catagenesis, and the limitations of laboratory pyrolysis experiments are all issues that complicate interpretation of experimental and field measurements of nitrogen isotope fractionation. As a result, there are a limited number of studies and a limited number of sample types in the literature. While we have listed some representative $\delta^{15}N$ values for a range of petroleum systems and petroleum-related samples (**Table 1**), it should be clear upon inspection that there are no universal $\delta^{15}N$ values or trends that characterize samples from petroleum systems. As with any interpretation of stable isotope data, the geological and geochemical context of particular samples are critical to understanding what processes might be represented by the $\delta^{15}N$ values.

In theory, alteration of the original water column $\delta^{15}N$ signal in petroleum systems can result *via* four possible pathways: inclusion of other organic matter compounds from alternate sources in the organic matter pool; alteration of the initial $\delta^{15}N$ signal during sedimentary diagenesis; alteration of the initial $\delta^{15}N$ signal during catagensis; and overprinting of the initial $\delta^{15}N$ signal through interaction with, or migration of, nitrogen-containing fluids. Each of these pathways has the potential to lead to misinterpretation of the initial environmental conditions and thus an inability to use bulk sedimentary nitrogen isotopes as a paleoredox proxy in petroleum systems.

Kerogen Type

In order for the bulk sedimentary $\delta^{15}N$ profiles to accurately represent paleoenvironmental conditions, the nitrogen measured should have originated from biological processes occurring in the water column, and not from outside sources. This would imply that petroleum systems containing kerogen with a large marine algal and phytoplankton input (Type I and Type II kerogen) would be more likely to reflect environmental water column nitrogen reactions than kerogen with a high terrestrial input (Type III kerogen). In addition to not reflecting water column processes, nitrogen isotope values of terrestrial organic material are often more variant and have a wider range of values than those from marine systems (Kendall, 1998 and references within). The influence of terrestrial input on the sedimentary organic matter can be traced through the C/N ratio, as terrestrial materials generally have a higher ratio than those of marine phytoplankton (Hedges and Mann, 1979). This is reflected in higher N_{org}/C_{org} ratios for Type II kerogen compared to Type III kerogen at comparable maturities even after nitrogen is lost preferentially to carbon during diagenesis (Boudou et al., 2008). This difference in source is reflected in the measured $\delta^{15}N$ values, with $\delta^{15}N$ values for Type II kerogen generally similar to that measured in black shale samples (~−2 to +2‰), and the $\delta^{15}N$ values for Type III kerogen closely resembling those for coal (~+2 to +6‰) (**Figure 2**; Boudou et al., 2008). Similarly, the $\delta^{15}N$ values x for coals and lacustrine and brackish-water oil shales are generally higher than for oil shales deposited under marine conditions, reflecting both organic matter source and the nitrogen utilization of the precursor organisms (Rigby and Batts, 1986). The $\delta^{15}N$ values of coals, in particular, reflect the organic matter source and composition rather than maturity or diagenesis (**Figure 2**; Rigby and Batts, 1986; Ding et al., 2018; Xie et al., 2021). These distinctions between the marine and terrestrial organic matter sources indicates that if the nitrogen source or kerogen type is unknown, caution must be used when interpreting $\delta^{15}N$ records in petroleum systems, as higher $\delta^{15}N$ values could be a consequence of suboxic conditions characterized by predominant water column denitrification or reflect the presence of significant amounts of terrestrial input. While this is also true of all sedimentary systems, the transformation of the initial organic material during diagenesis and catagenesis may make identification of terrestrial input through C/N ratios more difficult.

Diagenesis

The loss of organic nitrogen during diagenesis and catagenesis is well documented (e.g., Tissot and Welte, 1984; Prokopenko et al., 2006 and references within; Vandenbrouke and Largeau, 2007); however, how these processes alter the $\delta^{15}N$ signal in bulk sediment is not conclusive. **Figure 3** summarizes four different possible scenarios for the relationship between the N/C ratio of kerogen and the $\delta^{15}N_{kerogen}$ in sediments. As stated earlier, analysis of modern-day core top and particulate organic

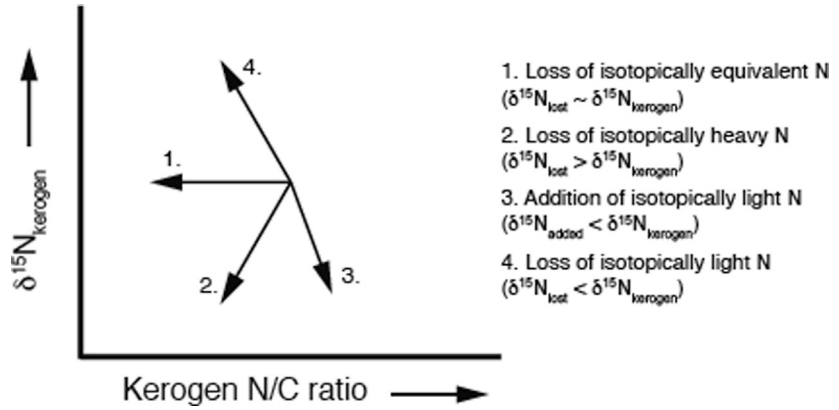

FIGURE 3 | The arrows illustrate the relationships between kerogen N/C ratio and the $\delta^{15}N_{kerogen}$ values for four possible diagenetic and catagenetic pathways. If nitrogen is lost that has a similar $\delta^{15}N$ value as the original kerogen, the N/C ratio will decrease without changing the $\delta^{15}N_{kerogen}$ (arrow 1). Loss of isotopically heavy N will result in decreasing values for both N/C ratio and $\delta^{15}N_{kerogen}$ (arrow 2). If diagenetic/catagenic processes result in the addition of N compounds that are isotopically light, $\delta^{15}N_{kerogen}$ will decrease while the N/C ratio increases (arrow 3). Removal of N compounds that have low $\delta^{15}N$ values from the kerogen will show an increase in $\delta^{15}N_{kerogen}$ values and a decrease in N/C ratio.

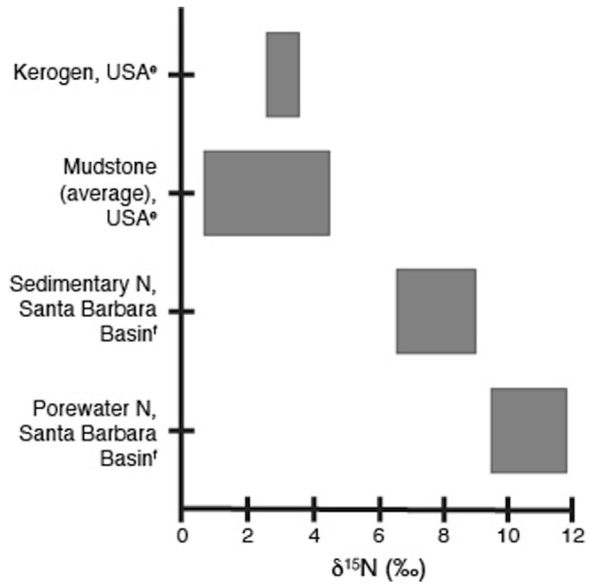

FIGURE 4 | Ranges of measured $\delta^{15}N$ values for kerogen, mudstone, sediment, and porewater samples, as referred to in the text. Values shown are from [e]Williams et al. 1995 and [f]Prokopenko et al. 2006; for analytical and sample details, please refer to the original articles.

matter indicates that in general, sedimentary $\delta^{15}N$ is an accurate recorder of water column processes, even when degradation has occurred (Peters et al., 1978; Altabet and Francois, 1994; Robinson et al., 2012 and references within). During diagenesis, organic nitrogen is converted to ammonium (NH_4^+) which can be trapped in the sediments, particularly in clay minerals. Detailed analysis of the nitrogen isotope values for the ammonium released provides conflicting information regarding fractionation during diagenesis. One scenario argues that since the NH_4^+ is generated from the organic nitrogen pool, the isotopic values are thought to be similar to the originating organic matter (Scholten 1991; Williams et al., 1995; Hoefs, 2004). Williams et al. (1995) compared the $\delta^{15}N$ values of clay-fixed NH_4^+ from mudstones with the $\delta^{15}N$ values of the associated kerogen and found no significant difference, leading them to conclude that the mudstones must be acting as a closed system (**Figure 4**). In this scenario, the $\delta^{15}N$ profile of the remaining sedimentary organic matter would be unchanged despite the loss of N as illustrated by arrow 1 in **Figure 3**, and thus primarily reflect processes that set the $\delta^{15}N$ values of the initial organic matter and not fractionation during diagenesis.

An alternative scenario is that nitrogen isotope fractionation does occur during the generation of NH_4^+, with the degree and direction of fractionation varying with environmental conditions during diagenesis. Incubation experiments under anoxic conditions show a decrease in the $\delta^{15}N$ values of organic matter of approximately 3‰ due to microbial degradation (Lehmann et al., 2002). Similarly, analysis of $\delta^{15}N$-NH_4^+ in pore water in the modern-day Santa Barbara Basin shows an enrichment of 1–3‰ compared to the residual organic matter (Prokopenko et al., 2006). Anoxic degradation appears to result in either the loss of a pool of organic nitrogen that is ^{15}N-enriched (**Figure 3**, arrow 2), or the addition of a ^{15}N-depleted fraction to the organic matter pool (**Figure 3**, arrow 3). Generation of heavy NH_4^+ *via* organic matter degradation could be due to anoxic diagenesis of more labile, isotopically enriched marine organic matter over more refractory, more depleted terrestrial nitrogen (Prokopenko et al., 2006). Incorporation of organic compounds generated by bacteria could be the source of lighter N to the organic matter pool (Lehmann et al., 2002). Unlike the incubation experiments, the loss of heavy nitrogen *via* diagenesis did not significantly change the $\delta^{15}N$ values of the sedimentary organic matter in the Santa Barbara Basin, likely due to sediment conditions favorable for good organic matter preservation (**Figure 4**; Prokopenko et al., 2006). It is probable that the

$\delta^{15}N$ values of organic matter could decrease during diagenesis if sediments had lower organic matter concentrations, slower sedimentation rates, and more oxic conditions, or in settings where the input of lower $\delta^{15}N$ compounds is significant. In contrast, oxic degradation increases the $\delta^{15}N$ value of organic matter (**Figure 3**, arrow 4) as ^{15}N-depleted nitrogen is preferentially lost as NH_4^+ during early diagenesis (Macko and Estep, 1984; Holmes et al., 1999; Freudenthal et al., 2001; Lehmann et al., 2002). The bulk sedimentary $\delta^{15}N$ signal appears to reflect the $\delta^{15}N$ values of organic matter and thus reflect water column processes in organic-rich areas with rapid accumulation rates. In contrast, sediments with low organic N concentrations and high NH_4^+ levels are more likely to have altered $\delta^{15}N$ profiles (Robinson et al., 2012 and references within). In a petroleum-generating system characterized by high organic matter concentrations and suboxic to anoxic environmental conditions, the use of $\delta^{15}N$ values as a redox proxy may be plausible. Plotting total organic carbon (TOC) concentrations vs total nitrogen (TN) concentrations for bulk sediment samples can provide information about excess inorganic N which may indicate whether significant diagenesis has occurred and that the $\delta^{15}N$ values for the bulk sediment may have been altered (Calvert, 2004).

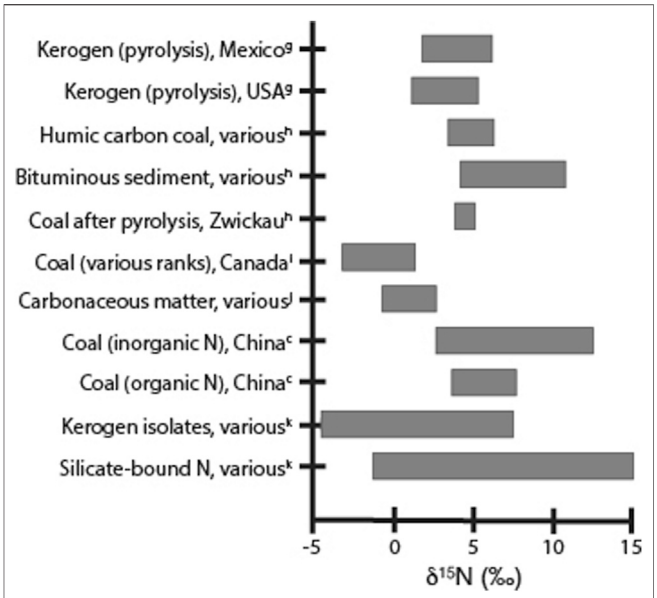

FIGURE 5 | Ranges of measured $\delta^{15}N$ values for kerogen, coal, and silicate-bound nitrogen samples, as referred to in the text. Values shown are from [g]Peters et al. 1981, [h]Stiehl and Lehmann 1980; [i]Whiticar 1996, [j]Ader et al. 2006, [c]Xie et al. 2021, and [k]Stüeken et al. 2017; for analytical and sample details, please refer to the original articles.

Catagenesis

Even after diagenesis, there is still nitrogen present in kerogen that can be lost during catagenesis, potentially resulting in additional nitrogen isotope fractionation. While modern-day systems can be used to evaluate alteration of $\delta^{15}N$ values during diagenesis, no such analogs exist for catagenesis. Changes in the nitrogen content and isotopic values due to catagenesis can only be evaluated through laboratory experiments or inferred through analysis of sediments from petroleum reservoirs. Though these analyses are imperfect due to the limitations of pyrolysis/thermal maturity experiments and the difficulty in isolating catagenic effects from other geological processes in petroleum-generating systems, all studies indicate that nitrogen is lost during catagenesis. Analysis of kerogen isolated from sediments after a series of thermal maturation experiments indicates that changes in nitrogen content with temperature were complex and varied with organic matter type, as algal-rich sediments showed a different pattern compared to more terrestrial peat-rich sediments (Peters et al., 1981). The amount of nitrogen lost during catagenesis also appeared to vary by kerogen maturity and on the method of evaluation. Analysis of nitrogen loss using pyrolysis results in low release of nitrogen from both Type I and Type II kerogen, generally less than 12% of the initial kerogen N concentration (Barth et al., 1996; Gillaizeau et al., 1997; Behar et al., 2000). In comparison, evaluation of C/N ratios and total N, organic N, and fixed-NH_4^+ concentrations of samples from both oil-producing and non-productive areas of the Santa Maria and San Joaquin Basins in California indicates that about half the nitrogen remaining after diagenesis is lost (Compton et al., 1992). Some of this difference may be due to a discrepancy in the inorganic N that is measured in the field versus what is measured in pyrolysis studies. The pyrolysis experiments found that the majority of the N released from kerogen was as N_2 gas, with little as NH_3 (Gillaizeau et al., 1997; Behar et al., 2000). In contrast, the field analyses generally measured NH_4^+ in the surrounding matrix, which could possibly have been brought in from outside the system, though C/N ratios document significant N loss (Compton et al., 1992). Field analyses in natural gas systems have measured N_2 levels, but it is unclear how much of the original kerogen-bound nitrogen was converted to gas (Zhu et al., 2000). Studies generally agree, however, that there is some amount of nitrogen in kerogen that is resistant to catagenic degradation, and that the majority of the nitrogen loss that does occur takes place at higher thermal maturities, with maximum NH_4^+ evolution in the peak oil generation stage and maximum N_2 release during gas generation (Compton, et al., 1992; Krooss et al., 1995; Littke et al., 1995; Barth et al., 1996; Gillaizeau et al., 1997; Behar et al., 2000). The degree and direction of nitrogen isotope fractionation that results from nitrogen loss during catagenesis is also highly variable (**Figure 5**). Some studies have found that increasing thermal maturity generally results in heavier $\delta^{15}N$ values for the remaining nitrogen in kerogen, since the light N is preferentially removed (**Figure 5**; Stiehl and Lehmann, 1980; Peters et al., 1981). In contrast, other evidence suggests that the $\delta^{15}N$ values for Type III kerogen and coals do not seem to change significantly with higher maturity levels even as N_{org} is lost, though the data for Type I and Type II kerogen is limited and inconclusive (**Figure 5**; Boudou et al., 1984; Rigby and Batts, 1986; Whiticar, 1996; Ader et al., 1998; Ader et al., 2006; Boudou et al., 2008; Xie et al., 2021). In other experiments, $\delta^{15}N_{kerogen}$

values decrease with increasing metamorphic grade, while the silicate-bound nitrogen becomes correspondingly heavier (**Figure 5**; Stüeken et al., 2017 and references within).

Fluid Migration

An additional difficulty in interpreting bulk $\delta^{15}N$ values in samples from petroleum systems is that these systems may experience nitrogen fractionation as a result of fluid interactions during migration, in addition to changes driven by diagenesis and catagenesis. Interaction with various fluids (e.g., during petroleum expulsion from source intervals, interaction with other non-petroleum fluids in reservoir intervals) can result in nitrogen exchange between kerogen and nitrogen compounds in fluids, which can alter the $\delta^{15}N$ values of kerogen depending on the source and type of N compounds present in the fluids (Schimmelmann and Lis, 2010). Exchange within a basin may have the effect of homogenizing the $\delta^{15}N$ values for different N pools and in different areas across the basin, eliminating any variations in $\delta^{15}N$ values that may be diagnostic of prior geochemical processes or original paleoenvironmental conditions (Schimmelmann and Lis, 2010). Isotopic analysis of NH_4^+ or N_2 generated by diagenesis and catagensis may also be impacted by infiltration of those compounds from other sources or subsequent reaction in the fluid phase (e.g., Williams et al., 1995; Zhu et al., 2000; Xie et al., 2021). In particular, loss of light nitrogen either as NH_3 (from the volatilisation of NH_4^+) or N_2 gas would result in enrichment for the remaining nitrogen in fluids (Williams et al., 1995; Ader et al., 1998; Krooss et al., 2005). Trapping of this heavy fluid nitrogen by clays could lead to higher $\delta^{15}N$ values for the bulk sediment in areas with significant concentrations of clay minerals (Charlesworth, 1986; Williams et al., 1995; Xie et al., 2021). The bulk sedimentary $\delta^{15}N$ values of petroleum reservoir sediments may also be influenced by the enrichment of the $\delta^{15}N$ values of organic nitrogen in petroleum due to migration (Williams et al., 1995 and references within).

Impact on Interpretation of $\delta^{15}N$ Data

Based on the previous paragraphs, it is clear that there is no consensus regarding the impact of kerogen type, diagenesis, catagenesis, fluid interaction, and migration on bulk sedimentary $\delta^{15}N$ values from petroleum systems. The heterogeneity of the organic matter, environmental conditions, and geological processes in petroleum systems make it complicated to interpret whether observed trends in bulk $\delta^{15}N$ values reflect initial nitrogen reactions and paleoredox conditions or if these trends indicate alteration (**Table 1**). If some broad conclusions can be drawn, the reliability of bulk sedimentary $\delta^{15}N$ records as redox proxies are higher if conditions are more conducive for organic matter preservation: high organic matter productivity, predominantly anoxic conditions, lower maturity, and minimal fluid interaction and migration.

Given all of the possible scenarios, it seems unlikely that the numerical value of bulk sedimentary $\delta^{15}N$ from petroleum systems is the same as the initial numerical value set during sediment deposition; however, it is possible that the relative relationships of $\delta^{15}N$ values within a sedimentary unit or location could be unchanged if the unit or location were subjected to similar geological processes over the interval in question. For example, this means that the presence of anoxic conditions could not be diagnosed based on a $\delta^{15}N$ value near 0‰, but an interval of lower $\delta^{15}N$ values within a profile of higher $\delta^{15}N$ values could be interpreted as an anoxic interval, particularly if supported by other geochemical and stratigraphic proxies. This means that it would be difficult to make direct comparisons of $\delta^{15}N$ values from sequences or locations that are too distant in either time or place, since they would likely be altered by different geological processes and therefore experience different influences with regards to isotopic fractionation. While there does seem to be some variation in sedimentary $\delta^{15}N$ values from unaltered systems through time on a global scale (Algeo et al., 2014), the potential fractionation due to catagenesis and migration likely make it inadvisable to draw global-scale conclusions from $\delta^{15}N$ measurements in petroleum systems.

NITROGEN ISOTOPE MEASUREMENT

Another potential complication in the comparison between $\delta^{15}N$ values for different locations and time periods is that the $\delta^{15}N$ values may also vary depending on the sediment fraction that is measured. The development of simpler and more sensitive isotope ratio mass spectrometer (IRMS) instrumentation in the last few decades means that the $\delta^{15}N$ of various nitrogen fractions can be measured relatively easily and using smaller sample sizes than in the past. The most basic measurement is bulk sedimentary $\delta^{15}N$, as the sediment samples simply need to be powdered, dried, and wrapped in tin capsules prior to combustion and analysis in an elemental analyzer (EA)-IRMS system, an improvement over the off-line Kjeldahl digestion or thermal oxidation methods previously used. This bulk sediment measurement can be referred to as $\delta^{15}N_{bulk}$, $\delta^{15}N_{sed}$, or $\delta^{15}N_{TN}$, and represents the $\delta^{15}N$ of the total nitrogen in the sediments, a sum of both the organic material and any inorganic N trapped in mineral matrices. This has become the most common measurement used for the $\delta^{15}N$ redox proxy and is generally thought to accurately represent the original $\delta^{15}N$ of organic matter in the water column as any NH_4^+ generated from the remineralization of organic matter is retained in the surrounding mineral matrix and included in the bulk measurement (Altabet and Francois, 1994; Higgins et al., 2012; Robinson et al., 2012).

In some samples, low organic matter concentrations or high amounts of detrital material may mean that nitrogen concentrations in the bulk sediments may be too low or too diluted to meet the detection limit of the IRMS. If the sediment is carbonate-rich, acidification methods can be used to reduce the sediment mass and concentrate the nitrogen. Acidification can either be performed in centrifuge tubes, with the residual sediments rinsed with water to remove acid then dried before analysis (rinse method), or on a smaller scale directly in silver capsules with the acid removed by evaporation (capsule method) (Brodie et al., 2011). The measured values for $\delta^{15}N_{acidified}$ are generally not the same as for $\delta^{15}N_{bulk}$ and the rinse method and the capsule method often return different $\delta^{15}N$ values. This

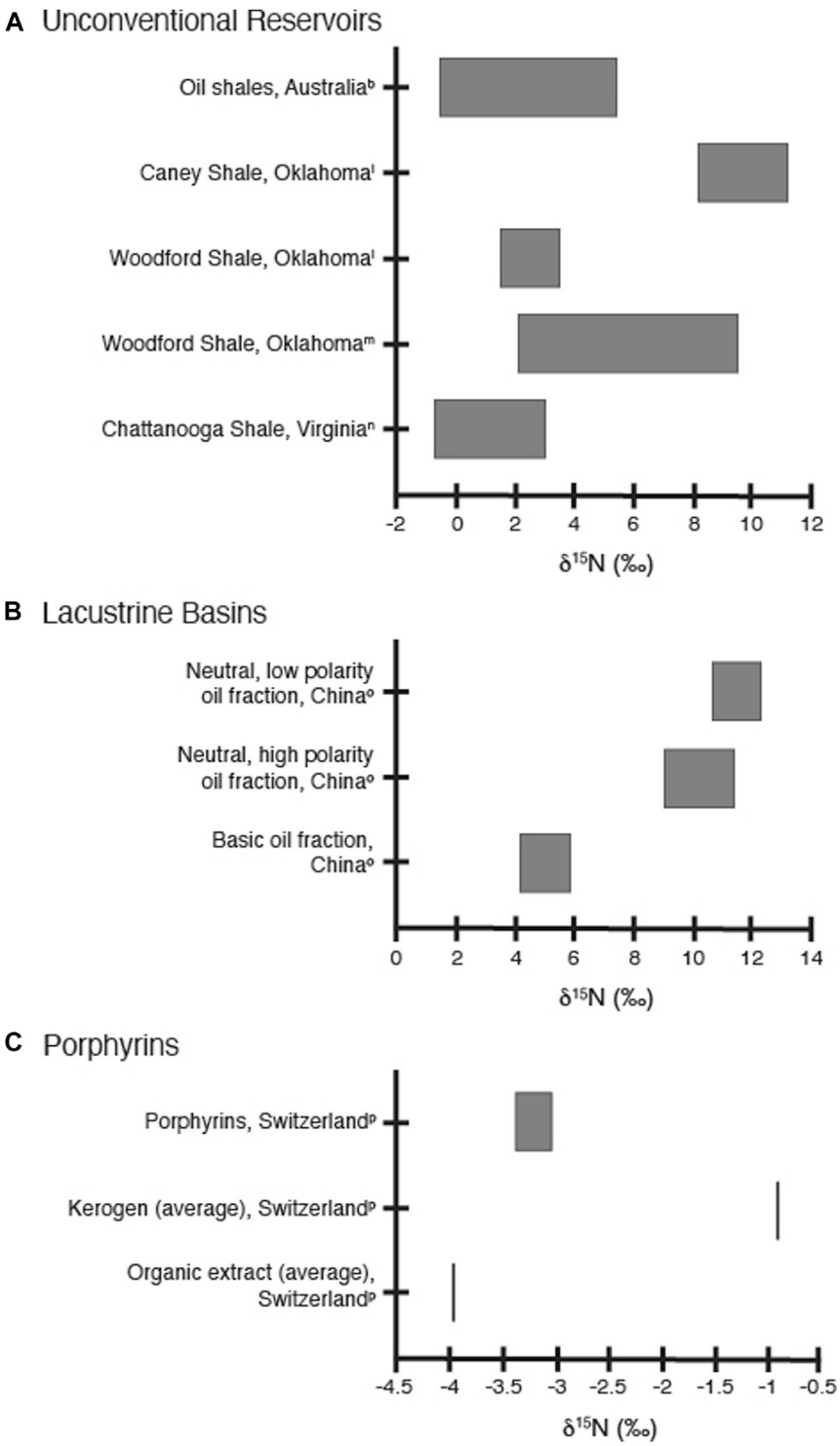

FIGURE 6 | (A): Ranges of measured $\delta^{15}N$ values for shale samples from unconventional reservoirs as referred to in the text. Values shown are from [b]Rigby and Batts 1986, [l]Quan et al. 2013, [m]Rivera et al. 2015, and [n]Tuite et al. 2019; for analytical and sample details, please refer to the original articles. **(B)**: Ranges of measured $\delta^{15}N$ values for lacustrine nitrogen fractions as referred to in the text. Values shown are from [o]Oldenburg et al. 2007; for analytical and sample details, please refer to the original article. **(C)**: Ranges of measured $\delta^{15}N$ values for porphyrin, kerogen, and organic extracts as referred to in the text. Values shown are from [p]Chicarelli et al. 1993; for analytical and sample details, please refer to the original article.

indicates that some nitrogen is lost during the acidification process, possibly through loss of volatile nitrogen or water-soluble nitrogen, though the exact identity of the lost nitrogen fraction is still undetermined (Brodie et al., 2011). Therefore, the $\delta^{15}N_{bulk}$ and $\delta^{15}N_{acidified}$ fractions are not equivalent, and numerical comparison of these values should be done with caution.

Nitrogen isotope measurements of the isolated kerogen fraction can capture the organic N isotope signal without the interference of inorganic nitrogen compounds. This $\delta^{15}N_{kerogen}$ can be measured using solvent-extracted rock powder or on the kerogen obtained after removal of carbonate minerals by acidification and silicate minerals by HF (e.g., Higgins et al., 2012; Stüeken et al., 2017). Other nitrogen fractions can also be measured for $\delta^{15}N$, including silicate-bound, foram-bound, inorganic, porphyrins, polar N compounds, and neutral N compounds, if they can be isolated from the bulk sediment. As each of these fractions measures specific nitrogen fractions, comparison between the various $\delta^{15}N$ values may provide additional information regarding the partitioning of nitrogen and nitrogen isotopes between these pools (e.g., Oldenburg et al., 2007; Stüeken et al., 2017).

INTERPRETATION OF $\delta^{15}N$ VALUES IN PETROLEUM SYSTEMS

The use of sedimentary nitrogen isotopes in the evaluation of petroleum reservoirs has increased in recent years as the use of $\delta^{15}N_{bulk}$ as a redox proxy has become more established. While there is still much more work to be done on the theory and systematics of nitrogen isotope partitioning and fractionation in such systems, $\delta^{15}N$ values of various fractions can still be used to interpret depositional paleoenvironmental conditions, nitrogen cycling, and organic matter sources. Here we present some examples to illustrate how sedimentary $\delta^{15}N$ has been used in a range of petroleum systems to evaluate paleoredox conditions, lacustrine settings, and organic matter fractions.

Unconventional Reservoirs

Unconventional reservoirs are petroleum systems characterized by low porosity and permeability, which often results in a lack of a clear density separation for the hydrocarbons and formation fluids contained within the reservoir unit (J. Puckette, personal communication). A significant amount of research has been done over the last couple of decades into the systematics, depositional conditions, and reservoir characteristics of these organic-rich shale, mudstone, and carbonate deposits. Due to their low permeability and porosity, the $\delta^{15}N_{bulk}$ values from unconventional reservoirs are likely to retain the isotopic fingerprint of water column nitrogen sources and processes during deposition, as these systems would experience minimal migration of either the organic or inorganic nitrogen pools. Rigby and Batts (1986) measured the $\delta^{15}N$ of oil shale samples from Australia and noted that the $\delta^{15}N_{bulk}$ values reflected the type of organic material, nitrogen source, and paleoenvironmental conditions during deposition, similar to unaltered sediments (**Figure 6A**). To evaluate whether $\delta^{15}N$ profiles could be used as a paleoproxy for water column redox state, the $\delta^{15}N_{bulk}$ values for two productive units from Oklahoma with similar geological histories but different depositional redox conditions were compared. The $\delta^{15}N_{bulk}$ values from the Woodford Shale, deposited under anoxic conditions, were found to be lower than those from the overlying suboxic Caney Shale, supporting the interpretation that $\delta^{15}N_{bulk}$ profiles can be used as a paleoredox proxy even for oil-mature unconventional formations (**Figure 6A**; Quan et al., 2013). Measurement of the $\delta^{15}N_{bulk}$ values from Woodford Shale samples taken from the Anadarko Basin (Oklahoma) found that there were no trends in $\delta^{15}N$ values with thermal maturity, as inferred from vitrinite reflectance measurements (**Figure 6A**; Rivera et al., 2015). Correlation of the $\delta^{15}N_{bulk}$ values with measured Fe and Mo concentrations once again indicated that the primary control on the $\delta^{15}N_{bulk}$ values appeared be depositional redox conditions (Rivera et al., 2015). Nitrogen isotope analysis of acidified samples from the oil-producing Huron, Three Lick, and Cleveland Shale formations identified variations that corresponded to two distinct depositional environments (**Figure 6A**; Tuite et al., 2019). Since paleoredox conditions also affect the predominant nitrogen reactions, the identification of these different redox regimes provided information about changing productivity, nutrient cycling, and water column stratification during alternating icehouse/greenhouse conditions (Tuite et al., 2019).

The results from these unconventional petroleum reservoir studies indicate that the sedimentary $\delta^{15}N$ values accurately reflect organic matter sources and redox conditions during deposition, which can be used to characterize the unconventional reservoir and evaluate its formation, evolution, and potential hydrocarbon yield. In addition, the $\delta^{15}N$ profiles from unconventional reservoir formations can also provide valuable information regarding past biogeochemical cycles, environmental conditions, and climate regimes even though these sediments have undergone significant catagenic alteration (Quan et al., 2013; Rivera et al., 2015; Tuite et al., 2019). This potentially expands the number of locations and geological formations that can be used to address paleoenvironmental and climatic questions, provided that the cores have robust age models and have not been influenced by loss of either organic or inorganic nitrogen phases.

Lacustrine Basins

Nitrogen reactions and their isotopic signatures are more complex in lacustrine and other freshwater systems due to the influence of terrestrial nutrients and organic matter, the smaller size of the water bodies, and the impacts of seasonal cycles (Talbot 2001 and references within; Quan and Falkowski, 2009 and references within). This means that the use of sedimentary $\delta^{15}N$ profiles to interpret paleoenvironmental conditions in lakes is not as well constrained as in marine environments, and evaluation of thermally mature lacustrine formations even less so. As mentioned above, the $\delta^{15}N$ values and C/N ratios for Type III kerogen and coals do reflect the influence of terrestrial organic material and are distinct from the Type I and Type II kerogen values (Rigby and Batts, 1986; Boudou et al., 2008; Ding et al., 2018; Xie et al., 2021). Analysis of two different lacustrine

source rocks from the Junggar Basin of China found that crude oils from brackish lacustrine basins were more enriched in pyrrolic-N containing compounds derived from biological sources than crude oils from alkaline lacustrine settings (Zhang et al., 2020). This observed enrichment was attributed to higher terrestrial plant contributions, particularly alkaloid and chlorophyll compounds, to the original organic matter deposits of the brackish lacustrine basin. While changes in N-compounds found in crude oils may also be a consequence of fractionation brought about by migration and thermal maturity, these were not considered to be the main processes responsible for differences in abundance and type of N-containing compounds seen in the end member oils derived from brackish vs. alkaline lacustrine settings (Zhang et al., 2020). Analysis of different organic nitrogen fractions extracted from a single crude oil sample from the Laohe Basin (China) indicated that the polar neutral nitrogen fraction (including pyrrolic-N compounds) was generally enriched in ^{15}N compared to basic nitrogen compounds by approximately 5‰ (**Figure 6B**; Oldenburg et al., 2007). While the $\delta^{15}N$ values of the crude oils from the Junggar Basin study were not measured, given the differences in organic matter sources and the enrichment of specific pyrrolic-N compounds, it would not be unexpected for the $\delta^{15}N_{oil}$ values to be significantly different in the brackish basins than the alkaline settings. Oldenburg et al. (2007) attributed the higher $\delta^{15}N$ values for pyrrolic-N compounds to be a result of increasing thermal maturity; however, Zhang et al. (2020) did not find higher concentrations of pyrrolic-N compounds in more mature samples. Resolution of this discrepancy by future studies may provide important information on the relative influence of organic matter source versus thermal maturity in lacustrine and freshwater systems. Given the complexity of processes that could potentially have a significant influence on the $\delta^{15}N$ signals in lacustrine systems, it is likely that the processes that impact lacustrine systems will vary depending on geologic setting and history of the particular paleolakes being studied.

Porphyrins

Porphyrins have traditionally been used as biomarker proxies for thermal maturity and to illustrate different depositional environmental conditions (Mawson et al., 2004). Since porphyrin compounds are direct breakdown products of chloropigments, the $\delta^{15}N$ values of porphyrins are considered to be a direct representation of the isotopic composition of those original chloropigments and thus of the original primary producers (e.g., Hayes et al., 1987; Boreham et al., 1989; Boreham et al., 1990; Chicarelli et al., 1993; Kashiyama et al., 2008). Porphyrins have been isolated in petroleum systems in samples with a wide range of maturities and retain the $\delta^{15}N$ signal of the original organic matter, so they could be a way to evaluate water column N reactions during deposition that would not be altered by post-depositional isotopic fractionation processes. Comparison of two different porphyrin fractions, kerogen, and total organic extract isolated from Serpiano oil shale sediments show that porphyrins fractions (average −3.1‰ and −3.3‰) are depleted in ^{15}N relative to the kerogen (average −0.9‰) and slightly enriched relative to the total extract (average −4.0‰) (**Figure 6C**; Chicarelli et al., 1993). While the depletion in the porphyrin fractions relative to the kerogen may indicate the influence of an additional nitrogen source, the low $\delta^{15}N$ values for all three fractions reflects the influence of predominant N_2 fixation to the original organic matter pool (Chicarelli et al., 1993). This indicates that $\delta^{15}N_{porphyrin}$ values can serve to determine whether isotopic fractionation has altered $\delta^{15}N_{kerogen}$ and/or $\delta^{15}N_{bulk}$ values for petroleum systems during catagenesis or migration. While the isolation and measurement of $\delta^{15}N$ for porphyrins is not trivial, it may be necessary if post-depositional fractionation processes are suspected and alteration of the $\delta^{15}N_{bulk}$ signal may have occurred.

CONCLUSION AND FUTURE WORK

In summary, nitrogen isotopes can be a powerful tool in petroleum systems, particularly for evaluating unconventional reservoirs, paleoenvironmental conditions, and organic matter sources. Uncertainties regarding how diagenesis, catagensis, hydrothermal fluids, and hydrocarbon migration processes may have fractionated the initial organic nitrogen deposits can result in significant caveats in terms of interpretation of the $\delta^{15}N$ values, and these may limit the use of $\delta^{15}N$ profiles as a redox and nitrogen cycle proxy for more complex petroleum systems. The more that is known about non-nitrogen parameters in the petroleum system being analyzed, such as fluid interactions, mineralogy, kerogen type, and porosity and permeability, the more constrained the interpretation of the $\delta^{15}N$ measurements can be, and the greater the potential to conclusively identify and characterize paleoenvironmental regimes and biogeochemical cycles. In addition to additional research to better constrain post-depositional nitrogen processes and fractionation, more $\delta^{15}N$ data from more locations, wider thermal maturity ranges, and different depositional environments is necessary to link measured $\delta^{15}N$ values to specific paleoenvironmental conditions and processes. While caution is advised against placing too much emphasis on specific $\delta^{15}N$ values in terms of interpretation, overall trends and excursions present in $\delta^{15}N$ profiles from petroleum systems can still provide critical information about reservoir characteristics, particularly depositional paleoredox conditions and organic matter sources.

AUTHOR CONTRIBUTIONS

All authors listed have made a substantial, direct, and intellectual contribution to the work and approved it for publication.

ACKNOWLEDGMENTS

The authors would like to thank J. Puckette for his contributions to the section on unconventional reservoirs. This is Oklahoma State University Boone Pickens School of Geology contribution #2021-123.

REFERENCES

Adeboye, O. O., Riedinger, N., Wu, T., Grammer, G. M., and Quan, T. M. (2020). Redox Conditions on the Anadarko Shelf of Oklahoma during the Deposition of the "Mississippian Limestone". *Mar. Pet. Geology.* 116, 104345. doi:10.1016/j.marpetgeo.2020.104345

Ader, M., Boudou, J.-P., Javoy, M., Goffe, B., and Daniels, E. (1998). Isotope Study on Organic Nitrogen of Westphalian Anthracites from the Western Middle Field of Pennsylvania (U.S.A.) and from the Bramsche Massif (Germany). *Org. Geochem.* 29, 315–323. doi:10.1016/s0146-6380(98)00072-2

Ader, M., Cartigny, P., Boudou, J.-P., Oh, J.-H., Petit, E., and Javoy, M. (2006). Nitrogen Isotopic Evolution of Carbonaceous Matter during Metamorphism: Methodology and Preliminary Results. *Chem. Geology.* 232, 152–169. doi:10.1016/j.chemgeo.2006.02.019

Ader, M., Thomazo, C., Sansjofre, P., Busigny, V., Papineau, D., Laffont, R., et al. (2016). Interpretation of the Nitrogen Isotopic Composition of Precambrian Sedimentary Rocks: Assumptions and Perspectives. *Chem. Geology.* 429, 93–110. doi:10.1016/j.chemgeo.2016.02.010

Algeo, T. J., Meyers, P. A., Robinson, R. S., Rowe, H., and Jiang, G. Q. (2014). Icehouse-GReenhouse Variations in Marine Denitrification. *Biogeosciences.* 11, 1273–1295. doi:10.5194/bg-11-1273-2014

Altabet, M. A., and Francois, R. (1994). Sedimentary Nitrogen Isotopic Ratio as a Recorder for Surface Ocean Nitrate Utilization. *Glob. Biogeochem. Cycles.* 8, 103–116. doi:10.1029/93gb03396

Barth, T., Rist, K., Huseby, B., and Ocampo, R. (1996). The Distribution of Nitrogen Between Bitumen, Water and Residue in Hydrous Pyrolysis of Extracted Messel Oil Shale. *Org. Geochem.* 24, 889–895. doi:10.1016/s0146-6380(96)00070-8

Bauersachs, T., Kremer, B., Schouten, S., and Sinninghe Damsté, J. S. (2009). A Biomarker and δ15N Study of Thermally Altered Silurian Cyanobacterial Mats. *Org. Geochem.* 40, 149–157. doi:10.1016/j.orggeochem.2008.11.008

Behar, F., Gillaizeau, B., Derenne, S., and Largeau, C. (2000). Nitrogen Distribution in the Pyrolysis Products of a Type II Kerogen (Cenomanian, Italy). Timing of Molecular Nitrogen Production versus Other Gases. *Energy Fuels.* 14, 431–440. doi:10.1021/ef990157g

Bokhoven, C., and Theeuwen, H. J. (1966). Determination of the Abundance of Carbon and Nitrogen Isotopes in Dutch Coals and Natural Gas. *Nature.* 211, 927–929. doi:10.1038/211927a0

Boreham, C. J., Fookes, C. J. R., Popp, B. N., and Hayes, J. M. (1990). Origin of Petroporphyrins. 2. Evidence From Stable Carbon Isotopes. *Energy Fuels.* 4, 658–661. doi:10.1021/ef00024a007

Boreham, C. J., Fookes, C. J. R., Popp, B. N., and Hayes, J. M. (1989). Origins of Etioporphyrins in Sediments: Evidence From Stable Carbon Isotopes. *Geochimica et Cosmochimica Acta.* 53, 2451–2455. doi:10.1016/0016-7037(89)90368-2

Boudou, J.-P., Mariotti, A., and Oudin, J.-L. (1984). Unexpected Enrichment of Nitrogen During the Diagenetic Evolution of Sedimentary Organic Matter. *Fuel.* 63, 1508–1510. doi:10.1016/0016-2361(84)90215-1

Boudou, J.-P., Schimmelmann, A., Ader, M., Mastalerz, M., Sebilo, M., and Gengembre, L. (2008). Organic Nitrogen Chemistry during Low-Grade Metamorphism. *Geochimica et Cosmochimica Acta.* 72, 1199–1221. doi:10.1016/j.gca.2007.12.004

Brodie, C. R., Heaton, T. H. E., Leng, M. J., Kendrick, C. P., Casford, J. S. L., and Lloyd, J. M. (2011). Evidence for Bias in Measured δ15N Values of Terrestrial and Aquatic Organic Materials Due to Pre-analysis Acid Treatment Methods. *Rapid Commun. Mass. Spectrom.* 25, 1089–1099. doi:10.1002/rcm.4970

Brunner, B., Contreras, S., Lehmann, M. F., Matantseva, O., Rollog, M., Kalvelage, T., et al. (2013). Nitrogen Isotope Effects Induced by Anammox Bacteria. *Proc. Natl. Acad. Sci.* 110, 18994–18999. doi:10.1073/pnas.1310488110

Calvert, S. E. (2004). Beware Intercepts: Interpreting Compositional Ratios in Multi-Component Sediments and Sedimentary Rocks. *Org. Geochem.* 35, 981–987. doi:10.1016/j.orggeochem.2004.03.001

Calvert, S. E., Pedersen, T. F., and Karlin, R. E. (2001). Geochemical and Isotopic Evidence for Post-Glacial Palaeoceanographic Changes in Saanich Inlet, British Columbia. *Mar. Geology.* 174, 278–305. doi:10.1016/s0025-3227(00)00156-0

Charlesworth, J. M. (1986). Interaction of clay Minerals With Organic Nitrogen Compounds Released by Kerogen Pyrolysis. *Geochimica et Cosmochimica Acta.* 50, 1431–1435. doi:10.1016/0016-7037(86)90316-9

Chen, C., Mei, B., and Cao, Y. (2005). Nitrogen Isotopic Geochemical Characteristics of Crude Oils in Several Basins of China. *Sci. China Ser. D-earth Sci.* 48, 1211–1219. doi:10.1360/03yd0180

Chicarelli, M. I., Hayes, J. M., Popp, B. N., Eckardt, C. B., and Maxwell, J. R. (1993). Carbon and Nitrogen Isotopic Compositions of Alkyl Porphyrins from the Triassic Serpiano Oil Shale. *Geochimica et Cosmochimica Acta.* 57, 1307–1311. doi:10.1016/0016-7037(93)90067-7

Compton, J. S., Williams, L. B., and Ferrell, R. E., Jr (1992). Mineralization of Organogenic Ammonium in the Monterey Formation, Santa Maria and San Joaquin Basins, California, USA. *Geochimica et Cosmochimica Acta.* 56, 1979–1991. doi:10.1016/0016-7037(92)90324-c

Danzelle, J., Riquier, L., Baudin, F., Thomazo, C., and Pucéat, E. (2020). Nitrogen and Carbon Cycle Perturbations Through the Cenomanian-Turonian Oceanic Anoxic Event 2 (~94 Ma) in the Vocontian Basin (SE France). *Palaeogeogr. Palaeoclimatol. Palaeoecol.* 538. doi:10.1016/j.palaeo.2019.109443

Delwiche, C. C., and Steyn, P. L. (1970). Nitrogen Isotope Fractionation in Soils and Microbial Reactions. *Environ. Sci. Technol.* 4, 929–935. doi:10.1021/es60046a004

Ding, D., Liu, G., Fu, B., and Wang, W. (2018). New Insights into the Nitrogen Isotope Compositions in Coals from the Huainan Coalfield, Anhui Province, China: Influence of the Distribution of Nitrogen Forms. *Energy Fuels.* 32, 9380–9387. doi:10.1021/acs.energyfuels.8b02467

Freudenthal, T., Wagner, T., Wenzhöfer, F., Zabel, M., and Wefer, G. (2001). Early Diagenesis of Organic Matter From Sediments of the Eastern Subtropical Atlantic: Evidence from Stable Nitrogen and Carbon Isotopes. *Geochimica et Cosmochimica Acta.* 65, 1795–1808. doi:10.1016/s0016-7037(01)00554-3

Froidl, F., Littke, R., Baniasad, A., Zheng, T., Röth, J., Böcker, J., et al. (2021). Peculiar Berriasian "Wealden" Shales of Northwest Germany: Organic Facies, Depositional Environment, Thermal Maturity and Kinetics of Petroleum Generation. *Mar. Pet. Geology.* 124, 104819. doi:10.1016/j.marpetgeo.2020.104819

Ganeshram, R. S., Pedersen, T. F., Calvert, S. E., and Murray, J. W. (1995). Large Changes in Oceanic Nutrient Inventories From Glacial to Interglacial Periods. *Nature.* 376, 755–758. doi:10.1038/376755a0

Gillaizeau, B., Behar, F., Derenne, S., and Largeau, C. (1997). Nitrogen Fate During Laboratory Maturation of a Type I Kerogen (Oligocene, Turkey) and Related Algaenan: Nitrogen Mass Balances and Timing of N2 Production versus Other Gases. *Energy Fuels.* 11, 1237–1249. doi:10.1021/ef970060z

Godfrey, L. V., and Falkowski, P. G. (2009). Nitrogen, its Cycle and Redox State in the Late Archaean Ocean. *Nat. Geosci.* 2, 725–729. doi:10.1038/ngeo633

Hayes, J. M., Takigiku, R., Ocampo, R., Callot, H. J., and Albrecht, P. (1987). Isotopic Compositions and Probable Origins of Organic Molecules in the Eocene Messel Shale. *Nature.* 329, 48–51. doi:10.1038/329048a0

Hedges, J. I., and Mann, D. C. (1979). The Characterization of Plant Tissues by Their Lignin Oxidation Products. *Geochimica et Cosmochimica Acta.* 43, 1803–1807. doi:10.1016/0016-7037(79)90028-0

Higgins, M. B., Robinson, R. S., Carter, S. J., and Pearson, A. (2010). Evidence From Chlorin Nitrogen Isotopes for Alternating Nutrient Regimes in the Eastern Mediterranean Sea. *Earth Planet. Sci. Lett.* 290, 102–107. doi:10.1016/j.epsl.2009.12.009

Higgins, M. B., Robinson, R. S., Husson, J. M., Carter, S. J., and Pearson, A. (2012). Dominant Eukaryotic export Production during Ocean Anoxic Events Reflects the Importance of Recycled NH4+. *Proc. Natl. Acad. Sci.* 109, 2269–2274. doi:10.1073/pnas.1104313109

Hoefs, J. (2004). *Stable Isotope Geochemistry*. Berlin Heidelberg: Springer-Verlag. doi:10.1007/978-3-662-05406-2

Hoering, T. C., and Moore, H. E. (1958). The Isotopic Composition of the Nitrogen in Natural Gases and Associated Crude Oils. *Geochimica et Cosmochimica Acta.* 13, 225–232. doi:10.1016/0016-7037(58)90024-3

Holloway, J. M., and Dahlgren, R. A. (2002). Nitrogen in Rock: Occurrences and Biogeochemical Implications. *Glob. Biogeochem. Cycles.* 16, 65–71. doi:10.1029/2002GB001862

Holmes, M. E., Eichner, C., Struck, U., Wefer, G., Fischer, G., and Wefer, G. (1999). "Reconstruction of Surface Ocean Nitrate Utilization Using Stable Nitrogen Isotopes in Sinking Particles and Sediments," in *The Use of Proxies in Paleoceanography: Examples from the South Atlantic* (Springer), 447–468. doi:10.1007/978-3-642-58646-0_18

Jenkyns, H. C., Gröcke, D. R., and Hesselbo, S. P. (2001). Nitrogen Isotope Evidence for Water Mass Denitrification During the Early Toarcian

(Jurassic) Oceanic Anoxic Event. *Paleoceanography.* 16, 593–603. doi:10.1029/2000pa000558

Kashiyama, Y., Ogawa, N. O., Shiro, M., Tada, R., Kitazato, H., and Ohkouchi, N. (2008). Reconstruction of the Biogeochemistry and Ecology of Photoautotrophs Based on the Nitrogen and Carbon Isotopic Compositions of Vanadyl Porphyrins from Miocene Siliceous Sediments. *Biogeosciences.* 5, 797–816. doi:10.5194/bg-5-797-2008

Kendall, C., and Caldwell, E. A. (1998). *Fundamentals of Isotope Geochemistry in Isotope Tracers in Catchment Hydrology*. Editors C. Kendall and J. J. McDonnell (Amsterdam: Elsevier Science B.V), 51–86. doi:10.1016/b978-0-444-81546-0.50009-4

Kendall, C. (1998). *Tracing Nitrogen Sources and Cycling in Catchments in Isotope Tracers in Catchment Hydrology*. Editors C. Kendall and J. J. McDonnell (Amsterdam: Elsevier Science B.V), 519–576. doi:10.1016/b978-0-444-81546-0.50023-9

Kotarba, M. J., Bilkiewicz, E., and Kosakowski, P. (2020). Origin of Hydrocarbon and Non-Hydrocarbon (H2S, CO2 and N2) Components of Natural Gas Accumulated in the Zechstein Main Dolomite Carbonate Reservoir of the Western Part of the Polish Sector of the Southern Permian Basin. *Chem. Geology.* 554, 119807. doi:10.1016/j.chemgeo.2020.119807

Krooss, B. M., Friberg, L., Gensterblum, Y., Hollenstein, J., Prinz, D., and Littke, R. (2005). Investigation of the Pyrolytic Liberation of Molecular Nitrogen from Palaeozoic Sedimentary Rocks. *Int. J. Earth Sci. (Geol Rundsch).* 94, 1023–1038. doi:10.1007/s00531-005-0012-3

Krooss, B. M., Littke, R., Müller, B., Frielingsdorf, J., Schwochau, K., and Idiz, E. F. (1995). Generation of Nitrogen and Methane from Sedimentary Organic Matter: Implications on the Dynamics of Natural Gas Accumulations. *Chem. Geology.* 126, 291–318. doi:10.1016/0009-2541(95)00124-7

Lee, C., Love, G. D., Hopkins, M. J., Kröger, B., Franeck, F., and Finnegan, S. (2019). Lipid Biomarker and Stable Isotopic Profiles through Early-Middle Ordovician Carbonates From Spitsbergen, Norway. *Org. Geochem.* 131, 5–18. doi:10.1016/j.orggeochem.2019.02.008

Lehmann, M. F., Bernasconi, S. M., Barbieri, A., and McKenzie, J. A. (2002). Preservation of Organic Matter and Alteration of its Carbon and Nitrogen Isotope Composition During Simulated and *In Situ* Early Sedimentary Diagenesis. *Geochimica et Cosmochimica Acta.* 66, 3573–3584. doi:10.1016/s0016-7037(02)00968-7

Littke, R., Krooss, B., Idiz, E., and Frielingsdorf, J. (1995). Molecular Nitrogen in Natural-Gas Accumulations - Generation From Sedimentary Organic-Matter at High-Temperatures. *Am. Assoc. Pet. Geologists Bull.* 79, 410–430. doi:10.1306/8D2B1548-171E-11D7-8645000102C1865D

Macko, S. A., and Estep, M. L. F. (1984). Microbial Alteration of Stable Nitrogen and Carbon Isotopic Compositions of Organic Matter. *Org. Geochem.* 6, 787–790. doi:10.1016/0146-6380(84)90100-1

Mawson, D. H., Walker, J. S., and Keely, B. J. (2004). Variations in the Distributions of Sedimentary Alkyl Porphyrins in the Mulhouse Basin in Response to Changing Environmental Conditions. *Org. Geochem.* 35, 1229–1241. doi:10.1016/j.orggeochem.2004.05.007

Meyers, P. A., Yum, J.-G., and Wise, S. W. (2009). Origins and Maturity of Organic Matter in Mid-Cretaceous Black Shales From ODP Site 1138 on the Kerguelen Plateau. *Mar. Pet. Geology.* 26, 909–915. doi:10.1016/j.marpetgeo.2008.09.003

Oldenburg, T. B. P., Larter, S. R., and Huang, H. (2007). Nitrogen Isotope Systematics of Petroleum Fractions of Differing Polarity - Neutral versus Basic Compounds. *Org. Geochem.* 38, 1789–1794. doi:10.1016/j.orggeochem.2007.05.016

Peters, K. E., Rohrback, B. G., and Kaplan, I. R. (1981). Geochemistry of Artificially Heated Humic and Sapropelic Sediments—I: Protokerogen. *AAPG Bull.* 65, 688–705. doi:10.4319/lo.1978.23.4.0598\

Peters, K. E., Sweeney, R. E., and Kaplan, I. R. (1978). Correlation of Carbon and Nitrogen Stable Isotope Ratios in Sedimentary Organic Matter. *Limnol. Oceanogr.* 23, 598–604. doi:10.4319/lo.1978.23.4.0598

Prokopenko, M., Hammond, D., Berelson, W., Bernhard, J., Stott, L., and Douglas, R. (2006). Nitrogen Cycling in the Sediments of Santa Barbara basin and Eastern Subtropical North Pacific: Nitrogen Isotopes, Diagenesis and Possible Chemosymbiosis Between Two Lithotrophs (Thioploca and Anammox)-"riding on a Glider". *Earth Planet. Sci. Lett.* 242, 186–204. doi:10.1016/j.epsl.2005.11.044

Quan, T. M., Adigwe, E. N., Riedinger, N., and Puckette, J. (2013). Evaluating Nitrogen Isotopes as Proxies for Depositional Environmental Conditions in Shales: Comparing Caney and Woodford Shales in the Arkoma Basin, Oklahoma. *Chem. Geology.* 360-361, 231–240. doi:10.1016/j.chemgeo.2013.10.017

Quan, T. M., and Falkowski, P. G. (2009). Redox Control of N:P Ratios in Aquatic Ecosystems. *Geobiology.* 7, 124–139. doi:10.1111/j.1472-4669.2008.00182.x

Quan, T. M., van de Schootbrugge, B., Field, M. P., Rosenthal, Y., and Falkowski, P. G. (2008). Nitrogen Isotope and Trace Metal Analyses from the Mingolsheim Core (Germany): Evidence for Redox Variations across the Triassic-Jurassic Boundary. *Glob. Biogeochem. Cycles.* 22, a–n. doi:10.1029/2007gb002981

Rigby, D., and Batts, B. D. (1986). The Isotopic Composition of Nitrogen in Australian Coals and Oil Shales. *Chem. Geology. Isotope Geosci. section.* 58, 273–282. doi:10.1016/0168-9622(86)90016-3

Rivera, K. T., Puckette, J., and Quan, T. M. (2015). Evaluation of Redox Versus thermal Maturity Controls on δ 15 N in Organic Rich Shales: A Case Study of the Woodford Shale, Anadarko Basin, Oklahoma, USA. *Org. Geochem.* 83-84, 127–139. doi:10.1016/j.orggeochem.2015.03.005

Robinson, R. S., Kienast, M., Luiza Albuquerque, A., Altabet, M., Contreras, S., De Pol Holz, R., et al. (2012). A Review of Nitrogen Isotopic Alteration in Marine Sediments. *Paleoceanography.* 27, PA4203. doi:10.1029/2012pa002321

Ryabenko, E., Kock, A., Bange, H. W., Altabet, M. A., and Wallace, D. W. R. (2012). Contrasting Biogeochemistry of Nitrogen in the Atlantic and Pacific Oxygen Minimum Zones. *Biogeosciences* 9, 203–215. doi:10.5194/bg-9-203-2012

Schimmelmann, A., and Lis, G. P. (2010). Nitrogen Isotopic Exchange During Maturation of Organic Matter. *Org. Geochem.* 41, 63–70. doi:10.1016/j.orggeochem.2009.01.005

Scholten, S. O. (1991). *The Distribution of Nitrogen Isotopes in Sediments*. Utrecht, Netherlands: PhD, University of Utrecht. doi:10.1142/9789814539166

Sigman, D. M., and Casciotti, K. L. (2001). Nitrogen Isotopes in the Ocean, in *Encyclopedia of Ocean Sciences*. Editors J. H. Steele, K. K. Turekain, and S. A. Thorpe (San Diego, CA: Academic Press), 1884–1894. doi:10.1006/rwos.2001.0172

Stiehl, G., and Lehmann, M. (1980). Isotopenvariationen des Stickstoffs Humoser und Bituminöser Natürlicher Organischer Substanzen. *Geochimica et Cosmochimica Acta.* 44, 1737–1746. doi:10.1016/0016-7037(80)90224-0

Stüeken, E. E., Zaloumis, J., Meixnerová, J., and Buick, R. (2017). Differential Metamorphic Effects on Nitrogen Isotopes in Kerogen Extracts and Bulk Rocks. *Geochimica et Cosmochimica Acta.* 217, 80–94. doi:10.1016/j.gca.2017.08.019

Talbot, M. R. (2001). "Nitrogen Isotopes in Palaeolimnology in *Tracking Environmental Change Using Lake Sediments*," in *Physical and Geochemical Methods. 2*. Editors W. M. Last and J. P. Smol (Dordrecht, Netherlands: Kluwer Academic Publishers), Vol. 2, 401–439.

Tissot, B. P., and Welte, D. H. (1984). *Petroleum Formation and Occurance*. Berlin: Springer-Verlag. doi:10.1007/978-3-642-87813-8

Tuite, M. L., Jr., Williford, K. H., and Macko, S. A. (2019). From Greenhouse to Icehouse: Nitrogen Biogeochemistry of an Epeiric Sea in the Context of the Oxygenation of the Late Devonian Atmosphere/ocean System. *Palaeogeogr. Palaeoclimatol. Palaeoecol.* 531, 109204. doi:10.1016/j.palaeo.2019.05.026

Vandenbrouke, M., and Largeau, C. (2007). Kerogen Origin, Evolution and Structure. *Org. Geochem.* 38, 719–833. doi:10.1016/j.orggeochem.2007.01.001

Wada, E., Goldberg, E. D., and Tokyo, Y. H. (1980). Nitrogen Isotope Fractionation and its Significance in Biogeochemical Processes Occuring in Marine Environments in Isotope Marine Chemistry. *Uchida Rokakuho Publ. Co. Ltd.*, 375–398.

Wada, E., Kadonaga, T., and Matsuo, S. (1975). ^{15}N Aboundance in Nitrogen of Naturally Occurring Substances and Global Assessment of Denitrification from Isotopic Viewpoint. *Geochem. J.* 9, 139–148. doi:10.2343/geochemj.9.139

Whiticar, M. J. (1996). Stable Isotope Geochemistry of Coals, Humic Kerogens and Related Natural Gases. *Int. J. Coal Geology.* 32, 191–215. doi:10.1016/s0166-5162(96)00042-0

Williams, L. B., Ferrell, R. E., Hutcheon, I., Bakel, A. J., Walsh, M. M., and Krouse, H. R. (1995). Nitrogen Isotope Geochemistry of Organic Matter and Minerals during Diagenesis and Hydrocarbon Migration. *Geochimica et Cosmochimica Acta.* 59, 765–779. doi:10.1016/0016-7037(95)00005-k

Xie, P., Dai, S., Hower, J. C., Nechaev, V. P., French, D., Graham, I. T., et al. (2021). Nitrogen Isotopic Compositions in NH_4^+-mineral-bearing Coal: Origin and Isotope Fractionation. *Chem. Geology.* 559. doi:10.1016/j.chemgeo.2020.119946

Zhang, J., Cao, J., Xia, L., Xiang, B., and Li, E. (2020). Investigating Biological Nitrogen Cycling in Lacustrine Systems by FT-ICR-MS Analysis of Nitrogen-Containing Compounds in Petroleum. *Palaeogeogr. Palaeoclimatol. Palaeoecol.* 556, 109887. doi:10.1016/j.palaeo.2020.109887

Zhu, Y., Shi, B., and Fang, C. (2000). The Isotopic Compositions of Molecular Nitrogen: Implications on Their Origins in Natural Gas Accumulations. *Chem. Geology.* 164, 321–330. doi:10.1016/s0009-2541(99)00151-5

Conflict of Interest: The authors declare that the research was conducted in the absence of any commercial or financial relationships that could be construed as a potential conflict of interest.

Publisher's Note: All claims expressed in this article are solely those of the authors and do not necessarily represent those of their affiliated organizations, or those of the publisher, the editors and the reviewers. Any product that may be evaluated in this article, or claim that may be made by its manufacturer, is not guaranteed or endorsed by the publisher.

frontiers in Earth Science

ORIGINAL RESEARCH
published: 13 August 2021
doi: 10.3389/feart.2021.703282

The Plenus Cold Event Record in the Abyssal DSDP Site 367 (Cape Verde, Central Atlantic): Environmental Perturbations and Impacts on the Nitrogen Cycle

Laurent Riquier[1]*, *Pierre Cadeau*[2,3], *Julien Danzelle*[1], *François Baudin*[1], *Emmanuelle Pucéat*[2] and *Christophe Thomazo*[2,4]

[1]UMR CNRS 7193 Institut des Sciences de la Terre de Paris (ISTeP), Sorbonne Université, Paris, France, [2]UMR 6282 Biogéosciences, Université de Bourgogne-Franche Comté, Dijon, France, [3]UMR 7154 Institut de physique du globe de Paris, Université de Paris, Paris, France, [4]Institut Universitaire de France, Paris, France

OPEN ACCESS

Edited by:
Eva Stüeken,
University of St Andrews,
United Kingdom

Reviewed by:
Jean-Carlos Montero-Serrano,
Université du Québec à Rimouski,
Canada
Xin-Yuan Zheng,
University of Minnesota Twin Cities,
United States

***Correspondence:**
Laurent Riquier
laurent.riquier@sorbonne-universite.fr

Specialty section:
This article was submitted to Geochemistry, a section of the journal Frontiers in Earth Science

Received: 30 April 2021
Accepted: 19 July 2021
Published: 13 August 2021

Citation:
Riquier L, Cadeau P, Danzelle J, Baudin F, Pucéat E and Thomazo C (2021) The Plenus Cold Event Record in the Abyssal DSDP Site 367 (Cape Verde, Central Atlantic): Environmental Perturbations and Impacts on the Nitrogen Cycle. Front. Earth Sci. 9:703282. doi: 10.3389/feart.2021.703282

The Oceanic Anoxic Event 2, at the Cenomanian-Turonian boundary (~93.9 Ma), was an episode of widespread burial of organic matter in marine sediments, underlined by a positive carbon-isotope ($\delta^{13}C$) excursion observed worldwide. Within this episode of O_2-depleted conditions, a short interval of cooling, termed as the Plenus Cold Event, has been recorded in many sites and sections in the northern hemisphere (Tethyan domain, Western Interior Seaway, proto-North Atlantic Ocean). But, its record and its impact on the biogeochemical cycles of carbon and nitrogen in the southern part of Central Atlantic Ocean has not been explored yet. Here, we present a detailed geochemical study of the Deep Sea Drilling Project site 367 (Cape Verde) based on a compilation of previous and new data of carbon and nitrogen isotope signals as well as trace element concentrations. The aim of this study is to better constrain the evolution of oxygenation in the water column and the associated changes in nitrogen cycle before and during the Oceanic Anoxic Event 2 in order to understand the paleoceanographic and environmental consequences of the Plenus Cold Event at one of the deepest site of the Central Atlantic Ocean. Our new dataset improves the resolution of the $\delta^{13}C$ curve for this site, and we propose a new chemo-stratigraphic frame of the carbon excursion allowing for a better identification of the short-term negative carbon isotope excursion associated to the Plenus Cold Event. The detailed evolution of redox-sensitive proxies (Mo, U, V, Fe, Cu, Ni enrichments and C_{org}/P_{total}) and isotopic signals ($\delta^{13}C_{org}$ and $\delta^{15}N_{total}$) evidence that this deep site was impacted by this cooling event. While anoxic conditions prevailed in bottom waters before and during the onset of the Oceanic Anoxic Event 2 characterized by euxinic NH_4^+-rich water column, this cooling event was accompanied by reoxygenation of the water column, which had affected the behavior of the redox-sensitive elements and caused changes in nitrogen biogeochemical cycling.

Keywords: cenomanian, turonian, carbon and nitrogen, trace metal elements, chemocline, reoxygenation

INTRODUCTION

The Cenomanian-Turonian boundary (CTB, ~93.9 Ma ago) is marked by a major environmental disturbance namely the Oceanic Anoxic Event 2 (OAE-2; Schlanger and Jenkyns, 1976). Among the numerous deoxygenation events developed in oceanic domains during the Jurassic and Cretaceous (Jenkyns, 2010 and references herein), OAE-2 has been extensively studied during the last decades because it is one of the most intense and most widespread event, and because of its particularly well preservation in the sedimentary record.

The geological evidence of this event lies primarily on the occurrence of black laminated organic-rich sediments (e.g., black shale) across a wide range of marine settings, ranging from deep ocean basins to shallow shelfal seas. The widespread deposition of these black shales is associated to a short-term (<1 Myr) perturbation of the carbon cycle marked in the case of OAE-2 by a positive carbon-isotope excursion (CIE) recorded in both the organic ($\delta^{13}C_{org}$, up to 6.0‰) and inorganic ($\delta^{13}C_{carb}$, up to 2.5‰) reservoirs (e.g., Scholle and Arthur, 1980; Schlanger et al., 1987; Arthur et al., 1988; Jenkyns et al., 1994; Kuypers et al., 2002; Tsikos et al., 2004; Bowman and Bralower, 2005; Erbacher et al., 2005; Sageman et al., 2006; Jarvis et al., 2011; Gale et al., 2019; Danzelle et al., 2020). The positive CIE, resulting from preferential burial of ^{12}C-rich organic carbon in marine sediments and observed in many marine DSDP-ODP-IODP sites and continental sections and cores, is used to define the extent of the biogeochemical OAE-2 (Gale et al., 1993; Kuypers et al., 2002).

This increased sedimentary organic matter (OM) burial rate is usually argued to reflect increasing nutrient delivery at basin scales leading to increasing primary productivity subsequently transferred to the sedimentary record by deposition of organic-rich deposits. Among possible drivers responsible for this increase in nutrient inputs, an accelerated hydrological cycle is frequently suggested as the leading hypothesis (Arthur et al., 1988; Jenkyns et al., 1994; Kuypers et al., 1999; Jarvis et al., 2011; van Helmond et al., 2014b). This intensification of the hydrological cycle, favoring continental weathering, is due to greenhouse conditions including high temperatures, high atmospheric pCO_2, and increases in humidity, as observed at the onset of the OAE-2 (Jarvis et al., 2011). This greenhouse paleoclimate has been directly related to intense volcanic activities associated to emplacement of submarine large igneous provinces (Caribbean and High-Artic) releasing vast quantities of CO_2 into the ocean and atmosphere (Sinton and Duncan, 1997; Jones and Jenkyns, 2001; Snow et al., 2005; van Bentum et al., 2012; Jenkyns et al., 2017). Seafloor hydrothermalism, associated with these large igneous provinces, and subaerial volcanism may also have supplied nutrients such as metals into seawater reservoirs, sustaining higher primary productivity (Orth et al., 1993; Kuroda et al., 2007; Turgeon and Creaser, 2008; Zheng et al., 2013; Du Vivier et al., 2015; Holmden et al., 2016). As a direct consequence of vigorous and sustained primary productivity, a profound deoxygenation of the water column in many parts of the world ocean, but particularly well expressed in the proto-North Atlantic and in the Central Atlantic (e.g., Sinninghe Damsté and Köster, 1998; Pearce et al., 2009; Jenkyns, 2010; van Helmond et al., 2014a; Westermann et al., 2014), is recorded in several biogeochemical cycling of elements including but not limited to nitrogen, sulfur, iron and trace metals such as molybdenum or uranium (Brumsack, 2006; Junium and Arthur, 2007; Owens et al., 2012, 2013; Ruvalcaba Baroni et al., 2015). Bottom water anoxia possibly affected up to 50% of the global ocean with local occurrences of euxinic conditions (Monteiro et al., 2012; Owens et al., 2013; Ostrander et al., 2017).

The positive CIE, associated with the OAE-2, is however interrupted by a short-term negative anomaly registered in many sites and sections and referred to as the Plenus carbon isotope excursion (P-CIE; O'Connor et al., 2020). The global distribution of this isotopic carbon anomaly argues for a global change of the carbon cycle. Based on pCO_2-dependent proxies ($\Delta^{13}C$; stomatal index, leaf-wax $\delta^{13}C$), the P-CIE has been interpreted as a short episode of pCO_2 rise during the $\delta^{13}C$ fall, followed by a decrease in pCO_2 up to the $\delta^{13}C$ maximum value (Kuypers et al., 1999; Sinninghe Damsté et al., 2008; Barclay et al., 2010; Sinninghe Damsté et al., 2010; Jarvis et al., 2011; Danzelle et al., 2020). These rapid oscillations of CO_2 concentration are thought to be linked to changes in temperature and oxygenation in oceanic domain. Geochemical evidences of oscillations in the oxygenation state of the water column include decrease in OM content and changes in the concentrations of redox–sensitive trace elements (RSTE: Mo, U, V, Cu) recorded within the P-CIE (Jarvis et al., 2011; van Helmond et al., 2014a; Clarkson et al., 2018; Danzelle et al., 2018, 2020; Gale et al., 2019). The reoxygenation interval is usually termed the benthic oxic zone and marked by repopulation of benthic fauna (Friedrich et al., 2006; Keller et al., 2008; Eldrett et al., 2014). The climatic perturbation is associated to the Plenus Cold Event (PCE; Gale and Christensen, 1996). This event, initially highlighted by the incursion of boreal marine fauna into the mid-latitudinal basins (Vocontian Basin, SE France; Jefferies, 1962, Jefferies, 1963), is now well defined in several basins and at all latitudes (see review of O'Connor et al., 2020 and references herein). The PCE is coeval to the second buildup of the $\delta^{13}C$ signal within the positive CIE and has been geochemically characterized by positive isotopic excursion of the $\delta^{18}O$ signal and by a decrease of dedicated biomarkers concentrations, such as the crenarchaeotal membrane lipid, linked to the TEX_{86}, a sea-surface temperature proxy (Jenkyns et al., 1994; Paul et al., 1999; Tsikos et al., 2004; Forster et al., 2007; Sinninghe Damsté et al., 2008; Takashima et al., 2009; Danzelle et al., 2020). The origin of this short-term carbon cycle event is still debated (atmospheric vs. oceanographic; regional *vs* global processes) because the triggering factors of CO_2 change are difficult to identify. The rise in pCO_2 is thought to be linked to the incursion of a cold oxygenated water mass in tropical to equatorial zones, associated to modification of oceanic circulation (Jenkyns et al., 2017). This oceanographic change would led to the remineralization of buried OM, which may cause trace metals released from the sediments into the water column and acidification. The PCE has been largely argued to reflect a drawdown in atmospheric pCO_2 of about 20–25% (Freeman and Hayes, 1992; Jarvis et al., 2011) with extreme estimate up

to 40–80% (Kuypers et al., 1999), resulting from a negative feedback caused by the combination of increased organic carbon burial, CO_2 consumption due to enhanced silicate weathering (Arthur et al., 1988; Sinninghe Damsté et al., 2010; Blättler et al., 2011; Jarvis et al., 2011; Pogge von Strandmann et al., 2013; Jenkyns et al., 2017) and potential cessation of volcanic outgassing (Kuroda et al., 2007).

While a causal relationship between carbon-cycle dynamics and cooling during the PCE is therefore largely documented and argued, especially in mid-latitude zones, little is known on the related biogeochemical cycle of nitrogen at this level of temporal resolution. Meanwhile, previous studies on the nitrogen isotopes record of OM during OAE-2 have proposed several hypotheses to explain commonly observed decrease in sedimentary $\delta^{15}N_{total}$ values such as depth variations of water column chemocline, hence activity and locus of nitrogen fixers and denitrifiers guilds (Kuypers et al., 2002; Junium and Arthur, 2007; Higgins et al., 2012) or changes in the pathway of diazotrophy (from canonical Mo-nitrogenase to alternative V-Fe or Fe-only nitrogenases; Zhang et al., 2014). According to the short residence time of fixed N in modern seawater (<3 kyr) (Tyrrell, 1999; Brandes and Devol, 2002) and to the estimated duration of the P-CIE ca. ~105 kyr (Charbonnier et al., 2018) comprising the ~40–60 kyr PCE as estimated for the boreal sites (Jarvis et al., 2011), high-resolution $\delta^{15}N_{total}$ record of the OAE-2 may offer a chance to better characterized the impact of rapid swings in temperatures on the nitrogen biogeochemical cycle. Moreover, within the context of the greenhouse OAE-2, the short lived PCE provides a unique opportunity to testify the hypothesis of Algeo et al. (2014), who proposed that the link between high temperatures and low $\delta^{15}N_{total}$ values observed on long times scale during greenhouse intervals may be potentially also observed during shorter event such as OAEs and should reflect lower integrated water-column denitrification rates in comparison to icehouse intervals.

Among the several sites, where the OAE-2 and the PCE has been recorded, the Deep Sea Drilling Project (DSDP) site 367 (Leg 41, Cape Verde, Central Atlantic) represents an interesting study case, characterized by a positive CIE of 6.0‰ (Arthur et al., 1988) and by a noticeable enrichment of organic carbon (up to 45%; after Herbin et al., 1986) deposited in abyssal environment in low latitude zone. Previous studies, mainly based on $\delta^{13}C$ and $\delta^{15}N_{total}$ isotopic signatures and biomarker identifications (Kuypers et al., 2002, Kuypers et al., 2004; Sinninghe Damsté et al., 2008), organic paleothermometer TEX_{86} (Schouten et al., 2003; Forster et al., 2007), iron speciation, $\delta^{56}Fe_T$, $\delta^{98/95}Mo$ isotopic signatures (Owens et al., 2012; Westermann et al., 2014; Dickson et al., 2016) and some trace element concentrations (Kuypers et al., 2002; Westermann et al., 2014) have been already realized on a few samples (14–17, except for Dickson et al. (2016), which was realized on 114 samples from the archive of half of the core) of this deep-water site. An integrated and detailed work is however needed to better constrain the primary signal of geochemical proxies, to reconstruct the paleo-environmental conditions during the OAE-2 and the PCE and to determine the impact of this event on the nitrogen cycle in one of the deepest settings of the CTB.

The aim of this work is thus to 1) achieve a detailed study of the OAE-2 in deep-sea context based on a multi-proxy study (including $\delta^{13}C_{org}$, $\delta^{15}N_{total}$, Rock-Eval and trace metals) of the DSDP 367 succession from Cape Verde, and 2) propose a model that account for the evolution of the biogeochemical cycle of nitrogen and its relation to environmental perturbations for the southeastern part of the Central Atlantic.

MATERIAL AND METHODS

Sampling Location

Site 367 (12°29.2′N; 20°02.8′W) was drilled in 1975 during the DSDP Leg 41 and is located off the coast of the Senegal in the Cape Verde Basin (**Figure 1**). This site shows an almost continuous sedimentary record from Upper Jurassic (Oxfordian-Kimmeridgian) up to Pleistocene (Lancelot et al., 1978). During the Cretaceous, this site belonged to the southern part of the Central Atlantic and a paleodepth of around 3,700 m has been estimated based on isostatic methods (Chenet and Francheteau, 1979). Thus, sediments were deposited in abyssal plain environment, probably below the Carbonate Compensation Depth (even if some traces of carbonate do exist, Chenet and Francheteau, 1979).

The studied succession, composed of cores 19 and 18, is about 13.5 m thick (from 650 to 636.5 m depth), with a coring hiatus of 2.2 m from 645.7 to 643.5 m depth. The sedimentary sequence is mainly composed of laminated black shales and terrigenous silicates. In details, in core 19, green and olive-grey calcareous clays are interbeded with laminated black shales whereas the core 18 is dominantly composed of laminated black shales, especially in the sections 5 and 1 (Mélières, 1978; Herbin et al., 1986). In some studied samples, some strong post-depositional oxidation of the pyrite within the sediments has been noticed and is underlined by the presence of abundant jarosite and iron oxides.

Methods

A total of 42 rock samples were collected every 5–20 cm according to sample availability as following: seven from the base of the studied interval up to the void (650.5–647.7 m depth) and 35 above the void (643.3–636.5 m depth). After cleaning, all rock samples were powdered manually in an agate mortar, at the Biogeosciences Laboratory of the University of Burgundy in Dijon (France).

Carbon and Nitrogen Analyses

Concentration and isotopic composition of organic carbon (C_{org}, $\delta^{13}C_{org}$) and total nitrogen (N_{total}, $\delta^{15}N_{total}$) were measured on carbonate free residues. Sample powders were rinsed by dichloromethane-ethanol (9:1) to remove any modern organic contaminant and reacted with hydrochloric acid (HCl; 6N) at room temperature overnight followed by 4 h at 80°C to remove carbonate phases. The residues were rinsed with deionized distilled water and centrifuged several times until neutral pH was reached and then dried at 60°C overnight in an oven. Aliquots of carbonate free samples (30–60 mg) were then weighed and

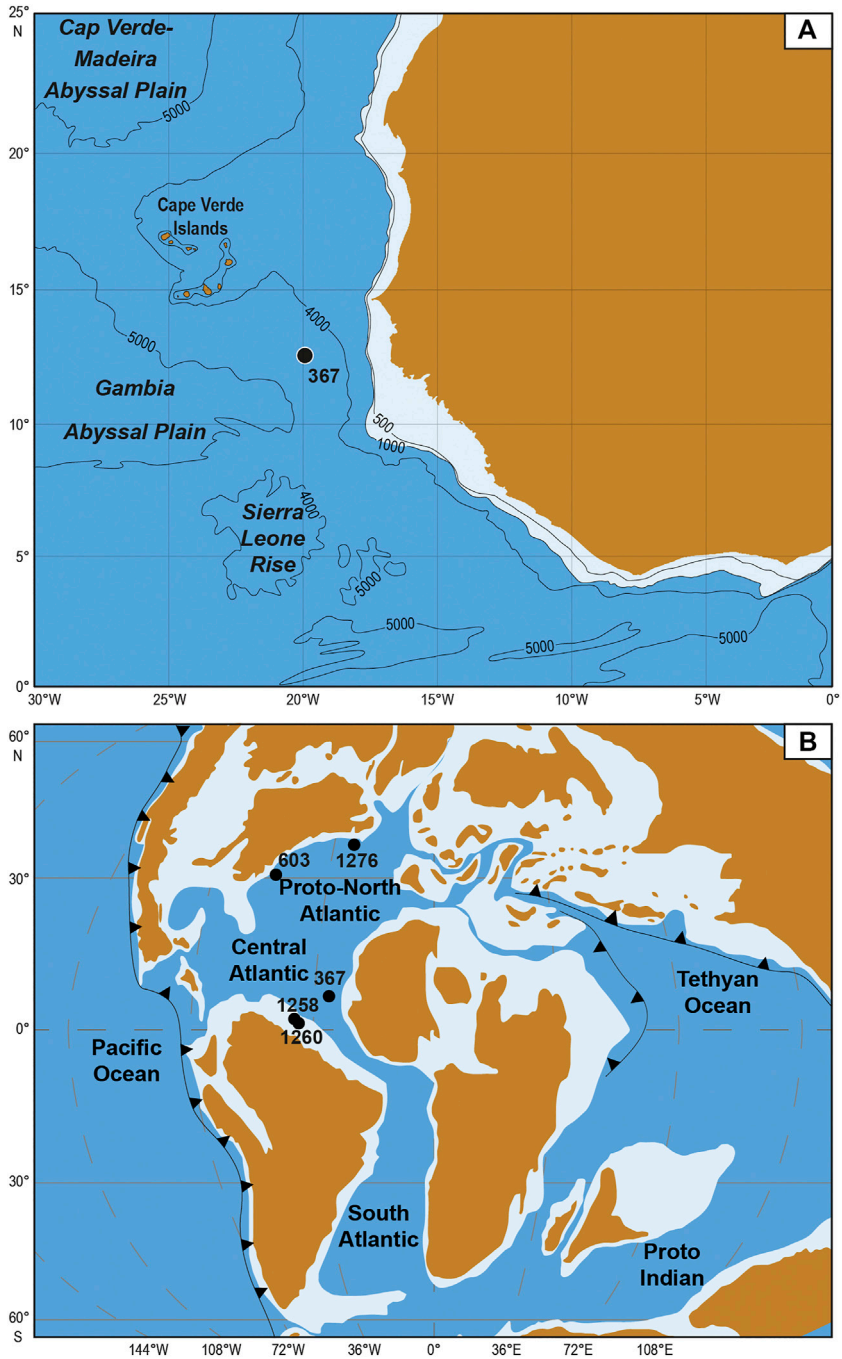

FIGURE 1 | Location of the DSDP site 367 in the Cape Verde Basin (modified from Lancelot et al., 1978) **(A)** and paleomap of the Cenomanian-Turonian Central Atlantic and proto-North Atlantic zones with the paleopositions of the site 367 and other DSDP/ODP sites (603, 1258, 1260, and 1276) mentioned in this paper (van Hinte et al., 1993; Erbacher et al., 2004a, Erbacher et al., 2004b; Tucholke et al., 2004) **(B)**.

poured in tin capsules. Isotopic measurements were performed at the Biogeosciences Laboratory, Dijon (France), on a vario Micro cube elemental analyser (Elementar) coupled to an IsoPrime stable isotope ratio mass spectrometer (Isoprime) in continuous flow mode. The carbon and nitrogen isotopic compositions are both expressed in delta notation and reported as the per mil (‰) deviation relative to the Vienna Pee Dee Belemnite (VPDB) standard for carbon and to AIR standard for nitrogen. USGS40 certified reference material (C = 40.8 wt%; N = 9.52 wt%; $\delta^{13}C_{VPDB}$ = −26.39‰, $\delta^{15}N_{AIR}$ = −4.52‰) was used for calibration. The organic carbon (C_{org}) and total nitrogen (N_{total}) content is expressed as dry weight

TABLE 1 | Correlation factor r between Al and major and minor elements.

	Fe	Mn	P	Si	Ba	Co	Cr	Cu	Mo	Ni	Th	U	V	Zn	Zr
Al	0.00	0.17	−0.45	0.96	−0.30	0.06	0.77	0.15	−0.65	−0.65	0.97	−0.68	0.03	0.02	0.93

percentage (wt%) of the total fraction. From these values, the molar C_{org}/N_{total} ratio was calculated. The external reproducibility based on duplicates analyses of carbonate free samples was better than ±0.15 wt% (1σ) for carbon and ±0.10 wt % (1σ) for nitrogen. External reproducibility based on duplicate analyses of the samples was better than ±0.05‰ and ±0.5‰ for carbon and nitrogen, respectively.

Rock-Eval Pyrolysis

Organic matter parameters, including Total Organic Carbon (TOC) content, Hydrogen Index (HI), Oxygen Index (OI) and temperature of the maximum yield of hydrocarbon (T_{max}) were obtained using 10–50 mg of bulk powder, on a Rock-Eval 6 Turbo at the ISTeP Laboratory of Sorbonne University in Paris (France), by sequential pyrolysis and oxidation treatment (Espitalié et al., 1985a; Espitalié et al., 1985b; Espitalié et al., 1986; Lafargue et al., 1998; Behar et al., 2001). Reproducibility was evaluated by replicates analyses of laboratory standards and was better than ±0.05 wt% (1σ) for TOC, ± 1.5°C (1σ) for T_{max}, ± 10 mg HC/g TOC (1σ) for HI, and ±10 mg CO_2/g TOC (1σ) for OI. The TOC (%) concentration, obtained by whole-rock analyses from the Rock-Eval method, is in agreement with this of C_{org}, determined on the carbonate-free fraction ($r = 0.97$) and show similar vertical distribution but with lower value compared to C_{org} (except for one sample).

Analysis of Major and Trace Elements

Major and trace elements analyses were performed using inductively coupled plasma mass spectrometry (ICP-MS) at the Activation Laboratory (Actlab) in Ancaster, Canada. Protocol information for the package 4Litho-Lithium Metaborate/Tetraborate Fusion ICP and ICP-MS can be found at www.actlabs.com. Reproducibility is better than 2% of the measured values (1σ) for major and trace elements.

To eliminate a possible detrital origin of selected elements (Ba, Co, Cr, Cu, Mo, Ni U, V, Zn Fe, Si, and P), the Al concentration was linearly correlated with each element and correlation coefficient r was calculated (**Table 1**). Aluminum is considered as an indicator of the aluminosilicate contribution to the sediments and is also a conservative element during secondary processes. Fort most of them (except for Si, Th, Zr and to a lesser extent Cr), no noticeable correlation or anti-correlation is observed, suggesting a non-detrital (i.e., authigenic) origin. In order to compare values obtained in this work with those of previous studies and from other Central and proto-North Atlantic sites, the concentration of major and trace elements were normalized to aluminum (El/Al) to correct for dilution effects by varying carbonate or OM contents. It is important to note here that although Al concentrations are always upper than 1%, fluctuating from 1.2 to 6.6%, they show a progressive decreasing trend from the base to the top of the studied interval (see **Supplementary Material**). So, for few samples, mainly located in the upper part of the studied sections (638.1; 638.7 and 640.35 m) and characterized by the lowest concentration of Al (<1.5%), normalization may lead to a slight exaggeration of El/Al values.

Lastly, the enrichment factor (EF) was also calculated following the formula: $EF = (Element/Al)_{sample}/(Element/Al)_{reference}$. This reference could be either the Post-Archean Average Shales (PAAS, Wedepohl, 1971) or the Upper Continental Crust (UCC, McLennan, 2001). For this work, the EFs were calculated using the UCC concentrations. As precised by Algeo and Tribovillard (2009), EF > 3 represents a detectable authigenic enrichment, whereas EF > 10 represents a substantial authigenic enrichment.

RESULTS

In order to have the highest resolution for geochemical signals, the results obtained in this study ($n = 42$) have been compiled with those of previous studies ($n = 17$ from Kuypers et al., 2002, Kuypers et al., 2004 and from H-J., Brumsack, unpublished data, for selected major and trace elements (Fe, Mn, P, Ni, Cu, Co, and Zn) on the same 17 samples; $n = 29$ from Forster et al., 2007 and $n = 14$ from Westermann et al., 2014).

Stable Isotopes

The $\delta^{13}C_{org}$ values of this study range from −28.5 to −21.2‰ (**Figure 2**) and are in agreement with the data reported by Kuypers et al. (2002) completed by Forster et al. (2007) for this site. After a phase of stability at the base of the section (649.6–642.0 m) with $\delta^{13}C_{org}$ values of ~ −27.8‰, an increasing trend of about +3.5‰ is observed up to 641.15 m, where $\delta^{13}C_{org}$ value reaches up to −24.3‰. This first increase is followed by a 1.45 m thick interval marked by lower values down to −25.8‰ at 640.8 m and a second phase of $\delta^{13}C_{org}$ increase with values up to −22.4‰ recorded at 639.7 m. A short plateau interrupts this second rapid increase with values close to -23.5‰ around 640.35 m. Upward (639.7–636.5 m), $\delta^{13}C_{org}$ values remain high oscillating between −22.5 and −21.2‰.

The $\delta^{15}N_{total}$ record of this study shows negative values ranging from −2.3 to −0.4‰, which also compare well to the $\delta^{15}N_{total}$ record of Kuypers et al. (2004) for this site (**Figure 2**). Unlike the $\delta^{13}C_{org}$, the $\delta^{15}N_{total}$ profile does not show interval of stable values at the base of the studied core. From 649.6 to 645.9 m and from 643.4 to 642.2 m, $\delta^{15}N_{total}$ values oscillate between −1.7 and 0.0‰ and between −1.6 and −0.4‰, respectively. It is important to note here that maximum value of $\delta^{15}N_{total}$ is reached at the base of the OAE-2, when $\delta^{13}C_{org}$ values are yet low. The rest of the studied core is characterized by lower $\delta^{15}N_{total}$ with values down to −1.5‰. However, unlike to

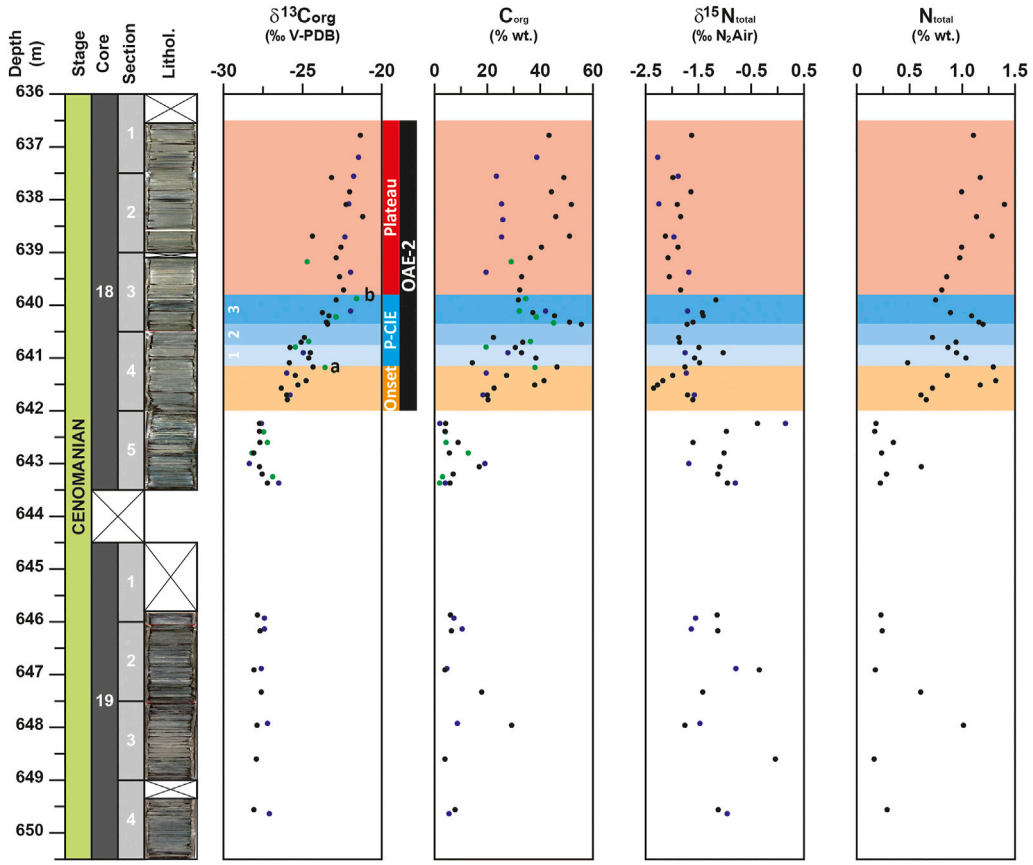

FIGURE 2 | Depth-profiles for $\delta^{13}C_{org}$, $\delta^{15}N_{total}$ signals, organic carbon (C_{org}) and total nitrogen (N_{total}) contents for the DSDP site 367. Data from the studies of Kuypers et al. (2002) and Kuypers et al. (2004) and Forster et al. (2007) are represented with blue and green circles respectively. OAE-2 interval is represented by the dark band determined on the base of the positive carbon isotope excursion. The OAE-2 interval is divided in three parts: the onset, represented by the orange band, the Plenus carbon isotope excursion (P-CIE), represented by the blue band and the plateau represented by the red band; a and b would correspond to the $\delta^{13}C_{carb}$ maxima, defined by Jarvis et al. (2011), that mark the limits between the onset and the P-CIE intervals and between the P-CIE and the plateau intervals. The P-CIE is subdivided in three subparts numbered 1, 2, and 3 and represented by gradual darker blue bands.

the $\delta^{15}N_{total}$ signal from Kuypers et al. (2004), which did not record noticeable variation from 642.0 to 636.5 m, two intervals can be recognized in the more detailed $\delta^{15}N_{total}$ record of this study. During the first interval (641.8–639.9 m), $\delta^{15}N_{total}$ values oscillate between −2.3 and −1.0‰, then from 639.7 to 636.5 m, a second interval of low $\delta^{15}N_{total}$ values (~−1.9‰) is recognized. In more details, the 1.9 m thick first interval (641.8–639.9 m) records a succession of two negative and two positive excursions of the $\delta^{15}N_{total}$. The first negative excursion of $\delta^{15}N_{total}$ broadly corresponds to the first buildup of $\delta^{13}C_{org}$ signal, the two positive excursions are recorded at the base and at the top of the 1.5 m thick interval marked by a slight trough and a second phase of rapid change in $\delta^{13}C_{org}$ values, corresponding to the P-CIE.

Carbon, Nitrogen, and Phosphorus Contents

In the core 19, the C_{org} profile is marked by a noticeable peak up to 29.3% at 648.0 m (**Figure 2**). At the base of the core 18, a slight increase of C_{org} values up to 17% is observed around 643.0 m. Similar trend with C_{org} values up to 20% was previously recorded for this site by Kuypers et al. (2002) and Forster et al. (2007). This is followed by a short interval of low values (down to 4% at 642.25 m) and a progressive increase of C_{org} values up to 46.4% at 641.2 m. After an episode of oscillating values, a short interval with the highest C_{org} values (between 45.5 and 55.5%) is recorded from 640.35 to 640.2 m, followed by a rapid decrease down to 31.8% recorded at 639.9 m. Lastly, a progressive increasing trend followed by a second interval of high C_{org} values (between 43.4 and 51.8%) is recorded from 638.7 m up to the end of the studied section. This second increasing trend and associated high values of C_{org} were not observed in Kuypers et al. (2002) and Forster et al. (2007). In these studies, a plateau of values around 25% marked this interval. The N_{total} profile, which oscillates from 0.16 to 1.40%, shows a similar evolution than the C_{org} ($r = 0.97$) with high values (>0.8%) recorded at 648.0 m in the core 19 and from 641.5 m onward in the core 18 (**Figure 2**).

The C_{org}/N_{total} ratio shows high values when compared to the Redfield ratio (i.e. 106/16 = 6.625, Redfield, 1958) and range

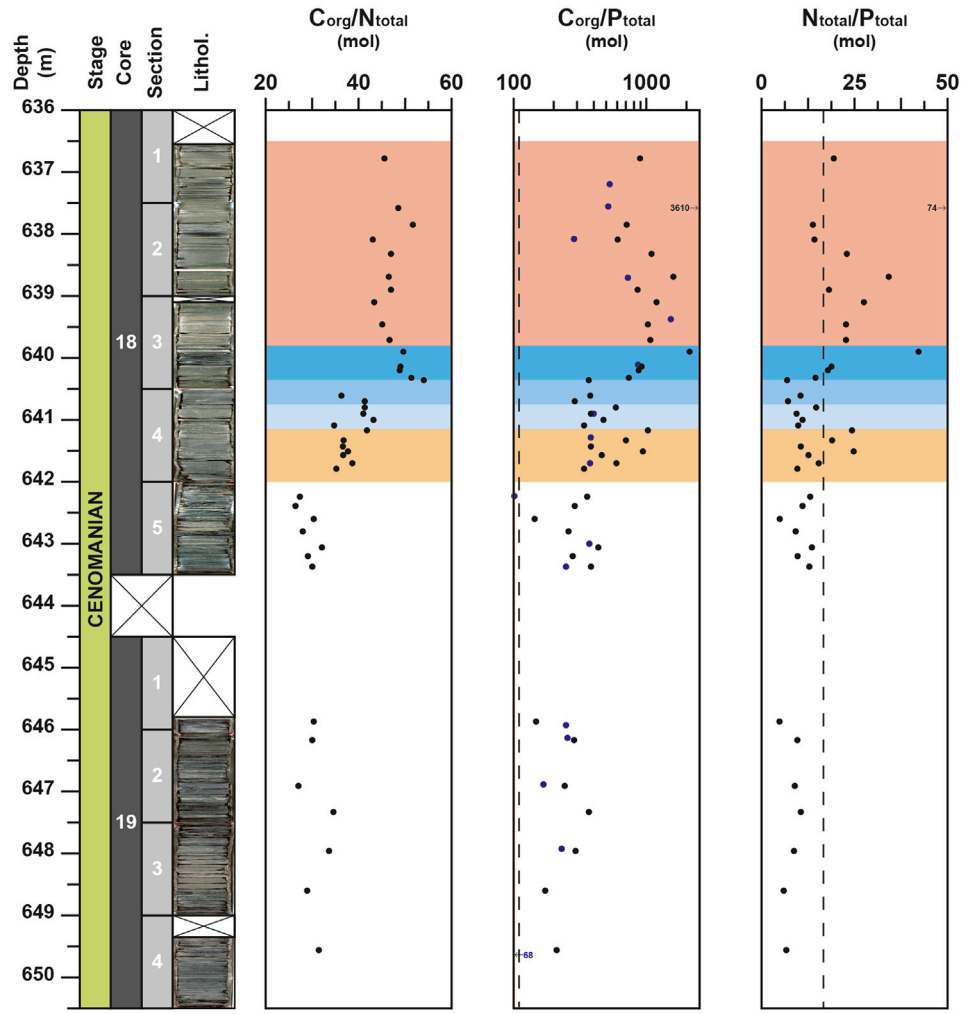

FIGURE 3 | Depth-profiles for C_{org}/N_{total}, C_{org}/P_{total} and N_{total}/P_{total} molar ratios for the DSDP site 367. Data from the studies of Kuypers et al., 2002 and Kuypers et al., 2004) are represented with blue circles. Vertical dotted lines represent the Redfield ratio value (106 for C_{org}/P_{total} and 16 for N_{total}/P_{total}).

between 26 and 54 (**Figure 3**). This range of values is comparable to those (25–50) usually recorded in Cretaceous black shale deposits (Rau et al., 1987; Junium and Arthur, 2007). Moreover, similar to the $\delta^{13}C_{org}$, the C_{org}/N_{total} profile shows three distinguished intervals in the studied cores. From 649.60 to 642.25 m, all values are lower than 35, then upward a noticeable increase the C_{org}/N_{total} ratio is recorded with the highest value (54) reached at 640.35 m. From this depth onward, the C_{org}/N_{total} values remain high oscillating between 43 and 52.

For the C_{org}/P_{total} molar ratio, all values are higher than the Redfield ratio (C_{org}/P_{total} = 106). In detail, the signal remains relatively constant from the base of the studied section up to 641.8 m with average value of 280. Then, an increasing trend is observed from 641.8 m up to 639.9 m, where the C_{org}/P_{total} molar ratio reaches 2093 (**Figure 3**). For the rest of the section, the C_{org}/P_{total} values tend to decrease but two noticeable peaks of 1,590 and 3,610 are recorded at 638.7 and 637.6 m, respectively.

The N_{total}/P_{total} molar ratio shows similar variations than the C_{org}/P_{total} molar ratio (r = 0.99). From 649.5 to 640.25 m, the N_{total}/P_{total} values are nearly constant with average values close to 10 (**Figure 3**). Only two peaks up to 24, due to increasing N content, are recorded at the base of the OAE-2 (at 641.5 and at 641.2 m). From 640.20 m onward, the N_{total}/P_{total} values sensibly increase, with most values exceeding the canonical Redfied ratio (i.e., N_{total}/P_{total} = 16).

Major and Trace Element Evolutions

Compared to the values of the UCC (McLennan, 2001), all the elements that are not linked to detrital fraction exhibit noticeable enrichment. The element to Al (El/Al) ratios exhibit contrasted evolutions depending on the considered element. For the core 19, most of elements record a positive peak of concentration and ratio at 648.0 m. This peak is particularly well expressed for U, V, Cd, Cu, and Zn (**Figures 4,5**) and corresponds to high C_{org} values (up to 29.3%).

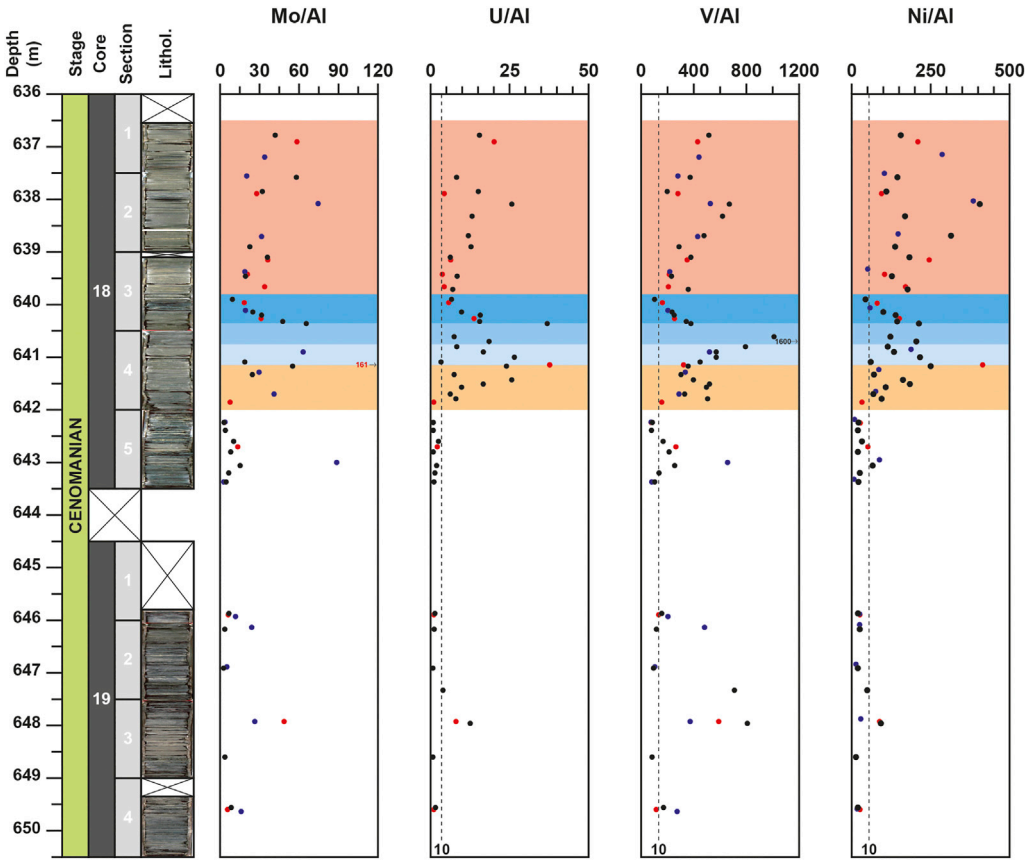

FIGURE 4 | Depth-profiles for Mo/Al, U/Al, V/Al, Ni/Al for the DSDP site 367, Data from the studies of Kuypers et al. (2002), coupled to unpublished data from H-J. Brumsack on the same samples, and Westermann et al. (2014) are represented with blue and red circles respectively. Vertical black dotted line, noted 10, represent the El/Al values corresponding to an EF equal to 10, respectively compared to the Upper Continental Crust (McLennan, 2001): 0.19 for Mo/Al; 0.35 for U/Al; 13.31 for V/Al and 5.47 for Ni/Al.

For the core 18, after a slight enrichment recorded around 643.0 m for only few elements (Mo, V, Ni, Zn, Ba), which was also observed in previous studies (Kuypers et al., 2002; Westermann et al., 2014), most elements are characterized by noticeable enrichments starting at 642.0 m and by an interval with the highest values from 640.8 to 640.35 m (**Figures 4–6**). This 45 cm-thick interval is well observed in the Al-normalized profiles of P, Cu, Zn, V, U, and Cd and corresponds to the highest values of C_{org} (up to 55.5%). Compared to previous studies (Kuypers et al., 2002; Westermann et al., 2014), the results obtained here allow to highlight for the first time this noticeable enrichment of these elements around 640.5 m depth. For most of them (P, Cu, Zn, V, U and Mo), this is followed by a noticeable decrease of El/Al values up to around 639.0 m depth. For few other elements, such as Ba, Ni, Co, and Fe, the highest values are observed upper in the core. For Ba, noticeable fluctuations are recorded from 642.0 m and the highest value are recorded around 639.0 m, whereas for Ni and Fe, the highest values are observed at 638.1 m and are coeval with peaks in the Al-normalized profiles of P, U, and V (**Figures 4–6**). Lastly, some elements, like Mn or Zr, do not show noticeable variations in the studied interval. These elements exhibit values mainly lower than the UCC value or close to it. Only one obvious positive peak at 640.9 m for Mn and a negative peak at 640.35 m for Zr are observed (**Figure 6**).

INTERPRETATIONS AND DISCUSSIONS

Identification of the Plenus Carbon Isotope Excursion Within the Deep Sea Drilling Project Site 367

Since the works of Gale et al. (1993), it is well established that the OAE-2 is defined by a positive stable CIE, composed of several spikes and nudges. This excursion is usually subdivided into three main phases: an earlier phase A, named rapid shift, characterized by an increase in $^{13}C/^{12}C$ ratio values from the pre-excursion background value and thus by an increase of $\delta^{13}C$ in both organic and carbonate fractions, a following phase B, corresponding to a plateau of high $\delta^{13}C$ values, and a final phase C, characterized by a gradual drop of $\delta^{13}C$ values toward pre-excursions level (Kuypers et al., 2002). As an OAE correspond by definition to the main phase of enhanced isotopically light organic carbon burial

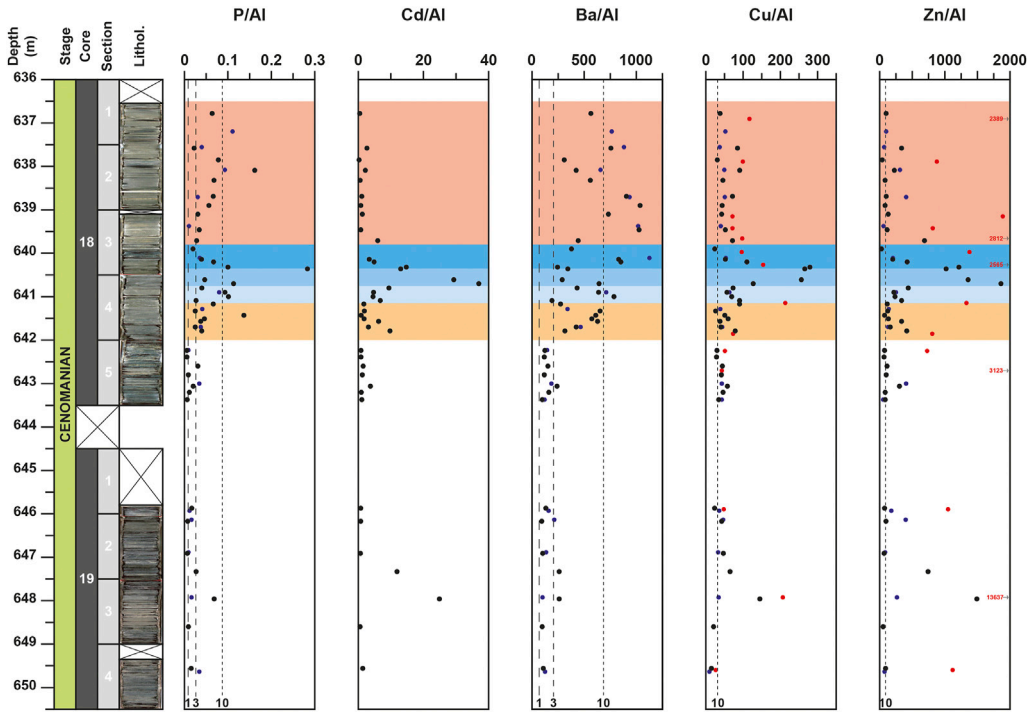

FIGURE 5 | Depth-profiles for P/Al, Cd/Al, Ba/Al, Cu/Al, Zn/Al for the DSDP site 367. Data from the studies of Kuypers et al. (2002), coupled to unpublished data from H-J. Brumsack on the same samples, and Westermann et al. (2014) are represented with blue and red circles respectively. Vertical black dotted lines, noted 1, 3 and 10, represent the El/Al value corresponding to an EF equal to 1, 3 and 10, respectively compared to the Upper Continental Crust (McLennan, 2001): 0.087 for P/Al; 0.01 for Cd/Al; 68.41 for Ba/Al; 3.11 for Cu/Al and 8.83 for Zn/Al.

(Arthur et al., 1988), the Cenomanian-Turonian OAE-2 is thus restricted to the phases A and B (Kuypers et al., 2002). In high-resolution isotope profiles, such as measured in Eastbourne (Paul et al., 1999); Lambruisse (Takashima et al., 2009; Danzelle et al., 2020) and Pont d'Issole (Jarvis et al., 2011), the phase A can be further subdivided in three intervals: an initial rise in $\delta^{13}C_{carb}$ value, corresponding to the first buildup, ended by a first maximum value ($\delta^{13}C_{carb}$ maxima a in Jarvis et al., 2011), followed by a slight decrease, associated to a trough interval, and a further rise, corresponding to the second buildup, to the maximum values of the CIE ($\delta^{13}C_{carb}$ maxima b in Jarvis et al., 2011) that define the beginning of the phase B (plateau interval). The short-lived interval, composed by a "trough interval" and the "second build-up", correspond to the P-CIE (O'Connor et al., 2020). This interval is associated with a cooling event, marked by a southerly incursion of boreal fauna (including the belemnite *Praeactinocamax plenus,* the bivalve *Oxytoma seminudum* and the serpulid worm *Hamulus sp.*) into mid-latitude areas (Jefferies, 1962; Gale and Christensen, 1996) and by positive oxygen isotopic excursion recorded in carbonates (Jarvis et al., 2011). This faunal and paleoclimatic event is referred to as the PCE (Gale and Christensen, 1996) and was identified from a number of paleo-temperature proxies at several European, North America and Atlantic sites. For the DSDP site 367, the PCE has been identified using the organic paleothermometer TEX_{86} signal which show low value (0.84) around 640.1 m (Schouten et al., 2003; Forster et al., 2007). In more details, the TEX_{86} signal records a ~1 m thick interval (640.35–639.40 m) marked by a negative excursion, interpreted as a sea surface temperature decline of about 4°C (Forster et al., 2007). Recently, based on low $\delta^{98}/^{95}$Mo values, Dickson et al. (2016) have reported in the same succession an 80 cm thick interval (640.86–640.05 m), slightly deeper to those defined by TEX_{86} signal corresponding to the PCE.

In agreement with previously OAE-2 carbon-isotope records (e.g., Paul et al., 1999), five distinctive phases can be recognized in the carbon-isotope signal of the DSDP site 367. The first phase of the $\delta^{13}C_{org}$ signal (649.5–642.0 m), with values clustering around −27.8‰, corresponds to the pre-excursion interval. The first rapid shift of $\delta^{13}C_{org}$ values up to −24.3‰ (642.00–641.15 m) corresponds to the first buildup, which marks the onset of the OAE-2, such as in typical CTB sections, like Eastbourne (Gale et al., 1993) and Pont d'Issole (Jarvis et al., 2011; Danzelle et al., 2018). The following 1.35 m thick interval (641.15–639.80 m) is interpreted as an equivalent of the P-CIE recorded in the Eastbourne section (O'Connor et al., 2020). The first 40 cm of this interval would represent the short trough and is referred here as the PCE-1 (641.15–640.75 m) and the last 95 cm would correspond to the second buildup. In this study, this interval is subdivided in two parts: a 40 cm thick interval referred here as the PCE-2 (640.75–640.35 m) and a 55 cm thick interval referred here as the PCE-3 (640.35–639.80 m). The limit between PCE-2 and PCE-3 corresponds to a short plateau of $\delta^{13}C$ values. The top of the core encompasses part of the isotopic plateau,

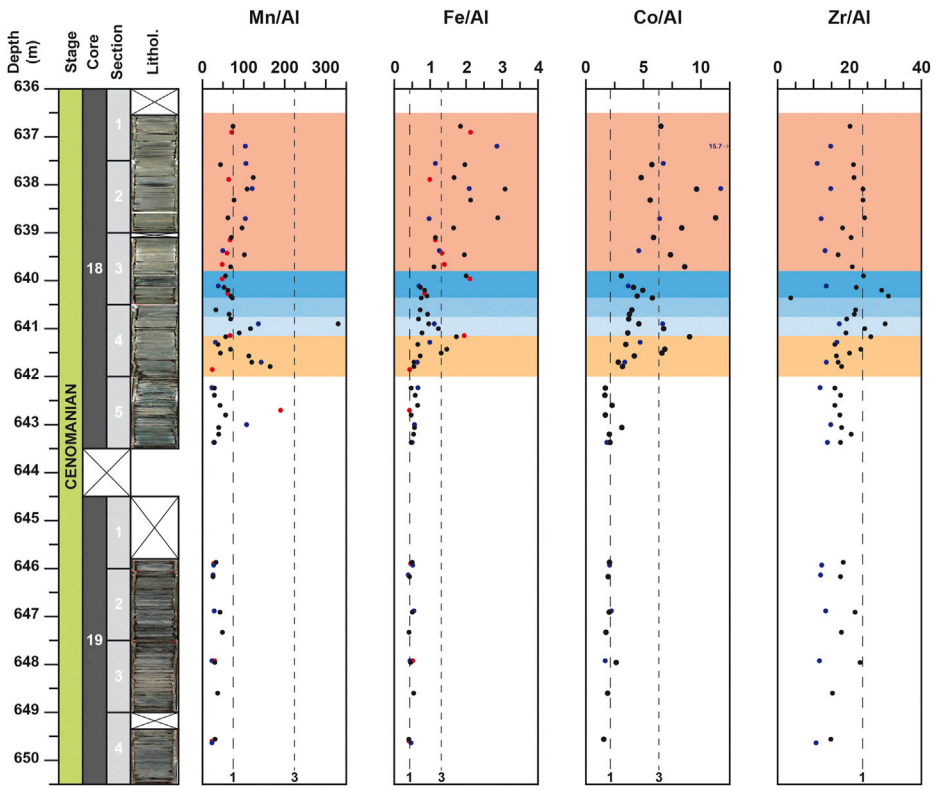

FIGURE 6 | Depth-profiles for Mn/Al, Fe/Al, Co/Al and Zr/Al for the DSDP site 367. Data from the studies of Kuypers et al. (2002), coupled to unpublished data from H-J. Brumsack on the same samples, and Westermann et al. (2014) are represented with blue and red circles respectively. Vertical black dotted lines, noted 1 and 3, represent the El/Al value corresponding to an EF equal to 1 and 3, respectively compared to the Upper Continental Crust (McLennan, 2001): 0.75 for Mn/Al; 0.44 for Fe/Al; 2.11 for Co/Al and 23.63 for Zr/Al.

corresponding to the phase B in Kuypers et al. (2002) and start at 639.80 m. The end of the phase B and the gradual return to pre-excursion values, which marks the CTB and corresponds to the phase C are not recorded in the DSDP site 367.

Based on the new $\delta^{13}C$ data, obtained in this study, the onset of the OAE-2 and the phase A should be moved from 643.0 m, as initially proposed by Kuypers et al. (1999), to 642.0 m depth. Even if the lowest values of $\delta^{13}C$ signal, −28.4‰ in Kuypers et al. (1999) and −28.1‰ in this study are respectively recorded at 643.0 and 642.8 m, the following values do not show noticeable increase before 642 m. They oscillate from −27.6 to −27.2‰ in Kuypers et al. (1999) and Forster et al. (2007) and are close to −27.7‰ in this study. The onset of the $\delta^{13}C_{org}$ shift is observed by a noticeable increase of 1.8‰ between 642.25 and 641.8 m in this study and 641.7 m in Kuypers et al. (1999). The A/B limit, marked by the first highest value of $\delta^{13}C$ recorded after the PCE, is located before 640 m, probably close to 639.8 m rather than at 640.1 m, as initially proposed by Kuypers et al. (2002). This new evolutionary frame agrees with data reported by Forster et al. (2007), which record the highest value of $\delta^{13}C_{org}$ of −21.6‰ at 639.9 m. Our results confirm that, as in other sites, the cooling, associated to the PCE, started after the onset of the P-CIE and the lowest temperature is recorded close to the isotopic A/B limit.

Organic Matter Source and Maturity

Both the C_{org} (%) and TOC (%) values calculated from carbonate free fraction and from bulk-rock by Rock-Eval pyrolysis show important enrichment of OM content (up to 55%, at 640.35 m). In both signals, a noticeable increase of organic carbon content, coeval with the onset of OAE-2 and associated with the $\delta^{13}C_{org}$ positive excursion, is observed from 642.0 m.

As shown in the modified van Krevelen diagram (**Figure 7A**), most samples have HI values higher than 400 mg HC/g TOC and are characterized by low OI values, which never exceed 65 mg CO_2/g TOC. In detail, pre-OAE-2 samples, with TOC mostly lower than 10%, record HI values lower than 350 mg HC/g TOC and OI values upper than 45 mg CO_2/g TOC. In the modified van Krevelen diagram, these values plot in the Type II and Type III domain, consisting theoretically of a mix of marine and terrestrial material. However, as demonstrated by previous studies based on molecular fossils (Kuypers et al., 1999; Kuypers et al., 2002; Sinninghe Damsté et al., 2008), OM is thought to have a dominant marine origin, even before the OAE-2. Molecular fossils of unambiguous terrestrial origin (i.e., leaf wax lipids and oleoananes) are present only in low abundance in the extractable OM (Kuypers et al., 2002). For these samples, it is likely that the marine OM had been partially oxidized with a

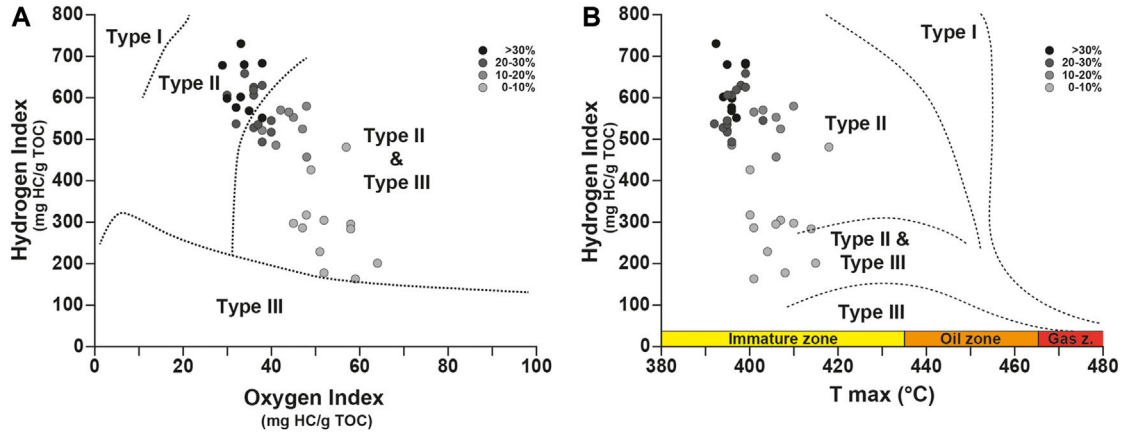

FIGURE 7 | Cross-plots of Hydrogen Index (HI) versus Oxygen Index (OI) **(A)** and versus T_{max} **(B)**.

consequence of a lowering of HI. The samples within the OAE-2 record the highest values of HI (up to 730 mg HC/g TOC) and the lowest values of OI (down to 30 mg CO_2/g TOC). For theses samples, these range of HI and OI values correspond to OM of Type II (marine origin), deriving from algal and bacterial sources. These data confirm the first results obtained by Herbin et al. (1986) on this site. Based on the significant covariation of $\delta^{13}C_{org}$ with $\delta^{13}C$ of the extended hopanoids and sulfur-bound phytane (r = 0.91), Kuypers et al. (2004) argue for the predominance of cyanobacteria in the phytoplanktonic community and thus in the sedimentary OM. The T_{max} values oscillate between 392 and 418°C, clearly indicating an immature OM (**Figure 7B**), hence a shallow burial of sediments. This result is in good agreement with the preservation of molecular fossils (see Kuypers et al., 2002; Sinninghe Damsté et al., 2008) within the studied site and indicates that the burial diagenesis might have been limited.

Evolution of the Oxygenation Conditions and of the Water Mass Restriction During the Oceanic Anoxic Event 2

Among the DSDP-ODP-IODP sites from the Central Atlantic, the DSPD site 367 is usually considered as being continually overlain by anoxic to euxinic water masses during the late Cenomanian times (Dickson et al., 2016). This is based on high value of C_{org}/P_{total} ratio (mostly >106; up to 1,536) and high values of Mo concentration (mostly >40 ppm and up to 630 ppm) obtained from previous studies (van Helmond et al., 2014a; Dickson et al., 2016). Occurrence of isorenieratene and chlorobactene, two biomarkers associated with sulfur phototrophic bacteria, within the OAE-2 interval would indicate that H_2S extended at least episodically into the photic zone (Sinninghe Damsté and Köster, 1998; Kuypers et al., 2002; Pancost et al., 2004; Sinninghe Damsté et al., 2008). By compiling and comparing the geochemical data ($\delta^{15}N_{total}$, C_{org}, trace metal concentrations) obtained as part of this study and from previous reports (Kuypers et al., 2002; Kuypers et al., 2004; Forster et al., 2007; van Helmond et al., 2014a; Westermann et al., 2014; Dickson et al., 2016) and unpublished data from H-J Brumsack for selected elements (Fe, Mn, P, Cu, Ni, Co, Zr), we propose below to bring further details in the oxygenation evolution of the DSDP site 367.

In the core 19, the El/Al record is only marked by a peak value at 648.0 m for some elements (V, Zn, Cd, Cu, U), associated to the first noticeable peak of C_{org} (29.3%), low values of $\delta^{15}N_{total}$ (−1.8‰) but without perturbation of $\delta^{13}C_{org}$ signal (**Figures 4,5**). All of these elements being redox-sensitive, it is likely that this short level of increasing OM burial, recorded few meter before the onset of the OAE-2, was associated to a short-term interval of O_2-depeted conditions. The peak of 2-methylhopanoid index, used as a marker of cyanobacterial oxygenic photosynthesis (Summons et al., 1999) recorded at 647.95 m in Kuypers et al. (2004) and the absence of isorenieratane, a biomarker of green sulfur cyanobacteria (Kuypers et al., 2002) argue for a well oxygenated photic zone. The water column extension of O_2-depleted conditions during this interval was probably limited, close to the sediment/water interface. The use of redox ratios, such as U/Th and V/Cr can further constraints the oxygenation level. Based on the dysoxic/anoxic thresholds (1.25 for U/Th, 4.25 for V/Cr), defined by Jones and Manning (1994), these ratios indicate anoxic conditions (**Figure 8**). Unfortunately, due to poor resolution of sampling around 648.0 m, the lower and upper limits of this interval cannot be precisely defined. Except for this short-term interval, the rest of the core 19 corresponds to dysoxic conditions.

In the core 18, the concentrations of O_2-sensitive elements (Mo, U, V, Zn, Ni) exhibit fluctuating values within the interval depth corresponding to the OAE-2 (642.0–636.5 m). The base of the OAE-2 (642.0–640.3 m), corresponding to the onset of $\delta^{13}C$ excursion, and the PCE-1-PCE-2 interval, is characterized by a progressive and noticeable increase in El/Al ratio for most of the RSTE (e.g., V, U, Ni) with peak value interval recorded around 640.5 m (**Figure 4**). Similar evolutions are observed for the redox V/Cr and U/Th ratios (**Figure 8**). The coeval increase of TOC values and most of the RSTE, associated with low values of $\delta^{15}N_{total}$ (mainly < −1.5‰), clearly indicate the onset of

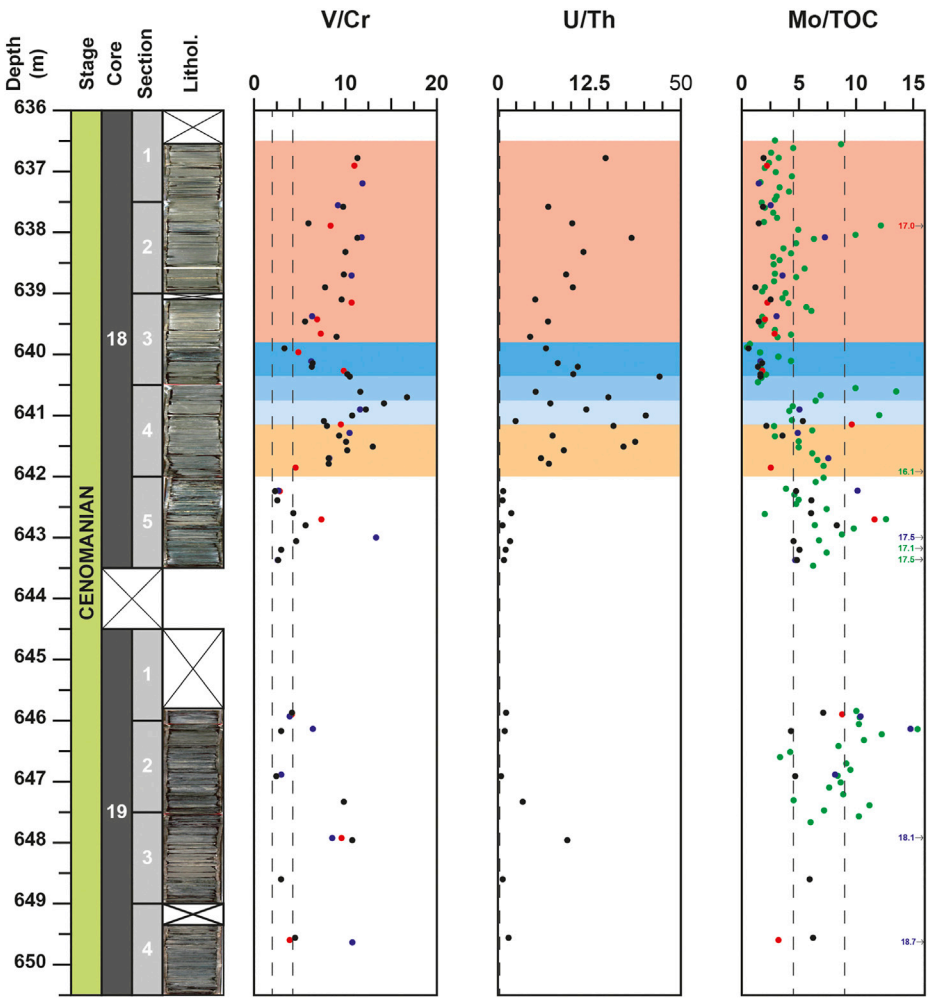

FIGURE 8 | Depth-profiles for V/Cr, U/Th and Mo/C_{org} redox ratios for the DSDP site 367. Data from the studies of Kuypers et al. (2002) and Kuypers et al. (2004), Westermann et al. (2014) and Dickson et al. (2016) are represented with blue, red and green circles respectively. Vertical dotted lines represent the threshold values (2.0 and 4.25 for V/Cr and 0.75 and 1.25 for U/Th) defined by Jones and Manning (1994) to distinguish oxic, dysoxic and anoxic conditions.

anoxic to euxinic conditions in the water column (**Figures 2**,**4**). The extent of O_2-depleted conditions is supported by cyanobacterial biomarkers (Kuypers et al., 2002). In this interval (642.0–640.35 m), the punctual occurrence of isorenieratane, associated with highest values of P, Cd and Cu (**Figure 5**) argue for an euxinic photic zone, which could be the result of an increase of O_2 demands by the phytoplankton associated with a rise of the chemocline to shallower depths (Kuypers et al., 2002).

This 1.5 m thick interval is followed by a 55 cm thick interval (640.35–639.80 m), corresponding to the PCE-3, that is underlined by an important drop of most of the RSTE (Mo, U, V, and Zn) for both concentrations and El/Al ratios, coeval with a decrease of TOC values of ~20% and an increasing trend of $\delta^{15}N_{total}$ values up to −1.2‰ (**Figures 2**,**4**). A similar organic-poor interval, characterized by low trace metal concentrations, was previously recorded in proto-North Atlantic deep sites: 1276 and 603 (van Helmond et al., 2014a) but never recognized at DSDP site 367. This short interval was interpreted at ODP sites 1276 and 603 as a temporary reoxygenation event of the bottom waters as a consequence of the PCE (van Helmond et al., 2014a). At the DSDP site 367, this interval (640.35–639.80 m) strictly correspond to the stratigraphic level where the lowest values of TEX_{86} were recorded by Forster et al. (2007) arguing for a cooling of see surface temperature episode and where a decrease of isorenieratane concentration was observed at 640.11 m in Kuypers et al. (2002). In this deeper site, the PCE thus likely triggered a transient decrease in concentration of dissolved H_2S in the photic zone and in bottom-water as well. The PCE would thus be associated to a short-term return toward non-euxinic conditions. This perturbation of redox conditions may have altered partially or totally the conversion of Mo, V, and Zn to thiomolybdates, oxides (V_2O_3 and $V(OH)_3$) and sulfides (ZnS), respectively (Tribovillard et al., 2006) and can account for noticeable decrease of El/Al ratio observed for most of the RSTE during this interval. As an alternative to redox

perturbation, enhanced drawdown of seawater trace metal reservoir has been suggested to explain the sizeable decrease of O_2/H_2S sensitive elements, as documented for two deep ODP sites (1258 and 1260) located in the south-western part of the Central Atlantic at Demerara Rise (Hetzel et al., 2009). For these two sites, the decline of elements concentrations is observed during the entire OAE-2, whereas for the DSDP site 367, this decline is observed only at the end of the P-CIE (for few elements, as Zn, Cu, and Cd continuing in the plateau interval). Most O_2/H_2S sensitive elements show either a slight enrichment in the plateau interval (e.g. Mo and U) or noticeable enrichment (e.g. V, Ni, and Fe) with the highest value recorded within the plateau interval at 638.1 m (**Figures 4**, **6**). The contrasted behavior of these elements between the DSDP site 367 (Cape Verde) and the ODP sites 1258–1260 (Demerara Rise) argue for a transient decrease in concentration of dissolved H_2S, associated to the PCE rather than for a drawdown of seawater trace metal reservoir at a global or regional scale. This transient episode of reoxygenation indeed likely replenish trace metals (Jenkyns et al., 2017). This inference is strengthened by the evolution of the C_{org}/P_{total} ratio and the $\delta^{15}N_{total}$ signal (**Figures 2**,**3**), which show respectively extremely high values (>1,000) and low values (<−1.6‰) within the plateau interval (this study) and by the high concentration of isorenieratane (>50 mg/g TOC) and high percentage of 2-methylhopanoid (>15%; Kuypers et al., 2004). All the geochemical data suggest that after a short-term episode of H_2S depletion during the PCE, the water column returns to anoxic-euxinic conditions during the plateau interval. Under these conditions, remobilization and regeneration of some elements like P (phosphate or organic phosphorus) and Ba (barite), during OM remineralization by sulfate reducing bacteria may occur (Van Capellen and Ingall, 1994; Krall et al., 2010). In contrast, in the presence of H_2S some other elements may form insoluble sulfide phase (CuS, CuS_2, CdS) or may be incorporated as solid solution (ZnS, NiS, CoS) in pyrite (FeS) (Huerta-Diaz and Morse, 1992). The absence of noticeable enrichment of Cu and Cd compared to those observed for Ni, Co and Fe suggests a preferential co-precipitation with FeS.

Since the work of Algeo and Lyons (2006) on the covariations of TOC and Mo concentration in modern euxinic basins (i.e., Black Sea, Cariaco Basin), the Mo/TOC ratio is considered as a reliable proxy to estimate intensity of restriction of water mass in silled basins and renewal time of the deep-water mass. By compiling all the Mo/TOC data for the DSDP site 367 (Kuypers et al., 2002; Westermann et al., 2014; Dickson et al., 2016; this study), an abrupt decrease of this ratio is clearly evidence from 440.5 m, with values mainly lower than 2.25 up to 636.5 m depth (**Figure 8**). This protracted shift toward lower values reflects a decline of Mo concentrations (mainly <100 ppm), associated to an increase of OM preservation (with TOC values >25%) recorded in samples from the top of the P-CIE (P-CIE-3) and the plateau intervals of the DSDP site 367. In details, the lowest values of Mo/TOC ratio are mainly recorded in the 1-m thick interval (640.5–639.5 m) corresponding to the PCE. This event, which lasted 40–65 kyr (O'Connor et al., 2020), record a reoxygenation of deep and shallow water domain and a cooling event (drop in sea-surface temperature of ~2.5–5.5°C, Forster et al., 2007) and likely corresponds here to an episode of water-masses renewal. We suggest that during this short-term event, the concentration of H_2S was too low to convert molybdate anions to particle-reactive thiomolybdates. Accordingly, we suggest that the low Mo/TOC values observed for the Cape Verde sediments during the PCE reflect an anoxic unrestricted environment, associated with dynamic water masses such as upwelling system rather than a restricted silled basin. For the remaining of the sedimentary record of the OAE-2, the Mo/TOC values mainly oscillate from 1 to 10 with an average value around 4.4, close to the regression slope value of 4.1, proposed by van Helmond et al. (2014a) for the deep proto-North Atlantic and the reference value of 4.5 obtained for the Black Sea (Algeo and Lyons, 2006), suggesting a water mass renewal period longer than 500 years.

General Framework of Nitrogen Isotope Signals Interpretations During the Oceanic Anoxic Event 2

Widespread changes of oxygen availability in the water column during the establishment of the OAE-2 have sensibly affected the cycle of N, which is considered as the main limiting nutrient with P and Fe. In general, extended anoxic conditions lead to an enhanced nitrogen loss through denitrification and ammonium oxidation processes, in which case an anoxic bottom part of the water column becomes NH_4^+-rich and N_2-fixation could overcome nitrate limitation to support biological productivity. Isotopic fractionation associated with atmospheric N_2-fixation by diazotrophs being low, the $\delta^{15}N_{total}$ values could tend towards ~0‰.

Changes of bioavailable dissolved nitrogen $\delta^{15}N_{total}$ over geological times mainly reflect the balance between the dominant nitrogen metabolic pathways regulating the nitrogen cycle alongside the water column structure (Sigman et al., 2009; Thomazo and Papineau, 2013; Ader et al., 2016; Stüeken et al., 2016). The Cretaceous Period is overall characterized by an elevated sea level and a warm climate, both affecting the water column stratification and dynamics and thus impacting the evolution of the sedimentary $\delta^{15}N_{total}$. Indeed, sea level variation is known to potentially change the locus of denitrification in oceanic settings (Deutsch et al., 2004). High sea level appears to enhance organic carbon burial in highly productive continental shelves by favouring sedimentary denitrification (Algeo et al., 2014). However, this highlighted correlation between sea level elevation and sedimentary $\delta^{15}N_{total}$ evolution through Greenhouse/Icehouse period might require to be nuanced concerning the OAE-2. Indeed, during this widespread anoxic event, numerous continental shelf environments appear to also evidence water column anoxic condition and hence active water column denitrification. It was also suggested that during the mid-Cretaceous Greenhouse period, high sea levels and the continental configuration favoured the formation by evaporation of warm and saline water masses in low latitude, inducing the formation of deep-water masses (Brass et al., 1982; Friedrich et al., 2006). This process could have favoured water column mixing and thus facilitated the input of NH_4^+-rich water masses to the surface. It probably occurred during the onset of the OAE-2 but was interrupted or at least highly reduced during the PCE, due to reduced evaporation and drier climate.

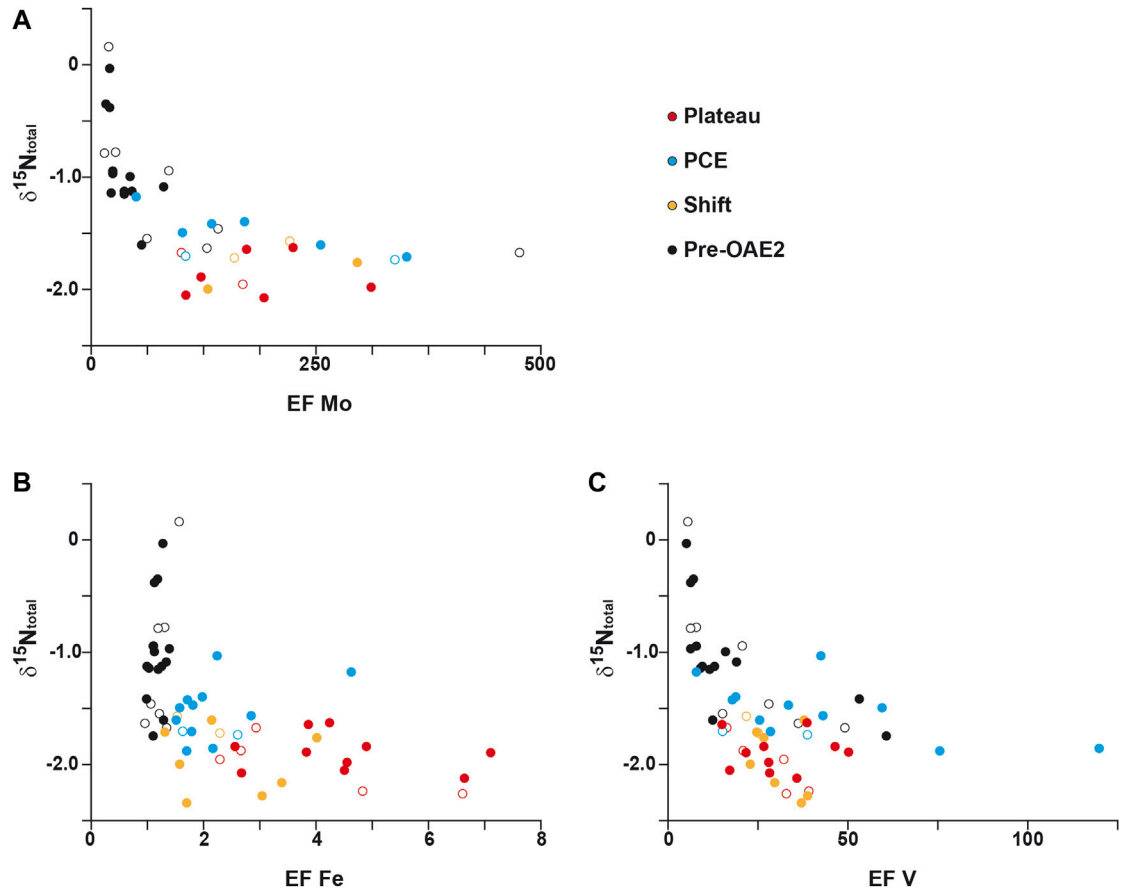

FIGURE 9 | Cross-plot of isotopic nitrogen compositions $\delta^{15}N_{total}$ versus, EF Mo **(A)**; EF Fe **(B)** and EF V **(C)** Open symbols correspond to the data from the study of Kuypers et al. (2002) for Mo and V and from unpublished data of H-J. Brumsack for Fe.

At the DSDP site 367, the low and negative $\delta^{15}N_{total}$ values (0 to −2.3‰) confirm the data previously obtained by Kuypers et al. (2004), and are consistent with the mainly negative $\delta^{15}N_{total}$ values reported in proto-North and Central Atlantic sites recording the OAE-2 (e.g., ODP sites 1260; 1261 and 1276), with $\delta^{15}N_{total}$ mostly comprised between −4 and 2‰ (Jenkyns et al., 2007; Junium and Arthur, 2007; Ruvalcaba Baroni et al., 2015). These isotopic values associated with elevated 2-methylhopanoid ratio at the DSDP site 367 have been initially attributed to a significant uptake of N_2 by diazotrophs (Kuypers et al., 2002). Such low $\delta^{15}N_{total}$ values are, however, significantly lower than $\delta^{15}N_{total}$ values observed in modern anoxic basins (e.g. Black Sea, Cariaco Basin) in which N_2-fixation is known to be significant (Fry et al., 1991; Thunell et al., 2004). To explain these negative $\delta^{15}N_{total}$ values, it was suggested that upwelling of anoxic and ammonium-rich deep waters have supported biological productivity by providing dissolved fixed-nitrogen to primary producers (Higgins et al., 2012).

During the OAE-2, deep oceanic settings, as the DSDP site 367, can indeed build up a large reservoir of NH_4^+, which can be the main *N* source for primary production (ammonia ocean scenario of Higgins et al., 2012). In such scenario, a combination of denitrification and anammox reactions at the chemocline quantitatively consumes the nitrate and nitrite reservoir, the primary productivity being supported by advection of ^{15}N-depleted NH_4^+, as well as other nutrient elements like PO_4^{3-}, from deep water up to the photic zone, especially during chemocline upward excursions. The ^{15}N-depleted NH_4^+ can be consumed through ammonium assimilation and ammonium oxidation (i.e., nitrification), which are both associated to a sizeable isotopic fractionation that generate a ^{15}N-depleted product and ^{15}N-enriched residual NH_4^+ reservoir. If the fractionation associated with ammonium assimilation outcompetes the isotopic enrichment caused by the combination of anammox/denitrification/nitrification processes, the biomass remains isotopically negative.

Alternative nitrogenases to N_2-fixation using Fe and V rather than Mo as enzymatic co-factor was also proposed to explain $\delta^{15}N_{total}$ values lower than −2‰ recorded during OAE-2 in the proto-North and Central Atlantic sites (Zhang et al., 2014). In this scenario, Mo is replaced in the active site of the metalloenzyme by Fe or V in response of the global oceanic drawdown of trace metals (especially Mo). These alternative nitrogenases can be expressed either by cyanobacteria in the photic zone or by anoxygenic phototrophs and would be favored during period

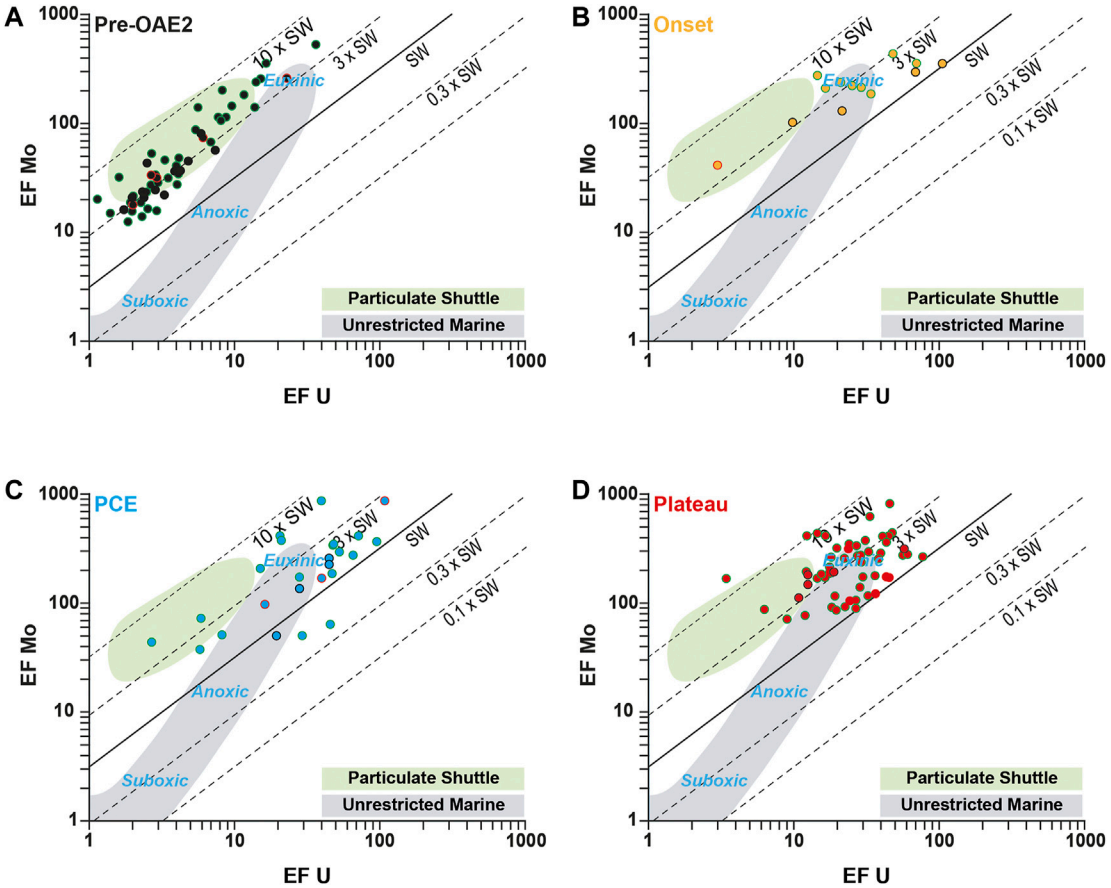

FIGURE 10 | Cross-plot of EF U versus, EF Mo for the Pre-OAE-2 interval **(A)**, the onset interval **(B)**, the PCE interval **(C)** and the plateau interval **(D)**. Data from the studies of Westermann et al. (2014) and Dickson et al. (2016) are represented with circles with red and green outline respectively.

of increase in the Fe/Mo ratio possibly linked to enhance hydrothermal activity and Mo scavenging. However, no clear difference is observed between Mo and Fe in a scatterplot with $\delta^{15}N_{total}$ values (**Figure 9**) in our dataset. Both elements are characterized by a nonlinear negative correlation with $\delta^{15}N_{total}$. Moreover, the alternative nitrogenase hypothesis implied a large $\delta^{15}N$ fractionation down to −7‰, while the minimum value recorded at DSDP site 367 is −2.3‰. We therefore suggest that the contribution of N_2-fixation through an alternative nitrogenase while possible could only represent a small proportion of $\delta^{15}N_{total}$ signal, due to both 1) mass balance considerations and 2) the reported high abundance of eukaryotic biomass at Demerara Rise, in a similar paleogeographical context and with equivalent $\delta^{15}N$ values during OAE-2 (Higgins et al., 2012).

Our $\delta^{15}N_{total}$ data, at the first order, seem to agree with the proposed combination of ^{15}N-depleted ammonium assimilation and N_2-fixation to explain the low and negative isotopic values observed. Moreover, our high-resolution $\delta^{15}N_{total}$ analysis revealed significant short-term $\delta^{15}N_{total}$ variations related to physical and chemical changes associated to both the OAE-2 and the PCE which are discussed below.

High Resolution Nitrogen Isotopes Variations Across Oceanic Anoxic Event 2 and Plenus Cold Event Records at Cape Verde

Pre-Oceanic Anoxic Event Nitrogen Cycle

The specificity of the Central Atlantic is to show evidences of deoxygenated conditions before the OAE-2. In the Cape Verde basin, this pre-OAE deoxygenation is expressed by continuous high amount of OM, detectable authigenic enrichments (3 < EF < 10) of most RSTE and evidences of an active phosphorus regeneration. Besides, high Mo enrichments compared to U suggest an active "Particulate shuttle" effect in water column (**Figure 10**), as reported for modern semi-enclosed basins (Algeo and Tribovillard, 2009; Tribovillard et al., 2012), hence suggesting that a strong and deep chemocline discriminates a well oxygenated upper water column from anoxic bottom waters. The redox conditions were, however, not stable during this Pre-OAE time, and periods of stronger deoxygenation standout such as within the section 3 of the core 19.

During this pre-OAE interval, constantly negative $\delta^{15}N$ values (−1.2 to 0‰) indicate that N_2-fixation outcompetes NO_3^-

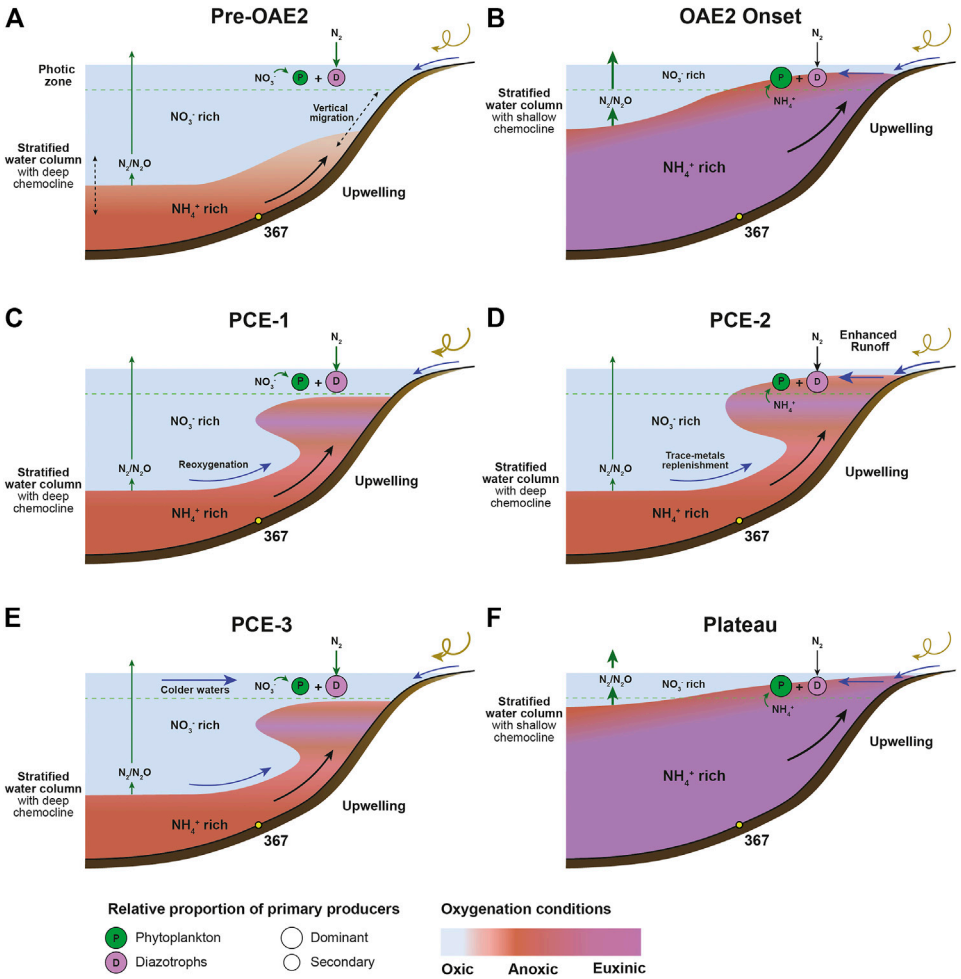

FIGURE 11 | Schematic representation of the nitrogen cycle and the resulting nitrogen isotopic imprint of marine sediments: Before the OAE-2 **(A)**, during the OAE-2 onset **(B)**, during the PCE-1 interval **(C)**, during the PCE-2 interval **(D)**, the PCE-3 interval **(E)**, during the plateau interval **(F)**. The red color indicates anoxic waters, the purple color euxinic waters and the blue color oxygenated waters (modified from Ader et al., 2014).

limitation in the photic zone (**Figure 11**). Within the framework of a stratified water column, quantitative N loss due to the combination of nitrification, heterotrophic denitrification and anammox occur at the chemocline while NH_4^+ could accumulate in the deeper basin.

While being presumably stratified before the OAE-2, oceanographic models (Trabucho Alexandre et al., 2010; Topper et al., 2011) proposed that during the mid-Cretaceous time the Southeastern part of the Central Atlantic basin was characterized by the presence of upwelling currents along margins bringing NH_4^+ rich waters from the deep ocean toward the surface, transiently reaching the photic zone. Anoxia in the photic zone preceding the OAE was previously proposed to account for punctual isorenieratane occurrences (Kuypers et al., 2002). In addition to the long term stratification of the Cape Verde basin, delivery of ^{15}N-depleted NH_4^+ in the photic zone from more proximal areas may have been assimilated by the phytoplankton and consequently participate to the lowest $\delta^{15}N$ values observed in the section 3 of the core 19 (down to −1.75‰). Other possible mechanisms of deep-water advection into the surface include eddy-circulation, which may have been particularly relevant of the mid-Cretaceous ice-free climate regime (Hay, 2008).

Oceanic Anoxic Event 2 Nitrogen Cycle

At DSDP site 367, the first $\delta^{13}C$ buildup and the plateau interval within the OAE-2 are characterized by an intensification of the deoxygenation as demonstrated by the substantial authigenic enrichment of the RSTE (e.g., U, Ni, V) leading to euxinic conditions in the basin. Large proportions of sulfide in the water column are also evidenced by exceptionally intense P recycling rate, marked by high C_{org}/P_{total} values (this study) and by a rapid positive excursion of the $\delta^{98/95}Mo$ (Westermann et al., 2014; Dickson et al., 2016), towards the typical seawater composition. The shallowing of the chemocline, and hence the invasion of the euxinic conditions from the bottom waters to the photic zone, was also demonstrated by the large concentrations of isorenieratane measured along the OAE-2 and mostly during the plateau interval (Kuypers et al., 2002).

At DSDP site 367, the Mo vs. U enrichments during the onset of the OAE-2 and the plateau intervals are mostly located in the "Euxinic" zone or even higher (**Figure 10**). Thus, the EF Mo/EF U values decrease during the two episodes of extreme deoxygenation approaching the values of today's seawater (~7.7). Significantly, while the plateau interval is the period characterized by the most intense and the most prolonged deoxygenated conditions of the OAE-2, enrichments in some RSTE as Mo, U or V are lower in this interval than during PCE, conversely to Fe. This observation, combined with low Mo/TOC values, suggests a drawdown of these elements in the water-column due to their scavenging in the sediments at the basin scale.

In the proto-North and Central Atlantic sites, negative $\delta^{15}N_{total}$ values during the OAE-2 has been largely reported in every part of the ocean (Kuypers et al., 2004; Junium and Arthur, 2007; Higgins et al., 2012; Ruvalcaba Baroni et al., 2015). This negative signal is consistent with a combination of both N_2-fixation and NH_4^+ partial assimilation processes in the N export production. While both N_2-fixation and NH_4^+ assimilation were important in the nitrogen exported production, a general lowering of the $\delta^{15}N_{total}$ value from North to South suggests that the NH_4^+ assimilation was particularly significant in the southern part (Ruvalcaba Baroni et al., 2015; Naafs et al., 2019) and could have been dominant, as evidenced by Higgins et al. (2012). The high C_{org}/N_{total} ratio, observed in the DSDP 367 site indicates an intense biological removal of amino groups from the OM in the sediments, releasing NH_4^+. The diffused NH_4^+ from the sediments would have further supplied a water column ammonium reservoir.

At DSDP site 367, the evolution of the $\delta^{15}N_{total}$ is fully consistent with the convecting redox-stratified ocean model proposed by Ader et al., 2014; Ader et al., 2016) where NH_4^+ invades the entire basin and NO_3^- reservoir is substantially reduced and limited in the photic zone far away from the coastal area (**Figure 11**). The limited $\delta^{15}N_{total}$ fluctuations during the plateau interval would therefore represent variations in the relative proportions between the eukaryotic and the denitrifying biomasses, which would be controlled by the position of the chemocline through the lower limit of the photic zone. The large variations in the Fe enrichments are coherent with fluctuations of the H_2S inventory of the water-column chemocline. Redox fluctuations with a similar pace were previously evidenced by oscillating $\delta^{98/95}$Mo, that were interpreted as the expression of orbital cycles controlling the continental-weathering and the delivery of nutrient in the basin (Dickson et al., 2016), suggesting a climate influence on oxygenation conditions and nitrogen cycle. Comparable variations in Fe chemistry, C_{org}/P_{total} ratio (Poulton et al., 2015) and $\delta^{98/95}$Mo variations (Goldberg et al., 2016) with those measured in the Cape Verde Basin were evidenced along the same continental margin in the Tarfaya Basin (Offshore Morocco), in a shelf setting. This observation highlights that the redox fluctuations described in the deep Cape Verde Basin are consistent with shallower settings and confirm that they are constrained by the regional redox structure of the entire southern proto-North Atlantic domain. Besides, continuous O_2-depleted conditions at intermediate bathymetry (>1,000 m for the deepest site) from pre-to post-OAE-2 at Demerara Rise (Hetzel et al., 2009) suggest that an expanded Oxygen-Minimum Zone impinged the southern part of the proto-North Atlantic, and we suggest that upwelling currents were active through the Cenomanian-Turonian interval in this region.

Nitrogen Cycle During the Plenus Cold Event

The high resolution of the $\delta^{15}N_{total}$ signal measured along the section not only allowed to distinguish the PCE during the OAE-2, but also to highlight large variations characterizing a complex N cycle during this swing in temperature. Indeed, the PCE interval is particularly well underlined by two spikes of heavier $\delta^{15}N_{total}$ values recorded during the PCE-1 and PCE-3. This period was also previously associated with a deepening of the chemocline based on a drop in the $\delta^{98/95}$Mo values (Dickson et al., 2016). However, still high enrichments in Mo, and in a lesser degree in U, argue for persistent anoxic to euxinic deep waters (**Figure 10**). Active upwelling currents bringing nutrients rich waters to the surface, hence maintaining a high primary production and C_{org} export to the sediments may have promoted the formation of an oxygen rich intermediate water mass along the Cape Verde basin margin.

We suggest that PCE-1 represents a period of better-ventilated intermediate waters. The rapid and large increase in $\delta^{15}N_{total}$ within the PCE-1 (+1.3‰) is consistent with a switch in the nitrogen cycle with higher ratio of nitrate *vs* ammonium assimilation the former expanding due to upwelling of oxygenated water masses (**Figure 11**). In both cases however, N_2-fixation likely represents the main source of N for primary producers, $\delta^{15}N_{total}$ remaining close to 0‰ value, as expected in stratified settings (**Figure 11**).

The PCE-2 is associated with lower $\delta^{15}N_{total}$ values (~−1.8‰) and many trace metal (Cd, Cu, Ni, V, Zn) enrichments (**Figures 3–5**). Such enrichments in an overall period of reoxygenation has previously been reported in the Western Interior Seaway (Eldrett et al., 2014) or in the English Chalk (Jenkyns et al., 2017), and were either interpreted has the advent of waters rich in hydrothermally-derived elements or by basin-scale re-oxidation of previously deposited organic- and sulfide-rich sediments. Oxygenated water masses may have been restricted "in sandwich" between two ammonium rich and nitrate poor water masses and the overall nitrogen cycle back to an isotopic signal of N_2-fixation and NH_4^+ partial assimilation state on proximal margin.

The second peak of heavier $\delta^{15}N_{total}$ values in the PCE-3 is accompanied with both a drop in sea-surface temperature (Forster et al., 2007) and a reoxygenation of the basin as demonstrated by the lowest trace metal enrichments. This transient cooling and reoxygenation may have cause a deepening of the chemocline and increase in the contribution of nitrate to the nitrogen isotope sedimentary signal. Compared to long-term secular variations observed during greenhouse-icehouse periods (Algeo et al., 2014), the PCE nitrogen cycling point out to a more complex picture. Indeed, if water column denitrification can expand during the PCE and imprint the geochemical sedimentary record due to an increasing contribution of cycled nitrate to the biomass, we suggest that associated changes in the $\delta^{15}N_{total}$ signal are primarily controlled by the ratio of bioavailable ammonium to nitrate rather than a change in the locus (sedimentary *vs* water column) of denitrification. This inference is supported by recent results of Earth System model which demonstrates that during the OAE-2 fundamental transitions in the species of nitrogen

dominating the fixed-N inventory, from nitrate to ammonium across deoxygenation, are anticipated (Naafs et al., 2019).

CONCLUSION

By combining newly generated and existing geochemical data from the DSDP site 367, our integrated study:

-confirms the burial of organic matter, dominantly marine in origin, associated to a positive carbon isotopic excursion of ~6.0‰. For this isotopic excursion, a detailed sequencing of $\delta^{13}C$ evolution has been proposed and a new subdivision within the Plenus carbon isotopic excursion in three sub-intervals (PCE-1, PCE-2, and PCE-3) is suggested.

-highlights the fluctuations of oxygenation in the water column especially during the Plenus carbon isotopic excursion for one the deepest site in the Central Atlantic. After a period of stability in concentration of redox sensitive trace elements and high $\delta^{15}N_{total}$ values (>−1.2‰), characterized by dysoxic to anoxic conditions before the OAE-2, the onset of this event, marked by noticeable enrichment of these elements and the lowest $\delta^{15}N_{total}$ values (<−2.0‰), is associated to euxinic conditions in bottom water. Within the OAE-2, the Plenus carbon isotopic excursion is associated to short-term O_2/H_2S fluctuations and three settings are distinguished. The PCE-1, characterized by decreasing trend of $\delta^{15}N_{total}$ values and contrasted record of redox sensitive trace elements, would correspond to a period of better-ventilated intermediate waters. The PCE-2, marked by noticeable enrichment of these elements and the lower $\delta^{15}N_{total}$ values (~−2.0‰), is characterized by water column O_2-depleted conditions, associated to potential hydrothermal enrichments. The PCE-3, marked by noticeable decreasing trend of both $\delta^{15}N_{total}$ values and redox sensitive trace elements, is interpreted as an interval of reoxygenation of water column, probably linked to input of cooler and oxygenated water from high latitudes. Lastly, the plateau interval is marked by the invasion of the euxinic conditions from the bottom waters up to the photic zone.

-discusses for the first time the impact of the Plenus Cold Event on the nitrogen cycle for this site and a model for the nitrogen cycle and the resulting nitrogen isotopic imprint of marine sediments is proposed. Before the OAE-2, a stratified water column model and a deep and strong chemocline, prevailed in NH_4^+-rich bottom water. The onset of the OAE-2 is characterized by the development in the water column of euxinic NH_4^+ rich water masses, and a restriction of the NO_3^- reservoir to the photic zone. These nitrogen cycle settings changed during the short-term climatic variations associated with the Plenus Cold Event. During cooling, a reoxygenation phase of the intermediate water due to active upwelling currents and accompanied by a deepening of a sulfide-rich chemocline temporally reshaped both the carbon and nitrogen cycles. These changes are remarkably well expressed in the nitrogen isotope record with swings in the $\delta^{15}N_{total}$ values, interpreted here as a tracer of ammonium to nitrate bioavailable inventory.

DATA AVAILABILITY STATEMENT

The original contributions presented in the study are included in the article/**Supplementary Materials**, further inquiries can be directed to the corresponding author/s.

AUTHOR CONTRIBUTIONS

PC performed the isotopic geochemical analysis and FB performed the organic geochemical analysis. LR, PC, FB, CT, and JD contributed to the interpretation of the results. LR organized the database and wrote the first draft of the manuscript. LR, PC, JD, and CT wrote sections of the manuscript. All authors contributed to manuscript revision, read, and approved the submitted version.

ACKNOWLEDGMENTS

We would like to thank Florence Savignac for her analytical assistance for Rock-Eval analysis, Marie-Jeanne Milloux for organic isotope measurements and Alexandre Lethiers for illustration support. Hans-Jürgen Brumsack is kindly thanked for sharing unpublished data for selected major and trace elements. We also thank J-C M-S and Y-U Z for providing constructive comments. This research used samples provided by the International Ocean Discovery Program. This study was funded by the project Anox-Sea ANR-12-BS06-0011 coordinated by EP. Data from this study can be found in the supplementary data file.

SUPPLEMENTARY MATERIAL

The Supplementary Material for this article can be found online at: https://www.frontiersin.org/articles/10.3389/feart.2021.703282/full#supplementary-material

REFERENCES

Ader, M., Sansjofre, P., Halverson, G. P., Busigny, V., Trindade, R. I. F., Kunzmann, M., et al. (2014). Ocean Redox Structure across the Late Neoproterozoic Oxygenation Event: a Nitrogen Isotope Perspective. *Earth Planet. Sci. Lett.* 396, 1–13. doi:10.1016/j.epsl.2014.03.042

Ader, M., Thomazo, C., Sansjofre, P., Busigny, V., Papineau, D., Laffont, R., et al. (2016). Interpretation of the Nitrogen Isotopic Composition of Precambrian Sedimentary Rocks: Assumptions and Perspectives. *Chem. Geology* 429, 93–110. doi:10.1016/j.chemgeo.2016.02.010

Algeo, T. J., and Lyons, T. W. (2006). Mo-Total Organic Carbon Covariation in Modern Anoxic marine Environments: Implications for Analysis of Paleoredox and Paleohydrographic Conditions. *Paleoceanography* 21, PA1016. doi:10.1029/PA00111210.1029/2004pa001112

Algeo, T. J., and Tribovillard, N. (2009). Environmental Analysis of Paleoceanographic Systems Based on Molybdenum-Uranium Covariation. *Chem. Geology* 268, 211–225. doi:10.1016/j.chemgeo.2009.09.001

Algeo, T. J., Meyers, P. A., Robinson, R. S., Rowe, H., and Jiang, G. Q. (2014). Icehouse-greenhouse Variations in marine Denitrification. *Biogeosciences* 11 (4), 1273–1295. doi:10.5194/bg-11-1273-2014

Arthur, M. A., Dean, W. E., and Pratt, L. M. (1988). Geochemical and Climatic Effects of Increased marine Organic Carbon Burial at the Cenomanian/Turonian Boundary. *Nature* 335, 714–717. doi:10.1038/335714a0

Barclay, R. S., McElwain, J. C., and Sageman, B. B. (2010). Carbon Sequestration Activated by a Volcanic CO2 Pulse during Ocean Anoxic Event 2. *Nat. Geosci.* 3 (3), 205–208. doi:10.1038/ngeo757

Behar, F., Beaumont, V., and De B. Penteado, H. L. (2001). Rock-Eval 6 Technology: Performances and Developments. *Oil Gas Sci. Technol. - Rev. IFP* 56, 111–134. doi:10.2516/ogst:2001013

Blättler, C. L., Jenkyns, H. C., Reynard, L. M., and Henderson, G. M. (2011). Significant Increases in Global Weathering during Oceanic Anoxic Events 1a and 2 Indicated by Calcium Isotopes. *Earth Planet. Sci. Lett.* 309 (1–2), 77–88. doi:10.1016/j.epsl.2011.06.029

Bowman, A. R., and Bralower, T. J. (2005). Paleoceanographic Significance of High-Resolution Carbon Isotope Records across the Cenomanian-Turonian Boundary in the Western Interior and New Jersey Coastal plain, USA. *Mar. Geology* 217 (3–4), 305–321. doi:10.1016/j.margeo.2005.02.010

Brandes, J. A., and Devol, A. H. (2002). A Global Marine-Fixed Nitrogen Isotopic Budget: Implications for Holocene Nitrogen Cycling. *Glob. Biogeochem. Cycles* 16 (4), 1120. doi:10.1029/2001GB001856

Brass, G. W., Southam, J. R., and Peterson, W. H. (1982). Warm saline Bottom Water in the Ancient Ocean. *Nature* 296, 620–623. doi:10.1038/296620a0

Brumsack, H.-J. (2006). The Trace Metal Content of Recent Organic Carbon-Rich Sediments: Implications for Cretaceous Black Shale Formation. *Palaeogeogr. Palaeoclimatol. Palaeoecol.* 232, 344–361. doi:10.1016/j.palaeo.2005.05.011

Charbonnier, G., Boulila, S., Spangenberg, J. E., Adatte, T., Föllmi, K. B., and Laskar, J. (2018). Obliquity Pacing of the Hydrological Cycle during the Oceanic Anoxic Event 2. *Earth Planet. Sci. Lett.* 499, 266–277. doi:10.1016/j.epsl.2018.07.029

Chenet, P-Y., and Francheteau, J. (1979). "Bathymetric Reconstruction Method : Application to the Central Atlantic Basin between 10°N and 40°N," in *Deep Sea Drilling Project Initial Report* (Washington, D. C: U.S. Gov. Print. Off.), 1501–1514. 51, 52, 53, Part 2.

Clarkson, M. O., Stirling, C. H., Jenkyns, H. C., Dickson, A. J., Porcelli, D., Moy, C. M., et al. (2018). Uranium Isotope Evidence for Two Episodes of Deoxygenation during Oceanic Anoxic Event 2. *Proc. Natl. Acad. Sci. USA* 115 (12), 2918–2923. doi:10.1073/pnas.1715278115

Danzelle, J., Riquier, L., Baudin, F., Thomazo, C., and Pucéat, E. (2018). Oscillating Redox Conditions in the Vocontian Basin (SE France) during Oceanic Anoxic Event 2 (OAE 2). *Chem. Geology* 493, 136–152. doi:10.1016/j.chemgeo.2018.05.039

Danzelle, J., Riquier, L., Baudin, F., Thomazo, C., and Pucéat, E. (2020). Nitrogen and Carbon Cycle Perturbations through the Cenomanian-Turonian Oceanic Anoxic Event 2 (~94 Ma) in the Vocontian Basin (SE France). *Palaeogeogr. Palaeoclimatol. Palaeoecol.* 538, 109443. doi:10.1016/j.palaeo.2019.109443

Deutsch, C., Sigman, D. M., Thunell, R. C., Meckler, A. N., and Haug, G. H. (2004). Isotopic Constraints on Glacial/interglacial Changes in the Oceanic Nitrogen Budget. *Glob. Biogeochem. Cycles* 18. doi:10.1029/2003GB002189

Dickson, A. J., Jenkyns, H. C., Porcelli, D., van den Boorn, S., and Idiz, E. (2016). Basin-Scale Controls on the Molybdenum-Isotope Composition of Seawater during Oceanic Anoxic Event 2 (Late Cretaceous). *Geochim. Cosmochim. Acta* 178, 291–306. doi:10.1016/j.gca.2015.12.036

Du Vivier, A. D. C., Selby, D., Condon, D. J., Takashima, R., and Nishi, H. (2015). Pacific 187 Os/188 Os Isotope Chemistry and U-Pb Geochronology: Synchroneity of Global Os Isotope Change Across OAE 2. *Earth Planet. Sci. Lett.* 428, 204–216. doi:10.1016/j.epsl.2015.07.020

Eldrett, J. S., Minisini, D., and Bergman, S. C. (2014). Decoupling of the Carbon Cycle During Ocean Anoxic Event 2. *Geology* 42 (7), 567–570. doi:10.1130/g35520.1

Erbacher, J., Mosher, D. C., Malone, M. J., Berti, D., Bice, K. L., Bostock, H., et al. (2004a). "Site 1258," in *Proc. ODP, Init. Repts*. Editors J. Erbacher, D. C. Mosher, and M.J. Malone (College Station, TX: Ocean Drilling Program), 207, 1–117. doi:10.2973/odp.proc.ir.207.105.2004

Erbacher, J., Mosher, D. C., Malone, M. J., Berti, D., Bice, K. L., Bostock, H., et al. (2004b). "Site 1260," in *Proc. ODP, Init. Repts*. Editors J. Erbacher, D. C. Mosher, and M. J. Malone (College Station, TX: Ocean Drilling Program), 207, 1–113. doi:10.2973/odp.proc.ir.207.107.2004

Erbacher, J., Friedrich, O., Wilson, P. A., Birch, H., and Mutterlose, J. (2005). Stable Organic Carbon Isotope Stratigraphy across Oceanic Anoxic Event 2 of Demerara Rise, Western Tropical Atlantic. *Geochem. Geophys. Geosyst.* 6, Q06010. doi:10.1029/2004GC000850

Espitalié, J., Deroo, G., and Marquis, F. (1985a). La pyrolyse Rock-Eval et ses applications. Première partie. *Rev. Inst. Fr. Pét.* 40, 563–579. doi:10.2516/ogst:1985035

Espitalié, J., Deroo, G., and Marquis, F. (1985b). La pyrolyse Rock-Eval et ses applications. Deuxième partie. *Rev. Inst. Fr. Pét.* 40, 755–784. doi:10.2516/ogst:1985045

Espitalié, J., Deroo, G., and Marquis, F. (1986). La pyrolyse Rock-Eval et ses applications. Troisième partie. *Rev. Inst. Fr. Pét.* 41, 73–89. doi:10.2516/ogst:1986003

Forster, A., Schouten, S., Moriya, K., Wilson, P. A., and Sinninghe Damste, S. (2007). Tropical Warming and Intermittent Cooling during the Cenomanian/Turonian Oceanic Anoxic Event 2: Sea Surface Temperature Record from the Equatorial Atlantic. *Paleoceanography* 22, 1219. doi:10.1029/PA001349

Freeman, K. H., and Hayes, J. M. (1992). Fractionation of Carbon Isotopes by Phytoplankton and Estimates of Ancient CO_2 levels. *Glob. Biogeochem. Cycles* 6 (2), 185–198. doi:10.1029/92gb00190

Friedrich, O., Erbacher, J., and Mutterlose, J. (2006). Paleoenvironmental Changes across the Cenomanian/Turonian Boundary Event (Oceanic Anoxic Event 2) as Indicated by Benthic Foraminifera from the Demerara Rise (ODP Leg 207). *Revue de Micropaléontol.* 49 (3), 121–139. doi:10.1016/j.revmic.2006.04.003

Fry, B., Jannasch, H. W., Molyneaux, S. J., Wirsen, C. O., Muramoto, J. A., and King, S. (1991). Stable Isotope Studies of the Carbon, Nitrogen and Sulfur Cycles in the Black Sea and the Cariaco Trench. *Deep Sea Res. A. Oceanographic Res. Pap.* 38, S1003–S1019. doi:10.1016/S0198-0149(10)80021-4

Gale, A. S., and Christensen, W. K. (1996). Occurrence of the Belemnite Actinocamax Plenus in the Cenomanian of SE France and its Significance. *bgsd* 43 (1), 68–77. doi:10.37570/bgsd-1996-43-08

Gale, A. S., Jenkyns, H. C., Kennedy, W. J., and Corfield, R. M. (1993). Chemostratigraphy versus Biostratigraphy: Data from Around the Cenomanian-Turonian Boundary. *J. Geol. Soc.*, 150, 29–32. doi:10.1144/gsjgs.150.1.0029

Gale, A. S., Jenkyns, H. C., Tsikos, H., van Breugel, Y., Sinninghe Damsté, J. S., Bottini, C., et al. (2019). High-resolution Bio- and Chemostratigraphy of an Expanded Record of Oceanic Anoxic Event 2 (Late Cenomanian-Early Turonian) at Clot Chevalier, Near Barrême, SE France (Vocontian Basin). *nos* 52 (1), 97–129. doi:10.1127/nos/2018/0445

Goldberg, T., Poulton, S. W., Wagner, T., Kolonic, S. F., and Rehkämper, M. (2016). Molybdenum Drawdown during Cretaceous Oceanic Anoxic Event 2. *Earth Planet. Sci. Lett.* 440, 81–91. doi:10.1016/j.epsl.2016.02.006

Hay, W. W. (2008). Evolving Ideas about the Cretaceous Climate and Ocean Circulation. *Cretaceous Res.* 29, 725–753. doi:10.1016/j.cretres.2008.05.025

Herbin, J. P., Montadert, L., Müller, C., Gomez, R., Thurow, J., and Wiedmann, J. (1986). Organic-Rich Sedimentation at the Cenomanian-Turonian Boundary in Oceanic and Coastal Basins in the North Atlantic and Tethys North Atlantic Palaeoceanography. *Spec. Publ. Geol. Soc.* 21, 389–422. doi:10.1144/GSL.SP.1986.021.01.28

Hetzel, A., Böttcher, M. E., Wortmann, U. G., and Brumsack, H.-J. (2009). Paleo-Redox Conditions during OAE 2 Reflected in Demerara Rise Sediment Geochemistry (ODP Leg 207). *Palaeogeogr. Palaeoclimatol. Palaeoecol.* 273, 302–328. doi:10.1016/j.palaeo.2008.11.005

Higgins, M. B., Robinson, R. S., Husson, J. M., Carter, S. J., and Pearson, A. (2012). Dominant Eukaryotic Export Production during Ocean Anoxic Events Reflects the Importance of Recycled NH4+. *Proc. Natl. Acad. Sci.* 109, 2269–2274. doi:10.1073/pnas.1104313109

Holmden, C., Jacobson, A. D., Sageman, B. B., and Hurtgen, M. T. (2016). Response of the Cr Isotope Proxy to Cretaceous Ocean Anoxic Event 2 in a Pelagic Carbonate Succession from the Western Interior Seaway. *Geochim. Cosmochim. Acta* 186, 277–295. doi:10.1016/j.gca.2016.04.039

Huerta-Diaz, M. A., and Morse, J. W. (1992). Pyritization of Trace Metals in Anoxic Marine Sediments. *Geochim. Cosmochim. Acta* 56, 2681–2702. doi:10.1016/0016-7037(92)90353-K

Jarvis, I., Lignum, J. S., Gröcke, D. R., Jenkyns, H. C., and Pearce, M. A. (2011). Black Shale Deposition, Atmospheric CO_2 drawdown, and Cooling during the

Cenomanian-Turonian Oceanic Anoxic Event. *Paleoceanography* 26 (3), PA3201. doi:10.1029/2010pa002081

Jefferies, R. P. S. (1962). The Paleoecology of the Actinocamax Plenus Subzone (Lowest Turonian) in the Anglo-Paris Basin. *Paleontology* 4 (4), 609–647.

Jefferies, R. P. S. (1963). The Stratigraphy of the Actinocamax Plenus Subzone (Turonian) in the Anglo-Paris Basin. *Proc. Geologists' Assoc.* 74, 1–IN4. doi:10.1016/S0016-7878(63)80011-5

Jenkyns, H. C., Gale, A. S., and Corfield, R. M. (1994). Carbon- and Oxygen-Isotope Stratigraphy of the English Chalk and Italian Scaglia and its Palaeoclimatic Significance. *Geol. Mag.* 131 (01), 1–34. doi:10.1017/s0016756800010451

Jenkyns, H. C., Matthews, A., Tsikos, H., and Erel, Y. (2007). Nitrate Reduction, Sulfate Reduction, and Sedimentary Iron Isotope Evolution during the Cenomanian-Turonian Oceanic Anoxic Event. *Paleoceanography* 22, PA3208. doi:10.1029/2006PA001355

Jenkyns, H. C., Dickson, A. J., Ruhl, M., and Boorn, S. H. J. M. (2017). Basalt-seawater Interaction, the Plenus Cold Event, Enhanced Weathering and Geochemical Change: Deconstructing Oceanic Anoxic Event 2 (Cenomanian-Turonian, Late Cretaceous). *Sedimentology* 64 (1), 16–43. doi:10.1111/sed.12305

Jenkyns, H. C. (2010). Geochemistry of Oceanic Anoxic Events. *Geochem. Geophys. Geosyst.* 11 (3), Q03004. doi:10.1029/2009GC002788

Jones, C. E., and Jenkyns, H. C. (2001). Seawater Strontium Isotopes, Oceanic Anoxic Events, and Seafloor Hydrothermal Activity in the Jurassic and Cretaceous. *Am. J. Sci.* 301, 112–149. doi:10.2475/ajs.301.2.112

Jones, B., and Manning, D. A. C. (1994). Comparison of Geochemical Indexes Used for the Interpretation of Palaeoredox Conditions in Ancient Mudstones. *Chem. Geol.* 111 (1-4), 111–129. doi:10.1016/0009-2541(94)90085-X

Junium, C. K., and Arthur, M. A. (2007). Nitrogen Cycling during the Cretaceous, Cenomanian-Turonian Oceanic Anoxic Event II. *Geochem. Geophys. Geosyst.* 8, 1–18. doi:10.1029/2006GC001328

Keller, G., Adatte, T., Berner, Z., Chellai, E. H., and Stueben, D. (2008). Oceanic Events and Biotic Effects of the Cenomanian-Turonian Anoxic Event, Tarfaya Basin, Morocco. *Cretaceous Res.* 29 (5–6), 976–994. doi:10.1016/j.cretres.2008.05.020

Krall, P., Slomp, C. P., Forster, A., and Kuypers, M. M. M. (2010). Phosphorus Cycling from the Margin to Abyssal Depths in the Proto-Atlantic during Oceanic Anoxic Event 2. *Palaeogeogr. Palaeodimatol., Palaeoecol.* 295, 42–58. doi:10.1016/j.palaeo.2010.05.014

Kuroda, J., Ogawa, N., Tanimizu, M., Coffin, M., Tokuyama, H., Kitazato, H., et al. (2007). Contemporaneous Massive Subaerial Volcanism and Late Cretaceous Oceanic Anoxic Event 2. *Earth Planet. Sci. Lett.* 256 (1–2), 211–223. doi:10.1016/j.epsl.2007.01.027

Kuypers, M. M. M., Pancost, R. D., and Damsté, J. S. S. (1999). A Large and Abrupt Fall in Atmospheric CO2 Concentration during Cretaceous Times. *Nature* 399, 342–345. doi:10.1038/20659

Kuypers, M. M. M., Pancost, R. D., Nijenhuis, I. A., and Sinninghe Damsté, J. S. (2002). Enhanced Productivity Led to Increased Organic Carbon Burial in the Euxinic North Atlantic basin during the Late Cenomanian Oceanic Anoxic Event. *Paleoceanography* 17, 1–13. doi:10.1029/2000PA000569

Kuypers, M. M. M., Lourens, L. J., Rijpstra, W. I. C., Pancost, R. D., Nijenhuis, I. A., and Sinninghe Damsté, J. S. (2004). Orbital Forcing of Organic Carbon Burial in the Proto-North Atlantic during Oceanic Anoxic Event 2. *Earth Planet. Sci. Lett.* 228, 465–482. doi:10.1130/G20458.110.1016/j.epsl.2004.09.037

Lafargue, E., Marquis, F., and Pillot, D. (1998). Rock-Eval 6 Applications in Hydrocarbon Exploration, Production, and Soil Contamination Studies. *Rev. Inst. Fr. Pét.* 53, 421–437. doi:10.2516/ogst:1998036

Lancelot, Y., Seibold, E., Cepek, P., Dean, W. E., Eremeev, V., Gardner, J., et al. (1978). "Site 367: Cape Verde Basin," in *Initial Reports of the Deep Sea Drilling Project*. 41, 163–232. doi:10.2973/dsdp.proc.41.103.1978

McLennan, S. M. (2001). Relationships between the Trace Element Composition of Sedimentary Rocks and Upper continental Crust. *Geochem. Geophys. Geosyst.* 2. doi:10.1029/2000GC000109

Mélières, F. (1978). "X-ray Mineralogy Studies, Leg 41, Deep Sea Drilling Project, Eastern North Atlantic Ocean," in *Initial Reports of the Deep Sea Drilling Project, 41*. Editor Y. Lancelot (Washington: U. S. Government Printing Office), 1065–1086. doi:10.2973/dsdp.proc.41.142.1978

Monteiro, F. M., Pancost, R. D., Ridgwell, A., and Donnadieu, Y. (2012). Nutrients as the Dominant Control on the Spread of Anoxia and Euxinia across the Cenomanian-Turonian Oceanic Anoxic Event (OAE2): Model-Data Comparison. *Paleoceanography* 27 (4), PA4209. doi:10.1029/2012pa002351

Naafs, B. D. A., Monteiro, F. M., Pearson, A., Higgins, M. B., Pancost, R. D., and Ridgwell, A. (2019). Fundamentally Different Global marine Nitrogen Cycling in Response to Severe Ocean Deoxygenation. *Proc. Natl. Acad. Sci. USA* 116 (24), 24979–24984. doi:10.1073/pnas.1905553116

O'Connor, L. K., Jenkyns, H. C., Robinson, S. A., Remmelzwaal, S. R. C., Batenburg, S. J., Parkinson, I. J., et al. (2020). A Re-Evaluation of the Plenus Cold Event, and the Links between CO 2 , Temperature, and Seawater Chemistry during OAE 2. *Paleoceanogr. Paleoclimatol.* 35, e2019PA003631. doi:10.1029/2019PA003631

Orth, C. J., Attrep, M., Quintana, L. R., Elder, W. P., Kauffman, E. G., Diner, R., et al. (1993). Elemental Abundance Anomalies in the Late Cenomanian Extinction Interval: A Search for the Source(s). *Earth Planet. Sci. Lett.* 117 (1–2), 189–204. doi:10.1016/0012-821x(93)90126-t

Ostrander, C. M., Owens, J. D., and Nielsen, S. G. (2017). Constraining the Rate of Oceanic Deoxygenation Leading up to a Cretaceous Oceanic Anoxic Event (OAE-2: ~94 Ma). *Sci. Adv.* 3 (8), e1701020. doi:10.1126/sciadv.1701020

Owens, J. D., Lyons, T. W., Li, X., Macleod, K. G., Gordon, G., Kuypers, M. M. M., et al. (2012). Iron Isotope and Trace Metal Records of Iron Cycling in the Proto-North Atlantic during the Cenomanian-Turonian Oceanic Anoxic Event (OAE-2). *Paleoceanography* 27, PA3223. doi:10.1029/2012PA002328

Owens, J. D., Gill, B. C., Jenkyns, H. C., Bates, S. M., Severmann, S., Kuypers, M. M. M., et al. (2013). Sulfur Isotopes Track the Global Extent and Dynamics of Euxinia during Cretaceous Oceanic Anoxic Event 2. *Proc. Natl. Acad. Sci.* 110 (46), 18407–18412. doi:10.1073/pnas.1305304110

Pancost, R. D., Crawford, N., Magness, S., Turner, A., Jenkyns, H. C., and Maxwell, J. R. (2004). Further Evidence for the Development of Photic-Zone Euxinic Conditions during Mesozoic Oceanic Anoxic Events. *J. Geol. Soc.* 161 (3), 353–364. doi:10.1144/0016764903-059

Paul, C. R. C., Lamolda, M. A., Mitchell, S. F., Vaziri, M. R., Gorostidi, A., and Marshall, J. D. (1999). The Cenomanian-Turonian Boundary at Eastbourne (Sussex, UK): a Proposed European Reference Section. *Palaeogeogr. Palaeoclimatol. Palaeoecol.* 150 (1–2), 83–121. doi:10.1016/s0031-0182(99)00009-7

Pearce, M. A., Jarvis, I., and Tocher, B. A. (2009). The Cenomanian-Turonian Boundary Event, OAE2 and Palaeoenvironmental Change in Epicontinental Seas: New Insights from the Dinocyst and Geochemical Records. *Palaeogeogr. Palaeoclimatol. Palaeoecol.* 280 (1–2), 207–234. doi:10.1016/j.paleo.2009.06.01210.1016/j.palaeo.2009.06.012

Pogge von Strandmann, P. A. E., Jenkyns, H. C., and Woodfine, R. G. (2013). Lithium Isotope Evidence for Enhanced Weathering during Oceanic Anoxic Event 2. *Nat. Geosci* 6 (8), 668–672. doi:10.1038/ngeo1875

Poulton, S. W., Henkel, S., März, C., Urquhart, H., Flögel, S., Kasten, S., et al. (2015). A continental-weathering Control on Orbitally Driven Redox-Nutrient Cycling during Cretaceous Oceanic Anoxic Event 2. *Geology* 43, 963–966. doi:10.1130/G36837.1

Rau, G. H., Arthur, M. A., and Dean, W. E. (1987). 15N/14N Variations in Cretaceous Atlantic Sedimentary Sequences: Implication for Past Changes in marine Nitrogen Biogeochemistry. *Earth Planet. Sci. Lett.* 82 (3), 269–279. doi:10.1016/0012-821X(87)90201-9

Redfield, A. C. (1958). The Biological Control of Chemical Factors in the Environment. *Am. Sci.* 46, 205–221.

Ruvalcaba Baroni, I., van Helmond, N. A. G. M., Tsandev, I., Middelburg, J. J., and Slomp, C. P. (2015). The Nitrogen Isotope Composition of Sediments from the Proto-North Atlantic during Oceanic Anoxic Event 2. *Paleoceanography* 30, 923–937. doi:10.1002/2014PA002744.5

Sageman, B. B., Meyers, S. R., and Arthur, M. A. (2006). Orbital Time Scale and New C-Isotope Record for Cenomanian-Turonian Boundary Stratotype. *Geol.* 34, 125–128. doi:10.1130/G22074.1

Schlanger, S. O., and Jenkyns, H. C. (1976). Cretaceous Anoxic Events: Causes and Consequences. *Geol. Mijnb.* 55, 179–184.

Schlanger, S. O., Arthur, M. A., Jenkyns, H. C., and Scholle, P. A. (1987). The Cenomanian-Turonian Oceanic Anoxic Event, I. Stratigraphy and Distribution of Organic Carbon-Rich Beds and the marine δ13C Excursion. *Geol. Soc. Lond. Spec. Publications* 26 (1), 371–399. doi:10.1144/gsl.sp.1987.026.01.24

Scholle, P. A., and Arthur, M. A. (1980). Carbon Isotope Fluctuations in Cretaceous Pelagic Limestones: Potential Stratigraphic and Petroleum Exploration Tool.

Am. Assoc. Pet. Geol. Bull. 60 (1), 67–87. doi:10.1306/2f91892d-16ce-11d7-8645000102c1865d

Schouten, S., Hopmans, E. C., Forster, A., van Breugel, Y., Kuypers, M. M. M., and Sinninghe Damsté, J. S. (2003). Extremely High Sea-Surface Temperatures at Low Latitudes during the Middle Cretaceous as Revealed by Archaeal Membrane Lipids. *Geol.* 31, 1069–1072. doi:10.1130/G19876.1

Sigman, D. M., Karsh, K. L., and Casciotti, K. L. (2009). "Nitrogen Isotopes in the Ocean," in *Encyclopedia of Ocean Sciences*. Editors J.H. Steele, S.A. Thorpe, and K.K. Turekian (Oxford: Academic Press), 40–54. doi:10.1016/b978-012374473-9.00632-9

Sinninghe Damsté, J. S., and Köster, J. (1998). A Euxinic Southern North Atlantic Ocean during the Cenomanian/Turonian Oceanic Anoxic Event. *Earth Planet. Sci. Lett.* 158, 165–173. doi:10.1016/S0012-821X(98)00052-1

Sinninghe Damsté, J. S. S., Kuypers, M. M. M., Pancost, R. D., and Schouten, S. (2008). The Carbon Isotopic Response of Algae, (Cyano)bacteria, Archaea and Higher Plants to the Late Cenomanian Perturbation of the Global Carbon Cycle: Insights from Biomarkers in Black Shales from the Cape Verde Basin (DSDP Site 367). *Org. Geochem.* 39, 1703–1718. doi:10.1016/j.orggeochem.2008.01.012

Sinninghe Damsté, J. S., van Bentum, E. C., Reichart, G.-J., Pross, J., and Schouten, S. (2010). A CO2 Decrease-Driven Cooling and Increased Latitudinal Temperature Gradient during the Mid-cretaceous Oceanic Anoxic Event 2. *Earth Planet. Sci. Lett.* 293 (1–2), 97–103. doi:10.1016/j.epsl.2010.02.027

Sinton, C. W., and Duncan, R. A. (1997). Potential Links between Ocean Plateau Volcanism and Global Ocean Anoxia at the Cenomanian-Turonian Boundary. *Econ. Geol.* 92, 836–842. doi:10.2113/gsecongeo.92.7-8.836

Snow, L. J., Duncan, R. A., and Bralower, T. J. (2005). Trace Element Abundances in the Rock Canyon Anticline, Pueblo, Colorado, marine Sedimentary Section and Their Relationship to Caribbean Plateau Construction and Oxygen Anoxic Event 2. *Paleoceanography* 20 (3), PA3005. doi:10.1029/2004pa00109310.1029/2005pa001222

Stüeken, E. E., Kipp, M. A., Koehler, M. C., and Buick, R. (2016). The Evolution of Earth's Biogeochemical Nitrogen Cycle. *Earth-Science Rev.* 160, 220–239. doi:10.1016/j.earscirev.2016.07.007

Summons, R. E., Jahnke, L. L., Hope, J. M., and Logan, G. A. (1999). 2-Methylhopanoids as Biomarkers for Cyanobacterial Oxygenic Photosynthesis. *Nature* 400, 554–557. doi:10.1038/23005

Takashima, R., Nishi, H., Hayashi, K., Okada, H., Kawahata, H., Yamanaka, T., et al. (2009). Litho-, Bio- and Chemostratigraphy across the Cenomanian/Turonian Boundary (OAE 2) in the Vocontian Basin of southeastern France. *Palaeogeogr. Palaeoclimatol. Palaeoecol.* 273, 61–74. doi:10.1016/j.paleo.2008.12.00110.1016/j.palaeo.2008.12.001

Thomazo, C., and Papineau, D. (2013). Biogeochemical Cycling of Nitrogen on the Early Earth. *Elements* 9, 345–351. doi:10.2113/gselements.9.5.345

Thunell, R. C., Sigman, D. M., Muller-Karger, F., Astor, Y., and Varela, R. (2004). Nitrogen Isotope Dynamics of the Cariaco Basin, Venezuela. *Glob. Biogeochem. Cycles* 18 (3), GB3001. doi:10.1029/2003GB002185

Topper, R. P. M., Trabucho Alexandre, J., Tuenter, E., and Meijer, P. T. (2011). A Regional Ocean Circulation Model for the Mid-cretaceous North Atlantic Basin: Implications for Black Shale Formation. *Clim. Past* 7, 277–297. doi:10.5194/cp-7-277-2011

Trabucho Alexandre, J., Tuenter, E., Henstra, G. A., van der Zwan, K. J., van de Wal, R. S. W., Dijkstra, H. A., et al. (2010). The Mid-cretaceous North Atlantic Nutrient Trap: Black Shales and OAEs. *Paleoceanography* 25, PA4201. doi:10.1029/2010PA001925

Tribovillard, N., Algeo, T. J., Lyons, T., and Riboulleau, A. (2006). Trace Metals as Paleoredox and Paleoproductivity Proxies: An Update. *Chem. Geology* 232, 12–32. doi:10.1016/j.chemgeo.2006.02.012

Tribovillard, N., Algeo, T. J., Baudin, F., and Riboulleau, A. (2012). Analysis of marine Environmental Conditions Based Onmolybdenum-Uranium Covariation-Applications to Mesozoic Paleoceanography. *Chem. Geology* 324-325, 46–58. doi:10.1016/j.chemgeo.2011.09.009

Tsikos, H., Jenkyns, H. C., Walsworth-Bell, B., Petrizzo, M. R., Forster, A., Kolonic, S., et al. (2004). Carbon-isotope Stratigraphy Recorded by the Cenomanian-Turonian Oceanic Anoxic Event: Correlation and Implications Based on Three Key Localities. *J. Geol. Soc.* 161 (4), 711–719. doi:10.1144/0016-764903-077

Tucholke, B. E., Sibuet, J.-C., Klaus, A., Arnaoldi, M., Delius, H., Engström, A. V., et al. (2004). "Site 1276,". *Proc. ODP, Init. Repts*. Editors B.E. Tucholke, J.-C. Sibuet, and A. Klaus (College Station, TX: Ocean Drilling Program), 210, 1–358. doi:10.2973/odp.proc.ir.210.103.2004

Turgeon, S. C., and Creaser, R. A. (2008). Cretaceous Oceanic Anoxic Event 2 Triggered by a Massive Magmatic Episode. *Nature* 454 (7202), 323–326. doi:10.1038/nature07076

Tyrrell, T. (1999). The Relative Influences of Nitrogen and Phosphorus on Oceanic Primary Production. *Nature* 400, 525–531. doi:10.1038/22941

van Bentum, E. C., Reichart, G.-J., Forster, A., and Sinninghe Damsté, J. S. (2012). Latitudinal Differences in the Amplitude of the OAE-2 Carbon Isotopic Excursion: pCO2 and Paleo Productivity. *Biogeosciences* 9 (2), 717–731. doi:10.5194/bg-9-717-2012

Van Capellen, P., and Ingall, E. D. (1994). Benthic Phosphorus Regeneration, Net Primary Production, and Ocean Anoxia: a Model of the Coupled marine Biogeochemical Cycles of Carbon and Phosphorus. *Paleoceanography* 9, 677–692. doi:10.1029/94PA01455

van Helmond, N. A. G. M., Ruvalcaba Baroni, I., Sluijs, A., Sinninghe Damsté, J. S., and Slomp, C. P. (2014a). Spatial Extent and Degree of Oxygen Depletion in the Deep Proto-North Atlantic basin during Oceanic Anoxic Event 2. *Geochem. Geophys. Geosyst.* 15 (11), 4254–4266. doi:10.1002/2014GC005528

van Helmond, N. A. G. M., Sluijs, A., Reichart, G.-J., Sinninghe Damsté, J. S., Slomp, C. P., and Brinkhuis, H. (2014b). A Perturbed Hydrological Cycle during Oceanic Anoxic Event 2. *Geology* 42, 123–126. doi:10.1130/G34929.1

van Hinte, J. E., Wise, S. W., Jr, Biart, B. N. M., Covington, J. M., Dunn, D. A., Haggerty, J. A., et al. (1993). "Site 603,". *Proc. DSDP, Init. Repts*. Editors J. E. van Hinte and S. W. WiseJr. (College Station, TX: Ocean Drilling Program), 93, 25–276. doi:10.2973/dsdp.proc.93.102.1987

Wedepohl, K. H. (1971). "Environmental Influences on the Chemicalcomposition of Shales and Clays," in *Physics and Chemistry of theEarth*. Editors L.H. Ahrens, F. Press, S.K. Runcorn, and H.C. Urey (Oxford: Pergamon), 305–333.

Westermann, S., Vance, D., Cameron, V., Archer, C., and Robinson, S. A. (2014). Heterogeneous Oxygenation States in the Atlantic and Tethys Oceans during Oceanic Anoxic Event 2. *Earth Planet. Sci. Lett.* 404, 178–189. doi:10.1016/j.epsl.2014.07.018

Zhang, X., Sigman, D. M., Morel, F. M. M., and Kraepiel, A. M. L. (2014). Nitrogen Isotope Fractionation by Alternative Nitrogenases and Past Ocean Anoxia. *Proc. Natl. Acad. Sci. USA* 111, 4782–4787. doi:10.1073/pnas.1402976111

Zheng, X.-Y., Jenkyns, H. C., Gale, A. S., Ward, D. J., and Henderson, G. M. (2013). Changing Ocean Circulation and Hydrothermal Inputs during Ocean Anoxic Event 2 (Cenomanian-Turonian): Evidence from Nd-Isotopes in the European Shelf Sea. *Earth Planet. Sci. Lett.* 375, 338–348. doi:10.1016/j.epsl.2013.05.053

Conflict of Interest: The authors declare that the research was conducted in the absence of any commercial or financial relationships that could be construed as a potential conflict of interest.

Publisher's Note: All claims expressed in this article are solely those of the authors and do not necessarily represent those of their affiliated organizations, or those of the publisher, the editors and the reviewers. Any product that may be evaluated in this article, or claim that may be made by its manufacturer, is not guaranteed or endorsed by the publisher.

frontiers in Earth Science

ORIGINAL RESEARCH
published: 10 September 2021
doi: 10.3389/feart.2021.706144

Redox-Controlled Ammonium Storage and Overturn in Ediacaran Oceans

Christian Hallmann[1†], Emmanuelle Grosjean[1†], Nathan D. Shapiro[1†], Yuichiro Kashiyama[2,3], Yoshito Chikaraishi[2,4], David A. Fike[1†], Naohiko Ohkouchi[2] and Roger E. Summons[1]*

[1]Department of Earth, Atmospheric and Planetary Sciences, Massachusetts Institute of Technology, Cambridge, MA, United States, [2]Japan Agency for Marine-Earth Science and Technology, Yokosuka, Japan, [3]Graduate School of Engineering, Fukui University of Technology, Fukui, Japan, [4]ILTS, Hokkaido University, Sapporo, Japan

As a key nutrient, nitrogen can limit primary productivity and carbon cycle dynamics, but also evolutionary progress. Given strong redox-dependency of its molecular speciation, environmental conditions can control nitrogen localization and bioavailability. This particularly applies to periods in Earth history with strong and frequent redox fluctuations, such as the Neoproterozoic. We here report on chlorophyll-derived porphyrins and maleimides in Ediacaran sediments from Oman. Exceptionally light $\delta^{15}N$ values (< −10‰) in maleimides derived from anoxygenic phototrophs point towards ammonium assimilation at the chemocline, whereas the isotopic offset between kerogens and chlorophyll-derivatives indicates a variable regime of cyanobacterial and eukaryotic primary production in surface waters. Biomarker and maleimide mass balance considerations imply shallow euxinia during the terminal Ediacaran and a stronger contribution of anoxygenic phototrophs to primary productivity, possibly as a consequence of nutrient 'lockup' in a large anoxic ammonium reservoir. Synchronous $\delta^{13}C$ and $\delta^{15}N$ anomalies at the Ediacaran–Cambrian boundary may reflect one in a series of overturn events, mixing ammonium and isotopically-light DIC into oxic surface waters. By modulating access to nitrogen, environmental redox conditions may have periodically affected Ediacaran primary productivity, carbon cycle perturbations, and possibly played a role in the timing of the metazoan radiation across the terminal Ediacaran and early Cambrian.

Keywords: ediacaran, ammonium, porphyrin, nutrient, nitrogen, animal evolution

OPEN ACCESS

Edited by:
Eva Stüeken, University of St Andrews, United Kingdom

Reviewed by:
Michael Kipp, California Institute of Technology, United States
Carina Lee, Universities Space Research Association (USRA), United States

****Correspondence:***
Christian Hallmann
Christian.hallmann@gfz-potsdam.de

†Present address:
Christian Hallmann, GFZ, German Research Center for Geosciences, Potsdam, Germany
Emmanuelle Grosjean, Geoscience Australia, Canberra, ACT, Australia
Nathan D. Shapiro, Vir Biotechnology, Inc., San Francisco, CA, United States
David A. Fike, Department of Earth and Planetary Sciences, Washington University, Saint Louis, MO, United States

Specialty section:
This article was submitted to Geochemistry, a section of the journal Frontiers in Earth Science

Received: *06 May 2021*
Accepted: *25 August 2021*
Published: *10 September 2021*

Citation:
Hallmann C, Grosjean E, Shapiro ND, Kashiyama Y, Chikaraishi Y, Fike DA, Ohkouchi N and Summons RE (2021) Redox-Controlled Ammonium Storage and Overturn in Ediacaran Oceans. Front. Earth Sci. 9:706144. doi: 10.3389/feart.2021.706144

INTRODUCTION

An increase in algal diversity during the Ediacaran (Knoll et al., 2006) and the advent of metazoan organismic complexity (Love et al., 2009) have traditionally been attributed to enhanced oxygen availability (e.g., Catling et al., 2005) or the demise of widespread marine sulfidic conditions (e.g. Cohen et al., 2009) toxic to complex eukaryotes. But the realisation that basal metazoan metabolism can proceed under exceedingly low oxygen partial pressures (Mills et al., 2014), a limited spatial extent of pervasive euxinia (Reinhard et al., 2013) and a slow oxygenation that continued into the early Paleozoic (Sperling, 2015) warrant revisiting these hypotheses. Only recently have researchers begun to examine the role of marine redox conditions in controlling the abundance of essential nutrients that could have retarded or stimulated evolutionary processes. While an increase in bioavailable phosphorus likely fueled the rise of eukaryotic algae to ecological significance during the Cryogenian (Brocks et al., 2017), P/Fe ratios in iron formations (Planavsky et al., 2010), P in fine-

grained sediments (Reinhard et al., 2017) and an abundance of late Neoproterozoic peritidal phosphate deposits (Brasier, 1990) suggest that phosphorus was likely widely bioavailable in the Ediacaran ocean. In terms of understanding the role that bioavailable nitrogen has played during the later Neoproterozoic, most studies have focused on measuring bulk $\delta^{15}N$ values (e.g., Ader et al., 2014; Zhang et al., 2017; Wang et al., 2017; Wang et al., 2018a,b; Chen et al., 2019) yet there are limits to the amount of information that can be gained from bulk $\delta^{15}N$ signals. Here we aim to address this limitation by studying compound-specific $\delta^{15}N$ signals.

Repeated imbalance of the Neoproterozoic marine carbon cycle is evident from frequent and extreme stable carbon isotope fluctuations recorded in Ediacaran carbonates and kerogens (e.g., Halverson and Shields-Zhou, 2011), yet relatively little is known about Neoproterozoic nitrogen cycling (Ader et al., 2014) or its availability as a potentially limiting nutrient. In modern oceans, the carbon and nitrogen cycles are tightly coupled through biological dependence on the fixed inorganic nitrogen species nitrate (NO_3^-) and ammonium (NH_4^+), which frequently limit primary productivity (Falkowski and Godfrey, 2008). The primary source of these nutrients is the cyanobacterial fixation of dissolved N_2, but the subsequent fate and transformation of nitrogen species is strongly dependent on environmental redox conditions (Canfield et al., 2010), thereby implying a tight connection between ecosystem diversity, environmental conditions and biogeochemical cycling. In particular the Neoproterozoic Era witnessed strong water column redox gradients and temporal fluctuations thereof (Li et al., 2010; Sperling et al., 2013). This has been recorded by a notable instability in the secular stable carbon isotope curve (e.g., Halverson and Shields-Zhou, 2011), with many anomalies and excursions that may reflect chemocline instability (e.g., Jiang et al., 2008) on shorter time scales or oxidative events (Rothman et al., 2003). One of these, the largest recorded negative carbon isotope anomaly, can be traced globally (Grotzinger et al., 2011) and occurred during deposition of the Shuram Formation in the South Oman Salt Basin (Fike et al., 2006). During such redox-driven perturbations, the speciation of fixed nitrogen and the nitrogen cycle would have been vulnerable to environmental factors. Ediacaran redox variability could thus have indirectly exerted a significant control on nitrogen nutrient availability and the marine carbon cycle, as well as on ecosystem structure and evolution.

The stable nitrogen isotopic composition of sedimentary organic matter can be used to constrain the nitrogen source as well as isotopic fractionation during assimilation of the precursor biomass (Ohkouchi and Takano, 2014). However, the $\delta^{15}N$ value of bulk organic matter represents an amalgamated signal of primary producing bacteria and algae, as well as heterotrophs—all of which fractionate nitrogen isotopes differently during assimilation (Higgins et al., 2008). Nitrogen in sedimentary porphyrins that represent the diagenetic product of chlorophylls is not only covalently bound and resistant to diagenetic overprinting, but also highly source-specific (Sachs et al., 1999). Yet the sensitivity of porphyrins to geothermal heating precludes their survival in most Precambrian rocks that have experienced deep burial (Baker et al., 1987). The South Oman Salt Basin (SOSB; **Figure 1**) hosts one of the most complete and thermally best preserved Ediacaran sedimentary sequences (**Figure 2**; Fike et al., 2006; Amthor et al., 2003; Grosjean et al., 2009) that was initially deposited under open marine conditions (Nafun Group) and subsequently in a restricted but marine fed epicratonic basin (Ara Group), witnessing periodic transgressive cycles that led to the deposition of six (A0–A5) shallow water carbonate-evaporite couplets (Amthor et al., 2003; Mattes and Conway-Morris, 1990). These are well developed on the southern carbonate platform (**Figure 1**), with carbonate 'stringers' sandwiched between sulphate and halite evaporites, but form a more continuous carbonate platform on the eastern flank. For more details of the geology of the SOSB the reader is referred to (Gorin et al., 1982) or (Loosveld and Terken, 1996). An ash bed in the A4 unit of the Ara Group was U-Pb dated at 541 ± 0.13 Ma (Bowring et al., 2007) and contains a $\delta^{13}C_{carbonate}$ excursion that marks the Precambrian–Cambrian boundary. Rifting around 543 Ma opened up a deeper sub-basin (Athel Basin) that hosts organic rich fine siliciclastics of the U Shale and Thuleilat Fm, as well as the somewhat enigmatic Athel Silicilite, which all were deposited synchronously with the platform A4 carbonate-evaporite unit (**Figures 1**, **2**) and thus also record the Ediacaran–Cambrian boundary. The Athel Fm (or, Al Shomou silicilyte) is a thick, finely laminated and organic rich quartz deposit deposited in deep waters, which stands in marked contrast to other Neoproterozoic silica sinks that are largely restricted to peritidal settings (Stolper et al., 2017). However the carbonates of its laterally equivalent shallow water facies appear to lack authigenic chert (e.g., Schröder et al., 2005; Stolper et al., 2017). To date, the origin and uniqueness of this formation remain debated (Ramseyer et al., 2013; Al Rajaibi et al., 2015; Stolper et al., 2017). We here report on porphyrins and maleimides recovered from basinal Ediacaran sediments of the South Oman Salt Basin and discuss their stable nitrogen isotope values in the context of biological assimilation pathways and different nitrogen reservoirs in the Ediacaran ocean.

METHODS

Cutting aliquots weighing between ca. 3 and 20 g (**Supplementary Table S1**) were powdered in a stainless steel puck mill and solvent extracted with dichloromethane/methanol (DCM/MeOH, 9:1) in a Dionex Accelerated Solvent Extractor (ASE) device. Asphaltenes were precipitated from the resulting bitumen extracts using *n*-pentane. Asphaltene-free fractions were treated with activated copper in order to remove elemental sulfur and separated into saturated hydrocarbons, aromatic hydrocarbons and a polar fraction by open column liquid chromatography over silica gel, eluting sequentially with

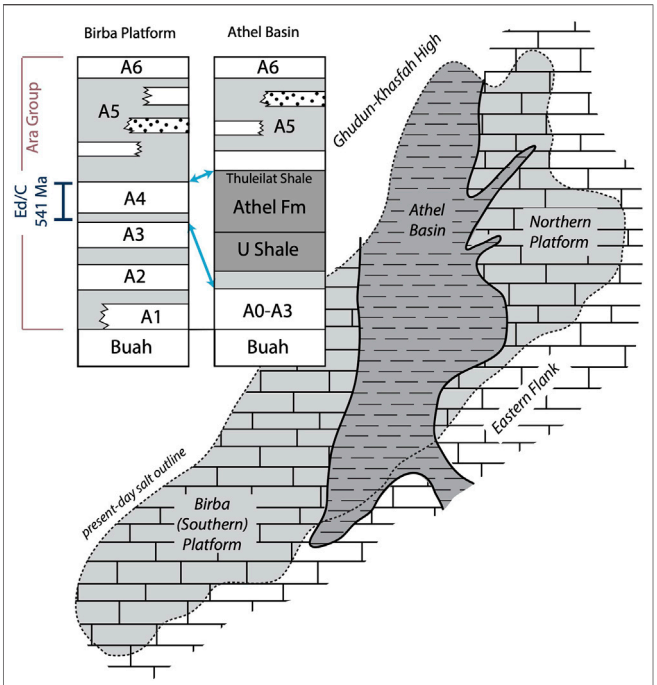

FIGURE 1 | Outline and stratigraphy of platform and basin in the South Oman Salt Basin. Deposits of the deep-water Athel subbasin are time equivalent to the A4 carbonate-evaporite couplet on the adjacent shallow platform. After Schröder et al. (2005).

n-hexane, *n*-hexane/DCM (1:1) and DCM/MeOH (1:1). The aromatic and polar fractions were further fractionated on a silica gel column to afford subfractions enriched in nickel and vanadyl porphyrins, respectively, by elution with DCM (Grice et al., 1996). Quantification of porphyrins was carried out on these enriched fractions using a UV-visible spectrophotometer as described in more detail elsewhere (Grosjean et al., 2004). While nickel porphyrins were not detected, vanadyl porphyrin concentrations were measured from visible spectra using an extinction coefficient of 31.6 L $mmol^{-1}$ cm^{-1} at 574 nm (Buchler et al., 1971; Mackenzie et al., 1981).

The porphyrin-enriched fractions were dissolved in DCM/MeOH (1:4 vol.) and analyzed on a Thermo Finnigan LCQ system fitted with a Hypersil BDS C_{18} column (4.6 × 150 mm) coupled to a UV photospectrometer and operated in full scan mode: *m/z* 400–1,500. During liquid chromatography samples were eluted at 0.8 ml/min with a concentration gradient from 100% MeOH (containing 0.1% formic acid) at t = 0–90% MeOH (containing 0.1% formic acid), 10% DCM at t = 15 min. Subsequently pure MeOH (containing 0.1% formic acid) was eluted for 10 further minutes.

A detailed procedure of the nitrogen isotope analysis of maleimides was described in (Chikaraishi et al., 2008) and is briefly described below. Porphyrin fractions were oxidized to maleimides using a 1:1 (v/v) mixture of 10% aqueous chromic acid and 15% aqueous H_2SO_4 at 0°C for 1 h and then at room temperature for 1 h (Nomoto et al., 2001). It was shown that this procedure involves no isotopic fractionation (Chikaraishi et al., 2008). Maleimides were extracted with benzene (5 x) from the solution. The extracts were then methyl-esterified and analyzed by GC-MS for screening. The nitrogen isotopic composition of maleimides was determined by GC-C-IRMS using an Agilent 6890N GC fitted with an Ultra-2 capillary column (25 m, 0.32 mm i.d., 0.52 μm film thickness) coupled to a Thermo Finnigan Delta Plus XP IRMS. The analytical error of repeated measurements was consistently better than 0.5‰. This number represents the average of analytical errors (1 sigma) of various in-house synthesized maleimide injections (also see Chikaraishi et al., 2008). The $\delta^{15}N$ values of these maleimides were independently determined at JAMSTEC on an EA/IRMS (described in Isaji et al., 2020) that was calibrated with IAEA authentic standards. Methyl-isobutyl-maleimides were below the limit of reliable analysis.

Bulk nitrogen isotope values shown in **Figure 2** ($\delta^{15}N_{org}$) and discussed in the context of the synchronicity of the $\delta^{13}C$ and $\delta^{15}N$ signals across the Ediacaran/Cambrian boundary derive from Chapter 4 in (Fike, 2007) and were determined at MIT on organic extracts (bitumens) in order to avoid falsification of the bulk organic $\delta^{15}N$ signal by nitrogen adsorbed on clay particles. Although likely to be offset from bulk $\delta^{15}N$ values, for samples of a similar range of moderate thermal maturity like the ones studied here, such offsets are likely small (Stueeken et al., 2017) and should not impact ensuing interpretations, especially if solely used to indicate stratigraphic trends (**Figure 2**). Bitumens were recovered by solvent extraction (dichloromethane/methanol 9:1 in a Dionex Accelerated Solvent Extractor), as described in (Fike, 2008), and the indigeneity of the bitumen was tested and asserted using biomarkers and stable isotope patterns. Bitumens were weighed into tin cups and flash combusted at 1,060°C in a Carlo Erba NA1500 Elemental Analyser fitted with an AS200 autosampler. The resulting gas, reduced to N_2 was analyzed in continuous flow mode using a Delta Plus XP Isotope Ratio Mass Spectrometer. Nitrogen isotope values are reported in units of per mil relative to Air after calibration using international standards and in-house references interspersed with the analysed samples (NBS-22, Acetanilide and Penn State kerogen).

Bulk $\delta^{15}N$ values shown in **Figure 5** and used for the calculation of ε values were determined at the Max-Planck-Institute for Biogeochemistry on kerogen isolates that were obtained after digestion of carbonates and silicates using aqueous HCl and HF, respectively. Despite an expected slight offset to whole-rock bulk $\delta^{15}N$ values, for the here studied unmetamorphosed rocks, both $\delta^{15}N_{kerogen}$ as well as $\delta^{15}N_{bulk}$ should be good approximations of $\delta^{15}N_{biomass}$ (Stueeken et al., 2017). Homogenized kerogen powders, weighed into tin cups, were flash combusted in an NA 1110 elemental analyser (CE Instruments) coupled to a Delta-Plus XL IRMS (Thermo Finnigan) *via* a ConFlow III. Nitrogen isotope values (averages of duplicate measurements) are reported in units of per mil relative to Air after calibration using in-house reference standards acetanilide ($\delta^{15}N$ = −1.51 ± 0.1 permit and caffeine ($\delta^{15}N$ = −15.46 ± 0.1 per mil). For further details of this method see (Werner and Brand, 2001).

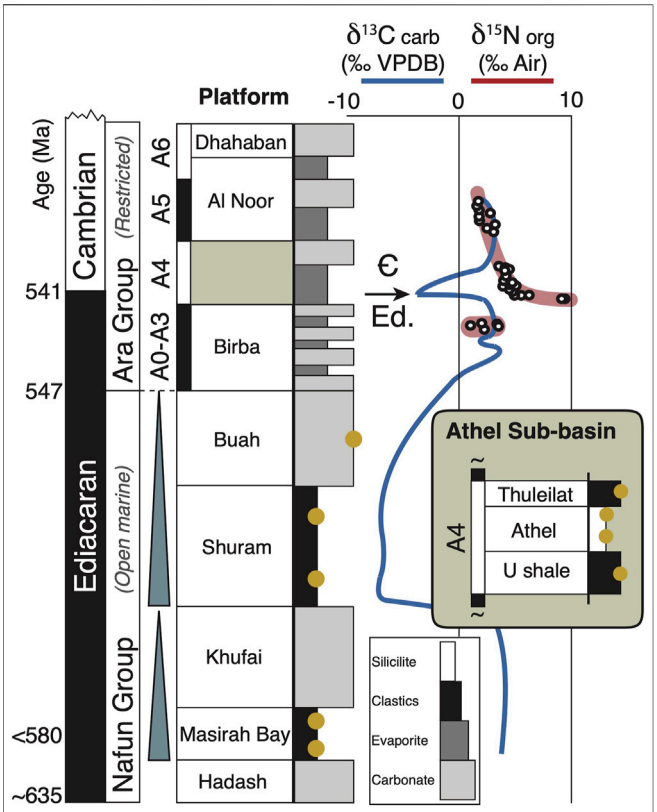

FIGURE 2 | Composite stratigraphy and stable isotope record of the South Oman Salt Basin. Studied samples (yellow circles) represent both open marine and more restricted basinal depositional environments. A composite stable carbon isotope curve (based on platform carbonates [after: Amthor et al., 2003] shows the Shuram anomaly and a characteristic excursion at the Ediacaran–Cambrian boundary. A precisely coincident positive nitrogen isotope anomaly first reported by Fike (2007) suggests a causal connectivity, interpreted as the consequence of sudden overturn and oxidation of a large deep-water pool of ammonium into shallow oxygenated surface waters. Shaded box shows deep-water equivalent strata to the A4 platform carbonates.

RESULTS AND DISCUSSION

Intact Preserved Neoproterozoic Porphyrins

LC-UVvis and LC-MS revealed the presence of intact porphyrin molecules in 18 of the 27 studied samples, with only vanadyl-complexed species and both DPEP (deoxophylloerythroetioporphyrins) and Etio (etioporphyrins) structures being present (**Figure 3**), which are characterised by a closed or opened pentacyclic ring, respectively. Given the conversion of DPEP to Etio during thermal maturation (Baker et al., 1987), we conclude that the observed VO-porphyrin dominance throughout the Ediacaran SOSB sedimentary sequence (**Table 1**) is not due to thermal destruction of the generally more labile Ni-porphyrins (Baker et al., 1987) but rather points to environmental conditions: sulfidic bottom waters in the SOSB may have periodically removed any available nickel by precipitation as insoluble sulfides (Lewan, 1984) and left an excess of vanadium to react with labile organic matter. On the basis of observed concentrations, only VO-chelates underwent detailed characterization as intact porphyrins. These revealed the highest concentrations of up to ~16 nmol/g rock in the youngest stratigraphic units that experienced the least burial (**Figure 4**), while porphyrin abundances decrease systematically with overall greater burial depth of older stratigraphic levels (**Figure 5**). Given a concomitant increase in hopanoid biomarker maturation parameters (based on 'Ts': 18α–22,29,30-trisnorneohopane and 'Tm': 17α–22,29,30-trisnorhopane), this decrease can be directly linked to progressive thermal destruction during sedimentary burial in the South Oman Salt Basin (**Figure 6A**). Oddly, silicilyte rocks of the Athel Formation are characterized by a paucity of porphyrins despite a suitable thermal maturation window (**Figures 5**, **6A**). The enigmatic nature and source of the Athel silica is subject to ongoing debate (e.g., Al Rajaibi et al., 2015; Stolper et al., 2017) and these results may suggest that the relative proportion of phototrophically derived organic matter in this stratigraphic unit was exceedingly small, thereby supporting the possibility of silica precipitation by nucleation on elevated levels of dissolved organic matter as a consequence of strongly enhanced heterotrophy (Ferris et al., 1988).

The detection of a wide range of VO-porphyrins, including structures > C_{33}, in all of the other stratigraphic units indicates an original input of both chlorophyll-a (*Chl-a*) and bacteriochlorophylls (*BChl*), including such structures adapted to light intensities at greater water depths and typically biosynthesized by anoxygenic phototrophs inhabiting chemoclines. To allow for their stable isotopic analyses, whole porphyrin fractions were oxidized to GC-amenable maleimides in the laboratory (**Figure 2**). This process involves no isotopic fractionation (Chikaraishi et al., 2008) and the retention of characteristic alkylation patterns allows for the recognition of precursor-product relationships. Structural and isotopic studies have previously shown that maleimides with a methyl-ethyl substitution pattern (MEM) are principally derived from *Chl-a* and thus largely representative of carbon and nitrogen fixation in surface waters, whereas both methyl-n-propyl (MPM) and methyl-isobutyl maleimides (MBM) largely derive from the same (Naeher et al., 2013) Chlorobi-derived *BChl-c*, *BChl-d* or *BChl-e* molecular precursors (Grice et al., 1996) that are indicative of processes occurring in anoxic waters below a chemocline.

Nitrogen Isotopes and Nutrient Assimilation in Surface Waters: Cyanobacteria and Algae

By knowing the stable nitrogen isotopic fractionation that occurs during porphyrin biosynthesis, the original composition of precursor biomass ($\delta^{15}N_{biomass}$) can be reconstructed from $\delta^{15}N_{porphyrin}$. By now several studies have focused on this biosynthetic fractionation ($\varepsilon_{por} = \delta^{15}N_{biomass}–\delta^{15}N_{porphyrn}$) and found that eukaryotic algae typically fractionate by 5–7‰ (Kennicutt et al., 1992; Sachs, 1997; Sachs et al., 1999; Sachs and Repeta, 1999; Sigman et al., 2009; Higgins et al., 2011) meaning that the pigments are depleted in ^{15}N relative to biomass. Negative epsilon values of freshwater cyanobacteria

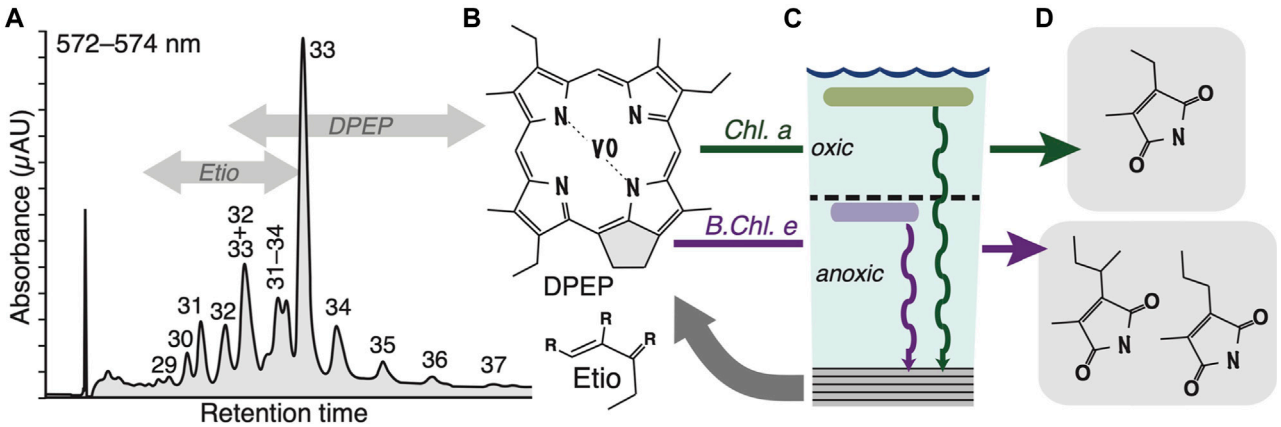

FIGURE 3 | Porphyrins and maleimides. Intact vanadyl porphyrins in SOSB sediments were characterized by LC-MS and quantified by UV*vis* spectrophotometry **(A,B)**. Chromatographic peaks in (a.) (sample OMR-11, Thuleilat Fm) are annotated by their corresponding carbon numbers. Porphyrins > C_{32} indicate the presence of both chlorophyll-a and bacteriochlorophyll-derived structures that were biosynthesized in surface waters and at the chemocline, respectively **(C)**. Oxidation to maleimides **(D)** does not affect the characteristic alkylation pattern, allowing the distinction of maleimides primarily deriving from surface water chlorophyll-a (MEM) versus structures deriving from bacteriochlorophyll-c, -d or-e (MPM, MBM), produced by anoxygenic phototrophs.

TABLE 1 | Organic carbon, hopanoid-derived thermal maturity (Ts and Tm) and normalized porphyrin concentrations in studied samples.

Unit	Sample	Depth min (m)	Depth max (m)	TOC (wt%)	Ts/(Ts + Tm)	Porphyrins (nmol/g rock)	(nmol/g TOC)
Masirah Bay	OMR027	2,280	2,295	3.8	0.25	0.0	0.0
Masirah Bay	OMR009	2,648	2,676	4.4	0.41	0.7	16.8
Masirah Bay	OMR015	2026	2060	4.7	0.31	0.8	17.7
Masirah Bay	OMR016	3,177	3,196	1.7	0.53	0.0	0.0
Shuram	OMR008	2,380	2,500	2.5	0.45	1.8	70.3
Shuram	OMR010	2,628	2,724	2.5	0.46	0.0	0.0
Shuram	OMR018	1,486	1,518	4.1	0.31	2.4	57.7
Shuram	OMR019	930	990	3.7	0.35	1.1	29.6
Shuram	OMR026	1905	1940	3.4	0.18	1.9	57.2
Shuram	OMR001	2,440	2,460	2.3	0.41	1.6	69.5
Buah	OMR002	2,344	2,374	1.6	0.31	4.5	281.5
Buah	OMR017	1,569	1,602	2.3	0.26	2.9	126.5
Buah	OMR020	4,411	_	3.1	0.53	0.0	0.0
U Shale	OMR005	1,425	1,527	3.5	0.21	10.1	288.4
U Shale	OMR006	1,527	1,650	4.9	0.16	9.9	202.5
U Shale	OMR007	1773	1872	5.7	0.27	8.4	146.8
U Shale	OMR014	2,420	2,460	6.4	0.34	4.7	74.0
U Shale	OMR025	1751	1833	4.0	0.3	3.3	82.5
Silicilyte	OMR004	1,198	1,425	3.4	0.22	0.0	0.0
Silicilyte	OMR013	2,240	2,352	2.3	0.21	0.0	0.0
Silicilyte	OMR024	1,628	1742	2.6	0.26	0.0	0.0
Silicilyte	OMR012	2,104	2,120	3.4	0.18	0.0	0.0
Silicilyte	OMR023	1,551	1,602	4.3	0.28	0.0	0.0
Thuleilat	OMR003	1,000	1,102	8.0	0.23	16.0	200.4
Thuleilat	OMR011	2068	2084	10.4	0.21	7.6	73.3
Thuleilat	OMR021	1,417.5	1,483	6.4	0.25	12.6	197.5
Thuleilat	OMR022	1,520	1,547	2.5	0.28	2.3	91.5

(Higgins et al., 2011; i.e. porphyrins heavier than biomass by ~10‰) are irrelevant to this study given that a marine depositional environment is well constrained for the studied deposits, whereas marine cyanobacteria tend to be characterized by exceedingly low ε_{por} values around 0‰ (Higgins et al., 2011). The variability of ε_{por} values appears to be independent of phylogeny (Higgins et al., 2011) and, because ε_{por} reflects intracellular partitioning of N isotopes downstream of glutamate, it is also independent of N substrate (Higgins et al., 2011, 2012). In the marine realm *Chl-a*, which is the principal molecular precursor to MEM, is predominantly biosynthesized by eukaryotic algae and cyanobacteria. Hence, when reconstructing $\delta^{15}N_{biomass}$ from $\delta^{15}N_{porphyrin}$ values we must consider both end-member options.

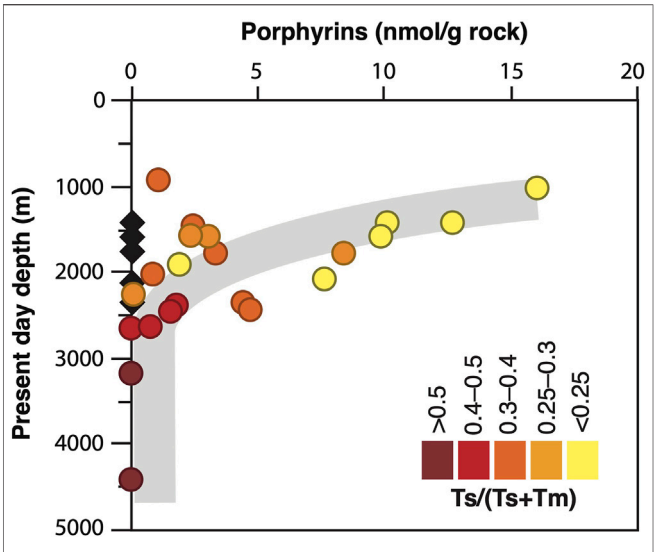

FIGURE 4 | Porphyrin preservation. Relationship between present-day burial depth of studied samples, their thermal maturity (*via* the hopanoids Ts and Tm) and porphyrin content. Overall, the porphyrin content decreases with increasing burial and thermal maturity, which corresponds to the stratigraphic trend shown in **Figure 5A**. Despite some variation, the oldest stratigraphic units have mostly also experienced the greatest burial (see **Table 1**). Black diamonds indicate samples from the Athel silicilyte, which contain no porphyrins despite a low thermal maturity (0.18–0.28 on the Ts/(Ts + Tm) scale).

In the studied SOSB samples, surface water derived MEM that principally reflect *Chl-a* exhibit $\delta^{15}N$ values ranging between −5.2‰ and +7.2‰ (Air) (**Figure 5**). If these maleimides were derived 100% from cyanobacteria, an identical range of values could be reconstructed for the bulk precursor biomass. Given an average $\delta^{15}N$ value of + 0.7‰ for dissolved marine N_2 and the fact that the nitrogenase enzyme typically fractionates by 0–2‰ ($\varepsilon_{assimilation}$, Higgins et al., 2011; Bauersachs et al., 2009), the biomass of diazotrophic marine cyanobacteria should carry average values around −1.3‰ (Higgins et al., 2011) and should not be lighter than −2‰ (Higgins et al., 2012). This implies that the lighter range of observed MEM values (i.e., those between −5.2‰ and ca. −2.0‰) cannot be attributed to nitrogen fixing cyanobacteria utilising the common and widespread Mo-based nitrogenase enzyme. These ^{15}N-depleted values may reflect the cyanobacterial use of a different substrate, a (partial) eukaryotic source of MEM or the activity of 'alternative' (i.e., Fe- or V-based) nitrogenases. The latter may have been more active under Mo-scarce conditions, as possibly induced by strong euxinia, and fractionate more strongly during nitrogen fixation, leading to lower $\delta^{15}N$ values (Zhang et al., 2014). Under the assumed environmental conditions, which will be discussed in more detail further below, such alternative nitrogenases could indeed have been relevant. However the role that such alternative nitrogenases have generally played in the geological past is unknown and debated, and it remains unresolved when they evolved (Boyd et al., 2011; Garcia et al., 2020). As will also be discussed in more detail further below, we consider the cyanobacterial use of different substrates—nitrate or, more likely, ammonium—as the most plausible source of the observed light isotopic values. Despite typically higher positive environmental $\delta^{15}N_{nitrate}$ values that are a consequence of microbial water-column denitrification (Sigman et al., 2009), a stronger fractionation during assimilation can generate cyanobacterial $\delta^{15}N_{biomass}$ values as light as −5.3‰ (corresponding to $\varepsilon_{assimilation}$ of 10.2‰, Higgins et al., 2012). Alternatively, cyanobacterial assimilation of ammonium may be considered, which can explain $\delta^{15}N_{biomass} < 2.0$ and lead to values as low as −5.0‰ ($\varepsilon_{assimilation}$ of 13.9‰) in Anabaena (Macko et al., 1987). In principle, the full range of $\delta^{15}N_{MEM}$ can plausibly be explained by a sole cyanobacterial source of primary produced organic matter in surface waters of the SOSB. Nevertheless, the studied deposits are not low in eukaryotic steranes, indicating that algae did provide a contribution to fossilized biomass.

Assuming a 100% contribution of eukaryotic algae to MEM, on the other hand, the precursor biomass can be reconstructed to $\delta^{15}N$ values between −0.2 and 12.2‰ (ε_{por} = ~5 ± 2‰, Sachs et al., 1999; Higgins et al., 2011). The heavier range of these values would be typical for nitrate-assimilating eukaryotic algae and zooplankton (e.g., Minagawa and Wada, 1984; Sigman et al., 2009) but these processes are incompatible with observed values around 0‰. Here again, the lighter range of values can be achieved when algae assimilate ammonium ($\varepsilon_{assimilation}$ of −6.7‰ to +7.2‰; average −0.92 ± 3.88‰; data from Table 1 in Higgins et al., 2011). Taking into account that we need to find an explanation for $\delta^{15}N_{MEM}$ between −5.2‰ and ca. −2.0‰ that likely cannot be attributed to diazotrophic cyanobacteria or to nitrate-assimilating algae, it appears likely that ammonium may have played a relevant role as a nitrogen substrate for Ediacaran primary producers, as will be discussed in more detail below.

Apart from allowing for the tentative reconstruction of the main nitrogen substrates used during assimilation, the wide range of observed values likely suggests that surface waters were inhabited by a mixed population of diazotrophic cyanobacteria, nitrate- or ammonium-assimilating cyanobacteria and eukaryotic algae. This is corroborated by ε_{por} values (kerogen–MEM)—i.e. $\Delta\delta^{15}N_{kerogen-MEM}$ that can yield further insight to the source of biomass under the assumption that $\delta^{15}N_{biomass} \approx {}^{15}N_{kerogen}$. In organic-rich sediments, such as the here-studied SOSB rocks (with total organic carbon [TOC] values between 1.6 and 10.4%: **Table 1**), $\delta^{15}N_{kerogen}$ is considered to faithfully reflect $\delta^{15}N_{biomass}$ (Robinson et al., 2012). The SOSB rocks (early-middle oil window) have never seen the advanced stages of thermal maturation during which $\delta^{15}N_{kerogen}$ values are significantly altered (Boudou et al., 2008). With the previously discussed knowledge—and under exclusion of freshwater cyanobacteria—the ε_{por} values can be used to tentatively differentiate between marine cyanobacterial and marine algal primary production (Higgins et al., 2011, 2012). The $\Delta\delta^{15}N_{kerogen-MEM}$ values obtained on SOSB samples range from −3.82 to +8.79 (**Figure 5**; **Table 2**), where the higher values are most likely characteristic of eukaryote-dominated primary productivity in surface waters (Higgins et al., 2011). This is not surprising, since a rise of mostly green algae (Hoshino et al., 2017) to ecological dominance was recorded at the onset of

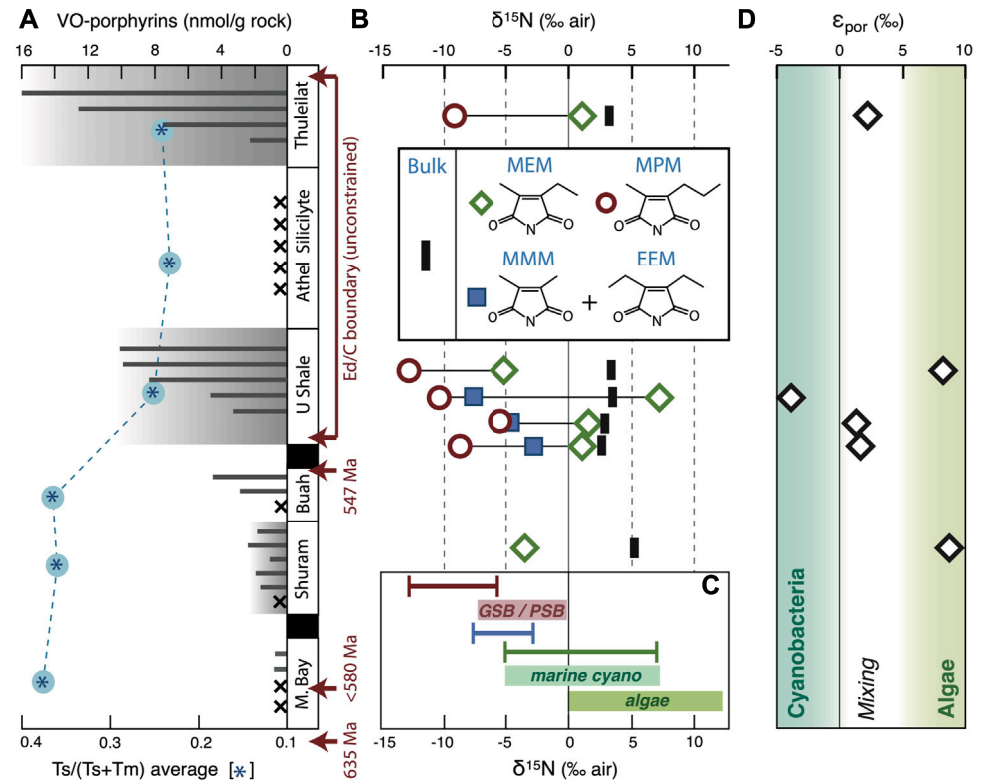

FIGURE 5 | Porphyrin abundances and maleimide nitrogen isotopes. **(A)** VO-porphyrin abundances (grey bars; plotted per stratigraphic unit irrespective of exact depth) decrease with burial and thermal maturity (blue asterisks; based on the hopanoids Ts and Tm: **Figure 6**). Crosses indicate absent porphyrins. **(B)** $\delta^{15}N$ values of kerogens and maleimides were determined for six samples only due to concentration and matrix interference. **(C)** Ranges of observed values (colored lines) and $\delta^{15}N_{biomass}$ values converted from $\delta^{15}N_{maleimide}$ based on known biosynthetic fractionation during porphyrin biosynthesis after Higgins et al., 2011 (annotated boxes) place constraints on nitrogen substrate and assimilatory processes. **(D)** The kerogen–MEM isotopic offset allows reconstructing the dominant primary producers (Higgins et al., 2011, 2012).

the Ediacaran (Brocks et al., 2017; van Maldegem et al., 2019) and C_{27}–C_{29} steranes are prominently present in all studied SOSB samples (Grosjean et al., 2009). The negative ε_{por} values observed in some samples, however imply primary productivity that is strongly shifted towards marine cyanobacteria (Higgins et al., 2011). While overall algae dominated marine productivity during the Ediacaran, the range of $\Delta\delta^{15}N_{kerogen-MEM}$ values observed here suggests that fluctuations in the composition of the primary producing community occurred during the course of the Ediacaran with periodic return to (cyano)bacterial dominance. In broad terms, this is in agreement with a strikingly large variation of bacterial hopanes over eukaryotic steranes observed throughout the Ediacaran (Brocks et al., 2017; Pehr et al., 2018; van Maldegem et al., 2019), which led to the suggestion that on regional scales primary productivity was likely modulated by local determinants such as nutrient supply (Pehr et al., 2018). It is also consistent with distributions of carotenoid pigments (Cui et al., 2020).

Nitrogen Isotopes and Nutrients at the Chemocline: Ammonium Assimilation

In contrast to MEM, deriving from cyanobacterial or algal *Chl-a* in surface waters, MPM is thought to largely derive from anoxygenic phototrophs thriving at a deeper chemocline. In contrast to MBM, which can *only* derive from anoxygenic phototrophs, but whose abundances were too low to allow for the reliable determination of $\delta^{15}N$ values in the here studied samples, MPM can theoretically represent a mixture of anoxygenic phototroph-derived MPM and an additional MPM-component deriving from *Chl*-a by phytyl ester hydrolysis and reduction of the resulting C-3 acid (Baker et al., 1987; Verne-Mismer et al., 1986). In principle, the relative contribution of anoxygenic phototrophs engaging in the rTCA cycle for carbon fixation to the pool of fossil MPM can be recognized on the basis of 'heavy' $\delta^{13}C$ values. Yet this was not achieved in the present study due to chromatographic co-elution: although we managed to purify the samples sufficiently to allow for the chromatographic baseline separation of individual maleimides from other nitrogen-bearing compounds, we could not achieve a baseline separation from other carbon-containing molecules. Nevertheless, in practical terms MPM and MBM seem to largely derive from the same biological precursors, which has been confirmed in multiple individual instances where MBM and MPM concentrations are linearly correlated with R^2 values of 0.95–0.99 (Naeher et al., 2013, 2015), confirming that these compounds either share the same origin or that populations of source bacteria thrive under the same, highly specific

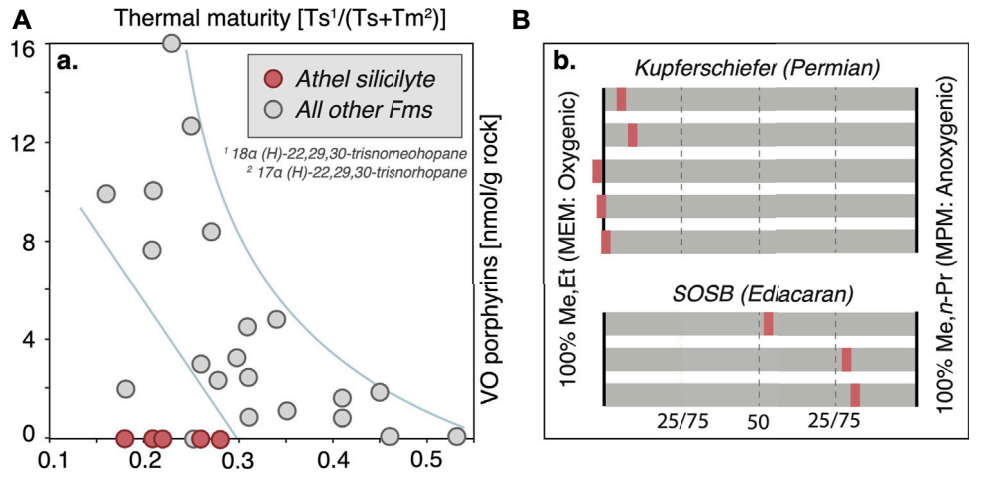

FIGURE 6 | Preservation of porphyrins and mass balance of autotrophy. **(A)** Porphyrin abundances are a function of preservation and thermal maturity (based on the hopanoids Ts and Tm; see main text). VO-porphyrins are systematically absent from the Athel Fm (red symbols) despite a suitable thermal maturity, pointing to strongly differing ecologies or environmental conditions. **(B)** Isotopic mass balance calculations (^{13}C for the Kupferschiefer after Grice et al., 1997: **Supplementary Table S3**; ^{15}N for the SOSB: **Table 2**) on the basis of comparing the isotope value of summed MMM and EEM to those of MEM and MPM end members can hint towards the relative proportion of oxygenic vs anoxygenic phototrophic biomass. SOSB primary productivity during deposition of the U-shale ($n = 3$) was shifted towards a markedly higher contribution of anoxygenic phototrophs. Negative values for some Kupferschiefer samples, i.e. $\delta^{13}C_{MMM+EEM}$ beyond the 0–100% spectrum spanned by $\delta^{13}C_{MEM}$ and $\delta^{13}C_{MPM}$, likely derive from analytical error.

TABLE 2 | Stable nitrogen isotopic composition of kerogen and maleimides in studied samples.

Unit	Sample	Depth min (m)	Depth max (m)	$\delta^{15}N$ (ker)	$\delta^{15}N$ maleimides (‰ air)			ε por (Ker–MEM)
					MEM	MPM	MMM + EEM	
U Shale	OMR006	1,527	1,650	2.7	1.1	−8.8	−2.8	1.6
U Shale	OMR007	1773	1872	2.8	1.5	−5.1	−5.0	1.3
U Shale	OMR014	2,420	2,460	3.4	7.2	−10.5	−7.7	−3.8
Thuleilat	OMR021	1,417.5	1,483	3.2	1.0	−9.3	n.a	2.2
U Shale	OMR025	1751	1833	3.1	-5.2	−13.0	n.a	8.3
Shuram	OMR026	1905	1940	5.20	-3.6	n.a	n.a	8.8

environmental conditions (Naeher et al., 2013). In samples of the Permian Kupferschiefer, (Grice et al., 1997), found MPM to be isotopically similar to MBM: with a simple mixing model of two samples characterized by $\delta^{13}C_{MBM}$ of −15.4‰ and −14.7‰, $\delta^{13}C_{MPM}$ of −17.0‰ and −17.3‰ and $\delta^{13}C_{MEM}$ of −26.2‰ and −25.9‰ (data from Table 3 and from Figure 8 in Grice et al., 1997) we can reconstruct that not more than 14.8–23.2% of all MPM in the Kupferschiefer samples (Grice et al., 1997) derives from a different biological source, implying that MPM sufficiently faithfully represents anoxygenic phototrophs.

Characterized by $\delta^{15}N$ values of −5.1‰ to −13.0‰, MPM in the here studied SOSB samples, largely reflecting nitrogen assimilation at the chemocline, carry some of the lightest biological stable nitrogen isotope values ever reported (**Figure 5**). These numbers systematically exclude either diazotrophy, which is rare in anoxygenic phototrophs (Madigan, 1995), or the assimilation of nitrate. Some cyanobacteria assimilating ammonium are known to fractionate strongly ($\varepsilon_{assimilation}$ of 13.9‰, Macko et al., 1987) but cyanobacteria tend to produce significantly more MEM than MPM and rarely generate $\delta^{15}N_{biomass}$ <−5‰ (*nota bene* that alternative nitrogenases may generate $\delta^{15}N_{biomass}$ as low as −7 or −8‰; Zhang et al., 2014), and hence even lighter porphyrins. Unfortunately, our knowledge of nitrogen isotope fractionation during assimilation and porphyrin biosynthesis by anoxygenic phototrophs is highly limited. As a best approximation, it has been shown that *Rhodobacter capsulatus*, a purple non-sulfur bacterium, fractionates by 0.8–1.8‰ ($\varepsilon_{assimilation}$) during photoautotrophic and photoheterotrophic growth on N_2, whereas these values increase to 10.6 and 12.4‰ during photoheterotrophic growth with NH_4^+ (Beaumont et al., 2000). Porphyrins synthesized during growth on ammonium were depleted relative to biomass (ε_{por}) by another 8.6–10.9‰, leading to *BChl-a* as light as −21.0‰ (Beaumont et al., 2000) despite much heavier biomass. Hence the presence of this process would never be visible in bulk $\delta^{15}N$ values of fossil organic matter. We conclude that the most likely explanation for observed light $\delta^{15}N_{MPM}$ values in the SOSB lies in a scenario involving assimilation of ammonium (Higgins et al., 2011, 2012; Vo et al., 2013) that likely accumulated in deep anoxic waters,

similar to what is frequently observed in modern stratified meromictic lakes such as Lake Cadagno and Lake Kaiike (e.g,. Ohkouchi et al., 2005, 2007; Halm et al., 2009). Although not providing a direct analog in terms of salinity and the presence of benthic phototrophic mats that were likely absent in deeper facies of the SOSB, stratified Lake Kaiike contains relevant amounts of dissolved ammonium below a chemocline inhabited by green and purple sulfur bacteria, whose *BChl-e* is characterized by similarly low $\delta^{15}N$ values to those found in the SOSB (Ohkouchi et al., 2005, 2007). At present, such a scenario provides the most plausible explanation for the anomalously light nitrogen isotopes encountered in MPM of the studied SOSB samples.

Isotope Mass Balance Suggests Significant Anoxygenic Productivity

Me, Me- and Et, Et-maleimides (MMM, EEM) are considered as source-unspecific since they can potentially derive from both *Chl-a* and from *BChls*. In modern, predominantly aerobic marine ecosystems, the relative proportion of anoxygenic phototrophs dwindles in comparison to oxygenic primary producers (Raven, 2009), which is evident from the molecular sedimentary remnants of phototrophic organisms: bacteriochlorophyll-derived porphyrins and farnesane are much less common than *Chl-a* derived porphyrins and phytyl hydrocarbons. Since independent of the nitrogen substrate used, MMM and EEM represent a mixture between a purely anoxygenic phototrophic source on one hand (*BChl*) and a mostly oxygenic phototrophic source (*Chl-a*) on the other, their stable isotopic composition—be it nitrogen *or* carbon—in comparison to those of MEM and MPM, can be used to establish a rough mass balance of phototrophic primary productivity.

Under modern aerobic conditions, the $\delta^{15}N$ value of MMM + EEM should lie close to that of MEM, given dominant oxygenic photosynthesis in surface waters, and such a constellation of values is even observed during episodes of mild euxinia (**Figure 6**), when reconstructing the predominant source of MMM and EEM using their $\delta^{13}C$ values in samples of the Permian Kupferschiefer (using data from Grice et al., 1997). Results from the SOSB that are based on $\delta^{15}N$ suggest that MMM and EEM are isotopically much more similar to MPM. Given the uncommon light $\delta^{15}N$ values of MPM that we attribute to chemocline-dwelling phototrophs, we posit that a significant portion of MMM and EEM is predominantly derived from *BChls* biosynthesized at the chemocline, and hence from anoxygenic phototrophs (**Figure 6B**). This appears to contradict the relatively low abundance of VO-porphyrins > C_{33} (**Figure 3**), but it must be kept in mind that the fate of *Chls* after demetallation is highly complex and that many different, yet uncharacterized chelates can form that evade characterization (Gueneli et al., 2018). Even if MPM do not constitute a pure anoxygenic phototrophic end member but contain some non-*BChl* sourced portion (e.g., up to ca. 25% as calculated for the Kupferschiefer), the SOSB ecosystem would still be remarkably different from modern oceans in that a sizable portion of productivity was performed by anoxygenic phototrophs in deeper waters. Considering the possibility of a preservational bias, a larger proportion of *Chl-a* produced in surface waters may indeed be oxidatively degraded than *BChl* produced at the chemocline, thereby artificially shifting the balance of preserved porphyrins towards anoxygenic phototrophs. However, episodic euxinia with a shallow chemocline was corroborated for deep-water facies of the SOSB by the presence of the molecular markers okenane and chlorobactane (French et al., 2015; Roussel et al., 2020). In the deep-water depositional environments of the SOSB, the observed carotenoid pigments cannot derive from benthic mats but must represent planktonic purple sulfur bacteria and the green strains of green sulfur bacteria, respectively—microbes requiring access to reduced sulfur and with high light requirements. In the absence of isorenieratane that derives from brown strains of green sulfur bacteria, and irrespective of the generally lesser ecological relevance of green sulfur bacteria prior to the Phanerozoic (Cui et al., 2020), these data point to persistent stratification and a shallow chemocline (<25 m, Brocks and Schaeffer, 2008). Given the short transit through oxygenated surface waters, any preferential degradation of surface-derived *Chl* may have been minimal. From this perspective the reconstructed mass balance would not require significant correction to account for preservational biases. On the other hand one could argue that remineralisation rates tend to be highest in the upper water column, where organic export fluxes are highest, whereas the maintenance of euxinic conditions requires a particularly high remineralisation rate in shallow waters in order to maintain anoxia. From this perspective a relevant preservation bias may be given. Nevertheless if such biases were large, they should have similarly affected the Kupferschiefer samples that are not shifted towards an anoxygenic phototrophic source of MMM and EEM despite only mild euxinia (Grice et al., 1997). Most recently, a study of fossil aromatic carotenoids in terminal Ediacaran SOSB sediments (Roussel et al., 2020) reported an elevated proportion of structures that were likely sourced by cyanobacteria rather than by anoxygenic phototrophs (Cui et al., 2020). However, the taphonomy of carotenoids is complicated by sulfide as a preferential preservative (e.g., Koopmans et al., 1996) and although we cannot exclude principally-cyanobacterial productivity in the SOSB, it is unlikely that ^{15}N-depleted MMM, EEM and *BChl*-derived MPM were all largely produced by cyanobacteria. Hence despite the paucity of comparative data, and accepting that we may face some degree of preservation bias, we posit that during the terminal Ediacaran a relevant portion of photosynthetic primary production in the distal facies of the SOSB (Athel subbasin) could have been taking place at the chemocline and not in surface waters.

While such conditions do not exist in modern oceans, the best modern analogue environments are shallow stratified lakes, where anoxygenic phototrophs can indeed dominate primary production (van Gemenden and Mas, 1995), and which are known to develop an ammonium reservoir in deeper anoxic waters (Ohkouchi et al., 2005). In trying to understand the here presented data, we hypothesize on a model where under persistently stratified conditions, sinking biomass of marine primary producers continuously contributed nitrogen to a deep-water ammonium pool in the SOSB, whose diffusion back up into the mixed zone would have been minimal. This

large pool of reduced nitrogen remained inaccessible to aerobic primary producers inhabiting surface waters. With an exceedingly shallow chemocline, suggested by the biomarkers okenane and chlorobactene, the biomass of diazotrophic cyanobacteria containing freshly fixed nitrogen would have rapidly exited the mixed layer, maintaining nitrogen scarcity in surface waters. This in turn would have led to a relative shift in overall primary productivity towards anoxygenic phototrophs inhabiting the chemocline and tapping into the deep pool of reduced nitrogen. In this scenario, the deep-water ammonium that is controlled by the redox structure of the water column represents a 'locked-up' nutrient reservoir capable of modulating primary productivity: under persistently stratified conditions, primary productivity will be throttled, whereas the overturn of such a setting will release abundant nutrients and stimulate surface water productivity.

Periodic Ammonium Overturn and Nutrient Release

The Ediacaran–Cambrian boundary in the SOSB not only records a characteristic and well-documented negative $\delta^{13}C_{CARB}$ anomaly (Halverson and Shields-Zhou, 2011; Fike et al., 2006; Amthor et al., 2003) but (Fike, 2007) also reported a positive $\delta^{15}N_{ORG}$ excursion with an exactly synchronous onset, which jumps abruptly from values around 1–3‰ to values close to 10‰ before gradually returning to pre-excursion values (**Figure 2**). Apart from the perfect synchronicity of their onset, nitrogen and carbon isotopes are not directly correlated (**Supplementary Table S2**), thereby rather excluding an explanation by coupled ammonium oxidation and methanotrophy (Thomazo et al., 2011). Rather than intense denitrification and depletion of the nitrate reservoir, as seen in modern low-productivity ocean regions (Sigman et al., 2009), we suggest that these heavy nitrogen isotopes may be the result of intense nitrate assimilation, which discriminates against ^{15}N with ~5‰, caused by enhanced productivity following basinal overturn and oxidation of a deep ammonium reservoir. Alternatively, direct cyanobacterial utilization of liberated ammonium—sourced from upwelling or overturn—could result in similar heavy values, as a consequence of Rayleigh fractionation of ammonium during anoxygenic photosynthetic assimilation. Such a situation was observed in meromictic Lake Kaiike (Ohkouchi et al., 2005) and may also provide an explanation for heavy MEM values (**Figure 5**). In the first scenario, availability of NO_3^- supplied by nitrification is eventually dependent on oxidant and NH_4^+ availability. Given persistent oxic surface waters as testified by the $\delta^{15}N$ of MEM and overall elevated ε_{por}, we suggest that Ediacaran surface water productivity could have been episodically limited by deep-water nutrient capture during stratified sulfidic conditions, and stimulated by overturn—the observed anomalies at the Ediacaran–Cambrian boundary (**Figure 1**) representing one such overturn event. Strong environmental redox fluctuations (e.g., Sperling et al., 2013; Li et al., 2010) could have exerted principal control on nitrogen nutrient availability by controlling the N supply pathway, thereby modulating primary productivity on shorter time scales and providing an explanation for the repeated return to cyanobacterial-dominated (Pehr et al., 2018) and mixed ecosystems (**Figure 5D**) during the Ediacaran. Models have suggested that the Ediacaran transition towards an oxygen-rich ocean-atmosphere system was inhibited or delayed by a need for elevated abundances of fixed nitrogen (Reinhard et al., 2017). The here suggested mechanistic link to redox-driven nitrogen nutrient dynamics may not only solve the timing of the latter, but also provides an explanation for the aberrant Neoproterozoic carbon cycle, while the progressive overturn of 'locked-up' nitrogen around the Ediacaran-Cambrian boundary could have contributed towards the enhanced nutrient requirements of an increasingly complex biosphere.

CONCLUSION

Together with previously published accounts of fossil pigments (French et al., 2015; Roussel et al., 2020), the distribution and stable nitrogen isotope composition of vanadyl porphyrins and porphyrin-derived maleimides in sediments of the Ediacaran SOSB is indicative of shallow euxinia. The $\delta^{15}N$ values of surface water (*Chl-a*) derived maleimides likely indicates the presence of both cyanobacteria as well as eukaryotic algae, as confirmed by steroid abundances in SOSB rocks (Grosjean et al., 2009), yet ranges into values that may point towards the use of ammonium as a nitrogen substrate. This notion is strengthened by $\delta^{15}N$ of chemocline (*BChl*) derived maleimides, whose exceptionally light values are best explained by the assimilation of ammonium by anoxygenic phototrophs (Beaumont et al., 2000; Vo et al., 2013), in analogy to the situation in some stratified meromictic lakes (Ohkouchi et al., 2005, 2007). Notably, such information would remain masked by bulk $\delta^{15}N$ analyses only. In such modern lake systems, a sizable portion of primary productivity can be shifted towards anoxygenic phototrophs. Using an isotope mass balance of maleimides we reconstruct a similar ecosystem structure for the SOSB and tentatively attribute this currently rare condition to the redox-controlled storage of ammonium-nitrogen in deep waters, which may have been periodically overturned. A coupled negative $\delta^{13}C$ and positive $\delta^{15}N$ excursion at the Ediacaran–Cambrian boundary (Fike, 2007) may reflect one such overturn event that released ^{13}C-depleted DIC and ammonium into surface waters, where it would be rapidly oxidized to nitrate and subjected to denitrification and algal assimilation. Our data may be explained by redox-controlled nitrogen scarceness in surface waters, which would have restricted eukaryotic, and reduced cyanobacterial activity. Under such conditions access to fixed nitrogen would have exerted fundamental control on phytoplankton community structure and possibly primary productivity (Johnston et al., 2009). Although more investigation is needed, such redox-driven nitrogen limitation may have played a role in delaying the transition to a fully oxygenated atmosphere-ocean system (Reinhard et al., 2017) and possibly the timing for the rise of animals.

DATA AVAILABILITY STATEMENT

The original contributions presented in the study are included in the article/**Supplementary Material**, further inquiries can be directed to the corresponding author.

AUTHOR CONTRIBUTIONS

EG, NO, DF, NS, YK, YC, and RS performed research and analyzed data; CH analyzed and interpreted data and wrote the paper with input from all others.

ACKNOWLEDGMENTS

Samples for this study were provided by Shell International E & P. Petroleum Development Oman provided financial support for the early stages of this work. Additional MIT research was supported by the NASA Astrobiology Institute NNA13AA90A Foundations of Complex Life. CH thanks the Agouron Institute for support. NO was financially supported by grants from JSPS. Petroleum Development Oman and the Oman Ministry of Oil and Gas are thanked for the permission to publish.

SUPPLEMENTARY MATERIAL

The Supplementary Material for this article can be found online at: https://www.frontiersin.org/articles/10.3389/feart.2021.706144/full#supplementary-material

REFERENCES

Ader, M., Sansjofre, P., Halverson, G. P., Busigny, V., Trindade, R. I. F., Kunzmann, M., et al. (2014). Ocean Redox Structure across the Late Neoproterozoic Oxygenation Event: a Nitrogen Isotope Perspective. *Earth Planet. Sci. Lett.* 396, 1–13. doi:10.1016/j.epsl.2014.03.042

Al Rajaibi, I. M., Hollis, C., and Macquaker, J. H. (2015). Origin and Variability of a Terminal Proterozoic Primary Silica Precipitate, Athel Silicilyte, South Oman Salt Basin, Sultanate of Oman. *Sedimentology* 62, 793–825. doi:10.1111/sed.12173

Amthor, J. E., Grotzinger, J. P., Schröder, S., Bowring, S. A., Ramezani, J., Martin, M. W., et al. (2003). Extinction of Cloudina and Namacalathus at the Precambrian-Cambrian Boundary in Oman. *Geol* 31, 431–434. doi:10.1130/0091-7613(2003)031<0431:eocana>2.0.co;2

Baker, E. W., William Louda, J., and Orr, W. L. (1987). Application of Metalloporphyrin Biomarkers as Petroleum Maturity Indicators: The Importance of Quantitation. *Org. Geochem.* 11, 303–309. doi:10.1016/0146-6380(87)90041-6

Bauersachs, T., Schouten, S., Compaoré, J., Wollenzien, U., Stal, L. J., and Sinninghe Damsteé, J. S. (2009). Nitrogen Isotopic Fractionation Associated with Growth on Dinitrogen Gas and Nitrate by Cyanobacteria. *Limnol. Oceanogr.* 54, 1403–1411. doi:10.4319/lo.2009.54.4.1403

Beaumont, V. I., Jahnke, L. L., and des Marais, D. J. (2000). Nitrogen Isotopic Fractionation in the Synthesis of Photosynthetic Pigments in Rhodobacter Capsulatus and Anabaena Cylindrica. *Org. Geochem.* 31, 1075–1085. doi:10.1016/s0146-6380(00)00133-9

Boudou, J.-P., Schimmelmann, A., Ader, M., Mastalerz, M., Sebilo, M., and Gengembre, L. (2008). Organic Nitrogen Chemistry during Low-Grade Metamorphism. *Geochimica et Cosmochimica Acta* 72, 1199–1221. doi:10.1016/j.gca.2007.12.004

Bowring, S. A., Grotzinger, J. P., Condon, D. J., Ramezani, J., Newall, M. J., Phillip, A., et al. (2007). Geochronological Constraints on the Chronostratigraphic Framework of the Neoproterozoic Huqf Supergroup, Sultanate of Oman. *Am. J. Sci.* 307, 1097–1145. doi:10.2475/10.2007.01

Boyd, E. S., Hamilton, T. L., and Peters, J. W. (2011). An Alternative Path for the Evolution of Biological Nitrogen Fixation. *Front. Microbio.* 2, 205. doi:10.3389/fmicb.2011.00205

Brasier, M. D. (1990). "Phosphogenic Events and Skeletal Preservation across the Precambrian-Cambrian Boundary Interval,". *Phosphorite Research and Development*. Editors A. J. G. Notholt and I. Jarvis (London: Geological society special publication), 52, 289–303. doi:10.1144/gsl.sp.1990.052.01.21

Brocks, J. J., Jarrett, A. J. M., Sirantoine, E., Hallmann, C., Hoshino, Y., and Liyanage, T. (2017). The Rise of Algae in Cryogenian Oceans and the Emergence of Animals. *Nature* 548, 578–581. doi:10.1038/nature23457

Brocks, J. J., and Schaeffer, P. (2008). Okenane, a Biomarker for Purple Sulfur Bacteria (Chromatiaceae), and Other New Carotenoid Derivatives from the 1640Ma Barney Creek Formation. *Geochimica et Cosmochimica Acta* 72, 1396–1414. doi:10.1016/j.gca.2007.12.006

Buchler, J. W., Eikelmann, G., Puppe, L., Rohbock, K., Schneehage, H. H., and Weck, D. (1971). Metallkomplexe mit Tetrapyrrol-Liganden, III. Darstellung von Metallkomplexen des Octaäthylporphins aus Metall-acetylacetonaten. *Justus Liebigs Ann. Chem.* 745, 135–151. doi:10.1002/jlac.19717450117

Canfield, D. E., Glazer, A. N., and Falkowski, P. G. (2010). The Evolution and Future of Earth's Nitrogen Cycle. *Science* 330, 192–196. doi:10.1126/science.1186120

Catling, D. C., Glein, C. R., Zahnle, K. J., and McKay, C. P. (2005). Why O2Is Required by Complex Life on Habitable Planets and the Concept of Planetary "Oxygenation Time". *Astrobiology* 5, 415–438. doi:10.1089/ast.2005.5.415

Chen, Y., Diamond, C. W., Stüeken, E. E., Cai, C., Gill, B. C., Zhang, F., et al. (2019). Coupled Evolution of Nitrogen Cycling and Redoxcline Dynamics on the Yangtze Block across the Ediacaran-Cambrian Transition. *Geochimica et Cosmochimica Acta* 257, 243–265. doi:10.1016/j.gca.2019.05.017

Chikaraishi, Y., Kashiyama, Y., Ogawa, N. O., Kitazato, H., Satoh, M., Nomoto, S., et al. (2008). A Compound-specific Isotope Method for Measuring the Stable Nitrogen Isotopic Composition of Tetrapyrroles. *Org. Geochem.* 39, 510–520. doi:10.1016/j.orggeochem.2007.08.010

Cohen, P. A., Knoll, A. H., and Kodner, R. B. (2009). Large Spinose Microfossils in Ediacaran Rocks as Resting Stages of Early Animals. *Proc. Natl. Acad. Sci.* 106, 6519–6524. doi:10.1073/pnas.0902322106

Cui, X., Liu, X.-L., Shen, G., Ma, J., Husain, F., Rocher, D., et al. (2020). Niche Expansion for Phototrophic Sulfur Bacteria at the Proterozoic-Phanerozoic Transition. *Proc. Natl. Acad. Sci. USA* 117, 17599–17606. doi:10.1073/pnas.2006379117

Falkowski, P. G., and Godfrey, L. V. (2008). Electrons, Life and the Evolution of Earth's Oxygen Cycle. *Phil. Trans. R. Soc. B* 363, 2705–2716. doi:10.1098/rstb.2008.0054

Ferris, F. G., Fyfe, W. S., and Beveridge, T. J. (1988). Metallic Ion Binding by Bacillus Subtilis: Implications for the Fossilization of Microorganisms. *Geol* 16, 149–152. doi:10.1130/0091-7613(1988)016<0149:mibbbs>2.3.co;2

Fike, D. A., Grotzinger, J. P., Pratt, L. M., and Summons, R. E. (2006). Oxidation of the Ediacaran Ocean. *Nature* 444, 744–747. doi:10.1038/nature05345

Fike, D. (2007). Carbon and Sulfur Isotopic Constraints on Ediacaran Biogeochemical Processes, Huqf Supergroup, Sultanate of Oman. PhD thesis. Cambridge, MA: Massachusetts Institute of Technology, 232.

French, K. L., Rocher, D., Zumberge, J. E., and Summons, R. E. (2015). Assessing the Distribution of Sedimentary C40carotenoids through Time. *Geobiology* 13, 139–151. doi:10.1111/gbi.12126

Garcia, A. K., McShea, H., Kolaczkowski, B., and Kaçar, B. (2020). Reconstructing the Evolutionary History of Nitrogenases: Evidence for Ancestral Molybdenum-Cofactor Utilization. *Geobiology* 18, 394–411. doi:10.1111/gbi.12381

Gorin, G. E., Racz, L. G., and Walter, M. R. (1982). Late Precambrian–Cambrian Sediments of the Huqf Group, Sultanate of Oman. *Am. Assoc. Pet. Geologists Bull.* 66, 2609–2627. doi:10.1306/03b5ac82-16d1-11d7-8645000102c1865d

Grice, K., Gibbison, R., Atkinson, J. E., Schwark, L., Eckardt, C. B., and Maxwell, J. R. (1996). Maleimides (1H-Pyrrole-2,5-Diones) as Molecular Indicators of Anoxygenic Photosynthesis in Ancient Water Columns. *Geochimica et Cosmochimica Acta* 60, 3913–3924. doi:10.1016/0016-7037(96)00199-8

Grice, K., Schaeffer, P., Schwark, L., and Maxwell, J. R. (1997). Changes in Palaeoenvironmental Conditions during Deposition of the Permian Kupferschiefer (Lower Rhine Basin, Northwest Germany) Inferred from Molecular and Isotopic Compositions of Biomarker Components. *Org. Geochem.* 26, 677–690. doi:10.1016/s0146-6380(97)00036-3

Grosjean, E., Adam, P., Connan, J., and Albrecht, P. (2004). Effects of Weathering on Nickel and Vanadyl Porphyrins of a Lower Toarcian Shale of the Paris Basin. *Geochimica et Cosmochimica Acta* 68, 789–804. doi:10.1016/s0016-7037(03)00496-4

Grosjean, E., Love, G. D., Stalvies, C., Fike, D. A., and Summons, R. E. (2009). Origin of Petroleum in the Neoproterozoic-Cambrian South Oman Salt Basin. *Org. Geochem.* 40, 87–110. doi:10.1016/j.orggeochem.2008.09.011

Grotzinger, J. P., Fike, D. A., and Fischer, W. W. (2011). Enigmatic Origin of the Largest-Known Carbon Isotope Excursion in Earth's History. *Nat. Geosci* 4, 285–292. doi:10.1038/ngeo1138

Gueneli, N., McKenna, A. M., Ohkouchi, N., Boreham, C. J., Beghin, J., Javaux, E. J., et al. (2018). 1.1-billion-year-old Porphyrins Establish a marine Ecosystem Dominated by Bacterial Primary Producers. *Proc. Natl. Acad. Sci. USA* 115, E6978–E6986. doi:10.1073/pnas.1803866115

Halm, H., Musat, N., Lam, P., Langlois, R., Musat, F., Peduzzi, S., et al. (2009). Co-occurrence of Denitrification and Nitrogen Fixation in a Meromictic lake, Lake Cadagno (Switzerland). *Environ. Microbiol.* 11, 1945–1958. doi:10.1111/j.1462-2920.2009.01917.x

Halverson, G. P., and Shields-Zhou, G. (2011). Chapter 4 Chemostratigraphy and the Neoproterozoic Glaciations. *Geol. Soc. Lond. Mem.* 36, 51–66. doi:10.1144/m36.4

Higgins, M. B., Robinson, R. S., Casciotti, K. L., McIlvin, M. R., and Pearson, A. (2008). A Method for Determining the Nitrogen Isotopic Composition of Porphyrins. *Anal. Chem.* 81, 184–192. doi:10.1021/ac8017185

Higgins, M. B., Robinson, R. S., Husson, J. M., Carter, S. J., and Pearson, A. (2012). Dominant Eukaryotic export Production during Ocean Anoxic Events Reflects the Importance of Recycled NH4+. *Proc. Natl. Acad. Sci.* 109, 2269–2274. doi:10.1073/pnas.1104313109

Higgins, M. B., Wolfe-Simon, F., Robinson, R. S., Qin, Y., Saito, M. A., and Pearson, A. (2011). Paleoenvironmental Implications of Taxonomic Variation Among δ15N Values of Chloropigments. *Geochimica et Cosmochimica Acta* 75, 7351–7363. doi:10.1016/j.gca.2011.04.024

Hoshino, Y., Poshibaeva, A., Meredith, W., Snape, C., Poshibaev, V., Versteegh, G. J. M., et al. (2017). Cryogenian Evolution of Stigmasteroid Biosynthesis. *Sci. Adv.* 3, e1700887. doi:10.1126/sciadv.1700887

Isaji, Y., Ogawa, N. O., Boreham, C. J., Kashiyama, Y., and Ohkouchi, N. (2020). Evaluation of δ13C and δ15N Uncertainties Associated with the Compound-specific Isotope Analysis of Geoporphyrins. *Anal. Chem.* 92, 3152–3160. doi:10.1021/acs.analchem.9b04843

Jiang, G., Zhang, S., Shi, X., and Wang, X. (2008). Chemocline Instability and Isotope Variations of the Ediacaran Doushantuo basin in South China. *Sci. China Ser. D-earth Sci.* 51, 1560–1569. doi:10.1007/s11430-008-0116-2

Johnston, D. T., Wolfe-Simon, F., Pearson, A., and Knoll, A. H. (2009). Anoxygenic Photosynthesis Modulated Proterozoic Oxygen and Sustained Earth's Middle Age. *Proc. Natl. Acad. Sci.* 106, 16925–16929. doi:10.1073/pnas.0909248106

Kennicutt, M. C., Bidigare, R. R., Macko, S. A., and Keeney-Kennicutt, W. L. (1992). The Stable Isotopic Composition of Photosynthetic Pigments and Related Biochemicals. *Chem. Geology. Isotope Geosci. section* 101, 235–245. doi:10.1016/0009-2541(92)90005-p

Knoll, A. H., Javaux, E. J., Hewitt, D., and Cohen, P. (2006). Eukaryotic Organisms in Proterozoic Oceans. *Phil. Trans. R. Soc. B* 361, 1023–1038. doi:10.1098/rstb.2006.1843

Koopmans, M. P., Köster, J., Van Kaam-Peters, H. M. E., Kenig, F., Schouten, S., Hartgers, W. A., et al. (1996). Diagenetic and Catagenetic Products of Isorenieratene: Molecular Indicators for Photic Zone Anoxia. *Geochimica et Cosmochimica Acta* 60, 4467–4496. doi:10.1016/s0016-7037(96)00238-4

Lewan, M. D. (1984). Factors Controlling the Proportionality of Vanadium to Nickel in Crude Oils. *Geochimica et Cosmochimica Acta* 48, 2231–2238. doi:10.1016/0016-7037(84)90219-9

Li, C., Love, G. D., Lyons, T. W., Fike, D. A., Sessions, A. L., and Chu, X. (2010). A Stratified Redox Model for the Ediacaran Ocean. *Science* 328, 80–83. doi:10.1126/science.1182369

LoosveldBell, R. A., and Terken, J. (1996). The Tectonic Evolution of interior Oman. *GeoArabia* 1, 28–51.

Love, G. D., Grosjean, E., Stalvies, C., Fike, D. A., Grotzinger, J. P., Bradley, A. S., et al. (2009). Fossil Steroids Record the Appearance of Demospongiae during the Cryogenian Period. *Nature* 457, 718–721. doi:10.1038/nature07673

Mackenzie, A. S., Patience, R. L., and Maxwell, J. R. (1981). "Molecular Changes and the Maturation of Sedimentary Organic Matter," in Proceedings of the Third Annual Karcher Symposium, Oklahoma, May 4 1979. Editors G. Atkinson and J. J. Zuckerman (Elsevier). doi:10.1016/b978-0-08-026179-9.50005-0

Macko, S. A., Fogel, M. L., Hare, P. E., and Hoering, T. C. (1987). Isotopic Fractionation of Nitrogen and Carbon in the Synthesis of Amino Acids by Microorganisms. *Chem. Geology. Isotope Geosci. section* 65, 79–92. doi:10.1016/0168-9622(87)90064-9

Madigan, M. T. (1995). "Microbiology of Nitrogen Fixation by Anoxygenic Photosynthetic Bacteria," in *Advances in Photosynthesis and Respiration. Anoxygenic Photosynthetic Bacteria*. Editors R. E. Blankenship, M. T. Madigan, and C. E. Bauer (Springer), Vol. 2, 915–928 .

Mattes, B. W., and Conway Morris, S. (1990). "Carbonate/evaporite Deposition in the Late Precambrian - Early Cambrian Ara Formation of Southern Oman,". *The Geology and Tectonics of the Oman Region*. Editor A. H. F. Robertson (London: Geological Society [London] Special Publication), 49, 617–636. doi:10.1144/gsl.sp.1992.049.01.37

Mills, D. B., Ward, L. M., Jones, C., Sweeten, B., Forth, M., Treusch, A. H., et al. (2014). Oxygen Requirements of the Earliest Animals. *Proc. Natl. Acad. Sci.* 111, 4168–4172. doi:10.1073/pnas.1400547111

Minagawa, M., and Wada, E. (1984). Stepwise Enrichment of 15N along Food Chains: Further Evidence and the Relation between δ15N and Animal Age. *Geochimica et Cosmochimica Acta* 48, 1135–1140. doi:10.1016/0016-7037(84)90204-7

Naeher, S., and Grice, K. (2015). Novel 1 H -Pyrrole-2,5-Dione (Maleimide) Proxies for the Assessment of Photic Zone Euxinia. *Chem. Geology.* 404, 100–109. doi:10.1016/j.chemgeo.2015.03.020

Naeher, S., Schaeffer, P., Adam, P., and Schubert, C. J. (2013). Maleimides in Recent Sediments - Using Chlorophyll Degradation Products for Palaeoenvironmental Reconstructions. *Geochimica et Cosmochimica Acta* 119, 248–263. doi:10.1016/j.gca.2013.06.004

Nomoto, S., Kozono, M., Mita, H., and Shimoyama, A. (2001). Structural Elucidation of an Oxidation Product of Sedimentary Porphyrins by One-Pot Synthesis of 3-methylphthalimide. *Bcsj* 74, 1975–1976. doi:10.1246/bcsj.74.1975

Ohkouchi, N., Nakajima, Y., Ogawa, N. O., and Chikaraishi, Y. (2007). Carbon Isotopic Composition of the Tetrapyrrole Nucleus in Chloropigments from a saline Meromictic lake: A Mechanistic View for Interpreting the Isotopic Signature of Alkyl Porphyrins in Geological Samples *Org. Geochem* 39, 521–531 .

Ohkouchi, N., Nakajima, Y., Okada, H., Ogawa, N. O., Suga, H., Oguri, K., et al. (2005). Biogeochemical Processes in the saline Meromictic Lake Kaiike, Japan: Implications from Molecular Isotopic Evidences of Photosynthetic Pigments. *Environ. Microbiol.* 7, 1009–1016. doi:10.1111/j.1462-2920.2005.00772.x

Ohkouchi, N., and Takano, Y. (2014). "Organic Nitrogen: Sources, Fates, and Chemistry," in *Treatise on Geochemistry. Organic Geochemistry*. Editors P. Falkowski and K. Freeman. second edition, 12, 251–289. doi:10.1016/b978-0-08-095975-7.01015-9

Pehr, K., Love, G. D., Kuznetsov, A., Podkovyrov, V., Junium, C. K., Shumlyanskyy, L., et al. (2018). Ediacara Biota Flourished in Oligotrophic and Bacterially Dominated marine Environments across Baltica. *Nat. Commun.* 9, 1807. doi:10.1038/s41467-018-04195-8

Planavsky, N. J., Rouxel, O. J., Bekker, A., Lalonde, S. V., Konhauser, K. O., Reinhard, C. T., et al. (2010). The Evolution of the marine Phosphate Reservoir. *Nature* 467, 1088–1090. doi:10.1038/nature09485

Ramseyer, K., Amthor, J. E., Matter, A., Pettke, T., Wille, M., and Fallick, A. E. (2013). Primary Silica Precipitate at the Precambrian/Cambrian Boundary in the South Oman Salt basin, Sultanate of Oman. *Mar. Pet. Geology.* 39, 187–197. doi:10.1016/j.marpetgeo.2012.08.006

Raven, J. (2009). Contributions of Anoxygenic and Oxygenic Phototrophy and Chemolithotrophy to Carbon and Oxygen Fluxes in Aquatic Environments. *Aquat. Microb. Ecol.* 56, 177–192. doi:10.3354/ame01315

Reinhard, C. T., Planavsky, N. J., Gill, B. C., Ozaki, K., Robbins, L. J., Lyons, T. W., et al. (2017). Evolution of the Global Phosphorus Cycle. *Nature* 541, 386–389. doi:10.1038/nature20772

Reinhard, C. T., Planavsky, N. J., Robbins, L. J., Partin, C. A., Gill, B. C., Lalonde, S. V., et al. (2013). Proterozoic Ocean Redox and Biogeochemical Stasis. *Proc. Natl. Acad. Sci.* 110, 5357–5362. doi:10.1073/pnas.1208622110

Robinson, R. S., Kienast, M., Albuquerque, A. L., Altabet, M., Contreras, S., Dubois, N., et al. (2012). A Review of Nitrogen Isotopic Alteration in marine Sediments. *Paleoceanography* 27, PA4203. doi:10.1029/2012pa002321

Rothman, D. H., Hayes, J. M., and Summons, R. E. (2003). Dynamics of the Neoproterozoic Carbon Cycle. *Pnas* 100, 8124–8129. doi:10.1073/pnas.0832439100

Roussel, A., Cui, X., and Summons, R. E. (2020). Biomarker Stratigraphy in the Athel Trough of the South Oman Salt Basin at the Ediacaran Cambrian Boundary. *Geobiology* 18, 663–681. doi:10.1111/gbi.12407

Sachs, J. P. (1997). Nitrogen Isotope Ratios in Chlorophyll and the Origin of Eastern Mediterranean Sapropels. Ph.D. Thesis. Cambridge, MA: Massachusetts Institute of Technology/Woods Hole Oceanographic Institute.

Sachs, J. P., Repeta, D. J., and Goericke, R. (1999). Nitrogen and Carbon Isotopic Ratios of Chlorophyll from marine Phytoplankton. *Geochimica et Cosmochimica Acta* 63, 1431–1441. doi:10.1016/s0016-7037(99)00097-6

Sachs, J. P., and Repeta, D. J. (1999). Oligotrophy and Nitrogen Fixation during Eastern Mediterranean Sapropel Events. *Science* 286, 2485–2488. doi:10.1126/science.286.5449.2485

Schröder, S., Grotzinger, J. P., Amthor, J. E., and Matter, A. (2005). Carbonate Deposition and Hydrocarbon Reservoir Development at the Precambrian-Cambrian Boundary: The Ara Group in South Oman. *Sediment. Geology.* 180, 1–28. doi:10.1016/j.sedgeo.2005.07.002

Sigman, D. M., Karsh, K. L., and Casciotti, K. L. (2009). "Nitrogen Isotopes in the Ocean," in *Encyclopedia of Ocean Sciences*. Editors J. H. Steele, S. A. Thorpe, and K. K. Turekian (Oxford: Academic Press), 40–54. doi:10.1016/b978-012374473-9.00632-9

Sperling, E. A., Halverson, G. P., Knoll, A. H., Macdonald, F. A., and Johnston, D. T. (2013). A basin Redox Transect at the Dawn of Animal Life. *Earth Planet. Sci. Lett.* 371-372, 143–155. doi:10.1016/j.epsl.2013.04.003

Sperling, E. A., Wolock, C. J., Morgan, A. S., Gill, B. C., Kunzmann, M., Halverson, G. P., et al. (2015). Statistical Analysis of Iron Geochemical Data Suggests Limited Late Proterozoic Oxygenation. *Nature* 523, 451–454. doi:10.1038/nature14589

Stolper, D. A., Love, G. D., Bates, S., Lyons, T. W., Young, E., Sessions, A. L., et al. (2017). Paleoecology and Paleoceanography of the Athel Silicilyte, Ediacaran-Cambrian Boundary, Sultanate of Oman. *Geobiology* 15, 401–426. doi:10.1111/gbi.12236

Stueeken, E. E., Zaloumis, J., Meixnerova, J., and Buick, R. (2017). Differential Metamorphic Effects on Nitrogen Isotopes in Kerogen Extracts and Bulk Rocks. *Geochimica et Cosmochimica Acta* 217, 80–94.

Thomazo, C., Ader, M., and Philippot, P. (2011). Extreme 15N-Enrichments in 2.72-Gyr-Old Sediments: Evidence for a Turning point in the Nitrogen Cycle. *Geobiology* 9, 107–120. doi:10.1111/j.1472-4669.2011.00271.x

van Gemenden, H., and Mas, J. (1995). in *Anoxygenic Photosynthetic Bacteria*. Editors R. E. Blankenship, M. T. Madigan, and C. Bauer (Springer), 49–85 .

van Maldegem, L. M., Sansjofre, P., Weijers, J. W. H., Wolkenstein, K., Strother, P. K., Wörmer, L., et al. (2019). Bisnorgammacerane Traces Predatory Pressure and the Persistent Rise of Algal Ecosystems after Snowball Earth. *Nat. Commun.* 10, 476. doi:10.1038/s41467-019-08306-x

Verne-Mismer, J., Ocampo, R., Callot, H. J., and Albrecht, P. (1986). Identification of a Novel C33 DPEP Petroporphyrin from Boscan Crude Oil : Evidence for Geochemical Reduction of Carboxylic Acids. *Tetrahedron Lett.* 27, 5257–5260. doi:10.1016/s0040-4039(00)85184-9

Vo, J., Inwood, W., Hayes, J. M., and Kustu, S. (2013). Mechanism for Nitrogen Isotope Fractionation during Ammonium Assimilation by Escherichia Coli K12. *Proc. Natl. Acad. Sci.* 110, 8696–8701. doi:10.1073/pnas.1216683110

Wang, D., Ling, H.-F., Struck, U., Zhu, X.-K., Zhu, M., He, T., et al. (2018a). Coupling of Ocean Redox and Animal Evolution during the Ediacaran-Cambrian Transition. *Nat. Commun.* 9, 2575. doi:10.1038/s41467-018-04980-5

Wang, W., Guan, C., Zhou, C., Peng, Y., Pratt, L. M., Chen, X., et al. (2017). Integrated Carbon, Sulfur, and Nitrogen Isotope Chemostratigraphy of the Ediacaran Lantian Formation in South China: Spatial Gradient, Ocean Redox Oscillation, and Fossil Distribution. *Geobiology* 15, 552–571. doi:10.1111/gbi.12226

Wang, X., Jiang, G., Shi, X., Peng, Y., and Morales, D. C. (2018b). Nitrogen Isotope Constraints on the Early Ediacaran Ocean Redox Structure. *Geochimica et Cosmochimica Acta* 240, 220–235. doi:10.1016/j.gca.2018.08.034

Werner, R. A., and Brand, W. A. (2001). Referencing Strategies and Techniques in Stable Isotope Ratio Analysis. *Rapid Commun. Mass. Spectrom.* 15, 501–519. doi:10.1002/rcm.258

Zhang, J., Fan, T., Zhang, Y., Lash, G. G., Li, Y., and Wu, Y. (2017). Heterogenous Oceanic Redox Conditions through the Ediacaran-Cambrian Boundary Limited the Metazoan Zonation. *Sci. Rep.* 7, 8550. doi:10.1038/s41598-017-07904-3

Zhang, X., Sigman, D. M., Morel, F. M. M., and Kraepiel, A. M. L. (2014). Nitrogen Isotope Fractionation by Alternative Nitrogenases and Past Ocean Anoxia. *Proc. Natl. Acad. Sci. USA* 111, 4782–4787. doi:10.1073/pnas.1402976111

Conflict of Interest: NS was employed by Vir Biotechnology, Inc.,

The remaining authors declare that the research was conducted in the absence of any commercial or financial relationships that could be construed as a potential conflict of interest

Publisher's Note: All claims expressed in this article are solely those of the authors and do not necessarily represent those of their affiliated organizations, or those of the publisher, the editors and the reviewers. Any product that may be evaluated in this article, or claim that may be made by its manufacturer, is not guaranteed or endorsed by the publisher.

frontiers in Earth Science

ORIGINAL RESEARCH
published: 23 December 2021
doi: 10.3389/feart.2021.787386

Nitrogen Isotope Discrepancy Between Primary Producers and Sediments in an Anoxic and Alkaline Lake

Pierre Cadeau[1], Magali Ader[1], Didier Jézéquel[1,2], Carine Chaduteau[1], Gérard Sarazin[1], Cécile Bernard[3] and Christophe Leboulanger[4]*

[1]*Université de Paris, Institut de physique du globe de Paris, CNRS, Paris, France,* [2]*UMR CARRTEL, INRAE & Université Savoie Mont Blanc, Annecy, France,* [3]*UMR 7245, MCAM, CNRS-MNHN, Muséum National d'Histoire Naturelle, Paris, France,* [4]*MARBEC, Université de Montpellier IRD CNRS Ifremer, Sète, France*

Nitrogen isotope compositions ($\delta^{15}N$) in sedimentary rocks are extensively used to investigate the biogeochemical nitrogen cycle through geological times. This use relies on the observation that, in modern continental platforms and anoxic basins, surface sediments faithfully record the $\delta^{15}N$ of primary producers, assuming that it was similar in the past. Over Earth's history, however, surface environments experienced profound changes, including the transition of ammonium-dominated to nitrate-dominated waters and the transition from exclusively microbial ecosystems to ecosystems including multicellularity, which make modern environments significantly different compared to earlier ones, potentially invalidating the fundamental assumption that surface sediments faithfully record the $\delta^{15}N$ of primary producers. In order to improve our understanding of the nitrogen isotopic information contained in the early Earth's sedimentary rock record, we investigate here the nitrogen isotope systematics in a microbial, nitrate free and ammonium-rich modern system, the Dziani Dzaha Lake. In this modern system, the $\delta^{15}N$ of the reduced dissolved inorganic nitrogen (i.e., NH_4^+ and NH_3) in the water column is close to ~7‰ . $\delta^{15}N$ of suspended particulate matter (SPM) show a similar average value in surface waters (i.e., where SPM is massively composed of active primary producers), but increases up to 14‰ in the deeper part of the water column during periods when it is enriched in dissolved reduced species (i.e., CH_4, H_2S/HS^- and NH_4^+/NH_3). Surface sediments $\delta^{15}N$, with values comprised between 10 and 14 ‰, seem to preferentially record these positive isotopic signatures, rather than those of active primary producers. We propose here that the observed isotopic pattern is mainly linked to the assimilation of ammonium strongly enriched in ^{15}N by isotope exchange with ammonia under basic conditions. Although ammonium assimilation seems here to be responsible for a significant isotopic enrichment due to the basic conditions, in neutral anoxic environments inhabited by similar microbial ecosystems, this process may also significantly impact the $\delta^{15}N$ of primary producers towards more negative values. This would have strong implications for our interpretation of the Precambrian sedimentary record as this finding challenges one the fundamental hypotheses underlying the use of sedimentary

OPEN ACCESS

Edited by:
Philippe Claeys,
Vrije Universiteit Brussel, Belgium

Reviewed by:
William Patrick Gilhooly III,
Indiana University—Purdue University Indianapolis, United States
Ichiro Tayasu,
Research Institute for Humanity and Nature, Japan

***Correspondence:**
Pierre Cadeau
pierre.cadeau@gmail.com

Specialty section:
This article was submitted to Geochemistry, a section of the journal Frontiers in Earth Science

Received: *30 September 2021*
Accepted: *26 November 2021*
Published: *23 December 2021*

Citation:
Cadeau P, Ader M, Jézéquel D, Chaduteau C, Sarazin G, Bernard C and Leboulanger C (2021) Nitrogen Isotope Discrepancy Between Primary Producers and Sediments in an Anoxic and Alkaline Lake. Front. Earth Sci. 9:787386. doi: 10.3389/feart.2021.787386

$\delta^{15}N$ in paleo-oceanographic reconstructions, *i.e.* that surface sediments faithfully record the $\delta^{15}N$ of active primary producers in the photic zone.

Keywords: nitrogen isotopes, Dziani Dzaha, ammonium assimilation, pH, basic condition, alkaline lake, 15N enrichment

INTRODUCTION

In continental margins and modern anoxic basins the nitrogen isotope compositions ($\delta^{15}N$) of surface sediments faithfully record the $\delta^{15}N$ of the nitrogen species assimilated by primary producers in surface waters (*e.g.* Thunell et al., 2004; Sigman et al., 2009; Robinson et al., 2012). In these environments, water column or sediment diagenesis processes were shown to have a limited impact on the primary producer's $\delta^{15}N$ (Lehmann et al., 2002; Chen et al., 2008; Mobius et al., 2010; Mobius, 2013), while in the oxic deep oceans ^{15}N enrichments compared to the primary producers have been reported in both surface sediments and particles sinking in the deep waters (i.e., 2–5‰ increase, Altabet and François, 1994; Mobius et al., 2010; Mobius et al., 2011; Robinson et al., 2012).

In the last decades, numerous studies have been conducted to improve our understanding of the biogeochemical nitrogen cycle and the diverse metabolic processes that regulate it (e.g., Sigman et al., 2009; Mobius, 2013; Bruner et al., 2013; Zhang et al., 2014). Overall, they show that nitrogen speciation and $\delta^{15}N$ in modern systems, including the open ocean (NO_3^- and on average 5 ‰, respectively), are mainly controlled by the balance in the dominant nitrogen metabolic pathways in the ocean (i.e., nitrogen fixation and denitrification), which are closely tied to the nutrient supply and water column redox structure (e.g., Galbraith et al., 2008; Sigman et al., 2009; Quan et al., 2013; Bruner et al., 2013; Mobius, 2013). It is based on these observations in modern systems that the sedimentary $\delta^{15}N$ record has been used to infer the evolution of both the biogeochemical nitrogen cycle and water column redox structures through geological times (e.g., see reviews in Ader et al., 2016; Stueken et al., 2016).

Yet, in contrast to modern environments where the main nitrogen species is nitrate, early Earth's environments must have been mainly dominated by ammonium (NH_4^+), at least before the ocean oxygenation during late Archean/early Proterozoic times (e.g., Beaumont and Robert, 1999; Canfield et al., 2010; Luo et al., 2018; Mettam et al., 2019; Yang et al., 2019). This has several implications for our understanding of the nitrogen isotope record of these time periods. First, ammonium assimilation is a well-known process associated with a large isotopic fractionation that may generate strongly ^{15}N-depleted organic matter (Pennock et al., 1996; Sigman et al., 2009; Vo et al., 2013). Although it was proposed to explain negative $\delta^{15}N$ values for some Cretaceous anoxic events (Higgins et al., 2012) or Archean and Proterozoic successions (Papineau et al., 2009; Mettam et al., 2019), there is still no known modern analogue to validate this scenario because their dissolved ammonium content is often limited, quantitatively assimilated or beyond reach of primary producers (e.g., Fuchsman et al., 2008). Second, the sediments of modern or past basic lacustrine environments often have strongly positive isotopic signatures (≥10 ‰) that have been interpreted as resulting from the NH_4^+/NH_3 chemical and isotope equilibrium and volatilization of the ^{15}N-depleted NH_3 (e.g., Talbot and Johannessen, 1992; Menzel et al., 2013; McLauchlan et al., 2013; Stueken et al., 2015). However, in-depth studies of the nitrogen isotope systematics in such modern systems are still lacking, preventing a comprehensive documentation of the processes controlling the elevated $\delta^{15}N$ values of sediments, including those related to the quality of preservation in the sedimentary record of the primary producer's signature. In order to explore this question further, we investigate here the nitrogen isotope systematics in a newly identified, and so far unique, microbial dominated, nitrate free and ammonium-rich modern lacustrine system, the Dziani Dzaha Lake.

MATERIALS AND METHODS

Study Site

The Dziani Dzaha Lake is a shallow tropical volcanic crater lake located on the Petite Terre Island of Mayotte (Comoros Archipelago, Indian Ocean, **Figure 1**). Its surface area is close to 2.36×105 m^2 and it is separated from the nearby seashore by a 220-m thick crater wall. The volcanic crater is approximately 1 km in diameter and 50–100 m high, resulting in a very restricted lake watershed. The average depth of the Dziani Dzaha water column is about 3 m with a narrow depression reaching 18 m depth, probably related to the phreatomagmatic eruption at the origin of this lake (i.e., between 9 and 4 ka, Zinke et al., 2003).

The Dziani Dzaha water column has a combination of physical, chemical and biological features that are atypical for a modern lacustrine system, which have been previously recently documented and are summarized here. Its waters probably originated from seawater and are now characterized by high salinity (i.e., ranging from 34 to 71 psu), strong alkalinity (i.e., ranging from 0.1 to 0.2 M), elevated pH value (i.e., comprised between 9 and 9.5), and very high primary productivity (i.e., 8 gC m^{-2} day^{-1} (Leboulanger et al., 2017; Sarazin et al., 2020). The lake ecosystem is dominated by microorganisms with a dense and perennial bloom of two photosynthetic species [i.e., *Picocystis salinarum* (Chlorophyta) and *Arthrospira fusiformis* (Cyanobacteria), Bernard et al., 2019]. The water column is permanently anoxic below *ca.* 1.5 m depth, with the anoxic water being periodically euxinic (i.e., presence of H_2S and HS^-) (e.g., Sarazin et al., 2020). The SO_4^{2-} content is relatively low compared to seawater (<3 mM, Sarazin et al., 2020). Organic matter in the anoxic waters is remineralized through both sulfate reduction, as evidenced by the periodic total consumption of SO_4^{2-}, when the lake becomes euxinic, and

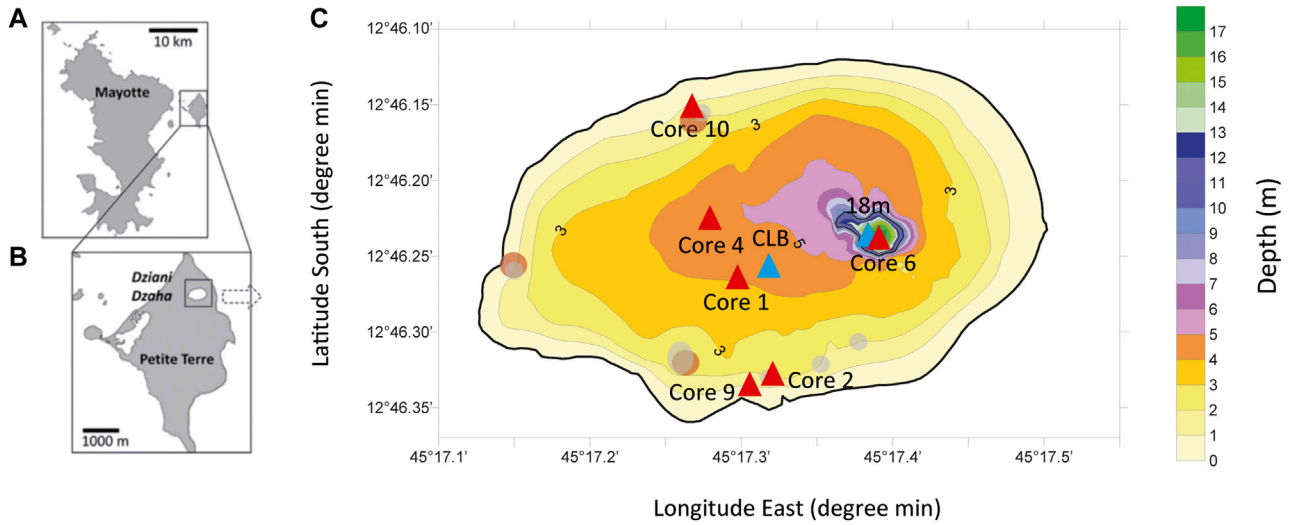

FIGURE 1 | Location **(A,B)** and bathymetric map **(C)** of the Dziani Dzaha. Water column (blue triangles) and sediment cores (red triangles) sampling locations.

methanogenesis, as indicated by the high concentration of CH_4 dissolved in the water column that degasses into the atmosphere (Cadeau et al., 2020). Finally, the water column is nitrate-free while the reduced dissolved nitrogen species (i.e., NH_4^+/NH_3) accumulate in the deeper part of the Dziani Dzaha lake (Bernard et al., 2019).

The physical and chemical structure of the Dziani Dzaha water column as well as the biological organism's distribution within it (mostly dominated by cyanobacteria), are closely related to the seasonal variations (Hugoni et al., 2018; Bernard et al., 2019; Sarazin et al., 2020). The water column is periodically stratified with a halocline at about 2 m depth due a decrease in surface water salinity driven by rainy season precipitation (**Figure 2**). A permanent chemocline was present at ca. 14 m depth in the depression. During the stratified period (**Figures 2**, **3**), salinity above the halocline was within 35–45 psu, alkalinity was close to 0.1 M, pH was close to 9.5, SO_4^{2-} was close to 3 mM, and only traces of NH_4^+/NH_3 were observed (<0.03 mM). Below the halocline the salinity and alkalinity increased up to 70 psu and 0.2 M, respectively, pH decreased to a value close to 9, no sulfates were observed, and reduced species accumulated. It is worth noting here while that HS^-/H_2S concentrations and CH_4 concentrations increased sharply at 2 m depth, i.e., across the halocline, up to 6 and 2 mM, respectively, and remained relatively constant down to the bottom, NH_4^+/NH_3 concentration increased in two steps, one up to 0.4 mM at 3 m depth (i.e., 1 m below the halocline) and another one up to 6 mM below the deep chemocline. Above the 2 m-depth halocline, the diversity was dominated by photosynthetic microorganisms, while below it, it was dominated by a dense and diverse population of archaea and heterotrophic bacteria (Hugoni et al., 2018). During the non-stratified period most of the physical, chemical and biological parameters were constant with depth down to the deep chemocline at 14 m depth, except for the dissolved oxygen that was only present down to a maximum of about 1 m depth (**Figures 2**, **3**). The salinity was close to 65 psu, the alkalinity close to 0.14 M, the pH close to 9.2, the SO_4^{2-} content close to 3 mM, NH_4^+/NH_3 content was lower than 0.03 mM, and the planktonic biomass was dominated by photosynthetic microorganisms. The biological and physico-chemical parameters of the waters underlying the deep chemocline during non-stratified periods resembled strongly to stratified periods, albeit with even higher concentrations of reduced species (Sarazin et al., 2020).

Methods

As shown by the above site description, many physical, chemical and biological parameters have been published previously [pH, T, Salinity, O_2, NH_4^+/NH_3 in Sarazin et al., 2020; SO_4^{2-}, H_2S/HS^- in Sarazin et al., 2020; Chlorophyll a before 2012 in Leboulanger et al., 2017; carbon biomass associated to photosynthetic cell abundance in Bernard et al., 2019]. In this section we will thus describe only the sampling and the analytical methods used to acquire the new data presented here; chlorophyll a (for samples taken since 2012) and C/N and nitrogen isotope compositions.

Sampling were performed at the end of the rainy season (April) in 2012, 2014 and 2015, and at the end of the dry season (October-November) in 2011, 2014 and 2015. The "CLB" and "18 m" names refer to the water column stations where samples were collected, throughout 4.5 m depth and 18 m depth respectively, as shown on the **Figure 1**. Water samples were collected using a horizontal 1.2 L Niskin bottles along a vertical profile at the CLB and 18 m stations (**Figure 1**) every 0.25–0.50 m depth for the first 4.5 m of water column and either every 50 cm across the deep chemocline (between 13 and 15 m depth), or every 1–2 m between 5 and 13 m depth where no significant variation was observed on the profiles from the multiparameter probe. An aliquot of sampled water for each depth was filtered onto precombusted (450°C–4 h) 47 mm Whatman GF/F glass fibre filters (0.7 µm porosity) to recover suspended particulate

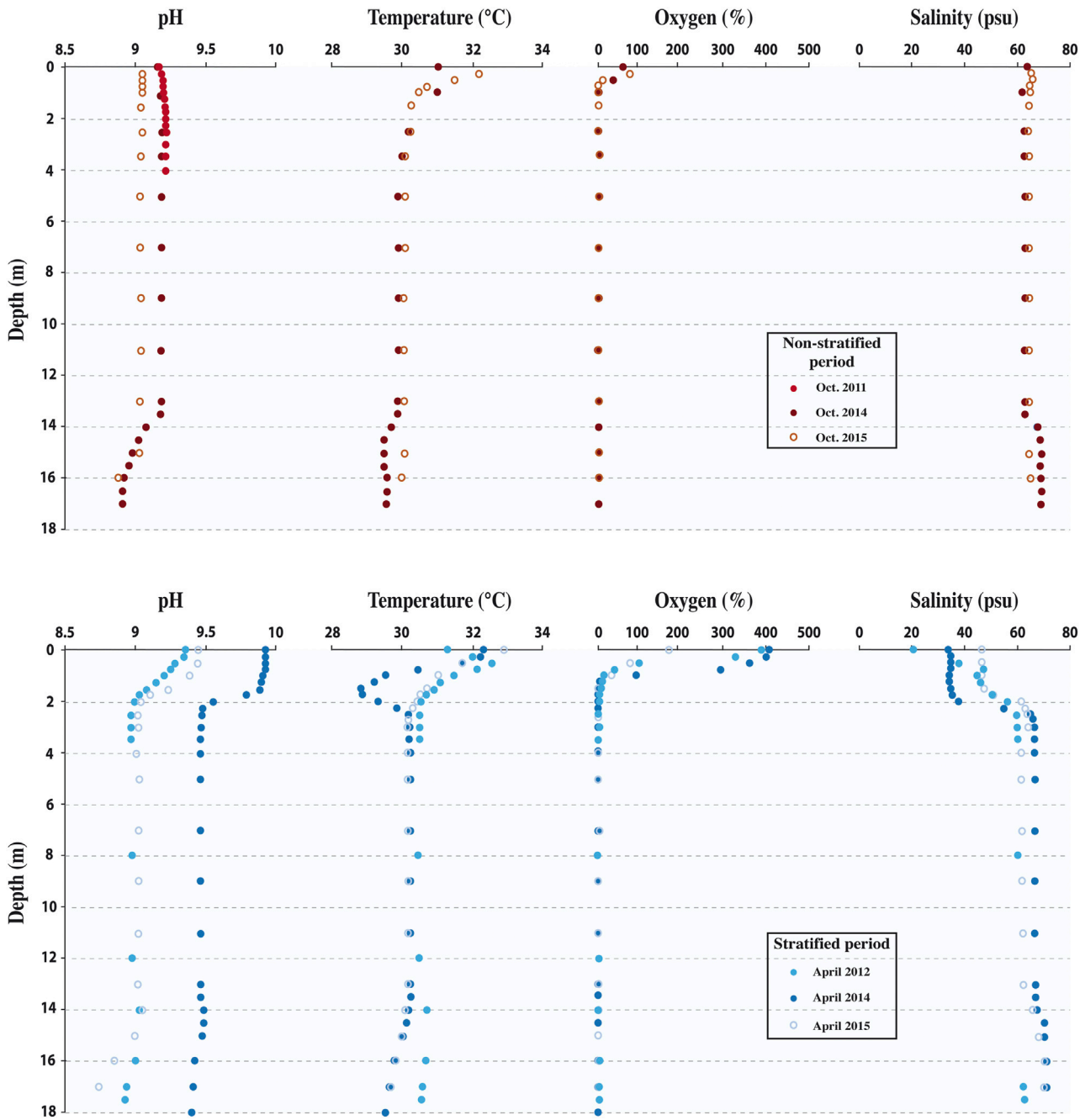

FIGURE 2 | Vertical profiles of physical and chemical parameters in the Dziani Dzaha water column. pH, temperature (°C), O_2 (%) and Salinity (psu) profiles during the non-stratified (2011, 2014 and 2015 in **top panel**) and stratified (2012, 2014 and 2015 in **bottom panel**) period (data from Sarazin et al., 2020).

matter for chlorophyll a, C/N and $\delta^{15}N$ analyses. Several sediment cores serially numbered from the first survey were collected at different depths (**Figure 1**), freeze-dried, rinsed with deionized water, centrifuged three times, and finally freeze-dried and crushed down to <80 µm.

The concentration of chlorophyll a was analyzed after a two-steps extraction, the extract being then filtered and the filtrate analyzed spectrophotometrically at 400–750 nm (Leboulanger et al., 2017). The concentration of chlorophyll a was calculated according to Camacho et al. (2009). Nitrogen isotope and C/N measurements were performed on the same samples as the carbon isotope analysis reported in Cadeau et al. (2020) (i.e., suspended particles and sediments), but during a different run dedicated to the $\delta^{15}N$ analyses and on bulk samples to avoid alterations of $\delta^{15}N$ signal during the acid decarbonatation required for $\delta^{13}C_{org}$ analyses (Brodie et al., 2011). Nitrogen isotope measurements of NH_4^+/

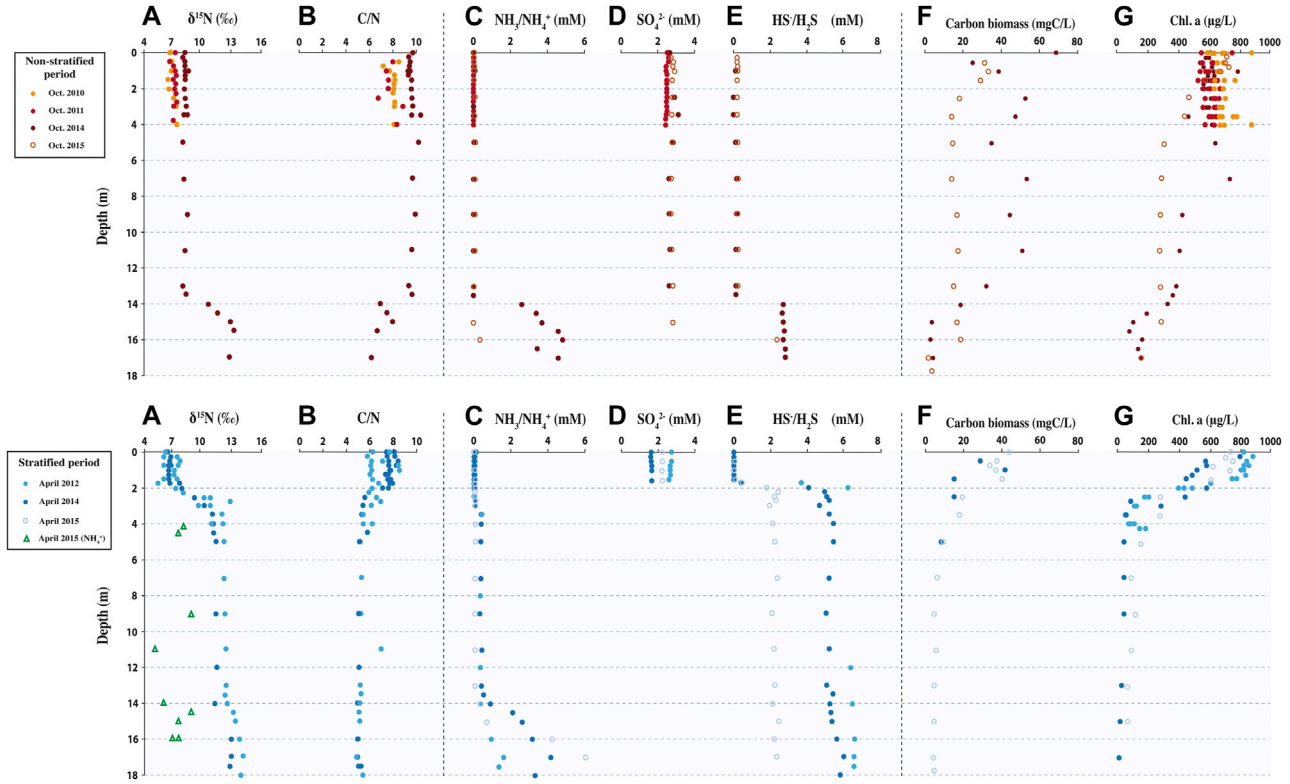

FIGURE 3 | Compilation of biogeochemical data in the Dziani Dzaha water column, including $\delta^{15}N_{SPM}$ and $\delta^{15}N$ of NH_4^+ **(A)**, C/N ratio **(B)**, (NH_4^+/NH_3) (data from Sarazin et al., 2020) **(C)**, (SO_4^{2-}) and (HS^-/H_2S) **(D,E)** (data from Sarazin et al., 2020), carbon biomass of the two main photosynthetic microorganisms (data from Bernard et al., 2019) **(F)**, and chlorophyll a (data this study and Leboulanger et al., 2017) **(G)**, during the non-stratified (2011, 2014 and 2015 in **top panel**) and stratified (2012, 2014 and 2015 in **bottom panel**) period.

NH_3 were performed using the ammonium diffusion method (Sebilo et al., 2004), which is based on the conversion of NH_4^+ to NH_3 by pH adjustments and subsequent trapping of the released NH_3 onto glass fibre filter. Nitrogen species retained on glass fibre filter (i.e., suspended particles, dissolved nitrogen trapped onto $(NH_4)_2SO_4$ form) and sediment samples were analyzed using a Flash EA1112 elemental analyser coupled to a Thermo Finnigan Delta^{plus} XP mass spectrometer via a Conflo IV interface (Thermo Fisher Scientific, Waltham, MA, United States). Nitrogen isotope ratios were calibrated against four internal standards of organic-rich soil or sediment included in the sample sequence and previously calibrated against the certified IAEA-N1 and IAEA-N2 international standards. The nitrogen isotopic signatures are expressed as ‰ relative to air with a reproducibility of ±0.3‰ (1σ). Routine replicate measurements on standards had internal deviations of ±0.15‰ (2σ) for $\delta^{15}N$ values, and less than 4% of the measured value for the nitrogen content.

RESULTS

In the Dziani Dzaha water column, the $\delta^{15}N$ values of suspended particulate matter ($\delta^{15}N_{SPM}$) ranged from 5.6 to 14.1‰, with an average value of 9.1 ± 2.6 ‰ (**Figure 3A**). When the lake was stratified, the $\delta^{15}N_{SPM}$ showed an average value of 6.9 ± 0.7‰ above the halocline that increased sharply across the halocline to an average value of 12.2 ± 1.1‰ below 2.5 m depth (**Figure 3A**). When the lake was non-stratified, a similar pattern was observed, but with a $\delta^{15}N_{SPM}$ average value of 7.4 ± 0.6‰ from the surface to the permanent deep chemocline at 14 m depth (**Figure 3A**) and an average value of 12.2 ± 1.1 ‰ below it. Sediment $\delta^{15}N$ values ranged from 11.0 to 12.9‰ with an average value of 12.1 ± 0.6‰ for the sediment core C6 (collected at 18 m depth, **Figure 1**); from 8.3 to 12.5‰ with an average value of 10.9 ± 1.0‰ for the cores C1 and C4 (collected at 4 m depth, **Figure 1**); and from 4.3 to 12.1‰ with an average value of 8.9 ± 2.0‰ for the cores C2, C9 and C10 (collected at 1 m depth, **Figures 1**, **4**). For all cores, sediment $\delta^{15}N$ values were similar to the high $\delta^{15}N_{SPM}$ observed below the halocline or deep chemocline depending on the water column stratification, than those observed in NH_4^+/NH_3 or surface water suspended particles (**Figure 3A**). The C/N ratio of suspended particulate matter seemed to be correlated to the $\delta^{15}N_{SPM}$ (**Figure 5**), with an average value of 5.5 ± 0.8 when the $\delta^{15}N_{SPM}$ was close to 12‰, and an average value of 7.8 ± 1.3 when the $\delta^{15}N_{SPM}$ was close to 7‰, in both stratified or non-stratified periods (**Figures 3B**, **5**). Finally, during the stratified period in 2015, the $\delta^{15}N$ of dissolved NH_4^+/NH_3 showed an average value of 7.7 ± 0.9 ‰ (**Figure 3A**). It is worth noting here that the depth of variations in $\delta^{15}N$ and C/N values are

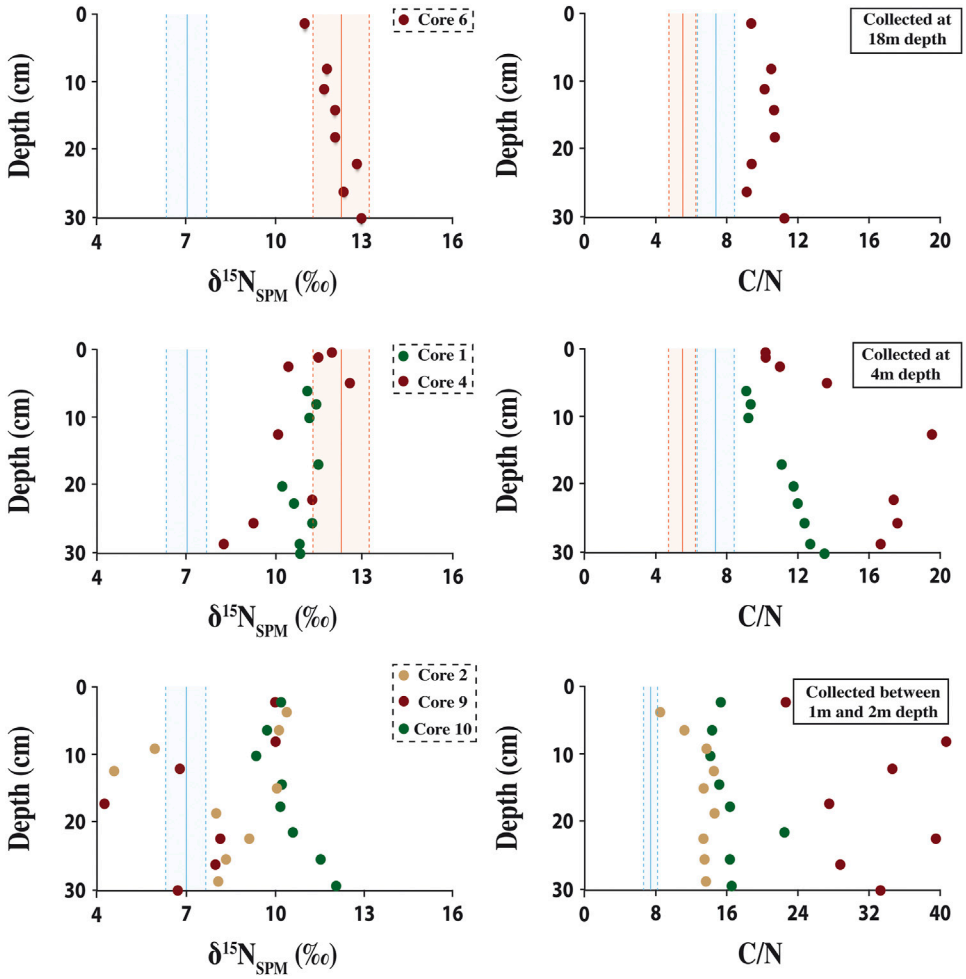

FIGURE 4 | Nitrogen isotope compositions and C/N ratio in the Dziani Dzaha surface sediment. The dashed blue areas represent the $\delta^{15}N_{SPM}$ and C/N average values observed in the water column above 2 or 14 m depth during stratified or non-stratified period, respectively. The dashed red areas represent the $\delta^{15}N_{SPM}$ and C/N average values observed in the water column below the mentioned depths.

more closely tied the depth of the halocline and chemocline than to those of the variations in NH_4^+/NH_3 concentration (**Figure 3C**).

Chlorophyll a content ranged from 6 to 875 µg/L within the water column (**Figure 3G**). When the lake was stratified, chlorophyll a content showed an average value of 704 ± 158 µg/L above the halocline, and decreased strongly to an average value of 115 ± 91 µg/L below 2 m-depth. When the lake was non-stratified, a similar pattern was observed with an average value of chlorophyll a content of 635 ± 75 µg/L from the surface to 4 m-depth, a decrease between 4 and 14 m-depth to an average value of 334 ± 53 µg/L, and a another below 14 m-depth to an average value of 158 ± 77 µg/L.

DISCUSSION

The three main results of this study are that, 1) the $\delta^{15}N$ of primary producers (given by the $\delta^{15}N_{SPM}$ from surface water during both stratified and non-stratified period) is on average of 7 ‰, 2) the $\delta^{15}N_{SPM}$ values are on average 5‰ higher in the euxinic (i.e., H_2S/HS^--rich) waters (i.e., below 2 m or 14 m depths during stratified periods or non-stratified periods, respectively), and 3) the sedimentary $\delta^{15}N$ values are closer to the $\delta^{15}N_{SPM}$ of euxinic bottom waters than to those of primary producers.

$\delta^{15}N$ values as high as 7‰ for dissolved inorganic nitrogen and primary producers in lakes have most often been interpreted as resulting from denitrification, anammox and/or NH_3 volatilization (e.g., Talbot and Johannessen, 1992; Lehmann et al., 2004; Bratkic et al., 2012; Menzel et al., 2013; Wenk et al., 2013; Wenk et al., 2014). Given that the Dziani Dzaha is both redox-stratified and alkaline, any combination these processes could account for the $\delta^{15}N$ average value of 7‰ in primary producers and NH_4^+/NH_3 (only measured in April 2015 for dissolved inorganic nitrogen). Addressing this question more thoroughly would require additional data, such as NH_3 fluxes at the water/air interface, or denitrification and anammox activities and is beyond the scope of this study. We will thus focus here on the possible processes that could account for the marked increase

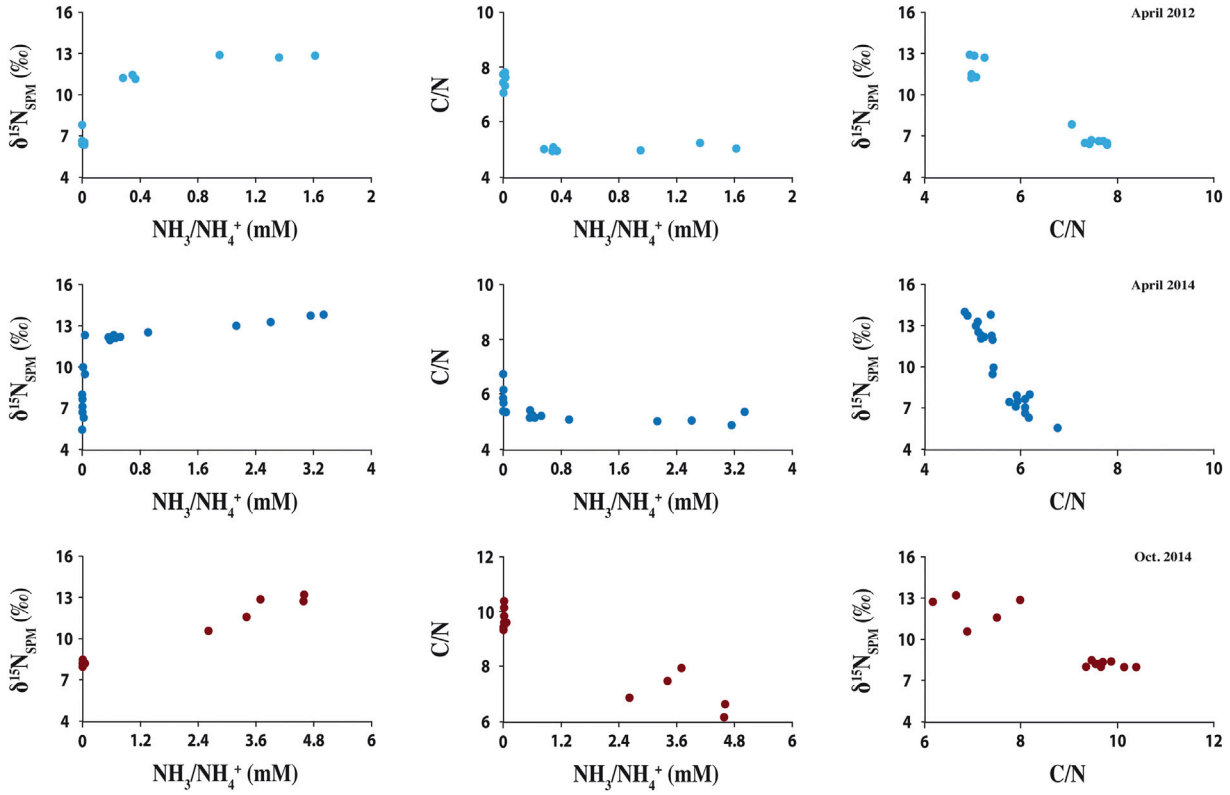

FIGURE 5 | Cross-plots of $\delta^{15}N_{SPM}$ vs. (NH_4^+/NH_3), C/N ratio *vs*. (NH_4^+/NH_3), and $\delta^{15}N_{SPM}$ vs. C/N ratio in the Dziani Dzaha water column during the stratified (2012 and 2014) and non-stratified (2014) periods at the 18 m water column station.

in $\delta^{15}N_{SPM}$ values in the euxinic waters and their transfer to the sediment.

Several processes are typically considered as being involved in modifying the $\delta^{15}N$ signature of primary producers during particulate matter sinking and/or deposition in surface sediments. They encompass 1) contribution of external sources of nitrogen to the particulate matter or sediment, 2) alteration of the $\delta^{15}N$ of primary producers during remineralization and 3) contribution of organic matter from non-photosynthetic organisms living in the water column or sediment, such as heterotrophs or chemolithotrophs. As discussed below, we conclude that none of these processes seem to account for the N-isotope pattern observed in the Dziani Dzaha. Instead, we propose that it results from NH_4^+ assimilation by the main organisms that compose the biomass in euxinic waters, i.e., cyanobacteria, together with a bias in the preservation of these N-enriched cyanobacteria.

Contribution of External Sources of ^{15}N-Enriched Nitrogen to the Euxinic Waters

Two types of external N-sources can be envisaged: an influx of dissolved nitrogen-rich fluids and/or a detrital input of terrestrial organic matter. An influx of dissolved nitrogen-rich fluid (from seawater or hydrothermal fluids) is unlikely based on physical and chemical measurements in the water column, no on-going water infiltrations were identified and, from a water balance point of view, this lake seems to be endoreic (Sarazin et al., 2020). Moreover, seawater entrance would only marginally affect the dissolved nitrogen budget and its $\delta^{15}N$ because the concentration of dissolved nitrate in the Indian Ocean (i.e., 5–15 µM up to 200 m depth, NOAA, 2017) are quite low compared to the concentration of dissolved reduced nitrogen species in euxinic waters of the Dziani Dzaha (i.e., mM range **Figure 2**) and the nitrate $\delta^{15}N$ in the Indian Ocean (~+6‰) is very close to that of the lake (~+7 ‰). For an external dissolved nitrogen source to contribute significantly to the lake NH_4^+/NH_3 budget, it would thus need to be sourced from NH_4^+/NH_3-rich hydrothermal fluids. However, that would still not explain the fact that in the euxinic and NH_4^+/NH_3-rich waters the $\delta^{15}N$ value of suspended particles and sediments are more positive than the dissolved NH_4^+/NH_3.

The supply of detrital organic matter from the surrounding catchment is also very unlikely to be responsible for the higher $\delta^{15}N_{SPM}$ values of the euxinic waters and $\delta^{15}N_{sed}$ values. The carbon and nitrogen contents and isotopic compositions of seven kinds of higher plants and soil sampled in the lake watershed (**Table 1**) exhibited $\delta^{15}N$ values that were lower than the lake primary producers (<7‰), except for the rush sample with a $\delta^{15}N$ value close to 9 ‰. This high value is best explained by the fact that rushes grow in the shallow waters of the lakeshore and are probably assimilating ^{15}N-enriched nitrogen from the lake

TABLE 1 | $\delta^{13}C$, $\delta^{15}N$ and C/N of organic terrestrial sources (Angiosperms leafs and soil humus) closely surrounding the Dziani Dzaha Lake.

Source sample	$\partial^{13}C_{org}$ (±0.2‰)	$\partial^{15}N_{org}$ (±0.2‰)	C/N
Ipomea sp. (Convolvulaceae, morning glory)	–25.7	6.3	14.5
Cocos nucifera (Arecaceae, coconut tree)	–25.5	1.7	47.1
Acacia sp. (Fabaceae)	–28.0	3.3	14.3
Juncus sp. (Juncaceae, rush)	–24.8	9.4	42.5
Musa sp. (Musaceae, banana tree)	–28.0	3.4	20.7
Undefined shrub	–26.4	5.6	26.1
Humus	–28.0	2.8	18.5

Rushes are developing mostly on the west and south shores of the lake, together with morning glory. A mix of cultivated (bananas, coconut trees) and wild plants forms a continous vegetation curtain around the lake.

sediment pore waters. In addition, the measured plants $\delta^{13}C$ and C/N values are significantly lower and higher, respectively, than those of suspended particulate matter and surface sediments (**Figures 3**, **4** and **Table 1**). A contribution of detrital organic matter to the suspended particulate matter or sediment would thus decrease their $\delta^{15}N$, rather than increase it. It would also decrease their $\delta^{13}C_{org}$ and increase their C/N, as observed in some samples of the shallow cores (i.e., C2 and C9, **Figure 4**), which we accordingly explain by a contribution of detrital organic matter.

Alteration of Particulate Matter $\delta^{15}N$ During Their Mineralisation

Isotopic alteration due to organic matter mineralisation in modern settings was relatively well investigated (e.g., Lehmann et al., 2002; Robinson et al., 2012; Tesdal et al., 2013; Katsev and Crowe, 2015). The extent of organic matter degradation as well as the early diagenesis processes, and subsequently the extent of isotopic alteration of the primary nitrogen isotope signature, appear to depend on the oxygen exposure time, water depth and organic matter availability (e.g., Lehmann et al., 2002; Thunell et al., 2004; Robinson et al., 2012). So far, increases in both $\delta^{15}N_{SPM}$ and $\delta^{15}N_{sed}$ of the order of a few per mil have only been reported in sinking particles in the deep ocean and have been interpreted as resulting from extensive organic matter remineralisation under oxic conditions (e.g., Lehmann et al., 2002; Gaye et al., 2009; Mobius et al., 2010; Mobius et al., 2011). It seems unlikely however that this process is applicable to the shallow and anoxic Dziani Dzaha for two reasons. First, ^{15}N enrichment in sinking particles and in the surface sediments through organic matter mineralisation is usually associated with an increase in C/N ratio, as nitrogen is preferentially lost over carbon (Lehmann et al., 2002; Fenchel et al., 2012). In the Dziani Dzaha, as shown in **Figure 4**, the increase in $\delta^{15}N_{SPM}$ is not associated with an increase in the C/N ratio but rather decreased with depth from approximately 7 to 5. Second, to our knowledge, such an isotopic increase with depth has never been reported so far in lacustrine systems (e.g., Lehmann et al., 2004; Menzel et al., 2013; McLauchlan et al., 2013) or in modern anoxic marine environments (e.g., Thunell et al., 2004; Fulton et al., 2012). In these systems, when $\delta^{15}N$-depths profiles were available, increases in the $\delta^{15}N$ of dissolved N species or suspended particles have been reported but they are either spatially limited to the vicinity of the chemocline (e.g., Cariaco Basin, Thunell et al., 2004; Black Sea, Fry et al., 1991; Lugano Lake, Wenk et al., 2014) or temporally limited to water column mixing events (e.g., Kinneret Lake, Hadas et al., 2009). They have been interpreted as resulting from denitrification and/or anammox together with assimilation of the enriched NO_3^- and/or NH_4^+ by chemoautotrophic organisms (Deutsch et al., 2001; Voss et al., 2001; Sigman et al., 2003; Thunell et al., 2004). These isotope signatures are however not transferred to the sinking particulate matter or the surface sediments, which both record the primary producer $\delta^{15}N$ values (Thunell et al., 2004).

Contribution of Organic Matter From Non-photosynthetic Organisms Living in the Euxinic Waters

The decrease in C/N ratio within euxinic waters coincides with a strong change in biological diversity (Hugoni et al., 2018). In terms of abundance, the biological communities are dominated by two primary producers (the picoeukaryote *Picocystis salinarum* and the cyanobacterium *Arthrospira fusiformis*) above the halocline at 2 m depth during stratified periods, or above the deep chemocline at 14 m depth during non-stratified periods, and by bacteria and archaea in euxinic waters below the halocline or deep chemocline (Leboulanger et al., 2017; Hugoni et al., 2018). The C/N value close to 7 in surface waters is consistent with the predominantly cyanobacterial biomass (Godfrey and Glass, 2011). Indeed, previous work on continuous cultures of *Arthrospira fusiformis* from Lake Chitu (Ethiopia) reported that the C/N ratio was stable in this species, around 6.25 (Kebede and Ahlgren 1996). The generally lower C/N values in the euxinic waters, sometimes approaching 5, are consistent with a predominantly bacterial or archaeal biomass (Muller, 1977; They et al., 2017). From there, it is tempting to imagine that both the decrease in C/N and the increase in $\delta^{15}N_{SPM}$ observed in the euxinic waters could be linked to a higher proportion of bacterial and archaea biomass, which would be characterized by a more positive $\delta^{15}N_{SPM}$ values than the cyanobacterial biomass. However, even if in euxinic waters bacteria and archaea are predominant in terms of number of individuals compared to cyanobacteria (Hugoni et al., 2018), biomass estimations from cells abundance measurements and biovolumes show that cyanobacteria remain by far the main constituent of the biomass (**Figure 3F**) and are responsible of most of the primary production in the lake (Leboulanger et al.,

2017). Therefore, in spite of their coincidence with a strong biodiversity change, the combined C/N decrease and $\delta^{15}N_{SPM}$ increase in euxinic waters are not directly related to it.

Ammonium Assimilation by Cyanobacteria in the Euxinic and Aphotic Bottom Waters

In this section, we investigate the possibility that the combined C/N decrease and $\delta^{15}N_{SPM}$ increase in the euxinic waters reflect NH_4^+ assimilation and storage by cyanobacteria (**Figure 3**). As previously shown in modern alkaline anoxic settings (e.g., Lonar Lake, Menzel et al., 2013), pH controls the dissolved reduced nitrogen speciation through the reaction of NH_4^+ dissociation to NH_3 (i.e., **Eq. 1** below, Li et al., 2012):

$$NH_4^+ = NH_3 + H^+ \quad (1)$$

At isotope equilibrium the isotope exchange between NH_4^+ and NH_3 is associated with a strong isotopic fractionation (i.e., of 45 ‰ at 23°C, Li et al., 2012), forming ^{15}N-depleted NH_3 and ^{15}N-enriched NH_4^+. Considering an average temperature of 30°C in the NH_4^+-rich part of the Dziani Dzaha water column (Sarazin et al., 2020; **Figure 2**), and based on the equations proposed in Li et al. (2012), the pKa of acid-base couple (**Eq. 1**) is of 9.09 in the Dziani Dzaha conditions. Considering this and the minimum and maximum pH values observed in the NH_4^+-rich and euxinic waters of the Dziani Dzaha (i.e., close to 9 in April 2012 and 9.5 in April 2014), between 45 and 72% of the NH_4^+ is dissociated in NH_3, enriching NH_4^+ in ^{15}N by about 20‰ and 32‰ , respectively at pH 9 and 9.5, compared to the total dissolved inorganic nitrogen. These values represent a qualitative estimation of the dissolved NH_4^+ isotopic signatures range in equilibrium with ammonia, which strongly depends on variations of both pH values and total dissolved inorganic nitrogen $\delta^{15}N$.

Arthrospira fusiformis, the main cyanobacteria species that constitute most of the biomass in the Dziani Dzaha, is known to harbour aerotopes (gas vacuoles) that enhance cell buoyancy, and cyanophycin-rich granules increasing nitrogen intracellular storage capacity (Cellamare et al., 2018). These characteristics are consistent with a vertical migration process where cells increase in density during photosynthesis in lit layer, which makes them sink in the NH_4^+/NH_3-rich water where they store nitrogen as cyanophycin or in phycobilisomes. When they reach aphotic waters, photosynthesis stops and respiration reduces their cell density, allowing them to move upward (Carey et al., 2012). However, when the lake is stratified and its deep waters are euxinic, this process could eventually lead to a death trap due the combination of the sulfide toxicity. The fact that the ^{15}N-enrichment and C/N decrease of suspended particles is limited to the euxinic waters at times of stratification could thus reflect the assimilation of this ^{15}N-enriched NH_4^+ by cyanobacteria, and their entrapment below the halocline. This would also be compatible with the delayed increase in NH_3/NH_4^+ concentration in the first meter below the halocline (compared to CH_4 and $H_2S^+/H\ S^-$) where cyanobacteria might still be active enough to assimilate NH_4^+ efficiently. In addition, $\delta^{15}N_{SPM}$ in the euxinic and NH_3/NH_4^+-rich waters shows an average value close to 12 ‰ (**Figure 3**), which represents an isotopic enrichment of only about 5 ‰ compared to the $\delta^{15}N_{SPM}$ observed in surface water despite the estimated $\delta^{15}N$ values of dissolved NH_4^+ in the NH_3/NH_4^+-rich waters comprised between 20‰ and 32 ‰. This is most likely related to the fact that NH_4^+ assimilation favours ^{14}N uptake (Pennock et al., 1996; Vo et al., 2013) and that only up to approximately 29% of the total nitrogen in the ^{15}N-enriched cyanobacterial biomass originated from assimilation of ^{15}N-enriched NH_4^+ according to the change in C/N ratio. Finally, $\delta^{15}N_{SPM}$ values in the euxinic waters vary by only 1 ‰ between 2012 and 2014 in spite of significant the variations of pH and NH_4^+/NH_3 dissolved concentrations which impact of the $\delta^{15}N$ of NH_4^+ may have balanced each other. Unfortunately, this cannot be assessed further here as in the absence of measurement of the total dissolved inorganic nitrogen $\delta^{15}N$ in 2012 and 2014.

Preservation Bias Towards ^{15}N-Enriched Cyanobacteria

Ammonium assimilation and storage by cyanobacteria, beyond accounting for the $\delta^{15}N_{SPM}$ increase in the euxinic waters, also explains the fact that the sediment $\delta^{15}N$ is biased towards the $\delta^{15}N$ of ^{15}N-enriched cyanobacteria, even at shallow depths where the water column remains oxic. The high buoyancy of cyanobacteria that allows them to move vertically in the water column when they are alive and active, also prevents them from sinking quickly to the surface sediment when they are dead. This is consistent with the fact that although the Dziani Dzaha is a highly productive and shallow lacustrine system exhibiting highly favourable conditions for the preservation of organic matter (e.g., Leboulanger et al., 2017), the proportion of the net primary production preserved in the sediments is only of 2.9% (Cadeau et al., 2020), e.g., only slightly higher than the maximum value estimated in the stratified and euxinic Black Sea basin (i.e., 0.5–1.8%, Karl and Knauer., 1991).

As shown by the chlorophyll a and biomass data (**Figures 3F,G**), when the water column is sulfide-free (i.e., up to 2 or 14 m depth according to the stratified or non-stratified period, respectively), most cyanobacteria are active and the amount of biomass is stable with depth. Their high buoyancy, together with the wind agitation of the surface waters that propagates down to the lake bottom when it is non-stratified (as shown by the similarity between surface and bottom water temperatures and their high amplitude temporal changes, Sarazin et al., 2020), probably limits the export of organic matter to the sediment. Preferential organic matter export would thus probably occur from the bottom waters when the lake is density stratified and the mixing dynamics of bottom waters strongly reduced (as shown by the very dissimilar surface and bottom water temperatures with constant temperatures in bottom waters unaffected by the high frequency changes in surface temperatures, Sarazin et al., 2020), allowing the dead or weakened cyanobacteria to sink in the water column and accumulate in the sediment.

In the shallow parts of the lake (i.e., up to 2 m depth), cyanobacteria remain active all year long, even when they settle down onto the water/sediment interface as suggested by observation of a green surface layer in the flocs resting on the top of the shallow sediment cores. Since the water column is never

euxinic and NH_4^+-rich at shallow depth, we would not expect shallow surface sediments to be ^{15}N-enriched, and yet they are. It is most probable that the interstitial waters of the colloidal floc and surface sediments are probably anoxic and NH_3/NH_4^+-rich and that ^{15}N-enriched NH_4^+ is assimilated by cyanobacteria when they reach the floc, explaining the increase observed in the sedimentary $\delta^{15}N$ values even at shallow sites.

Finally, NH_4^+ incorporation into clay minerals could also contribute to modifying the sediment $\delta^{15}N$ towards more positive values (Muller, 1977). Indeed, the shallowest sediment cores (e.g., C10) contain half the amount of organic matter than those collected at 4 and 18 m depths (i.e., C4 and C6 respectively) (Milesi et al., 2019), and a higher clay mineral (e.g., saponite) content (Milesi et al., 2019). Pore waters pH being basic within the first 30 cm studied here (Milesi et al., 2019; Milesi et al., 2020), NH_4^+ is also ^{15}N-enriched by isotope equilibrium with NH_3. An incorporation of ^{15}N-enriched ammonium into clay minerals by substituting for K^+ could make the sediments isotopically heavier in all sediment cores (Muller, 1977; Stueken et al., 2019), especially into the core C10 presenting a higher clay mineral content (Milesi et al., 2019). Still, although this process cannot be ignored, it is probably not significant compared to the nitrogen input from primary producers (at the surface or deep in the water column), because organic matter content in all sediment cores remains significant and the proportion of ammonium potentially incorporated into the clay mineral fraction would represent only a small fraction of the overall clay mineral content.

Nitrogen isotopic signatures recorded in the Dziani Dzaha surface sediments would then result from a combination of 1) the cyanobacterial initial biomass with its original $\delta^{15}N$ acquired from surface waters, 2) their nitrogen storage compartments with more positive $\delta^{15}N$ values acquired through ^{15}N-enriched ammonium assimilation in the euxinic part of the water column, in the floc or in the sediments interstitial waters, and possibly in a lesser extent 3) some abiotic incorporation of ^{15}N-enriched ammonium into authigenic silicates.

Implication for $\delta^{15}N$ Interpretations

As previously suggested, albeit for a different reason, these results confirm that basic pH conditions have a strong control on the sedimentary nitrogen isotopic signature, which hence represents an useful tool to track such geological settings over times (e.g., Stueken et al., 2019). However to date, the mechanisms envisioned to explain the overall ^{15}N enrichment of sediment in modern or past basic lakes are NH_4^+ isotope equilibrium with NH_3 coupled to NH_3 volatilization into the atmosphere and/or denitrification or anammox (e.g., Menzel et al., 2013; Stueken et al., 2015; Stueken et al., 2019; Stueken et al., 2020). Our results demonstrate that additional processes to those commonly used to explain these high values can contribute to increase the sedimentary $\delta^{15}N$. Indeed, in the Dziani Dzaha Lake a significant isotopic ^{15}N enrichment is observed at depths within the water column and/or directly within surface sediments. We propose here that it is mainly due to ^{15}N-enriched NH_4^+ assimilation by cyanobacteria either in the deep-water column or in surface sediments. The most important aspect of this result is that the primary producer $\delta^{15}N$ values observed in the surface water of the Dziani Dzaha Lake are not well recorded in surface sediments. This represents a strong contradiction with one of the main assumptions underlying the use of nitrogen isotope compositions as a tool for the reconstruction of the past nitrogen cycle: i.e., that sediment $\delta^{15}N$ values record those acquired by primary producers, themselves recording the $\delta^{15}N$ value of the nitrogen species assimilated in the photic zone (e.g., Ader et al., 2016). This hypothesis is well established for all previously studied modern continental platforms or anoxic basins, which are usually characterised by high export production, low oxygen content and high organic matter preservation (e.g., Pride et al., 1999; Altabet et al., 1999; Emmer and Thunell, 2000; Thunell and Kepple, 2004; Thunell et al., 2004). But our results show that it may not apply to ammonium replete environments or paleo-environments of the Precambrian, which are thought to have been inhabited by dominantly microbial ecosystems (e.g., Butterfield., 2015), in which cyanobacteria were responsible for the bulk of the primary productivity.

Depending on the water pH, the ability of cyanobacteria to assimilate ammonium when sinking in the water column may have various impacts on their initial $\delta^{15}N$. Although under basic settings, the large isotopic fractionation associated with NH_4^+ dissociation into NH_3 leads to ^{15}N enrichment through the assimilation of ^{15}N-enriched NH_4^+, NH_4^+ assimilation is associated with an isotopic fractionation that favours ^{14}N and is proportional to the NH_4^+ concentration (Pennock et al., 1996; Vo et al., 2013). Hence, under the neutral condition (i.e., without NH_4^+ dissociation into NH_3), NH_4^+ assimilation could modify the cyanobacteria $\delta^{15}N$ towards more negative isotopic values, leading, if ignored, to an underestimation of the assimilated nitrogen $\delta^{15}N$ in such settings. For instance, in the Dziani Dzaha Lake the total dissolved nitrogen $\delta^{15}N$ in the water column (i.e., NH_4^+ and NH_3) exhibits an isotopic value close to 7‰. If the pH values in the Dziani Dzaha were neutral, NH_4^+ assimilation could have modified the $\delta^{15}N$ of primary producers towards negative values. These findings require further consideration about the reliability of paleoenvironmental evidences provided by the $\delta^{15}N$ in such stratified and NH_4^+-rich settings.

CONCLUSION

The Dziani Dzaha is an atypical modern lacustrine system in which specific biological (e.g., predominantly cyanobacterial biomass) and chemical (e.g., low O_2, high NH_3/NH_4^+, euxinia and high pH) features appear to significantly modify both the C/N ratio and the nitrogen isotopic signature of primary producers during their export to the sediments.

Here we propose that this pattern is due to the assimilation and storage of ^{15}N-enriched NH_4^+ by cyanobacteria as they sink through the euxinic part of the water column and settle in the surface sediments. This observation challenges the basic assumption that systematically underlies the use of this

isotopic tool in paleoenvironmental reconstructions: i.e., that sediment $\delta^{15}N$ values record those that the primary producers have acquired in the photic zone. Although atypical compared to modern environments, the Dziani Dzaha features are likely representative of the past, especially before the advent of multicellular organisms and the oxygenation of the atmosphere and the ocean during the Proterozoic (Logan et al., 1995; Lenton et al., 2014; Lyons et al., 2014; Butterfield, 2015). While in the Dziani Dzaha case the basic pH conditions are responsible for an isotopic enrichment of the nitrogen isotopic composition of organic matter, the same process in a neutral environment would lead to a ^{15}N-depletion. Hence, more generally, NH_4^+ assimilation by cyanobacteria while they sink through an anoxic and NH_4^+-rich water column may shift the isotopic signatures of the sinking particulate matter to more positive or negative isotopic values than those initially acquired in surface waters, depending on the pH of the environment considered. This could have significant implications for the interpretation of $\delta^{15}N$ in the sedimentary record and hence for our understanding of the evolution of the nitrogen cycle over geological time.

DATA AVAILABILITY STATEMENT

The original contributions presented in the study are included in the article/Supplementary Material, further inquiries can be directed to the corresponding author.

AUTHOR CONTRIBUTIONS

MA and CL designed the study and supervised PC PhD thesis. DJ, CC, and MA performed ammonium isotopic analyses. PC performed all other isotopic analyses and took the lead in the interpretation and writing the original draft. All authors contributed to at least one fieldtrip mission and provided critical feedback in shaping both the research results and the manuscript.

REFERENCES

Ader, M., Thomazo, C., Sansjofre, P., Busigny, V., Papineau, D., Laffont, R., et al. (2016). Interpretation of the Nitrogen Isotopic Composition of Precambrian Sedimentary Rocks: Assumptions and Perspectives. *Chem. Geology.* 429, 93–110. doi:10.1016/j.chemgeo.2016.02.010

Altabet, M. A., and Francois, R. (1994). Sedimentary Nitrogen Isotopic Ratio as a Recorder for Surface Ocean Nitrate Utilization. *Glob. Biogeochem. Cycles* 8 (1), 103–116. doi:10.1029/93gb03396

Altabet, M. A., Pilskaln, C., Thunell, R., Pride, C., Sigman, D., Chavez, F., et al. (1999). The Nitrogen Isotope Biogeochemistry of Sinking Particles from the Margin of the Eastern North Pacific. *Deep Sea Res. Oceanographic Res. Pap.* 46 (4), 655–679. doi:10.1016/s0967-0637(98)00084-3

Beaumont, V., and Robert, F. (1999). Nitrogen Isotope Ratios of Kerogens in Precambrian Cherts: a Record of the Evolution of Atmosphere Chemistry? *Precambrian Res.* 96 (1-2), 63–82. doi:10.1016/s0301-9268(99)00005-4

Bernard, C., Escalas, A., Villeriot, N., Agogué, H., Hugoni, M., Duval, C., et al. (2019). Very Low Phytoplankton Diversity in a Tropical saline-alkaline lake, with Co-dominance of Arthrospira Fusiformis (Cyanobacteria) and Picocystis Salinarum (Chlorophyta). *Microb. Ecol.* 78 (3), 603–617. doi:10.1007/s00248-019-01332-8

Bratkič, A., Šturm, M., Faganeli, J., and Ogrinc, N. (2012). Semi-annual Carbon and Nitrogen Isotope Variations in the Water Column of Lake Bled, NW Slovenia. *Biogeosciences* 9 (1), 1–11. doi:10.5194/bg-9-1-2012

Brodie, C. R., Casford, J. S., Lloyd, J. M., Leng, M. J., Heaton, T. H., Kendrick, C. P., et al. (2011). Evidence for Bias in C/N, δ13C and δ15N Values of Bulk Organic Matter, and on Environmental Interpretation, from a lake Sedimentary Sequence by Pre-analysis Acid Treatment Methods. *Quat. Sci. Rev.* 30 (21-22), 3076–3087. doi:10.1016/j.quascirev.2011.07.003

Brunner, B., Contreras, S., Lehmann, M. F., Matantseva, O., Rollog, M., Kalvelage, T., et al. (2013). Nitrogen Isotope Effects Induced by Anammox Bacteria. *Proc. Natl. Acad. Sci.* 110 (47), 18994–18999. doi:10.1073/pnas.1310488110

Butterfield, N. J. (2015). Early Evolution of the Eukaryota. *Palaeontology* 58 (1), 5–17. doi:10.1111/pala.12139

Cadeau, P., Jézéquel, D., Leboulanger, C., Fouilland, E., Le Floc'h, E., Chaduteau, C., et al. (2020). Carbon Isotope Evidence for Large Methane Emissions to the Proterozoic Atmosphere. *Sci. Rep.* 10 (1), 18186. doi:10.1038/s41598-020-75100-x

Camacho, C., Coulouris, G., Avagyan, V., Ma, N., Papadopoulos, J., Bealer, K., et al. (2009). BLAST+: Architecture and Applications. *BMC bioinformatics* 10 (1), 421–429. doi:10.1186/1471-2105-10-421

Canfield, D. E., Glazer, A. N., and Falkowski, P. G. (2010). The Evolution and Future of Earth's Nitrogen Cycle. *science* 330 (6001), 192–196. doi:10.1126/science.1186120

Carey, C. C., Ibelings, B. W., Hoffmann, E. P., Hamilton, D. P., and Brookes, J. D. (2012). Eco-physiological Adaptations that Favour Freshwater Cyanobacteria in a Changing Climate. *Water Res.* 46 (5), 1394–1407. doi:10.1016/j.watres.2011.12.016

Cellamare, M., Duval, C., Drelin, Y., Djediat, C., Touibi, N., Agogué, H., et al. (2018). Characterization of Phototrophic Microorganisms and Description of New Cyanobacteria Isolated from the saline-alkaline Crater-lake Dziani Dzaha (Mayotte, Indian Ocean). *FEMS Microbiol. Ecol.* 94 (8), fiy108. doi:10.1093/femsec/fiy108

Chen, F., Zhang, L., Yang, Y., and Zhang, D. (2008). Chemical and Isotopic Alteration of Organic Matter during Early Diagenesis: Evidence from the Coastal Area Off-Shore the Pearl River Estuary, south China. *J. Mar. Syst.* 74 (1-2), 372–380. doi:10.1016/j.jmarsys.2008.02.004

Deutsch, C., Gruber, N., Key, R. M., Sarmiento, J. L., and Ganachaud, A. (2001). Denitrification and N2fixation in the Pacific Ocean. *Glob. Biogeochem. Cycles* 15 (2), 483–506. doi:10.1029/2000gb001291

Emmer, E., and Thunell, R. C. (2000). Nitrogen Isotope Variations in Santa Barbara Basin Sediments: Implications for Denitrification in the Eastern Tropical North Pacific during the Last 50,000 Years. *Paleoceanography* 15 (4), 377–387. doi:10.1029/1999pa000417

Fenchel, T., Blackburn, H., King, G. M., and Blackburn, T. H. (2012). *Bacterial Biogeochemistry: The Ecophysiology of mineral Cycling*. Cambridge: Academic Press.

Fry, B., Jannasch, H. W., Molyneaux, S. J., Wirsen, C. O., Muramoto, J. A., and King, S. (1991). Stable Isotope Studies of the Carbon, Nitrogen and Sulfur Cycles in the Black Sea and the Cariaco Trench. Deep Sea Research Part A. *Deep Sea Res. A. Oceanographic Res. Pap.* 38, S1003–S1019. doi:10.1016/s0198-0149(10)80021-4

Fuchsman, C. A., Murray, J. W., and Konovalov, S. K. (2008). Concentration and Natural Stable Isotope Profiles of Nitrogen Species in theBlack Sea. *Mar. Chem.* 111 (1-2), 90–105. doi:10.1016/j.marchem.2008.04.009

Fulton, J. M., Arthur, M. A., and Freeman, K. H. (2012). Black Sea Nitrogen Cycling and the Preservation of Phytoplankton δ15N Signals during the Holocene. *Glob. Biogeochem. Cycles* 26 (2), 1–15. doi:10.1029/2011gb004196

Galbraith, E. D., Sigman, D. M., Robinson, R. S., and Pedersen, T. F. (2008). Nitrogen in Past marine Environments. *Nitrogen Mar. Environ.* 2, 1497–1535. doi:10.1016/b978-0-12-372522-6.00034-7

Gaye, B., Wiesner, M. G., and Lahajnar, N. (2009). Nitrogen Sources in the South China Sea, as Discerned from Stable Nitrogen Isotopic Ratios in Rivers, Sinking Particles, and Sediments. *Mar. Chem.* 114 (3-4), 72–85. doi:10.1016/j.marchem.2009.04.003

Godfrey, L. V., and Glass, J. B. (2011). The Geochemical Record of the Ancient Nitrogen Cycle, Nitrogen Isotopes, and Metal Cofactors. *Methods Enzymol.* 486, 483–506. doi:10.1016/b978-0-12-381294-0.00022-5

Hadas, O., Altabet, M. A., and Agnihotri, R. (2009). Seasonally Varying Nitrogen Isotope Biogeochemistry of Particulate Organic Matter in Lake Kinneret, Israel. *Limnol. Oceanogr.* 54 (1), 75–85. doi:10.4319/lo.2009.54.1.0075

Higgins, M. B., Robinson, R. S., Husson, J. M., Carter, S. J., and Pearson, A. (2012). Dominant Eukaryotic export Production during Ocean Anoxic Events Reflects the Importance of Recycled NH4+. *Proc. Natl. Acad. Sci.* 109 (7), 2269–2274. doi:10.1073/pnas.1104313109

Hugoni, M., Escalas, A., Bernard, C., Nicolas, S., Jézéquel, D., Vazzoler, F., et al. (2018). Spatiotemporal Variations in Microbial Diversity across the Three Domains of Life in a Tropical Thalassohaline lake (Dziani Dzaha, Mayotte Island). *Mol. Ecol.* 27 (23), 4775–4786. doi:10.1111/mec.14901

Karl, D. M., and Knauer, G. A. (1991). Microbial Production and Particle Flux in the Upper 350 M of the Black Sea. Deep Sea Research Part A. *Deep Sea Res. Part A. Oceanographic Res. Pap.* 38, S921–S942. doi:10.1016/s0198-0149(10)80017-2

Katsev, S., and Crowe, S. A. (2015). Organic Carbon Burial Efficiencies in Sediments: The Power Law of Mineralization Revisited. *Geology* 43 (7), 607–610. doi:10.1130/g36626.1

Kebede, E., and Ahlgren, G. (1996). Optimum Growth Conditions and Light Utilization Efficiency of Spirulina Platensis (= Arthrospira Fusiformis) (Cyanophyta) from Lake Chitu, Ethiopia. *Hydrobiologia* 332 (2), 99–109. doi:10.1007/bf00016689

Leboulanger, C., Agogué, H., Bernard, C., Bouvy, M., Carré, C., Cellamare, M., et al. (2017). Microbial Diversity and Cyanobacterial Production in Dziani Dzaha Crater lake, a Unique Tropical Thalassohaline Environment. *PLoS One* 12 (1), e0168879. doi:10.1371/journal.pone.0168879

Lehmann, M. F., Bernasconi, S. M., Barbieri, A., and McKenzie, J. A. (2002). Preservation of Organic Matter and Alteration of its Carbon and Nitrogen Isotope Composition during Simulated and *In Situ* Early Sedimentary Diagenesis. *Geochimica et Cosmochimica Acta* 66 (20), 3573–3584. doi:10.1016/s0016-7037(02)00968-7

Lehmann, M. F., Sigman, D. M., and Berelson, W. M. (2004). Coupling the 15N/14N and 18O/16O of Nitrate as a Constraint on Benthic Nitrogen Cycling. *Mar. Chem.* 88 (1-2), 1–20. doi:10.1016/j.marchem.2004.02.001

Lenton, T. M., Boyle, R. A., Poulton, S. W., Shields-Zhou, G. A., and Butterfield, N. J. (2014). Co-evolution of Eukaryotes and Ocean Oxygenation in the Neoproterozoic Era. *Nat. Geosci* 7 (4), 257–265. doi:10.1038/ngeo2108

Li, L., Lollar, B. S., Li, H., Wortmann, U. G., and Lacrampe-Couloume, G. (2012). Ammonium Stability and Nitrogen Isotope Fractionations for -NH3(aq)-NH3(gas) Systems at 20-70°C and pH of 2-13: Applications to Habitability and Nitrogen Cycling in Low-Temperature Hydrothermal Systems. *Geochimica et Cosmochimica Acta* 84, 280–296. doi:10.1016/j.gca.2012.01.040

Logan, G. A., Hayes, J. M., Hieshima, G. B., and Summons, R. E. (1995). Terminal Proterozoic Reorganization of Biogeochemical Cycles. *Nature* 376 (6535), 53–56. doi:10.1038/376053a0

Luo, G., Junium, C. K., Izon, G., Ono, S., Beukes, N. J., Algeo, T. J., Cui, Y., Xie, S., and Summons, R. E. (2018). Nitrogen Fixation Sustained Productivity in the Wake of the Palaeoproterozoic Great Oxygenation Event. *Nat. Commun.* 9 (1), 978–979. doi:10.1038/s41467-018-03361-2

Lyons, T. W., Reinhard, C. T., and Planavsky, N. J. (2014). The Rise of Oxygen in Earth's Early Ocean and Atmosphere. *Nature* 506 (7488), 307–315. doi:10.1038/nature13068

McLauchlan, K. K., Williams, J. J., Craine, J. M., and Jeffers, E. S. (2013). Changes in Global Nitrogen Cycling during the Holocene Epoch. *Nature* 495 (7441), 352–355. doi:10.1038/nature11916

Menzel, P., Gaye, B., Wiesner, M. G., Prasad, S., Stebich, M., Das, B. K., et al. (2013). Influence of Bottom Water Anoxia on Nitrogen Isotopic Ratios and Amino Acid Contributions of Recent Sediments from Small Eutrophic Lonar Lake, central India. *Limnol. Oceanogr.* 58 (3), 1061–1074. doi:10.4319/lo.2013.58.3.1061

Mettam, C., Zerkle, A. L., Claire, M. W., Prave, A. R., Poulton, S. W., and Junium, C. K. (2019). Anaerobic Nitrogen Cycling on a Neoarchaean Ocean Margin. *Earth Planet. Sci. Lett.* 527, 115800. doi:10.1016/j.epsl.2019.115800

Milesi, V. P., Debure, M., Marty, N. C. M., Capano, M., Jézéquel, D., Steefel, C., et al. (2020). Early Diagenesis of Lacustrine Carbonates in Volcanic Settings: the Role of Magmatic CO2 (Lake Dziani Dzaha, Mayotte, Indian Ocean). *ACS Earth Space Chem.* 4 (3), 363–378. doi:10.1021/acsearthspacechem.9b00279

Milesi, V. P., Jézéquel, D., Debure, M., Cadeau, P., Guyot, F., Sarazin, G., et al. (2019). Formation of Magnesium-smectite during Lacustrine Carbonates Early Diagenesis: Study Case of the Volcanic Crater lake Dziani Dzaha (Mayotte–Indian Ocean). *Sedimentology* 66 (3), 983–1001. doi:10.1111/sed.12531

Möbius, J., Gaye, B., Lahajnar, N., Bahlmann, E., and Emeis, K. C. (2011). Influence of Diagenesis on Sedimentary δ15N in the Arabian Sea over the Last 130 Kyr. *Mar. Geology.* 284 (1-4), 127–138. doi:10.1016/j.margeo.2011.03.013

Möbius, J. (2013). Isotope Fractionation during Nitrogen Remineralization (Ammonification): Implications for Nitrogen Isotope Biogeochemistry. *Geochimica et Cosmochimica Acta* 105, 422–432. doi:10.1016/j.gca.2012.11.048

Möbius, J., Lahajnar, N., and Emeis, K. C. (2010). Diagenetic Control of Nitrogen Isotope Ratios in Holocene Sapropels and Recent Sediments from the Eastern Mediterranean Sea. *Biogeosciences* 7 (11), 3901–3914. doi:10.5194/bg-7-3901-2010

Müller, P. J. (1977). CN Ratios in Pacific Deep-Sea Sediments: Effect of Inorganic Ammonium and Organic Nitrogen Compounds Sorbed by Clays. *Geochimica et Cosmochimica Acta* 41 (6), 765–776.

NOAA (2017). National Oceanic and Atmospheric Administration. Available at: https://www.nodc.noaa.gov/.

Papineau, D., Purohit, R., Goldberg, T., Pi, D., Shields, G. A., Bhu, H., et al. (2009). High Primary Productivity and Nitrogen Cycling after the Paleoproterozoic Phosphogenic Event in the Aravalli Supergroup, India. *Precambrian Res.* 171 (1-4), 37–56. doi:10.1016/j.precamres.2009.03.005

Pennock, J. R., Velinsky, D. J., Ludlam, J. M., Sharp, J. H., and Fogel, M. L. (1996). Isotopic Fractionation of Ammonium and Nitrate during Uptake by Skeletonema Costatum : Implications for δ15N Dynamics under Bloom Conditions. *Limnol. Oceanogr.* 41 (3), 451–459. doi:10.4319/lo.1996.41.3.0451

Pride, C., Thunell, R., Sigman, D., Keigwin, L., Altabet, M., and Tappa, E. (1999). Nitrogen Isotopic Variations in the Gulf of California since the Last Deglaciation: Response to Global Climate Change. *Paleoceanography* 14 (3), 397–409. doi:10.1029/1999pa900004

Quan, T. M., Wright, J. D., and Falkowski, P. G. (2013). Co-variation of Nitrogen Isotopes and Redox States through Glacial-Interglacial Cycles in the Black Sea. *Geochimica et Cosmochimica Acta* 112, 305–320. doi:10.1016/j.gca.2013.02.029

Robinson, R. S., Kienast, M., Luiza Albuquerque, A., Altabet, M., Contreras, S., De Pol Holz, R., et al. (2012). A Review of Nitrogen Isotopic Alteration in marine Sediments. *Paleoceanography* 27 (4), 1–13. doi:10.1029/2012pa002321

Sarazin, G., Jezequel, D., Leboulanger, C., Fouilland, E., Le Floc'h, E., Bouvy, M., et al. (2020). Geochemistry of an Endorheic Thalassohaline Ecosystem: the Dziani Dzaha Crater lake (Mayotte Archipelago, Indian Ocean). Comptes Rendus. *Géoscience* 352 (8), 559–577. doi:10.5802/crgeos.43

Sebilo, M., Mayer, B., Grably, M., Billiou, D., and Mariotti, A. (2004). The Use of the 'Ammonium Diffusion' Method for δ15N-NH4+ and δ15N-NO3 - Measurements: Comparison with Other Techniques. *Environ. Chem.* 1 (2), 99–103. doi:10.1071/en04037

Sigman, D. M., Karsh, K. L., and Casciotti, K. L. (2009). "Ocean Process Tracers: Nitrogen Isotopes in the Ocean," in *Encyclopedia of Ocean Sciences*. 2nd Edition (Cambridge: Academic Press), 40–54. doi:10.1016/b978-012374473-9.00632-9

Sigman, D. M., Robinson, R., Knapp, A. N., Van Geen, A., McCorkle, D. C., Brandes, J. A., et al. (2003). Distinguishing between Water Column and Sedimentary Denitrification in the Santa Barbara Basin Using the Stable Isotopes of Nitrate. *Geochem. Geophys. Geosystems* 4 (5), 1–20. doi:10.1029/2002gc000384

Stüeken, E. E., Tino, C., Arp, G., Jung, D., and Lyons, T. W. (2020). Nitrogen Isotope Ratios Trace High-pH Conditions in a Terrestrial Mars Analog Site. *Sci. Adv.* 6 (9), eaay3440. doi:10.1126/sciadv.aay3440

Stüeken, E. E., Buick, R., and Schauer, A. J. (2015). Nitrogen Isotope Evidence for Alkaline Lakes on Late Archean Continents. *Earth Planet. Sci. Lett.* 411, 1–10. doi:10.1016/j.epsl.2014.11.037

Stüeken, E. E., Kipp, M. A., Koehler, M. C., and Buick, R. (2016). The Evolution of Earth's Biogeochemical Nitrogen Cycle. *Earth-Science Rev.* 160, 220–239. doi:10.1016/j.earscirev.2016.07.007

Stüeken, E. E., Martinez, A., Love, G., Olsen, P. E., Bates, S., and Lyons, T. W. (2019). Effects of pH on Redox Proxies in a Jurassic Rift lake: Implications for Interpreting Environmental Records in Deep Time. *Geochimica et Cosmochimica Acta* 252, 240–267. doi:10.1016/j.gca.2019.03.014

Talbot, M. R., and Johannessen, T. (1992). A High Resolution Palaeoclimatic Record for the Last 27,500 Years in Tropical West Africa from the Carbon and Nitrogen Isotopic Composition of Lacustrine Organic Matter. *Earth Planet. Sci. Lett.* 110 (1-4), 23–37. doi:10.1016/0012-821x(92)90036-u

Tesdal, J.-E., Galbraith, E. D., and Kienast, M. (2013). Nitrogen Isotopes in Bulk marine Sediment: Linking Seafloor Observations with Subseafloor Records. *Biogeosciences* 10 (1), 101–118. doi:10.5194/bg-10-101-2013

They, N. H., Amado, A. M., and Cotner, J. B. (2017). Redfield Ratios in Inland Waters: Higher Biological Control of C:N:P Ratios in Tropical Semi-arid High Water Residence Time Lakes. *Front. Microbiol.* 8, 1505. doi:10.3389/fmicb.2017.01505

Thunell, R. C., and Kepple, A. B. (2004). Glacial-Holocene δ15N Record from the Gulf of Tehuantepec, Mexico: Implications for Denitrification in the Eastern Equatorial Pacific and Changes in Atmospheric N2O. *Glob. Biogeochem. Cycles* 18 (1), 1–12. doi:10.1029/2002gb002028

Thunell, R. C., Sigman, D. M., Muller-Karger, F., Astor, Y., and Varela, R. (2004). Nitrogen Isotope Dynamics of the Cariaco Basin, Venezuela. *Glob. Biogeochem. Cycles* 18 (3), 1–15. doi:10.1029/2003gb002185

Vo, J., Inwood, W., Hayes, J. M., and Kustu, S. (2013). Mechanism for Nitrogen Isotope Fractionation during Ammonium Assimilation by *Escherichia coli* K12. *Proc. Natl. Acad. Sci.* 110 (21), 8696–8701. doi:10.1073/pnas.1216683110

Voss, M., Dippner, J. W., and Montoya, J. P. (2001). Nitrogen Isotope Patterns in the Oxygen-Deficient Waters of the Eastern Tropical North Pacific Ocean. *Deep Sea Res. Part Oceanographic Res. Pap.* 48 (8), 1905–1921. doi:10.1016/s0967-0637(00)00110-2

Wenk, C. B., Blees, J., Zopfi, J., Veronesi, M., Bourbonnais, A., Schubert, C. J., et al. (2013). Anaerobic Ammonium Oxidation (Anammox) Bacteria and Sulfide-dependent Denitrifiers Coexist in the Water Column of a Meromictic South-alpine lake. *Limnol. Oceanogr.* 58 (1), 1–12. doi:10.4319/lo.2013.58.1.0001

Wenk, C. B., Zopfi, J., Blees, J., Veronesi, M., Niemann, H., and Lehmann, M. F. (2014). Community N and O Isotope Fractionation by Sulfide-dependent Denitrification and Anammox in a Stratified Lacustrine Water Column. *Geochimica et cosmochimica acta* 125, 551–563. doi:10.1016/j.gca.2013.10.034

Yang, J., Junium, C. K., Grassineau, N. V., Nisbet, E. G., Izon, G., Mettam, C., et al. (2019). Ammonium Availability in the Late Archaean Nitrogen Cycle. *Nat. Geosci.* 12 (7), 553–557. doi:10.1038/s41561-019-0371-1

Zhang, X., Sigman, D. M., Morel, F. M. M., and Kraepiel, A. M. L. (2014). Nitrogen Isotope Fractionation by Alternative Nitrogenases and Past Ocean Anoxia. *Proc. Natl. Acad. Sci. USA* 111 (13), 4782–4787. doi:10.1073/pnas.1402976111

Zinke, J., Reijmer, J. J. G., and Thomassin, B. A. (2003). Systems Tracts Sedimentology in the Lagoon of Mayotte Associated with the Holocene Transgression. *Sediment. Geology.* 160 (1-3), 57–79. doi:10.1016/s0037-0738(02)00336-6

Conflict of Interest: The authors declare that the research was conducted in the absence of any commercial or financial relationships that could be construed as a potential conflict of interest.

Publisher's Note: All claims expressed in this article are solely those of the authors and do not necessarily represent those of their affiliated organizations, or those of the publisher, the editors and the reviewers. Any product that may be evaluated in this article, or claim that may be made by its manufacturer, is not guaranteed or endorsed by the publisher.

frontiers in Earth Science

ORIGINAL RESEARCH
published: 14 February 2022
doi: 10.3389/feart.2021.727971

N and C Isotope Variations Along an Extreme Eutrophication and Salinity Gradient in the Coorong Lagoon, South Australia

Stacey C. Priestley[1], Jonathan Tyler[1], Savannah R. Liebelt[1], Luke M. Mosley[2], Wei Wen Wong[3], Yuexiao Shao[1], Zara Woolston[1], Mark Farrell[4], David T. Welsh[5,6], Justin D. Brookes[2], Alan S. Collins[1], Chris Keneally[2] and Juraj Farkaš[1]*

[1]Department of Earth Sciences, University of Adelaide, Adelaide, SA, Australia, [2]School of Biological Sciences, University of Adelaide, Adelaide, SA, Australia, [3]Water Studies, School of Chemistry, Monash University, Melbourne, VIC, Australia, [4]CSIRO Agriculture and Food, Glen Osmond, SA, Australia, [5]School of Environment and Science, Griffiths University, Southport, QLD, Australia, [6]Future Industry Institute, University of South Australia, Adelaide, SA, Australia

OPEN ACCESS

Edited by:
Magali Ader, UMR7154 Institut de Physique du Globe de Paris (IPGP), France

Reviewed by:
Naohiko Ohkouchi, Japan Agency for Marine-Earth Science and Technology (JAMSTEC), Japan
Zhanfei Liu, University of Texas at Austin, United States
Christopher Junium, Syracuse University, United States

***Correspondence:**
Stacey C. Priestley
stacey.priestley@adelaide.edu.au

Specialty section:
This article was submitted to Geochemistry, a section of the journal Frontiers in Earth Science

Received: *20 June 2021*
Accepted: *14 December 2021*
Published: *14 February 2022*

Citation:
Priestley SC, Tyler J, Liebelt SR, Mosley LM, Wong WW, Shao Y, Woolston Z, Farrell M, Welsh DT, Brookes JD, Collins AS, Keneally C and Farkaš J (2022) N and C Isotope Variations Along an Extreme Eutrophication and Salinity Gradient in the Coorong Lagoon, South Australia. Front. Earth Sci. 9:727971. doi: 10.3389/feart.2021.727971

The Coorong Lagoon is a unique hydrological and depositional system at the terminus of the Murray–Darling Basin, the largest river system in Australia. It exhibits large salinity, nutrient, and organic matter gradients, providing a modern analogue to study and validate the use of $\delta^{15}N$ and $\delta^{13}C$ as tracers of past and contemporary geochemical cycles in estuarine environments. To this end, water and surface sediment samples were analyzed for particulate organic nitrogen (PON) and carbon (POC) concentrations, and the respective $\delta^{15}N$ and $\delta^{13}C$ signatures of particulate nitrogen and carbon. PON and POC exhibited positive relationships to chlorophyll-a, indicating the dominance of phytoplankton production upon suspended organic matter. There was also a general trend of increasing $\delta^{15}N$ of PON ($\delta^{15}N_{PON}$) values and decreasing $\delta^{13}C$ of particulate carbon ($\delta^{13}C_{PC}$) values with increasing salinity and eutrophication in the restricted South Lagoon. In a multiple linear regression for $\delta^{15}N_{PON}$, the best two predictors in combination are PON and C:N molar ratio, highlighting the importance of productivity and the type or source of organic matter. For $\delta^{13}C_{PC}$, the best two predictors are total dissolved phosphorus and latitude, suggesting influences from productivity and proximity to the ocean. Sediment $\delta^{15}N$ values across the Coorong Lagoon overlap with the $\delta^{15}N_{PON}$ in the water column, suggesting that PON derived from algal material represents the main source of nitrogen to lagoon sediments. We hypothesize that limited N loss via denitrification leads to PON being recycled almost exclusively to ammonium, due to low rates of nitrification and dominance of dissimilatory nitrate reduction to ammonium (DNRA). We propose that preferential volatilization of ^{14}N in ammonia increases the $\delta^{15}N$ of ammonium assimilated by phytoplankton, thereby increasing the $\delta^{15}N$ within suspended organic matter and surface sediment in the South Lagoon. By contrast, the gradient exhibited in $\delta^{13}C_{PC}$ data was countered by a relatively constant sedimentary organic carbon $\delta^{13}C$. Data from the Coorong, therefore, suggest that $\delta^{15}N$ values in sediments can be used to infer palaeoproductivity in this hypereutrophic and hypersaline depositional environment,

however, the measured $\delta^{13}C_{PC}$ may be influenced by $\delta^{13}C_{DIC}$ or preferential loss of ^{13}C during sedimentation that alter the sedimentary $\delta^{13}C$ record of organic carbon.

Keywords: $\delta^{15}N$, $\delta^{13}C$, particulate organic matter, palaeoenvironment, hypersaline, hypereutrophic, Coorong Lagoon, Australia

INTRODUCTION

Nitrogen and carbon are bioessential elements and key constituents of living organisms and accumulated organic matter in both marine and terrestrial environments. The isotopic compositions of these elements can provide source and process-related information for both modern and past depositional environments (Casciotti 2016; DeNiro and Epstein 1978; Mettam and Zerkle 2021; Miyake and Wada 1967; Ohkouchi, et al., 2015; Sigman and Casciotti 2001). Nitrogen stable isotope ($\delta^{15}N$) composition in sedimentary archives are used to infer changes in the biogeochemical nitrogen cycle, water column redox, anoxia/euxinia, and nutrient conditions in past marine and coastal environments (e.g., Sigman and Casciotti, 2001; Wang et al., 2018; Cox et al., 2019; Davis et al., 2019; Isaji et al., 2019; Obrist-Farner et al., 2019; Tuite et al., 2019; Zhu et al., 2020). The stable isotope composition of carbon ($\delta^{13}C$) in marine sedimentary archives, including both carbonates and organic sediments, is also interpreted to reflect aquatic productivity and carbon cycling from local to global scales, as well as to assess the relative contributions of terrestrial and marine organic matter, and marine vs. freshwater mixing in past aquatic environments (e.g., Popp et al., 1997; Meyers and Lallier-Verges 1999; Wilson et al., 2005; Lamb et al., 2006). Sediment $\delta^{13}C$ records have also been used to determine relative sea level fluctuations in marine, coastal, and estuarine environments (e.g., Chmura and Aharon et al., 1995; Lamb et al., 2006; Goslin et al., 2017). Carbon and nitrogen isotope analyses are often complimented by the molar ratio of C:N within sediments, which represents an index for primary producers in the system, where higher C:N ratios (>20) are usually found in organic matter with a higher lignin or cellulose content, namely, derived from higher plant matter (Elser et al., 2000). By contrast, C:N ratios <10 are more commonly found in algal, bacterial, and cyanobacterial biomass due to the absence of reinforced cell walls and, thus, the greater relative contribution of amino acids and pigments to the total molecular composition (Meyers and Lallier-Verges 1999; Cadd et al., 2018).

Interpretation of $\delta^{15}N$ and $\delta^{13}C$ from sedimentary archives, however, requires a detailed understanding of the above processes and their impacts on the isotopic fractionation and cycling of nutrient and carbon species in modern marine and coastal systems (Casciotti 2016; Mettam and Zerkle 2021). This is particularly important in hypersaline and eutrophic environments, which are common in coastal and lacustrine settings, where the state and composition of the biological community is strongly affected by changes in the physiochemical parameters (Brookes, et al., 2009; Isaji, et al., 2019; Tweedley, et al., 2019). Nevertheless, to date, only a limited number of studies have examined variability in the $\delta^{15}N$ and $\delta^{13}C$ of organic matter within modern depositional systems characterized by extreme hypersaline and hypereutrophic conditions (e.g., Chen et al., 2017; Isaji, et al., 2019; Šajnović, et al., 2020). Rather, studies in hypersaline environments have predominantly focused on using $\delta^{13}C$ in diatoms, ostracods, microbial mat deposits, and carbonates, or sedimentary facies and evaporate deposits as proxies of palaeoclimate and palaeosalinity (e.g., Sylvestre et al., 2005; Frantz et al., 2014; Schröder et al., 2018; Buongiorno et al., 2019; Cuna-Rodriguez et al., 2020).

The Coorong Lagoon and Murray Mouth Estuary in South Australia, the terminus of the largest river system in Australia (the Murray–Darling Basin), is a Ramsar-listed wetland of international importance. It comprises a unique coastal aquatic and depositional system that exhibits a strong salinity gradient, ranging from fresh in the northern end, which receives riverine inflows to hypersaline in the south (e.g., 3–160 PSU). There is also a progressive increase in total nutrient and organic matter stocks in the more restricted and hypersaline South Lagoon, which reaches hypereutrophic conditions due to reduced freshwater flushing and nutrient retention (Mosley, et al., 2020). The transition to hypereutrophic conditions has caused deposition of organic rich sulfidic black muds in the modern system (Herczeg et al., 2001; Fitzpatrick et al., 2019; Haynes et al., 2019). The natural salinity and eutrophication gradient, existence of both terrestrial and marine water and nutrient sources, and current depositional environment makes the Coorong Lagoon an interesting analogue to aid interpretations of sedimentary $\delta^{15}N$ and $\delta^{13}C$ proxy records from ancient coastal lagoon systems and euxinic ocean conditions.

The aim of this study is to investigate the variability in the $\delta^{15}N$ and $\delta^{13}C$ of organic matter in the waters and surface sediments of the Coorong Lagoon in the context of a broad salinity and nutrient gradient. These findings are intended to support the interpretation of $\delta^{15}N$ and $\delta^{13}C$ data from sedimentary archives rich in organic matter (e.g., organic-rich shales), with implications for ancient hypersaline and hypereutrophic environments in euxinic ocean and semi-restricted coastal settings.

STUDY AREA

The Coorong Lagoon is a shallow (~1.3 m deep) and narrow (~2 km wide) lagoon system that runs northwest to southeast along the South Australian coast for approximately 110 km, separated from the ocean by a sand barrier (**Figure 1**). A narrow constriction (~100 m wide) in the middle of the Coorong Lagoon, at Parnka Point, separates the lagoon into

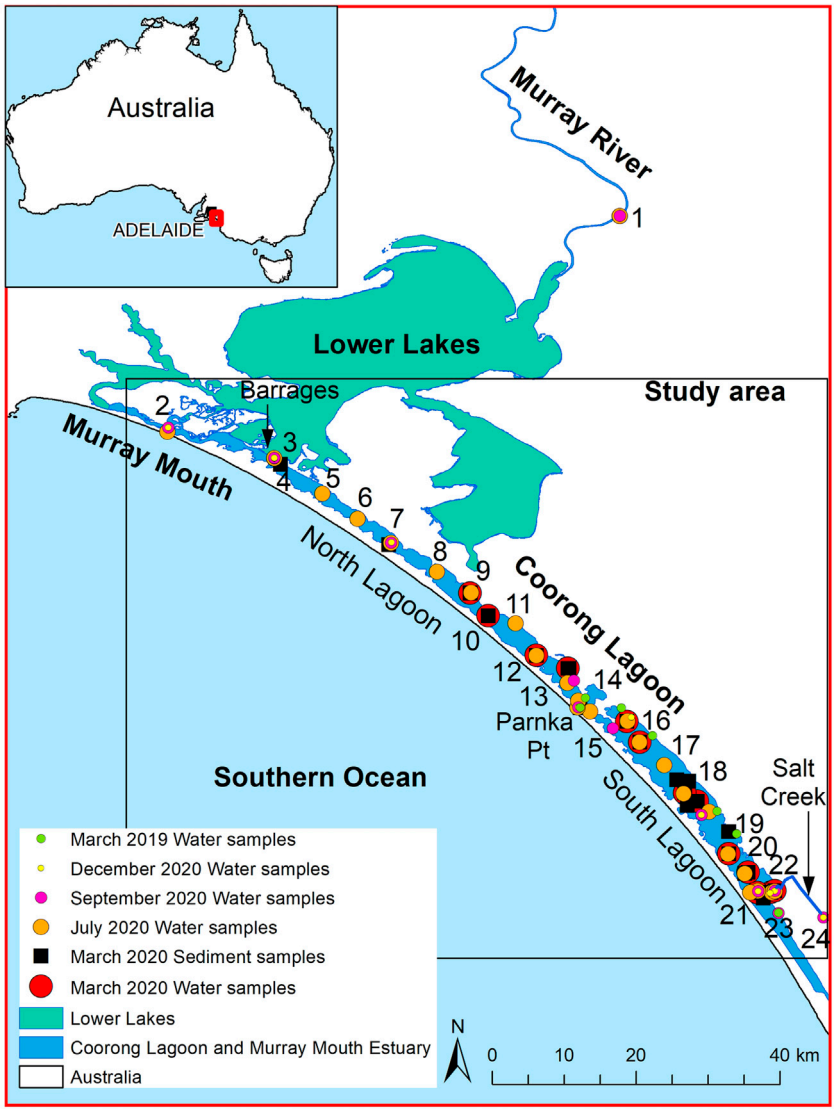

FIGURE 1 | Map of the Coorong Lagoon including location of water and sediment sampling sites. Parnka Point is located at site number 14 and Policeman's point is located at site number 19.

two: the North Lagoon and South Lagoon (**Figure 1**; Mosley, 2016; Stone et al., 2016; Gibbs et al., 2019).

The Murray Mouth, a constricted outlet to the Southern Ocean at the northwestern end of the Coorong Lagoon, allows exchange of seawater into the North Lagoon, influencing water levels in the Coorong Lagoon (Kingsford, et al., 2011). To the east of the Murray Mouth, Murray River waters enter the Coorong Lagoon via the Lower Lakes from regulated barrage structures along the Lower Lakes–Murray Mouth connection, with the Tauwitchere barrage (site 3; **Figure 1**) being the largest and closest to the Coorong Lagoon (Mosley, 2016). Rising tides and high freshwater flows from the Murray River refill the lagoon and lower salinities throughout the Coorong Lagoon in winter (Brookes et al., 2009; Brookes et al., 2020; Ryan, 2019). Fresh to brackish continental waters also enter the southern end of the endorheic South Lagoon from Salt Creek, however, flows are not sufficient to counter evaporation and to lower salinity in this "terminal" lagoon with no major outflows (**Figure 1**). Thus, the Coorong operates as a reverse estuary with salinity increasing from the Murray Mouth toward the South Lagoon (Geddes and Butler, 1984; Geddes et al., 2016: **Figure 2**). While there is a latitudinal gradient, the water column is well mixed vertically with no salinity or other gradients present due to strong wind mixing in the shallow lagoon (Mosley et al., 2019).

Prior to European settlement, there is evidence that the Coorong was less saline, less turbid, and had lower nutrient concentrations compared with the system today (Dick, et al., 2011; Krull, et al., 2009; McKirdy, et al., 2010). Annual sedimentation rates during the Holocene ranged from 1.6 mm in the North Lagoon to <1 mm in the South Lagoon (Haynes

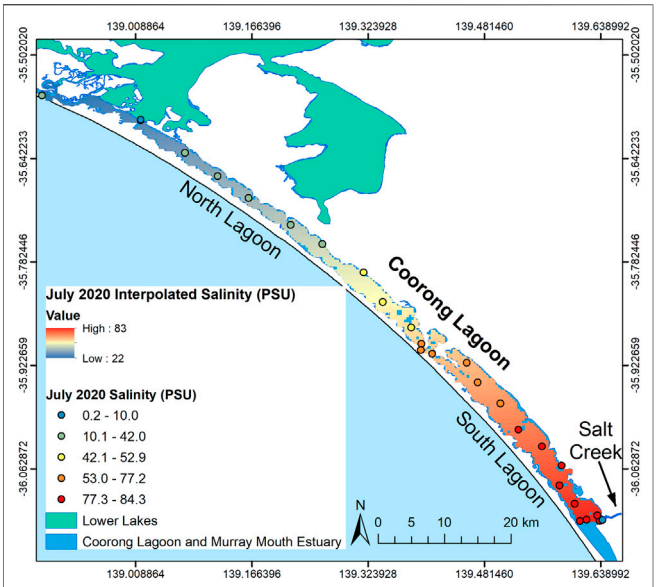

FIGURE 2 | Winter July 2020 salinity measurements and interpolated surface (linear trend in ArcGIS).

et al., 2019). Since European settlement, waters from the Murray–Darling Basin have been diverted, and the rivers within the basin have become highly regulated with streamflow reduced by 60% (Aldridge, et al., 2019; Ryan, 2019).

Currently, the lack of fresh water flushing and evaporation of the lagoon water concentrates salts, nutrients, and other solutes in the water column, especially in the South Lagoon, and has accelerated sedimentation rates. The impact of these reduced flows, land-use changes, and evaporation of the lagoon water has caused increasing trends in salinity, total nutrients, and chlorophyll-a, and a shift to a system dominated by phytoplankton rather than submerged aquatic plants (Herczeg, et al., 2001; Mosley, et al., 2020; Reeves, et al., 2015; Stone, et al., 2016). Consequently, a large proportion of the nutrient inputs from the Murray River and Salt Creek are retained within the lagoon, especially the South Lagoon, and not exported to the ocean (Cook, et al., 2010; Stone, et al., 2016). Thus, the Coorong Lagoon is hypereutrophic with high total nutrient loads and very high algal loads all increasing southward, although dissolved nutrients are low due to rapid uptake by algae (Aldridge, et al., 2019; Ford 2007; Geddes and Butler 1984; Stone, et al., 2016). These impacts have led to a shift in the phytoplankton community from microalgae to cyanobacteria dominated throughout the lagoon, with filamentous green algae blooms becoming an ongoing problem in the South Lagoon (Leterme et al., 2015; Collier et al., 2017; Aldridge et al., 2019). Additionally, sedimentation rates have exponentially increased throughout the Coorong Lagoon due to anoxic preservation of the increased organic matter, and these changes are reflected in the deposition of organic-rich sulfidic black muds since the 1950s (Herczeg et al., 2001; Fitzpatrick et al., 2019; Haynes et al., 2019).

METHODS

Sample collection and preservation

Coorong Lagoon water samples were collected in March 2019; and March, July, September, and December 2020, and sediment samples were collected in March 2020. As the water column throughout the Coorong Lagoon is shallow and well mixed, representative water samples were collected from ~50 cm below the water surface. Onsite measurements of physical and chemical water properties were recorded using a calibrated YSI™ Pro DSS Sonde and handheld meter, including the temperature, dissolved oxygen concentration, salinity, turbidity, and pH. Most samples were collected by boat; however, due to inclement weather and/or boat access issues, some samples were collected by wading from the northern shore. The location of all samples collected in these field trips are shown in **Figure 1**, and the sampling methods used are specified in **Supplementary Table S1**.

For isotope analysis of particulate N and C, aliquots of unfiltered water samples were passed separately through PALL type A/E glass fiber filters with a 1-µm pore size. For total dissolved nitrogen (TDN), total dissolved phosphorus (TDP), and NH_4^+ concentrations, water samples were filtered using 0.2-µm PES syringe filters into acid-cleaned HDPE bottles. All samples including filters containing particulate matter were stored frozen until analysis.

Sediment samples, with a water column of approximately 1 m above, were collected using a "Russian D" auger to a depth of approximately 50 cm. Some shallow shoreline samples were collected with a polycarbonate core tube pushed into the sediment. To investigate the recent transition to hypersaline and eutrophic conditions in the Coorong Lagoon subsamples of the surface (0–2 or 0–5 cm layer), "modern" sediment identified by the organic rich layer, due to rapid mixing in the top up to 5 cm (Krull et al., 2009), were homogenized at the time of sampling for analysis. Samples were immediately placed in sealed vials with no air gap and cooled on ice. Upon return to the laboratory (within 48 h), samples were frozen at −20°C until analysis.

Additionally, *Ruppia tuberosa* (hereafter Ruppia) and cyanobacteria mat biomass samples were collected from Noonamenna, and Ruppia and filamentous algae samples were collected from Salt Creek sampling sites in March 2020.

Analytical procedure for nutrient concentrations and isotopes in water samples

Analyses for total particulate nitrogen and carbon concentration, $^{15}N/^{14}N$ ratio and $^{13}C/^{12}C$ ratio were analyzed from the PALL type A/E glass fibe filters at Monash University analytical and stable isotope facility using a continuous flow isotope ratio mass spectrometer (CF-IRMS; Sercon Ltd., UK; Russell et al., 2018).

The C/N molar ratio was estimated based on beam area using internal standards with known amount of carbon and nitrogen along with the samples for each analysis. Previous comparisons between the concentrations of organic carbon and total carbon suspended in Coorong waters indicated that inorganic carbon accounted for a minor (undetectable) fraction of the suspended load. As a consequence, due to the small sample sizes available, and due to the primary focus of this study being the nitrogen isotope system, particulate carbon samples were not acidified prior to isotope analysis. As a consequence, the suspended carbon isotope data reported here are strictly "total particulate carbon;" however, we interpret this signal to primarily reflect the $^{13}C/^{12}C$ of particulate organic carbon. The isotopic and elemental composition of these samples, as described below, supports this interpretation. Concentrations of NH_4^+, TDN, and TDP were analyzed at Monash University analytical and stable isotope facility. Nutrient concentrations were quantified spectrophotometrically following the procedures in Standard Methods for Water and Wastewater (APHA 2005), using a Lachat QuikChem 8000 Flow Injection Analyzer (FIA). Samples for TDN and TDP were digested with alkaline persulfate prior to analysis via FIA. Dissolved phosphorus was measured as orthophosphate using method 4500-P G as described in APHA (2005). The accuracy of these analyses was within ±2%. Chlorophyll-a were measured at the Australian Water Quality Centre (AWQC), South Australia, a National Association of Testing Authorities (NATA) accredited laboratory.

Analytical procedure for nutrient concentrations and isotopes in sediment and aquatic plant samples

Total carbon and nitrogen concentrations were measured via high-temperature combustion and infrared detection using a LECO CNS TruMAC Analyzer in the Environmental Analysis Laboratory, Lismore, Australia. Total organic carbon ($\%C_{org}$) was measured using the same analytical method following pretreatment of the sample with dilute HCl to remove inorganic carbon. The $^{15}N/^{14}N$ and $^{13}C/^{12}C$ ratios of sedimentary organic matter were analyzed by EA-IRMS in the Environmental Analysis Laboratory, Lismore, Australia, with HCl pretreatment prior to carbon isotope analysis as above. All carbon and nitrogen isotope data are reported using the standard delta notation, relative to the standards of air for nitrogen and PDB for carbon.

Ruppia, cyanobacteria, and filamentous algae samples were dried at 60°C, pulverized, and weighed into tin cups before being analyzed at Monash University on an ANCA GSL2 elemental analyzer interfaced to a Hydra 20–22 continuous-flow isotope ratio mass spectrometer (Sercon Ltd. UK). Quality control was carried out using four internal standards (ammonium sulfate, sucrose, gelatine, and bream), which were calibrated against internationally recognized reference materials including USGS 40, USGS 41, IAEA N1, USGS 25, USGS 26, and IAEAC-6. The internal standards were used to correct for any variations as a result of peak size linearity and instrumental drift with typical reproducibility of ±0.2‰ for both $\delta^{13}C$ and $\delta^{15}N$. Based on these internal standards, the accuracy of our data was calculated to fall within ±0.3‰ for $\delta^{15}N$ and ±0.2‰ for $\delta^{13}C$.

Statistical analysis

Processes controlling water column nutrient and POM concentrations were explored through principal component analysis (PCA; Jackson 1992) of the variable latitude, salinity, pH, DO, temperature, turbidity, alkalinity, chlorophyll-a, PON, POC, TOC, DOC, TN, TDN, DON, TKN, TP, TDP, FRP, and C:N molar ratio (**Supplemental Analysis and Results; Supplementary Table S1**) using the *vegan* package (Oksanen, et al., 2020) in R. Best subset regression was performed using the *regsubsets* function in the package *leaps3.1* for R (Lumley, 2020) to guide exploratory data analysis to identify the best single and combination of variables that explain variability in $\delta^{15}N_{PON}$ and $\delta^{13}C_{PC}$. These proposed relationships were then explored using classical multiple linear regression, with model significance tests conducted using analysis of variance (ANOVA; Chambers and Hastie, 1992), and only models that were significant with variance inflation factors (VIF) close to 1 are kept and presented (Fox and Monette 1992; Fox and Weisberg 2018).

RESULTS

Water column results

There is a general pattern of increasing salinity (**Figure 3A**), and PON (**Figure 3B**) and POC concentrations (**Figure 3C**) from the North Lagoon to the South Lagoon. PON and POC concentrations increase from the North Lagoon (~0.2 mg L^{-1} N and ~1.4 mg L^{-1} C, respectively) to the South Lagoon (up to 0.9 mg L^{-1} N and 6.7 mg L^{-1} C; **Figures 3B, C**). In the warmer seasons, salinity in the South Lagoon can become concentrated by evaporation to >100 PSU (**Figure 3A**), however, PON and POC do not appear to increase in concentration to a similar extent (**Figure 3D**).

In general, salinity, PON and POC concentrations in the Murray River are low (<1 PSU, <0.2 mg L^{-1} N, and <0.5 mg L^{-1} C, respectively), although relatively high PON and POC concentrations occur in the Lower Lakes (upstream of Tauwitchere barrage; up to 1.1 mg L^{-1} N and 11 mg L^{-1} C, respectively; **Figures 3B, C**) and salinities in the Murray Mouth can reach that of seawater (~35 PSU). Finally, salinity, PON and POC concentrations in Salt Creek are generally low compared with the South Lagoon (<15 PSU, <0.2 mg L^{-1} N, and <2.8 mg L^{-1} C, respectively). However, during the March sampling period, PON and POC concentrations were similar to that of the South Lagoon (0.8 mg L^{-1} N and 6 mg L^{-1} C, respectively).

C:N molar ratios of POM average 9 ± 4 in the North Lagoon, 9 ± 1 in the South Lagoon, 9 ± 4 in Salt Creek, 8 ± 4 in the Murray River, with larger C:N ratios in the Lower Lakes (14 ± 2) and Murray Mouth (14 ± 8; **Supplementary Table S2**). These are all higher than the Redfield C:N ratio of 6.6 and represent phytoplankton.

The $\delta^{15}N_{PON}$ values average 4.3 ± 2.9‰ (**Figure 4A**; **Supplementary Table S2**), and the $\delta^{13}C_{PC}$ values average −26.5 ± 1.9‰ in the Coorong (**Figure 4B**; **Supplementary Table S2**). The $\delta^{15}N_{PON}$ and $\delta^{13}C_{PC}$ values in the Coorong show opposite trends with $\delta^{15}N_{PON}$ increasing from the North

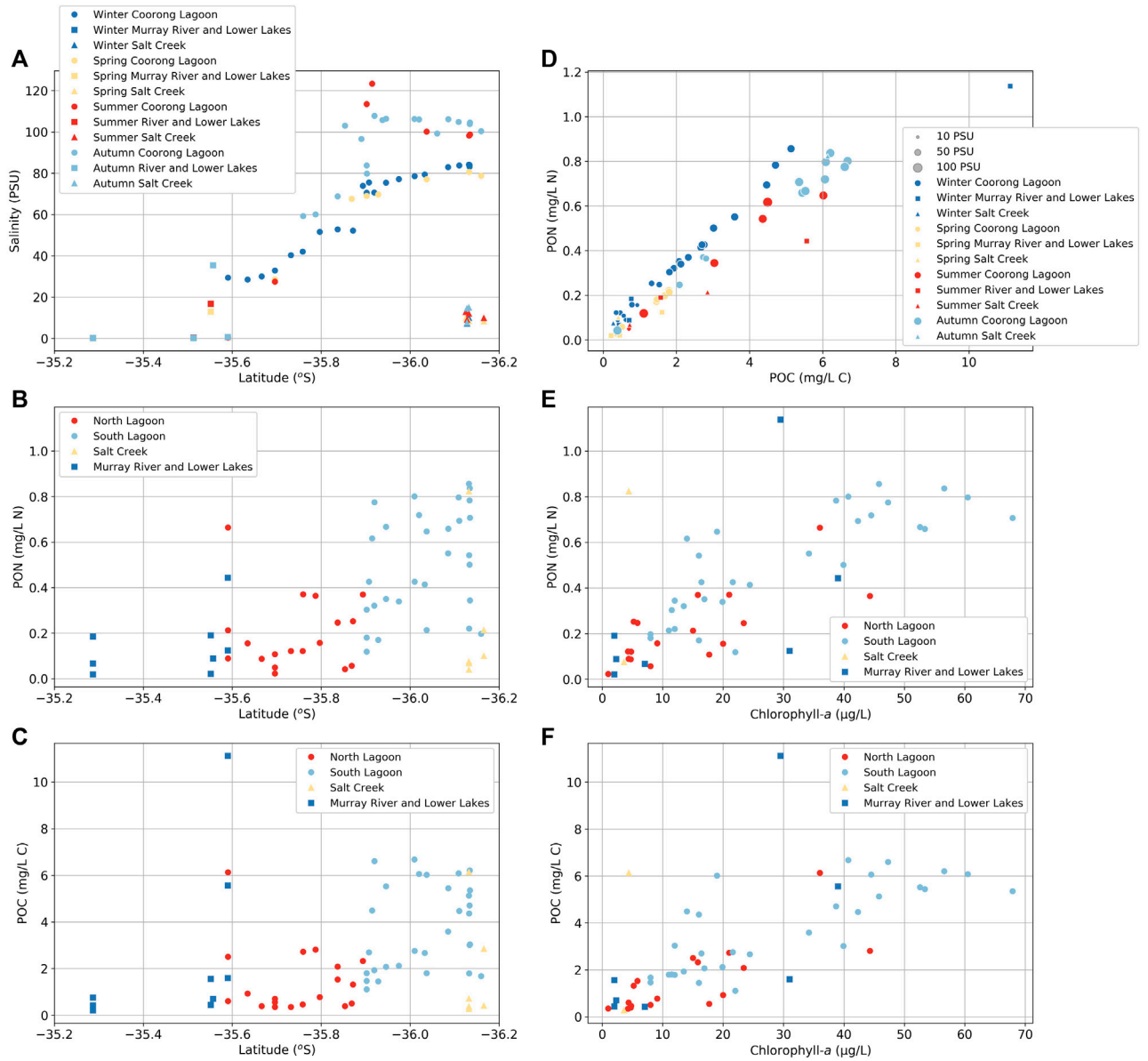

FIGURE 3 | (A) Salinity plotted along sample latitude showing sampling season. **(B)** Particulate organic nitrogen (PON) concentrations and **(C)** particulate organic carbon (POC) concentrations plotted against sample latitude. **(D)** PON against POC showing sampling season. **(E)** PON concentrations and **(F)** POC concentrations plotted against chlorophyll-a concentrations.

Lagoon to South Lagoon, and $\delta^{13}C_{PC}$ values decreasing across the same latitudinal gradient. The average $\delta^{15}N_{PON}$ in the South Lagoon (+4.5 ± 1‰) is ~1‰ higher compared with the North Lagoon (+3.8 ± 2‰; **Supplementary Table S2**). There is also a 2‰ increase in $\delta^{13}C_{PC}$ values from the South Lagoon (−27.4 ± 1.5‰) to the North Lagoon (−25.2 ± 1.8‰; **Supplementary Table S2**). Lower Lakes $\delta^{13}C_{PC}$ values also average −25.1 ± 0.7‰, whereas the Murray River $\delta^{13}C_{PC}$ values average −29.3 ± 0.9‰, and the Salt Creek $\delta^{13}C_{PC}$ values average −25.3 ± 2‰. The $\delta^{15}N_{PON}$ values in Salt Creek and Murray River are (+3.43 ± 1.5‰ and +3.9 ± 3.5‰, respectively). Ruppia from the North Lagoon and Salt Creek regulator had $\delta^{13}C$ values of −13.8‰ and −15.3‰, whereas filamentous algae from the Salt Creek regulator had $\delta^{13}C$ values of −12.5‰ and a cyanobacterial mat from Noonamenna in the North Lagoon had $\delta^{13}C$ values of −18.1‰ (**Supplementary Table S2**).

N and C isotope results for sediments

Total organic carbon and total nitrogen in the South Lagoon sediments (6.6 ± 2.6% and 0.4 ± 0.3%, respectively) are double

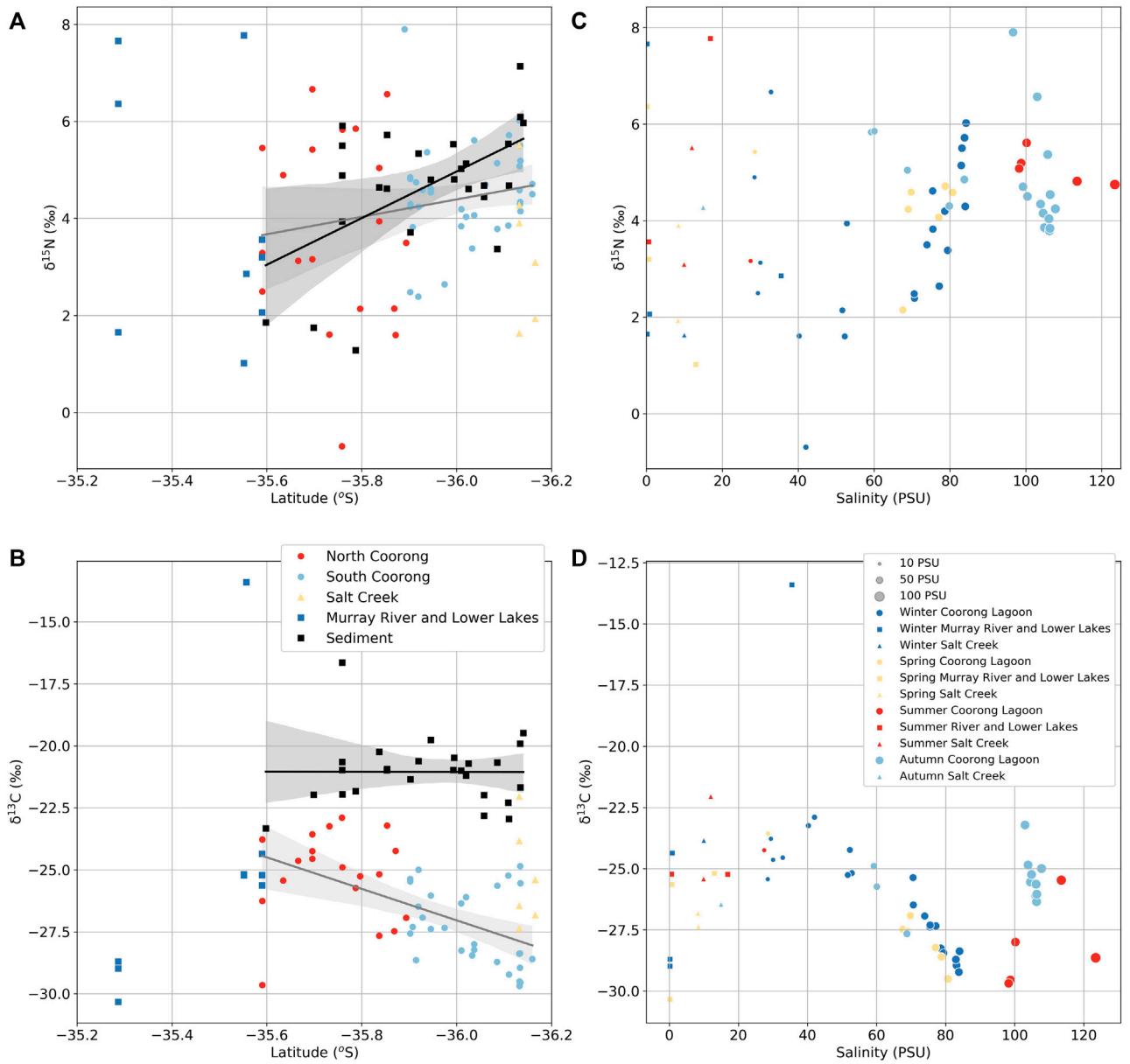

FIGURE 4 | (A) PON and bulk sediment $\delta^{15}N$ results and **(B)** particulate carbon (PC) and bulk sediment $\delta^{13}C$ results against sample latitude. Legend in **(B)** applies to **(A)** as well. **(C)** $\delta^{15}N_{PON}$ results and **(D)** $\delta^{13}C_{PC}$ results against salinity. In both, the gray regression line represents all Coorong Lagoon POM isotope values and black regression line represents the bulk sediment isotope values. Legend in **(D)** applies to **(C)** as well.

that of the North Lagoon sediments (1.8 ± 1.8% and 0.2 ± 0.2%, respectively; **Supplementary Table S3**). The C:N molar ratios of both the North Lagoon and South Lagoon are 9 ± 2 (**Supplementary Table S3**).

Sedimentary organic matter $\delta^{15}N$ values range from +1.3‰ up to +7.1‰ and increase from the North Lagoon (+4.0 ± 1.7‰) to South Lagoon (+5.1 ± 0.9‰; **Figure 4A**; **Supplementary Table S3**). By contrast, there is no significant difference between the North Lagoon (−21 ± 1.8‰) and South Lagoon (−21 ± 1.0‰) bulk sediment $\delta^{13}C$ values, with the full range from −16.6‰ to −23.3‰ (**Figure 4B**).

DISCUSSION

Processes controlling water column nutrient and POM concentrations

Salinity increases from north to south along the Coorong Lagoon (**Figure 2**) with higher concentrations of dissolved ions in summer compared with winter, especially in the South Lagoon (**Figure 3A**), due to evaporation and the lack of seasonal flushing owing to the Coorong Lagoon being a reverse estuary (Webster 2010). Similar trends to those seen for salinity are also shown for PON, POC (**Figures 3B, C**), and other nutrient concentrations,

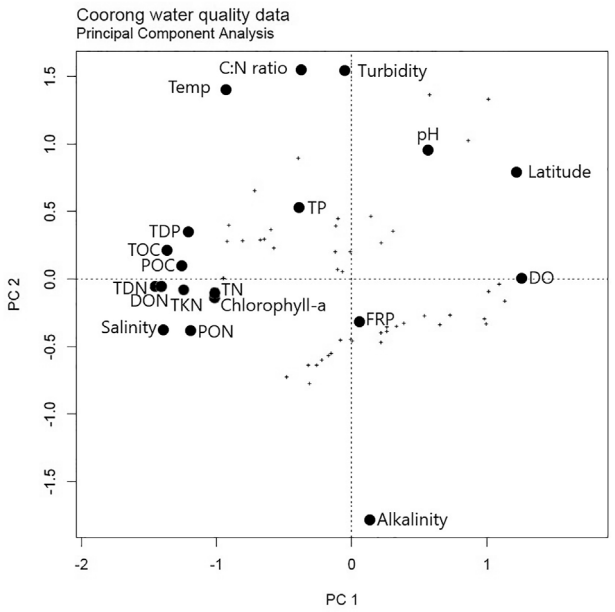

FIGURE 5 | Principal component analysis (PCA) results for the Coorong Lagoon water dataset (**Supplementary Table S1**).

such as TN, TOC, and DOC, which also exhibit increasing concentrations from north to south, as previously reported (e.g., Aldridge et al., 2019). Interestingly, the range of variability in PON and POC across the latitudinal gradient is greater than that of salinity, and they do not increase in concentration to a similar extent in summer compared with winter (**Figure 3D**). Instead, the variability in PON and POC across the lagoon primarily reflects phytoplankton biomass, as reflected by the correlation with chlorophyll-a concentration (**Figures 3E, F**), whereby biomass is higher in the South Lagoon (Mosley et al., 2019; Mosley et al., 2020). Carbon: chlorophyll-a ratios of ~50:1 support this interpretation, and that of Ford (2007), who found that most of the POC in the Coorong can be accounted for by phytoplankton production (Reynolds 1997). Additionally, the C:N molar ratios (9 ± 3; **Supplementary Table S2**) of POM throughout the North and South Lagoons are consistent with predominantly phytoplankton-derived suspended organic matter (cellulose, lipid, and protein, etc.; Cadd et al., 2018; Huang et al., 2020; Meyers and Lallier-Vergès 1999; Tyson 1995).

Principal components analysis (PCA) of the water chemistry data shows that chlorophyll-a, PON, POC, DON, TDN, TKN, TN, TOC, and salinity all covary with the first principal component (**Figure 5**). This confirms that nutrient concentrations are the primary driver for productivity and, hence, PON and POC concentrations in Coorong waters. Additionally, covariation of salinity with nutrient, chlorophyll-a, and POM concentrations highlights that all are primarily controlled by the lack of flushing. Thus, the overall increase in productivity and nutrient concentrations from north to south in the Coorong appears to primarily be controlled by the lack of flushing due to hydrological restriction of the South Lagoon that acts as an endorheic system, or a "closed basin" with no major outflows.

A lack of flushing ensures that the nutrients, suspended load, and sediments are inefficiently removed from the lagoon system into the ocean, further exacerbating their progressive accumulation in the South Lagoon. The reduced amount of flushing over recent years is linked to the shallowing of the South Lagoon due to enhanced evaporation, and physical restrictions caused by the buildup of sediments in the narrower channels of the Coorong (Haynes et al., 2019). The high salinity also inhibits macroinvertebrate survival and bioturbation (Dittmann et al., 2015; Remaili et al., 2018), thus promoting anoxia and sulfate reduction in the surface sediments, especially in the South Lagoon. Thus, we hypothesize that this lack of flushing and restriction of the South Lagoon are one of the fundamental causes of its salinization, the accumulation of nutrients, enhanced productivity, and hence, the buildup of particulate organic matter, all of which contribute to local sediment anoxia, especially in the South Lagoon (Mosley et al., 2020).

Processes controlling POM isotope values

The combined effects of flushing, salinization, and eutrophication also appear to affect the $\delta^{15}N_{PON}$ and $\delta^{13}C_{PC}$ isotope values throughout the entire Coorong Lagoon (**Figure 4**). There is a general decrease in $\delta^{13}C_{PC}$ from north to south with increasing salinity (**Figures 4B, D**). However, the $\delta^{13}C_{PC}$ values of samples near Salt Creek are higher (~26‰) compared with the rest of the South Lagoon samples (**Figures 4B, D**). Likewise, there is a subtle increase in average $\delta^{15}N_{PON}$ from north to south with increasing salinity (**Figures 4A, C**).

Redundancy analysis (RDA) and best subsets regression were used to preliminarily explore which of the environmental variables in the Coorong best predict variability in $\delta^{15}N_{PON}$ and $\delta^{13}C_{PC}$. These observations were then formally tested using multiple linear regression, with models validated using model-to-model ANOVA tests and by rejecting models with variance inflation factors >1.5. The best single predictor of $\delta^{15}N_{PON}$ was POC (R^2 = 0.15, p = 0.004; **Table 1**), followed closely by PON (R^2 = 0.13, p = 0.006; **Table 1**). The best two predictors for $\delta^{15}N_{PON}$ in a multiple linear regression are PON and C:N molar ratio (R^2 = 0.26, ANOVA p-value < 0.001; **Table 1**), beyond which more complex models failed to meet significance test criteria. This suggests that of the measured variables, phytoplankton biomass or productivity, in addition to the composition of the suspended organic matter—either

TABLE 1 | Redundancy analysis and best subsets regression analysis results.

Variable	Predictors	R^2	p-Value
$\delta^{15}N_{PON}$	Particulate organic carbon (POC)	0.15	0.004
$\delta^{15}N_{PON}$	Particulate organic nitrogen (PON)	0.13	0.006
$\delta^{15}N_{PON}$	PON and C:N atomic ratio	0.26	<0.001
$\delta^{13}C_{PC}$	Total Kjeldahl nitrogen (TKN)	0.35	<0.001
$\delta^{13}C_{PC}$	Total dissolved phosphorus (TDP) and latitude	0.44	0.006

taxonomic make up or input from other sources—are the principal controls over $\delta^{15}N_{PON}$, although with a large amount of variance unexplained. The correlation between $\delta^{15}N_{PON}$ and biomass can be potentially explained by the higher productivity and recycling of nitrogen between the sediment and water column in the South Lagoon. Additionally, changes in nitrification/denitrification, as well as the Rayleigh fractionation of nitrogen during assimilation, may also promote an increase in $\delta^{15}N_{PON}$ by preferentially removing ^{14}N from the lagoonal water (e.g., Wada 1980; Zanden and Rasmussen 1999; Ohkouchi et al., 2015). Overall, our data from the Coorong Lagoon suggest that variability in suspended PON concentration and $\delta^{15}N_{PON}$ are best interpreted as tracers of productivity and associated nitrogen cycling.

The best single predictor of $\delta^{13}C_{PC}$ is total Kjeldahl nitrogen (TKN), a measure of the total concentration of organic nitrogen and ammonia ($R^2 = 0.35$, p-value < 0.001; **Table 1**). In a multiple linear regression, the best two predictors in combination are TDP and latitude ($R^2 = 0.44$, ANOVA p-value = 0.006; **Table 1**). Broadly speaking, this relationship between $\delta^{13}C_{PC}$, TDP, and latitude is best explained by proximity to marine carbon sources, in combination with a complex array of factors linked to nutrient driven productivity (Krull, et al., 2009; McKirdy, et al., 2010). The influence of marine–freshwater mixing on $\delta^{13}C_{PC}$ values is manifested by the higher, marine-like $\delta^{13}C$ values near the Murray Mouth (Middelburg and Nieuwenhuize 1998), which decline with both increasing or decreasing salinity (**Figure 4D**). This marine effect is likely countered by possible kinetic isotopic fractionation during CO_2 hydration and hydroxylation during periods of intense productivity in hypersaline waters, which could contribute to observed ^{13}C-depleted DIC values and the trend of the decreasing $\delta^{13}C_{PC}$ at salinities between 40 and 100 PSU (**Figure 4D**) (Clark, et al., 1992; Lazar and Erez 1992). The higher $\delta^{13}C_{PC}$ values of the hypersaline (>100 PSU) South Lagoon in summer and autumn sampling periods are more readily interpreted in the context of eutrophication and changes in phytoplankton composition as progression to filamentous algae ($\delta^{13}C_{PC}$ = −12.5‰) dominance during high evaporation periods in the South Lagoon (Leterme et al., 2015; Collier et al., 2017) could lead to increased $\delta^{13}C_{PC}$. Additionally, higher $\delta^{13}C_{PC}$ values could be due to decreased photosynthetic carbon isotope fractionation at higher phytoplankton growth rates (e.g., Laws et al., 1995; Zanden and Rasmussen 1999; Ohkouchi et al., 2015). Nevertheless, several other potential mechanisms and processes may contribute to the relationship between $\delta^{13}C_{PC}$ and nutrient concentration, which require further investigation. For example, in organic rich sediments, higher $\delta^{13}C_{PC}$ can be linked to microbial mineralization of detrital organic matter, leading to the release of ^{13}C enriched carbon into the water column. In addition, it is known that the South Lagoon receives a considerable amount of dissolved Sr from Salt Creek and/or via groundwater inputs (Shao, et al., 2018; Shao, et al., 2021), and thus it is also plausible that such alkaline continental water inputs also contain ^{13}C-enriched DIC, which may thus contribute to the higher $\delta^{13}C_{PC}$ observed in the southernmost part of the Coorong Lagoon (**Figure 4D**). Future research into $\delta^{13}C$ of DIC is required to verify this hypothesis.

Processes controlling sediment N and C isotope values

Before delving into the sediment $\delta^{15}N$ and $\delta^{13}C$ results, it is important to note that the South Lagoon sediments have a greater proportion of total organic carbon and total nitrogen than those in the North Lagoon (**Supplementary Table S3**), reflecting higher net deposition of organic matter in the South Lagoon (Haynes et al., 2019). In fact, the total organic carbon contents in the South Lagoon sediments are approaching those of black shales.

It has been determined above that water column $\delta^{15}N_{PON}$ and $\delta^{13}C_{PC}$ values, and the total organic carbon and total nitrogen in the sediment, throughout the Coorong Lagoon are affected by nutrient concentrations and associated productivity, as well as proximity to the ocean. However, for sediment-derived $\delta^{15}N$ and $\delta^{13}C$ proxy signals to be useful tracers of the above processes in palaeolagoon or coastal systems, it is essential to understand the preservation and "transfer" of $\delta^{15}N_{PON}$ and $\delta^{13}C_{PC}$ signals into a local sediment.

Comparison of $\delta^{15}N_{PON}$ and sediment $\delta^{15}N$ values (**Figure 4A**) shows that generally sediment $\delta^{15}N$ overlaps with the "long-term" average $\delta^{15}N_{PON}$ suggesting autochthonous phytoplankton-derived nitrogen represents the primary source of N to the lagoon sediment. This is consistent with algal deposition from a highly eutrophic water column (Pérez-Ruzafa, et al., 2019) and previous research using nitrogen and carbon isotopic biomarkers (Krull et al., 2009; McKirdy et al., 2010). In fact, McKirdy et al. (2010) found South Lagoon sediments to be continuously richer in total nitrogen reflecting higher productivity and hence net deposition of organic matter and nutrients compared with the North Lagoon during the mid-to-late Holocene. They also found a decrease in $\delta^{15}N$ in the upper ~50 cm due to a greater contribution by halotolerant cyanobacteria, and this is also preserved in our data with an increase in sediment $\delta^{15}N$ from 3.9‰ to 5.5‰ from 0–2 to 5–10 cm from a site in the North Lagoon (**Supplementary Table S3**).

Currently, it is likely that the sediment $\delta^{15}N$ values are not significantly altered from the $\delta^{15}N_{PON}$ values due to the shallow water column (Tesdal, et al., 2013). Nitrification of ammonium is also likely severely limited in the oxygen-poor, organic matter and sulfide-rich sediments, as nitrifying bacteria have a lower affinity for oxygen than aerobic heterotrophs and other chemoautotrophs and are outcompeted by these under oxygen-limited conditions (Kemp, et al., 1990). This effect would be reinforced by the extremely low macroinvertebrate diversity and abundance in the South Lagoon sediments (Dittmann, et al., 2015; Tweedley, et al., 2019), as the presence of macrofauna typically enhances benthic nitrification by increasing sediment oxygenation and the provision of aerobic niches for nitrifying bacteria in their burrow wall sediments (Welsh, 2003; Stief, 2013). Limited nitrification rates would also intrinsically limit N-losses from the lagoon as gaseous products via denitrification and competition with the alternative nitrate reduction process dissimilatory nitrate

reduction to ammonium (DNRA) would further decrease N-loss (An and Gardner 2002; Ford 2007; Valiente et al., 2022). DNRA competes with denitrification and, therefore, limits N-loss as N_2 by recycling the nitrate produced from ammonium by nitrification back to ammonium leading to enhanced retention of nitrogen in the system (e.g., Burgin and Hamilton 2007; Giblin et al., 2013; Hardison, et al., 2015; Magri, et al., 2020). The organic matter-rich, highly reduced sediments that are present in the South lagoon would favor DNRA over denitrification as a nitrate reduction process (An and Gardner, 2002; Nizzoli et al., 2006; Molnar et al., 2013). Thus, overall benthic N-cycling is dominated by processes that favor the retention, accumulation, and recycling of N, rather than N-loss processes and thereby supporting ongoing eutrophication of the South Lagoon. This hypothesis is supported by the higher nitrogen content in sediments in the South Lagoon (**Supplementary Table S3**), as well as high NH_4^+ concentrations (up to 10 mg L^{-1}: **Supplementary Table S1**) measured in sediment pore waters in the South Lagoon, which would support high diffusive fluxes of ammonium to the overlying water to fuel phytoplankton production and further PON loads to the sediment. Additionally, in the absence of other quantitatively significant N-loss processes (flushing and denitrification) volatilization of ammonia (NH_3) to the atmosphere may be a quantitatively important N-loss process, which would be facilitated by the Coorong water with pH values >8 (**Supplementary Table S1**). This would also result in isotopic fractionation due to preferential volatilization of light $^{14}NH_3$ compared with $^{15}NH_3$ (Li et al., 2012). This would result in the residual dissolved ammonium available for phytoplankton being ^{15}N-enriched and the ammonium regenerated during remineralization of this phytoplankton biomass also being ^{15}N-enriched. Thus, progressively over time repeated cycles of ammonium assimilation and remineralization, isotopic fractionation during ammonia volatilization may have contributed to the heavy $\delta^{15}N$ values (5.6‰–6.8‰) in sediment and PON in the South Lagoon, and the overlap in the sediment and PON $\delta^{15}N$ values (**Figure 4A**).

The transfer of $\delta^{13}C_{PC}$ variability into the sediment $\delta^{13}C$ record appears more complex. The sediment $\delta^{13}C$ signatures are consistently higher (5‰–7‰) and less geographically variable compared with $\delta^{13}C_{PC}$ (**Figure 4B**), with the $\delta^{13}C$ of sedimentary TOC varying around −21 ± 1‰ (**Figure 4B**). It is possible that the sediment $\delta^{13}C$ values represent a mixture between aquatic plant and algae deposition, since the Ruppia, cyanobacterial mat, and filamentous algae $\delta^{13}C$ values range between −12.5‰ and −18.1‰. However, this observation contrasts with the general absence of aquatic plants in the majority of the South Lagoon presently due to hypersalinity and light limitations due to turbidity and phytoplankton blooms (Dick, et al., 2011, Kim, et al., 2013; Aldridge et al., 2019). An alternative interpretation is that terrestrial detritus from areas bordering the lagoons also contributes to the sedimentary pool (Middelburg and Nieuwenhuize 1998). However, isotope signatures for local terrestrial plants ($\delta^{13}C$ values between −25‰ and −30‰; Krull et al., 2009) indicate that this mixture cannot entirely explain the observed sediment $\delta^{13}C$ values. Also, a previous study at nearby Lake Alexandrina showed that <10% of organic matter preserved in sediments was from terrestrial plants (Herczeg, et al., 2001). Instead, it is also possible that isotopically light carbon could have been lost from the sediment due to methanogenesis or preferential microbial mineralization of ^{12}C. Conversely, if isotopically heavy carbon is delivered to the lagoon sediment as carbonate, whereupon it dissolves in the low pH environment of the sediment, the isotopically heavy CO_2 produced could be assimilated by phytoplankton and bacteria. Alternatively, it is possible that the $\delta^{13}C$ of sedimentary carbon reflects a contribution by a large mass of recalcitrant carbon (i.e., resistant to decomposition) preserved from the now absent macrophyte communities. However, Krull et al. (2009) found that *Ruppia megacarpa* ($\delta^{13}C$ of −13‰) was the predominant source of organic carbon in the North Lagoon prior to the 1950s. They determined that the upper modern 0–5 cm of sediment organic matter $\delta^{13}C$, which fluctuates around −22 ± 1.2‰ and is identical within error to our analyses of −21 ± 1.3‰ (**Supplementary Table S3**), is predominantly degraded phytoplankton. In addition, the sediment C:N ratios of 9 ± 2 are consistent with a phytoplankton source (Krull et al., 2009; McKirdy et al., 2010). Thus, it is possible that the $\delta^{13}C_{PC}$ measured in this study is influenced by DIC and the sediment organic $\delta^{13}C$ carbon is a result of algal deposition similar to the sediment $\delta^{15}N$ values. The above interpretations to explain the observed $\delta^{13}C$ variability in sedimentary carbon archives across the Coorong Lagoon thus need further process-based investigations to corroborate the validity of these different hypotheses and scenarios.

Implications for palaeo-environmental reconstructions based on $\delta^{15}N$-$\delta^{13}C$ proxies

The acquired data from the restricted, hypersaline, and hypereutrophic Coorong Lagoon represent a useful case study to test the sensitivity and fidelity of $\delta^{15}N$ and $\delta^{13}C$ proxies as tracers of past environmental conditions and their temporal changes in lagoonal and coastal systems. Here we show that the $\delta^{15}N$ in both suspended and sedimentary organic matter is sensitive to spatial variability in phytoplankton biomass, which, in turn, is primarily controlled by local nitrogen mineralization or recycling with eutrophication primarily being driven by internal processes not external nutrient inputs. In part, this is linked to the hypersalinity and eutrophic conditions related to lagoon restriction and the associated decrease in flushing of nutrient-rich lagoonal waters, which yielded progressively higher $\delta^{15}N$ signatures (up to +8‰) in the South Lagoon. Furthermore, surficial lagoon sediment $\delta^{15}N$ values follow the same general pattern as the overlying water column $\delta^{15}N_{PON}$ suggesting that processes that determine $\delta^{15}N$ in the water column are also reflected in the sediments. This is due to a high degree of dominance of internal processes, as N assimilation into PON is being regenerated by breakdown of PON in the sediment. Whereas, if the $\delta^{15}N_{PON}$ was driven by external nutrient inputs, then $\delta^{15}N_{PON}$ would be intermediate between that of these inputs and the ammonium coming from the sediment. Thus, the correlation between $\delta^{15}N_{PON}$ and sediment $\delta^{15}N$ values representing modern sediment (Krull et al., 2009) is mostly a function of the unique restricted, hypersaline, and hypereutrophic conditions characteristics of the Coorong

Lagoon, and especially for its southern parts. However, there is greater variance in the $\delta^{15}N_{PON}$ values compared with the sediment $\delta^{15}N$ values suggesting that the sediment is an integration of the relatively long-term signals derived from the water column. Therefore, based on this case study, it would appear that $\delta^{15}N_{PON}$ is largely recorded and preserved in the sediment $\delta^{15}N$ archives in these types of lagoonal and coastal systems, and that nitrogen isotope analysis of ancient estuarine/lagoon or coastal marine sediments has the potential to be used as a proxy for palaeo-productivity in hypersaline and hypereutrophic depositional systems. These results also have relevance for understanding deep time sedimentary systems, particularly the ancient anoxic (Archean) sediments where organic matter and N may be preserved from the water column sources.

In contrast, the $\delta^{13}C$ of the surficial sediments in the Coorong does not directly reflect that of $\delta^{13}C_{PC}$, suggesting the $\delta^{13}C_{PC}$ is influenced by variable $\delta^{13}C_{DIC}$. An additional hypothesis is that preferential mineralization of nitrogen over carbon is occurring, where carbon spends relatively more time tied up as sediment organic matter. Additionally, the $\delta^{13}C$ of the surficial sediments could be the result of diagenetic alteration on $\delta^{13}C$ at sediment–water interface upon the deposition of local organic matter. If the former is the case, it is conceivable that $\delta^{13}C$ of sediment organic matter is autochthonous phytoplankton derived carbon. In order to verify these effects more research is needed into the influence of various inputs, sources, and local biogeochemical cycling of both inorganic and organic carbon in the Coorong Lagoon.

Overall, the Coorong Lagoon with its extreme gradient in environmental conditions and processes, and deposition of organic rich sulfidic sediments, can provide potential insights into ancient ocean conditions in relation to nitrogen and carbon isotope patterns under highly sulfidic conditions with no significant bioturbation. Similar conditions are considered to have occurred during ocean anoxic events and the deposition of ancient black shale environments in deep time (Meyer and Kump 2008; Rickard, 2012). Thus, the Coorong Lagoon represents a useful analogue to better understand C and N isotope records and redox conditions during deposition of organic-rich sediments in ancient and redox-stratified basins.

CONCLUSION

Investigations into contemporary carbon and nitrogen cycles and associated isotope variability are essential for interpreting sedimentary $\delta^{15}N$ and $\delta^{13}C$ records in the context of past salinity and nutrient conditions in restricted estuarine/lagoonal and coastal systems. To this end, the $\delta^{15}N$ and $\delta^{13}C$ of suspended particulate matter and underlying sediments were investigated in the Coorong Lagoon, South Australia, to test the effect of eutrophication and increased salinity across a wide natural environmental gradient.

In the highly restricted Coorong Lagoon, the lack of freshwater flushing and high evaporation rates causes hypersalinity and eutrophication of local lagoonal waters, particularly in the South Lagoon. This lack of flushing causes a north–south trend of increasing nutrient load, which is also reflected by increasing POM and chlorophyll-a concentrations due to increased phytoplankton productivity in more restricted and nutrient-rich parts of the lagoon. This nutrient-productivity gradient, in addition to changes in marine–freshwater mixing and differences in organic matter composition, is reflected by both the $\delta^{15}N$ and $\delta^{13}C$ of suspended particulate matter in the water column.

Importantly, this water column $\delta^{15}N$ signal or an isotope gradient of particulate organic matter ($\delta^{15}N_{PON}$) is also effectively transferred and recorded in local sediment archives deposited in the Coorong Lagoon. By contrast, $\delta^{13}C$ differs markedly between suspended particulate matter and surficial lagoon sediments, suggesting the influence of either recalcitrant legacy organic matter derived from now absent aquatic macrophytes, or the effects of diagenetic processes and carbon remineralization at the sediment–water interface. Overall, our results suggest that variability in the $\delta^{15}N$ of sediment organic matter could provide a robust proxy for palaeo-productivity in the Coorong and/or similar coastal lagoon/estuarine systems elsewhere. It is possible that, similar to the sediment $\delta^{15}N$ values, sediment organic $\delta^{13}C$ carbon is a result of algal deposition and $\delta^{13}C_{PC}$ measured in this study is influenced by variable $\delta^{13}C_{DIC}$. However, if $\delta^{13}C_{PC}$ is not influenced by DIC sedimentary organic $\delta^{13}C$ signal and archives in this system offers a more complex record of past environmental change, which may be still representative of previous conditions, or instead considerably modified and altered by diagenetic processes.

DATA AVAILABILITY STATEMENT

The original contributions presented in the study are included in the article/**Supplementary Material**. Further inquiries can be directed to the corresponding author.

AUTHOR CONTRIBUTIONS

SP, JT, LM, and JF contributed to the conception and design of the study. WW performed the sample analysis. SL, YS, and ZW contributed to the data collection. SP wrote the first draft of the manuscript. All authors contributed to manuscript revision, read, and approved the submitted version.

FUNDING

This project is funded as part of the South Australian Government's Healthy Coorong, Healthy Basin Program, which is jointly funded by the Australian and South Australian governments. Initial calibrations and pilot studies on N isotope proxies in Coorong waters and anoxic sediments were also supported via ARC Linkage Grant LP160101353.

ACKNOWLEDGMENTS

The Coorong Lagoon and surrounding lands are the home of the Ngarrindjeri Nations and First Nations of the South East

peoples, and we, therefore, pay respect to their elders past and present, and acknowledge the longstanding and continued link between these lands and their traditional owners. The authors would like to also acknowledge the Goyder Institute for Water Research for supporting this project. The Goyder Institute for Water Research is the delivery partner for research components of Healthy Coorong, Healthy Basin, providing independent research to inform future management decisions for the region. The authors would like to thank Dr. Sebastien Lamontagne (CSIRO land and water, Australia) for helpful and productive discussions. Garry Hera-Singh and Glen Hill are kindly thanked for boat driving support and sharing their local knowledge.

SUPPLEMENTARY MATERIAL

The Supplementary Material for this article can be found online at: https://www.frontiersin.org/articles/10.3389/feart.2021.727971/full#supplementary-material

REFERENCES

Aldridge, K., Mosley, L., and Oliver, R. (2019). Water quality in the Coorong Lower Lakes and Murray Mouth. *Natural History of the Coorong, Lower Lakes, and Murray Mouth Region (Yarluwar-Ruwe)*. (Editors) L. Mosley, Q. Ye, S. Sheperd, S. Hemming, and R. Fitzpatrick. Adelaide, South Australia: University of Adelaide Press.

An, S., and Gardner, W. (2002). Dissimilatory Nitrate Reduction to Ammonium (DNRA) as a Nitrogen Link, versus Denitrification as a Sink in a Shallow Estuary (Laguna Madre/Baffin Bay, Texas). *Mar. Ecol. Prog. Ser.* 237, 41–50. doi:10.3354/meps237041

APHA (2005). *Standard Methods for the Examination of Water and Waste Water. Standard Methods for the Examination of Water and Waste Water*. Washington DC: American Public Health Association, American Water Works Association, and Water Environment Federation.

Brookes, J., Lamontagne, S., Aldridge, K., Benger, S., Bissett, A., Bucater, L., et al. (2009). *An Ecosystem Assessment Framework to Guide Management of the Coorong. Final Report of the CLLAMMecology Research Cluster. An Ecosystem Assessment Framework to Guide Management of the Coorong*. Final Report of the CLLAMMecology Research Cluster. Canberra, Australia: CSIRO.

Brookes, J., Aldridge, K., Hipsey, M., Busch, B., Ye, Q., Gibbs, M., et al. (2020). Ecological condition of the Lower Lakes and Coorong. *Murray Darling Basin Australia: Its future management*. Australia: Elsevier.

Buongiorno, J., Gomez, F. J., Fike, D. A., and Kah, L. C. (2019). Mineralized Microbialites as Archives of Environmental Evolution, Laguna Negra, Catamarca Province, Argentina. *Geobiology* 17, 199–222. doi:10.1111/gbi.12327

Burgin, A. J., and Hamilton, S. K. (2007). Have We Overemphasized the Role of Denitrification in Aquatic Ecosystems? A Review of Nitrate Removal Pathways. *Front. Ecol. Environ.* 5, 89–96. doi:10.1890/1540-9295(2007)5[89:hwotro]2.0.co;2

Cadd, H. R., Tibby, J., Barr, C., Tyler, J., Unger, L., Leng, M. J., et al. (2018). Development of a Southern Hemisphere Subtropical Wetland (Welsby Lagoon, South-East Queensland, Australia) through the Last Glacial Cycle. *Quat. Sci. Rev.* 202, 53–65. doi:10.1016/j.quascirev.2018.09.010

Casciotti, K. L. (2016). Nitrogen and Oxygen Isotopic Studies of the Marine Nitrogen Cycle. *Annu. Rev. Mar. Sci.* 8, 379–407. doi:10.1146/annurev-marine-010213-135052

Chambers, J. M., and Hastie, T. J. (1992). *Statistical Models in S*. Boca Raton: Routledge.

Chen, X., McGowan, S., Zeng, L., Xu, L., and Yang, X. (2017). Changes in Carbon and Nitrogen Cycling in a Floodplain lake over Recent Decades Linked to Littoral Expansion, Declining Riverine Influx, and Eutrophication. *Hydrological Process.* 31, 3110–3121. doi:10.1002/hyp.11254

Chmura, G. L., and Aharon, P. (1995). Stable Carbon Isotope Signatures of Sedimentary Carbon in Coastal Wetlands as Indicators of Salinity Regime. *J. Coastal Res.* 11, 124–135.

Clark, I. D., Fontes, J.-C., and Fritz, P. (1992). Stable Isotope Disequilibria in Travertine from High pH Waters: Laboratory Investigations and Field Observations from Oman. *Geochimica et Cosmochimica Acta* 56, 2041–2050. doi:10.1016/0016-7037(92)90328-g

Collier, C., van Dijk, K-J., Erftemeijer, P., Foster, N., Hipsey, M., O'Loughlin, E., et al. (2017). Optimising Coorong Ruppia Habitat: Strategies to Improve Habitat Conditions for Ruppia Tuberosa in the Coorong (South Australia) Based on Literature Review, Manipulative Experiments and Predictive Modelling. *Reports to Department of Environment and Natural Resources (DEWNR). (Editor) M. Waycott.* Adelaide, South Australia: University of Adelaide, School of Biological Sciences, Adelaide.

Cook, P. L. M., Aldridge, K. T., Lamontagne, S., and Brookes, J. D. (2010). Retention of Nitrogen, Phosphorus and Silicon in a Large Semi-arid Riverine lake System. *Biogeochemistry* 99, 49–63. doi:10.1007/s10533-009-9389-6

Cox, G. M., Sansjofre, P., Blades, M. L., Farkaš, J., and Collins, A. S. (2019). Dynamic Interaction between basin Redox and the Biogeochemical Nitrogen Cycle in an Unconventional Proterozoic Petroleum System. *Sci. Rep.* 9, 5200. doi:10.1038/s41598-019-40783-4

Cuña-Rodríguez, C., Piovano, E. L., García-Rodríguez, F., Sylvestre, F., Rostek, F., Bernasconi, S. M., et al. (2020). Paleolimnological Record of the Pampean plains (Argentina) as a Natural Archive of South American Hydroclimatic Variability since the LGM to the Current Warm Period. *Quat. Sci. Rev.* 250, 106675. doi:10.1016/j.quascirev.2020.106675

Davis, C. V., Ontiveros-Cuadras, J. F., Benitez-Nelson, C., Schmittner, A., Tappa, E. J., Osborne, E., et al. (2019). Ongoing Increase in Eastern Tropical North Pacific Denitrification as Interpreted through the Santa Barbara Basin Sedimentary δ 15 N Record. *Paleoceanography and Paleoclimatology* 34, 1554–1567. doi:10.1029/2019pa003578

DeNiro, M. J., and Epstein, S. (1978). Influence of Diet on the Distribution of Carbon Isotopes in Animals. *Geochimica et Cosmochimica Acta* 42, 495–506. doi:10.1016/0016-7037(78)90199-0

Dick, J., Haynes, D., Tibby, J., Garcia, A., and Gell, P. (2011). A History of Aquatic Plants in the Coorong, a Ramsar-Listed Coastal Wetland, South Australia. *J. Paleolimnol* 46, 623–635. doi:10.1007/s10933-011-9510-4

Dittmann, S., Baring, R., Baggalley, S., Cantin, A., Earl, J., Gannon, R., et al. (2015). Drought and Flood Effects on Macrobenthic Communities in the Estuary of Australia's Largest River System. *Estuarine, Coastal Shelf Sci.* 165, 36–51. doi:10.1016/j.ecss.2015.08.023

Elser, J. J., Fagan, W. F., and Denno, R. F. (2000). Nutritional constraints in terrestrial and freshwater food webs. *Nature* 408, 578–580.

Fitzpatrick, R. W., Shand, P., and Mosley, L. M. (2019). Soils in the Coorong, Lower Lakes and Murray Mouth Region. *Natural History of the Coorong, Lower Lakes, and Murray Mouth Region (Yarluwar-Ruwe)*. (Editors) L. Mosley, Q. Ye, S. Shepherd, S. Hemming, and R. Fitzpatrick. Adelaide, South Australia: University of Adelaide Press.

Ford, P. W. (2007). *Biogeochemistry of the Coorong. Review and Identification of Future Research Requirements*. Canberra, Australia: CSIRO.

Fox, J., and Weisberg, S. (20182018). Visualizing Fit and Lack of Fit in Complex Regression Models with Predictor. *Effect Plots and Partial Residuals* 87, 27. doi:10.18637/jss.v087.i09

Fox, J., and Monette, G. (1992). Generalized Collinearity Diagnostics. *J. Am. Stat. Assoc.* 87, 178–183. doi:10.1080/01621459.1992.10475190

Frantz, C. M., Petryshyn, V. A., Marenco, P. J., Tripati, A., Berelson, W. M., and Corsetti, F. A. (2014). Dramatic Local Environmental Change during the Early Eocene Climatic Optimum Detected Using High Resolution Chemical Analyses of Green River Formation Stromatolites. *Palaeogeogr. Palaeoclimatol. Palaeoecol.* 405, 1–15. doi:10.1016/j.palaeo.2014.04.001

Geddes, M., Shiel, R., and Francis, J. (2016). Zooplankton in the Murray Estuary and Coorong during Flow and No-Flow Periods. *Trans. R. Soc. South Aust.* 140, 1–16. doi:10.1080/03721426.2016.1151497

Geddes, M. C., and Butler, A. J. (1984). Physicochemical and Biological Studies on the Coorong Lagoons, South Australia, and the Effect of Salinity on the Distribution of the Macrobenthos. *Trans. R. Soc. South Aust.* 108, 51–62.

Gibbs, M., Joehnk, K., Webster, I., and Heneker, T. (2019). Hydrology and Hydrodynamics of the Lower Lakes, Coorong and Murray Mouth. *Natural History of the Coorong, Lower Lakes, and Murray Mouth Region (Yarluwar-Ruwe)*. (Editors) L. Mosley, Q. Ye, S. Shepherd, S. Hemming, and R. Fitzpatrick. Adelaide, South Australia: University of Adelaide Press.

Giblin, A., Tobias, C., Song, B., Weston, N., Banta, G., and Rivera-Monroy, V. (2013). The Importance of Dissimilatory Nitrate Reduction to Ammonium (DNRA) in the Nitrogen Cycle of Coastal Ecosystems. *Oceanog* 26, 124–131. doi:10.5670/oceanog.2013.54

Goslin, J., Sansjofre, P., Van Vliet-Lanoë, B., and Delacourt, C. (2017). Carbon Stable Isotope (δ13 C) and Elemental (TOC, TN) Geochemistry in Saltmarsh Surface Sediments (Western Brittany, France): a Useful Tool for Reconstructing Holocene Relative Sea-Level. *J. Quat. Sci.* 32, 989–1007. doi:10.1002/jqs.2971

Hardison, A. K., Algar, C. K., Giblin, A. E., and Rich, J. J. (2015). Influence of Organic Carbon and Nitrate Loading on Partitioning between Dissimilatory Nitrate Reduction to Ammonium (DNRA) and N2 Production. *Geochimica et Cosmochimica Acta* 164, 146–160. doi:10.1016/j.gca.2015.04.049

Haynes, D., Tibby, J., Fluin, J., and Skinner, R. (2019). Palaeolimnology of the Lower Lakes and Coorong Lagoon. *Natural History of the Coorong, Lower Lakes, and Murray Mouth Region (Yarluwar-Ruwe)*. (Editors) L. Mosley, Q. Ye, S. Shepherd, S. Hemming, and R. Fitzpatrick. Adelaide, South Australia: University of Adelaide Press.

Herczeg, A. L., Dogramaci, S. S., and Leaney, F. W. J. (2001). Origin of Dissolved Salts in a Large, Semi-arid Groundwater System: Murray Basin, Australia. *Mar. Freshw. Res.* 52, 41–52. doi:10.1071/mf00040

Huang, C., Chen, F., Zhang, S., Chen, C., Meng, Y., Zhu, Q., et al. (2020). Carbon and Nitrogen Isotopic Composition of Particulate Organic Matter in the Pearl River Estuary and the Adjacent Shelf. *Estuarine, Coastal Shelf Sci.* 246, 107003. doi:10.1016/j.ecss.2020.107003

Isaji, Y., Kawahata, H., Ogawa, N. O., Kuroda, J., Yoshimura, T., Jiménez-Espejo, F. J., et al. (2019). Efficient Recycling of Nutrients in Modern and Past Hypersaline Environments. *Sci. Rep.* 9, 3718. doi:10.1038/s41598-019-40174-9

Jackson, J. E. (1992). *A User's Guide to Principal Components. A User's Guide to Principal Components*. New York: John Wiley & Sons.

Kemp, W. M., Sampou, P., Caffrey, J., Mayer, M., Henriksen, K., and Boynton, W. R. (1990). Ammonium Recycling versus Denitrification in Chesapeake Bay Sediments. *Limnol. Oceanogr.* 35, 1545–1563. doi:10.4319/lo.1990.35.7.1545

Kim, D. H., Aldridge, K. T., Brookes, J. D., and Ganf, G. G. (2013). The Effect of Salinity on the Germination of Ruppia Tuberosa and Ruppia Megacarpa and Implications for the Coorong: A Coastal Lagoon of Southern Australia. *Aquat. Bot.* 111, 81–88. doi:10.1016/j.aquabot.2013.06.008

Kingsford, R. T., Walker, K. F., Lester, R. E., Young, W. J., Fairweather, P. G., Sammut, J., et al. (2011). A Ramsar Wetland in Crisis - the Coorong, Lower Lakes and Murray Mouth, Australia. *Mar. Freshw. Res.* 62, 255–265. doi:10.1071/mf09315

Krull, E., Haynes, D., Lamontagne, S., Gell, P., McKirdy, D., Hancock, G., et al. (2009). Changes in the Chemistry of Sedimentary Organic Matter within the Coorong over Space and Time. *Biogeochemistry* 92, 9–25. doi:10.1007/s10533-008-9236-1

Lamb, A. L., Wilson, G. P., and Leng, M. J. (2006). A Review of Coastal Palaeoclimate and Relative Sea-Level Reconstructions Using $\delta^{13}C$ and C/N Ratios in Organic Material. *Earth-Science Rev.* 75, 29–57. doi:10.1016/j.earscirev.2005.10.003

Laws, E. A., Popp, B. N., Bidigare, R. R., Kennicutt, M. C., and Macko, S. A. (1995). Dependence of Phytoplankton Carbon Isotopic Composition on Growth Rate and [CO2)aq: Theoretical Considerations and Experimental Results. *Geochimica et Cosmochimica Acta* 59, 1131–1138. doi:10.1016/0016-7037(95)00030-4

Lazar, B., and Erez, J. (1992). Carbon Geochemistry of marine-derived Brines: I. ^{13}C Depletions Due to Intense Photosynthesis. *Geochimica et Cosmochimica Acta* 56, 335–345. doi:10.1016/0016-7037(92)90137-8

Leterme, S. C., Allais, L., Jendyk, J., Hemraj, D. A., Newton, K., Mitchell, J., et al. (2015). Drought Conditions and Recovery in the Coorong Wetland, South Australia in 1997-2013. *Estuarine, Coastal Shelf Sci.* 163, 175–184. doi:10.1016/j.ecss.2015.06.009

Li, L., Lollar, B. S., Li, H., Wortmann, U. G., and Lacrampe-Couloume, G. (2012). Ammonium Stability and Nitrogen Isotope Fractionations for NH_4^+-$NH_{3(aq)}$-$NH_{3(gas)}$ Systems at 20-70°C and pH of 2-13: Applications to Habitability and Nitrogen Cycling in Low-Temperature Hydrothermal Systems. *Geochimica et Cosmochimica Acta* 84, 280–296. doi:10.1016/j.gca.2012.01.040

Lumley, T. (2020). Package 'leaps'. Version 3.1. Available at: https://CRAN.R-project.org/package=leaps.

Magri, M., Benelli, S., Bonaglia, S., Zilius, M., Castaldelli, G., and Bartoli, M. (2020). The Effects of Hydrological Extremes on Denitrification, Dissimilatory Nitrate Reduction to Ammonium (DNRA) and Mineralization in a Coastal Lagoon. *Sci. Total Environ.* 740, 140169. doi:10.1016/j.scitotenv.2020.140169

McKirdy, D. M., Thorpe, C. S., Haynes, D. E., Grice, K., Krull, E. S., Halverson, G. P., et al. (2010). The Biogeochemical Evolution of the Coorong during the Mid- to Late Holocene: An Elemental, Isotopic and Biomarker Perspective. *Org. Geochem.* 41, 96–110. doi:10.1016/j.orggeochem.2009.07.010

Mettam, C., and Zerkle, A. L. (2021). *Nitrogen Isotopes in Deep Time*. Cambridge: Cambridge University Press.

Meyer, K. M., and Kump, L. R. (2008). Oceanic Euxinia in Earth History: Causes and Consequences. *Annu. Rev. Earth Planet. Sci.* 36, 251–288. doi:10.1146/annurev.earth.36.031207.124256

Meyers, P. A., and Lallier-vergés, E. (1999). Lacustrine Sedimentary Organic Matter Records of Late Quaternary Paleoclimates. *J. Paleolimnology* 21, 345–372. doi:10.1023/a:1008073732192

Middelburg, J. J., and Nieuwenhuize, J. (1998). Carbon and Nitrogen Stable Isotopes in Suspended Matter and Sediments from the Schelde Estuary. *Mar. Chem.* 60, 217–225. doi:10.1016/s0304-4203(97)00104-7

Miyake, Y., and Wada, E. (1967). The Abundance Ratio of $^{15}N/^{14}N$ in marine Environments. *Rec. oceanographic works Jpn.* 9, 176–192.

Molnar, N., Welsh, D. T., Marchand, C., Deborde, J., and Meziane, T. (2013). Impacts of Shrimp Farm Effluent on Water Quality, Benthic Metabolism and N-Dynamics in a Mangrove forest (New Caledonia). *Estuarine, Coastal Shelf Sci.* 117, 12–21. doi:10.1016/j.ecss.2012.07.012

Mosley, L., Gaget, V., and Furst, D. (2019). *Healthy Coorong, Healthy Basin – Water Quality Monitoring Requirements Review*. Adelaide. South Australia: Royal Society of South Australia.

Mosley, L., Priestley, S., Brookes, J., Dittmann, S., Farkaš, J., Farrell, M., et al. (2020). *Coorong Water Quality Synthesis with a Focus on the Drivers of Eutrophication*. Adelaide, South Australia: Goyder Institute for Water Research Technical Report Series No. 20/10.

Mosley, L. (2016). *Barrage Release Optimisation Trial August 2015: Assessment of Environmental Outcomes and Achievement of Management Objectives*. Adelaide, Australia: University of Adelaide.

Nizzoli, D., Welsh, D., Fano, E., and Viaroli, P. (2006). Impact of Clam and Mussel Farming on Benthic Metabolism and Nitrogen Cycling, with Emphasis on Nitrate Reduction Pathways. *Mar. Ecol. Prog. Ser.* 315, 151–165. doi:10.3354/meps315151

Obrist-Farner, J., Brenner, M., Curtis, J. H., Kenney, W. F., and Salvinelli, C. (2019). Recent Onset of Eutrophication in Lake Izabal, the Largest Water Body in Guatemala. *J. Paleolimnol* 62, 359–372. doi:10.1007/s10933-019-00091-3

Ohkouchi, N., Ogawa, N. O., Chikaraishi, Y., Tanaka, H., and Wada, E. (2015). Biochemical and Physiological Bases for the Use of Carbon and Nitrogen Isotopes in Environmental and Ecological Studies. *Prog. Earth Planet. Sci.* 2, 1. doi:10.1186/s40645-015-0032-y

Oksanen, J., Blanchet, F. G., Friendly, M., Kindt, R., Legendre, P., McGlinn, D., et al. (2020). *Vegan Community Ecology Package Version 2.5-7 November 2020*.

Pérez-Ruzafa, A., Campillo, S., Fernández-Palacios, J. M., García-Lacunza, A., García-Oliva, M., Ibañez, H., et al. (2019). Long-Term Dynamic in Nutrients, Chlorophyll a, and Water Quality Parameters in a Coastal Lagoon during a Process of Eutrophication for Decades, a Sudden Break and a Relatively Rapid Recovery. *Front. Mar. Sci.* 6, 26. doi:10.3389/fmars.2019.00026

Popp, B. N., Parekh, P., Tilbrook, B., Bidigare, R. R., and Laws, E. A. (1997). Organic Carbon $\delta^{13}C$ Variations in Sedimentary Rocks as Chemostratigraphic and Paleoenvironmental Tools. *Palaeogeogr. Palaeoclimatol. Palaeoecol.* 132, 119–132. doi:10.1016/s0031-0182(97)00061-8

Reeves, J. M., Haynes, D., García, A., and Gell, P. A. (2015). Hydrological Change in the Coorong Estuary, Australia, Past and Present: Evidence from Fossil Invertebrate and Algal Assemblages. *Estuaries and Coasts* 38, 2101–2116. doi:10.1007/s12237-014-9920-4

Remaili, T. M., Simpson, S. L., Bennett, W. W., King, J. J., Mosley, L. M., Welsh, D. T., et al. (2018). Assisted Natural Recovery of Hypersaline Sediments: Salinity Thresholds for the Establishment of a Community of Bioturbating Organisms. *Environ. Sci. Process. Impacts* 20, 1244–1253. doi:10.1039/c8em00092a

Reynolds, C. S. (1997). Vegetation Processes in the Pelagic: a Model for Ecosystem Theory. Xxvii, 371 P. Oldendorf/Luhe, Germany: Ecology Institute, 1997. (Excellence in Ecology No. 9). Price DM 68.00. *J. Mar. Biol. Assoc. United Kingdom* 77, 919.

Rickard, D. (2012). Chapter 13 - Euxinic Systems. *Developments in Sedimentology*. (Editor) D. Rickard. Amsterdam, Netherlands: Elsevier.

Russell, D. G., Wong, W. W., and Cook, P. L. M. (2018). Negligible Isotopic Fractionation of Nitrogen within Temperate Zostera Spp. Meadows. *Biogeosciences* 15, 7225–7234. doi:10.5194/bg-15-7225-2018

Ryan, D. (2019). The Role of Climate in Shaping the Coorong, Lower Lakes and Murray Mouth. *Natural History of the Coorong, Lower Lakes, and Murray Mouth Region (Yarluwar-Ruwe)*. (Editors) L. Mosley, Q. Ye, S. Shepherd, S. Hemming, and R. Fitzpatrick. Adelaide, South Australia: University of Adelaide Press.

Šajnović, A., Grba, N., and Neubauer, F. (2020). Geochemistry of Sediments from the Lopare Basin (Bosnia and Herzegovina): Implications for Paleoclimate, Paleosalinity, Paleoredox and Provenance. *Acta Geologica Sinica - English Edition* 94, 1591–1618. doi:10.1111/1755-6724.14324

Schröder, T., van 't Hoff, J., Ortiz, J. E., de Torres Pèrez-Hidalgo, T. J., López-Sáez, J. A., Melles, M., et al. (2018). Shallow Hypersaline Lakes as Paleoclimate Archives: A Case Study from the Laguna Salada, Málaga Province, Southern Spain. *Quat. Int.* 485, 76–88. doi:10.1016/j.quaint.2017.08.006

Shao, Y., Farkaš, J., Holmden, C., Mosley, L., Kell-Duivestein, I., Izzo, C., et al. (2018). Calcium and Strontium Isotope Systematics in the Lagoon-Estuarine Environments of South Australia: Implications for Water Source Mixing, Carbonate Fluxes and Fish Migration. *Geochimica et Cosmochimica Acta* 239, 90–108. doi:10.1016/j.gca.2018.07.036

Shao, Y., Farkaš, J., Mosley, L., Tyler, J., Wong, H., Chamberlayne, B., et al. (2021). Impact of Salinity and Carbonate Saturation on Stable Sr Isotopes ($\delta^{88/86}$Sr) in a Lagoon-Estuarine System. *Geochimica et Cosmochimica Acta* 293, 461–476. doi:10.1016/j.gca.2020.11.014

Sigman, D. M., and Casciotti, K. L. (2001). Nitrogen Isotopes in the Ocean. *Encyclopedia of Ocean Sciences*. (Editor) J. H. Steele. Oxford: Academic Press.

Stief, P. (2013). Stimulation of Microbial Nitrogen Cycling in Aquatic Ecosystems by Benthic Macrofauna: Mechanisms and Environmental Implications. *Biogeosciences* 10, 7829–7846. doi:10.5194/bg-10-7829-2013

Stone, D., Palmer, D., Hamilton, B., Cooney, C., and Mosley, L. (2016). *Coorong, Lower Lakes and Murray Mouth Water Quality Monitoring Program 2009—2016: Summary Report*. South Australia: Environment Protection Authority.

Sylvestre, F., Sifeddine, A., Turcq, B., Gil, I. M., Albuquerque, A. L. S., Lallier-Verges, E., et al. (2005). Hydrological Changes Related to the Variability of Tropical South American Climate from the Cabo Frio Lagoonal System (Brazil) during the Last 5000 Years. *The Holocene* 15, 625–630. doi:10.1191/0959683605hl823rr

Tesdal, J.-E., Galbraith, E. D., and Kienast, M. (2013). Nitrogen Isotopes in Bulk marine Sediment: Linking Seafloor Observations with Subseafloor Records. *Biogeosciences* 10, 101–118. doi:10.5194/bg-10-101-2013

Tuite, M. L., Williford, K. H., and Macko, S. A. (2019). From Greenhouse to Icehouse: Nitrogen Biogeochemistry of an Epeiric Sea in the Context of the Oxygenation of the Late Devonian Atmosphere/ocean System. *Palaeogeogr. Palaeoclimatol. Palaeoecol.* 531, 109204. doi:10.1016/j.palaeo.2019.05.026

Tweedley, J. R., Dittmann, S. R., Whitfield, A. K., Withers, K., Hoeksema, S. D., and Potter, I. C. (2019). Chapter 30 - Hypersalinity: Global Distribution, Causes, and Present and Future Effects on the Biota of Estuaries and Lagoons. (Editors) E. Wolanski, J. W. Day, M. Elliott, and R. Ramachandran. *Coasts and Estuaries*. Amsterdam, Netherlands: Elsevier.

Tyson, R. V. (1995). *Sedimentary Organic Matter. Sedimentary Organic Matter*. London: Chapman & Hall.

Valiente, N., Jirsa, F., Hein, T., Wanek, W., Prommer, J., Bonin, P., et al. (2022). The Role of Coupled DNRA-Anammox during Nitrate Removal in a Highly saline lake. *Sci. Total Environ.* 806, 150726. doi:10.1016/j.scitotenv.2021.150726

Wada, E. (1980). Nitrogen Isotope Fractionation and its Significance in Biogeochemical Processes Occurring in marine Environments. *Isotope Mar. Chem.*, 375–398.

Wang, T., Ravelo, A. C., Ren, H., Dang, H., Jin, H., Liu, J., et al. (2018). Nitrogen Isotope Variations in the Northern South China Sea since Marine Isotopic Stage 3: Reconstructed from Foraminifera-Bound and Bulk Sedimentary Nitrogen. *Paleoceanography and Paleoclimatology* 33, 594–605. doi:10.1029/2018pa003344

Webster, I. T. (2010). The Hydrodynamics and Salinity Regime of a Coastal Lagoon - the Coorong, Australia - Seasonal to Multi-Decadal Timescales. *Estuarine, Coastal Shelf Sci.* 90, 264–274. doi:10.1016/j.ecss.2010.09.007

Welsh, D. T. (2003). It's a Dirty Job but Someone Has to Do it: The Role of marine Benthic Macrofauna in Organic Matter Turnover and Nutrient Recycling to the Water Column. *Chem. Ecol.* 19, 321–342. doi:10.1080/0275754031000155474

Wilson, G. P., Lamb, A. L., Leng, M. J., Gonzalez, S., and Huddart, D. (2005). δ^{13}C and C/N as Potential Coastal Palaeoenvironmental Indicators in the Mersey Estuary, UK. *Quat. Sci. Rev.* 24, 2015–2029. doi:10.1016/j.quascirev.2004.11.014

Zanden, M. J. V., and Rasmussen, J. B. (1999). Primary consumer δ^{13}C and δ^{15}N and the trophic position of aquatic consumers. *Ecology* 80, 1395–1404. doi:10.1890/0012-9658(1999)080[1395:pccana]2.0.co;2

Zhu, X., Jia, G., Xu, W., Zheng, X., Liu, J., Tian, Y., et al. (2020). Sedimentary Records of Nitrogen Isotope in the Western Tropical Pacific Linked to the Eastern Tropical Pacific Denitrification during the Last Deglacial Time. *Geo-mar Lett.* 40, 89–99. doi:10.1007/s00367-020-00637-9

Conflict of Interest: The authors declare that the research was conducted in the absence of any commercial or financial relationships that could be construed as a potential conflict of interest.

Publisher's Note: All claims expressed in this article are solely those of the authors and do not necessarily represent those of their affiliated organizations, or those of the publisher, the editors, and the reviewers. Any product that may be evaluated in this article, or claim that may be made by its manufacturer, is not guaranteed or endorsed by the publisher.

frontiers | Frontiers in Earth Science

ORIGINAL RESEARCH
published: 13 June 2022
doi: 10.3389/feart.2022.745830

Combining Nitrogen Isotopes and Redox Proxies Strengthens Paleoenvironmental Interpretations: Examples From Neoproterozoic Snowball Earth Sediments

Benjamin W. Johnson[1]*, *Colin Mettam*[2] and *Simon W. Poulton*[3]

[1]Earth System Evolution Laboratory, Iowa State University, Department of Geological and Atmospheric Sciences, Ames, IA, United States, [2]Department of Earth Sciences, University College London, London, United Kingdom, [3]School of Earth and Environment, University of Leeds, Leeds, United Kingdom

The history of the nitrogen cycle on Earth is linked to the redox evolution of the surface environment. Many nitrogen cycle fluxes are microbially mediated, and the particular fluxes operating at any given time in an ecosystem depend on the presence, absence or abundance of oxygen. However, interpreting this relationship is complicated as several isotopic fractionations associated with N-cycling are not diagnostic of a particular redox state. Thus, linking nitrogen isotopic analyses with redox-sensitive proxies is essential when interpretating past environments. Specifically, we use concentrations of U, V and Mo, along with Fe-speciation, to augment and contextualize nitrogen isotopic measurements. As an example, we consider samples from the Neoproterozoic Cryogenian period to suggest that there was oxygenated water, with associated aerobic N cycle fluxes. This interpretation is based on positive $\delta^{15}N$ values between 4 to $8^{0}/_{00}$, Fe-speciation data consistent with anoxic bottom water during the Snowball ocean and oxygenated after, and redox-sensitive trace metals indicative of oxic weathering and surface water. Typically, high $\delta^{15}N$ values are interpreted to reflect enhanced denitrification. We propose potential causes including a post-Snowball freshwater melt lid that suppressed deep water ventilation and that denitrification occurred more rapidly at high temperatures after the Snowball. These interpretations are buttressed by combined N isotope and redox analyses. This approach is especially useful during times of dynamic redox in the ocean-atmosphere system to interpret biologic isotopic signals.

Keywords: nitrogen, isotope, Neoproterozoic, redox, Snowball Earth

OPEN ACCESS

Edited by:
Pierre Sansjofre, Muséum National d'Histoire Naturelle, France

Reviewed by:
Julien Danzelle, Sorbonne Universités, France
Vincent Busigny, UMR7154 Institut de Physique du Globe de Paris,France

***Correspondence:**
Benjamin W. Johnson
bwj@iastate.edu

Specialty section:
This article was submitted to Biogeoscience, a section of the journal Frontiers in Earth Science

Received: *22 July 2021*
Accepted: *29 April 2022*
Published: *13 June 2022*

Citation:
Johnson BW, Mettam C and Poulton SW (2022) Combining Nitrogen Isotopes and Redox Proxies Strengthens Paleoenvironmental Interpretations: Examples From Neoproterozoic Snowball Earth Sediments. Front. Earth Sci. 10:745830. doi: 10.3389/feart.2022.745830

1 NITROGEN AND REDOX BIOGEOCHEMISTRY

Nitrogen is a key nutrient for life, a major component of the atmosphere, and tracks connections between the biosphere, atmosphere, and geosphere over long time scales (Zerkle and Mikhail, 2017). It is possible to investigate changes in the evolution and operation of the ancient nitrogen cycle via stable isotope geochemistry[1] as nitrogen undergoes a number of biologically mediated, redox sensitive transformations, each of which is associated with an isotopic fractionation (see Stüeken et al., 2016a).

Atmospheric N_2 enters the biosphere via nitrogen fixation by diazotrophic organisms. Such fixing splits the triple bond in N_2 using the nitrogenase enzyme. The most common enzyme (Fe - Mo nitrogenase) produces a minimal isotopic effect (Zhang et al., 2014). Nitrogen which is then remineralised from diazotrophic biomass can be stable and bioavailable in the environment as NH_4^+ or, in the presence of oxygen, is transformed by microbes to NO_3^- via nitrification. Nitrification has a significant isotopic effect, with product NO_3^- being enriched by 13 to $38^0/_{00}$ compared to substrate NH_4^+ (e.g., Casciotti et al., 2003, 2011). Typically, in modern oxygenated waters, nitrification is complete, such that all available NH_4^+ is converted, and thus there is no net isotopic effect recorded in the resultant NO_3^-.

Denitrification and anammox, which are microbially mediated respiration reactions that transform NO_3^- to N_2 (with minor N_2O), imparts a large net isotope effect where product N_2 is about $25^0/_{00}$ depleted compared to reactant NO_3^-. In the modern ocean, water column denitrification occurs primarily in oxygen minimum zones, but is only *partial* as the wider ocean is oxygenated, leaving a residual pool of NO_3^- with an average $\delta^{15}N$ of 5 to $7^0/_{00}$ (Sigman et al., 2009). By contrast, in modern marine sediments, there is no net isotopic effect on the bioavailable N pool, as here conversion to N_2 is quantitative (Sigman et al., 2009). The same isotopic pattern would result from anaerobic ammonium oxidation (anammox), especially in the geologic record (Brunner et al., 2013).

We can observe in modern oceans that sedimentary N-isotope values reflect the integrated signal of nitrogen cycling by organisms in the water column (Tesdal et al., 2013). However, interpretation of N-isotope values is complicated by the fact that fractionations produced by transitions between N compounds are not diagnostic (Busigny et al., 2013; Ader et al., 2014, 2016; Stüeken et al., 2016b). For example, a bulk ecosystem $\delta^{15}N$ value of $0^0/_{00}$ typically indicates anaerobic conditions (e.g., Garvin et al., 2009), but could also reflect quantitative nitrification without any denitrification. The latter case could occur in a completely aerobic environment, and thus the same bulk $\delta^{15}N$ value could be produced under completely opposite redox conditions in the water column. These issues are amplified in ancient sediments and rocks, since we cannot measure contemporaneous water conditions during sediment deposition.

In the Precambrian, most measured $\delta^{15}N$ values from sediments are positive (Stüeken et al., 2016a). During this time, anoxic water and potential oxyclines were more widespread. As a result there are multiple scenarios which could lead to positive $\delta^{15}N$ values. For example, in a study of the Archean Mount McRae Shale and Brockman Iron Formations Busigny et al. (2013) measured variable but consistently positive $\delta^{15}N$ values. Such positive values could reflect partial assimilation of NH_4^+ enriched in ^{15}N due to partial oxidation to NO_2^-. Such oxidation could occur in a fully anoxic water column via reactions with Fe or mediated biologically in local oxygen "oases" or in pervasively oxygenated shallow water (Busigny et al., 2013).

Previous nitrogen isotope studies of Neoproterozoic sedimentary rocks observed mostly positive $\delta^{15}N$ values (Ader et al., 2014; Wang et al., 2017; Stüeken et al., 2019a). Such values have mostly been interpreted to reflect an aerobic nitrogen cycle, due to the similarity of measured $\delta^{15}N$ to the modern ocean. As discussed, however, the relationship between N-isotopes as recorded in sediments and water column redox state is not straightforward. There are multiple potential environmental redox structures that can produce similar $\delta^{15}N$ values in sediments.

Thus, in order to interpret nitrogen isotope data it is essential to independently establish redox conditions in the depositional environment. This ideally includes both water column and sediment-water interface proxy data. Previous work has combined redox proxies with carbon isotopes (e.g., Kunzmann et al., 2015), and some have combined redox proxies with nitrogen isotopes (Quan et al., 2008, 2013; Zerkle et al., 2017; Stüeken et al., 2019b). This is crucial, given the strong connection between nitrogen cycling and oxygen. In this contribution, we combined redox proxies - redox sensitive trace elements and Fe-speciation - and nitrogen isotopes. Specifically, we apply this approach to sediments from the Neoproterozoic Snowball Earth ocean with new measurements from the Mineral Fork and Kelley Canyon Formations in Utah, United States. We further compare our results to previous data from the Ghaub Formation (Johnson et al., 2017b) and find that syn-glacial sediments have consistently positive $\delta^{15}N$ values which increase after the glaciation. Iron speciation suggests mostly anoxic bottom water during the glaciation and oxygenated bottom water after. Redox sensitive trace element concentrations suggest oxic weathering and an oxygenated upper water column throughout both the glaciation and afterwards. Combining all data, we suggest persistent oxygenated shallow water during Snowball glaciations which expands in depth after the glaciations. This finding supports previous interpretations of the Neoproterozoic ocean redox structure, and provides additional evidence for oxygenated water in the syn-glacial ocean.

2 GEOLOGIC SETTING AND SAMPLE DESCRIPTIONS

Samples presented in this study are from the Marinoan Ghaub Formation, Namibia (Johnson et al., 2017b) and the Mineral Fork

[1]Nitrogen isotopes are presented in delta notation (per mil, $^0/_{00}$), where

$$\delta^{15}N = \left[\frac{^{15}N/^{14}N_{sample} - ^{15}N/^{14}N_{standard}}{^{15}N/^{14}N_{standard}}\right]1000 \qquad (1)$$

The standard for N isotopes is atmospheric N_2, which is set to $0^0/_{00}$ definition.

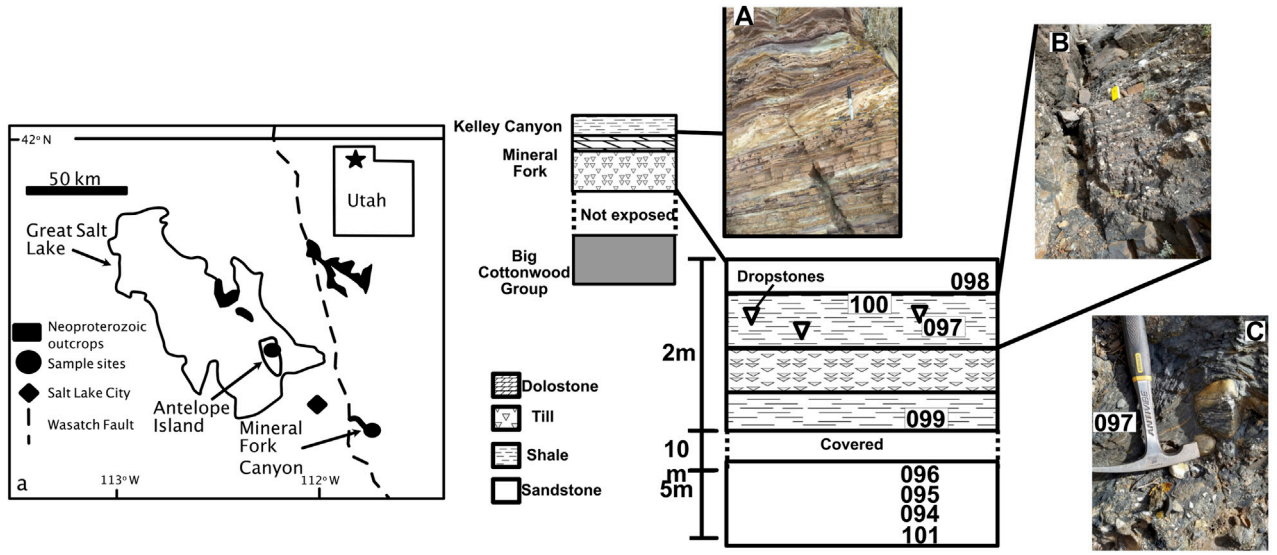

FIGURE 1 | Generalized map showing outcrop area of Neoproterozoic strata in Utah, United States. Map is after Crittenden et al. (1983) and (Young, 2002). Generalized cross section is shown, with detail of Mineral Fork Canyon showing sample locations. Photo **(A)** shows Kelley Canyon Formation, and **(B)** and **(C)** show outcrop photos from Mineral Fork Canyon. Samples were taken from finely laminated units away from draping, as seen in photo c.

Tillite and Kelley Canyon Formation, Utah, USA (**Figure 1**). Detailed description of the Ghaub samples are in Johnson et al. (2017b), but briefly these units are interpreted to be glacial outwash deposited below the ice-grounding line. The sequence was deposited during the Marinoan (~ 650*to*635 Ma), though exactly when during this interval is unclear. The sampled unit unconformably overlies the Naarchams Member, and conformably grades upwards into the overlying cap carbonate, the Keilberg Member. In detail, the Ghaub Formation is predominantly detrital carbonate (Hoffman, 2016), as the glaciers in this area were eroding an underlying carbonate platform. Specifically, samples were taken from the Fransfontein Homocline (Hoffman, 2011).

The Mineral Fork Formation is found in the central Wastach Range and on Antelope Island in Utah, United States. The unit comprises interbedded diamictites, sandstones and mudstones (Ojakangas and Matsch, 1980; Christie-Blick, 1982). The diamictite is typically massive, while the sandstone is subfeldspathic to quartzose, and includes laminated and cross-bedded facies; mudstones contain rare dropstones, several Fe-rich layers (Young, 2002), and carbonaceous layers with microfossils (Knoll et al., 1981). The unit is interpreted as having been deposited in a marginal marine setting, with dynamic glacial activity and periodic connection to the open ocean (Crittenden et al., 1983). Further, the overall geologic setting is consistent with a rifted margin creating accommodation space, but the depositional rate of the diamictite could have been more rapid than the accumulation of space due to tectonic activity (Hoffman P. F. et al., 2017). The relationship between glaciation, rifting, and deposition during the Sturtian in western North America may be complex (e.g., Kennedy and Eyles, 2021). We assume, however, for this study, that the Mineral Fork Formation is the result of glacial deposition in a marginal marine environment.

Age constraints are relatively poor. The Mineral Fork overlies the Big Cottonwood Formation, which is stratigraphically correlated with the ~ 766 Ma Uinta Mountain Group (Link and Christie-Blick, 2011). High Fe content supports association with Sturtian glaciation successions in North America (Young, 2002). The cap carbonate above the Mineral Fork Formation, however, is visually and texturally similar to the Keilberg Member in Namibia, supportive of a Marinoan age. Detrital zircons from the Kelley Canyon Formation yield maximum deposition ages for the till of 703 ± 6 Ma and an overlying graywacke of 667 ± 5 Ma (Balgord et al., 2013). There are no strong minimum age constraints. Thus, while existing geochronology does not rule out a younger, Marinoan age, these data more strongly support that the Mineral Fork tillite is Sturtian in age.

The paleogeographic location and tectonic setting of the Mineral Fork Formation is also not well constrained, due to its uncertain age. If the Mineral Fork is Sturtian, it is likely that it was deposited in a rift basin (Li et al., 2013; Merdith et al., 2017). Such a setting is more likely to have been a restricted basin, and thus would not record global oceanic geochemical conditions. If, however, the Mineral Fork is Marinoan, it was more likely deposited in a basin that was better connected to the global ocean (Li et al., 2013; Merdith et al., 2017). Regardless of this under-constrained geological setting, the main purpose of this study is to demonstrate that interpreting N isotopes in the geologic record is strengthened by combined consideration of independent redox proxies. Providing better constraints on the age of the Mineral Fork Formation, and whether or not these samples represent local or global signals, are beyond the scope of this paper.

We also analyzed samples from the Kelley Canyon Formation, which includes a post-Marinoan cap dolomite and a slate

TABLE 1 | Sample location and geologic information.

Sample	Latitude	Longitude	Formation	Lithology
BWJ18094	40° 36′ 59.8″	111° 40′ 45.3″	Mineral Fork	Massive till with cm clasts
BWJ18095	40° 36′ 39.9″	111° 40′ 46.2″	Mineral Fork	Coarse sandstone, cross-bedding
BWJ18096	40° 36′ 39.9″	111° 40′ 35.4″	Mineral Fork	Fine sandstone, ripple marks
BWJ18097	40° 36′ 39.9″	111° 40′ 35.4″	Mineral Fork	Fine grained sedimentary drape over dropstone
BWJ18098	40° 36′ 39.9″	111° 40′ 35.4″	Mineral Fork	Sandstone
BWJ18099	40° 36′ 39.9″	111° 40′ 35.4″	Mineral Fork	Fine grained black shale
BWJ18100	40° 36′ 39.9″	111° 40′ 35.4″	Mineral Fork	Fine grained black shale
BWJ18101	40° 36′ 39.9″	111° 40′ 35.4″	Mineral Fork	Fine grained black shale
BWJ18102	40° 59′ 1.62″	112° 12′ 49.32″	Kelley Canyon	Shale/slate, purple and resistant
BWJ18103	40° 59′ 1.62″	112° 12′ 49.32″	Kelley Canyon	Shale/slate, tan and resistant
BWJ18104	40° 59′ 1.62″	112° 12′ 49.32″	Kelley Canyon	Shale/slate, green-gray and recessive

member (**Table 1**). Specifically, samples are from the slate member and from three distinct facies. The three facies contain layers that are purple and resistant, tan and resistant, and green-gray recessive. Bedding in all facies is thin (~1–3 cm), supporting a depositional setting that is below wave-base (**Table 1**).

3 ANALYTIC TECHNIQUES

For all samples, we collected specimens free of obvious weathering or alteration. Prior to analyses, weathered edges of hand samples were trimmed with a rock saw. Samples were broken into smaller pieces with a rock hammer, and crushed to a powder in a motorized agate mortar and pestle. As detailed later, we argue that analyzed values represent primary values. Regional metamorphism was greenschist facies or lower (Yonkee et al., 2014), and measured values are very similar to previous work (Johnson et al., 2017b).

3.1 Nitrogen Concentration and Isotopes

Nitrogen isotopic techniques for the Namibian samples are presented in (Johnson et al., 2017b), and are similar for Mineral Fork and Kelley Canyon Formation samples. Nitrogen concentration and isotope ratios for the Mineral Fork Formation were characterized at the University of Colorado Boulder Earth Systems Stable Isotope Lab (CUBES-SIL), and values for the Kelley Canyon Formation were determined, using identical protocol, at the Earth System Evolution Lab (EaSEL) at Iowa State University. Carbon concentrations were obtained during the same runs as N concentration and isotopic analyses, using the same standards.

Sample powders were decarbonated via reaction with 5 ml of 6 N HCl. Samples were then sonicated for 30 min. All tubes were then placed in a 60°C oven overnight. The next day, samples were centrifuged to settle all undissolved material. Acid was poured off, fresh acid was added as before, and samples sat in the oven overnight. This acid refresh was repeated once more. To clean samples, all were rinsed three times with DI H_2O, centrifuging between each rinse. Sample powders then dried at 60 °C for 2 days; all vials containing multiples of the same sample powder were combined and homogenized after drying.

Samples were then analyzed on a Thermo Delta V after combustion in a Thermo Elemental Analyzer at CUBES-SIL and on a Thermo Delta V Plus following combustion in a Thermo Isolink EA at EaSEL. Between 50 and 100 mg of sample powder was weighed into a Sn capsule, as well as standards: two acetanilides (act1, $\delta^{15}N = 1.18^0/_{00} \pm 0.02$ and act2, $\delta^{15}N = 19.56^0/_{00} \pm 0.03$) and pugel ($\delta^{15}N = 5.45^0/_{00} \pm 0.1$) at CUBES-SIL and urea (internal, $\delta^{15}N = -2.60 \pm 0.2^0/_{00}$) and caffeine (USGS62, $\delta^{15}N = 20.17 \pm 0.1^0/_{00}$) at EaSEL. All samples were flash-combusted with an excess of O_2 at 1,020° C in a combustion column packed with cobaltous oxide (combustion aid) and silvered cobaltous oxide (sulphur scrubber). Combustion products were passed over a reduced copper to reduce all N to N_2 and absorb excess O_2. Finally, sample gas was passed through a magnesium perchlorate trap to absorb water and a 3 m gas chromatography column to separate N_2 from CO_2. All analyses were quantified using IsoDat software and the Isoreader pipeline (Kopf et al., 2021). Errors reported are standard deviations from repeated analyses.

While the dominant mineralogy of the Ghaub at this location is carbonate, the geochemical results presented here, and in Johnson et al. (2017b), reflect analysis of the siliciclastic portion of the Ghaub sediment. Carbonate was removed via dissolution, so that the clay minerals could be analyzed directly. Clays record both the N signal (Ader et al., 2016) and the trace metal budget (Tribovillard et al., 2006; Johnson et al., 2017b).

Mineral Fork and Kelley Canyon samples were analyzed in the same run as previously measured glacial till samples (Timeball Hill and Blaubeker) from published work (Gaschnig et al., 2016; Johnson et al., 2017b). Measured N and $\delta^{15}N$ for Timeball (250 ppm, $5.06^0/_{00}$) and Blaubeker (158 ppm, $4.1^0/_{00}$) are similar to published values: 305 ± 5 ppm and $4.9 \pm 0.3^0/_{00}$ for Timeball Hill; and 90 ± 20 ppm and $4.4 \pm 0.2^0/_{00}$ for Blaubeker. We note that agreement in $\delta^{15}N$ values is quite good, though there are differences in N concentration outside uncertainty. Further, we also ensured that organic standards (urea, acetanilide, pugel, and caffeine) used to calculate N concentration included very small standard amounts (< 10 μg total mass) to capture relatively low N content in these rocks. The overall N concentrations are in the 100s of ppm, which is a

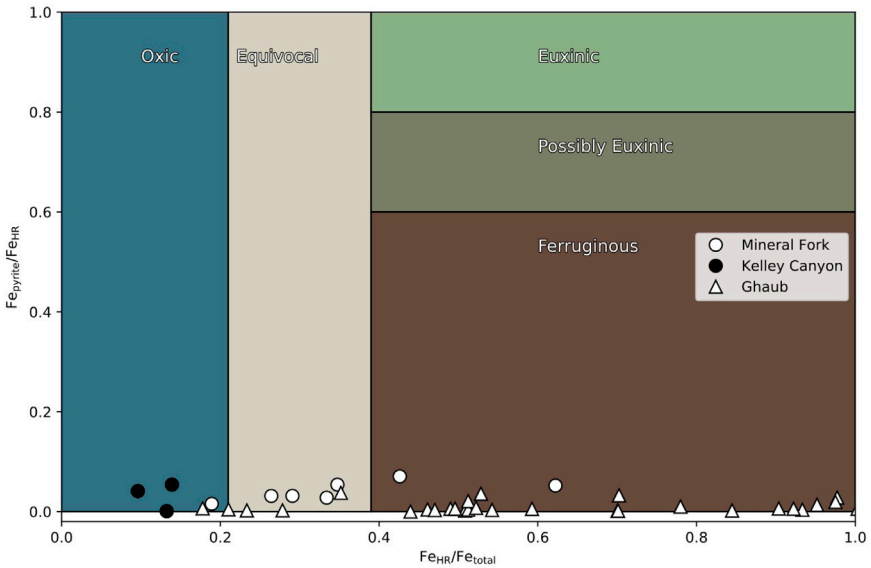

FIGURE 2 | Iron speciation data from the Mineral fork tillite (circles), Kelley Canyon Formation (filled circles) and the Ghaub Formation (triangles). Some samples from both settings plot in the fields characteristic of oxic bottom waters. Specifically, Kelley Canyon samples reflect oxic bottom waters with some samples from the Ghaub formation as well.

reasonable N content suitable for EA-IRMS analysis (Bräuer and Hahne, 2005; Boocock et al., 2020).

3.2 Redox Proxies

The Fe speciation method targets operationally defined Fe pools, including carbonate-associated Fe (Fe_{carb}), ferric oxide Fe (Fe_{ox}), magnetite Fe (Fe_{mag}) and pyrite Fe (Fe_{py}). Extractions were performed according to well-established protocols (Poulton and Canfield, 2005, 2011; Poulton, 2021), with subsequent analysis via atomic absorption spectroscopy (AAS) for Fe_{carb}, Fe_{ox} and Fe_{mag} at the University of Leeds. Fe_{py} was determined gravimetrically following chromous chloride distillation at the University of St Andrew's. Previous studies have shown reproducibility of better than ±2% (Mettam et al., 2017). Total Fe (Fe_T) was determined after HF–$HClO_4$–HNO_3 dissolution via AAS. All Fe extractions gave a relative standard deviation (RSD) of $< 5\%$ based on replicate analyses, and sequential extraction analyses were within 5% of the international Fe-speciation reference material WHIT (Alcott et al., 2020). Total dissolution of international sediment standards (USGS; SGR-1bl; USGS SBC-1) gave an Fe recovery of $> 98\%$.

The sum of Fe_{carb}, Fe_{ox}, Fe_{mag} and Fe_{py} defines a highly reactive (Fe_{HR}) pool, which is considered to represent Fe that is biogeochemically reactive during deposition and early diagenesis (Raiswell and Canfield, 1998; Poulton et al., 2004). Anoxic waters commonly have Fe_{HR}/Fe_T ratios > 0.38, in contrast to oxic depositional conditions where ratios are generally < 0.22 (Poulton and Canfield, 2011). Elevated Fe_{HR}/Fe_T ratios in anoxic settings arise from the additional water column formation of pyrite in euxinic (sulphidic) settings, or unsulphidized Fe_{HR} minerals in ferruginous (Fe-containing) settings. Thus, for anoxic samples (i.e., $Fe_{HR}/Fe_T > 0.38$) the ratio of Fe_{py}/Fe_{HR} distinguishes euxinic ($Fe_{py}/Fe_{HR} > 0.8$) from ferruginous ($Fe_{py}/Fe_{FR} < 0.6$) water column conditions (Poulton and Canfield, 2011; Benkovitz et al., 2020; Poulton, 2021). Fe_{HR}/Fe_T ratios of 0.22–0.38 are considered equivocal, and may occur due to the masking of water column enrichments via rapid sedimentation (e.g., during turbidite deposition Canfield et al., 1996), or due to transformation of unsulphidized Fe_{HR} to clay minerals during diagenesis and metamorphism (e.g., Poulton et al., 2010). This second possibility can be evaluated by considering Fe/Al ratios, since Fe_T is preserved even if Fe_{HR} is lost to clay minerals. In this case, normal oxic marine shales tend to have Fe/Al ratios of 0.55 ± 0.11, and thus Fe/Al > 0.66 is considered to provide a robust indication of water column anoxia (Clarkson et al., 2014).

Trace element composition was determined by ActLabs following their Ultratrace 4 protocol (https://actlabs.com/geochemistry/exploration-geochemistry/4-acid-near-total-digestion/). This is a total digestion using HF, HNO_3 and HCl, followed by analysis via ICP-MS. All measured values are above stated detection limits which are 0.1, 1 and 0.05 ppm for U, V and Mo, respectively. Reported accuracy for all elements are within 1–5% compared to certified standards (GXR-4, SDC-1, DNC-1a, and SBC-1). Reported precisions are ±0.3 ppm for U, ± 2 ppm for V, and ±0.1 ppm for Mo.

4 RESULTS AND INTERPRETATION

We will first discuss the Fe-speciation and U, V and Mo redox proxy data. These establish the geochemical boundary conditions that govern the nitrogen cycle, and within which N isotope data can be interpreted. Then, we place the N isotopic data within this

TABLE 2 | Geochemical data presented in text. Nitrogen and trace element concentrations are given in ppm, while Al and Fe speciation data are in weight percent. Nitrogen isotope values are in permil (%), compared to atmospheric N_2.

Sample name	N	$\delta^{15}N$	V	Mo	U	Zr	Al	Fe_{carb}	Fe_{ox}	Fe_{mag}	Fe_{pyrite}	Fe_{total}	Fe/Al
BWJ18094	212	4.1	56.0	0.2	1.4	38.0	4.36						
BWJ18095	130		20.0	0.2	0.4	20.0	1.89	0.10	0.56	0.03	0.04	1.17	0.62
BWJ18096	220	7.7	64.0	4.8	1.9	69.0	5.41	1.58	0.55	0.84	0.23	7.50	1.39
BWJ18097	353	7.6	56.0	0.1	3.2	57.0	7.69	0.35	0.86	0.22	0.08	4.35	0.57
BWJ18098	302	7.0	72.0	0.2	3.6	91.0	8.50	0.50	0.40	0.61	0.02	8.11	0.95
BWJ18099	326	6.2	34.0	0.0	2.9	55.0	7.62	0.29	0.60	0.29	0.04	4.19	0.55
BWJ18100	402	6.8	67.0	0.1	2.5	57.0	8.11	0.20	0.64	0.25	0.04	4.26	0.53
BWJ18101	393	4.8	42.0	0.0	2.8	66.0	8.94	0.21	0.87	0.16	0.04	3.82	0.43
BWJ18102	166	6.7	56.0	0.1	6.0	74.0	10.00	0.06	0.85	0.16	0.00	8.09	0.81
BWJ18103	101	8.2	25.0	0.0	4.4	134.0	7.62	0.22	0.05	0.01	0.02	2.13	0.28
BWJ18104	118	8.9	50.0	0.1	4.8	161.0	9.64	0.05	0.16	0.00	0.01	2.28	0.24

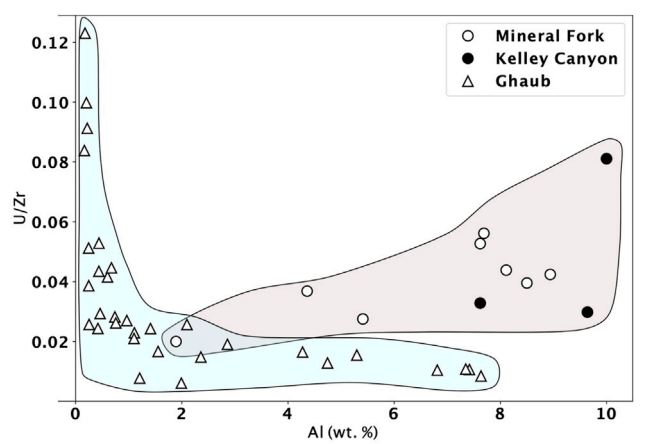

FIGURE 3 | U/Zr ratio from the Mineral fork tillite (circles) and the Ghaub Formation (triangles) plotted against Al concentration. Uranium and Zr are similar geochemically, except U is redox sensitive and Zr is not. Therefore, correlation of this ratio with Al, a proxy for detrital influence, can distinguish between changing U concentrations caused by detrital input or redox evolution. We suggest that only moderate control of U concentration by detrital input is evident in samples from Utah (Mineral Fork and Kelley Canyon). In contrast, Ghaub samples show authigenic enrichment in U, with high U at low Al content. Ghaub and Utah samples show a distinct trend, highlighted by the blue and peach fields.

geochemical context. We also include data from Johnson et al. (2017b).

4.1 Redox Proxies

Iron speciation data from the Ghaub Formation are characteristic of anoxic, ferruginous bottom water (**Figure 2**), with Fe_{pyrite}/Fe_{HR} ratios below 0.1 and Fe_{HR}/Fe_{total} above 0.38. The Mineral fork and Kelly Canyon Formations, however, have Fe speciation data ranging from ferruginous to oxic conditions. In both Utah and Namibia, there appears to be minor fluctuations between anoxic and possibly oxic conditions, but in the samples from the Kelley Canyon Formation reflect oxygenated bottom waters after the Snowball glaciation (**Table 2**).

In all Utah samples, Mo is low, between detection limit of 0.05 ppm and 0.24 ppm, with the exception of one sample at 4.8 ppm. Vanadium ranges from 20–72 ppm, and U ranges from 0.4 to 6 ppm, with most values above 2.5 ppm (**Table 2**). These variations are only partially due to differential detrital input, as seen by plotting U normalized to Zr as a function of Al (**Figure 3**). Zirconium is geochemically similar to U, but Zr is non redox-active, and when plotted against Al (a proxy for detrital input), it is apparent that there is a weak correlation ($r^2 = 0.36$). This indicates that some variation in trace metal abundance may be related to detrital input into the basin, but it is likely not the primary control. In contrast, we observe high U values at low Al concentration in Ghaub samples, indicating authigenic enrichment of U in this location.

There is no clear correlation, however, between the trace element concentration (U and Mo), normalized to Post-Archean Average Shale (PAAS), and total organic carbon (TOC) (**Figure 4**). By normalizing to PAAS, we are showing whether or not each trace element is enriched compared to the average over time. Such an "enrichment factor", when plotted as a function of TOC, is an effective redox proxy (Algeo and Liu, 2020). Specifically, this indicates that scavenging by organic carbon during burial is unlikely to be the primary control on trace element abundance. Rather, the abundance of trace elements indicate oxic weathering and delivery of soluble forms of these elements to the water column.

Johnson et al. (2017b) interpreted the Mo, U and V data from Namibia to reflect oxic weathering on the continents, followed by delivery to the ocean and scavenging in ferruginous bottom waters. While U supply is controlled by detrital input, by normalizing to Al (**Figure 3**), Johnson et al. (2017b) demonstrated that changing U concentrations were not due to changing detrital input alone, and were consistent with iron speciation data. Similarly, these redox-sensitive elements from Utah are present in similar concentrations (**Figure 5**). Uranium, specifically, also displays a negative correlation with Fe_{HR}/Fe_{Total}, consistent with higher U concentrations reflecting a more pervasively oxygenated water column.

There is no enrichment, however, in Mo or V observed from the Mineral Fork or Kelley Canyon formation. Recent work from the early Cambrian of South China has suggested that in settings with a well developed, dynamic redox-cline, the behavior of Mo, V, and U may be decoupled (Han et al., 2018). Specifically, the

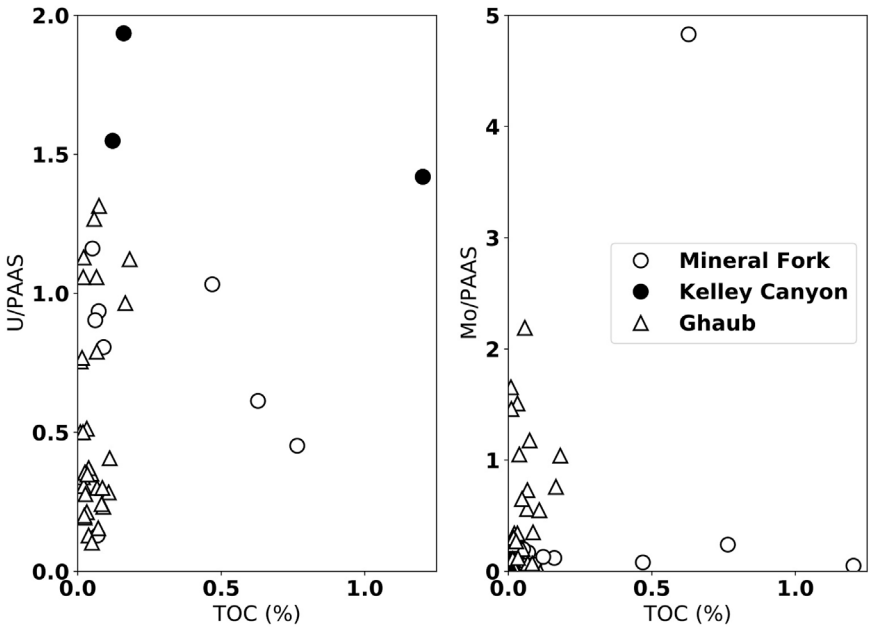

FIGURE 4 | Uranium and Mo concentrations, normalized to Post-Archean Average Shale (PAAS), plotted against carbon concentration (ppm) from the Mineral fork (open circles), Kelley Canyon (closed circles), and the Ghaub Formation (triangles). There is no clear correlation between either, suggesting limited influence of organic carbon availability on trace metal concentration in sediments.

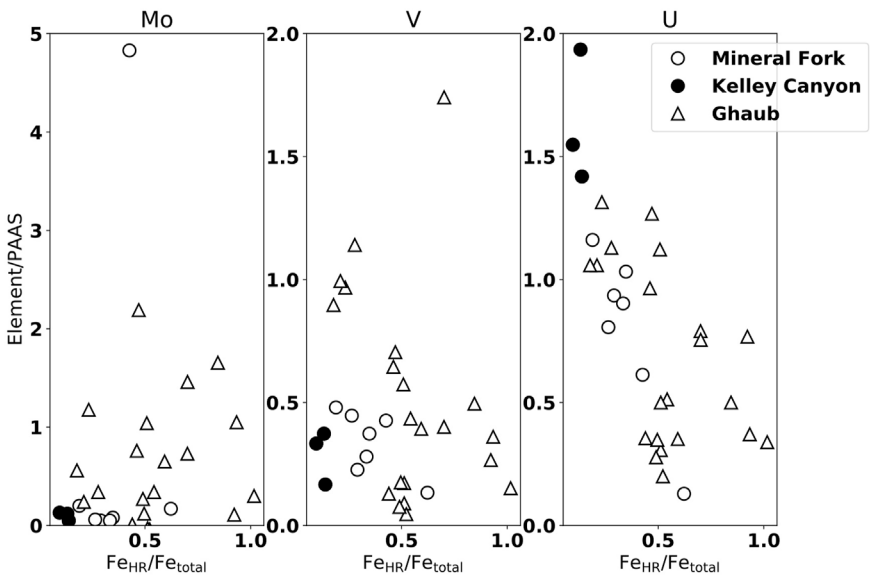

FIGURE 5 | Trace element concentrations normalized to Post-Archean Average Shale (PAAS), plotted against iron speciation data from the Mineral Fork (open circles), Kelley Canyon (closed circles), and the Ghaub Formation (triangles). In general, the Ghaub Formation has higher enrichments in all redox sensitive trace elements, but values above one indicate oxic weathering of continental crust (e.g., Algeo and Tribovillard, 2009; Johnson et al., 2017b). Uranium is enriched relative to PAAS in the samples from Utah, while V and Mo are not.

presence of a zone of Fe-Mn particulate formation can preferentially enrich sediments in V. If such a zone is absent, or sediments sampled are from shallower water, such V enrichment could be missing. It is likely that the Mineral Fork samples were deposited near the ice-grounding line (Christie-Blick, 1982), and perhaps the water column at this location did

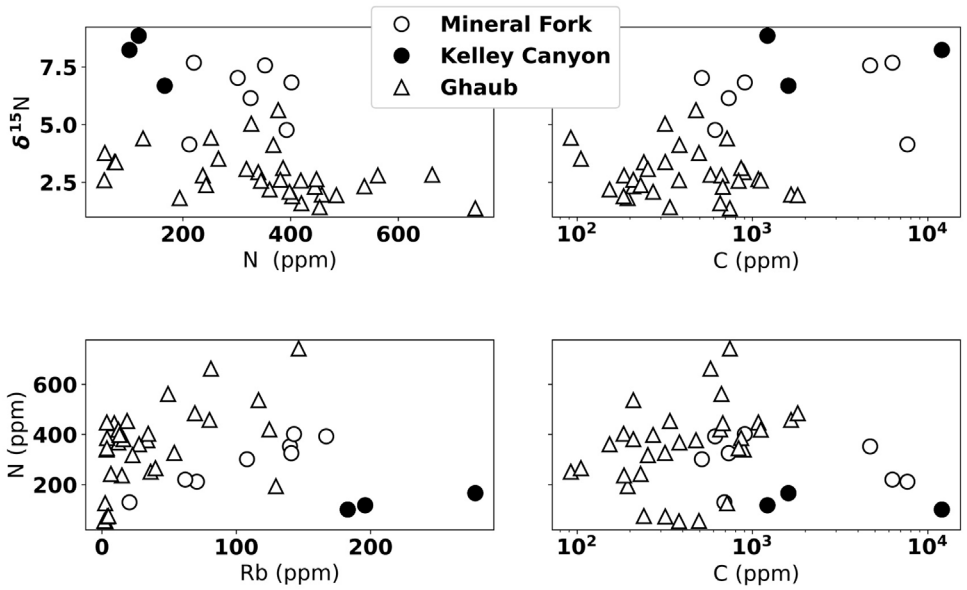

FIGURE 6 | Nitrogen isotope and concentration data shown in comparison to C and Rb concentration. We note no clear correlation between $\delta^{15}N$ and N or C, indicating no significant N loss due to metamorphism or fluid loss. Slight correlation between N and Rb concentration indicates there is some mineralogic control on the amount of N, but this is not influencing the $\delta^{15}N$.

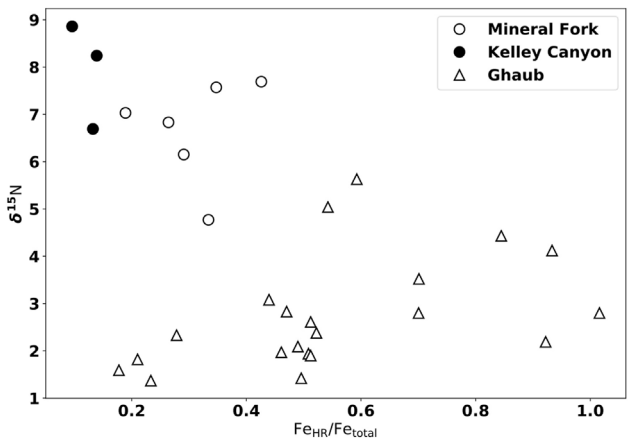

FIGURE 7 | Iron speciation data from the Mineral Fork Formation (open circles), Kelley Canyon Formation (closed circles), and the Ghaub Formation triangles). Mineral Fork samples with the highest $\delta^{15}N$ values have the lowest Fe_{HR}/Fe_{total}, consistent with oxygenated waters and partial denitrification. In contrast, samples from the Ghaub Formation show no clear correlation, consistent with an more anoxic water column.

not contain a Fe-Mn particulate shuttle, leading to low V concentrations.

Overall concentrations of these elements observed from Utah and Namibia are similar to other work focused on the Cryogenian. For example, a section spanning both Sturtian and Marinoan from the Zavkhan Terrane, southwest Mongolia finds U concentrations of between 0.05 and 2 ppm, very similar to our measurements (Lau et al., 2017). Trace element measurements from the Doushantuo Formation of South China, deposited after the Marinoan glacial period, display quite high concentrations of U (up to 30 ppm), V (1,000 ppm), and Mo (200 ppm) in the immediate deglacial period, with values decreasing rapidly up-section (Sahoo et al., 2012). Since the Kelley Canyon formation overlies the cap carbonate, it would have been deposited sometime after the deglaciation, and thus likely does not capture the immediate deglaciation.

4.2 Nitrogen Isotopes

We present N concentration and isotope data in **Figure 6**. $\delta^{15}N$ in both Namibia and Utah are positive, between about 1 to $5^0/_{00}$ from the Ghaub and 4.1 to $7.6^0/_{00}$ in the Mineral Fork (**Figures 6**, **7**). Values from the Kelley Canyon Formation are higher, between 6.7 to $8.9^0/_{00}$. Nitrogen concentration is similar in units from Namibia and Utah, ranging from 100 to 650 ppm. As noted in **Section 3.1**, analysis of previously measured till samples from the Timeball Hill and Blaubeker formations produced nearly identical $\delta^{15}N$ values but different N concentrations. Previous work has noted that within-sample heterogeneity may be an issue for N measurements (Johnson et al., 2017a). Rock hosted N can potentially exist as different species (e.g., NH_4^+, NO_3^-, N_2) and in different organic or mineral phases. So, it is possible that small scale heterogeneity, or slightly different analytical conditions/techniques may be liberating different pools of N. Bulk N isotope values, however, seem to be robust even if measured N concentrations vary (Bräuer and Hahne, 2005; Boocock et al., 2020).

To assess the potential influence of metamorphic alteration of N content and isotopic signals, we show $\delta^{15}N$ plotted against

N concentration, Rb concentration, and C concentration (**Figure 6**). We observe no correlation between $\delta^{15}N$ and N concentration, suggesting that higher $\delta^{15}N$ values are not caused by progressive N loss during metamorphism (Bebout and Fogel, 1992). There is a rough correlation between N and Rb concentration, suggesting some variation in N content could be related to detrital input. The lack of correlation, however, between $\delta^{15}N$ and N concentration again indicates that while there might be some lithologic control on total N, this does not influence isotope values. There is not a clear correlation between C and N content, which is different than previous work on the non-glacial Neoproterozoic (e.g., Ader et al., 2014), but similar to previous analyses of syn-glacial units (Johnson et al., 2017b). This suggests that there may be either differential preservation of N and C in these units, or that the N and C cycles are differently coupled during Snowball glaciations than the non-glacial intervals of the Cryogenian.

Assuming atmospheric N_2 was at $0^0/_{00}$ during the Cryogenian (Stüeken et al., 2016b), enriched $\delta^{15}N$ values, given the evidence of persistent O_2 availability provided by redox-sensitive element data, are consistent with the presence of partial, water-column denitrification during the Snowball glaciation. That is, there must have been sufficient O_2 present to support nitrification, with denitrification occurring at boundaries between oxygenated and low-oxygen waters, with a likely chemocline location in bottom waters. The similarity of Mineral Fork $\delta^{15}N$ values to average modern marine values (5 to $7^0/_{00}$) indicates that a similar relative amount of partial denitrification (~ 20%) was occurring in the water column (Tesdal et al., 2013).

After the glaciation, as preserved by the Kelley Canyon formation, samples have the highest $\delta^{15}N$ values measured. These values are typically interpreted to indicate more extensive denitrification, and lower water-column O_2, to drive residual N to higher $\delta^{15}N$ values. Yet, Fe-speciation data indicates oxygenated bottom waters during the deposition of the Kelley Canyon Formation (**Figures 2**, **7**). Kelley Canyon units also have the highest U concentrations of any samples presented (**Figure 5**), suggesting oxic weathering and delivery of U to the site of deposition. Thus, we require an interpretation that can explain both higher $\delta^{15}N$ values and a pervasively oxygenated water column. We propose two potential explanations: oceanographic circulation shifts and biologic responses to deglaciation.

A similar pattern, positive but low and then increasing several permil, in $\delta^{15}N$ values in sediments has been observed in a number of locations during the Pleistocene-Holocene deglaciation (Galbraith and Kienast, 2013). Several sites are near-shore environments, including one off the coast of northern Chile (De Pol-Holz et al., 2006). De Pol-Holz et al. (2006) observed an increase in sedimentary $\delta^{15}N$ values from 8 to $12^0/_{00}$ across the deglaciation, and attributed this increase to melting of the Patagonian Ice Sheet. The influx of freshwater slowed formation of intermediate water, which in turn decreased deep water ventilation. This oceanographic reorganization could have resulted in upwelled N that was enriched in ^{15}N, due to removal by denitrification, compared to the glacial maximum with a less well developed oxygen minimum zone. The Snowball deglaciation would have produced a large meltwater lid (Hoffman PF. et al., 2017), which could affect ocean circulation in a similar way: limited deep-water ventilation, increased denitrification at a chemocline underlying a well oxygenated upper water column.

In the wake of both the Sturtian and the Marinoan glaciations, the ocean appears to have become more oxygen rich and the surface temperature increased (Hoffman PF. et al., 2017; Lechte et al., 2019). There are many studies on contemporary denitrifying bacteria, both in the field and in culture, that demonstrate an increase in denitrification activity at higher temperatures (Nowicki, 1994; Veraart et al., 2011). Thus, we would expect to observe an increase in $\delta^{15}N$ in post-Snowball warm oceans, observed in both the Ghaub and Mineral Fork-Kelley Canyon Formations. While an increase in water column oxygen may seem anathema to increased denitrification, modern denitrifiers do function in oxygenated water. Specifically, by using the Nap reductase enzyme, instead of the Nar enzyme (Berks et al., 2001), organisms can perform aerobic denitrification (Ji et al., 2015). Perhaps, then, the combined effect of high temperatures and aerobic denitrification caused an increase in $\delta^{15}N$ values in the post-Snowball ocean, even in the presence of higher water column O_2.

Alternately, it is possible that enriched $\delta^{15}N$ values could reflect partial nitrification followed by complete denitrification. This scenario was proposed to explain very positive $\delta^{15}N$ values from the 2.7 Ga Tumbiana Formation (Thomazo et al., 2011), though an alternate explanation has been proposed suggesting high values could be caused by alkaline conditions and degassing of NH_3 (Stüeken et al., 2015). Nitrification to nitrite has a pronounced isotopic effect, with product NO_2^- depleted between 13 to $38^0/_{00}$ compared to reactant NH_4^+ (Casciotti et al., 2003). If, then, NO_2^- is quantitatively removed via anammox, the residual N pool would be comprised of isotopically enriched NH_4^+. In the modern ocean, this scenario has been observed in sediments of the Bering Sea (e.g., Morales et al., 2014). There is, however, a much wider range in sediment $\delta^{15}N$ values ($+2^0/_{00}$ to $+ 18^0/_{00}$), reflecting the transient nature of the geochemical conditions necessary for this to occur. Since the N isotope data from both Cryogenian sections are more tightly coupled with evidence for persistent oxic weathering, we suggest that they instead reflect less transient redox conditions, and likely complete nitrification followed by partial denitrification.

Additionally, we note that $\delta^{15}N$ values are generally lower in samples with Fe_{HR}/Fe_{total} values that are 'equivocal' compared to those that clearly plot in the ferruginous field (**Figure 2**, **7**). Since this potential trend is not strongly correlated ($r^2 = 0.13$), any interpretations at this point are speculative. It is possible that samples with low Fe_{total}, and therefore higher Fe_{HR}/Fe_{total}, represent upwelling into oxygenated conditions, driving denitrification and increasing $\delta^{15}N$ values. However, iron speciation data does not allow for quantitative interpretation of bottom water conditions within fields, but rather serves to distinguish between overarching redox conditions. Future work, either observational or geochemical modeling, could be valuable to investigate any controls on patterns within Fe-speciation fields.

5 IMPLICATIONS FOR SNOWBALL OCEAN AND REDOX-BIOLOGIC INTERPRETATIONS

There are two major implications from this work. First, we present further support for periods of oxygenated water during the Snowball Earth glaciations based on Fe-speciation, redox sensitive trace elements and enriched $\delta^{15}N$ values. Second, we suggest corroborating evidence for a relatively rapid increase in oxygen content in the post-Snowball ocean set against a background of variable redox conditions (Kunzmann et al., 2017; Lau et al., 2017) while also providing hypotheses to explain positive $\delta^{15}N$ during the Snowball ocean that increased after the glaciation.

Previous data from Namibia, combining N isotopes and redox proxies, had suggested pockets of oxygenated water with active photosynthesis and aerobic N cycling during the Marinoan (Johnson et al., 2017b). Our work herein records similar geochemical values, consistent with a similar water-column redox/nutrient state. Thus, in at least two locations - during a Snowball ocean - there is geochemical evidence for oxygenated water. What is unclear, though, is whether samples from Namibia and Utah represent contemporaneous time periods. Age control from Namibia is relatively tight (Hoffman et al., 2021), clearly indicating the Ghaub Formation is Marinoan in age.

As previously mentioned, the age of the Mineral Fork is crucial for any interpretation linking this site to broader global patterns of redox structure. If the Mineral Fork is Sturtian, it is likely that it was deposited in a rifting basin (e.g., Balgord et al., 2013). The similarity of N and redox geochemical values from Mineral Fork and the Ghaub suggest that they record broadly similar ocean conditions. We cannot say to what extent this might be a global signal during each glaciation, since at present these are the only sites with N and redox data synchronous with the Snowball ocean. Perhaps, then, marginal marine settings during the Marinoan and Sturtian glaciations were geochemically similar. While it is beyond the scope of this paper to determine global ocean redox, our work does demonstrate that combining proxies from geographically distributed samples can help fill in this picture. We suggest long-lived open water and/or ample photosynthesis to keep the atmosphere and at least parts of the upper ocean oxygenated. There may even have been periodic bottom water oxygenation during the deposition of the Mineral Fork Formation.

Comparison to other geochemical and observational work also indicates the presence of persistent oxygenated environments throughout the Snowball ocean. For example, geochemical analyses of iron formations (IFs) indicate that subglacial meltwater would have provided O_2 to marginal marine settings (Lechte et al., 2019). Measurements of cyclicity in banded IFs are consistent with ice sheets responding dynamically to orbital forcing (Mitchell et al., 2021). A potential consequence of such orbital forcing is that dynamic ice could have facilitated oxygenation of the surface ocean via air-sea gas exchange upon either ice retreat or advancement (Mitchell et al., 2021).

Our work demonstrates the utility of the combined redox proxy-N isotope analytical strategy for characterizing Precambrian units. This is especially useful during times of dynamic fluctuations in oxygen, both in the atmosphere and ocean (Sperling et al., 2015; Wei et al., 2021). For example, previous work has demonstrated that different oceanic redox structures can result in similar ranges of $\delta^{15}N$ values recorded in sediment (Ader et al., 2014). Values above approximately $0^0/_{00}$ could be generated in the water column, and therefore recorded in sediments, either from modern-like conditions or strongly redox stratified conditions. For the former, this is the result of complete nitrification followed by partial denitrification. For the latter, higher than zero $\delta^{15}N$ values can be caused by a combination of ammonification and partial assimilation (Ader et al., 2014). Such a redox-cline can either be shallow or deep, and still produce similar $\delta^{15}N$ values.

Thus, water column redox reconstructions are crucial for interpretation of N isotopes. Specifically, using Fe-speciation for bottom water redox and redox-sensitive trace elements for surface water/atmospheric redox conditions can contextualize N isotopes values. As more work utilizes N isotope measurements as a tool to investigate both biologic and redox activity (e.g., Peng et al., 2020), placing such biologically controlled signals into a redox context will be crucial.

6 CONCLUSION

The evolution of ocean redox and water column nutrient cycling are closely intertwined over Earth history. There are a number of redox proxies, including redox sensitive trace metal abundance and iron speciation, that can be used to investigate oxygenation of the ancient atmosphere and oceans. Stable isotope ratios of major nutrients, such as carbon and nitrogen, are often used to reconstruct ancient microbial ecosystems and metabolisms. Nitrogen isotopes are commonly measured in ancient sediments, but produce non-diagnostic signals. Indeed, there is more than one pathway or combination of fluxes in the nitrogen cycle that could produce the same bulk $\delta^{15}N$ signal. Due to the tight relationship between the nitrogen cycle and oxygen availability, combining redox proxies with isotopic measurements provides insight and context into the redox environment crucial for interpreting isotopic signals.

We utilized a combined redox and N-isotope approach to specifically highlight the nitrogen cycle during the Neoproterozoic Snowball Earth glaciations. We analyzed deposits from Utah, USA likely preserving the Sturtian (Mineral Fork Formation) and post-Sturtian (Kelley Canyon Formation) time periods, and show previous work from the Ghaub Formation in Namibia for comparison (Johnson et al., 2017b). We find that redox proxies (U, V and Mo concentrations, and Fe speciation) are consistent with the presence of oxygenated water near the surface and potentially near the sediment water interface as well. Nitrogen isotope ratios are all above $0^0/_{00}$,

and given redox constraints, are indicative of nitrification followed by partial denitrification in the water column. The geochemical proxies are quite similar between the two field sites, suggesting similar water conditions at different paleogeographic locations and times. That is, we present evidence for oxygenated water during Cryogenian glaciations. More broadly, our work shows that combining these two approaches yields a deeper insight into ancient ecosystems and water conditions over Earth history. We also highlight the importance of considering oceanographic and biologic interpretations of redox data, as these are important factors controlling N isotope signals in biomass and sediments through time.

DATA AVAILABILITY STATEMENT

The original contributions presented in the study are included in the article/**Supplementary Materials**, further inquiries can be directed to the corresponding author.

AUTHOR CONTRIBUTIONS

BJ designed the study, collected the samples, conducted N isotopic measurements, interpreted results, and prepared the manuscript. SP conducted Fe-speciation work, interpreted results, and prepared the manuscrpit. CM conducted Fe-speciation work, interpreted results, and prepared the manuscript.

FUNDING

BJ was supported by an NSF EAR postdoctoral fellowship (EAR-PF 1725784), as well as startup funding from Iowa State University.

SUPPLEMENTARY MATERIAL

The Supplementary Material for this article can be found online at: https://www.frontiersin.org/articles/10.3389/feart.2022.745830/full#supplementary-material

REFERENCES

Ader, M., Sansjofre, P., Halverson, G. P., Busigny, V., Trindade, R. I. F., Kunzmann, M., et al. (2014). Ocean Redox Structure across the Late Neoproterozoic Oxygenation Event: a Nitrogen Isotope Perspective. *Earth Planet. Sci. Lett.* 396, 1–13. doi:10.1016/j.epsl.2014.03.042

Ader, M., Thomazo, C., Sansjofre, P., Busigny, V., Papineau, D., Laffont, R., et al. (2016). Interpretation of the Nitrogen Isotopic Composition of Precambrian Sedimentary Rocks: Assumptions and Perspectives. *Chem. Geol.* 429, 93–110. doi:10.1016/j.chemgeo.2016.02.010

Alcott, L. J., Krause, A. J., Hammarlund, E. U., Bjerrum, C. J., Scholz, F., Xiong, Y., et al. (2020). Development of Iron Speciation Reference Materials for Palaeoredox Analysis. *Geostand. Geoanal Res.* 44, 581–591. doi:10.1111/ggr.12342

Algeo, T. J., and Liu, J. (2020). A Re-assessment of Elemental Proxies for Paleoredox Analysis. *Chem. Geol.* 540, 119549. doi:10.1016/j.chemgeo.2020.119549

Algeo, T. J., and Tribovillard, N. (2009). Environmental Analysis of Paleoceanographic Systems Based on Molybdenum-Uranium Covariation. *Chem. Geol.* 268, 211–225. doi:10.1016/j.chemgeo.2009.09.001

Balgord, E. A., Yonkee, W. A., Link, P. K., and Fanning, C. M. (2013). Stratigraphic, Geochronologic, and Geochemical Record of the Cryogenian Perry Canyon Formation, Northern Utah: Implications for Rodinia Rifting and Snowball Earth Glaciation. *Geol. Soc. Am. Bull.* 125, 1442–1467. doi:10.1130/b30860.1

Bebout, G. E., and Fogel, M. L. (1992). Nitrogen-isotope Compositions of Metasedimentary Rocks in the Catalina Schist, California: Implications for Metamorphic Devolatilization History. *Geochimica Cosmochimica Acta* 56, 2839–2849. doi:10.1016/0016-7037(92)90363-N

Benkovitz, A., Matthews, A., Teutsch, N., Poulton, S. W., Bar-Matthews, M., and Almogi-Labin, A. (2020). Tracing Water Column Euxinia in Eastern Mediterranean Sapropels S5 and S7. *Chem. Geol.* 545, 119627. doi:10.1016/j.chemgeo.2020.119627

Boocock, T. J., Mikhail, S., Prytulak, J., Di Rocco, T., and Stüeken, E. E. (2020). Nitrogen Mass Fraction and Stable Isotope Ratios for Fourteen Geological Reference Materials: Evaluating the Applicability of Elemental Analyser versus Sealed Tube Combustion Methods. *Geostand. Geoanal Res.* 44, 537–551. doi:10.1111/ggr.12345

Bräuer, K., and Hahne, K. (2005). Methodical Aspects of the 15N-Analysis of Precambrian and Palaeozoic Sediments Rich in Organic Matter. *Chem. Geol.* 218, 361–368. doi:10.1016/j.chemgeo.2005.01.004

Brunner, B., Contreras, S., Lehmann, M. F., Matantseva, O., Rollog, M., Kalvelage, T., et al. (2013). Nitrogen Isotope Effects Induced by Anammox Bacteria. *Proc. Natl. Acad. Sci. U.S.A.* 110, 18994–18999. doi:10.1073/pnas.1310488110

Busigny, V., Lebeau, O., Ader, M., Krapež, B., and Bekker, A. (2013). Nitrogen Cycle in the Late Archean Ferruginous Ocean. *Chem. Geol.* 362, 115–130. doi:10.1016/j.chemgeo.2013.06.023

Canfield, D. E., Lyons, T. W., and Raiswell, R. (1996). A Model for Iron Deposition to Euxinic Black Sea Sediments. *Am. J. Sci.* 296, 818–834. doi:10.2475/ajs.296.7.818

Casciotti, K. L., Buchwald, C., Santoro, A. E., and Frame, C. (2011). Assessment of Nitrogen and Oxygen Isotopic Fractionation during Nitrification and its Expression in the Marine Environment. *Methods Enzym. (Elsevier)* 486, 253–280. doi:10.1016/b978-0-12-381294-0.00011-0

Casciotti, K. L., Sigman, D. M., and Ward, B. B. (2003). Linking Diversity and Stable Isotope Fractionation in Ammonia-Oxidizing Bacteria. *Geomicrobiol. J.* 20, 335–353. doi:10.1080/01490450303895

Christie-Blick, N. (1982). Upper Proterozoic and Lower Cambrian Rocks of the Sheeprock Mountains, Utah: Regional Correlation and Significance. *Geol. Soc. Am. Bull.* 93, 735–750. doi:10.1130/0016-7606(1982)93<735:upalcr>2.0.co;2

Clarkson, M. O., Poulton, S. W., Guilbaud, R., and Wood, R. A. (2014). Assessing the Utility of Fe/Al and Fe-Speciation to Record Water Column Redox Conditions in Carbonate-Rich Sediments. *Chem. Geol.* 382, 111–122. doi:10.1016/j.chemgeo.2014.05.031

Crittenden, M. D., Jr, Christie-buck, N., and Karl Link, P. (1983). Evidence for Two Pulses of Glaciation during the Late Proterozoic in Northern Utah and Southeastern Idaho. *Geol. Soc. Am. Bull.* 94, 437–450. doi:10.1130/0016-7606(1983)94<437:eftpog>2.0.co;2

De Pol-Holz, R., Ulloa, O., Dezileau, L., Kaiser, J., Lamy, F., and Hebbeln, D. (2006). Melting of the Patagonian Ice Sheet and Deglacial Perturbations of the Nitrogen Cycle in the Eastern South Pacific. *Geophys. Res. Lett.* 33, 24477. doi:10.1029/2005gl024477

Galbraith, E. D., Kienast, M., and Kienast, M. (2013). The Acceleration of Oceanic Denitrification during Deglacial Warming. *Nat. Geosci.* 6, 579–584. doi:10.1038/ngeo1832

Garvin, J., Buick, R., Anbar, A. D., Arnold, G. L., and Kaufman, A. J. (2009). Isotopic Evidence for an Aerobic Nitrogen Cycle in the Latest Archean. *Science* 323, 1045–1048. doi:10.1126/science.1165675

Gaschnig, R. M., Rudnick, R. L., McDonough, W. F., Kaufman, A. J., Valley, J. W., Hu, Z., et al. (2016). Compositional Evolution of the Upper Continental Crust through Time, as Constrained by Ancient Glacial Diamictites. *Geochimica Cosmochimica Acta* 186, 316–343. doi:10.1016/j.gca.2016.03.020

Han, T., Fan, H., and Wen, H. (2018). Dwindling Vanadium in Seawater during the Early Cambrian, South China. *Chem. Geol.* 492, 20–29. doi:10.1016/j.chemgeo.2018.05.022

Hoffman, P. F., Abbot, D. S., Ashkenazy, Y., Benn, D. I., Brocks, J. J., Cohen, P. A., et al. (2017a). Snowball Earth Climate Dynamics and Cryogenian Geology-Geobiology. *Sci. Adv.* 3, e1600983. doi:10.1126/sciadv.1600983

Hoffman, P. F. (2016). Cryoconite Pans on Snowball Earth: Supraglacial Oases for Cryogenian Eukaryotes? *Geobiology* 14, 531–542. doi:10.1111/gbi.12191

Hoffman, P. F., Halverson, G. P., Schrag, D. P., Higgins, J. A., Domack, E. W., Macdonald, F. A., et al. (2021). Snowballs in Africa: Sectioning a Long-Lived Neoproterozoic Carbonate Platform and its Bathyal Foreslope (NW Namibia). *Earth Sci. Rev.* 2021, 103616. doi:10.1016/j.earscirev.2021.103616

Hoffman, P. F., Lamothe, K. G., LoBianco, S. J. C., Hodgskiss, M. S. W., Bellefroid, E. J., Johnson, B. W., et al. (2017b). Sedimentary Depocenters on Snowball Earth: Case Studies from the Sturtian Chuos Formation in Northern Namibia. *Geosphere* 13, 811–837. doi:10.1130/ges01457.1

Hoffman, P. F. (2011). Strange Bedfellows: Glacial Diamictite and Cap Carbonate from the Marinoan (635 Ma) Glaciation in Namibia. *Sedimentology* 58, 57–119. doi:10.1111/j.1365-3091.2010.01206.x

Ji, B., Yang, K., Zhu, L., Jiang, Y., Wang, H., Zhou, J., et al. (2015). Aerobic Denitrification: a Review of Important Advances of the Last 30 Years. *Biotechnol. Bioproc E* 20, 643–651. doi:10.1007/s12257-015-0009-0

Johnson, B. W., Drage, N., Spence, J., Hanson, N., El-Sabaawi, R., and Goldblatt, C. (2017a). Measurement of Geologic Nitrogen Using Mass Spectrometry, Colorimetry, and a Newly Adapted Fluorometry Technique. *Solid earth.* 8, 307–318. doi:10.5194/se-8-307-2017

Johnson, B. W., Poulton, S. W., and Goldblatt, C. (2017b). Marine Oxygen Production and Open Water Supported an Active Nitrogen Cycle during the Marinoan Snowball Earth. *Nat. Commun.* 8, 1316. doi:10.1038/s41467-017-01453-z

Kennedy, K., and Eyles, N. (2021). Syn-rift Mass Flow Generated 'tectonofacies' and 'tectonosequences' of the Kingston Peak Formation, Death Valley, California, and Their Bearing on Supposed Neoproterozoic Panglacial Climates. *Sedimentology* 68, 352–381. doi:10.1111/sed.12781

Kopf, S., Davidheiser-Kroll, B., and Kocken, I. (2021). Isoreader: An R Package to Read Stable Isotope Data Files for Reproducible Research. *Joss* 6, 2878. doi:10.21105/joss.02878

Kunzmann, M., Gibson, T. M., Halverson, G. P., Hodgskiss, M. S. W., Bui, T. H., Carozza, D. A., et al. (2017). Iron Isotope Biogeochemistry of Neoproterozoic Marine Shales. *Geochimica Cosmochimica Acta* 209, 85–105. doi:10.1016/j.gca.2017.04.003

Kunzmann, M., Halverson, G. P., Scott, C., Minarik, W. G., and Wing, B. A. (2015). Geochemistry of Neoproterozoic Black Shales from Svalbard: Implications for Oceanic Redox Conditions Spanning Cryogenian Glaciations. *Chem. Geol.* 417, 383–393. doi:10.1016/j.chemgeo.2015.10.022

Lau, K. V., Macdonald, F. A., Maher, K., and Payne, J. L. (2017). Uranium Isotope Evidence for Temporary Ocean Oxygenation in the Aftermath of the Sturtian Snowball Earth. *Earth Planet. Sci. Lett.* 458, 282–292. doi:10.1016/j.epsl.2016.10.043

Lechte, M. A., Wallace, M. W., Hood, A. v. S., Li, W., Jiang, G., Halverson, G. P., et al. (2019). Subglacial Meltwater Supported Aerobic Marine Habitats during Snowball Earth. *Proc. Natl. Acad. Sci. U.S.A.* 116, 25478–25483. doi:10.1073/pnas.1909165116

Li, Y., Wiedenbeck, M., Shcheka, S., and Keppler, H. (2013). Nitrogen Solubility in Upper Mantle Minerals. *Earth Planet. Sci. Lett.* 377-378, 311–323. doi:10.1016/j.epsl.2013.07.013

Link, P. K., and Christie-Blick, N. (2011). Chapter 38 Neoproterozoic Strata of Southeastern Idaho and Utah: Record of Cryogenian Rifting and Glaciation. *Geol. Soc. Lond. Memoirs* 36, 425–436. doi:10.1144/m36.38

Merdith, A. S., Collins, A. S., Williams, S. E., Pisarevsky, S., Foden, J. D., Archibald, D. B., et al. (2017). A Full-Plate Global Reconstruction of the Neoproterozoic. *Gondwana Res.* 50, 84–134. doi:10.1016/j.gr.2017.04.001

Mettam, C., Zerkle, A. L., Claire, M. W., Izon, G., Junium, C. J., and Twitchett, R. J. (2017). High-frequency Fluctuations in Redox Conditions during the Latest Permian Mass Extinction. *Palaeogeogr. Palaeoclimatol. Palaeoecol.* 485, 210–223. doi:10.1016/j.palaeo.2017.06.014

Mitchell, R. N., Gernon, T. M., Cox, G. M., Nordsvan, A. R., Kirscher, U., Xuan, C., et al. (2021). Orbital Forcing of Ice Sheets during Snowball Earth. *Nat. Commun.* 12, 4187–4189. doi:10.1038/s41467-021-24439-4

Morales, L. V., Granger, J., Chang, B. X., Prokopenko, M. G., Plessen, B., Gradinger, R., et al. (2014). Elevated 15N/14N in Particulate Organic Matter, Zooplankton, and Diatom Frustule-Bound Nitrogen in the Ice-Covered Water Column of the Bering Sea Eastern Shelf. *Deep Sea Res. Part II Top. Stud. Oceanogr.* 109, 100–111. doi:10.1016/j.dsr2.2014.05.008

Nowicki, B. L. (1994). The Effect of Temperature, Oxygen, Salinity, and Nutrient Enrichment on Estuarine Denitrification Rates Measured with a Modified Nitrogen Gas Flux Technique. *Estuar. Coast. Shelf Sci.* 38, 137–156. doi:10.1006/ecss.1994.1009

Ojakangas, R. W., and Matsch, C. L. (1980). Upper Precambrian (Eocambrian) Mineral Fork Tillite of Utah: a Continental Glacial and Glaciomarine Sequence. *Geol. Soc. Am. Bull.* 91, 495–501. doi:10.1130/0016-7606(1980)91<495:upemft>2.0.co;2

Peng, Y., Dong, L., Ma, H., Wang, R., Lang, X., Peng, Y., et al. (2020). Surface Ocean Nitrate-Limitation in the Aftermath of Marinoan Snowball Earth: Evidence from the Ediacaran Doushantuo Formation in the Western Margin of the Yangtze Block, South China. *Precambrian Res.* 347, 105846. doi:10.1016/j.precamres.2020.105846

Poulton, S. W., and Canfield, D. E. (2005). Development of a Sequential Extraction Procedure for Iron: Implications for Iron Partitioning in Continentally Derived Particulates. *Chem. Geol.* 214, 209–221. doi:10.1016/j.chemgeo.2004.09.003

Poulton, S. W., and Canfield, D. E. (2011). Ferruginous Conditions: A Dominant Feature of the Ocean through Earth's History. *Elements* 7, 107–112. doi:10.2113/gselements.7.2.107

Poulton, S. W., Fralick, P. W., and Canfield, D. E. (2010). Spatial Variability in Oceanic Redox Structure 1.8 Billion Years Ago. *Nat. Geosci.* 3, 486–490. doi:10.1038/ngeo889

Poulton, S. W., Fralick, P. W., and Canfield, D. E. (2004). The Transition to a Sulphidic Ocean ~ 1.84 Billion Years Ago. *Nature* 431, 173–177. doi:10.1038/nature02912

Poulton, S. W. (2021). *The Iron Speciation Paleoredox Proxy*. Cambridge: Cambridge University Press.

Quan, T. M., van de Schootbrugge, B., Field, M. P., Rosenthal, Y., and Falkowski, P. G. (2008). Nitrogen Isotope and Trace Metal Analyses from the Mingolsheim Core (Germany): Evidence for Redox Variations across the Triassic-Jurassic Boundary. *Glob. Biogeochem. Cycles* 22, a–n. doi:10.1029/2007GB002981

Quan, T. M., Wright, J. D., and Falkowski, P. G. (2013). Co-variation of Nitrogen Isotopes and Redox States through Glacial-Interglacial Cycles in the Black Sea. *Geochimica Cosmochimica Acta* 112, 305–320. doi:10.1016/j.gca.2013.02.029

Raiswell, R., and Canfield, D. E. (1998). Sources of Iron for Pyrite Formation in Marine Sediments. *Am. J. Sci.* 298, 219–245. doi:10.2475/ajs.298.3.219

Richardson, D. J., Berks, B. C., Russell, D. A., Spiro, S., and Taylor, C. J. (2001). Functional, Biochemical and Genetic Diversity of Prokaryotic Nitrate Reductases. *Cell. Mol. Life Sci.* 58, 165–178. doi:10.1007/PL00000845

Sahoo, S. K., Planavsky, N. J., Kendall, B., Wang, X., Shi, X., Scott, C., et al. (2012). Ocean Oxygenation in the Wake of the Marinoan Glaciation. *Nature* 489, 546–549. doi:10.1038/nature11445

Sigman, D. M., DiFiore, P. J., Hain, M. P., Deutsch, C., Wang, Y., Karl, D. M., et al. (2009). The Dual Isotopes of Deep Nitrate as a Constraint on the Cycle and Budget of Oceanic Fixed Nitrogen. *Deep Sea Res. Part I Oceanogr. Res. Pap.* 56, 1419–1439. doi:10.1016/j.dsr.2009.04.007

Sperling, E. A., Wolock, C. J., Morgan, A. S., Gill, B. C., Kunzmann, M., Halverson, G. P., et al. (2015). Statistical Analysis of Iron Geochemical Data Suggests Limited Late Proterozoic Oxygenation. *Nature* 523, 451–454. doi:10.1038/nature14589

Stüeken, E. E., Buick, R., Guy, B. M., and Koehler, M. C. (2015). Isotopic Evidence for Biological Nitrogen Fixation by Molybdenum-Nitrogenase from 3.2 Gyr. *Nature* 520, 666–669. doi:10.1038/nature14180

Stüeken, E. E., Buick, R., and Lyons, T. W. (2019a). Revisiting the Depositional Environment of the Neoproterozoic Callanna Group, South Australia. *Precambrian Res.* 334, 105474. doi:10.1016/j.precamres.2019.105474

Stüeken, E. E., Kipp, M. A., Koehler, M. C., and Buick, R. (2016b). The Evolution of Earth's Biogeochemical Nitrogen Cycle. *Earth-Science Rev.* 160, 220–239. doi:10.1016/j.earscirev.2016.07.007

Stüeken, E. E., Kipp, M. A., Koehler, M. C., Schwieterman, E. W., Johnson, B., and Buick, R. (2016a). Modeling pN2 through Geological Time: Implications for Planetary Climates and Atmospheric Biosignatures. *Astrobiology* 16, 949–963. doi:10.1089/ast.2016.1537

Stüeken, E. E., Martinez, A., Love, G., Olsen, P. E., Bates, S., and Lyons, T. W. (2019b). Effects of pH on Redox Proxies in a Jurassic Rift Lake: Implications for Interpreting Environmental Records in Deep Time. *Geochimica Cosmochimica Acta* 252, 240–267. doi:10.1016/j.gca.2019.03.014

Tesdal, J.-E., Galbraith, E. D., and Kienast, M. (2013). Nitrogen Isotopes in Bulk Marine Sediment: Linking Seafloor Observations with Subseafloor Records. *Biogeosciences* 10, 101–118. doi:10.5194/bg-10-101-2013

Thomazo, C., Ader, M., and Philippot, P. (2011). Extreme 15N-Enrichments in 2.72-Gyr-Old Sediments: Evidence for a Turning Point in the Nitrogen Cycle. *Geobiology* 9, 107–120. doi:10.1111/j.1472-4669.2011.00271.x

Tribovillard, N., Algeo, T. J., Lyons, T., and Riboulleau, A. (2006). Trace Metals as Paleoredox and Paleoproductivity Proxies: an Update. *Chem. Geol.* 232, 12–32. doi:10.1016/j.chemgeo.2006.02.012

Veraart, A. J., De Klein, J. J. M., and Scheffer, M. (2011). Warming Can Boost Denitrification Disproportionately Due to Altered Oxygen Dynamics. *PLoS One* 6, e18508. doi:10.1371/journal.pone.0018508

Wang, W., Guan, C., Zhou, C., Peng, Y., Pratt, L. M., Chen, X., et al. (2017). Integrated Carbon, Sulfur, and Nitrogen Isotope Chemostratigraphy of the Ediacaran Lantian Formation in South China: Spatial Gradient, Ocean Redox Oscillation, and Fossil Distribution. *Geobiology* 15, 552–571. doi:10.1111/gbi.12226

Wei, G.-Y., Planavsky, N. J., He, T., Zhang, F., Stockey, R. G., Cole, D. B., et al. (2021). Global Marine Redox Evolution from the Late Neoproterozoic to the Early Paleozoic Constrained by the Integration of Mo and U Isotope Records. *Earth-Science Rev.* 214, 103506. doi:10.1016/j.earscirev.2021.103506

Yonkee, W. A., Dehler, C. D., Link, P. K., Balgord, E. A., Keeley, J. A., Hayes, D. S., et al. (2014). Tectono-stratigraphic Framework of Neoproterozoic to Cambrian Strata, West-Central U.S.: Protracted Rifting, Glaciation, and Evolution of the North American Cordilleran Margin. *Earth-Science Rev.* 136, 59–95. doi:10.1016/j.earscirev.2014.05.004

Young, G. M. (2002). Geochemical Investigation of a Neoproterozoic Glacial Unit: the Mineral Fork Formation in the Wasatch Range, Utah. *Geol. Soc. Am. Bull.* 114, 387–399. doi:10.1130/0016-7606(2002)114<0387:gioang>2.0.co;2

Zerkle, A. L., and Mikhail, S. (2017). The Geobiological Nitrogen Cycle: From Microbes to the Mantle. *Geobiology* 15, 343–352. doi:10.1111/gbi.12228

Zerkle, A. L., Poulton, S. W., Newton, R. J., Mettam, C., Claire, M. W., Bekker, A., et al. (2017). Onset of the Aerobic Nitrogen Cycle during the Great Oxidation Event. *Nature* 542, 465–467. doi:10.1038/nature20826

Zhang, X., Sigman, D. M., Morel, F. M. M., and Kraepiel, A. M. L. (2014). Nitrogen Isotope Fractionation by Alternative Nitrogenases and Past Ocean Anoxia. *Proc. Natl. Acad. Sci. U.S.A.* 111, 4782–4787. doi:10.1073/pnas.1402976111

Conflict of Interest: The authors declare that the research was conducted in the absence of any commercial or financial relationships that could be construed as a potential conflict of interest.

Publisher's Note: All claims expressed in this article are solely those of the authors and do not necessarily represent those of their affiliated organizations, or those of the publisher, the editors and the reviewers. Any product that may be evaluated in this article, or claim that may be made by its manufacturer, is not guaranteed or endorsed by the publisher.The standard for N isotopes is atmospheric N_2, which is set to $0^0/_{00}$ by definition.

Advantages of publishing in Frontiers

OPEN ACCESS
Articles are free to read for greatest visibility and readership

FAST PUBLICATION
Around 90 days from submission to decision

HIGH QUALITY PEER-REVIEW
Rigorous, collaborative, and constructive peer-review

TRANSPARENT PEER-REVIEW
Editors and reviewers acknowledged by name on published articles

Frontiers
Avenue du Tribunal-Fédéral 34
1005 Lausanne | Switzerland

Visit us: www.frontiersin.org
Contact us: frontiersin.org/about/contact

REPRODUCIBILITY OF RESEARCH
Support open data and methods to enhance research reproducibility

DIGITAL PUBLISHING
Articles designed for optimal readership across devices

FOLLOW US
@frontiersin

IMPACT METRICS
Advanced article metrics track visibility across digital media

EXTENSIVE PROMOTION
Marketing and promotion of impactful research

LOOP RESEARCH NETWORK
Our network increases your article's readership